THERMAL DECOMPOSITION OF CHARRING MATERIALS

By

Said Nurbakhsh

A DISSERTATION

Submitted to
Michigan State University
in partial fulfillment of the requirements
for the degree of

DOCTOR OF PHILOSOPHY

Department of Mechanical Engineering

1989

ABSTRACT

THERMAL DECOMPOSITION OF CHARRING MATERIALS

By

Said Nurbakhsh

In this work, the complex process of pyrolysis of charring solids was studied. Experimental techniques and methods were developed to investigate the transient process of wood pyrolysis under different levels of external radiation, moisture content of the wood sample, and oxygen concentration of the ambient atmosphere. A unique small-scale combustion-wind tunnel was constructed to conduct the pyrolysis experiments and to obtain the time dependent gasification mass flux, surface and in-depth temperatures, and evolved products of pyrolysis (CO, CO_2, H_2O, and total hydrocarbons [THC]) for thermally thick samples of Douglas-fir. Experiments were performed both in inert atmosphere (nitrogen), and in air at several different heat fluxes and three different moisture contents of wood. Time dependent empirical chemical composition, char yield, and the heat of combustion of the pyrolysis products were determined.

The experimental results indicate that the presence of moisture reduces the pyrolysis mass flux and delays the occurrence of its maxima. Presence of oxygen drastically increases the pyrolysis mass flux but its effect specially at lower temperatures depends on the experimental conditions such as the boundary layer thickness over the wood surface. Char yield, chemical composition of the volatiles, and the heat of combustion were not found to be constant, instead they vary during the pyrolysis process and with changes in the environmental conditions and wood moisture content. The results also show that the asymptotic fall-off of the pyrolysis mass flux is not proportional to the negative one-half power of time as predicted by

some simple models.

In the theoretical part of this work, the 'pyrolysis temperature' assumption often used for the simplified modeling of wood pyrolysis was examined in detail by considering two otherwise identical models; one with infinitely fast decomposition kinetics and the other with finite rate chemistry. The pyrolysis temperature used in the pyrolysis temperature model was determined by enforcing conservation of mass and energy in an integral sense between the two models. It was found that although the surface and in-depth temperatures predicted by both the models were in reasonable agreement, significant differences were found in the mass evolution rate of volatiles. Different pyrolysis temperatures were required to balance mass and energy each time the heat loss boundary conditions or the incident heat flux was altered. It was concluded that the pyrolysis temperature is not a material property and different pyrolysis temperatures are needed for every problem.

To the Memory of My Mother

Acknowledgement

The author is greatly thankful to his advisor Professor Arvind Atreya for introducing him to the area of wood pyrolysis and fire research. His constant guidance, encouragement and direct involvement in every step of the work was of invaluable help in the completion of this work. I deeply appreciate his patience and and his friendship. I am also very grateful to Professors John R. Lloyd, James V. Beck, and David Yen, members of my Ph.D. Guidance Committee, for their helpful comments, suggestions, and encouragements.

I would like to thank Mr. Leonard Eisele and Mr. Paul Faeth for construction of the combustion-wind tunnel. I also wish to thank Mr. Robert Rose for his ever generous helps in many details of the electrical components of my experimental facility. Without their help this work would not have been possible. Many thanks to my colleagues and friends; Mr. Kamel El Mekki for his help in conducting experiments and Mr. Charles Gendrich for developing the data acquisition system. Finally, I am thankful to my dear wife, Hengameh, for her patience during this work.

This work was supported by the National Science Foundation under Grant # CBT - 8415423.

TABLE OF CONTENTS

LIST OF TABLES

LIST OF FIGURES

Appendix A

Appendix B

Appendix C

NOMENCLATURE

A = Pre-exponential factor, 1/sec
b_1 = Variable in equation (B-3)
b_2 = Variable in equation (B-3)
b_3 = Variable in equation (B-3)
C_p = Specific Heat, J/kg.K
E = Energy, W/cm^2
E_p = Activation Enegy, J/Kg.mole
f_s = Energy going into the solid, W/cm^2
F = Externally applied heat flux, W/cm^2
h = Conductive heat transfer coefficient, W/cm^2 . K
ΔH_c = Heat of combustion per unit mass of O_2, KJ/gm
ΔH_v = Heat of combustion of pyrolysis products, KJ/gm
k = $\Delta\eta$
K = Thermal conductivity, J/ m . K . sec
L = Length, m
N = Number of nodal points
$\dot{m}''$ = Mass flux, g/cm^2.sec
$\dot{q}''$ = Heat flux, W/cm^2
Q = Heat of pyrolysis, cal/gm
r = $\Delta\tau/\Delta\eta^2$
R = Universal gas constant, Cal/ gm mole K
s = Non-dimensional distance
T = Temperature, °C or K
t = Time, sec
t_c = Time constant, sec
w = Nodal points adjacent to char-wood interface
x = Distance, cm
X = Distance, cm
X_1 = Variable in equation (B-12)
Y = Mole fraction
Y_c = Char yield

Greek

α = Thermal diffusivity (Chapter 5)
α = A constant (Chapter 4)
β = α_w/α_c
η = x/L
γ = k_c/k_w
Γ = Gamma function
ρ = Density
τ = Non-dimensional time, equation (B-1)
θ = T/Tsun$_\infty$

Subscripts

a = Active material
c = Char
f = Final
f = Fuel
in = Incident
i = Space coordinate
j = Time coordinate
og = Out with gases
p = Pyrolysis
py = Pyrolysis
s = Solid
w = Wood
∞ = Ambient
st = Stored

Chapter One

Introduction and Literature Review

The burning of wood and other cellulosic materials has long been recognized as being of central importance in fire research. These materials are very important sources of fuel and the potential for energy and chemicals production from these renewable sources has established great interest in their thermal behavior. A fundamental understanding of the thermal degradation and combustion of cellulosic materials and possible methods for controlling them is essential for protection and better utilization of these materials.

The combustion of charring materials is a complex process. A major feature of these materials is that the solid upon heating, undergoes a thermal degradation process which generates the fuel gases to sustain a diffusion flame and leaves behind a layer of

char. The formation and growth of this char layer complicates the flaming combustion of thick pieces of wood. The propagation of the pyrolysis front into the solid presents a Stefan-type problem which introduces nonlinear coupling between the gas phase combustion and the solid phase decomposition. For a realistic prediction of the pyrolysis rate it is necessary to have data on the amount of char produced at any instant (i.e. the char yield) and changes in the thermal properties of burning wood and char.

In this work the transient thermal decomposition process of thick samples of wood is studied under different levels of external radiation, moisture content, and oxygen concentration of the ambient atmosphere. Experimental techniques and methods were developed for this study. Numerous experiments were done on specially prepared and instrumented samples of wood in an attempt to obtain reliable data for the determination of the transient changes in the overall composition of the volatile gases and the char yield.

1.1 Description of the Physical Problem

Consider a slab of wood initially at ambient temperature exposed to heat from other burning objects in a furnace or a fireplace. Upon heating of wood, first the adsorbed water is released (desorption), and then thermal degradation or pyrolysis of wood provides a highly reactive carbonaceous char and a mixture of gaseous, volatile, and tarry products. In the presence of oxygen, oxidation of char in the solid phase produces glowing combustion, whereas the mixture of volatiles and tarry particles (condensible hydrocarbons) that are carried out to the gas phase can produce flaming combustion if the mixture of fuel and oxygen is ignited. Figure 1.1 shows a qualitative diagram of the pyrolysis mass flux history. During this process a pyrolysis zone will be developed in the solid [corresponds to the initial rise of the mass flux curve (Figure 1.1)] and begins to propagate into the material [corresponds to the gradual decay in

the ma

layer a

heat in

surface

wood i

of woo

In

coupled

the over

thermal

be addre

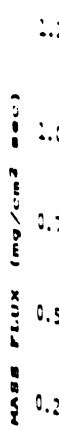

the mass flux curve (Figure 1.1)] leaving behind an insulating layer of char. This char layer attenuates the fuel evolution rate, by acting as a barrier against conduction of heat into the solid, and also radiates away part of the incident radiation to the surface. If wood is heated in an inert atmosphere, this process continues until all of the wood is pyrolyzed. In an oxygen containing atmosphere, non-flaming gasification rate of wood will be increased by char oxidation.

In the burning of a charring solid, the gas phase flaming combustion is directly coupled with the solid phase decomposition process. For a complete understanding of the overall combustion, one needs to study the phenomena in each phase. In this work thermal decomposition of wood - the phenomenon occurring in the solid phase – will be addressed.

Figure 1.1 Qualitative diagram of pyrolysis mass flux.

Background and Literature Review

1.2 Physical Properties and Chemical Components of Wood

Wood is a highly porous material made up of cells and fibers that are vessels and channels for transportation of water and gases. They also provide the mechanical strength of wood. The porosity (ratio of the volume of pores to the volume occupied by the cell wall) of the wood lies somewhere in the range of 40-75%. It is mainly made up of two major chemical components carbohydrates (65-70%) and lignin (18-35%). Minor amounts of extraneous materials, mostly in the form of organic and inorganic minerals (ash), are also present in wood.

The carbohydrate portion of wood comprises of cellulose and hemicellulose. Cellulose (a polymer of glucosan $(C_6H_{10}O_5)_n$) ranges from 40 to 45% of the dry wood weight, and hemicellulose (a polysacharide producing wood sugars) ranges from 25 to 35%. The other major component of wood, i.e. lignin, is a multi ring compound whose molecular weight exceeds one thousand.

Unless wood is dried, it usually contains some moisture. The moisture in wood is in three forms: (1) Free water which is mechanically held - by surface tension - to the walls of the cell cavities in the structure of wood. The energy needed to release this water is only slightly over the latent heat of water. (2) Adsorbed or bound water which is limited to approximately 30% of the oven dry weight of the wood. Here the water molecules are attached to the cell walls via hydrogen bonds and it needs some more energy to be released for lower moisture content. (3) The water of constitution which is formed and liberated along with the other pyrolysis products of wood. Primarily absorbed and adsorbed water are liberated within the early stages of heating of wood. In general, it is not possible to distinguish between different kinds of moisture being released. Practically, at any depth in wood, decomposition starts soon after the free and bound water are evaporated. Furthermore, upon heating of wood,

the release of water occurs in depth and the vapor need not all be driven to the surface to escape. Some may move inward and recondense in cooler interior portions of the solid. Thus even before decomposition starts the nature of the solid may be modified by the heat.

To obtain "dry" wood, generally, it is not possible to remove all the moisture content of wood without initiating any pyrolysis. However, theoretically when all non-constitution water is evaporated the wood could be termed as "dry". This, of course, will take a very long demoisturizing treatment of wood in a well controlled humidity chamber to be achieved.

1.3 Thermal Decomposition of Wood

As it was mentioned earlier, cellulose is the major component of wood and other cellulosic materials as well as the major source of combustible fuel for the flaming combustion. Hence, the chemistry of pyrolysis and formation of volatile products from cellulose could well represent the corresponding processes occurring in wood. In this section the pyrolysis of cellulose within thermally thick slabs of the solid is described briefly.

Pyrolysis of cellulose occurs in two distinct pathways [Shafizadeh (1981)]. At lower temperatures (200 - 280°C) dehydration of cellulose produces dehydrocellulose and water. This process is slightly endothermic (except in the presence of oxygen) and leads to the formation of char, water, and volatile gases such as CO_2, CO, and hydrocarbons. The gases evolved in the dehydrocellulose route are primarily noncombustible and the char which remains can oxidize through a surface (glowing) combustion. At higher temperatures (280 - 340°C) endothermic depolymerization of cellulose leads to the formation of tarry products which are highly condensible and constitute the main gaseous fuel to support a gas-phase flame. On further raising the temperature, the tar-forming reactions accelerate rapidly and overshadow the

production of char and gases. The tarry products of primary reactions may undergo further decomposition as they pass through the hot porous char. In fact, the analysis of the pyrolysis products of cellulose show different yields of char and tar in vacuum and in atmospheric pressure [Shafizadeh (1981)]. This is due to the much lower residence time of evolved gases when they travel through the hot char matrix in vacuum than in atmospheric pressure. These pathways and observations were summarized by Atreya (1983) in the following scheme which is consistent with the works of other investigators [Madorsky (1975), Shafizadeh (1981), Martin (1965), Panton et al. (1971), and Broido (1976)].

1.4 Formation of Char and Its Effects on Pyrolysis Process

As shown in Figure 1.2, char may be produced by direct thermal degradation of wood. It may also be produced from dehydration and condensation of the volatile pyrolysis products (tar) in the active material. The porous char matrix is a highly reactive substance which can have different compositions and properties at various stages of charring. The reactivity of char depends on the interactions between the char matrix and the volatile gases at different stages of pyrolysis [Shafizadeh (1981)]. The temperature history, the type of ambient atmosphere, and heat treatment conditions of wood will change the rate of char yield and to some extent properties of char.

In the presence of oxygen, oxidation of char can lead to smoldering or glowing combustion. The latter one, occurs in the presence of more oxygen and at higher temperatures. Smoldering combustion occurs at lower temperatures and " incomplete " oxidation of char leads to formation of CO and CO_2 and generation of new reactive cites. Oxidation of char causes the char surface to regress. However, the rate of char consumption is not as fast as the rate of pyrolysis of the substrate [Shafizadeh (1981)].

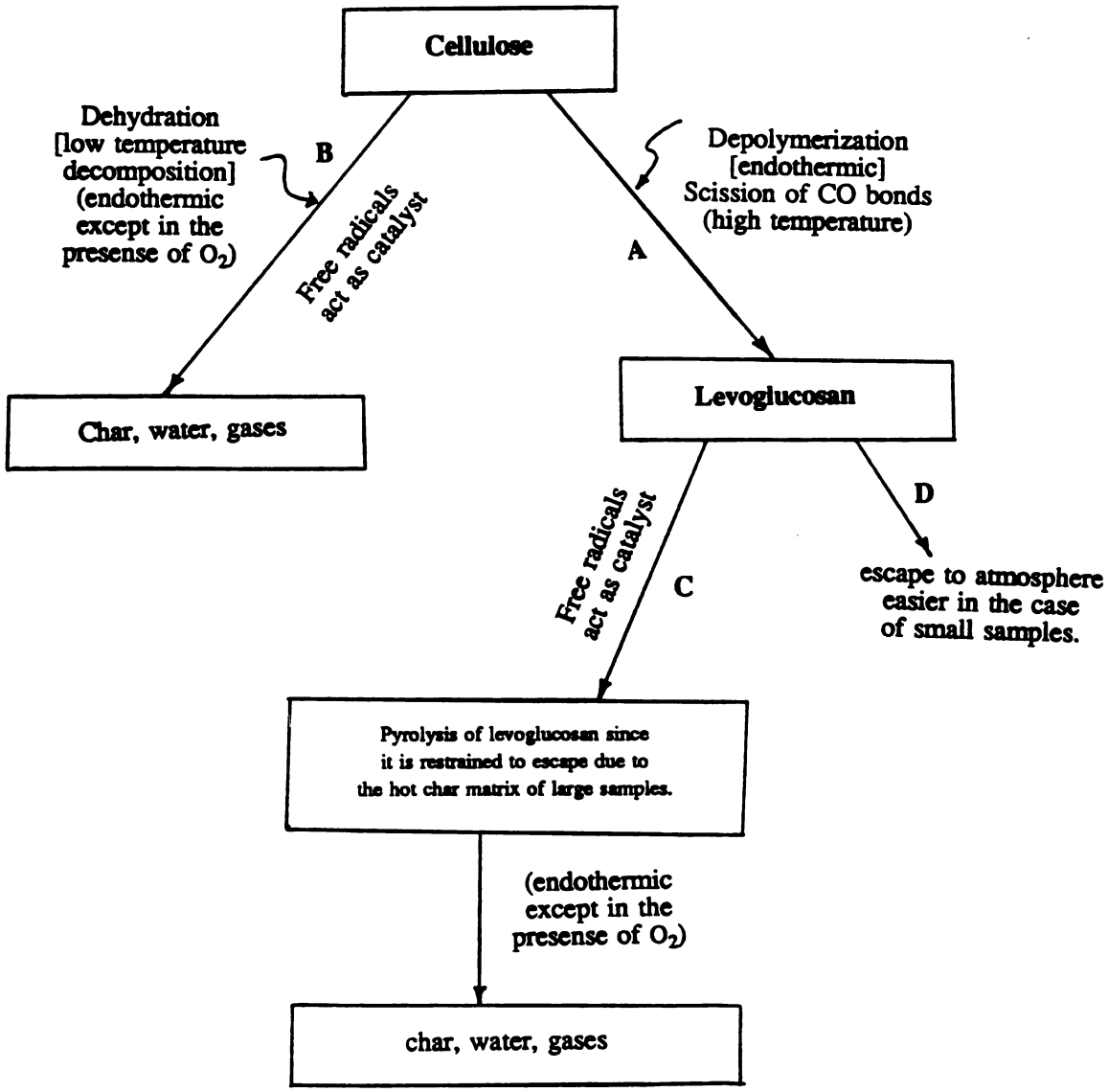

Figure 1.2 Two alternative routes for the decomposition of cellulose.

As the pyrolysis continues and the thickness of the char layer increases fine cracks begin to appear on the surface. The solid surface continuously shrinks and the cracks grow in size. The direction and size of the cracks are different for different types of wood and even for different samples of the same type of wood. The appearance of these cracks may have a significant effect on the pyrolysis of the remaining material because they alter the course of heating of the solid and the motion of volatiles within the char matrix by reducing heat exchange between the gases and the solid [Atreya (1983)]. The shrinkage of the solid, which is more significant at high heat fluxes, causes the actual temporal variations in the densities to be different from those obtained based on the initial volume of the solid.

1.5 Energetics of Thermal Decomposition

The overall solid-phase decomposition process involves the following phenomena: energy transport by conduction; kinetics of thermal decomposition; outward migration of moisture and pyrolysis products and its interaction with the solid; convective heat transfer and possibly* chemical reactions between the fuel volatiles and the char matrix; inward migration, condensation, and regasification of volatile fuel gases; pressure build up in the interior of the solid due to the generation and migration of these gases; radiative exchange within the porous cells of the char matrix; shrinkage and cracking of the char which alters some of the above processes. The physical and chemical properties of both char and wood also change as the temperature of the solid changes.

---

* The controversy over the occurrence of secondary exothermic reactions between the hot char and the fuel gases is not yet completely resolved. Atreya (1983), by recording the temperature of the gas phase very close to the surface of the pyrolyzing wood, showed that the exothermic reactions indeed occur not inside the solid but outside between oxygen and fuel gases. This issue will be addressed in this work.

Inclusion of all these parameters into a single analytical or even numerical model will be extremely difficult because of the nonlinearities associated with all the rate processes. A detail theoretical model must include variations of thermal properties (ρ, C_p, K) of the solid and char yield in the pyrolysis of wood. For polymeric fuels property variations associted with chemical decomposition are very significant. However, wood is a highly anisotropic and inhomogeneous porous solid and its thermal properties are different in each direction. Hence, the transient process of wood pyrolysis is very hard to be completely reproduced. Accurate reliable data on temperature dependent thermal properties of wood and char, char yield and changes in the empirical chemical composition of pyrolysis products are lacking.

1.6 Previous Work

Extensive experimental and theoretical work has been done on chemical and physical processes occurring during pyrolysis of solid materials. A considerable amount of this work have been focussed on "vaporizing" solids such as PMMA (Polymethylmetacrylate). Many investigators studied pyrolysis of charring solids such as wood. However, most of their attempts have been focussed on determination of thermal and kinetic parameters (such as heat of pyrolysis, activation energy, and frequency factor) that were incorporated in the models that describe pyrolysis process. Several reviews have been published on the subject [Welker (1970), Roberts (1970), Zardy and Pyle (1982)]. Since these works have been recently reviewed by Atreya (1983), only relevant aspects are presented here. In Section 1.6.1 the history of the previous experimental work is reviewed and work on pyrolysis of thick specimens of wood is described in more detail. In Section 1.6.2 the past theoretical work is discussed briefly.

1.6

and

sam

Da

gra

par

dec

The

Sh

[Ta

Sca

and

losse

cylin

as th

sensi

mate

weig

energ

which

I

differe

same

each c

1.6.1 Experimental Work

experiments on pyrolysis of wood and its components (cellulose, hemicellulose, and lignin) may be divided into two major categories: (1) Data obtained on small samples (i.e. thermally thin with almost no temperature gradient within the solid). (2) Data obtained on large samples (i.e. thermally thick with an effective temperature gradient inside the solid). These were reviewed by Atreya (1983) and Chan (1983).

In the first category several techniques are used to determine the relevant parameters related to the physics of pyrolysis (heat of pyrolysis), or chemistry of decomposition (activation energy and frequency factor). These techniques are: (1) Thermogravimetric Analysis (TGA) [Tang (1967), Rogers and Ohlemiller (1980), Shafizadeh (1968) and several other authors]; Differential Thermal Analysis (DTA) [Tang and Neil (1964), Broido (1966) and several other authors]; and Differential Scanning Calorimetery (DSC).

In the DTA method, the electrical power required to keep a wood test cylinder and a compensation cylinder at the same surface temperature to assure equal heat losses to the surrounding is measured. The difference in the power supplied to the test cylinder as compared to the compensation cylinder is due to the sensible heat as well as the heat of decomposition. This is called "energy capacity". By assuming the sensible heat portion of the energy capacity to be proportional to the amount of solid material left, the value of the energy capacity can be multiplied by the percentage of weight remaining at a given temperature to estimate the sensible heat portion of the energy capacity. Several authors have used this technique to measure heat of pyrolysis, which is reported in a review by Welker (1970).

In differential scanning calorimetery energy differences rather than temperature differences are measured. Both the sample and the reference cells are maintained at the same temperature during the analysis by adjusting the electrical power dissipated in each case in the required manner. Havens et al. (1971) used this method to measure

heat of pyrolysis.

In thermal gravimetric studies of wood decomposition weight loss versus time is measured at a series of constant temperatures over the desired range (isothermal TGA), or weight loss is measured as a function of time while the sample is heated so as to effect a linear temperature rise (dynamic TGA). From these data, the frequency factor A and activation energy E are determined to find a first order Arrhenius reaction equation for the weight loss (or density change) as a function of temperature

$$\frac{dm}{dt} = A\, m\, e^{-\frac{E}{RT}}$$

Several authors have used this method [Tang (1967), Shafizadeh (1968), Rogers and Ohlemiller (1980), and others].

In the second category, the pyrolysis of large samples of wood have been studied. Large samples are thermally thick, resulting in a temperature gradient inside the solid which plays a significant role in the decomposition process, composition of pyrolysis products, and the char yield. In this type of pyrolysis, wood gasification is controlled by heat and mass transfer processes and is affected by other physical variables such as moisture content, grain direction, and sample orientation. Only a few studies on thick samples have been reported in the past and most of them have been focussed on the determination of physical and kinetic parameters controlling the pyrolysis process. Some of the most relevant work which has been done in the past is briefly reviewed in the following paragraphs.

Bamford et al. (1945) heated thick slabs of wood by luminous gas flames and measured the spontaneous ignition time and the temperature at the center of the solid and calculated the heat of decomposition per unit mass of volatiles. Roberts and Clough (1963) conducted experiments on wood cylinders under controlled atmosphere in nitrogen to study the overall kinetics of the decomposition reactions. The rise in the central temperature of the wood cylinder above the surface temperature was attributed

to the exothermic reactions within the solid. Their results showed that for experiments in which the weight loss was high and the central temperature exceeded 350°C the activation energy E was 15,000 cal/gm-mole and the frequency factor A was 9.0×10^4 1/min. For lower temperature and weight loss E=25,000 cal/gm and A=2.6×10^9 1/min. This was attributed to the difference between the early and later stages of the reaction. From their experimental data they concluded that primary decomposition of wood has low heat of reaction but when gases travel outwards through the hot char, secondary decomposition of gases occurs, solid char acting as catalyst. Thus the exothermic heat of reaction increases rapidly with distance from the axis and then becomes approximately constant.

Kilzer and Broido (1965) analyzed data for pyrolysis of wood and suggested two competing sequences of reactions. One a slightly endothermic dehydration to "dehydrocellulose" followed by an endothermic sequence of reactions yielding char and various gaseous products. The other one an endothermic depolymerization of cellulose to produce volatile products. They concluded that under some conditions, such as reduced pressure, the primary pyrolysis of wood can be endothermic. Under normal conditions, at atmospheric pressure the primary pyrolysis of wood is exothermic. They speculated that the difference may be caused by a change in the reaction mechanism of cellulose due to catalytic or autocatalytic effects.

The wide discrepancy of reported values and even sign of the heat of decomposition was considerably narrowed by the work of Kung and Kalelkar (1973). They used a mathematical model describing the essential processes taking place in wood pyrolysis, i.e., conduction, outward migration of volatiles, and a first order reaction kinetics to compare with the experimental data of Roberts and Clough and deduce the values of heat of pyrolysis. The values of Q_p, A, and E which gave the best fit to all experimental data were -48.4 cal/gm (endothermic), 1.19×10^5 1/min and 15140 cal/mole. They found that for a pyrolyzing cylinder the central temperature

could rise above the surface temperature which might erroneously lead one to believe that it is caused by exothermic reactions of wood pyrolysis. By expanding the energy equation for the pyrolysing solid they showed that the effective local heat of vaporization not only involves the endothermic heat of pyrolysis, but also includes the energy carried away by the fuel volatiles and changes in the enthalpy of the solid due to the thermal decomposition. These three components represent the instantaneous local energy absorption associated with the generation of volatiles. The effective heat of vaporization for wood decreases with temperature and in some cases it could even become negative (exothermic) at high temperatures leading to the possibility of a thermal runaway. They deduced that, this phenomena caused the temperature in the central portion of the wooden pellets to be greater than the surface temperature at the end of the pyrolysis process. Similar analysis was also adopted later by Atreya (1983) who demonstrated that an exothermic heat of reaction could eventually lead to the thermal explosion, a phenomenon that has never been observed for wood.

Lee et al. (1976) studied pyrolysis of 2 cm diameter wood pellets heated by a CO_2 laser between 3 and 8 W/cm^2. They found that a pyrolysis zone (about 1 cm thick) can be divided into three zones. (i) An endothermic primary decomposition zone at $T < 250°C$. (ii) An exothermic partial char (active pyrolysis) zone at $250 < T < 340°C$. (iii) An endothermic surface char zone $340 < T < 520°C$. The overall effective heat of pyrolysis was determined to be -146 cal/gm (endothermic). It was found that the rate of pyrolysis depends on the heating rate and that the pyrolysis zone is thiner and progresses faster if heat flux is perpendicular to the grain direction. This could be related to the samples' much lower gas permeability in the perpendicular direction than in the parallel grain direction relative to the heat flux. The evidence was appearance of more cracks in the parallel grain direction than the normal direction. In the latter case, high pressures up to 0.3 psig are generated within the solid as it decomposes. This pressure is much smaller in the case of parallel grain direction and gases are released

much more easier resulting in lower solid temperatures. Their data indicated that the pyrolysis of wood is a rather complex process which is strongly influenced by the endothermic and exothermic reactions, wood and char structural and thermal properties, and the heating rate. Atreya (1983) suggested that the wide discrepancy in the the reported values of heat of reaction could be due to either exothermic gas phase reactions with oxygen, or to endothermic desorption of even small amount of moisture. However, this question could be answered only when experiments were repeated in an inert atmosphere, which eliminates the role of gas phase reactions.

Kanury and Blackshear (1967) reported temperature and density profiles in a cellulosic pellet heated in air. They used the time-temperature history of pyrolyzing cylinders to determine local heat source and sink strengths. They found that decomposition is endothermic at 300-400°C, and is exothermic above 500°C. They also found that gases produced by the endothermic pyrolysis of the solid in the interior of the specimen undergoes exothermic pyrolysis in the hot char near the surface.

The effects of absorbed water on the pyrolysis and ignition of wood was investigated by Lee and Diehl (1981). They soaked wood samples in the water to obtain up to 60% water content and then exposed it to the fire level radiation of 2 cal/cm^2 heat flux. They found that the absorbed water mainly delays the temperature rise in the wet wood and the vaporized water convectively cools the pyrolyzing solid.

There are very few studies that have reported the measurements of products of pyrolysis and until very recently no *transient* measurements of these products had been reported. Chan (1983) studied the product distribution as a function of physical variables such as wood density, length, grain direction, and substrate composition (cellulose, hemicellulose, lignin). His results indicated that heat flux has the strongest influence on temperature and product distribution. Although the products of different components of wood behave differently as temperature changes, however, the chemical composition of wood does not alter the general trends for increase or decrease of the

pyrolysis products as a function of temperature. He also found that the char yield generally decreases with high heating rate and temperature, but increases with longer residence time. The reverse is true for the gas yield. The tar yield increases with higher temperature but may either increase or decrease with increasing heating rate depending on the temperature. High temperatures, high heating rate and short gas residence time would increase tar yield. Low temperature and low heating rate would maximize char yield while high temperature, high heating rate and short gas residence time would maximize gas yield. He quantitatively demonstrated the validity of these findings.

The only study in which transient measurements of major products of pyrolysis of thick slabs of wood has been reported, is the work of Kashiwagi et al. (1987). They studied the effects of oxygen concentration of the ambient atmosphere and the external heat flux on the rate of pyrolysis and the evolution rate of evolved products, namely, [THC], CO_2, CO, H_2O and tar. However, due to the difficulties in measurement of H_2O, the study failed to quantitatively measure the water and tar evolution rates.

1.6.2 Theoretical Work

The process of formation and growth of a char layer which protects the decomposition zone and the virgin material involves many physical and chemical parameters that makes it very difficult to develop even a numerical solution which contains all these effects. In the past several attempts have been made to develop realistic models for this complex phenomena and compare with experimental results. The investigators considered different kinds of simplifying assumptions in their theoretical models. The simplest models are pure thermal models that only consider the heat transfer within the pyrolyzing solid. Attempts to model the pyrolysis reaction rates are mostly limited to a single first order reaction scheme. Few authors have considered higher or multiple first order reactions [Shafizadeh and Bradbury (1979)]. The

modeling of pyrolysis becomes more difficult when large samples of wood are considered. Often simultaneous solutions of mass, energy, and reaction kinetics that involve highly nonlinear terms are involved. In the following paragraphs some the most relevant theoretical work that has been done in the past is briefly reviewed.

Tinney (1965) studied the pyrolysis of wooden dowels heated in air using the Fourier conduction equation with a source term accounting for the exothermicity of pyrolysis. Thermal properties were assumed constant and the convective heat transfer of volatiles were neglected. Matsumoto et al. (1969) studied the thermal decomposition of plastics which has some similarities with wood pyrolysis. They included the temperature and degree of pyrolysis dependence of properties and convection of fuel volatiles. The time-space region was divided into three distinct regions; namely, char, pyrolysis, and virgin material zones. Kanury (1971) showed that a pure transient conduction model (pyrolysis temperature model) overestimates the burning rate and slightly underestimates its dependency on element thickness, i.e. predicts less than experimental data. This is because of neglecting internal convection, detailed pyrolysis kinetics, pyrolysis endothermicity, and thermal property variations with degree of charring. Kung (1972) assumed thermal properties of the solid to vary continuously from their values for virgin wood to their values for char. Kung and Kalelkar (1976) used this model to study the experimental data of Robert and Clough (1963) and in a detailed analysis of the energies associated with pyrolysis process explained the reasons that caused misinterpretations of those data in the past. This was described in the previous section.

Kansa et al. (1977) included a momentum equation for the motion of gases relative to the solid and obtained good agreement with Lee et al.'s (1976) experimental data for low heat fluxes. At high heat fluxes, however, poor agreement was obtained that was attributed to ignoring effects of structural changes (shrinkage and cracking) and to the assumption of a single step pyrolysis reaction. All these models have used

a global first order Arrhenius pyrolysis rate relation. The effect of evaporation and inward propagation of moisture have often been ignored. Atreya (1983) included the kinetics of moisture evaporation and migration in his numerical model. The effects of cracking of char was simulated by shutting off the term representing the outward convection of volatiles at a specified temperature of the solid when cracking was expected to occur (650°K). A simple analytical model was developed by Delichatsios and deRis (1983) which predicted the asymptotic pyrolysis rate for constant heat flux after pyrolysis is initiated at a pyrolysis temperature T_P at time $t=t_p$. At large times the pyrolysis decays proportional to $(t-t_p)^{-\frac{1}{2}}$, that is negative half-power of time. However, none of the available models, numerical or analytical, are detailed enough to correctly predict the fuel generation for wood.

1.7 This Work

Experiments on the decomposition of thermally thick samples of charring polymers are usually conducted by exposing the sample to a known heat flux and measuring its weight loss. Uncertainties in the interpretation of these results arise due to (i) spectral absorptance of the polymer surface relative to the spectral quality of the incident radiation [Wesson et al. (1971)], (ii) changes in surface radiative properties during decomposition, (iii) absorption of incident radiation by the decomposition products [Kashiwagi (1981)], (iv) exothermic reactions in the gas phase [Atreya (1983)], (v) endothermic moisture desorption effects in natural polymers [Atreya (1983)], (vi) variations in char yield during decomposition [Atreya (1983), Broido and Nelson (1975)], and (vii) lack of knowledge about changes in the physical properties with temperature and decomposition.

The net effect of (i) to (iv) is that the boundary conditions at the polymer surface are no longer precisely known. Uncertainties due to (i), (ii) and (iii) can be eliminated by using surface temperature instead of the incident heat flux. A method of

continuously measuring the surface temperature during decomposition has been developed by Atreya (1983) and is described in Chapter 2. As mentioned before, (iv) may be eliminated by conducting the experiments in an inert atmosphere. However, items (v), (vi), and (vii) are processes occurring in the solid phase and need to be understood and modeled.

In the studies in which chemistry of wood pyrolysis is investigated, usually samples of the pyrolysis products are periodically extracted and analyzed [Chan (1983)], or to prevent the condensation of heavy molecule hydrocarbons, they are condensed in a cold trap and analyzed later. This approach preserves the chemical composition of the fuel gases, but results in the loss of transient information. Thus an alternative approach which allows the transient determination of carbon, hydrogen, and oxygen atoms in the products of pyrolysis without preserving the chemical form is adopted in this work. Experiments are performed in N_2 atmosphere and in air. For N_2 atmosphere, a known flow rate of oxygen is introduced to the boundary layer flow downstream of the wood sample and a small sample of the resulting mixture is passed through a high temperature catalytic combustor to produce water vapor and carbon dioxide which are continuously measured.

1.7.1 Experimental Work

A small scale combustion-wind tunnel was designed and constructed to conduct the pyrolysis experiments. Wind-aided and wind-opposed flame spread experiments in the floor as well as ceiling configuration can also be performed in this facility. The main features of this tunnel are: (1) It provides variable external radiation. (2) It allows transient measurements of many physical and chemical parameters, such as temperature of solid and gas, concentrations of evolved gases, and weight loss of the wood sample. (3) It provides a well controlled atmosphere over the wood sample to conduct the pyrolysis experiments. Detail description of the experimental facility is

given in Chapter 2.

The pyrolysis experiments were conducted to determine the evolved mass flux as a function of applied heat flux. The objectives were: (i) to identify the dominant chemical and physical processes that occur during the decomposition process, (ii) to determine the amount of char formed at any instant under given environmental condition, and (iii) to obtain time dependent empirical chemical composition of the pyrolysis products.

The newly constructed tunnel was extensively tested prior to conducting any pyrolysis experiments. The results of these tests are described in detail in Chapter 2. Also, a large number of experiments (>50) were conducted in order to identify various factors that influence the experimental process and the accuracy of the results. These factors were partly due to the nature of wood and partly due to the ability of the instruments to do the measurements. For instance, accurate weight loss and chemical species measurements were of utmost importance. For every experiment, the accuracy of the results were determined from the temporal and overall mass recovery in that experiment. Experimental procedure had to be improved and/or modified in order to obtain reliable qualitative data. In these experiments, simultaneous measurements of several physical and chemical quantities were made. The results of the preliminary experiments and the final procedures adopted to conduct the experiments are described in Chapter 3.

1.7.2 Theoretical Work

As mentioned earlier, pyrolysis of thick samples of wood involves both the physics of heat and mass transfer and the kinetics of thermal decomposition. In the past, several attempts have been made to develop a simple model of this complex phenomena with the objective of predicting the mass evolution rate of the volatiles. The approach most often used to simplify the model equations is to assume

infinitely fast decomposition chemistry at a specified temperature called the "pyrolysis temperature." In this work the "pyrolysis temperature" assumption is examined in detail by considering two otherwise identical models; one with infinitely fast decomposition kinetics and the other with finite rate chemistry. The pyrolysis temperature used in the first model is determined by enforcing conservation of mass and energy in an integral sense between the two models. Chapter 4 describes the formulation of the governing equations and results of the numerical calculations. Derivation of finite-difference equations and the methods of solution are presented in Appendix B.

1.8 Objectives

The purpose of this work is to identify the dominant chemical and physical processes that occur during the thermal decomposition of wood. The specific objectives are:

(i) To study the effects of external heat flux, oxygen concentration of the ambient atmosphere, and the moisture content of the samples on wood pyrolysis.

(ii) To obtain transient data on the evolution mass flux of pyrolysis products, temperature profiles inside the solid, and the total pyrolysis mass flux.

(iii) To determine instantaneous fraction of wood that is left behind as char.

(iv) To determine changes in the empirical chemical composition of the pyrolysis products with the growth of the char layer; and

(v) To obtain the instantaneous heating value of the pyrolysis products.

To achieve these objectives, a series of systematic experiments were performed on samples of Douglas-fir with different moisture contents under different external radiation levels in air and in nitrogen atmospheres. The results of these experiments are presented and discussed in Chapter 3.

Chapter Two

Experimental Apparatus

2.1 Purpose

The primary objective of the pyrolysis experiments is to understand and obtain reliable data on relationship between evolved mass flux and externally applied heat flux under different environmental conditions encountered in a furnace or a home fire. Upon heating by a neighboring fire, wood undergoes thermal decomposition producing fuel gases (volatiles) and char. In this work, external radiation from a fire is simulated by using electrical radiant heaters. In this chapter, the apparatus and the procedure employed, the data processing methods, and the errors encountered in the experiments are described in detail.

2.2 Experimental Facility

A schematic of all the components of the apparatus used in this work is shown in Figure 2.1. This facility consists of three main units:

(i) A small scale combustion-wind tunnel which provides a well controlled environment for performing the pyrolysis experiments and allows detail transient measurements of physical and chemical variables; to the actual experiments.

(ii) Gas analysis equipment, to measure concentrations of chemical species in the flow;

(iii) Data acquisition equipment to collect, store and process the data. The products of pyrolysis were measured once directly as they were produced and once after they were burned inside a high temperature combustion tube that was attached to the tunnel.

Small Scale Combustion-Wind Tunnel

The thermal decomposition experiments were performed in a small scale combustion wind tunnel. This tunnel can also be used for ignition, flame spread, and extinction experiments. This facility was designed by the primary investigator of the project and the technical drawings, modifications and construction of the tunnel was carried on and supervised by the author. Figure 2.2 shows the pictorial view of the tunnel which is rigidly mounted on a frame. The moving belt shown in this figure is for the future flame spread experiments and it was substituted with an adjustable table and an electronic balance for the pyrolysis experiments. The cross-sectional view of the tunnel is shown in Figure 2.3.

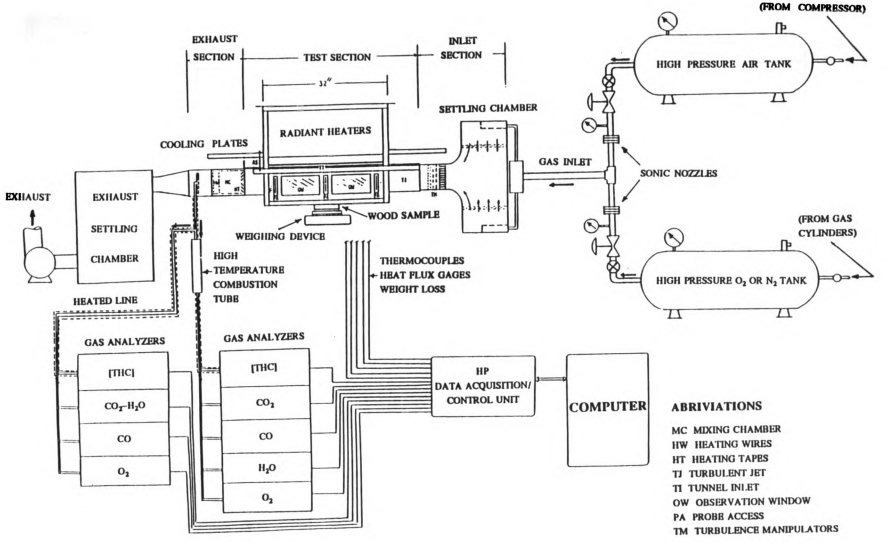

Figure 2.1 Schematic diagram of the experimental facility

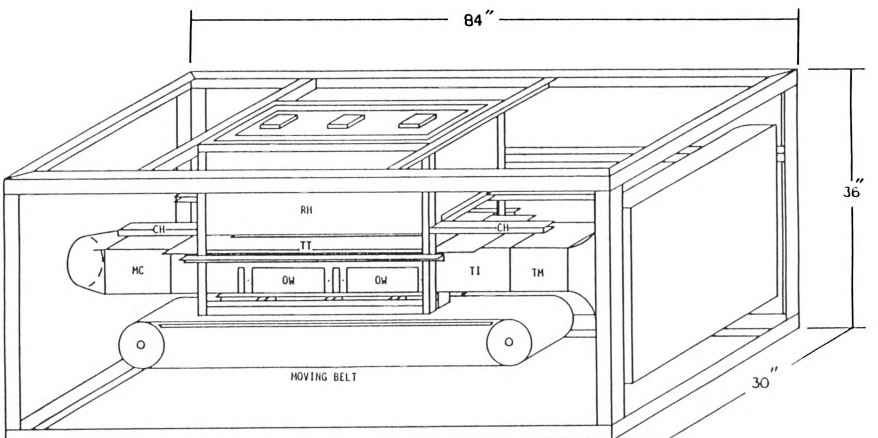

Figure 2.2 Pictorial view of the tunnel.
(Not all the support structures are shown here for clearity)

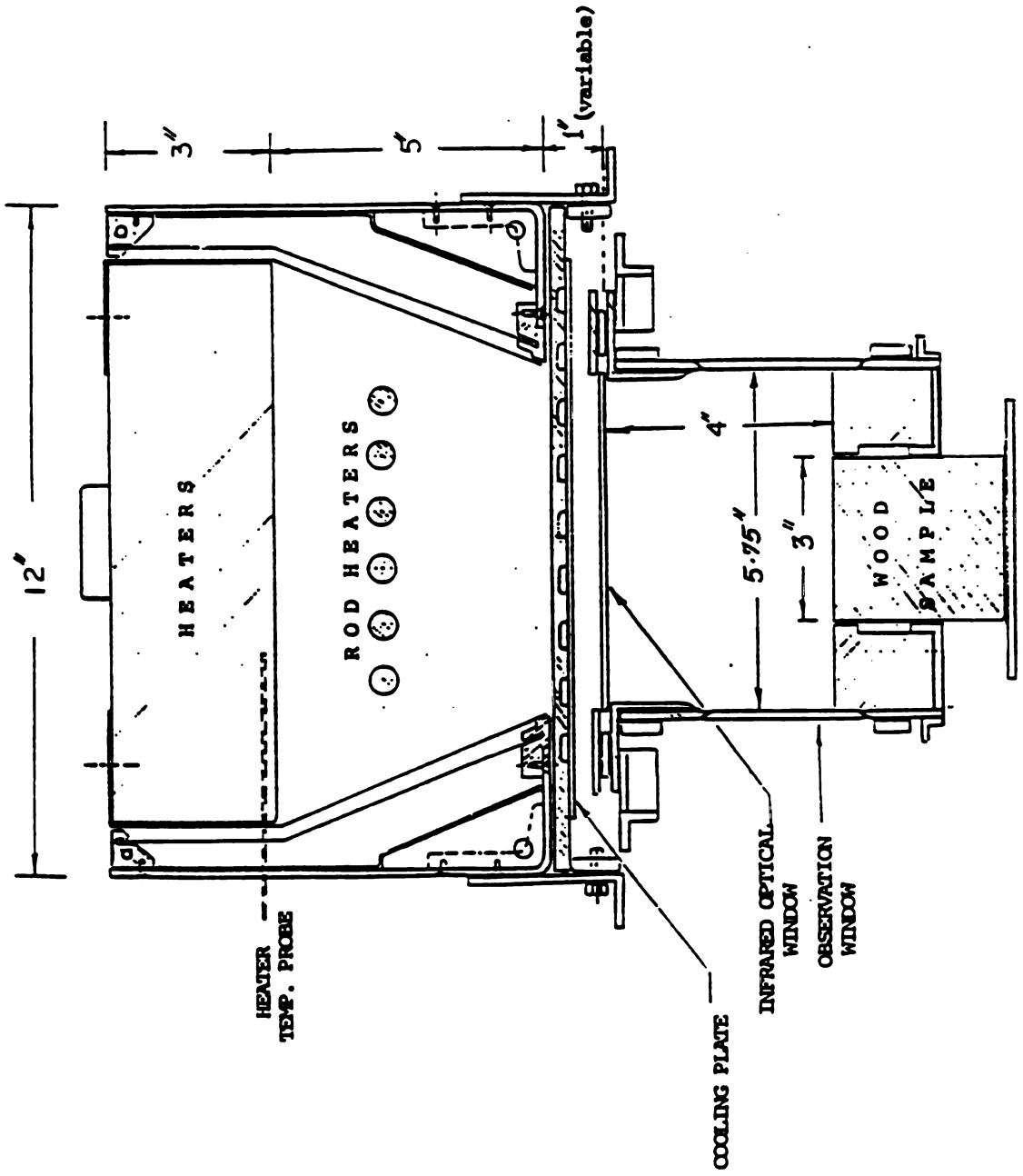

Figure 2.3 Cross sectional view of the tunnel.

This unique facility is comprised of several sections such that each section could be detached and modified separately. These sections are: 1) inlet section and accessories, 2) turbulence manipulation section, 3) test section, 4) radiant heaters, 5) tunnel-top, and 6) exhaust section and accessories.

2.2.1 Inlet Section and Accessories

As illustrated in the schematic diagram of the experimental facility, Figure 2.1, the inlet gases are provided by two separate routes to the tunnel, namely, compressed air route and pressurized nitrogen and/or oxygen route. The compressed air which is obtained from the main air pipe lines of the building first enters a large pressure tank. The mechanical oscillations of the air flow initiated at the compressor are damped in this tank. After passing through a set of globe and control valves, air enters a sonic (critical) nozzle. The sonic orifice maintains desired certain flow rate if the inlet (upstream) pressure controlled within the critical range. The temperature of the air is measured by a thermocouple installed through a small well at the nozzle location. The flow rate of the air can be calculated knowing the diameter of the nozzle, upstream pressure and the temperature of the air. The downstream pressure of the sonic orifice is nearly atmospheric and is controlled to obtain the desired pressure at the sample location. The sonic nozzles were calibrated by employing a tracer gas technique. A small known flow rate of pure methane was introduced upstream of the orifice and the mole fraction of the methane in the resulting air-methane mixture was measured. The discharge coefficient of each nozzle was carefully determined from the flow rate measurements. Figure 2.4 shows calibration curve of a sonic orifice. A similar procedure was used for introducing cylinder nitrogen and/or oxygen gases.

The inlet air enters a distribution manifold and flows into the settling chamber through eight pipes which branch out of the manifold at equal angles. Within the settling chamber, the high velocity incoming jets strike baffles which are symmetrically

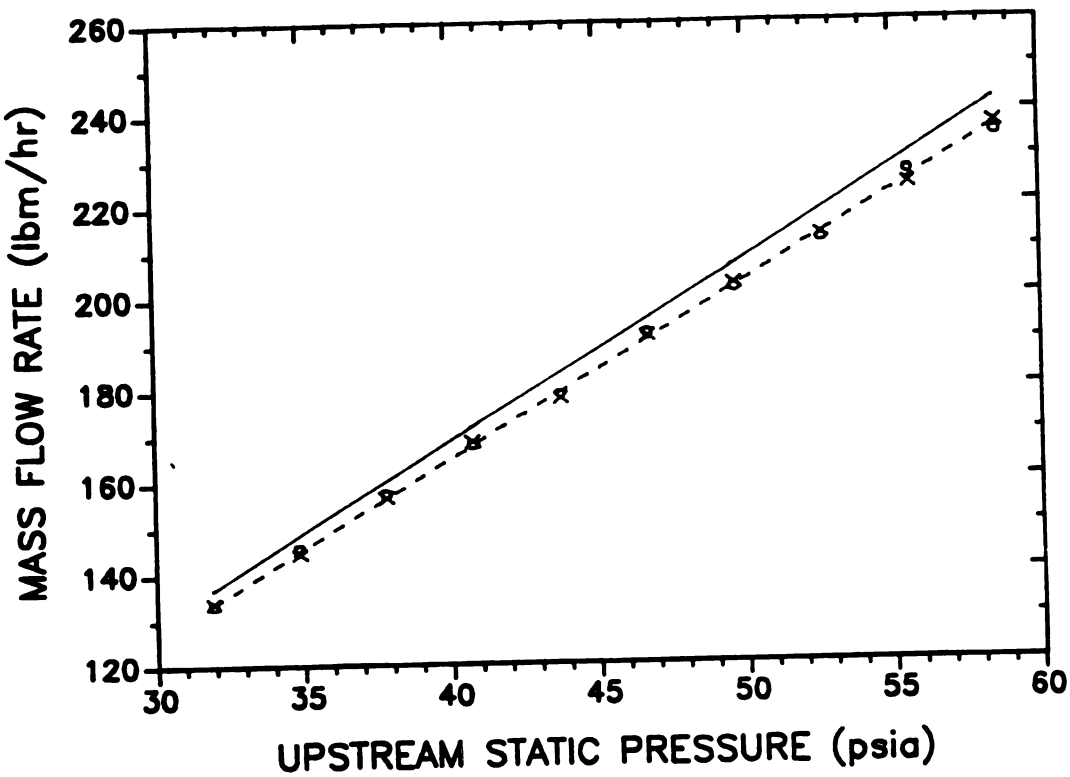

Figure 2.4 Calibration of a sonic orifice.

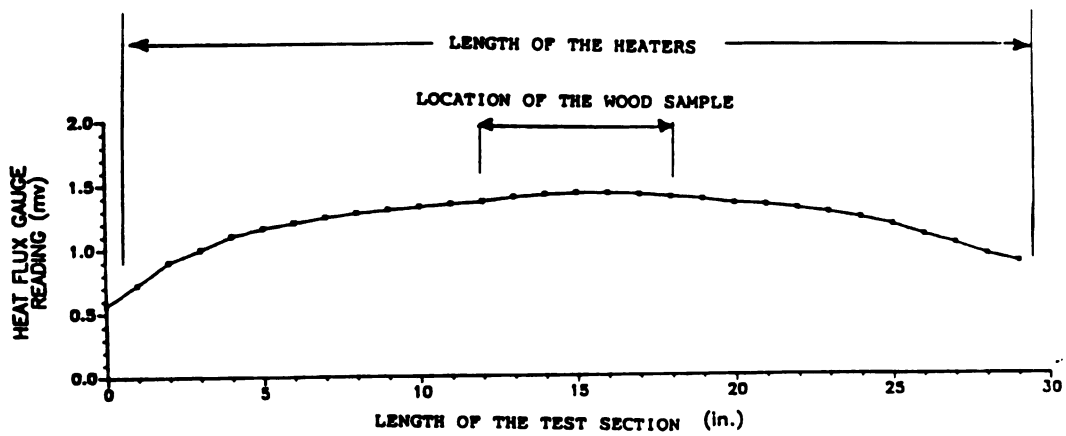

Figure 2.5 Heat flux distribution along the test section.

installed in the chamber opposing the air jets. The air looses its momentum and the pressurized air flows into the tunnel through a set of canvas and metal screens. The cylindrical settling chamber is made such that part of the cylinder can be detached and slided out. The screens can then be cleaned or replaced if necessary. This combination, therefore, creates a slightly pressurized flow of gases while helps damping out most of the oscillatory motions of the flow.

2.2.2 Turbulence Manipulation Section

The turbulence manipulation section consists of a two-inch wide honeycomb and three fine wire screens installed two inches apart. The first screen is attached to the outlet plane of the honeycomb and the others are installed 2 inches apart. Screens are carefully made in a way not to disturb the flow. They are tightly held in a metal frame which is inserted inside a slot grooved on the side , bottom, and top of the tunnel. The large scale turbulent eddies are damped in the honey comb section, and the smaller scale eddies are dissipated by the wire screens. In addition, the two-inch wide open space between the first and the second screen is filled with 4 mm diameter glass beads, which provides more uniformity for the flow and damps the oscillations even further. According to Nagib's (1976) turbulence reduction mechanisms, this combination fulfills the task of turbulence reduction and creating a uniform flow which is particularly significant for flame spread experiments as well as for weight loss measurements in pyrolysis experiments.

2.2.3 Test Section

The test section of the tunnel consists of three modules: (1) The external radiation source, (2) the tunnel-top, and (3) the main-frame of the tunnel.

2.2.3.1 Radiant Heaters (RH)

Two types of electrical radiant heaters were combined and employed to maintain the external radiation for the pyrolysis and flame spread experiments. Three high temperature (maximum fillament temperature = 1230°K)) quartz electrical heaters were mounted in a metal frame [RH, Figure 2.2]. The three 10" x 10" square heaters were configured at the top of a metal box to create a 10" x 30" infrared heat source. In addition six U shaped Chromlox coil heaters (Chromlox 3/8" dia. Incoloy sheath, type UTU each 1.8 KW) were added beneath the quartz heaters. Each group of the heaters were controlled separately by a 3-phase 440 volt variable transformer. As shown in Figure 2.3 a series of highly reflective aluminum sheets were installed as radiation shields within the side walls of the heaters frame. The space within the walls of the box were filled with ceramic fiber insulating material to minimize the heat loss to the surrounding.

As shown in the cross-sectional view of the entire heating system [Figure 2.3], the 10-inch width was reduced to about 6-1/2 inches by two reflective chromium plated (mirror finish) stainless steel sheets. The resulting combination acted as a furnace providing a highly directional radiative heat flux towards the base of the tunnel where the wood sample is located. The warm up time of the quartz heaters was approximately 30 minutes. During this warm up time, a pair of water cooled blackened aluminum plates [Figure 2.2] were used to intercept the radiation from the heaters. These cooling plates slided out on several pairs of small ball-bearings which were attached to the side walls of the heaters via two longitudinal L shape holders. These cooling plates were used to expose the sample to external radiation. The radiant heater module could be raised and lowered by two jacks which held the heater box and were firmly attached to the main frame of the facility.

2.2.3.2 Top-Tunnel

The top (ceiling) section of the tunnel was constructed as a separate module which was hinged at the tunnel inlet. This water-cooled plate housed five 6" x 6" x 2mm pieces of infrared optical glass plates [Figure 2.2, KODAK IRTRAN II]. The combination of the five pieces made a 6" x 30" window which was transparent to the infrared radiation. The IRTRAN glasses were lined with flexible silicon rubber to allow for expansion. During the exposure of the glasses to external radiation a plane jet of air was blown on the top, by a compressed air manifold, to convectively cool the glasses. This high velocity air jet, however, caused entrainment of air into the heater box and reduced the temperature of the heating rods. This was partially compensated by increasing the electrical power to the heaters and raising the heater box slightly above the air jet.

The entire tunnel top could be lifted at the downstream side of the tunnel by an adjusting mechanism. This increases the cross-sectional area of the tunnel at the exhaust end to compensate for acceleration of the gas core due to the boundary layer growth and gas expansion from combustion heat release. By experimentally adjusting the height of the top-tunnel it is possible to obtain a constant free stream velocity (U_∞).

To prevent leakage of the gases into or out of the tunnel through any possible gap between tunnel-top and the main frame, two 1.5 inch wide 1/8 inch thick chromium plated (mirror finish) bars were attached to the top tunnel next to the side walls of the tunnel [Figure 2.3]. They were tightly in contact with the side walls and prevented leakage when top tunnel was lifted. The mirror finish surface of these bars helped to enhance radiation as well.

2.2.3.3 Tunnel Mainframe

The 48-inch long mainframe consisted of three sections: inlet, test, and outlet sections which were 10, 32, and 6 inches long, respectively. The water-cooled side walls were made of 1/8" brass plates and they house two observation windows and three probe access slots on each side. Pyrex glass was used for these windows and it was lined with a thin sheet of flexible silicon rubber on the frame edges to allow for expansion and prevent cracking. Some static pressure probes were also installed on the side walls. The probe access slots were also lined with silicon rubber to prevent leakage and allowing the probe to transverse up and down for velocity profile measurements. The base of the 10 inch long inlet section of the mainframe was also water-cooled. This was done to ensure that the inlet air and the entering wood samples (for future flame spread experiments) were at the ambient temperature.

The cross-sectional area of the tunnel is shown in Figure 2.3. The configuration and the dimensions were selected to satisfy several objectives: (1) To obtain a uniform heat flux across (3" wide) and along (6" long) wood sample for pyrolysis and moisture desorption experiments. (2) To prevent the interference of the side wall boundary layers with the boundary layer over the charring solid at the presence of a flame. (3) To minimize the consumption rate of the inlet gases (nitrogen and oxygen). Two 1.5" wide noncombustible blocks (Kawool insulating board from Babcok & Wilcox, type 3000 sprayed with a rigidizer and baked in oven at 400°C) mounted flush with the wood sample surface, were placed symmetrically on both sides of the sample. For pyrolysis experiments all but the middle 6 inches of the 32-inch long sample space was covered with the insulating board. In addition a 1/2" thick Kawool board was used to cover entire tunnel base except for the sample location, and a 1/16" thick aluminum plate with a sample size opening covered this board. This combination created a laminar boundary layer over the flat plate and brought the sample a little closer to the heaters to increase the heat flux. The radiative heat flux was also slightly augmented

by the presence of the metal plate.

2.2.4 Exhaust Section

The main part of the exhaust section was the mixing chamber [MC, Figure 2.2]. This chamber was made as a separate detachable module. The primary purpose of this chamber was to mix the stratified boundary layer flow carrying the pyrolysis or flaming combustion gases before reaching the sampling probe. This was necessary in order to obtain a well mixed and uniform sample of gases for chemical measurements. In this chamber the gases were also heated to prevent any condensation of the heavy hydrocarbons (tar) on their way to the gas analyzers.

Mixing and heating in the mixing chamber were achieved in several steps. The incoming flow passed through three baffles installed at the inlet, middle, and outlet of the mixing chamber. Large scale mixing of the stratified gases was accomplished when they passed through these baffles and a series of electrical tapes installed in staggered position and up and down along the flow. In addition, further downstream of the mixing chamber a net of electrical resistance wire [Figure 2.6] was used to provide mixing on a small scale. At the outlet of the mixing chamber a metal louver was installed to finally assure mixing of the gasses.

The mixing chamber was made of stainless steel and was lined with oven treated Kawool insulating boards. Quartz tubings reinforced with metal bars were used as the holders for the heating tapes and wires. The input power to the heaters was controlled by a small variable transformer.

A sample of the gases was extracted through a spatially integrating sampling probe. This cross-shaped probe, with holes distributed along its four arms, further assured a representative sampling of the product gasses for chemical analysis. A 12" extension was attached to the MC which emptied the exhaust gases into a 4' x 2' x 2' metalic chamber [Figure 2.1]. The gases were then sucked from the chamber by an

exhaust pump and were exhausted through the roof vent. The 16 ft^3 exhaust tank was used to suppress the mechanical oscillations which were created by the exhaust fan and were reflected back upstream into the flow and disturbed the boundary layer flow and the weight loss measurements.

The presence of all of the above mentioned components, i.e., heating tapes and wires, baffles, louver, and the exhaust chamber, substantially increased the pressure drop. This resistance against the flow was overcome by the exhaust fan. A motor driven adjustable slot was installed on the exhaust side of this fan to vary the outlet area. This outlet area was carefully adjusted until the pressure inside the tunnel at the sample location was almost atmospheric.

The entire tunnel was rigidly secured by to a solid metal frame made of angle iron bars. This allowed the tunnel to be used in the horizontal, vertical, and ceiling configurations.

2.2.5 Catalytic Combustion Tube

A part of the sample gas from the tunnel flow was passed through a high temperature catalytic combustor (combustion tube) in which the fuel gases were burned with oxygen and converted to CO_2 and H_2O. The combustion tube and the gas sampling lines are schematically shown in Figure 2.6. A heating element (Nichrome resistance wire and a piece of platinum wire attached in series) was made as a coil and installed inside a ceramic tube. The inlet and outlet of the ceramic tube were tightly sealed using several layers of high temperature ceramic adhesives. The ends of the wire were passed through two small holes that were made close to the inlet and the outlet of the ceramic tube. These holes were tightly sealed as well. The entire tube was completely insulated from outside by ceramic fiber insulation. Temperatures of the outside of the tube were measured at three different locations. The input power was adjusted by a variable transformer to achieve the desired temperature. The premixed

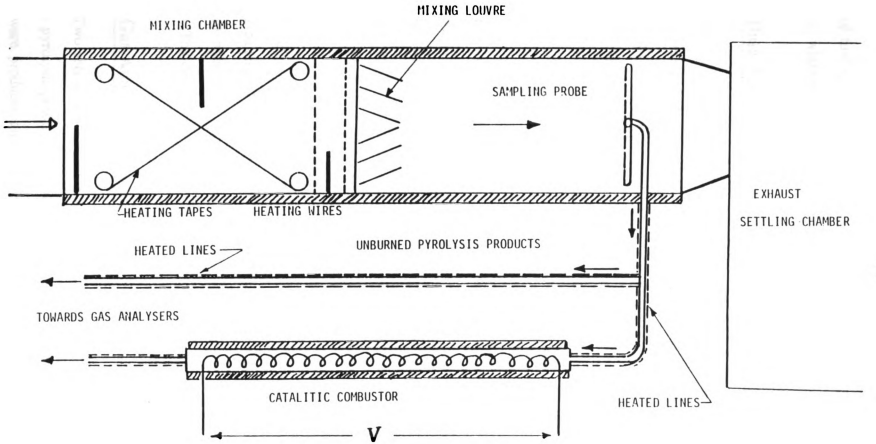

Figure 2.6 Schematic of the tunnel outlet and the catalytic combustor.

flow of fuel and oxygen came into direct contact with the high temperature (>1000°C) element while passing through the combustion tube.

2.3 Data Acquisition Equipment

All the analog signals from the thermocouples, gas analyzers, and the heat flux gauges were collected and stored with the help of a DEC PDP11-73 computer running RSX-11M+ operating system. The analog signals were first fed into a HP 3497A controller digital voltmeter which was interfaced with the computer via an IEQ-11 interface board so that the two machines could exchange information. The electronic balance, was directly interfaced with the computer to record the transient weight loss data.

Two separate data acquisition algorithms were developed, namely, a single buffered (slow scan) option and a multi buffered (fast scan) option. The slow scan acquired data at approximately eleven readings per second. The fast scan version could take up to 20 readings per second (time constant of the system about 1/20 seconds). The accuracy of the acquired data was about 5-1/2 digits. The transient weight loss data were obtained at a rate of about 5-6 data points per second.

A single computer program named ACQ invoked both the HP controller and the digital balance. The system time was recorded at the start of both data to enable the user to match the starting time of both weight loss and the other group of data points. The data were stored on floppy diskettes.

2.4 Gas Analysis Equipment

Two sets of gas analyzers were used to continuously measure the concentrations of the pyrolysis products. One set was used for direct measurement of these species as they were produced and the second set measured the mole fraction of the gases after they burned in the high temperature catalytic combustor. A small sample of the tunnel

flow was extracted and passed through each set of the gas analyzers to continuously measure the concentrations of the total hydrocarbons [THC], CO_2, CO, O_2, and H_2O. The sampling lines were all heated up to about 100°C via electrical heating tapes. The transport times for the gases to reach the analyzers, (i.e., the lag time) were measured for each equipment. A schematic of the gas analysis system is shown in Figure 2.7.

A high temperature vacuum pump (Metal Bellows model MB-601HT) was used on side one (before combustion tube) to transport sampled gases to the gas analyzers via 1/4 inch O.D. stainless steel and teflon tubings which were insulated all the way to the analyzers. One port of the pump was used to feed the CO_2-H_2O analyzer and the other port fed the hydrocarbon, CO, and O_2 meters. The hydrocarbon analyzer was equiped with a built-in pressure regulator that maintained the desired pressure throughout the system. Needle valves on the lines were used to control the flow to all analyzers and the flow rates were monitored by rotameters.

On side two (after combustion tube), the selected sample was pumped into all analyzers by a Metal Bellows vacuum pump (model P-40). The pressure on the system was controlled by the 6" height of water inside a container that acted as a pressure regulator. The sample gases supplied to the CO–CO_2 and O_2 analyzers as well as the CO analyzer of set number one passed through a cold trap and was cooled to -5°C and dried. The cold bath was cooled by a Neslab U-cool immersion cooler. All sample lines which fed the [THC] and H_2O analyzers were electrically heated from their entrance to the system to the analyzer entrances to prevent condensation of [THC] and H_2O.

2.4.1 The Gas Analyzers

Total Hydrocarbons [THC]

In both sets the total hydrocarbons were measured by using a Flame Ionization Detector (FID). On side one a Beckman hydrocarbon analyzer model 400 and on side two a Shimadzu gas chromatograph GC-3BF was used as a [THC] detector. The response time of both [THC] meters was very small (< 1 sec.). Both FIDs were fueled with a 40%H_2-60%He mixture to minimize the effect of O_2 in the sample flow. The response of the FID for a constant concentration of [THC] is a weak function of O_2 concentration in the sample stream. The FID response with 20% O_2 in the sample gas was 97% of the response for the same concentration of CH_4 and no O_2. However, since the [THC] meters were calibrated using methane, the measured value was considered as equivalent of CH_4 concentration. The time constant of the Beckman [THC] analyzer was 1.0 second and that of the Shimadzu analyzer was 0.86 seconds.

CO–CO_2 *Analyzers*

On side one a dual analyzer (ANARD Series 600 nondispersive infrared) was used to measure CO_2 and H_2O. It measured the concentration of a selected gas specie in a multi-component gas mixture by measuring the infrared absorption of the selected component in the mixture. The meter could measure CO_2 up to 5% and H_2O up to 1%. The response time of the analyzer was very small. The sample flow was filtered before entering this analyzer. A Beckman CO analyzer (model 315B Infrared)was used to measure CO on this side.

On side two an Infrared IR702 nondispersive dual gas analyzer was used for CO_2 (F.S. 0-20%, 0-6%) and CO (F.S. 0-12%, 0-3%) analysis. The time constant of this analyzer was about 2.6 seconds at about 2 liters/sec flow and the accuracy was ±1% of the Full scale. The analyzer required a water free sample.

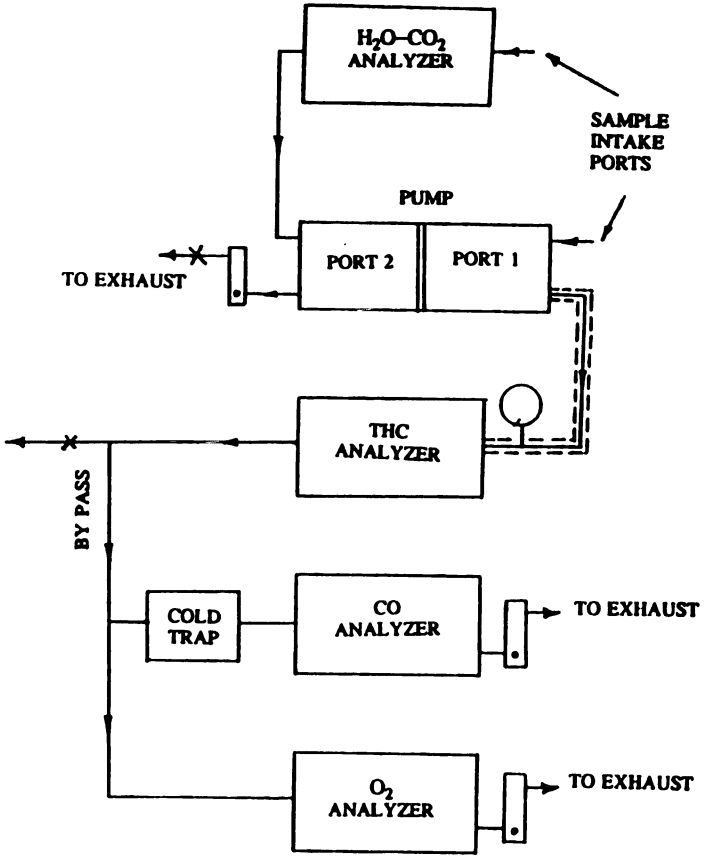

Side 1: Direct measurement.

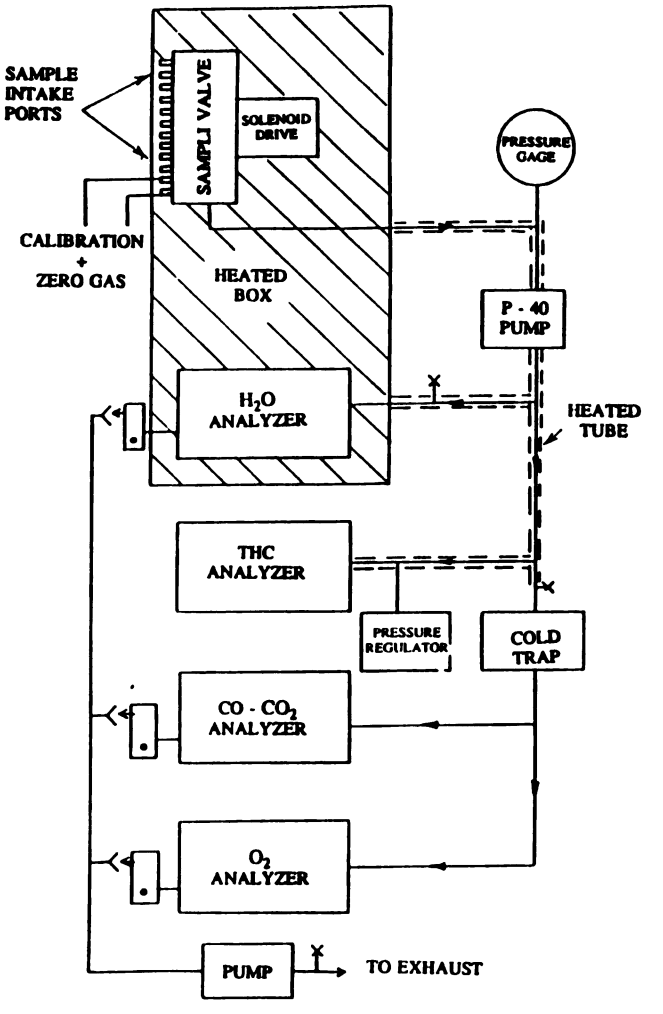

Side 2: After catalytic combustion

Figure 2.7 Gas analysis equipment

H_2O *Meter*

On side two a General Eastern 1200APS Condensation Dew-Point hygrometer was used to measure the water. This equipment measured the dew point temperature of the sample stream by optically detecting the condensation on a temperature-controlled mirror surface. The instrument was accurate to ±0.2°C when the mirror was clean (no condensible contaminant). It was very sensitive to the presence of any condensible other than water. The time constant was approximately 10 seconds at 1 liter/sec.

O_2 *Analyzer*

On side one, a Beckman oxygen analyzer Model 778 was used. This analyzer measures the partial pressure of oxygen which diffuses into a layer of potassium chloride gel through a Teflon membrane. The gel electrically connects the cathode of the sensor to the anode. This analyzer had a lot of electrical noise. The response time was about 2 seconds and the accuracy was ±1% full scale at constant temperature.

On side two, a Beckman OM-11 a polarographic analyzer, was used for O_2 analysis. The time constant was about 1.5 seconds at 0.5 liters/sec flow and the instrument had a short term (10 minute) accuracy of ±0.05% (±0.15% long term). The analyzer required a dry sample a 15-40°C.

2.5 Sample Preparation

The wood samples for pyrolysis experiments were cut from 1'x1'x1.5" boards of Douglas-fir which was supplied by the USDA Forest Products Laboratory (Madison Wisconsin). Samples of approximately 3" x 6" x 1.5" in dimensions were carefully machined to obtain right angles and smooth surfaces. Prior to the experiments, the samples were instrumented by very fine thermocouples (type K, 0.002" Alumel-Chromel) both on the top and the bottom surfaces. The surface thermocouples were installed using the method developed and successfully used by Atreya (1983). In this

method, a very thin layer of wood surface was skinned off carefully by a sharp razor blade. The thermocouple leads were then burried under this 1-2 mm wide skin and glued to the surface by wood glue. It was then left to dry out under a heavy weight for several hours. As a result, the flatened thermocouple bead was well attached to the surface. At high heat fluxes and/or high moisture contents of wood, some thermocouples were installed in depth of the sample at the designated locations. For these thermocouples, a very fine hole (0.8 mm diameter) was drilled to about 1 inch depth on the side wall of the wood sample. A very fine ceramic thermocouple insulator tubing with two holes were used to secure the thermocouple leads inside wood and maintain strength for thermocouple wires. The thermocouple leads were carefully imbeded in fine grooves made on the side walls of the wood sample and were glued to stay tight in their position. This prevented the thermocouple wires to hang loosely about the sample and disturb the weight loss measurement.

For moisture contents different from room condition the samples were conditioned in a humidity control chamber to the desired moisture content. The samples were first heated in an air tight insulated electrical oven at a well controlled temperature of about 104 °C for about two days. During this drying process a flow of pure nitrogen was maintained in the oven. This procedure resulted in drying the samples in a very well controlled atmosphere with a known temperature and relative humidity. The condition of the wood, therefore, was well known at the time of removal from the oven. Samples treated in this manner were considered as "dry". For cases other than "dry" a temperature-humidity test chamber (model TH-3 from BMA, Inc.) was used. The controllable humidity range of this chamber was 20% to 95% and the controllable temperature range was +2 to 85°C. This was limited by a ±2°C dew point temperature. For humidification, a vapor generator system incorporating a stainless steel heater was used to introduce water vapor into the chamber. The chamber was carefully tested and calibrated prior to its use. Also, before starting the

condition

was obs

assure th

usually

steadine

For

the sam

because

move al

produces

the numb

the gase

informat

to obtain

2.6 Sys

In

physical

of the py

necessary

this secti

2.6.1 D

The

a HP-Re

which m

were pe

conditioning of the samples the history of the moisture gain with time was recorded. It was observed that it was necessary to condition the samples for at least 4 weeks to assure that they had reached the desired moisture content. However, the samples were usually conditioned for about two months to obtain the best uniformity and steadiness. The samples were usually conditioned at 20°C dry-bulb temperature.

For the pyrolysis and moisture desorption experiments all but the top surfaces of the sample were covered with aluminum self-adhesive tape. This was necessary because upon heating, some of the desorbed water and condensed volatiles tended to move along the grain direction within the wood and drip out of the sample. These products would remain unaccounted if they were not evaporated and carried away by the tunnel flow. It should be emphasized that any other method by which water and/or fuel gases were collected and evaporated later, would have resulted in loss of transient information about the products of pyrolysis of wood. Also, this procedure is necessary to obtain a true 1-D experiment, i.e. an infinite slab.

2.6 System Diagnostics Tests and Preliminary Experiments

In order to ensure the validity and applicability of the experimental results, all physical and dynamical aspects of the tunnel were examined in detail prior to the start of the pyrolysis experiments. Every component of the tunnel was tested carefully and necessary improvements or modifications were carried out. These tests are described in this section.

2.6.1 Dynamics of the Flow in the Tunnel

The turbulence fluctuation intensity of the flow in the tunnel was monitored using a HP-Real Time Analyzer. This device can differentiate the mechanical oscillations, which may exist in the flow, from the turbulence fluctuations. Large number of tests were performed and flow fluctuations were carefully detected in all possible


Non-Dimensional
Fluctuating Velocities

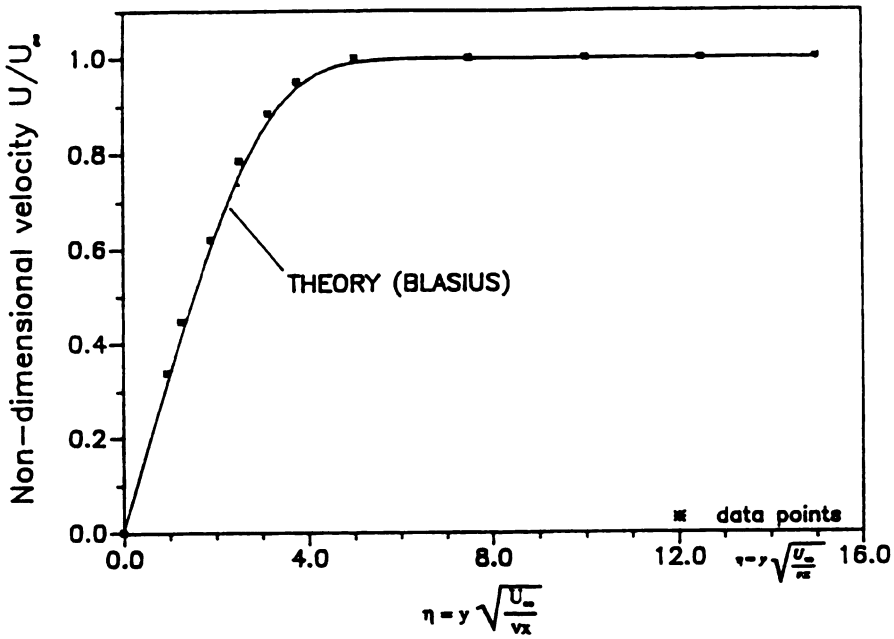

Figure 2.8 Velocity profile inside the tunnel.

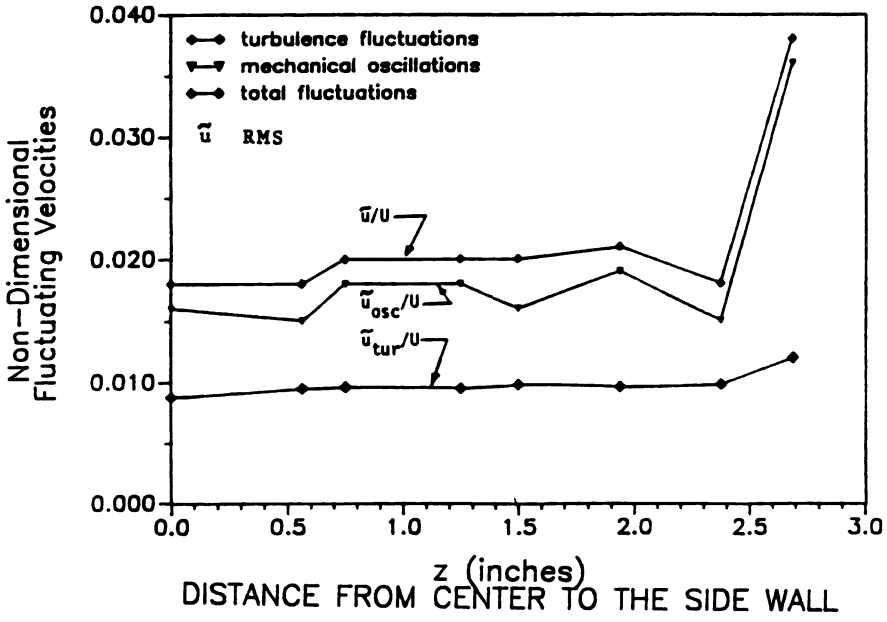

Figure 2.9 Air flow fluctuations in the tunnel.

combinati

flow, exh

when the

upstream

Figure 2.

on Blasi

turbulence

percent. A

tunnels [

indicating

2.6.2 T

Know

infrared g

Also the

tunnel gl

temperatu

planar jet

absorbed

of the IR

under sim

the permis

combinations of all mechanical parts connected to the system (inlet pressure driven flow, exhaust fan, and roof fan). For instance, the flow fluctuations were recorded when the exhaust and roof fans were off and the flow was driven into the tunnel by its upstream pressure. Then the exhaust fan was turned on and data were recorded. Figure 2.8 compares the gas velocity profile inside the tunnel with that obtained based on Blasius theory [Potter and Foss (1975)]. Figure 2.9 shows that the typical turbulence fluctuations along the flow direction $(\frac{\tilde{u}}{U_\infty})$ are less than one percent. According to the existing literature on the characteristics of small scale wind-tunnels [Mitchel and Frobel (1988)], this is a well reasonable turbulence level, indicating that the flow in the tunnel is laminar.

2.6.2 Temperature Distribution Along Top-Tunnel Glasses

Knowledge of the temperature distribution along and across the top-tunnel infrared glasses is important to prevent them from cracking under high heat fluxes. Also the maximum temperature of these glasses must not exceed 200°C. Thus the top-tunnel glasses were first replaced by pyrex glasses of the same size and their temperature distribution was measured while they were convectively cooled by a planar jet of air. From the calculation of the comparison of the total radiation absorbed by each type of the glass, it was determined that the maximum temperature of the IRTRAN II glasses would not exceed the maximum permissible temperature under similar conditions. The temperature gradient across the glasses was also within the permissible range that was specified by the manufacturer.

2.6.3 Mixing of the Pyrolysis Products

Extraction of a well mixed representative sample of the gases produced during pyrolysis is of great importance for chemical analysis. This was one of the most difficult tasks of this work. The flow of the gases in the tunnel tended to be highly stratified. Most of the product gases were carried by the free stream close to the bottom of the tunnel. To quantify the mixing achieved in the mixing chamber, detailed tests were performed by injecting a small known amount of pure methane after the sonic nozzle into the air flow. This methane was completely mixed with the air during its travel in the pipe connecting the sonic nozzle to the tunnel inlet. The mole fraction of the methane in a sample of this flow was recorded by the gas chromatograph. Then the same amount of methane was introduced at the sample location to be mixed with the main flow in the tunnel. The recorded mole fraction of methane in this flow was compared with the previous one which was considered as the reference point. The difference between the two measured methane concentration was less than 5%. These measurements were used to improve the mixing of the gases in the mixing chamber (see Section 2.2.4). The final result was satisfactory. The mixing was very good specially at low flow rates.

2.7 Calibrations

2.7.1 Radiant Heat Flux

The incident radiant heat flux at the sample location was calibrated against the incident radiation at the inlet of the test section (Figure 2.10). This was done both with and without the top-tunnel infrared glasses. The calibration curves in both cases were linear and were in good agreement. This indicated that the effect of geometry or refraction of radiation on the heat flux readings due to the presence of the glasses was very small.

As sho

heat flux ga

of convectiv

was investig

the blowing

determining

2.7.2 Gas

The ar

very small

heat fluxes.

accuracy of

needed spec

of condensi

was used a

CO_2 and H

Prior

calibrated

calibration

experiment

tunnel whil

location. Th

reached a s

point (zero

value of ox

into the tu

experiment

As shown in Figure 2.10, the thermal boundary layer starts after the water cooled heat flux gauge. Thus, this gauge measures only the incident radiation. The possibility of convective cooling of the heat flux sensor due to the flow of gases inside the tunnel was investigated. The change in the heat flux measured by this heat flux gauge due to the blowing of air, was negligible (maximum 1.5%.) This was accounted for when determining the radiative heat flux at the sample location.

2.7.2 Gas Analyzers

The amount of gases produced by thermal decomposition of wood samples were very small compared to the main flow in the tunnel (less than 5%), specially at low heat fluxes. Thus, measurement of each chemical component was very sensitive to the accuracy of calibration of the gas analyzers. Furthermore, the measurement of H_2O needed special care. The dew-point hygrometer was extremely sensitive to the presence of condensible hydrocarbons and to the temperature of its surroundings. This analyzer was used after the combustion tube where all the fuel was burned and converted to CO_2 and H_{2O}.

Prior to the start of experiments, first [THC], CO_2, CO, and O_2 analyzers were calibrated using a 'zero gas' (21.3% oxygen and the balance nitrogen) and a calibration gas (0.2% CH_4, 2.01% CO_2, 0.195% CO, and the rest N_2). Then for the experiments conducted in the nitrogen atmosphere, first nitrogen was flown into the tunnel while an inert block (the size of the wood sample) was placed at the sample location. The dew point and oxygen concentration of the flow was monitored until it reached a steady value. The steady value of the dew point was taken as the reference point (zero line) for the moisture produced later during wood pyrolysis. The steady value of oxygen recorded during this time was used to determine the leakage of the air into the tunnel. The amount of air leakage (assumed to remain constant during the experiment) was used in the calculation of volatile mass fluxes. All the recorded data

during pyrolysis were corrected for this leakage.

2.8 Experimental Procedure

As the dew point and oxygen readings reached steady values, indicating that the initial conditions for the experiment were all known, the wood sample was placed and positioned properly such that it did not touch the tunnel. This was done as quickly as possible to: (i) minimize further leakage of the air into the tunnel and, (ii) to minimize the surface desorption (or adsorption) of moisture out of (or into) the wood sample. Then, as soon as the analyzers reached steady readings again, the heating of the sample and the data collection was started. A schematic diagram of the thermal decomposition process occurring in the tunnel is shown in Figure 2.10. Here, it should be emphasized that, if a uniform external heat flux [Figure 2.7] is maintained over the entire surface area of the wood sample, the mass flux of the products evolving from wood would also be spatially uniform [Figure 2.10]. As shown, the velocity boundary layer starts considerably ahead of the entrance edge of the sample and the thermal boundary layer starts after the heat flux sensor which is water-cooled. Thus, the convective heat transfer is nearly constant along the length of the sample and the system is convectively well defined. Also, the heat flux gauge is not convectively affected by the incoming flow which is at the same temperature as the gauge, thus it records only the incident radiation.

2.9 Data Reduction

The data collection by the computer was started a few seconds before exposing the wood sample to the external radiation. This was done to record the initial conditions (reference points) of the data recorded by the gas analyzers during the experiments. The data for weight loss was recorded in one data file and all other data (temperatures, heat flux, and chemical measurements) were stored in another file. As a

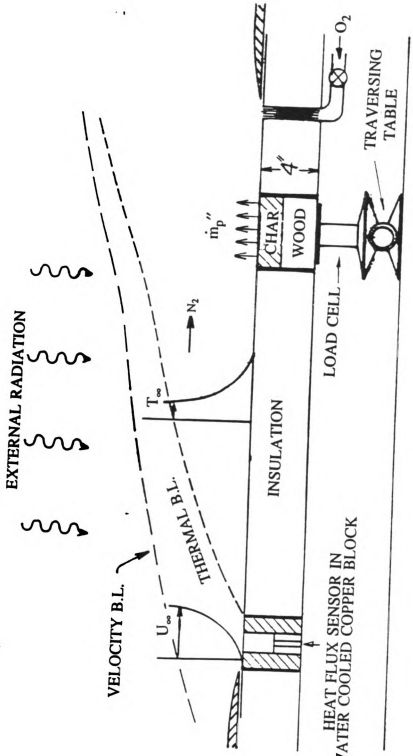

Figure 2.10 Schematic of the decomposition process occurring in the tunnel.

first step, these data were converted into a tabulated form (value vs. time) and were plotted for a preliminary analysis. From these curves the offset (base line) of each chemical measurement was determined. This was used for the final data processing and calculations which were performed in several steps.

There were two types of disturbances in the experimental data which had to be distinguished from the actual pyrolysis data. The first type, was the electrical noise that existed in most of the gas analyzer outputs. The second type, were the disturbances caused partially by the fluctuations in the tunnel flow and partially by the motion of the ambient air due to the exhaust fan and air circulation in the room. The latter mostly affected the weight loss measurements. The output signals, therefore, had to be smoothed in such a way so as to preserve the overall characteristics of the phenomena while filtering out the noise. As stated by Atreya [1983], to do this on a computer, we must use a procedure flexible enough to keep the important trends, but not too flexible so as to include the noises.

The smoothing was also necessary to obtain the weight loss rate (pyrolysis mass flux) and other derived quantities [Chapter 3]. In addition, the data is never recorded simultaneously for all channels, and yet, for calculation procedure the value of all signals at specified time intervals is needed. This was done by interpolating the data by fitting appropriate polynomials through them. The procedure used for lag and response time corrections, smoothing, and curve fitting is the one used by Atreya [1983] and is described in Appendix A.

The final output of this data processing procedure was a tabulated form of all measured quantities corrected for offsets, time lags, and response times at specified time intervals. Further calculations were done to obtain derived quantities like empirical chemical compositions of the pyrolysis products and the char yield. These are described in Chapter 3. Finally, these corrected data and derived quantities were plotted using a plotting routine called PlotIT furnished by the College of

Engineering. The data processing and plots were carried out on a Micro VAX computer.

2.10 Experimental Errors

The difference between the true value (unknown) and the result of measurements (best experimentally determined value) is the error. Generally, two types of experimental error may be recognized; systematic errors and random errors. Systematic errors are repetitive and usually of fixed value such as calibration errors that occur consistently every time the measurement is made. These errors are not susceptible to statistical analysis. Random errors are of inconsistent nature and may change from one experiment to another, such as some errors due to the nature of the material being investigated and environment and human errors. For example, electrical noise in the output signal of gas analyzers or disturbances in the weight loss measurements caused by the motion of the air, are of this type. These noises can be removed by a data processing routine.

There are several sources of experimental errors in the pyrolysis experiments. Different types of error may assume different significance during the course of wood pyrolysis. For instance, at early times, wood decomposition occurs very rapidly and small errors in the weight loss measurement (caused by air flow disturbances) may translate to large discrepancies in the pyrolysis mass flux that is numerically calculated from the weight loss data. At larger times, shrinkage and cracking of the solid changes the effective surface area of the sample, which in turn affects the calculated total mass flux. In addition, the derived quantities of interest, such as char yield, are often determined using several measured values. They incorporated all errors existing in those measured quantities.

The errors encountered in the experimental results can be categorized in three broad groups [Atreya (1983)] as:

(i) Errors in the measurements of basic quantities;

(ii) Errors in the derived quantities;

(iii) Errors due to the response time of the instruments.

2.10.1 Errors in Measurements

In every experiment three types of data were obtained. (i) Weight loss data; (ii) Chemical measurements; (iii) Temperature measurements.

1. Errors in Weight Measurement

Weight loss measurements were disrupted by disturbances induced by the flow of gases inside the tunnel and the motion of air in the room. These fluctuations caused a random error in weight loss measurement. The electronic balance was able to measure the weight up to 0.01 grams with an accuracy of ±0.005. The typical disturbances were in the range of ±0.02 grams. The noise in the weight loss measurements was highly magnified in the calculation of the weight loss rate which was obtained by numerically differentiating the weight loss data. The data smoothing scheme (Appendix A) maintains the continuity of the data but it is not possible to fully maintain the continuity of their derivative with respect to time. Thus, sudden changes in the measured quantities may cause discontinuities in the mass flux curves. The maximum error in the calculated weight loss rate was less than ±20%.

2. Instrument Errors

Several sources of error existed in the measurements of the chemical species. The errors due to the electrical noises, calibration, and the accuracy of each analyzer were specially important at the times when the measured quantities were very small. For instance the lower range of the CO_2 analyzer was 0-6% while the gas

concentrations ranged from zero to 2%. At low heat fluxes the concentration of gases were usually very small and became comparable with the accuracy of the instrument (±1% full scale). In the measurement of total hydrocarbons [THC] another error was introduced due to the use of the flame ionization detector (FID). This instrument basically responds to the presense of C atoms in the sample stream and is usually calibrated with pure methane. The response of FID per carbon atom is altered if oxygen atoms are present in the sample gas. For the calculations of the mass flow rates of [THC] the measured concentrations were assumed to be equivalent to that of CH_4.

3. Errors Due to the Nature of Experiments

Some systematic errors were caused due to the nature of wood and pyrolysis products. For instance, the condensation of the heavy molecule hydrocarbons (tar) in the tunnel and in the tubes, slightly changed the concentrations of other gases reaching the analyzers. However, as explained in Chapter 3, since the pyrolysis products were highly diluted with the carrier gas in the tunnel, the contribution of this error was negligible. Also, internal pressures generated inside the wood and the char matrix (Chapter 3) may cause random *local* variations in the weight loss data as the gases evolved from the wood surface. These variations could not be distinguished from weight losses due to the evolution of water or fuel volatiles.

Other errors in the measured chemical quantities were due to the imperfections of the experimental apparatus. A possible source of error was the imperfect mixing of the gases before reaching the entrance of the sampling probe. The error due to the incomplete mixing of the gases was not more than ±5%. Another type of error was introduced due to the leakage of the air into the tunnel specially at higher heat fluxes when the top-tunnel glasses had to be removed. The flow rate of this incoming air was determined using the tracer gas technique and was accounted for in the calculations. The accuracy of the results depended on the accuracy of the measurement

of t

amo

effec

this

nanc

4. E

grad

as th

large

therm

assur

surfac

more

2.10.

F

of co

measu

The sy

such a

values.

a know

evolutio

compos

Append

of the leakage. In the experiments conducted in the nitrogen atmosphere, since the amount of air leakage was very small compared to the main flow (less than 5%), its effect on the calculated mass fluxes was very small. In experiments performed in air this effect was more significant because more leakage had to be allowed into the tunnel (up to 20%).

4. Errors In Temperature Measurements

During pyrolysis, as the wood chars it cracks and shrinks and its surface recedes gradually. The location of the surface and in-depth thermocouples, therefore, changes as the pyrolysis continues. This effect is more at higher external radiations and also is larger in air than in nitrogen atmosphere due to char oxidation. The position of thermocouples can be measured at the end of experiment. A linear correction may be assumed for the intermediate times. However, the change in the heat flux at the wood surface due to surface regression was not significant because the regression was not more than a few millimeters even at high heat fluxes.

2.10.2 Errors in the Derived Quantities

From the equations for the char yield, chemical composition of volatiles, and heat of combustion of pyrolysis volatiles (Chapter 3), it is seen that the errors in the measurement of the pyrolysis mass flux and the gas concentrations were accumulated. The systematic errors due to the assumptions made in derivation of these quantities, such as a constant compositions of char and wood, also affected the determined values. The accuracy of these calculation was experimentally determined by injecting a known fuel (propane) into the tunnel at the sample location which simulated the evolution of volatile gases from the wood. The total mass balance and chemical composition of the products of combustion was calculated. The results are presented in Appendix C [Figures ERxx] and are discussed in chapter 3.

L

prese

combu

condi

pyroly

detail.

time i

of pyr

combu

proble

Chapter Three

Pyrolysis of Wood

In this chapter the pyrolysis experiments are described and the results are presented and discussed in detail. In sections 3.1 through 3.5 preliminary experiments, combustion efficiency test, difficulties in the pyrolysis experiments, experimental conditions and derived quantities are described. Section 3.6 analyzes the data on pyrolysis mass flux and examines the effects of all variable parameters in detail. Products of pyrolysis are discussed in section 3.7, and section 3.8 describes the time integrated mass of these products. Char yield and empirical chemical composition of pyrolysis products are examined in section 3.9. In section 3.10 the results of heat of combustion of pyrolysis products are presented, and finally the sample temperature profile is discused in section 3.11.

orde
meas
balar
volat
by t
condu
therm
chem
of
meas
dew-p
stream
is coo
water
amoun
measu
liters
have
meter
sensit
liters
respon
quant
quant
deplet

3.1 Preliminary Experiments

As mentioned in Chapter 2, a large number of experiments were performed in order to obtain reliable and accurate weight loss and chemical species measurements. The main focus was on obtaining a reasonably acceptable overall mass balance within every single experiment. That is, the sum of the mass flux of all volatiles leaving the wood sample had to be equal to the pyrolysis mass flux measured by the electronic balance at any time. The major difficulty encountered was the condensation of the heavy molecular weight hydrocarbons (tar) that left the wood upon thermal decomposition. The importance of this parameter and its effect on other chemical measurements were not originally known to the investigator. The presence of condensible tar in the sample stream significantly affected water measurement. Initially, water content of the pyrolysis products was measured by a dew-point hygrometer. This analyzer measures the dew-point temperature of water in a stream of gases by letting the water condense on a small flat gold mirror (sensor) that is cooled (or heated) by a heat pump. The meter, however, can not distinguish between water and any other condensible molecules. As a result, presence of even minor amounts of condensibles in the sample stream would considerably alter the water measurements. The readings were usually higher than that was expected. Even filteration of the sample stream did not eliminate this problem. Kashiwagi et al.(1987) have also encountered similar difficulties. After extensive investigations, a new water meter was purchased and employed. Although the new system was also somewhat sensitive to the presense of high concentrations of contaminants, however, by proper filtering of the sample gas stream (which removed larger particles without affecting the response time of the analyzer), the water measurement data were much more quantitatively accurate. The system is described in Chapter 2. Thus *transient quantitative* measurement of permanent gases {[THC], CO_2, CO} , H_2O and O_2 depletion were successfully obtained before and after catalytic combustion tube

(Sectio

calculat

3.2 'C

A

tempera

CO_2 an

describe

after ca

pyrolysi

combust

the pyr

answere

calculate

to obtai

combust

A l

location.

surface

tunnel g

minutes

the heati

and H_2O

shown, d

(Section 3.2). The mass flux of condensible portion of the pyrolysis products was then calculated by difference, i.e.,

$$\dot{m}_{tar} = \dot{m}_{p} - (\dot{m}_{[THC]} + \dot{m}_{CO_2} + \dot{m}_{CO} + \dot{m}_{H_2O}) \qquad (3\text{-}1)$$

3.2 'Combustion Efficiency' Experiment

A sample of the tunnel gases was extracted and passed through the high temperature catalytic combustion tube where it was burned with oxygen producing CO_2 and H_2O and trace amounts of CO and [THC]. The catalytic combustion tube is described in Chapter 2. As will be discussed later, from the measurements of products after catalytic combustion, the char yield and empirical chemical composition of the pyrolysis gases were calculated. The relevant question was "how complete is the combustion process in the tube", and whether all reactants were oxidized or not. Since the pyrolysis products contain many unknown hydrocarbons, this question could be answered only by using a gaseous fuel with known chemical composition. The calculated chemical composition of the fuel was compared with the actual composition to obtain a measure of the efficiency of the combustion process in the catalytic combustor. Propane (C_3H_8) was found to be a very suitable fuel for this purpose.

A known flow rate of propane was introduced into the tunnel at the wood sample location. This closely simulated the evolution of the volatile products from the wood surface during pyrolysis experiments including any effects of imperfect mixing of the tunnel flow before reaching the sampling probe. The data were collected for a few minutes without heating the combustion tube and then power was suddenly applied to the heating element resulting in the combustion of the propane and production of CO_2 and H_2O and depletion of O_2. This corresponds to $t \approx 150$ sec in Figure 3.1. As shown, during the warm up time of the heating element, fuel concentration gradually

decreases while concentration of CO_2 increases. The corresponding increase in concentration of H_2O and depletion of O_2 is shown in Figure 3.2. Initially, temperature is not high enough for complete oxidation of propane, thus small amount of CO is generated which diminishes as temperature rises. The steady burning of propane continues until the power is cut-off at $t \approx 570$ sec where the combustion process stops and fuel concentration increases. In this experiment due to the lack of equipments (a very sensitive pressure regulator or control valve) it was very difficult to maintain a constant flow rate of the fuel. The flow rate of propane slightly decreased during the test (see Figure 3.1). This is the reason for the difference between the initial and final concentrations of [THC] in Figure 3.1. The data shown in Figures 3.1 and 3.2 are the recorded gas concentrations and are not corrected for the zero shift, lag and response time (Appendix A). Assuming the chemical composition of the fuel (treated as an unknown) to be C_xH (normalized with respect to the number of H atoms), then the combustion process within the catalytic combustor can be represented by

$$C_xH + O_2 \rightarrow CO_2 + CO + [THC] + H_2O + O_2. \qquad (3\text{-}2)$$

This expression is merely a symbolic representation of the reaction occurring in the combustor and *does not* represent an actual chemical reaction equation. Here, [THC] represents the unburned portion of propane. However, the total hydrocarbon analyzer (FID) was calibrated with CH_4 and the resulting data indicates the mole fraction of the leftover fuel "equivalent" to CH_4. From the measured mole fractions the mass flux of the products [$\dot{m}_{CO_2}$, $\dot{m}_{CO}$, $\dot{m}_{[THC]}$ and $\dot{m}_{H_2O}$] were calculated. These were used to determine x from carbon balance as follows

$$x = \frac{\frac{1}{44}\dot{m}_{CO_2} + \frac{1}{28}\dot{m}_{CO} + \frac{1}{16}\dot{m}_{[THC]}}{[\dot{m}_f - 12(\frac{1}{44}\dot{m}_{CO_2} + \frac{1}{28}\dot{m}_{CO} + \frac{1}{16}\dot{m}_{H_2O})]}. \qquad (3\text{-}3)$$

Here $\dot{m}_f$ represents the mass flux of propane. The calculated values of x (multiply by 8) are shown in Figure 3.3. The sudden discontinuities appearing at the beginning and end of the combustion process, i.e. times around 150 and 570 seconds, are caused by the very sharp rise (or fall) of the gas concentrations due to suddenly applying (or cutting-off) of the electrical power. This results in small over-prediction of gas concentrations at these "cut-off" times (after correcting for lag and response time - not shown here). These errors in the mass flow rates of chemical species accumulate in the calculated value of x through equation (3-3) and cause large discrepancies at the cut-off at times in x values (Figure 3.3). Beyond that, the predicted numbers of carbons are very close to the expected constant value of 3 in C_3H_8 and the overall agreement is quite satisfactory. The total mass balance, i.e. sum of the mass fluxes of CO_2, CO, H_2O, and [THC] is also plotted against input mass flow rate of propane (Figure 3.4). The difference is less than 10%. This demonstrates that the overall performance of the catalytic combustion tube is satisfactory and the values calculated from the measured quantities are accurate within the errors of experiments (i.e. ±10%).

3.3 Pyrolysis Experiments

The main parameters of the pyrolysis experiments were: external radiation, oxygen content of the ambient atmosphere, and the moisture content of wood. Experiments were conducted in two major groups: (1) in inert atmosphere , and (2) in air. In each group three different moisture contents of wood, (i.e., oven-dry (considered as containing 0% adsorbed moisture), wood at "room" condition (8-9% moisture content), and "moist" (about 17% moisture content) were examined under 4 different external radiation levels of 1, 2, 3, and 4 W/cm^2.

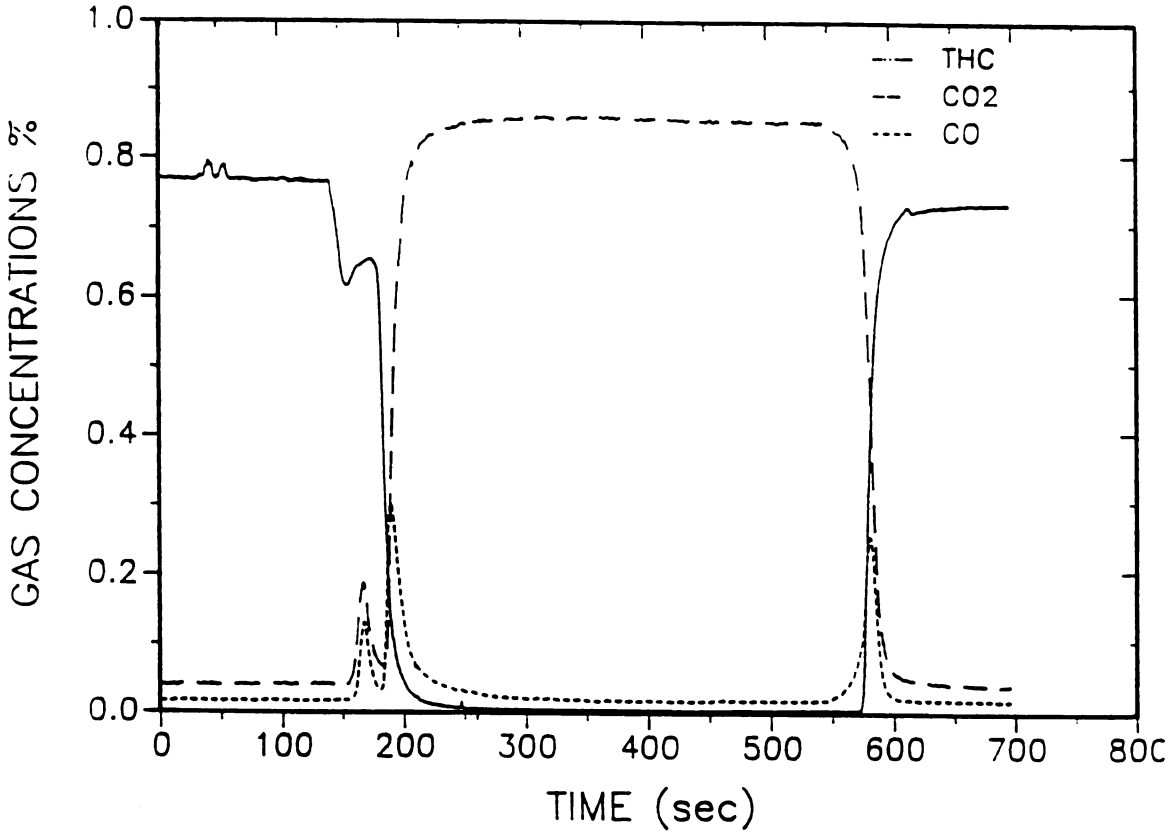

Fig. 3.1 C_3H_8, CO_2, and CO in the combustion of C_3H_8.

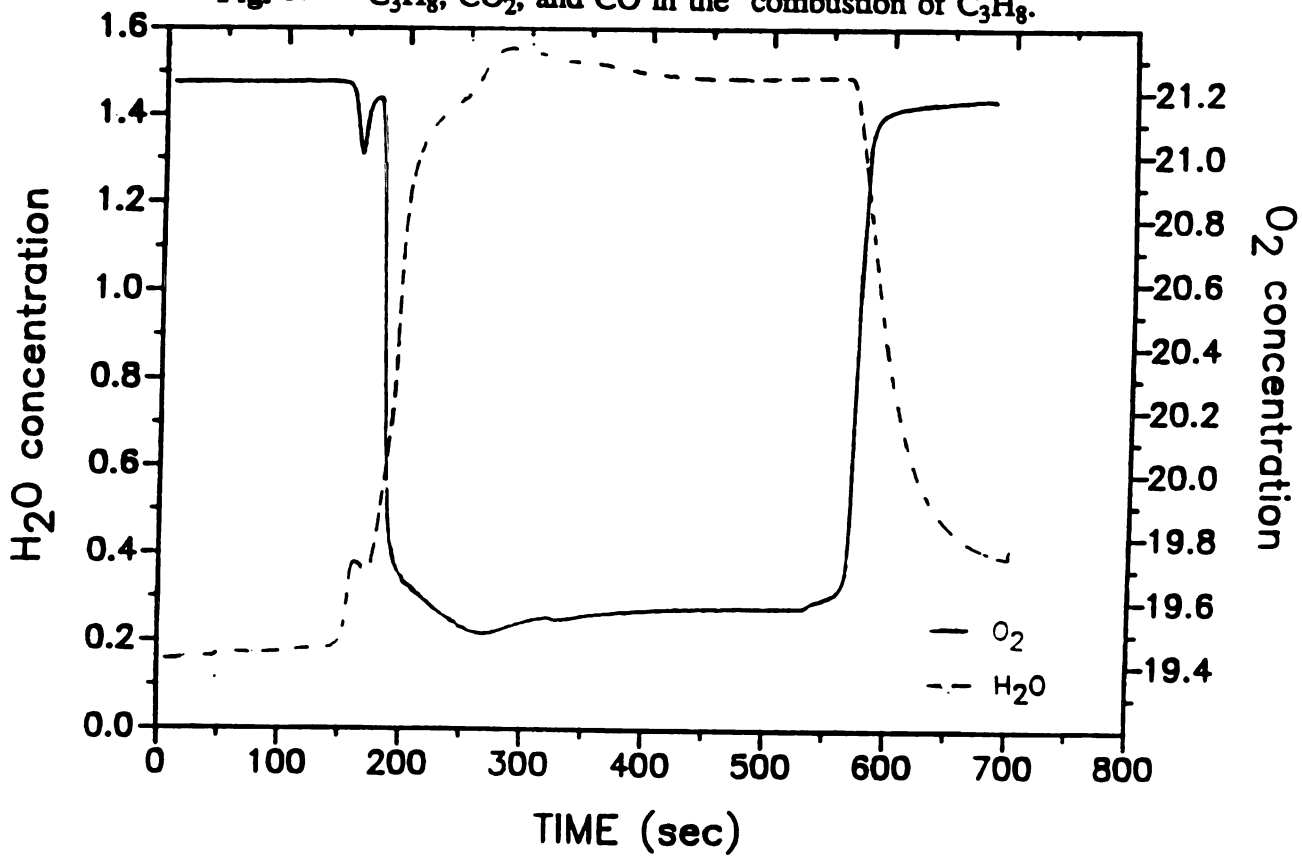

Fig. 3.2 H_2O and O_2 in the combustion of C_3H_8.

TOTAL MASS FLOW RATE (mg/cm²)

Fig. 3.

OF CARBON ATOMS, IN C_xH_8

Fig. 3.

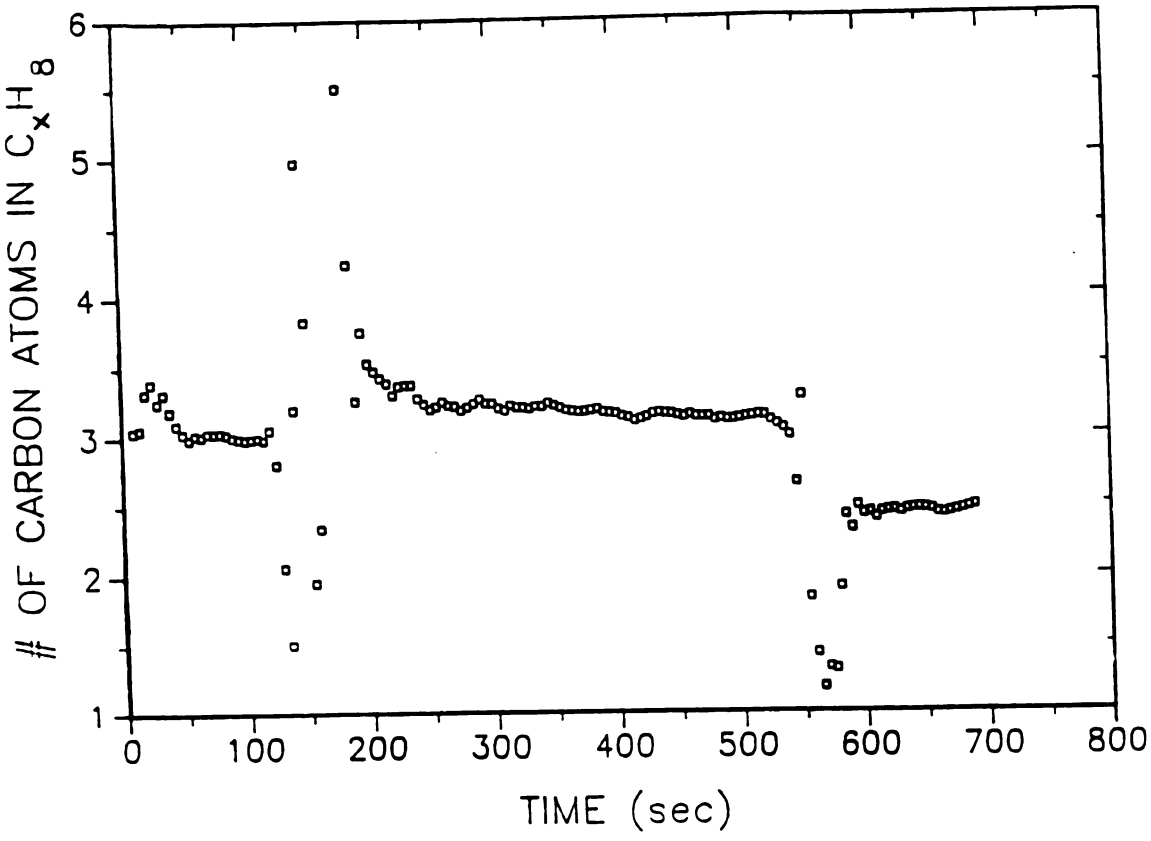

Fig. 3.3 Number of carbon atoms calculated from products of combustion of C_3H_8.

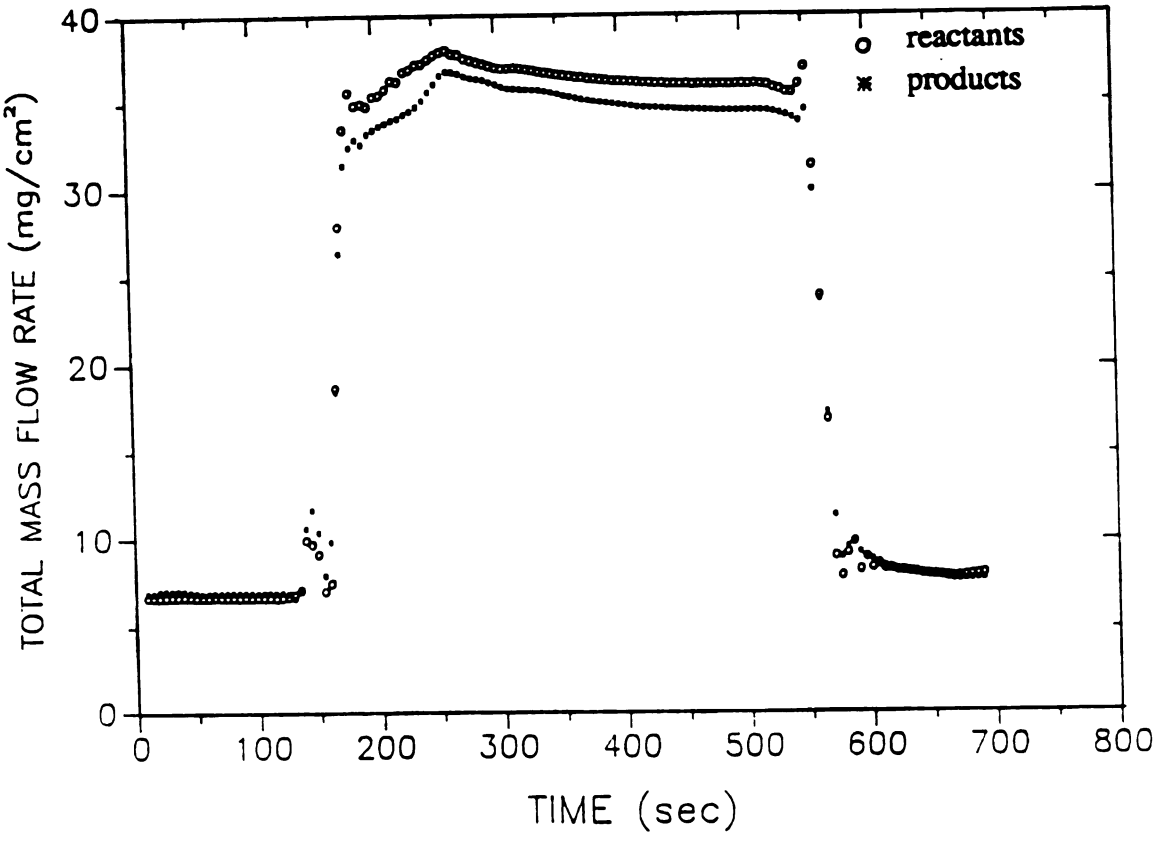

Fig. 3.4 Total mass flux of reactants and products of combustion of C_3H_8.

exp

(4 r

very

exa

be c

will

pow

simp

corre

micro

Wi

cond

'R+A

wood

were

exper

for i

additi

Wi

experi

data,

where

o this

The maximum external heat flux was limited due to the capability of the experimental facility. Moreover, although the heaters were warmed up for a long time (4 to 8 hours) before the start of the experiments, it was very difficult to maintain a very constant heat flux and, more importantly, closely reproduce the same level of external radiation for similar experiments. This was because some experiments had to be conducted under special condition i.e. without the tunnel-top infrared glasses (which will be discussed later), and possibly there were variations in the current of the main power supply to the laboratory (from time to time). However, for the sake of simplicity and convenience, the experiments are nominally coded for their corresponding heat flux levels at each moisture content of wood in either air or nitrogen atmospheres. For example, the experiment conducted on dry wood at 2 W/cm^2 in nitrogen is called experiment 'D2N'. The experiment conducted on wood conditioned in "room" moisture condition at 4 W/cm^2 in air is termed as experiment 'R4A'. The experiment on wood with 17% moisture content (herein termed as "moist wood") at 1 W/cm^2 in nitrogen is considered as experiment 'M1N'.

In addition, to improve the weight loss measurements, most of the experiments were conducted with only front and back surface thermocouples installed. Separate experiments with samples instrumented with in-depth thermocouples were carried out for in-depth temperature measurements. These experiments are coded with an additional letter 'T'. For example, TD3A represents an experiment on dry wood at 3 W/cm^2 in air with only temperature measurements. These nominal classification of the experiments are summarized in Table 3.1. Due to the large amount of experimental data, most of the results are presented in Appendix C. In the following sections wherever a reference is made to the Figures from Appendix C it is explicitly referred to this Appendix. Otherwise the Figures are shown in this chapter.

Table 3.1

CODES FOR PYROLYSIS EXPERIMENTS							
Atmosphere		Nitrogen			Air		
Moisture Content		Dry	8-9%	17%	Dry	8-9%	17%
External Heat Flux (W/cm^2)	1	D1N	R1N	M1N	D1A	R1A	M1A
	2	D2N	R2N	M2N	D2A	R2A	M2A
	3	D3N	R3N	M3N	D3A	R3A	M3A
	4	D4N	R4N	M4N	D4A	R4A	M4A

3.4 Experimental Conditions

Unfortunately, even after adding extra heating coils to the external radiation source [RH in Figure 3.2], it was not possible to obtain 4 W/cm^2 at the sample surface in the presence of the infrared glasses. Thus, for experiments conducted at more than 2 W/cm^2 external radiation the top-tunnel infrared glasses were removed. This allowed us to obtain more than 4 W/cm^2 heat flux on the wood sample. In this condition, the 1" gap between the top-tunnel and the cooling plate [Figure 3.3] was sealed with insulating boards, and the tunnel flow rate and the exhaust suction were adjusted to eliminate leakages of volatile pyrolysis products out of the tunnel. The boundary layer over the sample surface was not significantly altered in this condition. Small leakages of the ambient air into the tunnel were measured by tracing gas technique prior to the start of every experiment and were accounted for in the subsequent calculations.

mo

ca

des

py

ea

im

we

exp

10

the

3.5

and

spe

mea

mea

basi

mea

conv

In the absence of the top-tunnel glasses, however, the inside of the radiant heater module was likely to be filled with smoke, specially at the start of the pyrolysis. This caused partial blockage of radiation and reduced the magnitude of heat flux from its desired constant values. Figures HFxx show the measured heat flux values during the pyrolysis experiments. The maximum reduction in the heat flux was about 15% at the early seconds of the experiments performed at 3 and 4 W/cm^2. The condition improved as the pyrolysis continued and as the tarry contents of the pyrolysis products were reduced. The external radiation was much more constant at 1 and 2 W/cm^2 experiments as can be observed from Figures HFxx (maximum change less than 10%). The slight fall off of heat flux in some of these cases was due to the cooling of the heating rods [Figure 3.3] by the air jets used to cool the infrared glasses.

3.5 Derived Quantities

The measured output of the continuous gas analyzers were corrected for lag time and instrument response time [Appendix A] to obtain mole fractions of the measured species as a function of time when they were produced. Since the instruments used to measure O_2 , CO_2, and CO after catalytic combustor and CO on the direct measurement line required a dry sample stream, the measured values were on a dry basis. To obtain the real mole fractions, they were converted to a wet basis using the measured mole fraction of water, i.e.,

$$\text{(mole fraction on wet basis)} = \text{(measured mole fraction on dry basis)} \times \text{(1.0 – mole fraction of water removed by the drier).} \qquad (3\text{-}4)$$

The corrected mole fractions of all the species (major constituents) were then converted into mass production rates by using the exhaust mass flow rate [mass flow

rate c

pyroly

oxyge

!

(1982

(descr

combu

is con

amoun

potenti

Ir

combu

consum

multip

(1980)

time

where,

In

the pyr

formula

may be

of woo

rate of nitrogen (or air) determined from the sonic nozzle relations + mass flow rate of pyrolysis products determined from weight loss measurements + mass flow rate of oxygen (for experiments in nitrogen) + mass flow rate of air leaking into the tunnel].

Methods of determining the empirical formula of the pyrolysis products [Susott (1982), Parker (1985)] are in principle similar to the method adopted in this work (described below). In these methods, which are used to determine the heat of combustion of volatiles and the kinetic parameters as well, a small flow of the volatiles is completely oxidized in a catalytic converter to carbon dioxide and water. The amount of oxygen consumed in this process is measured and used to calculate the potential rate of heat release and the heat of combustion.

In this work, the difference between the input mass flow rate of O_2 before combustion tube and mass flux of O_2 after combustion tube is the amount of oxygen consumed by the complete combustion of the pyrolysis products. This difference multiplied by the nearly constant heat of combustion per unit mass of O_2 [Hugget (1980)], determines the heat of combustion of the pyrolysis products as a function of time

$$\Delta H_v = \dot{m}_{\Delta O_2} \cdot \Delta H_c \qquad (3\text{-}5)$$

where, ΔH_c is the heat of combustion of fuels per unit mass of oxygen.

Instantaneous char yield and the time varying empirical chemical composition of the pyrolysis products are calculated as follows. Let C_uH_vO represent the empirical formula for wood, and C_pH_qO represent the empirical chemical formula for char (these may be obtained from elemental analysis), then the thermal decomposition of a gram of wood can be written as

$$1 \text{ gram of } (C_uH_vO) \rightarrow Y_c \text{ gram of } (C_pH_qO) + (1 - Y_c) \text{ gram of } C_xH_yO \quad (3\text{-}6)$$

where, Y_c is the char yield (grams of char formed per gram of wood) and C_xH_yO is the empirical chemical composition of the pyrolysis products.

These pyrolysis products are later burned to CO_2 and H_2O and trace amounts of CO, (neglecting [THC] which was practically zero after the combustion tube). This reaction is represented by

$$C_xH_yO + O_2 \rightarrow CO_2 + CO + H_2O. \quad (3\text{-}7)$$

The two unknowns x and y in expression (3-7) are easily obtained from the two equations for carbon and hydrogen balance in terms of the species mass production rate as:

$$x = \frac{\frac{4}{11}\dot{m}_{CO_2} + \frac{4}{7}\dot{m}_{CO}}{\dot{m}_p - \left[\frac{3}{11}\dot{m}_{CO_2} + \frac{3}{7}\dot{m}_{CO} + \frac{1}{9}\dot{m}_{H_2O}\right]}; \quad (3\text{-}8)$$

and

$$y = \frac{\frac{16}{9}\dot{m}_{H_2O}}{\dot{m}_p - \left[\frac{3}{11}\dot{m}_{CO_2} + \frac{3}{7}\dot{m}_{CO} + \frac{1}{9}\dot{m}_{H_2O}\right]}. \quad (3\text{-}9)$$

The instantaneous char yield can now be obtained from equation (3-6). Since the composition of wood is unknown and is assumed to be invariant, u and v are known constants. Hence we are left with three unknowns Y_c, p, and q and only two equations (for the carbon and hydrogen balance; oxygen does not yield an independent equation because the empirical formulas are normalized with respect to

oxygen). However, previous investigations [Atreya (1983)] shows that the char composition is very nearly constant during the decomposition process and the only variable effectively changing the composition of the wood volatiles is the char yield. Thus, p and q can be determined from elemental analysis and assumed to be constants. Hence char yield can be obtained from the expression

$$Y_c = \left[\frac{(12\,p + q + 16)}{(12\,u + v + 16)}\right] \cdot \left[\frac{12\,(x - u) + (y - v)}{12\,(x - p) + (y - q)}\right] \tag{3-10}$$

From the calculated empirical composition of the pyrolysis products the amount of oxygen needed for complete combustion in the combustion tube can be determined from the reaction

$$C_xH_yO + \left(x + \frac{y}{4} - \frac{1}{2}\right) O_2 \rightarrow x\,CO_2 + \frac{y}{2}\,H_2O, \tag{3-11}$$

as

$$\dot{m}_{\Delta O_2} = \frac{32\left(x + \frac{y}{4} - \frac{1}{2}\right)}{(12\,x + y + 16)}\,\dot{m}_{p.} \tag{3-12}$$

This serves as a criterion for checking the accuracy of gas composition measurements.

Experimental Results and Discussion

3.6 Pyrolysis Mass Flux

The mass flux curves represent the single most important characteristic of pyrolysis of wood, because the ignition, gas phase flame propagation, steady burning, and extinction phenomena are all primarily controlled by the rate at which the solid can provide fuel to the gas phase. Also physical and kinetic quantities such as heat of pyrolysis, activation energy, and reaction rates are obtained from models which best fit these curves. Experimental data of pyrolysis mass flux, specially the ones that represent short and long term behavior of the solid, are often lacking. Before discussing the effects of each parameter on the pyrolysis mass flux the general characteristics of these curves are described.

The pyrolysis mass flux data was obtained by numerically differentiating the weight loss data vs. time and dividing it by the original surface area of wood that was exposed to the external radiation. This was a difficult task because disturbances were caused in weight loss measurements due to both the nature of the wood and the experimental conditions. Two sources of disturbances existed in the weight loss measurements. The first included the mechanical fluctuations and small level of turbulence that exist in any tunnel flow, and are harder to eliminate in small scale tunnel flows [Michel and Froibel (1988)]. These "noises" were mostly smoothed out by the data fitting technique described in Appendix A. Care was taken to smooth the data in such a way that the fundamental characters of the phenomenon was preserved. The second source of fluctuations in the weight loss data originated from the nature of the wood and the physics of pyrolysis. It has been shown [Lee et al. (1976), Fredlund (1988)] that high pressures are generated inside wood as the pyrolysis zone propagates

within the solid. Moisture and fuel volatiles travel outward through the pores of wood and char, and burst out of the surface in an irregular fashion. At higher temperatures occasionally cracks appear on the char surface and fuel gases are released through these cracks more freely. Wood is also an inhomogeneous material. Grain direction and density growth rings [Atreya (1983)] have significant effect on how easily the pyrolysis products are liberated from the front surface. These two groups of parameters caused some *local* variations within the pyrolysis mass flux curves (Figures 3.6-3.17). It is not possible to distinguish between the variations caused by each of these factors at any time. No further attempts were taken to smooth these curves any more.

Another common problem with the mass loss curves is that in most experiments the first few seconds of data are not generally reliable. This is due to practical reasons that have existed in other investigations as well [Atreya (1983)]. For example, in the preliminary experiments, it was found that a sudden exposure of the tunnel to external radiation increased temperature and pressure of the gases inside the tunnel, thus disturbing the weight loss measurements. This situation was significantly improved by modifying the procedure for starting the experiments. A thin flat aluminum plate slightly larger than the wood sample size was laid down over the sample location such that it covered the sample without touching it. The cooling plates were removed and the tunnel was exposed to radiation moments before the start of the experiments. After a few seconds the flat plate covering the wood surface was removed without contacting with the sample. This was done successfully in most experiments. However, due to the extremely rapid pyrolysis and water desorption, disturbances at the initial times, could not be totally eliminated. To demonstrate the reproducibility of pyrolysis experiments, three similar experiments were performed on three wood samples. In Figure 3.5 the pyrolysis mass fluxes of these experiments (wood heated in air at 2 W/cm^2) are compared. Considering all experimental problems associated with wood

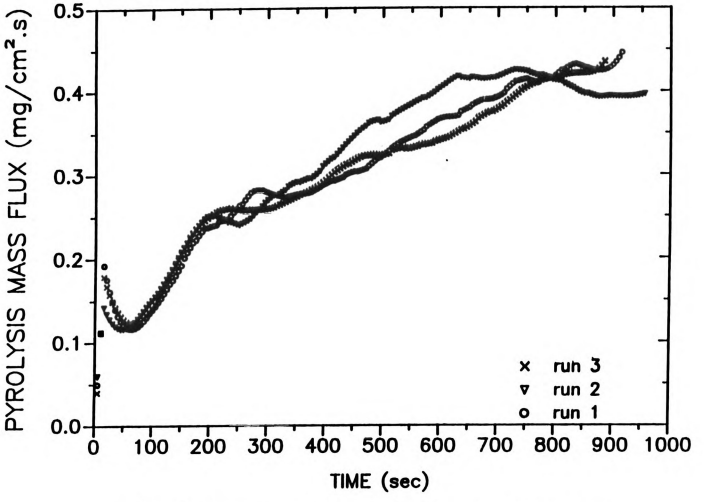

Fig. 3.5 Pyrolysis mass flux obtained in three runs of an experiment on 8-9% moist wood at 2 W/cm^2 in air (reproducibilty test).

pyrolysis, the agreement is encouraging.

In order to capture both the small time and the large time characteristics of the pyrolysis process, the majority of experiments were continued up to 30 minutes. This is about twice the duration of similar experiments conducted by other investigators [Kashiwagi et al. (1987)]. The mass flux curves for each group of conditions are shown in Figures 3.6-3.17. These data are also plotted on log-log coordinates in order to observe some of their characteristics more clearly. The most striking observation about all mass flux curves conditions is that the gradual decline of the pyrolysis mass flux following the rapid initial rise, does not show a negative one-half power dependence on time as is assumed by many investigators and is predicted by simple theoretical models (Chapter 4). Such dependence is observed rarely and for short periods such as in Figures 3.18-3.23. For the time duration of most of these experiments the mass flux, after the rapid initial rise and the subsequent gradual fall-off, decreases very slowly and in some cases tends to increase and becomes almost constant. The sudden rise and gradual fall-off type behavior of mass loss curves was previously observed [Lee et al. (1976), Chan & Kreiger (1980), Kashiwagi et al. (1987)] and is predicted by numerical models of wood pyrolysis (see Chapter 4). However, in all the experiments performed in this work, the fall off in mass flux curves does not appear to be proportional to the negative one-half power of time for the entire duration of the experiment, on Douglas-fir. Although other types of wood and different grain direction relative to the incident radiation may cause quantitative variations in the mass flux, it seems unlikely that the characteristic behavior will be significantly different. Atreya (1983) examined many types of wood and this trend, i.e. decreasing the pyrolysis mass flux proportional to the negative one-half power of time, was not observed. Kashiwagi et al. (1987) reported the pyrolysis mass flux data for similar experiments performed on white pine. In their data it appears that the fall-off of the pyrolysis mass flux is closely related to the negative one-half power of

time. For this reason, while for similar experiments (e.g. experiment at 4 W/cm^2 in N_2) the mass flux values in the initial times are in reasonable agreement with our data (considering the two different woods), the large time values are consistently smaller. Although these data and Kashiwagi's data (some of the original data were available) were examined in detail, the main reasons for this difference are not yet fully known to the author. However, it appears that the flow geometry may be a major source for this different behavior in the rate of gasification. As it will be discussed in more detail in section 3.6.1.2 (for experiments in air), in their experiments the boundary layer over the wood sample starts from the sample edge resulting in highly non-uniform convective heat transfer over the wood sample. The convective heat transfer coefficient along the length of their sample (3.8 cm) is very high and the sample is convectively cooled. In fact, even at the early times of heating, the results show that the mass flux in our experiments typically rises faster than their experiments. As the surface temperature rises, which corresponds to the charring regime of pyrolysis process, the effect of this non-uniform convective cooling becomes more significant. Thus, the mass flux falls-off more rapidly than in our experiments where the boundary layer is almost fully developed and is uniform along the entire length of the sample. This flow geometry has even a more significant effect for experiments conducted in air, where the char oxidation occurs. This will be discussed later. A second reason for higher mass fluxes in our experiments could be the oxidative effect of minor amount of oxygen (typically less than 1%) into the tunnel in experiments conducted in N_2. Of course, no char oxidation was visually observed even at high heat fluxes and the effect of this small amount of O_2 can not be significant. But, possibly some oxygen may have diffused into the hot char pores and reacted with it. The extent of this effect, if any, can not be quantified.

3.6.1.1 Effect of External Heat Flux

Obviously, the rate of pyrolysis (for the same ambient conditions and moisture content of wood) increases as the external heat flux increases. As shown in Figures 3.5-3.17, the maximum in the mass flux curves occurs earlier for higher heat fluxes. This is also predicted by theoretical models.

A. Dry Wood

For oven-dry wood heated in inert atmosphere, the mass flux rises rapidly and only one sharp mass flux peak appears (Figure 3.6). This peak corresponds to approximately 375°C (range of 350-400°C). The initial early peak appearing in mass flux curve at 1 W/cm^2 is not believed to accurately represent mass flux values. This could be partly due to the desorption of small amount of moisture that might have diffused into the surface layer of wood during the short period of time that the sample was made ready for experiment. It could also be caused in part by the previously mentioned initial disturbances that are significant compared with the mass flux values at low heat fluxes. This problem generally exists at low external heat flux experiments where the mass loss rate is so low that the experimental errors become comparable with the actual data.

In air, the experiments performed at 4 W/cm^2 heat flux show a very rapid rise in mass flux followed by a sharp increase in surface temperature (Figure 3.31). The sample spontaneously ignited after about 82 seconds. This corresponds to the surface temperature of about 510°C which is followed by a sharp temperature rise of up to about 700°C. Similar experiments on wood with 8-9% and 17% moisture content also ignited at surface temperature of about 500 - 540°C. The ignition was delayed due to the desorption of water. The sample with 8-9% moisture content ignited after 127 seconds, and the one with 17% moisture ignited 150 seconds after the start of heating. After ignition, the pulsating motions of the flame caused the mass flux to be very

oscillatory. These flaming conditions are not of interest here because they can not be compared with the non-flaming conditions; since, the heat flux impinging upon the surface of wood changes drastically in the presence of the flame.

B. Moist Wood

For moist wood at 4 W/cm^2 also only one peak was observed in both air and nitrogen atmospheres. The first small hump in experiment R4A [Figure 3.14] at about 120 seconds is likely to be caused by disturbances and does not represent actual mass loss. However, for 17% moisture content, the successive steps of drying, thermal decomposition (tar evolution), and char production can be distinguished [Figures 3.10 and 3.16]. For example, in Figure 3.16 for experiment M4A the first peak corresponds to the maximum moisture evolution rate, whereas the second one represents the maximum pyrolysis mass flux and the formation of char. The effects of moisture content of wood are discussed in more detail in section 3.7.2.

3.6.1.2 Effect of Ambient Oxygen

In oxygen containing atmosphere char oxidation and exothermic gas phase reactions between volatile products and oxygen at the vicinity of the surface contribute to the energy which enters the solid. This energy supplements the external heat flux so that the mass flux increase is due both to increased pyrolysis and char gasification. Like the external heat flux, the char oxidation heat in confined to a thin surface zone. However, the char does not oxidize as fast as the inward moving pyrolysis wave produces char; thus the pyrolysis mass flux falls-off with time in much the same manner as in pure nitrogen atmosphere.

At lower heat fluxes, under non-flaming condition in air [Figures 3.12-3.17], an early hump appears in the mass flux curves followed by less rapid rise to a second larger peak which is followed by very gradual decline of mass flux rates as the

pyrolysis continues. This is a very interesting phenomenon. To explain this behavior, we should note that in these experiments the velocity and thermal boundary layer starts ahead of the edge of the sample. Thus, the boundary layer is thick and almost fully developed over the sample. In this situation less O_2 can diffuse into the surface of the hot char compared with a thin boundary layer. Then, let's compare experiments D2N and D2A as well as experiments R2N and R2A with each other. In these experiments the external heat fluxes are almost equal to 2 W/cm^2 and are nearly constant during entire duration of experiment [Figures 3.7 and 3.13]. In both experiments D2N and D2A it took approximately 100 seconds before the mass flux reached the first peak. In both cases, this corresponds to the surface temperature of about 375-400°C. The first peaks of experiments in air, however, are smaller than those in nitrogen. This is likely in part due to the chemisorption of oxygen into the surface of freshly produced reactive hot char at lower temperatures, and in part due to the less complete char oxidation in the absence of enough O_2. Notice that at earlier times, e.g. at t=50 sec., when the surface temperature is almost equal in both cases (= 300°C) [Figures TD2N and TD2A, (Appendix C)] the magnitude of mass flux is nearly equal. As the temperature of porous char, which is highly reactive, increases and before significant oxidation of char is initiated, oxygen molecules are absorbed into the char surface and consequently the weight loss rate at this point is relatively lower than the similar situation in inert atmosphere. Upon formation of char, in experiment D2N the pyrolysis mass flux decreases rapidly after the peak appears. In experiment D2A the mass flux slightly decreases (due to formation of char), but begins to increase again with a slower rate than the early times. This increase continues until about 560 seconds where the mass flux starts to decline due to the growing char thickness. This peak is slightly higher than that of D2N experiment but occurs at a much later time.

This phenomenon is closely related to the smoldering combustion and involves the formation of reactive char by pyrolysis, chemisorption of O_2, evolution of CO,

CO_2, and generation of new reactive cites [Shafizadeh (1980)]. This process, which is accompanied by evolution of incompletely oxidized volatile pyrolysis products at relatively low temperatures; is usually distinguished from the more rapid and incandescent combustion of char (*glowing combustion*) at higher temperatures and in the presence of more O_2.

This phenomenon does not appear in the work of Kashiwagi et al. (1987). The mass flux curves in air do not show such early shorter humps and the sharp peaks of the curves are always higher and occur faster in oxygen containing atmospheres than in nitrogen. The reasons are not yet fully known to the author. However, different experimental conditions are likely to have considerable effect on the pyrolysis process. In their experiments the boundary layer starts at the lower edge of the sample which is heated vertically. The boundary layer is thin over the length of the sample and is even thinner over part of the sample before its thickness grows. Thus, the amount of oxygen diffusing into the surface of the char from the free stream flow is higher than our condition resulting in the rapid oxidation of char. The pyrolysis mass flux, therefore, rises quickly and reaches its maximum. Chan and Kreiger (1980) also obtained different gas evolution patterns than those of Kashiwagi et al. (1987). This problem is not yet well understood and needs more experimental verification.

The second peak in these mass flux curves [Figures 3.12-3.17] corresponds to the "thick char" regime [Wichman and Atreya (1986)], in that further decomposition is hampered by the formation and growth of an insulating layer of char. The consumption of the char in the glowing combustion, however, continues. Therefore, after the second peak in the mass loss curves the rate of weight loss is much higher than the similar case in nitrogen atmosphere. The surface temperature of the solid [Figure 3.31] shows an inflection point after the start of char oxidation which results in much higher temperatures in air than in nitrogen. The effects of oxygen on the surface temperature will be discussed later in more details. Similar phenomena are observed in

experiments R2N and R2A, i.e., experiments on 8-9% moist wood at 2 W/cm^2 in nitrogen and air respectively [Figures 3.6-3.11 and 3.12-3.17]. In these experiments the very early humps are due to the desorption of adsorbed water upon heating of the sample. The second peak is the time when rapid decomposition leads to the formation of char, after which the one in nitrogen decreases monotonically. The magnitude of this peak in experiment R2A is smaller than that of experiment R2N (due to chemisorption of O_2). The experiment in air experiences a very small decline for a short time after the first pyrolysis peak, followed by gradual increase leading to the second peak. This phenomenon is also observed in experiments conducted under 3 W/cm^2 external heat flux in air as well. The second peak is very clear in the experiment D3A and occurs earlier than in experiment D2A, as expected. The experiment R3A is not very clear due to the excessive disturbances in the weight loss data caused perhaps by moisture evolution. The magnitude of the highest peak of the mass loss rate curves for the same moisture content is much higher in air than the maximum mass flux in nitrogen atmosphere. The difference is larger at higher heat fluxes. Thus, the pyrolysis mass flux for wood samples degrading in air is considerably larger than those decomposing in inert atmosphere, even when the char layer becomes thick.

To summarize, the pyrolysis mass flux increases with an increase in ambient oxygen concentration. The chemisorption of the oxygen on the reactive char surface, smoldering and then glowing combustion significantly change the physics of pyrolysis and the weight loss rate. The actual energy going into the solid in oxygen containing atmosphere is the external heat flux plus the exothermic energy released by the char oxidation and exothermic chemical reactions in the gas phase above the wood surface.

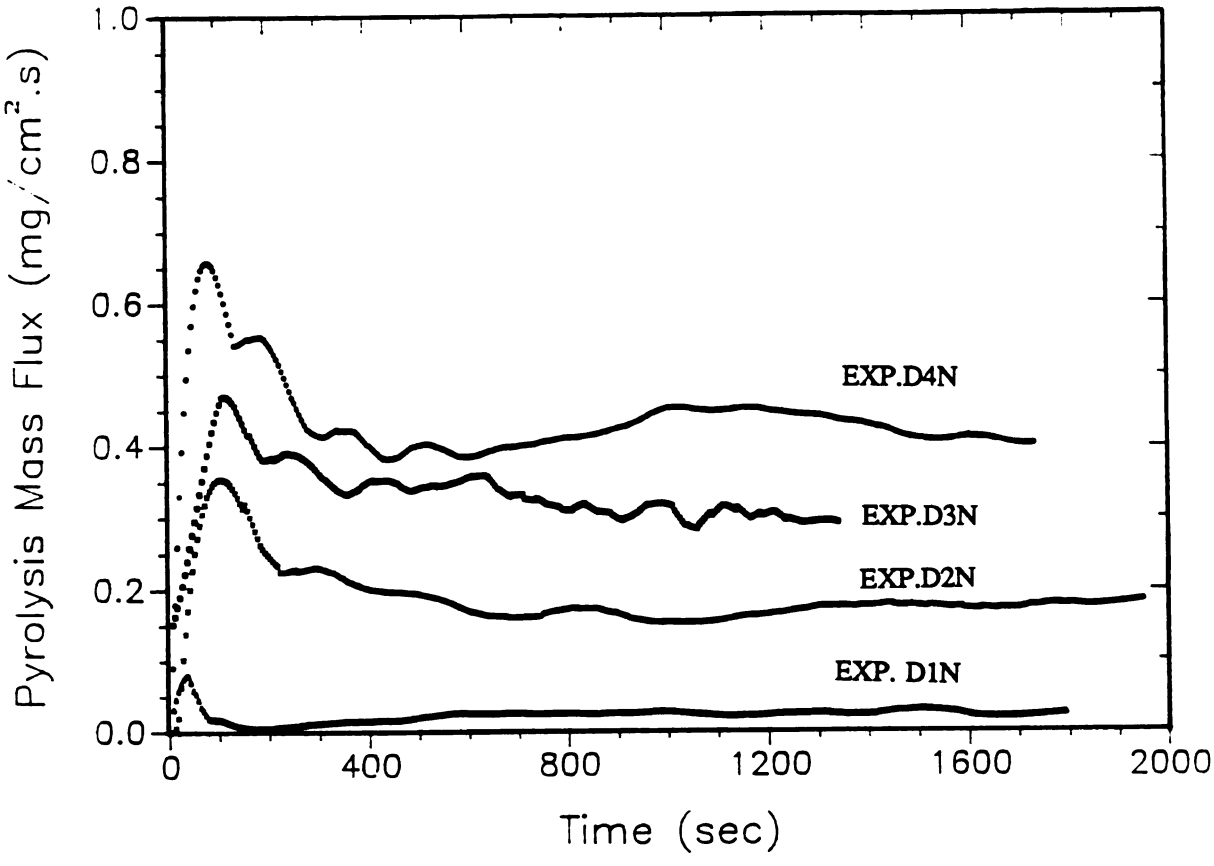

Fig. 3.6 Pyrolysis mass flux for experiments on dry wood in N_2.

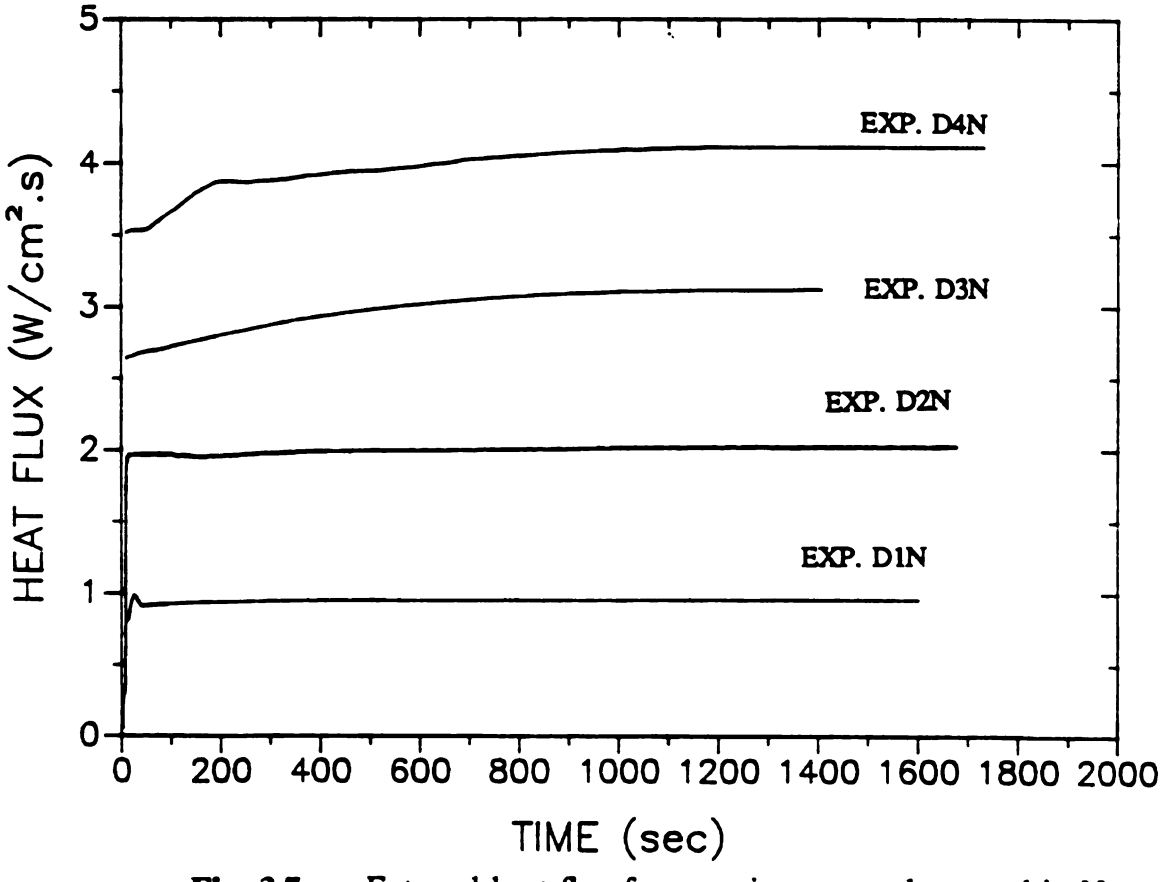

Fig. 3.7 External heat flux for experiments on dry wood in N_2.

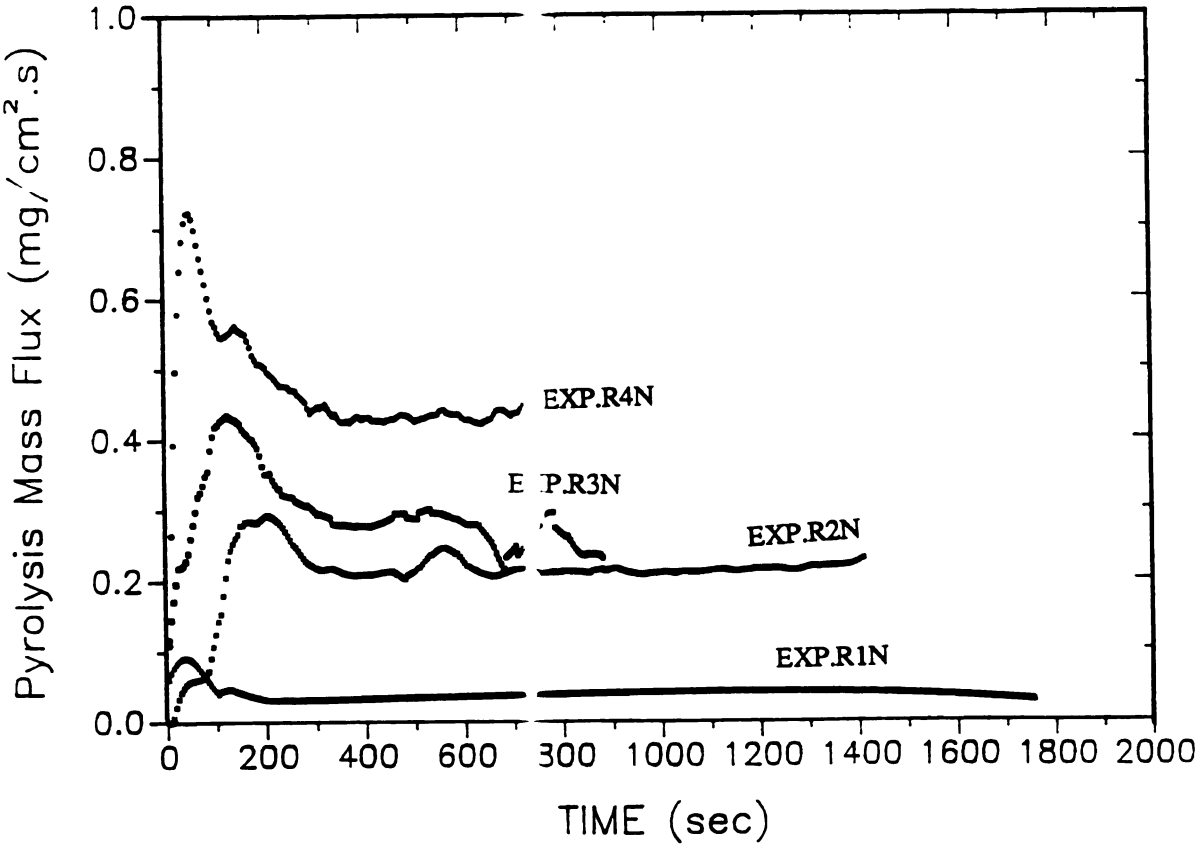

Fig. 3.8 Pyrolysis mass flux for experiments on 8-9% moist wood in N_2.

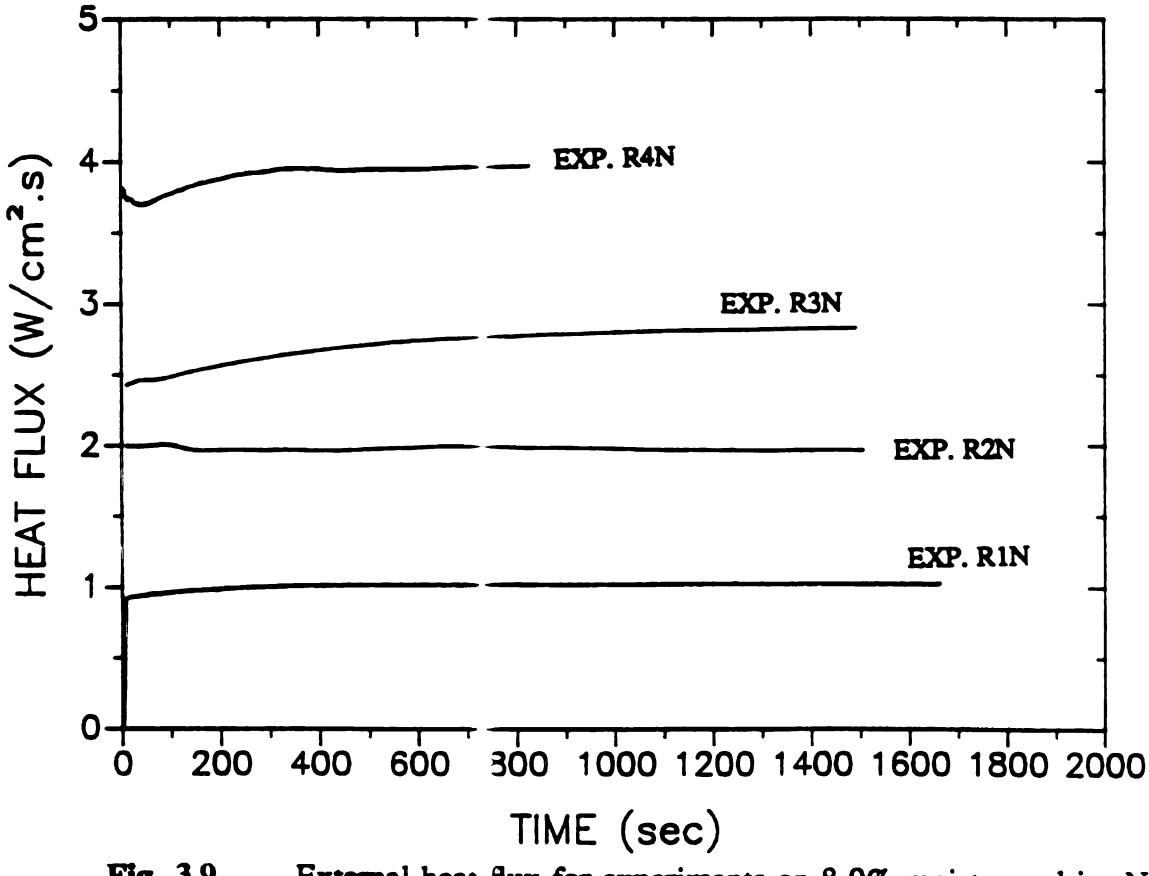

Fig. 3.9 External heat flux for experiments on 8-9% moist wood in N_2.

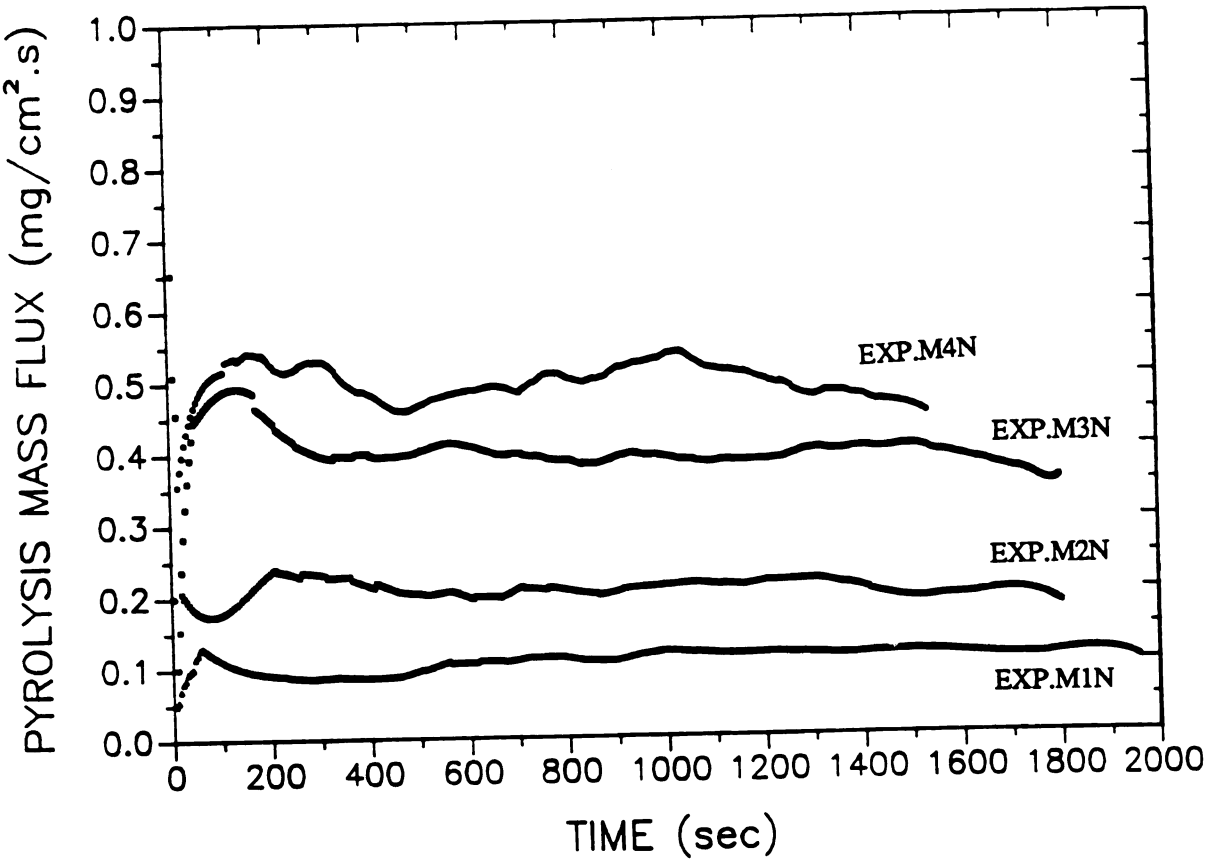

Fig. 3.10 Pyrolysis mass flux for experiments on 17% moist wood in N_2.

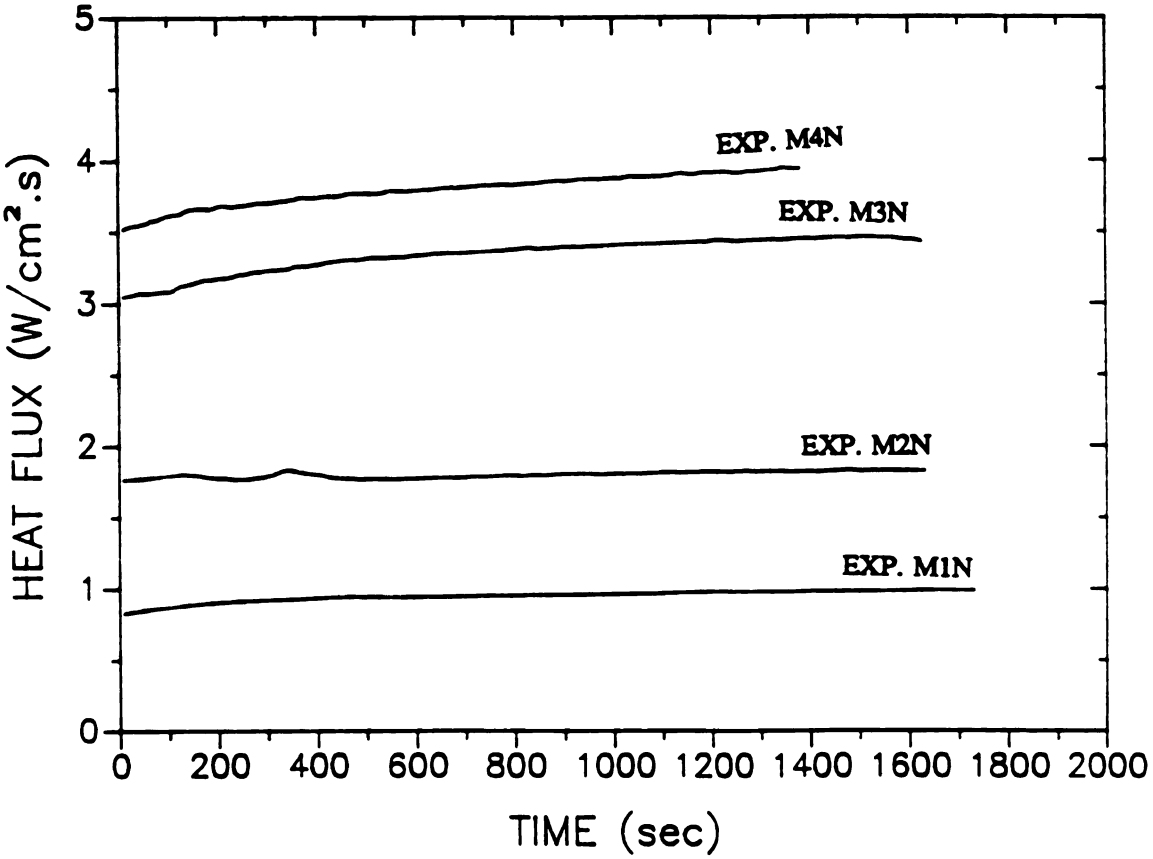

Fig. 3.11 External heat flux for experiments on 17% moist wood in N_2.

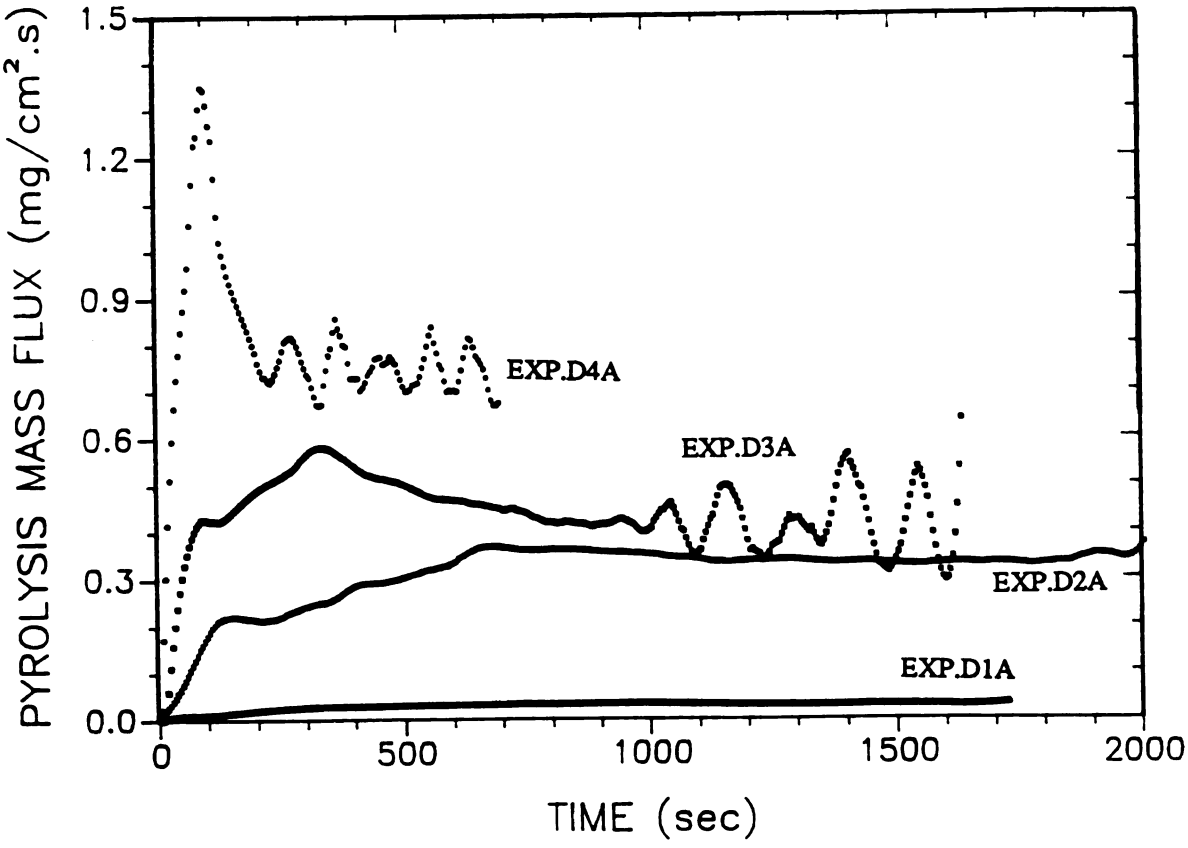

Fig. 3.12 Pyrolysis mass flux for experiments on dry wood in air.

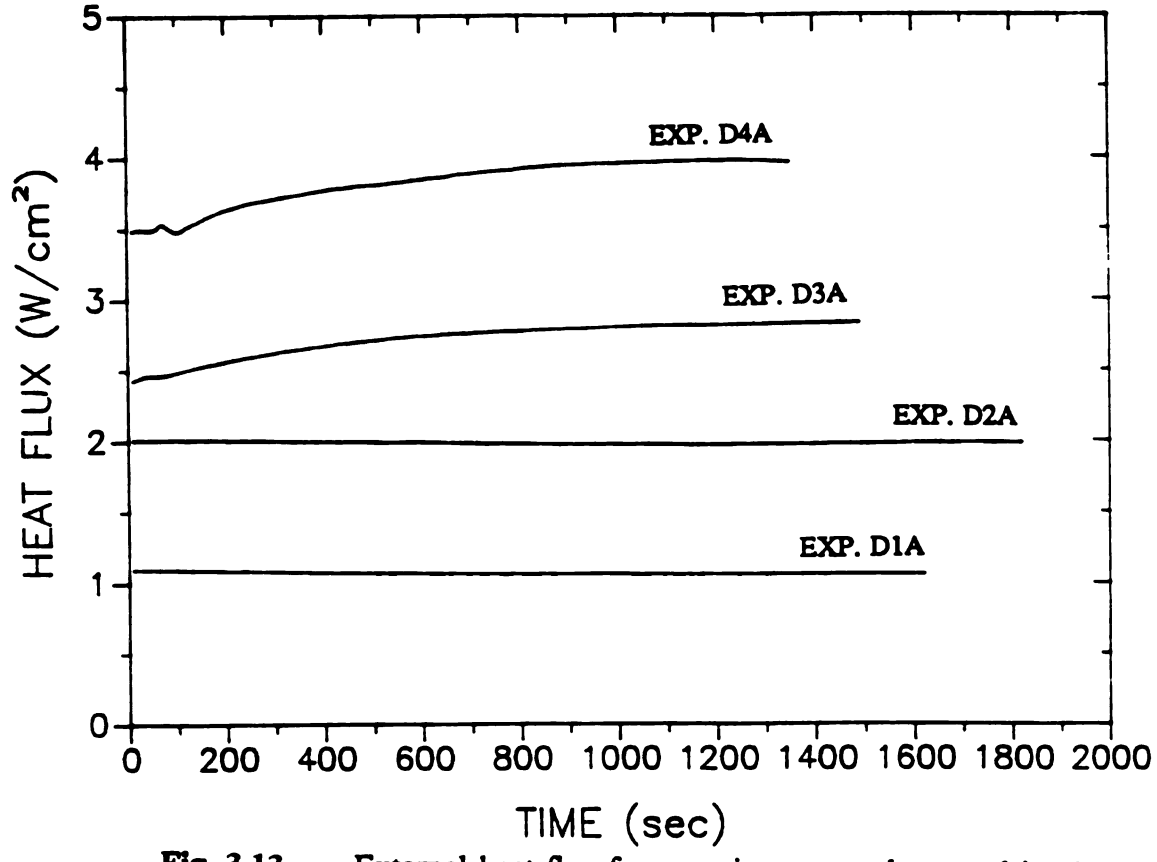

Fig. 3.13 External heat flux for experiments on dry wood in air.

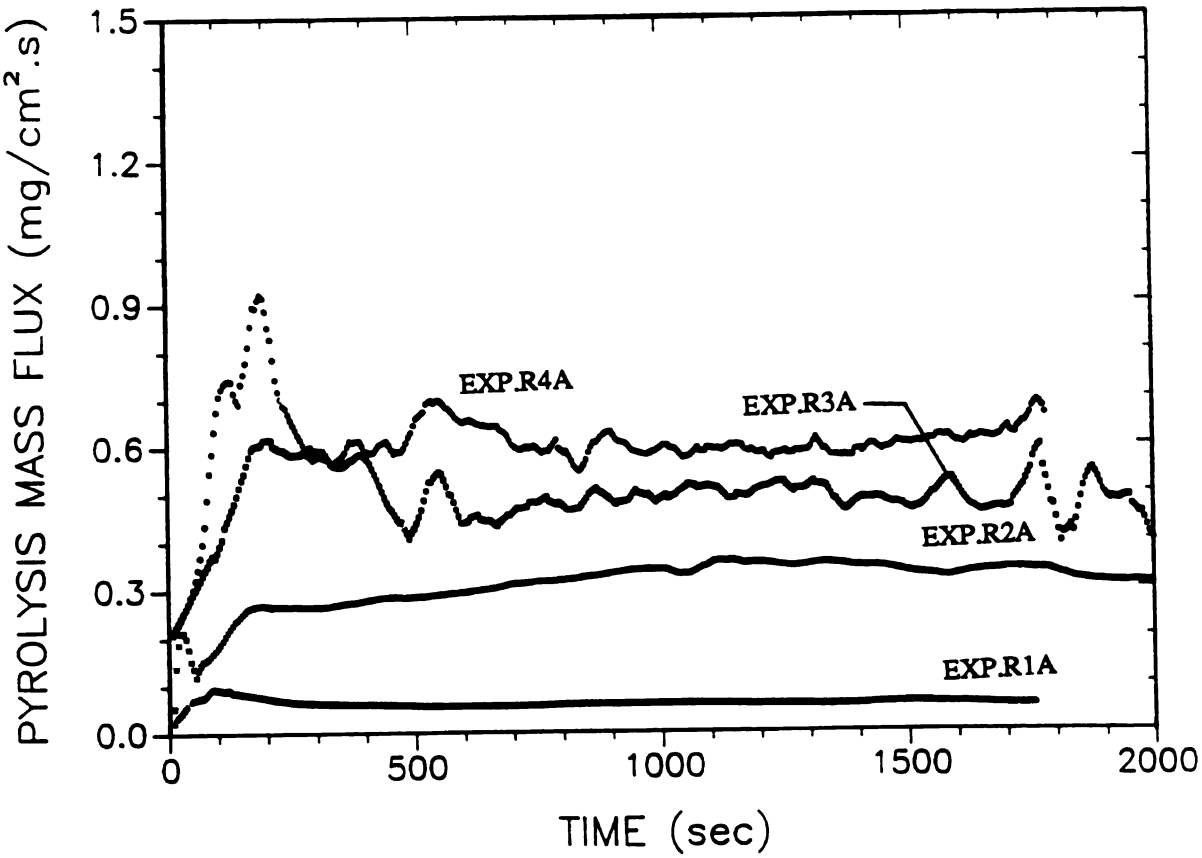

Fig. 3.14 Pyrolysis mass flux for experiments on 8-9% moist wood in air.

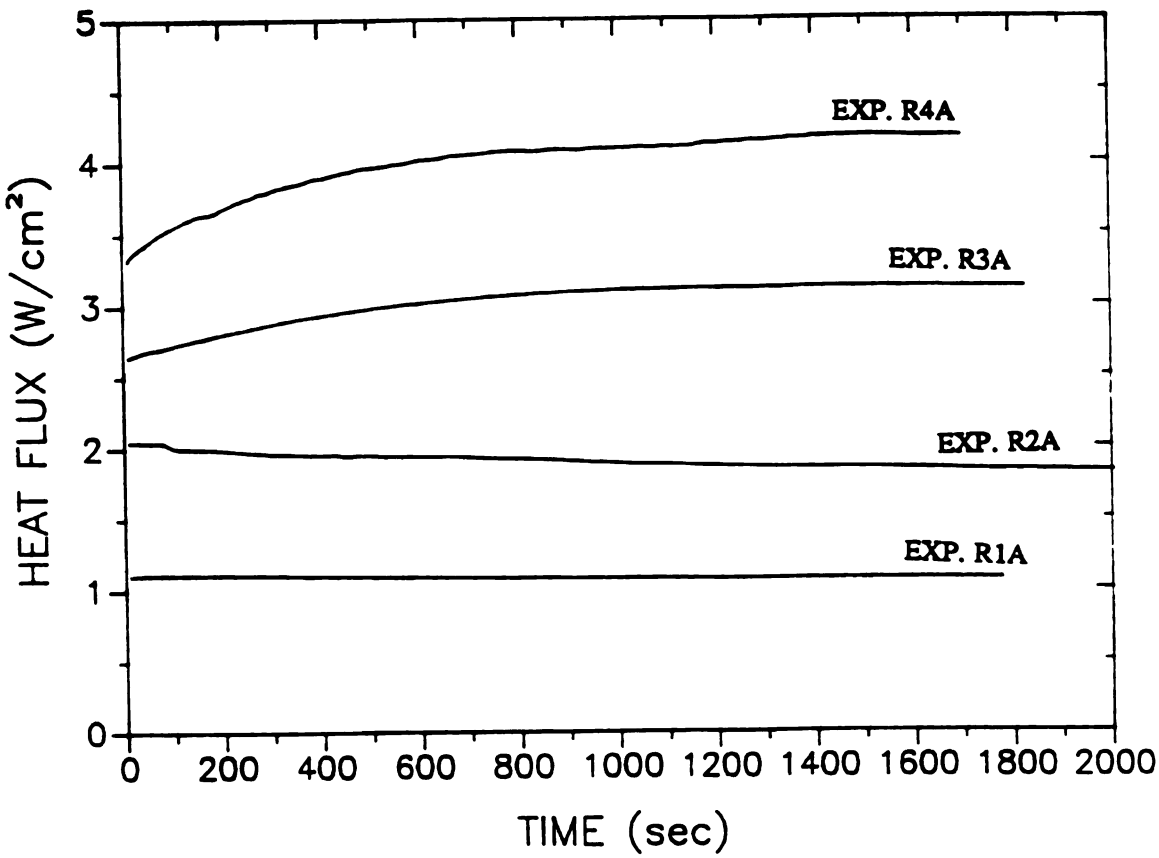

Fig. 3.15 External heat flux for experiments on 8-9% moist wood in air.

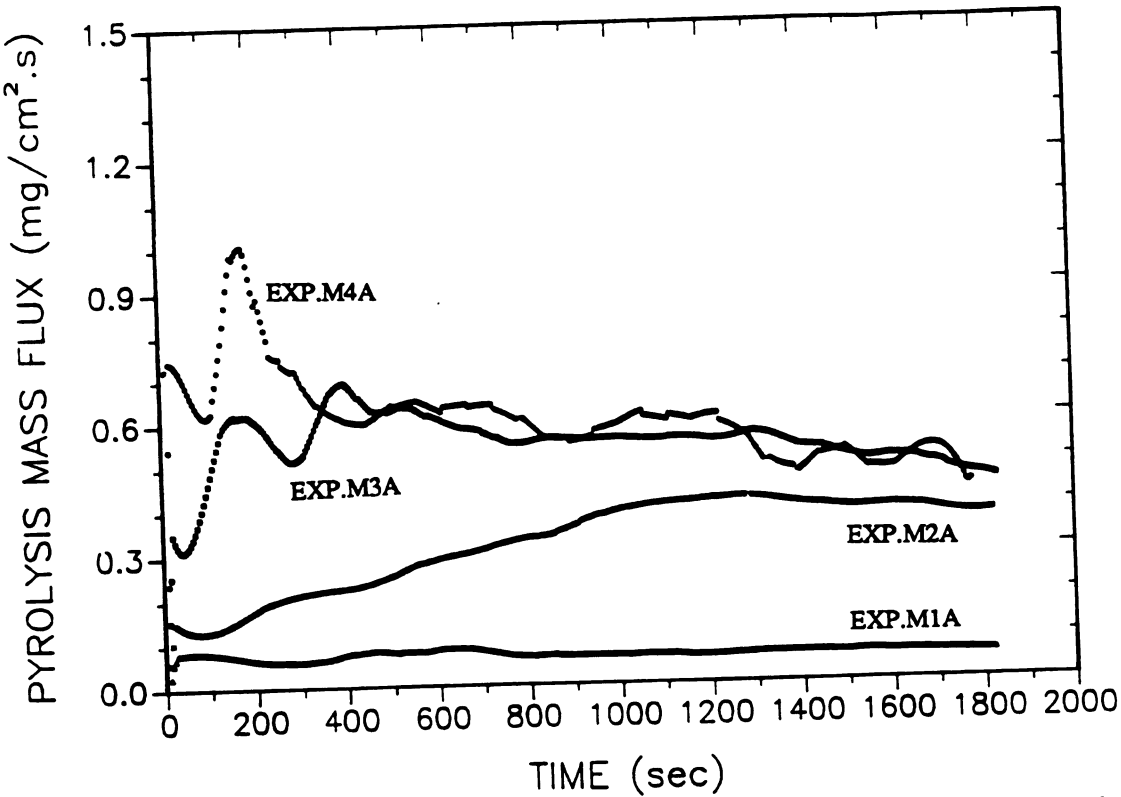

Fig. 3.16 Pyrolysis mass flux for experiments on 17% moist wood in air.

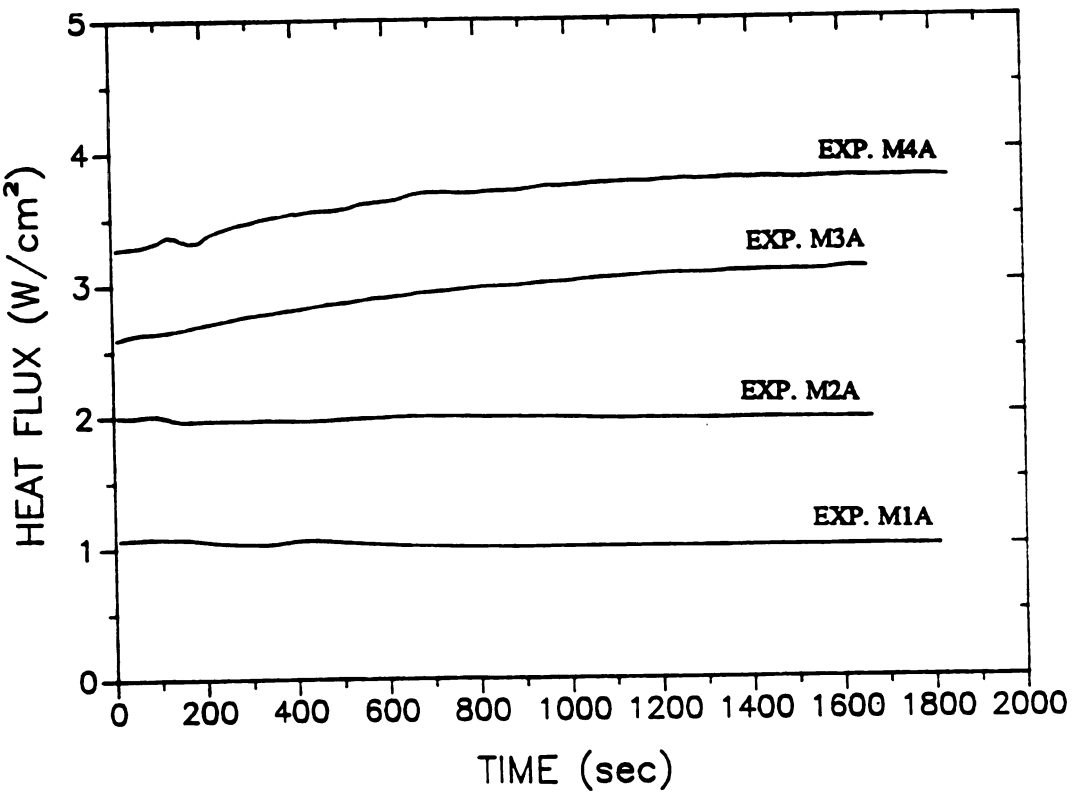

Fig. 3.17 External heat flux for experiments on 17% moist wood in air.

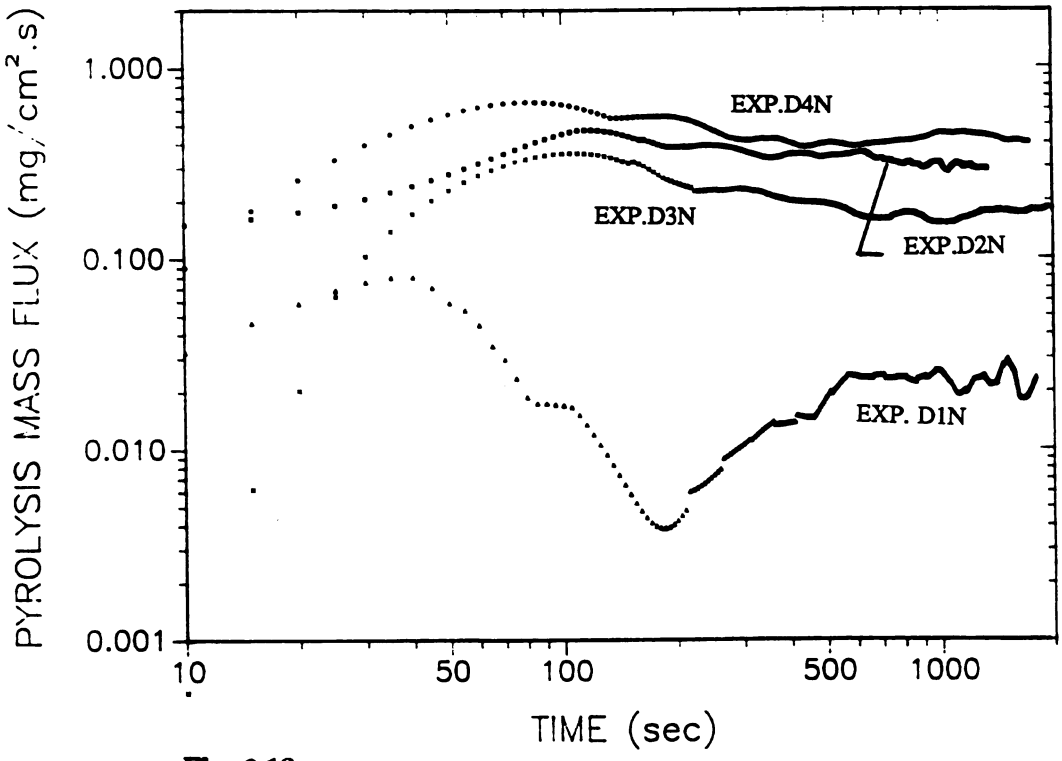

Fig. 3.18 Pyrolysis mass flux for experiments on dry wood in N_2.

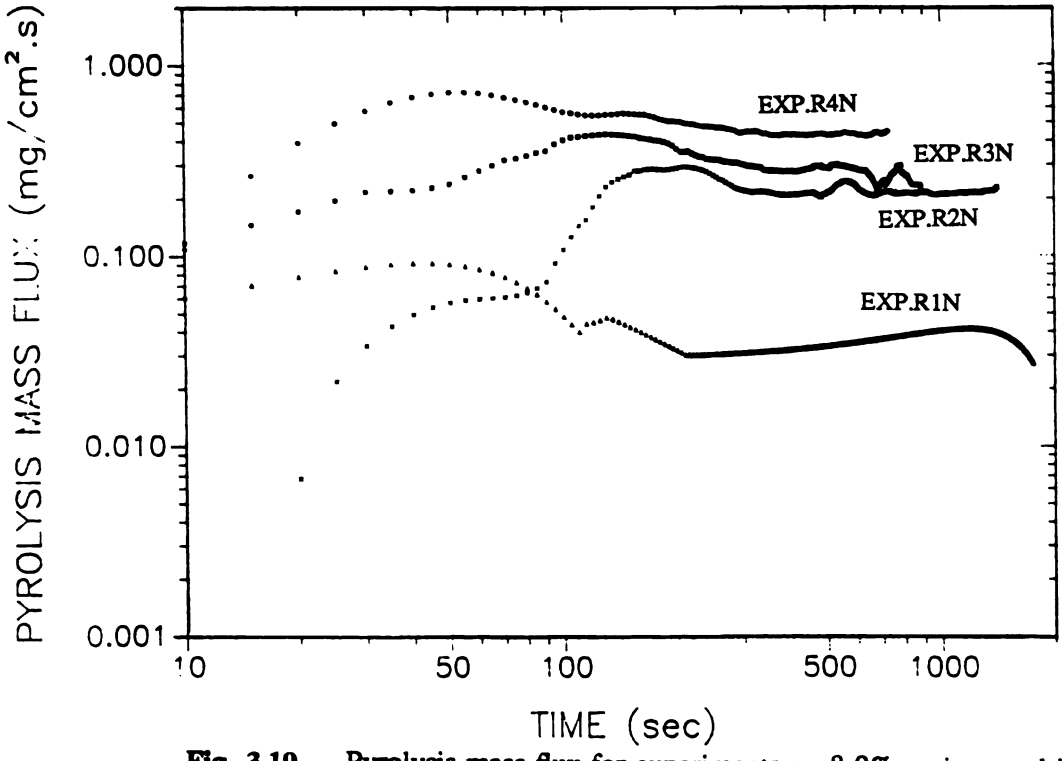

Fig. 3.19 Pyrolysis mass flux for experiments on 8-9% moist wood in N_2.

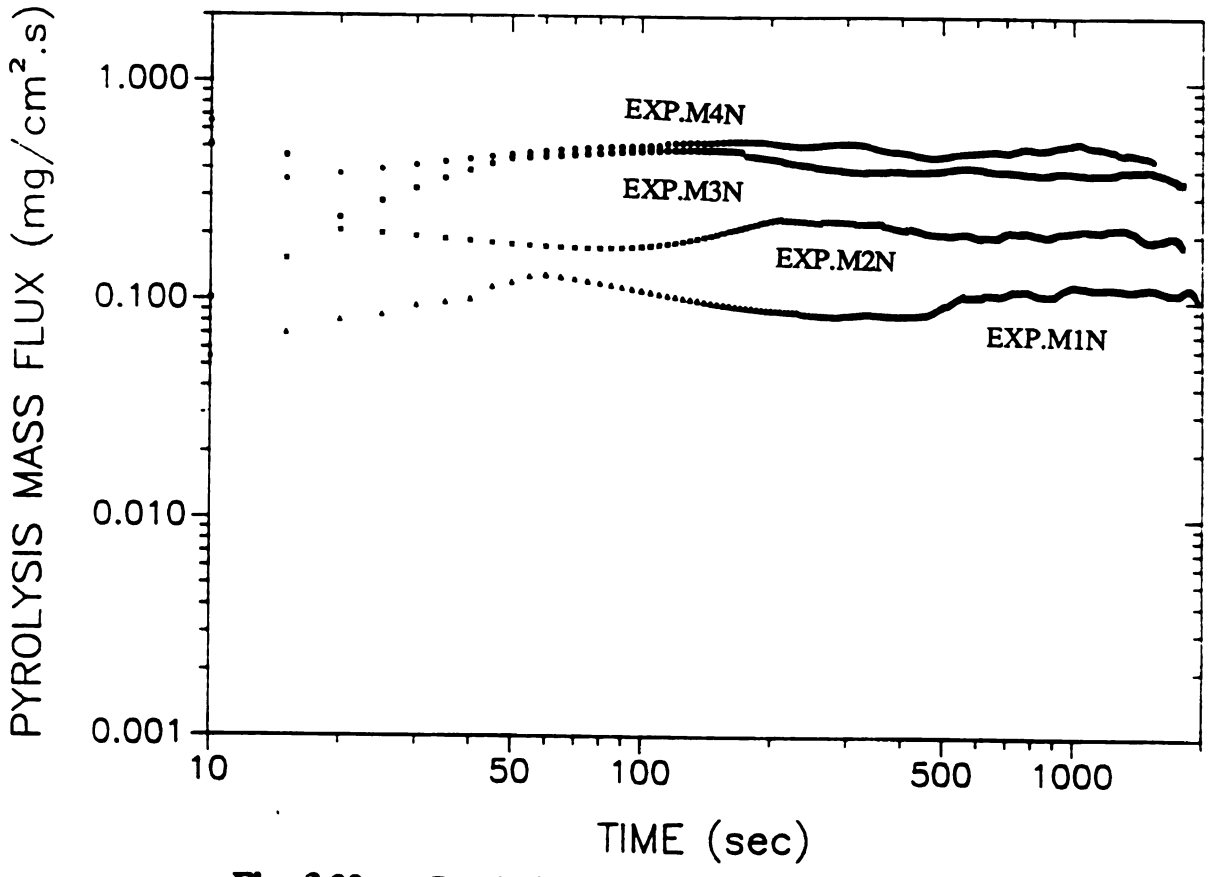

Fig. 3.20 Pyrolysis mass flux for experiments on 17% moist wood in N_2.

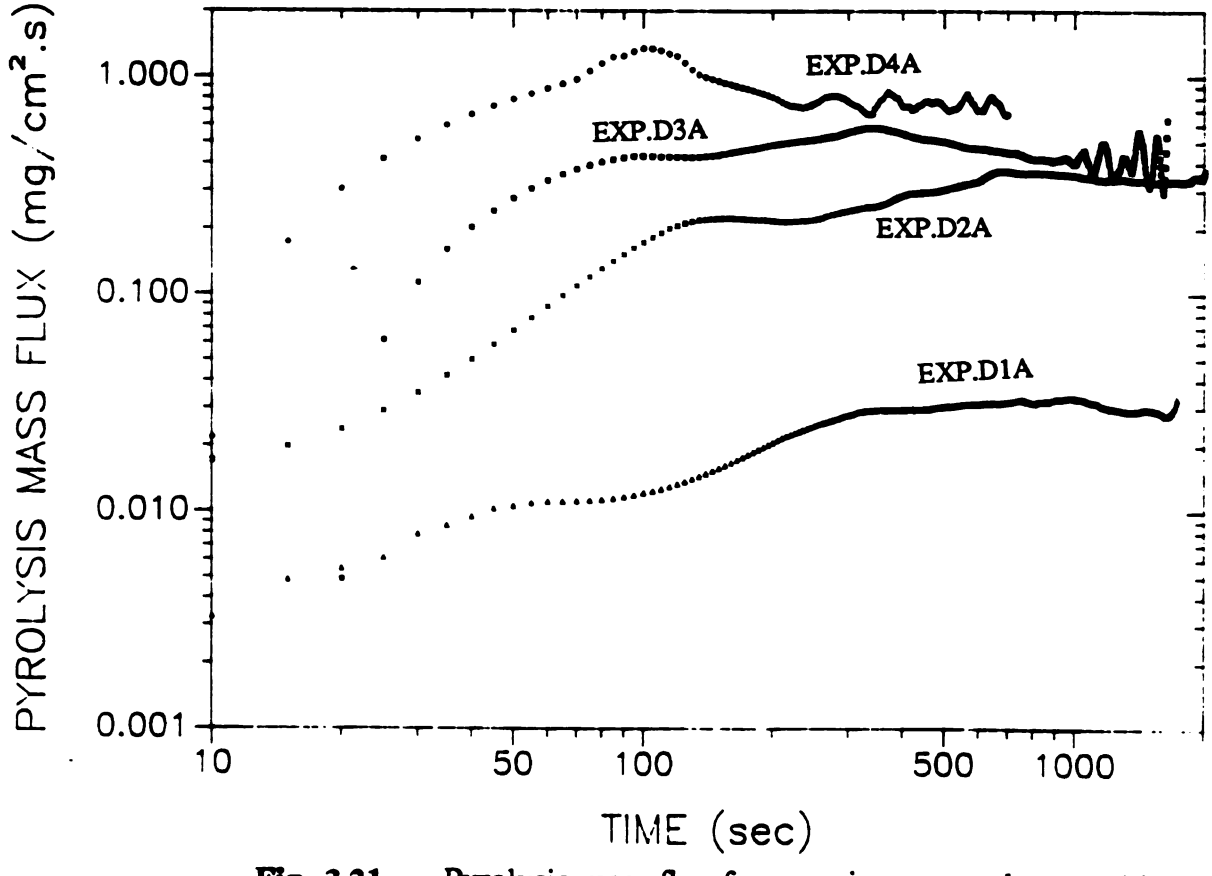

Fig. 3.21 Pyrolysis mass flux for experiments on dry wood in air.

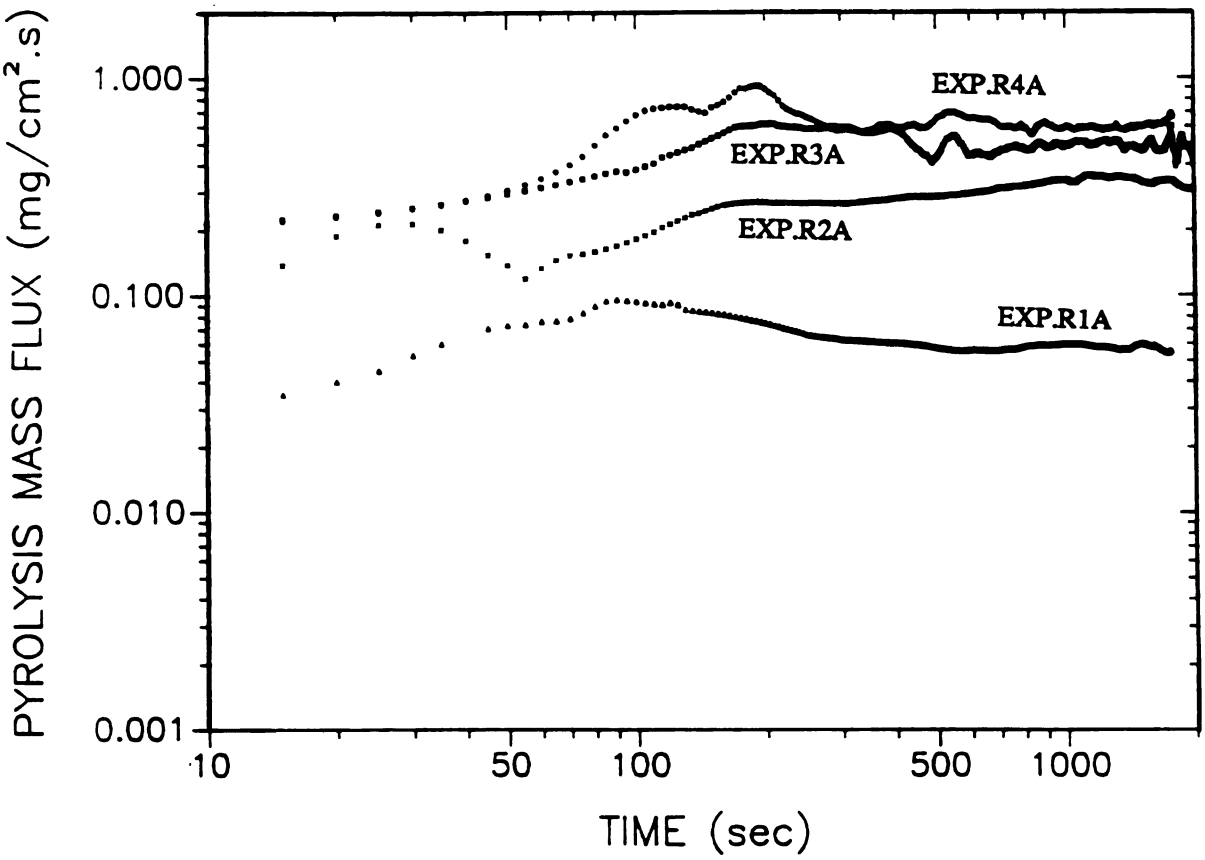

Fig. 3.22 Pyrolysis mass flux for experiments on 8-9% moist wood in air.

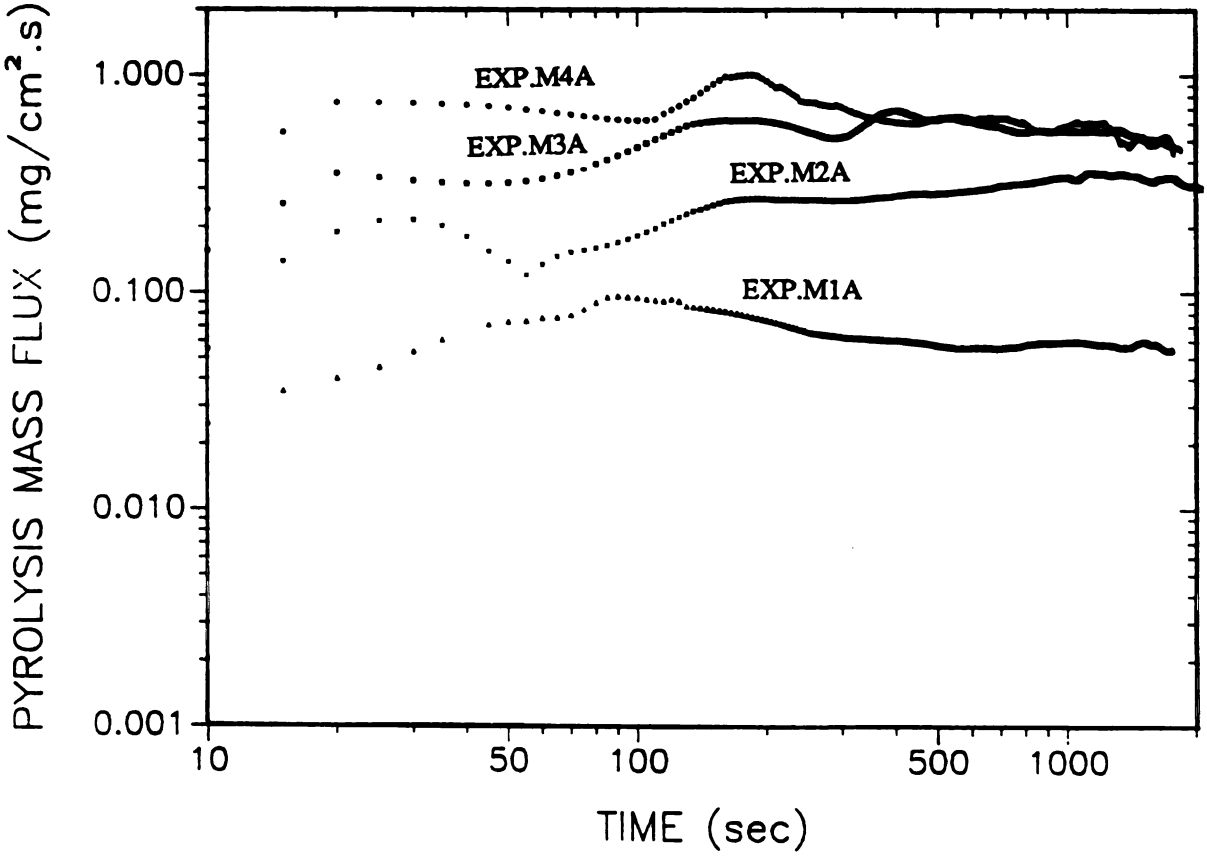

Fig. 3.23 Pyrolysis mass flux for experiments on 17% moist wood in air.

3.7 Products of Pyrolysis

Data from transient measurements of the products of pyrolysis of wood are plotted in Figures S1xxx (Appendix C). These data are also plotted as a percentage of total mass flux in Figures PSxxx (Appendix C). In theses Figures, xxx stands for every experiment and is consistent with the nomenclature described previously. As mentioned earlier, the mass flux of total organic condensibles (tar) was not measured directly. It was calculated by subtracting the sum of the mass fluxes of [THC], CO_2, CO, and H_2O, from the pyrolysis mass flux. This is exactly true for the experiments in nitrogen atmosphere. In air, however, due to the char oxidation the total mass flux of the produced gases is more than the pyrolysis mass flux and the mass recovery is more than 100%. At higher heat fluxes part of CO and CO_2 are the products of char oxidation rather than thermal decomposition of wood. Thus, generally for the experiments in air, mass flux of tar is not shown except at low heat fluxes where the surface oxidation is not expected to be significant, tar is plotted for comparison with experiments in inert atmosphere. It is important to note that for data obtained in nitrogen atmosphere, the only errors in the products mass fluxes and their trend are the experimental (measurement) errors. The sample weight loss is directly measured and the mass of tar is whatever that has not been measured by the gas analysis equipment. Thus, these curves represent *quantitative transient* data for the pyrolysis of wood in inert atmosphere. In a recent study [Kashiwagi et al. (1987)], water and therefore tar data, were only qualitative. In most cases, the magnitudes and sometimes even the trends were not closely confirmed by this study.

In these measurements, all the sample lines were electrically heated at least up to 100°C. Nevertheless, it was not possible to completely prevent the condensation of tar even inside the tunnel where it was exposed to the external heat flux and the temperature was even higher. However, since the total mass flux of the pyrolysis products was never more than 5% of the main flow in the tunnel (nitrogen or air), the

changes in the concentrations of the permanent gases due to any tar condensation before they reached the analyzers were negligible. Thus, the recorded mole fractions of CO_2, CO, H_2O, and [THC] very closely represent the actual mole fractions in the mixture of the tunnel flow.

In some experiments specially those at high heat fluxes, the water meter reading on the direct measurement side was slightly shifted upwards. Thus, at the beginning of every experiment, the line filter was replaced and the meter was set back to zero. At the end of the test, the reading of the meter for a "zero gas" was recorded and the entire curve was linearly corrected for this shift.

For "dry" wood a large portion of the volatile pyrolysis products consisted of organic condensibles (tar) [Figures S1DxN]. Although the wood is termed as "dry" the initial mass evolved (for the first few seconds) is water followed by a rapid and large outflow of fuel gases. Thus, most of this water is water of constitution which is a product of direct pyrolysis of wood and is possibly produced as fuel volatiles pass through the hot char matrix and are cracked down to lower molecular weight hydrocarbons, CO_2, CO and H_2O. The peak of these curves obviously corresponds closely to the peak of pyrolysis mass flux curves and occur at temperature about 375°C. In all cases the tar mass flux falls off rapidly and is responsible for the rapid fall-off of the pyrolysis mass flux after the peak.

In nitrogen atmosphere [Figures S1xxN (Appendix C)] the interesting feature is the downward turn in the tar evolution which is steeper than the corresponding mass flux at larger times. For example, from experiment D3N one gets about 0.175 mg/cm^2.sec tar at 400 sec while the pyrolysis mass flux at this time is about 0.35 mg/cm^2.sec (Figure 3.6). This difference is much larger as the moisture content of wood is higher. For instance, the corresponding proportions in experiments R3N and M3N are 0.075 to 0.3 and 0.1 to 0.4 respectively. This type of behavior was also observed by Kashiwagi et al. [1987]. This is consistent with the phenomenon

explained in Chapter 1, that the chemical composition of the pyrolytic products is altered as they pass through the growing hot char layer by cracking into small hydrocarbons or by polymerization to char. Thus, as heating continues, more permanent gases (CO_2, CO, and noncondensible hydrocarbons) and water are produced while production of tars generally decreases. An exception was the experiment D4N (dry wood at 4 W/cm^2 in nitrogen) as is shown in Figure 3.6. In this experiment the pyrolysis mass flux and the corresponding tar [Figure S1D4N (Appendix C)] increases again after the rapid fall-off and a second peak appears at about 1000 sec. An opposite trend has occurred in the H_2O curve (same Figure). This experiment was conducted twice and both times the second rise in mass flux was observed. It is likely to be due to the appearance of huge cracks on the char surface at high heat flux that allows more pyrolytic tar to escape without contact with the hot char. Less condensible molecules were cracked down and also more radiation penetrated further inside the solid. Thus, more tar and less water were produced. Later as thickness of char increases, the rate of tar production reduces again. The same trend, although to a lesser extent, is observed in Figure S2D4N, which shows the products after the combustion tube. Here, a second peak similar to that of the mass flux curve is observed in both CO_2 and H_2O curves. This indicates that indeed more fuel has been generated resulting in more CO_2 and water on this route. Of course, not all of the produced hydrocarbons entered the catalytic combustor due to the condensation of tar. Thus, the second up and down trend in these curves are less steep than in Figure S1D4N. This type of trend was not observed in the work of Kashiwagi et al. (1987). In their experiments the heating period was 12-15 minutes and they used different type of wood and the heat flux was parallel to the grain direction (in this work it was always perpendicular.) Of course, different woods have different densities and rosin contents, and other properties may differ as well. This observation signifies the importance of the effect of the cracking of char specially at high heat fluxes. Therefore, cracking of char not only alters the

heat transfer between the outgoing volatiles and the hot char, but it also could change the mass flux as well as the chemical composition of the pyrolysis products. For a detailed theoretical model of wood pyrolysis, therefore, it will be important to include the effect of char cracking.

3.7.1 Permanent Gases

As the heat flux increases the evolved mass flux of permanent gases ([THC], CO_2, CO) generally increases [Figures S2xxN and S2xxA (Appendix C)]. When the sample is heated in air the evolution rate of all permanent gases is larger than those in nitrogen atmosphere. The most significant increase is in production of CO_2. Since the wood samples in experiments at 4 W/cm^2 in air all ignited, they can not be compared with the similar experiments in nitrogen atmosphere. Figure S1R3N and S1R3A (Appendix C) show such experiments at 3 W/cm^2 in N_2 and in air on wood with 8-9% moisture content. At about 900 seconds mass flux of CO_2 in nitrogen and air are 0.035 and 0.15 mg /cm^2.sec respectively. These correspond to 10% and 35% of their pyrolysis mass fluxes, respectively [Figures PSR3N and PSR3A Appendix C)]. Those at 2 W/cm^2 heat flux [Figures S1R2N and S1R2A (Appendix C)] are 0.045 and 0.01 mg/cm^2.sec, respectively. These correspond to 2.5% and 14% of their pyrolysis mass flux respectively [Figures PSR2N and PSR2A (Appendix C)]. Production rate of [THC] increases only slightly in air and part of it is possibly consumed in endothermic gas phase reactions occurrng at the vicinity of the char surface. Mass flux of the evolved [THC] in experiments R2N and R2A at 900 seconds is 0.02 and 0.035 mg/cm^2 (corresponding to 6% and 10% of the pyrolysis mass flux), respectively [Figures S1R2N, S1R2A, PSR2N and PSR2A]. Since the differences in percentage values are within the ranges of experimental error, distinct conclusions may not be derived from these values. CO also shows increase in oxygen containing atmosphere. It is about 5% and 15% in R2N and R2A experiments, and 9% and 18% in R3N and

R3A experiments respectively. In most of these experiments the production rates of permanent gases (Figures S1xxA) remained almost constant after initial rise. Thus, since the pyrolysis mass flux (total) was gradually decreasing, the mass fraction rates (percentages) of production of these components show a gradual increase (Figures PSxxA). The continuous increase in the production rate of CO_2 with time that was reported for wood with 5% moisture content by Kashiwagi et al. (1987), was not observed in these results. As it was discussed in section 3.6.1.2, in their experiments the boundary layer started from the edge of the wood sample, whereas, in these experiments the sample was located in the middle of the boundary layer and far away from its leading edge. As a result, for similar heat fluxes, the wood surface was exposed to different amount of oxygen in each case, resulting in different amounts of products. This shows that when the boundary layer starts from the sample edge, the process in not convectively (heat and mass transfer) well defined, and the magnitude and history of the pyrolysis mass flux will be affected.

3.7.2 Water Mass Flux and Effects of Moisture Content of Wood

In this section the moisture desorption rate and the effects of moisture content on energetics of pyrolysis and combustion of the solid is discussed. Although, adsorbed moisture plays an important role in pyrolysis and in ignition of wood, it has often been ignored in the theoretical models. Atreya (1983) showed that unless the wood is completely "dry" the terms related to moisture in the model equations for the pyrolysis process must be retained. Considerable improvement in the theoretical prediction of pyrolysis mass flux were obtained by including moisture desorption in his model.

In this work, samples with three different moisture contents, ("dry" ≈ 0%, room ≈8-9%, and moist ≈17%) were examined. All the water measured in nitrogen atmosphere experiments (direct measurements) represents the water produced during pyrolysis. This consists of adsorbed moisture and water of constitution. For

experiments in oxygen containing atmosphere, a part of the evolved water vapor, specially at higher heat fluxes, is generated by char oxidation and exothermic gas phase reactions between fuel volatiles and oxygen above the char surface. For example, in experiment R3N (8-9% moist wood in N_2) the water mass flux at t=400 sec is 0.14 mg/cm^2.sec (Figure S1R3N), while that of experiment R3A (in air) is 0.2 mg/cm^2.sec (Figure S1R3A), an increase of about 40%. Part of this extra water is produced in the gas phase reactions. Other part is generated from drying and pyrolysis of the solid due to the heat of char oxidation conducted into the solid. The corresponding values for experiments R2N and R2A at t=1000 sec [Figures S1R2N and S1R2A Appendix C] are 0.035 and 0.075 mg/cm^2.sec, respectively.

As mentioned earlier, almost all of the water appearing in experiments DxN (dry wood in nitrogen) is the water of constitution which is a product of thermal degradation of wood. At higher moisture contents, as wood is heated, first the desorbed water is evaporated and then pyrolysis starts. The mass flux curve of evolved moisture is very similar to the pyrolysis mass flux curve indicating that the desorption of water is also affected by the formation and growth of the char. The adsorbed moisture is a few molecules thick layer of water molecules that are attached to the cell walls within the micro-pores of wood via hydrogen bonds.

Moisture content of wood primarily changes physics of pyrolysis and ignition and its effect on the chemistry of pyrolysis is not significant. Some of the effects of moisture on the energetics of the thermal decomposition and ignition of wood are discussed in the following paragraphs. Water (depending on the magnitude that is adsorbed or absorbed) delays the process of pyrolysis and dilutes the products of pyrolysis of wood. For example, we can compare products of pyrolysis for experiments conducted on samples with three different moisture contents at 2 W/cm^2 [Figures S1D2N, S1R2N, and S1M2N]. These data indicate that while the trend of production of each species at different moisture contents are alike, suggesting that they follow the

same type of reaction kinetics, the mass flux and time of occurrence of their peak is different. In these experiments the magnitude and time of maximum mass flux of tar for dry, 8-9% moist, and 17% moist wood are 0.28 mg/cm^2.sec (at t=100 sec), 0.135 mg/cm^2.sec (at t=180 sec), and 0.08 mg/cm^2.sec (at 210 sec), respectively. That is, the evolution of tar is reduced and delayed as moisture content of wood increases. An opposite trend in the production of water can be observed in these Figures. Similar trend can be observed in other experiments as well as for experiments conducted in air. As a result, the flammibility of wood is decreased as more water is adsorbed (or absorbed) in it. As mentioned previously, in experiments conducted in air at 4 W/cm^2, the samples ignited and the ignition was delayed as moisture content of wood increased.

Comparison of pyrolysis mass flux curves [Figure 3.6-3.11] also shows that at each external heat flux, the magnitude of the mass flux reduces as the moisture content of wood increases, while the time of occurrence of the pyrolysis peak (i.e. tar evolution) increases. Only at very low heat flux, where thermal decomposition of wood is very small, mass flux increases with moisture content of wood. For example, for experiments at 1 W/cm^2, the weight loss rate increased as wood contained more moisture indicating that most of the weight loss was due to the moisture evaporation [Figures SxD1N, SxR1N, SxM1N (Appendix C)]. In fact, while for dry wood in nitrogen atmosphere [experiment D1N, Figures SxD1N], some degree of pyrolysis has occurred and some tar and small amounts of other pyrolysis products have been generated, for 8-9% moist wood [Experiment R1N] mostly water and small amounts of fuel gases were produced. For 17% moist wood [Experiment M1N], almost all of the weight loss of the sample was due to the water desorption and very little tar and consequently small amount of char were produced (Figure S1M1N). The same effects is observed in experiments in air [Figure S1M1A].

The effect of moisture is basically cooling the solid by absorbing energy from it for its desorption and during its outward migration. A comparison of the surface temperature of the pyrolyzing solid can demonstrate this effect. Figures TD4N, TR4N and TTM4N (Appendix C) represent the surface and in-depth temperature history of samples heated in N_2 at 4 W/cm^2. At t=200 sec the surface temperature of dry, 8-9%, and 17% moist wood are 620, 580, and 460°C, respectively. For similar experiments conducted at 2 W/cm^2 in N_2 [Figures TD2N, TR2N, and TTM2N (Appendix C)], the surface temperatures at t=200 sec are 420, 390, and 360°C, respectively. The presence of moisture changes thermal capacity of the solid and therefore changes the heat transfer and hence the temperature rise history of the solid. The thermal conductivity, specific heat, and density of dry wood are normally less than those of moist wood. Hence the surface temperature, which is proportional to $(\rho Ck)^{-0.5}$ [Carslaw and Jaeger (1959)], will be higher for dry wood than for moist wood. This will cause delay in the pyrolysis process (and ignition) of moist wood. Finally, heat is transferred directly by inward and outward migration of water. Forward migration and condensation of the moisture ahead of the arrival of the pyrolysis zone, changes wood properties even before decomposition starts.

3.8 Time Integrated (Total) Mass of Pyrolysis Products

Since the pyrolysis mass flux was calculated numerically and tar mass flux was obtained by difference, the data on tar involves both errors in the measurement of permanent gas concentrations and errors in pyrolysis mass flux as well. An alternative way of studying the effects of each parameter on the mass evolution rate of pyrolysis products is the comparison of the total amounts of each product after a specified duration of heating time. The total amounts of each product was obtained by integrating their mass evolution rate. Here, since some experiments were continued for only 15 minutes, although majority of experiments were carried out up to 30 minutes,

all evolved rates were integrated for only 15 minutes. This also allows us to compare these results with the data on other types of woods [e.g. with Ohlemiller et al. (1987)]. Figures 3.24-3.29 show the results for nitrogen and air. The heat fluxes shown on these curves represent the average values obtained from Figures 3.7-3.17.

The results indicate that for experiments in nitrogen atmosphere the amount of all major products of pyrolysis increases with the heat flux, while their corresponding percentages relative to the total mass flux do not show a similar trend. For dry wood [Figure 3.24], the percentage of tar shows a slight decrease with increase in heat flux while more water in generated except for experiment at 4 W/cm^2. For experiments at 1, 2 and 3 W/cm^2, this is due to cracking of heavy molecule hydrocarbons as they pass through the hot char. For experiment D4N, as it was described earlier, formation of huge cracks is likely to be responsible for escape of more tar without contacting the hot char. As a result, less total amount water is also observed. Increase in the total percentage of CO is not significant, but more CO_2 is generated at higher heat fluxes. For moist wood, water accounts for most of the products at low heat fluxes and it decreases at higher fluxes. For moist wood, production of tar generally increases with heat flux, except at the highest heat flux [Figures 3.25 and 3.26]. It is because for moist wood specially at lower heat fluxes, the desorption of moisture is the dominant process and as heating continues more fuel volatiles are generated. At 4 W/cm^2, however, due to the rapid rise in the surface temperature, the drying process occurs very rapidly and thermal decomposition of wood continues more similar to that of dry wood. Again, the total amount of CO_2 increases at higher fluxes and increase in the production of CO is not significant, except for 17% moist wood in which more CO is produced at 4 W/cm^2. This is because water dilutes the mixture of products and reduces the solid temperature altering the trend of cracking of tar while passing through the char matrix.

For samples heated in air since all samples at 4 W/cm^2 ignited, obviously almost all of the products are CO_2 and H_2O. Therefore, basically only experiments at heat fluxes lower than 4 W/cm^2 are compared. In all of these experiments because of the char oxidation the mass recovery is more than 100 percent. Moreover, the gas phase reactions with oxygen produce some products that are not products of pyrolysis. Production of CO and CO_2 show considerable increase compared with nitrogen atmosphere. Also, generally increase in the production of CO_2 in air is more significant than changes in CO yield indicating that CO is mostly a product of pyrolysis not incomplete oxidation.

The final char depths in the pyrolysis experiments are shown in Table 3.2. These were found by cutting the sample in half in the middle and measuring the char depth from the original surface of the wood sample to the sharp black char-wood interface. Often, specially at higher temperatures, gases evolved from the sample even after removing the external radiation. Thus the values represent the approximate char depths at the final instant. The numbers are correct within ±0.5 mm. In some cases, due to the structure of that particular piece of wood, huge longitudinal cracks appeared which significantly altered the normal heating rate and the final char depths were much higher. The general trend is higher char depth at higher heat fluxes. Also more char is produced in air than in nitrogen at similar external radiations.

Table 3.2 Final Char Depth For Pyrolysis Experiments at Different Conditions. (in mm)

(For 30 minutes heating time unless specified in parenthesis)

Atmosphere		Nitrogen			Air		
Moisture Content		Dry	8-9%	17%	Dry	8-9%	17%*
External	2	10.0 (32)	5.0 (20)	4.0	15.0	15.0	16.0
Radiation	3	5.0 (20)	7.0 (5)	6.4	19.5	18.0	19.5
W/cm^2	4	18.0	7.0 (12)	10.5	24.0	19.5	21.5

* Large longitudinal cracks appeared.

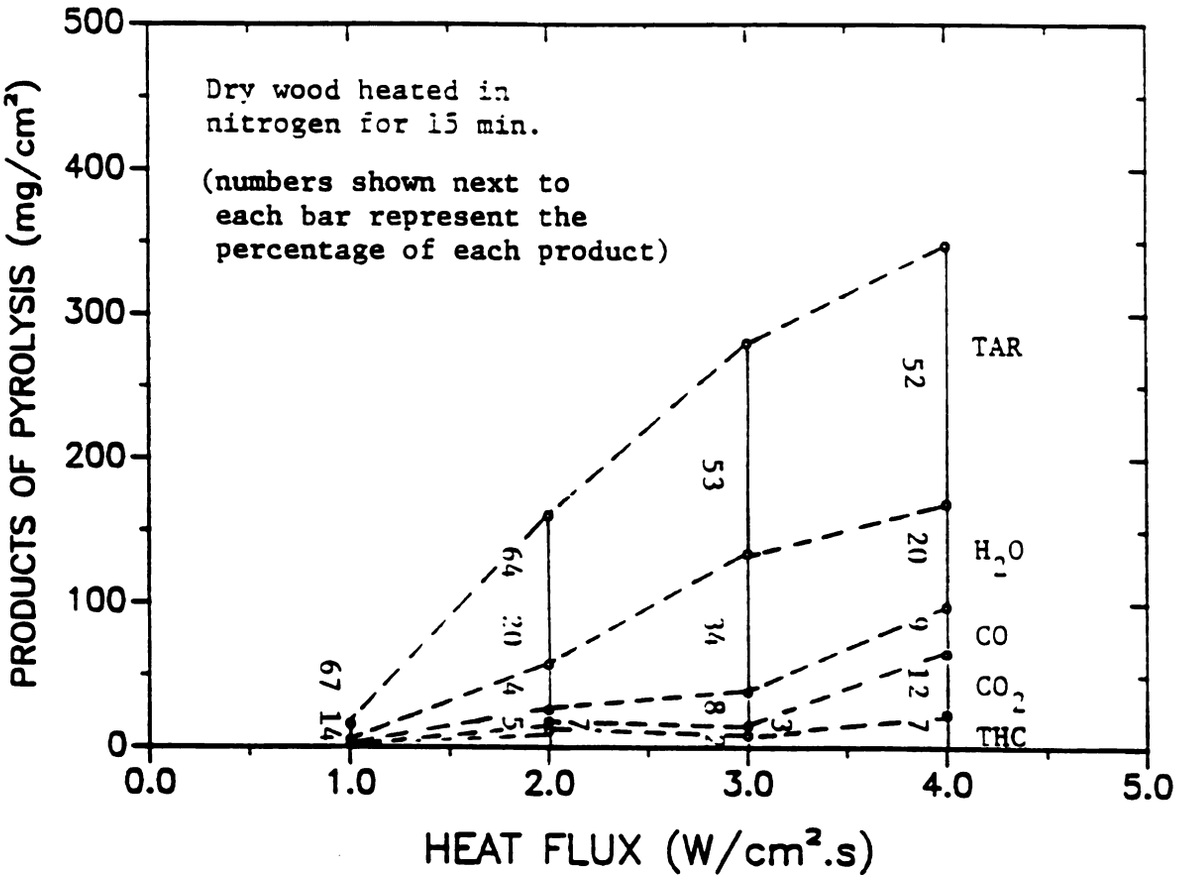

Fig. 3.24 Time integrated mass of pyrolysis products as a function of incident heat flux.

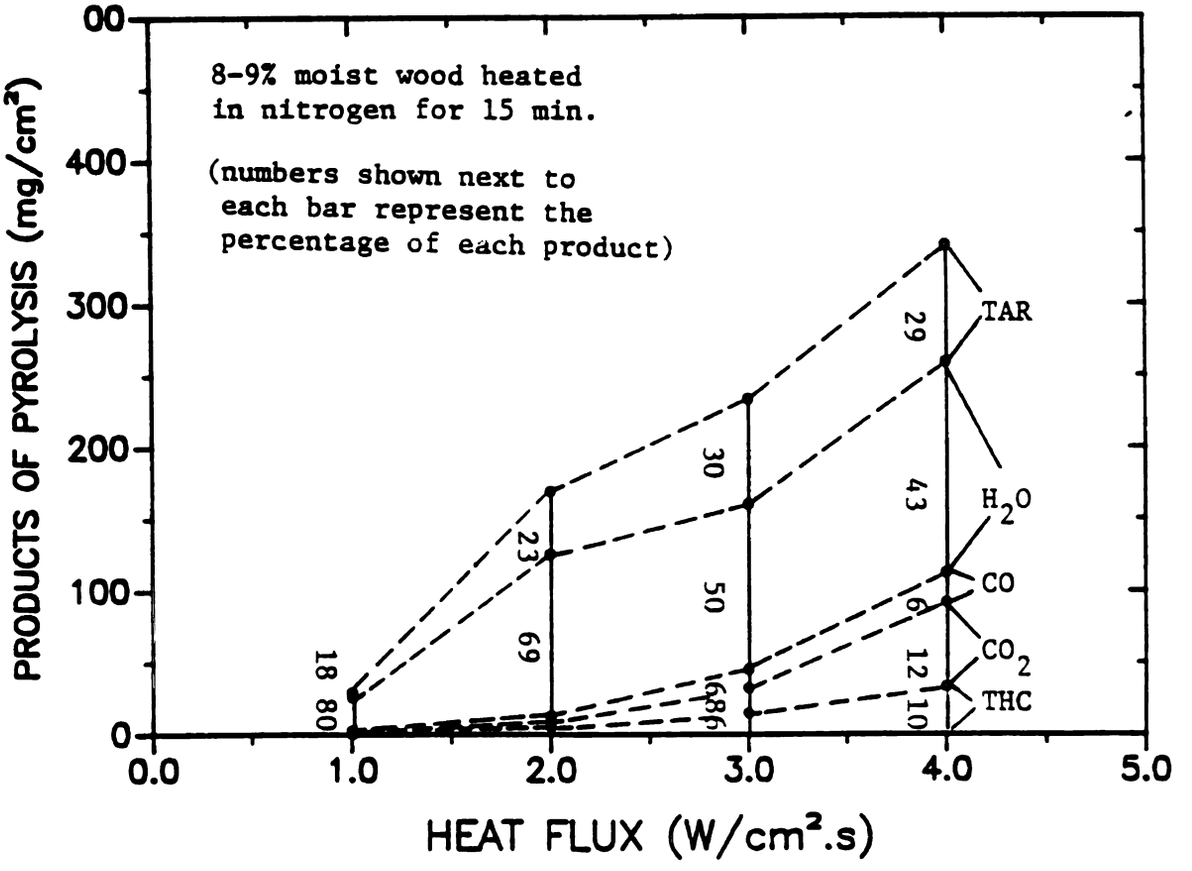

Fig. 3.25 Time integrated mass of pyrolysis products as a function of incident heat flux.

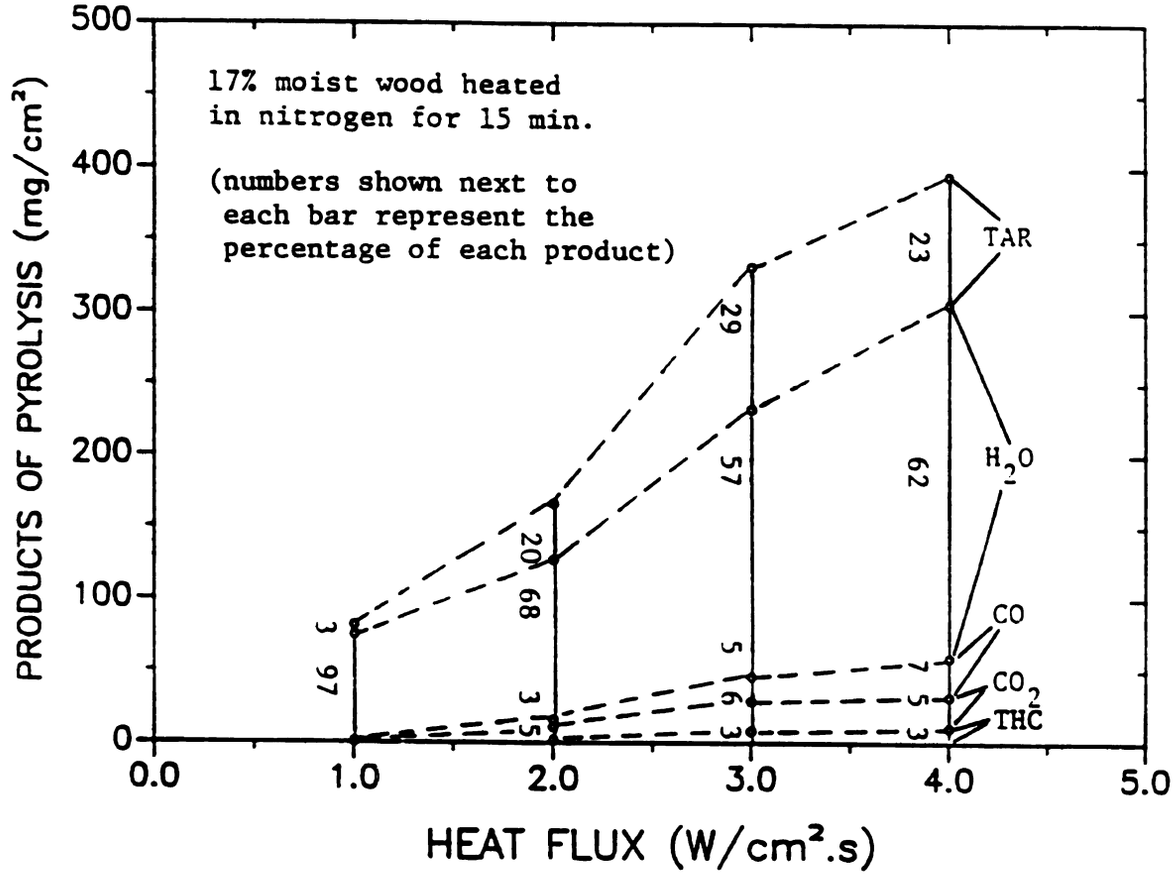

Fig. 3.26 Time integrated mass of pyrolysis products as a function of incident heat flux.

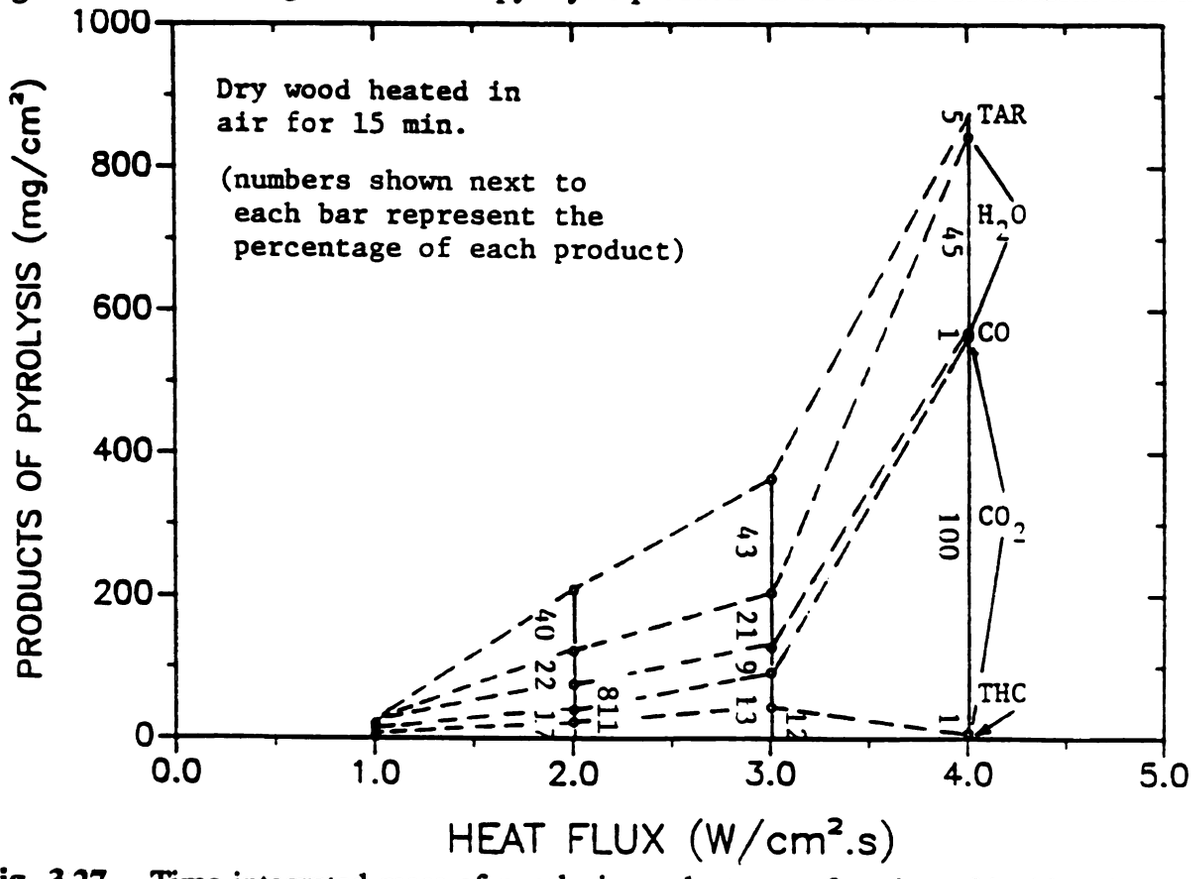

Fig. 3.27 Time integrated mass of pyrolysis products as a function of incident heat flux.

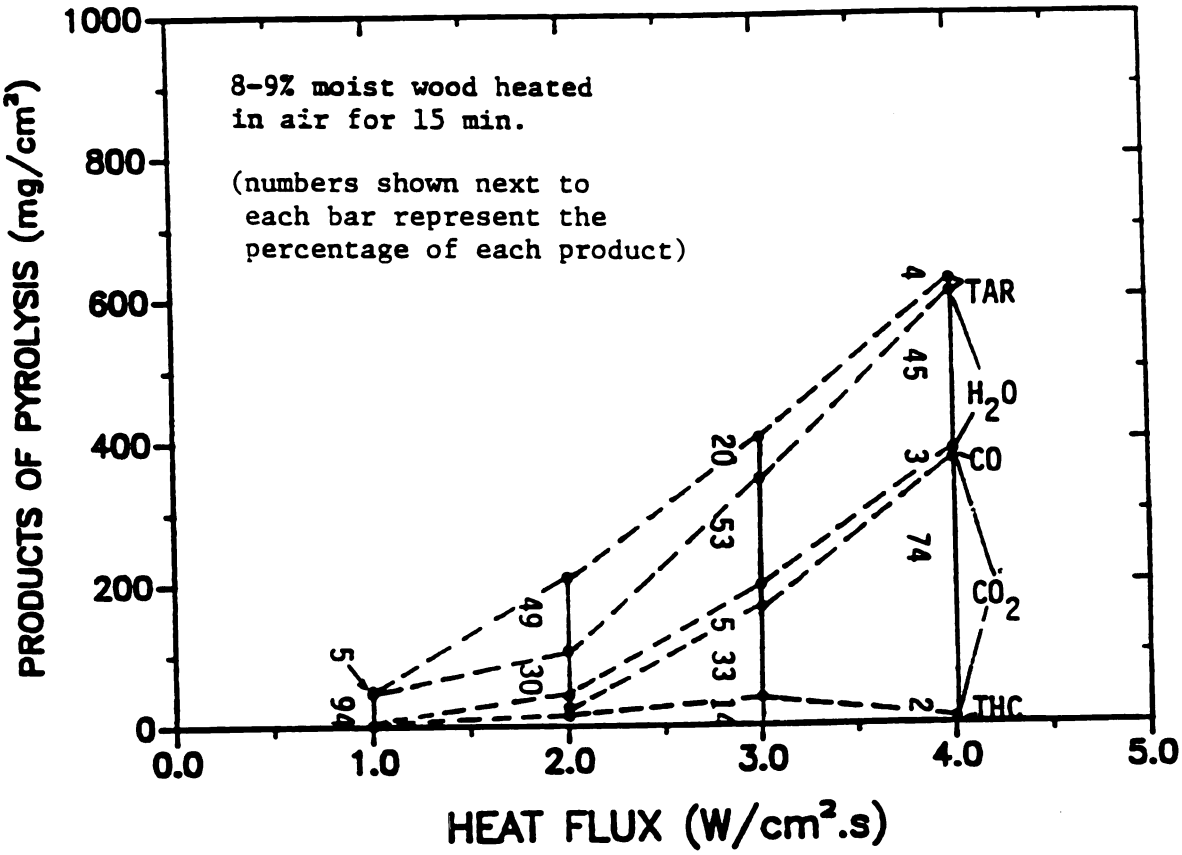

Fig. 3.28 Time integrated mass of pyrolysis products as a function of incident heat flux.

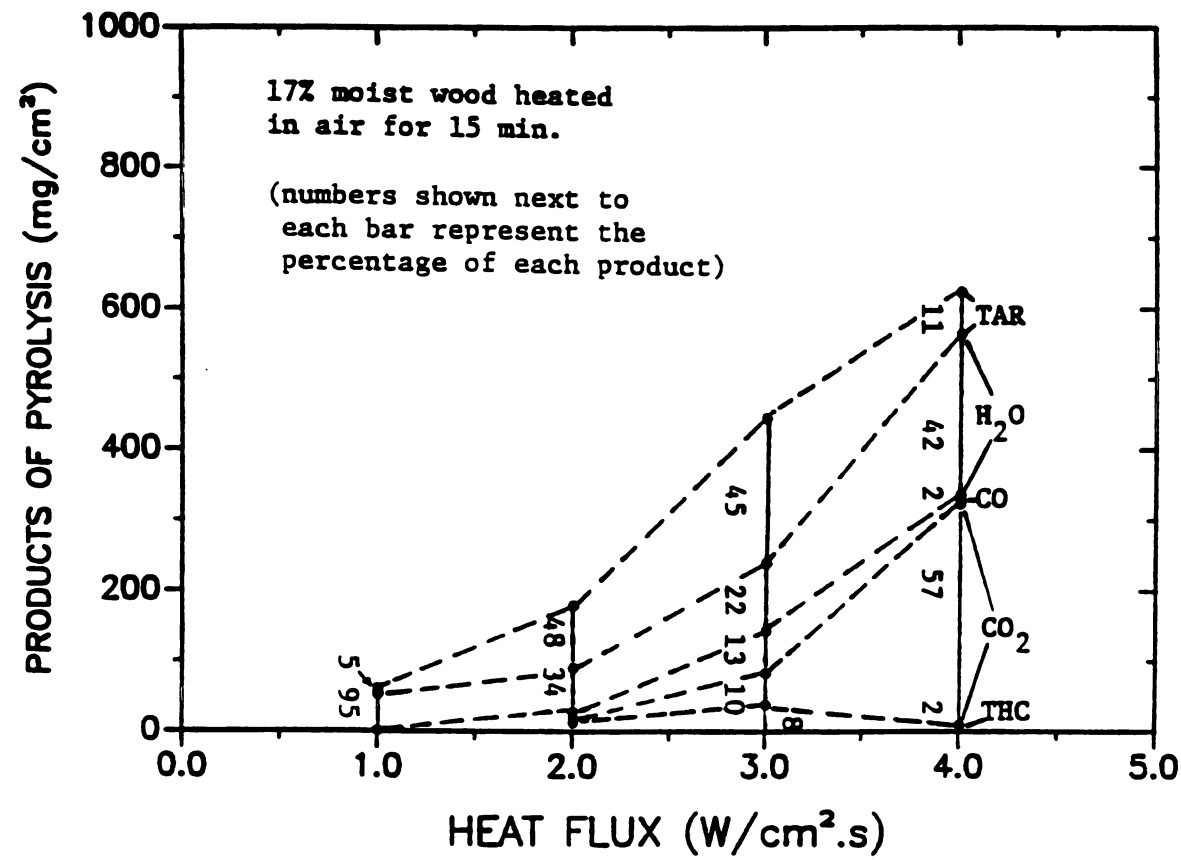

Fig. 3.29 Time integrated mass of pyrolysis products as a function of incident heat flux.

3.9 Char Yield and Empirical Chemical Composition of Pyrolysis Products

Char yield (Y_c) was calculated using equation (3-12) and the results are shown in Figures YCxxx (Appendix C). The values of x and y in C_xH_yO were determined from relations (3-8) and (3-9) and are plotted in Figures CHxxx (Appendix C). Figures S2xxx show the mass fluxes of the products of combustion of pyrolysis volatiles in the catalytic combustion tube. These products are mainly CO_2 and H_2O, and the amount of CO is usually negligible indicating nearly complete combustion. Only at the start of the combustion for a short period of time higher amounts of CO are detected. This was because the mixture of fuel gases and oxygen was not yet fully ignited. The most significant source of error in these data is the condensation of the heavy hydrocarbons (tar) before the sample gas enters the combustion tube. As described in Chapter 2, considerable care was taken to minimize the condensation by heating all the components of the tunnel and the connecting lines. Nevertheless, some tar always condensed on the interior surfaces of the tunnel and the sample lines and never reached the combustion tube. To determine the extent of this partial loss of tar, the total mass balance was calculated from the measurements of CO_2, CO, and H_2O after the combustion tube. For this calculation the amount of oxygen consumed in the combustion process was determined from the difference between the mass fluxes of oxygen before and after the combustor. Figures TMxxx (Appendix C), represent comparison between the measured pyrolysis mass flux and the computed total mass flux of the gases $[(\dot{m}_{CO_2} + \dot{m}_{CO} + \dot{m}_{H_2O}) - \dot{m}_{\Delta O_2}]$ after combustion. Figures ERxxx (Appendix C) show the percentage of the difference between the two curves. As expected, the highest degree of error in the total mass balance occurs at the early times of the pyrolysis process where most of the tar is generated (see Figures S1xxx, Appendix C). As the char layer thickens, less condensibles are liberated and the total

mass balance considerably improves. This "lost" tar is not obviously accounted for in determining the empirical chemical composition of the pyrolysis products and the char yield.

To analyze the data for Y_c, and number of C and H atoms in C_xH_yO, consider the processes that occurs during wood pyrolysis. As described in Chapter 1, the pyrolysis of cellulose (major component of wood) starts with the dehydration process at low temperatures which leads to the formation of char, water, and fuel gases. At higher temperatures depolymerization of cellulose produces levoglucosan which is further pyrolyzed in large samples, while passing through the hot char matrix. In these processes, the rate and composition of the pyrolysis products changes with the heating rate and temperature. As the pyrolysis takes place deeper inside the solid, the products of pyrolysis contain less 'carbon' and 'hydrogen' atoms relative to the number of oxygen atoms, due to the cracking of heavy molecules while passing through the hot char. These products are reported by several authors [Goos(1952), Madorsky (1975), Hileman et al. (1976), Chan (1980), Kashiwagi et al. (1987)]. The average empirical chemical composition, char yield, and heat of combustion of volatiles of various woods are reported in the literature. These were summerized by Atreya (1983) in a review of pyrolysis of wood. The average formula reported for pyrolysis products of Douglas-fir is $C_{1.04}H_{2.38}O$. The average char yield is 0.36 and the lower heat of complete combustion of $C_{1.04}H_{2.38}O$ is determined to be 15.33 KJ/gm (same reference).

In our data [Figures CHxxx and Ycxxx (Appendix c)], the complete prediction of time variations of char yield Y_c and number of 'C' and 'H' atoms during the heating period of wood, was hampered by the condensation of tar. Since the heaviest organic volatiles, containing the largest number of carbon atoms, escape during the early stages of pyrolysis and they are partially condensed, error in the calculated values of x, y, Y_c and the heat of combustion is higher at the early times. This error is consistent with the trend of errors in the total mass balance [Figures ERxxx (Appendix C)]. The

difference between the two curves in Figures TMxxx (Appendix C), specially around the peak of the mass flux curves, represents mainly the amount of tar which has been lost by condensation and was not accounted for.

Experimental data [Broido and Nelson (1975), Shafizadeh (1981)] shows that char yield increases with decrease in temperature and also the extent of the sample exposure to lower temperatures. Under different experimental conditions char yield on heating of cellulose for one hour at 370°C varied by a factor of five [Broido and Nelson (1975)]. According to Shafizadeh's (1981) data for cellulose, $(\frac{\rho_f}{\rho_w})$ (final density of char/density of wood) varies from 21% at 300°C to 3% at 500°C. From equations (4-8 through 4-10) it is evident that the variations in the chemical composition of the pyrolysis products is closely related to the variations in the char yield. The calculated values of 'C', 'H', and Y_c in these experiments at larger times generally become closer to the values reported in the literature and was mentioned above. Figures CHD4N and YCD4N (Appendix C) are good example of variations of these parameters during an experiment with relatively low total mass balance error. Except for early stages of pyrolysis, for this high heat flux experiment on dry wood, the average char yield is about 0.35 which is very close to the average value reported in the literature. Almost similar values (average) are obtained for 4 W/cm^2 experiment performed on dry wood in air. In air, of course, due to the char oxidation char yield is expected to be lower. The discrepancy is due to higher experimental error for experiments conducted in air (because of more air leakage).

Theoretically, the char yield right at the start of heating (i.e. at time=0), must be unity because no carbon has left the wood as yet. This point can not be obtained experimentally due to the uncertainties in all quantities involved at the first few seconds of each experiment. Then, char yield increases monotonically during the rapid rise and fall-off of the pyrolysis mass flux [Figures 3.6-3.17], because as char thickens

more 'carbon' atoms are caught in the char matrix as the pyrolysis products travel outwards. However, the trend observed specially at the early stages of char yield and 'C' and 'H' data are opposite to the expected trend. This is obviously the consequence of the condensation of that portion of tar that never entered the combustion process, and seemed as if it remained in the solid and was converted to char. The magnitude of this error is different in different experiments depending on how much tar has been condensed. However, generally at lower heat fluxes and higher moisture contents, the values of 'C' and 'H' and Y_c appear to improve significantly [Figures CHx1x, YCx1x (Appendix C]. The results for each group of experiments show that for the same ambient condition and moisture content, char yield increases with decrease in heat flux (and consequently with decrease in the solid temperature). Moreover, the results indicate that the char yield increases by moisture content of wood*. For example, a comparison of the 'average' char yield in experiments at 4 W/cm^2 in nitrogen [Figures YCx4N (Appendix C)] shows that char yield increases with increase in the moisture content of wood. In low heat flux experiments on 17% moist wood in nitrogen, where small amounts of tar are generated and mostly water is released [Figures YCM2N and YCM1N], the char yield is almost invariable and is about 0.65, indicating that ρ_f and ρ_w basically represents densities of dry and wet wood. Notice that C_xH_yO, empirically represents those gases which left the wood. Thus, the char yield, as calculated from relation (3-4), is a measure of the 'carbon' (and 'H' and 'O') atoms which stayed in the solid.

The values of gram C/gram of C_xH_yO and gram H/gram of C_xH_yO are also plotted in Figures GGxxx (Appendix C). From the average reported empirical formula of Douglas-fir volatiles, i.e. $C_{1.04}H_{2.38}O$, the average values of $\frac{\text{gm C}}{\text{gm } C_xH_yO}$, $\frac{\text{gm H}}{\text{gm } C_xH_yO}$, and $\frac{\text{gm O}}{\text{gm } C_xH_yO}$ are 0.404, 0.077, and 0.519

* Deviations from these general observations are due to the experimental errors in any particular experiment.

respectively. The results show good agreement and the errors follow the same trend as in the other data.

To summerize, although due to the condensation of tar the overall time variations of Y_c, 'C', and 'H' for the entire period of heating was not completely obtained, the results confirm the fact that char yield and chemical composition of pyrolysis products are not constant and they vary with time, temperature, and heating rate. Moisture content of wood also dilutes the pyrolysis products and increases the char yield.

3.10 Heat of Combustion of Pyrolysis Products

For the determination of combustion efficiency we need to know the lower heat of complete combustion. Hugget (1980) found that for most hydrocarbons, which included polymers, organic liquids, and natural materials, the amount of heat released per unit mass of oxygen consumed for their combustion is almost constant. A value of 13.1 KJ heat released per gram of oxygen consumed was a close approximation. Deviations from this average value were typically on the order of ±5%. In this work, the value 13.5 was considered which is the constant heat of combustion of fuel per unit mass of O_2 required for the complete oxidation of a unit mass of fuel obtained from Atreya (1983). The heat of combustion of pyrolysis products is determined from the relation

$$\Delta H_v = 13.5 \frac{\dot{m}_{\Delta O_2}}{\dot{m}_p}$$

in which ΔH_v (KJ/g) is the heat of combustion of volatile products, $\dot{m}_{\Delta O_2}$ (mg/cm^2.sec) is mass flow rate of oxygen consumed for the combustion of pyrolysis products, and $\dot{m}_p$ is the pyrolysis mass flux (mg/cm^2.sec).

.PP Figures HVxxx (Appendix C) show the calculated values of lower heat of combustion of pyrolysis products. These data include the error due to the condensation

of that part of the heavy hydrocarbons which did not enter the catalytic combustor. However, average large time values are mostly within the ranges reported in the literature. The average reported lower heat of combustion of Douglas-fir volatiles is 15.33 KJ/g [Atreya (1983)] which may be determined from complete combustion of $C_{1.04}H_{2.38}O$ (average empirical formula for products of pyrolysis of Douglas-fir). The results show that for higher moisture content of wood, the heat of combustion of volatiles is lower. This is due to the presence of more water in the evolved products which dilutes the mixture. Higher heat fluxes also yield higher heat of combustion of volatiles which is due to the presence of more heavy hydrocarbons in the pyrolysis products.

3.11 Sample Temperature Profile

In most of the experiments, temperature at specified locations in the samples along with the front and back surface temperatures were measured. The distance between the in-depth thermocouples was greater as they were located further away from the heated surface. This was done because these measurements provide data for the calculation of thermal properties of the pyrolyzing solid and their variations with time. Sensitivity of these calculations to the changes in the temperatures larger for higher temperature gradients closer to the hot surface than to the back surface. The surface thermocouple usually remained in place for most of the duration of experiments in nitrogen atmosphere. In air, however, due to the oxidation and more frequent cracking of the char, surface thermocouples came off the solid much faster. Moreover, the location of the in-depth thermocouples could not be maintained the same in all samples because the growth rings of the wood samples made it impossible to drill a straight fine hole for the insertion of the thermocouples. For this reason direct comparison of the in-depth temperatures is not made. However, the exact location of the thermocouple beads were determined and recorded. The temperature

versus time measurements are shown in Figures Txxx in Appendix C.

From the in-depth temperature-time profiles, it is clear that the temperature histories of the solid are profoundly altered by some nonconductive processes. For moist wood there is a characteristic plateau at about 100°C. Such plateau does not appear in the temperature profiles of dry wood [Figure TD4N, Appendix C]. The time of occurrence and duration of these plateaux increase as the distance from the heated surface increases. These plateaux are distinctly visible in experiments on wood with 17% moisture content [Figure 3.30 and Figures TMxN Appendix C]. Such an endothermic effect is quite characteristic in pyrolyzing organics and is due to the diffusion, condensation, and re-evaporation of adsorbed moisture.

A second plateau, although not very distinctly clear, can be observed at temperature range of 350-400°C [Figures Txxx (Appendix C)]. As the wood is heated and the surface of the sample is pyrolyzed, while most of the volatile products of pyrolysis move into the the boundary layer outside of the solid, some of them are driven (and diffuse) into the cooler interior of the solid. These gases carry energy from regions of higher temperature to the relatively cooler inner layers and they condense where the temperature is as low as their condensation temperature. The energy released in this process heats up the intact solid prior to the arrival of the pyrolyzing zone. As heating continues, energy is conducted into these regions which causes re-evaporation of condensed pyrolysis volatiles.

The in-depth temperatures continuously increase with time while the rate of temperature increase reduces as the char layer thickens. The surface temperature, however, first shows a rapid increase and then the rate of increase reduces drastically and becomes almost constant. This is because although the absorptivity of the char is higher than wood and its conductivity is low, both of which result in increasing the surface temperature, however, the surface emissivity increases as well and much of the incident heat flux is reradiated from the surface. These two effects offset each other

and the surface temperature tends to remain constant and even occasionally decreases.

Heat flux has the most significant effect on the temperature distribution along the sample thickness. Figures Txxx (Appendix C) show that as heat flux increases temperature increases. Appearance of cracks may alter the surface and in-depth temperatures. In general, temperature decreases with increasing sample depth and so does the temperature gradient.

Ambient oxygen significantly increases the surface as well as the in-depth temperatures at any given time [Kashiwagi et al. (1987) obtained data for interior temperatures measured at *equal* distances in three different ambient oxygen concentrations. They also observed these effects]. The most important effect of ambient oxygen is on the surface temperature.

Surface temperature considerably increases in the presence of oxygen. This appears at all levels of external heat fluxes and the effect is higher at higher heat fluxes [Figures 3.13-3.14 and Figures Txxx (Appendix C)]. The surface temperature of the solid decomposing in air, however, shows an inflection point followed by sharp increase before it gradually becomes flat (Figures 3.31-3.32). This is due to the occurrence of exothermic gas phase reactions between the fuel gases and oxygen adjacent to the surface [Atreya (1983)] followed by oxidation of char. Other investigators [Shivadev (1974), Quintiere et al. (1982)] have also observed such inflection points in their surface temperature data. Atreya's (1983) data showed that the inflection point in the surface temperature corresponds to the deviation in the required heat flux (calculated from the measured surface temperature) from that measured by the heat flux sensor. Further oxidation of the char surface and the glowing combustion increases the surface temperature drastically. In all experiments at 4 W/cm^2 heat flux in air, the wood was ignited and flaming combustion continued.

The increase in the interior temperatures in the presence of oxygen is mainly due to increased heat conduction through the sample from a higher surface temperature

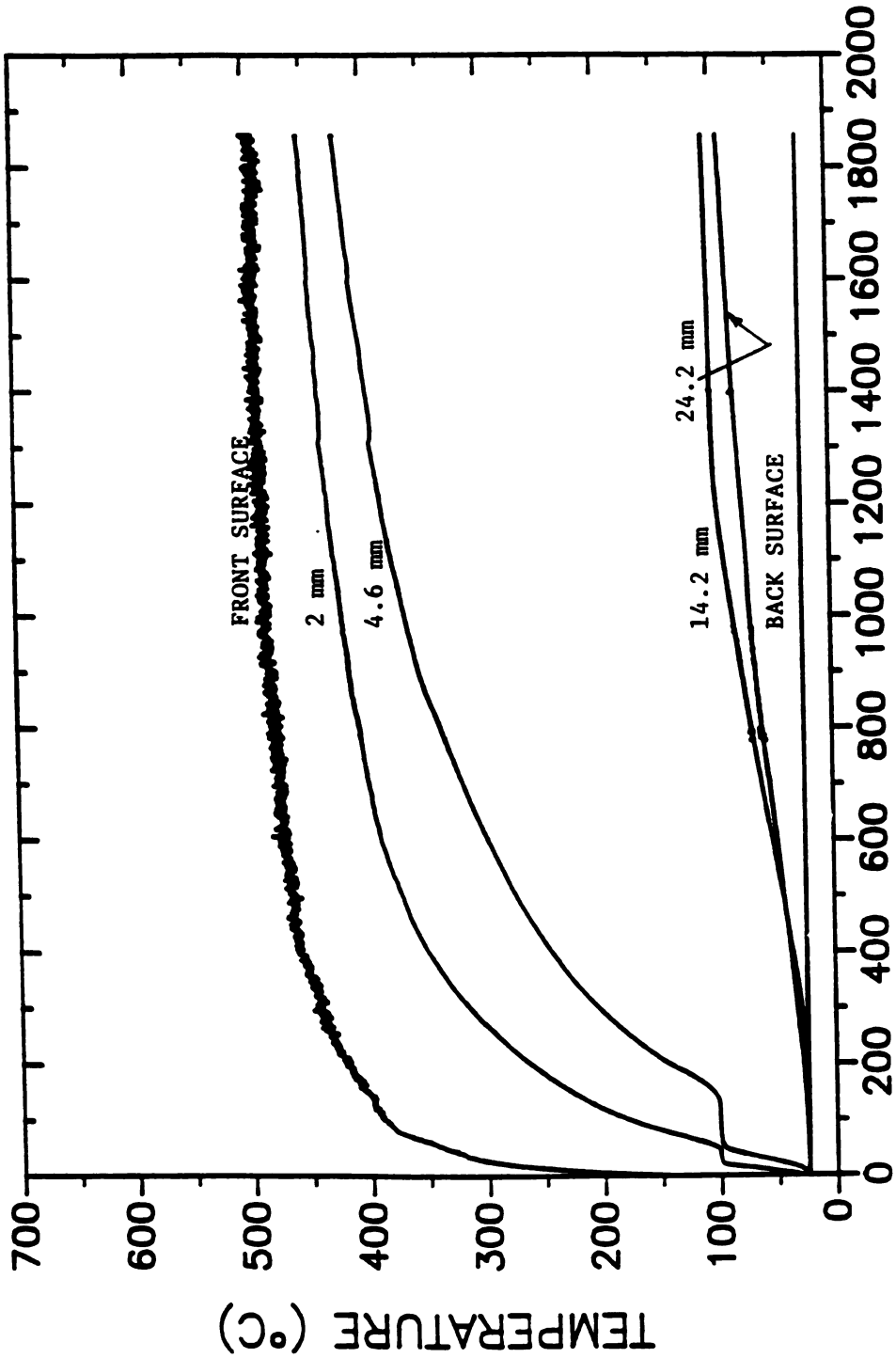

Fig. 3.30 Temperature vs. time at various locations isnside the wood; EXP. TM3N.

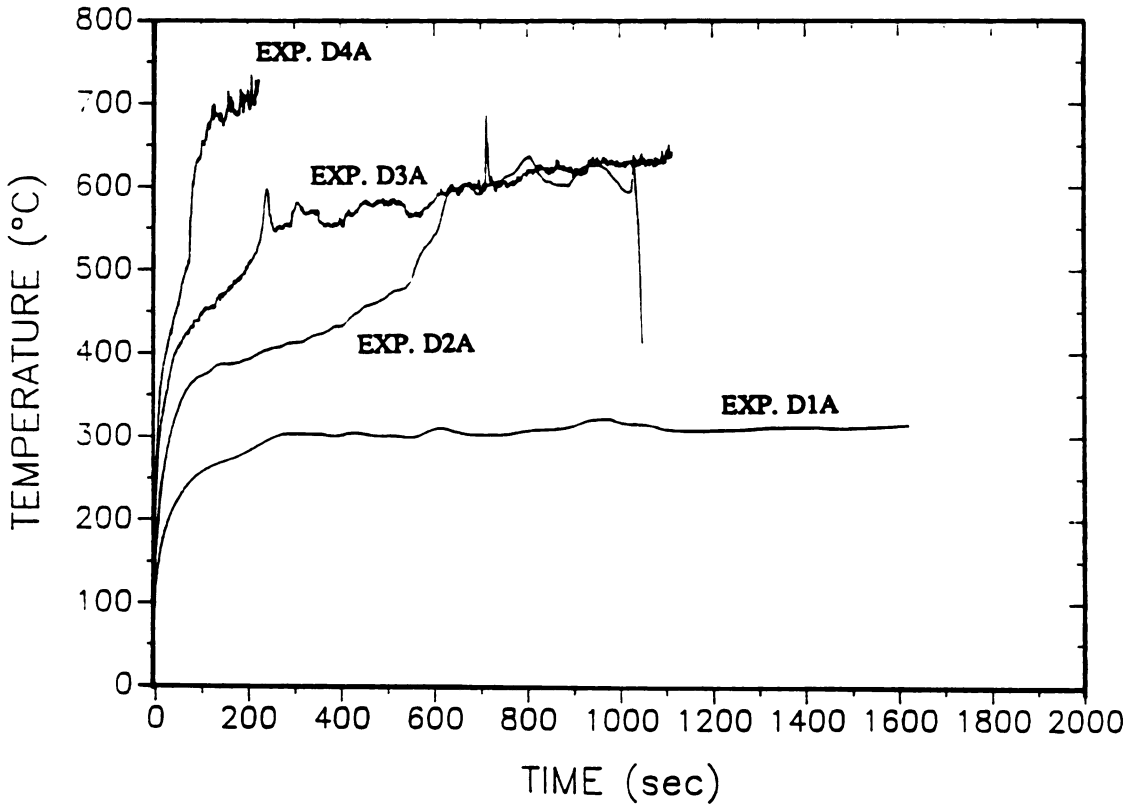

Fig. 3.31 Surface temperatures for experiments on dry wood in air.

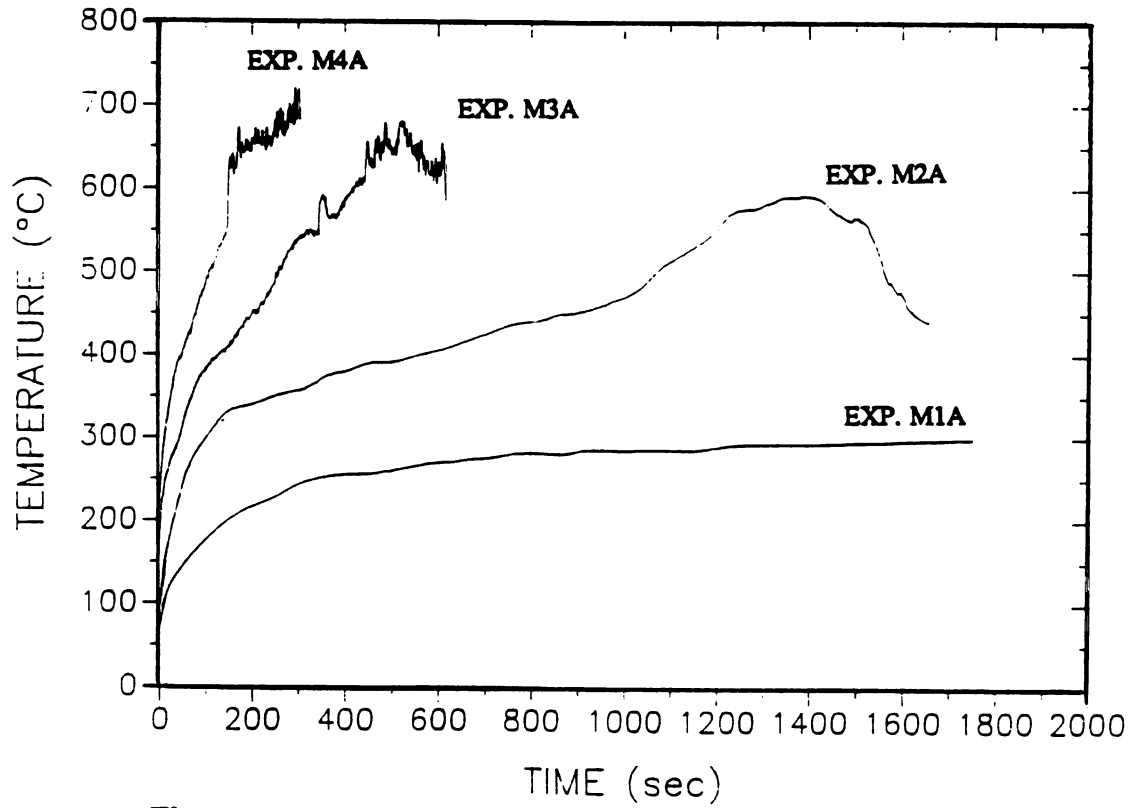

Fig. 3.32 Surface temperatures for experiments on 17% moist wood in air.

caused by the oxidation of char. It may also be partially caused by the increased penetration of external radiation inside the solid through cracks. Oxidative degradation of wood due to the diffusion of oxygen into the solid does not seem likely to be significant. Because the penetration of oxygen into the solid is mostly overcome by the outward flow of the volatiles and it is also mostly consumed by the char oxidation reactions. Indeed, the upward trends in the interior temperatures follow the same route as the surface temperature when the conduction wave reaches those thermocouples, indicating that no significant 'extra' source of heat (due to the exothermic reactions between char and O_2) has been present at those locations. This is also observed in the data obtained by Kashiwagi et al. (1987). Thus, the exothermic secondary reactions occur outside not inside the solid.

3.12 DATA CORRELATION

In an actual fire environment, it is very helpful to be able to even approximately predict the burning rate of the objects from the surface temperature information, without resorting to a detailed theoretical calculation. In an attempt to find an empirical correlation for the experimental results, the solution to the problem of 1-D conduction of heat in a semi-infinite inert solid initially at a fixed temperature is considered. The conduction of heat in the solid at time $t > 0$, initially at a constant temperature of T_∞, is described by the equation

$$\rho C_p \frac{\partial \theta}{\partial t} = k \frac{\partial^2 \theta}{\partial x^2} \qquad ; x > 0 \quad t > 0, \tag{3-13}$$

where

and a generalized heat flux boundary condition is given by

$$-k\frac{\partial\theta}{\partial x} = f_s(\theta_s, T_\infty, t) = \varepsilon[F - h\theta_s - \sigma((\theta_s + T_\infty)^4 - T_\infty^4)]. \qquad (3\text{-}14)$$

where F is the externally applied heat flux, and f_s is the heat flux going into the solid at the surface. Other symbols are defined in the nomenclature. Atreya (1983) obtained an approximate integral solution for equation (3-13) with the generalized boundary condition (3-14) using Duhamel's theorem and assuming that $f_s = a\,t^{\alpha}$, where a and α are real constants. For a constant heat flux boundary condition, $\alpha = 0$, whereas for a constant temperature boundary condition $\alpha = -1/2$. The details of the derivations are given by Atreya (1983) and will not be repeated here. From the resulting equations, it was found that

$$t = A^2\rho C_p k\left(\frac{\theta^2}{f_s^2}\right) \qquad (3\text{-}15)$$

where $A = \Gamma(\alpha+\frac{3}{2})/\Gamma(\alpha+1)$, in which $\Gamma(\,)$ is the gamma function. The total energy stored per unit area in the semi-infinite solid, E", is given by

$$E'' = \int_0^t f_s(t)dt = \frac{A^2\rho C_p k}{\alpha+1}\left(\frac{\theta_s^2}{f_s}\right). \qquad (3\text{-}16)$$

Even though these equations were derived for a semi-infinite inert solid, they collapse the pyrolysis data very well. Figure 3.33 shows the resulting correlation. In this figure, the heat flux f_s is the net heat actually going into the solid and is given by

$$f_s = \varepsilon[\, F - \sigma\,(T_s^4 - T_\infty^4) - h\,(T_s - T_\infty)E(b)] - C_{pg}\dot{m}''(T_s - T_\infty). \qquad (3\text{-}17)$$

where F is the prescribed incident heat flux, T_s is the surface temperature, h is the convective heat transfer coefficient, and C_{pg} is the specific heat of evolved gases. In this equation, E(b) and $C_{pg}\dot{m}''(T_s - T_\infty)$, respectively, are the required corrections due to the blowing and the enthalpy carried by the pyrolysis gases; E(b) [deRis (1978)] is given by

$$E(b) = \frac{b}{(e^b - 1)} \qquad \text{and} \qquad b = \frac{\dot{m}''C_{pg}}{h} \qquad (3\text{-}18)$$

The abscissa of this figure, TIME(--), is

$$\text{TIME}\ (\text{---}) = \left(\frac{\theta_s}{T_\infty}\right)^2 / \left(\frac{f_s}{F}\right)^2$$

where $\theta = T - T_\infty$, and T_∞ is the ambient temperature.

The pyrolysis mass fluxes of 9 experiments performed in nitrogen at 2, 3, and 4 W/cm^2 on wood samples with three different moisture contents are included in this Figure. Due to the large number of data points all the graphs are plotted with the same symbol. The mass flux changes from being proportional to θ_s^2/f_s, which may be interpreted as the instantaneous energy content of the solid , to being proportional to $\theta_s^{1.65}/f_s^{1.12}$. The correlation provides a very convenient tool for approximate prediction of the burning rate in an actual fire given the incident heat flux and the surface temperature of the solid.

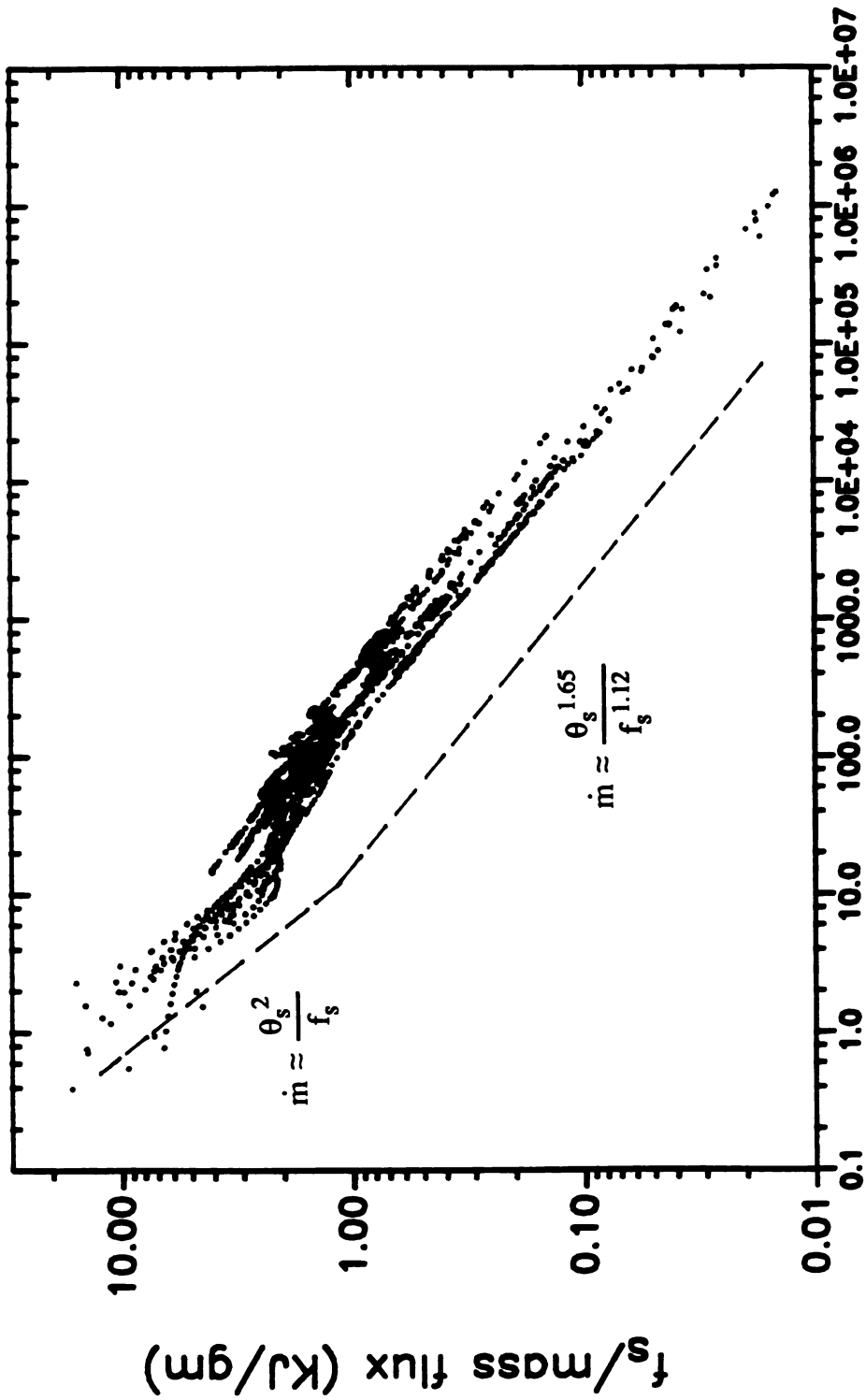

Fig. 4.33 Apparent Latent Heat of Pyrolysis (Experiments in N_2)

Chapter Four

The Effect of Thermal Decomposition Kinetics on the Mass Evolution Rate of Charring Materials

As it was discussed in Chapter 3, previous theoretical studies can generally be divided into two categories. The first category contains detailed numerical studies [Kansa et.al (1977), Kung (1972), Atreya (1983), Chan and Kreiger (1984)] that attempt to provide comprehensive description of wood pyrolysis by including as many heat and mass transfer processes as possible. Single-step overall apparent decomposition chemistry is often used to describe the complex decomposition kinetics. The second category contains simplified analytical studies [Kanury (1972), Delichstios and de Ris (1983), Wichman and Atreya (1987)] that attempt to develop practical and useful formulas for important quantities such as the evolved fuel mass flux and surface temperature. Such models are purely thermal and treat thermal decomposition as a phase change process, in which wood abruptly converts to char at

a specified pyrolysis temperature. Recently, an attempt has also been made to obtain an analytical solution to a simplified set of equations that include Arrhenius decomposition kinetics [Wichman and Atreya (1987)]. Formulas for volatile mass efflux were derived for the initial stages (kinetically controlled regime) of pyrolysis. Also, as expected, it was found that for the later stages (diffusion controlled regime) the results were similar to those obtained by the pyrolysis temperature (thermal) models [Delichaetios and de Ris (1983)]. However, obtaining a unified analytical description of the entire process was not possible and a pyrolysis temperature had to be assumed in the diffusion controlled regime. Pyrolysis temperature models are often used when seeking simplified formulas for predicting the evolved fuel mass flux and the sample surface temperature which are needed for solving complex problems such as fire growth in buildings. This chapter examines their validity by considering two otherwise identical models; one with infinitely fast decomposition kinetics (i.e. assuming a pyrolysis temperature) and the other with finite rate decomposition kinetics. The dependence of pyrolysis temperature on various parameters is also examined. For simplicity, the solid is assumed free of moisture and changes in thermophysical properties with temperature are ignored for both the models.

4.1 Model Formulation

Consider a "dry" infinite slab of wood of thickness L and initially at ambient temperature, T_∞. At times $t > 0$, let one face of this slab be subjected to a constant heat flux, $\dot{q}_{in}''$, and let the other face be well insulated. Thus, as heating proceeds, the temperature throughout the solid gradually increases. At some time a pyrolysis zone begins to develop at the surface and then propagates slowly into the interior of the solid leaving behind a thermally insulating layer of char.

The thickness of the pyrolysis zone depends upon the decomposition kinetics. For infinitely fast decomposition reactions, this thickness tends to zero and a pyrolysis

front propagates through the solid. This sharp front is associated with a temperature (T_p), at which wood abruptly converts into char. For finite rate decomposition kinetics, the density of the solid in the pyrolyzing zone continuously changes from the initial density of wood (ρ_w) to the final density of char (ρ_f). At any instant, a partially pyrolyzed element of wood in this zone may be considered to consist of char distributed through the unpyrolyzed active material. Since zero shrinkage is assumed, all densities used in this work are based on the original volume of the wood element. Thus, $\rho_s\,(x,t) = \rho_a\,(x,t) + \rho_c\,(x,t)$, where ρ_a and ρ_c are the densities of the active wood material and char respectively. Also, at $t = 0$, $\rho_s = \rho_a\,(x,0) = \rho_w$ and at $t = \infty$, $\rho_s = \rho_c\,(x,\infty) = \rho_f$ and $\rho_a\,(x,\infty) = 0$. For constant char yield (i.e. $\frac{\rho_f}{\rho_w}$ = constant), ρ_s is linearly related to ρ_a according to:

$$\rho_s\,(x,t) = (1 - \frac{\rho_f}{\rho_w})\,\rho_a\,(x,t) + \rho_f. \tag{4-1}$$

Similarly, a linear variation with density for the thermal conductivity (k_s) of the solid in the pyrolyzing zone is assumed;

$$k_s = \left[\frac{\rho_a}{\rho_w}\right] k_w + \left[\frac{\rho_c}{\rho_f}\right] k_c. \tag{4-2}$$

Here, k_w and k_c are the thermal conductivities of unpyrolyzed wood and char respectively. These are assumed constant and independent of temperature. Also, for temperature independent thermal properties, the enthalpy per unit volume of an element in the pyrolysis zone is given by;

$$\rho_s h_s = \rho_s C_{ps} T = (\rho_w C_{pw} + \rho_c C_{pc})T. \tag{4-3}$$

where, C_{pw} and C_{pc} are the specific heats of unpyrolyzed wood and char respectively.

Assuming no heat transfer between the pyrolysis gases and the char matrix, the energy equation describing the process becomes;

$$\frac{\partial}{\partial t}(\rho_s h_s) = \frac{\partial}{\partial x}\left[k_s \frac{\partial T}{\partial x}\right] + Q. \tag{4-4}$$

where Q is the rate at which energy is released per unit volume during the decomposition process. For a single first-order overall decomposition reaction, Q is given by

$$Q = Q_p \frac{\partial \rho_s}{\partial t} = -A\, Q_p\, (\rho_s - \rho_f)\, \exp\left(-\frac{E}{RT}\right). \tag{4-5}$$

whereas, for an infinitely fast decomposition reaction (i.e. a propagating pyrolysis front) Q is given by

$$Q = -\, Q_p\, (\rho_w - \rho_f)\, \frac{dx_p}{dt}\, \delta\,(x - x_p). \tag{4-6}$$

Here, Q_p is the heat of pyrolysis per unit mass of volatiles (positive when endothermic) and x_p is the location of the pyrolysis front. The other symbols are defined in the nomenclature.

The associated boundary and initial conditions are:

at t = 0:

$$T(x,0) = T_\infty; \quad \rho_c(x,0) = 0; \quad \rho_s(x,0) = \rho_w = \rho_a\,(x,0); \tag{4-7}$$

at x = 0, t > 0 :

$$-k_s \frac{\partial T}{\partial x}\bigg|_{x=0} = \dot{q}_{in}'' - h\,[T(0,t) - T_\infty] - \varepsilon\sigma\,[T^4(0,t) - T_\infty^4]; \tag{4-8}$$

and at x = L, t > 0 :

$$-k_s \frac{\partial T}{\partial x}\bigg|_{x=L} = 0. \tag{4-9}$$

4.1.1 The Pyrolysis Temperature Model

For infinitely fast decomposition kinetics, equations (4-4) and (4-6) reduce to the conventional formulation of the phase change problem. Note that for $0 < x < x_p$ (i.e. in the char), $Q = 0$, $\rho_s h_s = \rho_f C_{pc} T$ and $k_s = k_c$. For $x_p < x < L$ (i.e. in unpyrolyzed wood), $Q = 0$, $\rho_s h_s = \rho_w C_{pw} T$ and $k_s = k_w$. Thus the energy conservation equations for wood and char with temperature independent thermal properties become:

$$\rho_w C_{pw} \frac{\partial T_w}{\partial t} = k_w \frac{\partial^2 T_w}{\partial x^2}; \tag{4-10}$$

and

$$\rho_c C_{pc} \frac{\partial T_c}{\partial t} = k_c \frac{\partial^2 T_c}{\partial x^2}. \tag{4-11}$$

At the wood-char interface (i.e. $x = x_p$), the temperature is continuous and is equal to the pyrolysis temperature, T_p, viz.,

$$x = x_p \; ; \; T_w = T_c = T_p \tag{4-12}$$

The energy balance at the interface may be obtained by integrating equations (4-4) and (4-6) from $x = x_p(t) - \varepsilon$ to $x = x_p(t) + \varepsilon$ and letting $\varepsilon \rightarrow 0$. This procedure yields,

$$k_w \frac{\partial T_w}{\partial x}\bigg|_{x = x_p + \varepsilon} - k_c \frac{\partial T_c}{\partial x}\bigg|_{x = x_p - \varepsilon} = Q_p \, (\rho_w - \rho_c) \, \frac{dx_p}{dt.} \tag{4-13}$$

Equations (4-10) through (4-13) along with the boundary and initial conditions given by equations (4-7) through (4-9) were solved numerically by using the Crank-Nicolson finite difference method. Special, completely implicit finite difference equations were used for the start and end of charring of the boundary nodes and the nodes adjacent to the char-wood interface. The numerical procedure is similar to that described by Elhrich [1958]. The numerical code was verified against Neumann's exact solution [Carslaw and Jaeger (1959)]. The results were in excellent agreement. The finite difference equations and methods of solution are described in Appendix B.

4.1.2 The Finite Rate Decomposition Model

As noted earlier, for finite rate decomposition kinetics, the density and therefore the thermal properties change gradually from their values for wood to their values for char inside the pyrolyzing zone. Equations (4-1), (4-2) and (4-3) show the linear variation assumed. Thus, equation (4-4) may be rewritten as:

$$(\rho_a C_{pw} + \rho_c C_{pc}) \frac{\partial T}{\partial t} = \frac{\partial}{\partial x}\left[k_s \frac{\partial T}{\partial x}\right] + \frac{\partial \rho_s}{\partial t}\left[Q_p - \frac{(C_{pc} - \rho_f C_{pc})}{(\rho_w - \rho_s)}(T - T_\infty)\right] \quad (4\text{-}14)$$

Here, the last term is the energy required to produce a unit mass of volatiles minus the energy carried away by this unit mass of volatiles. In the pyrolysis temperature model this energetic process occurs solely at the wood-char interface.

Equations (4-14) and (4-5) along with the boundary and initial conditions given by the equations (4-7), (4-8) and (4-9) were numerically solved. A finite difference form of these equations was obtained by using the Crank-Nicolson method to express the derivatives. A simplified version of the computer program developed by Atreya [1983] was used for this purpose. This program has been previously tested for accuracy against the analytical calculations of the same reference.

4.2 Overall Energy and Mass Balance

Overall energy and mass balances were used as criteria to check the accuracy of both models and to enable comparison between them. Various terms in the energy balance are schematically indicated in Figure 1. Let t_f be the time it takes to completely pyrolyze a slab of wood of thickness, L. Then, the total mass of volatile gases produced during the time t_f and the sum of all energies lost, stored and absorbed during the pyrolysis process must be the same as the total input energy and also the same for both the models.

For constant values of initial (ρ_w) and final (ρ_f) densities, the total mass evolved per unit area [$(\rho_w - \rho_f)L$] is automatically balanced. However, for the energy balance various terms need to be considered separately. These are:

(i) Total input energy per unit area (J/cm^2)

$$E_{in} = \dot{q}_{in}'' \, (t_f - t_0). \tag{4-15}$$

(ii) Enthalpy remaining in the system at the end of charring (J/cm^2)

$$E_{st} = \rho_f \, C_{pc} \int_0^L [T(x,t_f) - T_\infty] \, dx. \tag{4-16}$$

(iii) Energy consumed during thermal decomposition (J/cm^2)

$$E_{py} = Q_p \, (\rho_w - \rho_f \,) \, L. \tag{4-17}$$

(iv) Convective and radiative heat losses from the surface (J/cm^2)

$$E_{loss} = \int_{t_0}^{t_f} \left[\varepsilon\sigma \, (T_s^4(t) - T_\infty^4 \,) + h \, (T_s(t) - T_\infty) \right] dt. \tag{4-18}$$

(v) Energy carried out by the products of pyrolysis (J/cm^2)

(from equation (14));

$$E_{og} = - \int_{t_0}^{t_f} \int_0^L \frac{\partial \rho_s}{\partial t} \, \frac{(\rho_w C_{pw} - \rho_f C_{pc})}{(\rho_w - \rho_f)} \, [T(x,t) - T_\infty] \, dx \, dt. \tag{4-19}$$

For the pyrolysis temperature model $\frac{\partial \rho_s}{\partial t}$ may be calculated from Equations (4-5) and (4-6), and using $T(x_p,t) = T_p$, whereby

$$E_{og} = (\rho_w C_{pc} - \rho_f C_{pc}) (T_p - T_\infty) L. \qquad (4\text{-}20)$$

Thus for the overall energy balance the sum of the terms given by equations (4-16) through (4-19) must be equal equation (4-15). For the pyrolysis temperature model, equation (4-20) must be used instead of equation (4-19). All of these terms were calculated for both the models for the purpose of comparison.

4.3 Results and Discussion

Property values used in the calculations are listed in Table 4.1 for both the kinetic and pyrolysis temperature models. Calculations were performed with both the models for four different incident heat fluxes and four different heat loss boundary conditions on the front surface. The boundary conditions used on the front surface were; (i) no heat losses, (ii) only convective heat losses, (iii) only radiative heat losses, and (iv) combined convective and radiative heat losses. For purposes of comparison, the case with no heat losses is taken as the base case. An appropriate pyrolysis temperature was determined by enforcing the overall energy and mass balances between the pyrolysis temperature and the kinetic models. The influence of the heat of pyrolysis was also investigated.

Figures 4a-d show the history of total weight loss, front and back surface temperatures and the weight loss rate for the cases with no heat losses at the front surface. This is the base case. The solid lines are the results of calculations performed by using the kinetic model, whereas the dotted lines are for the pyrolysis temperature model. The pyrolysis temperature used in these calculations was

determined by matching the energy and mass balances between the two models for the case with 3 W/cm^2 incident heat flux, giving T_p = 425°C. In these cases, the only variable is the incident heat flux. The front and back surface temperatures predicted by both the models are in reasonable agreement. The curves deviate only slightly as the incident heat flux is varied. This is expected because the boundary conditions and the thermal properties used in the two models are identical. However, the total weight loss (which is directly proportional to char depth) and thus the volatile mass flux predicted by the two models differ significantly with the incident heat flux. The deviations in the mass flux curves calculated by two methods are more pronounced at the early times (corresponding to ignition) and the later times (corresponding to extinction).

Next, more realistic cases with surface heat losses were considered. The accuracy of both the numerical schemes was determined by performing the overall energy balance described in Section 4.2. Table 4.2 shows the percentage errors in the total energy balance within each numerical scheme. The pyrolysis temperature model has more computational error, because of the abrupt conversion of wood to char. This error is introduced during the time step in which the pyrolysis front crosses a nodal boundary. In this time step, the location of the pyrolysis front is iteratively determined by satisfying Equation (4-13). If the pyrolysis front is within a small prescribed distance from the nodal boundary, its location is taken as the nodal boundary. Thus, an error is introduced in the energy balance. This error may be reduced by reducing the time step. However, it was considered acceptable for the present purpose.

Table 4.3 shows the percentage difference between the total input energies for the two models. This difference was minimized to determine the energy-balanced pyrolysis temperature for each of the cases listed in the table. The pyrolysis temperature was found by trial and error by enforcing the condition that the total energy for the front model be equal to that of the kinetic model. Also shown in Table 4.3 (in the last

column) is the percentage difference in the total input energy between the two models when the pyrolysis temperature was held constant (T_p = 425°C). As can be seen, for the most realistic case with convective and radiative heat losses, the error in the energy balance is 33%. In order to reduce this error to 6.9% the pyrolysis temperature had to be lowered by 75°C to 350°C. It is possible to obtain even better agreement between the two models by further lowering the pyrolysis temperature. As a general rule, higher the net heat flux into the solid (i.e. $k(\frac{\partial T}{\partial x})$) at x = 0 the higher is the pyrolysis temperature required for balancing the energy. Thus, the pyrolysis temperature is clearly not a material property. Instead, it varies considerably with the net heat flux into the solid, which may be altered either by changing the heat losses from the sample surface or by changing the incident heat flux to the sample surface.

Figures 4-3a to 4-3e show the time histories of front and back surface temperatures, total weight loss and the weight loss rate, as calculated by the two models for different front surface heat losses. Once again, front and back surface temperatures predicted by both the models are in good agreement when identical boundary conditions are used. The effect of decomposition kinetics on the total weight loss and the weight loss rate can be seen from Figures 4-3c, 4-3d and 4-3e. The agreement between the decomposition kinetics model and the pyrolysis front model is excellent for Case 1, i.e. with no heat losses. However , it deteriorates when larger heat losses are permitted at the front surface; even for the cases where the energy-balanced T_p was used. For the case with nonlinear radiative heat losses, the error in the mass balance (Figure 4-3c) at 500 seconds is 27% when the energy-balanced T_p is used (Case 3) and is 51% when T_p is kept fixed at 425°C (Case 6). This error is clearly unacceptable for predicting fire growth in practical problems. Furthermore, even with a T_p that satisfies the energy balance requirements, it is not possible to predict the correct pyrolysis mass flux (as evidenced by Figures 4-3d and 4-3e) specially in the initial and final stages. Thus, pyrolysis temperature models cannot be

used to predict ignition and extinction phenomena. Figure 4-3f shows the difference between the mass flux predicted by the pyrolysis temperature model and that predicted by the decomposition kinetics model at early times using a T_p that satisfies the energy balance requirements. The pyrolysis temperature model predicts that both piloted and spontaneous ignition will occur at 30 seconds when the mass flux sharply rises to 0.8 $mg/cm^2.sec$ and that the surface temperature at that instant is equal to the pyrolysis temperature. These predictions do not agree even qualitatively with the experimental observations. Figure 4-3g shows the in-depth temperature and density profiles for the case with radiative heat losses at the front surface and with the back surface insulated. Three different calculations are compared at two instances; 300 and 600 seconds. These calculations correspond to: (1) decomposition kinetics model, (ii) pyrolysis temperature model with energy-balanced T_p = 375°C, and (iii) pyrolysis temperature model with fixed T_p = 425°C. As can be seen, although the front and back surface temperatures are reasonably close the temperature and density profiles inside the solid are substantially different. This difference accounts for the large differences observed in the volatile mass flux shown in Figures 4-3d and 4-3e.

The effect of the controversial heat of pyrolysis on volatile mass flux is shown in Figure 4-4. Three different values of the endothermic heat of pyrolysis were used. For a fixed pyrolysis temperature (T_p = 425°C), the total energy between the two models balanced to within 3%. The volatile mass flux predicted by the two models (Figure 4-4) also shows good agreement except at the initial and final times. Thus, heat of pyrolysis does not have a significant effect on the pyrolysis temperature. The front and back surface temperature histories presented in the Figures 4-2a, 4-2b, 4-3a and 4-3b show that there is relatively small difference between the predictions of the two models. This is because identical boundary conditions are used. Thus, the heat loss term [Equation (18)] in the overall energy balance is essentially identical for both kinetic and pyrolysis temperature models. Energy consumed during thermal

decomposition [Equation (4-17)] is also the same for both the models. The enthalpy remaining in the system at the end of charring [Equation (16)] is very small compared with the other terms in the energy balance; hence, any differences in energy between the two models may be ignored. Thus, the primary difference in the energy balance is the energy carried out by the products of pyrolysis, i.e. Equations (4-19) and (4-20). Thus, for a given problem, an approximate energy-balanced pyrolysis temperature may be found from the terms (4-19) and (4-20), viz,

$$\Theta_p = A^* \int_0^{11}\int_0^{} \rho^*_s \exp\left(-\frac{\phi}{(\Theta + 1)}\right) d\eta d\tau^* \qquad (4\text{-}21)$$

where

$$\Theta = \frac{(T - T_\infty)}{T_\infty}\ ,\ \eta = \frac{x}{L}\ ,\ \tau^* = \frac{t}{t_f}\ ,\ \rho^*_s = \frac{(\rho_s(x,t) - \rho_f)}{(\rho_w - \rho_f)}\ ,\ \phi = \frac{E}{RT_\infty}\ ,\ A^* = At_f$$

and t_0 is taken as zero. Clearly, the non-dimensional Θ_p depends upon the history of the pyrolysis process. The higher the average temperature, Θ, at which pyrolysis occurs (i.e. higher incident heat fluxes), the higher is the value of Θ_p. Equation (4-21) has to be solved numerically since it requires the knowledge of $\rho^*_s(x,t)$, and $\Theta(x,t)$, which must satisfy Equations (4-4) and (4-5).

Table 4.1 Constants used for the calculations.

$A = 250 \times 10^6$	$\frac{1}{sec}$
$C_{pc} = 712$	$\frac{J}{Kg.°K}$
$C_{pw} = 1465.1$	$\frac{J}{Kg.°K}$
$E = 125.58 \times 10^8$	$\frac{J}{Kg.°K}$
$K_c = 0.0712$	$\frac{J}{m.°K.sec}$
$K_w = 0.1675$	$\frac{J}{m.°K.sec}$
$L = 1$	cm
$h = 11.4$	$\frac{W}{cm^2.°K}$
$Q_p = 30$	$\frac{cal}{gm}$
$T_\infty = 25$	°C
$\varepsilon = 0.95$	(surface emissivity)
$\sigma = 5.67 \times 10^{-8}$	$\frac{W}{cm^2.K^4}$
$\rho_w = 676$	$\frac{Kg}{m^3}$
$\rho_c = 162.24$	$\frac{Kg}{m^3}$

Table 4.2 Percentage errors in the total energy balance within each numerical scheme.

CONDITIONS:

External Heat Flux = 3 W/cm^2
Q_p = 30 cal/mg
Insulated back surface.

$\text{Percentage error} = \frac{E_{in} - (E_{og} + E_{loss} + E_{py} + E_{st})}{E_{in}} \times 100$		
	KINETIC MODEL	PYROLYSIS TEMPERATURE MODEL
1) no surface heat losses	0.002	1.45 (T_p = 425°C)
2) convective heat losses	0.06	3.00 (T_p = 405°C)
3) radiative heat losses	0.9	2.20 (T_p = 375°C)
4) convective & radiative heat losses	1.64	1.95 (T_p = 350°C)

Table 4.3: Percnetage difference between the total input energies (E_{in}) for the two models. This was used to determine the pyrolysis temperature T_p.

CONDITIONS:

External Heat Flux = 3 W/cm^2
Q_p = 30 cal/mg
Insulated back surface.

	Total input energy (Joules)			Percentage difference	
	Kinetic (1)	Pyrolysis Temperature (2)	Pyrolysis Temperature (3)	(1) & (2)	(1) & (3)
1) no surface heat losses	6.100E+6	5.985E+6 (T_p = 425°C)	5.985E+6 (T_p = 425°C)	1.87	1.87
2) convective heat losses	8.640E+6	8.500E+6 (T_p = 405°C)	8.820E+6 (T_p = 425°C)	1.62	2.08
3) radiative heat losses	19.800E+6	20.000E+6 (T_p = 375°C)	24.600E+6 (T_p = 425°C)	1.01	24.24
4) convective & radiative heat losses	22.679E+6	21.110E+6 (T_p = 350°C)	30.200E+6 (T_p = 425°C)	6.90	33.05

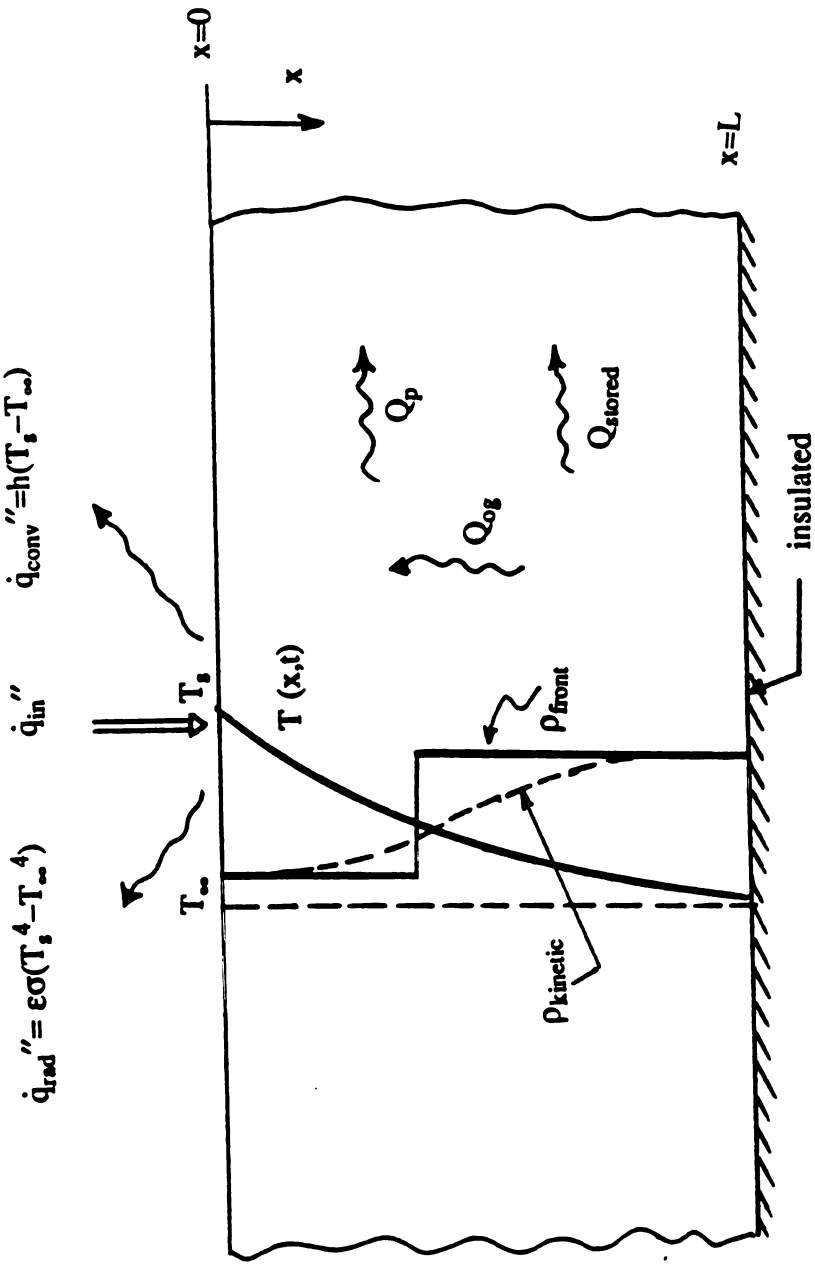

Figure 4.1 Physical configuration of thermal decomposition problem showing all energy transfers.

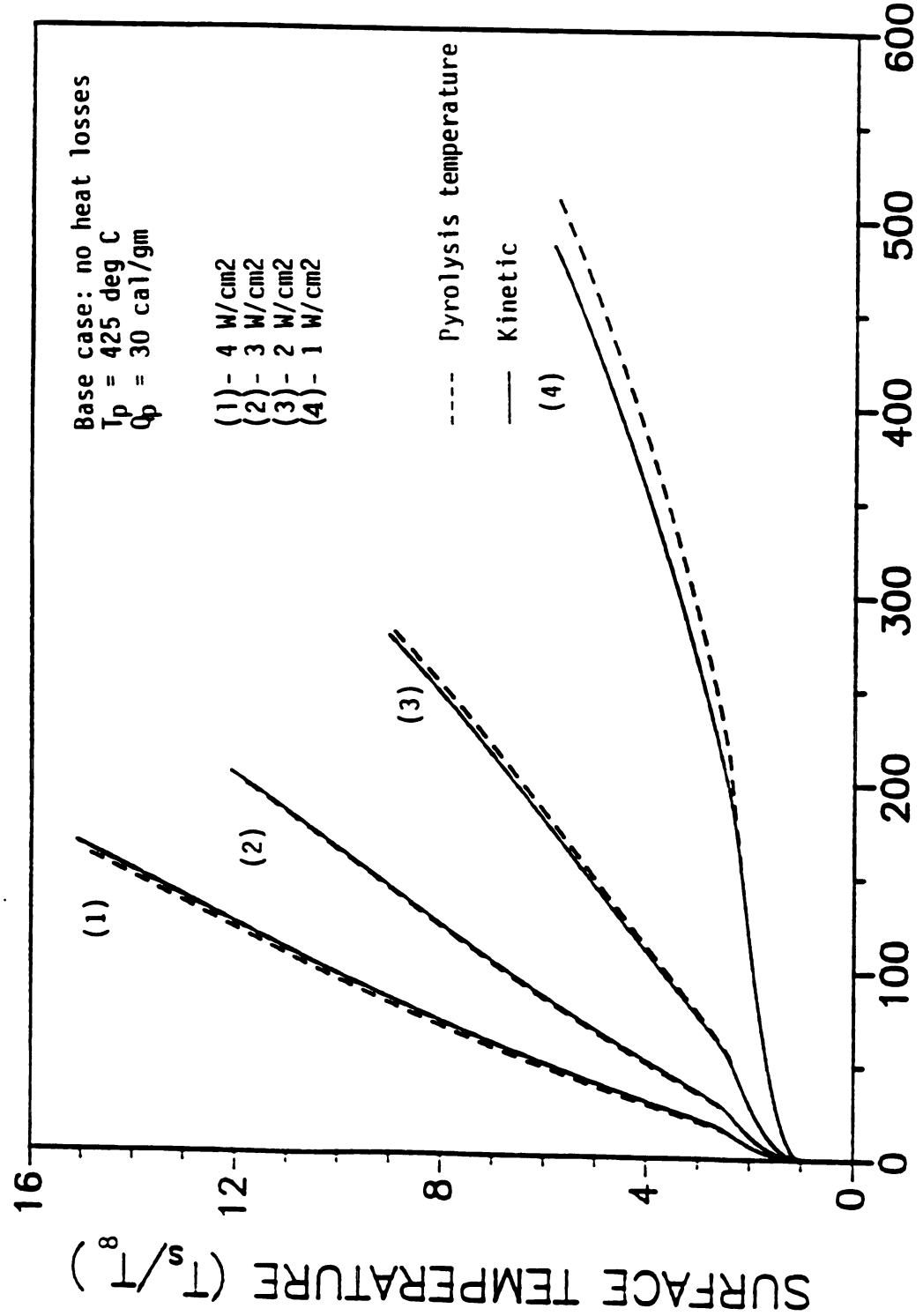

Figure 4.2a Front surface temperatures, with no heat losses at the front and back surface.

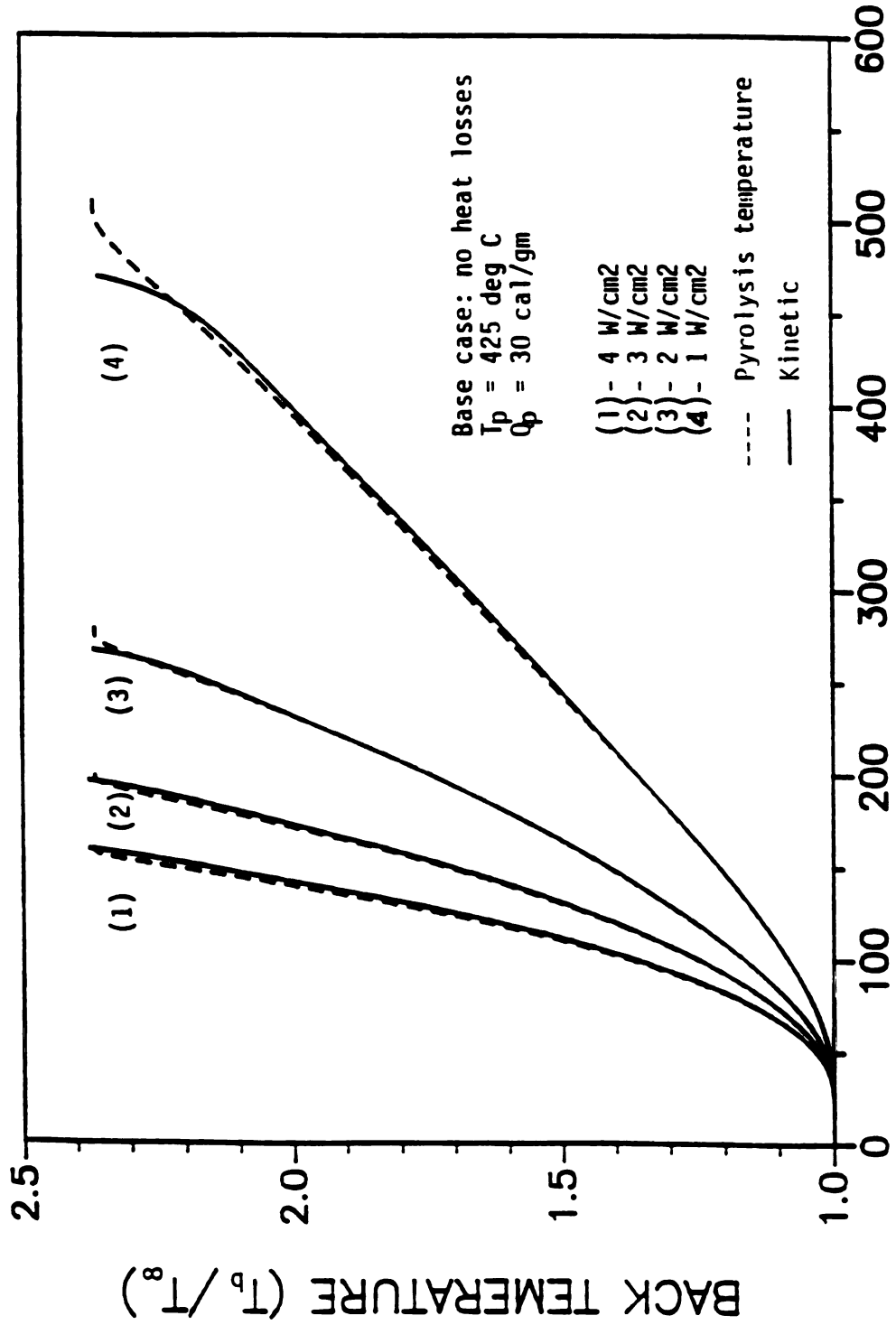

Figure 4.2b Back surface temperature, with no heat losses at the front and back surfaces.

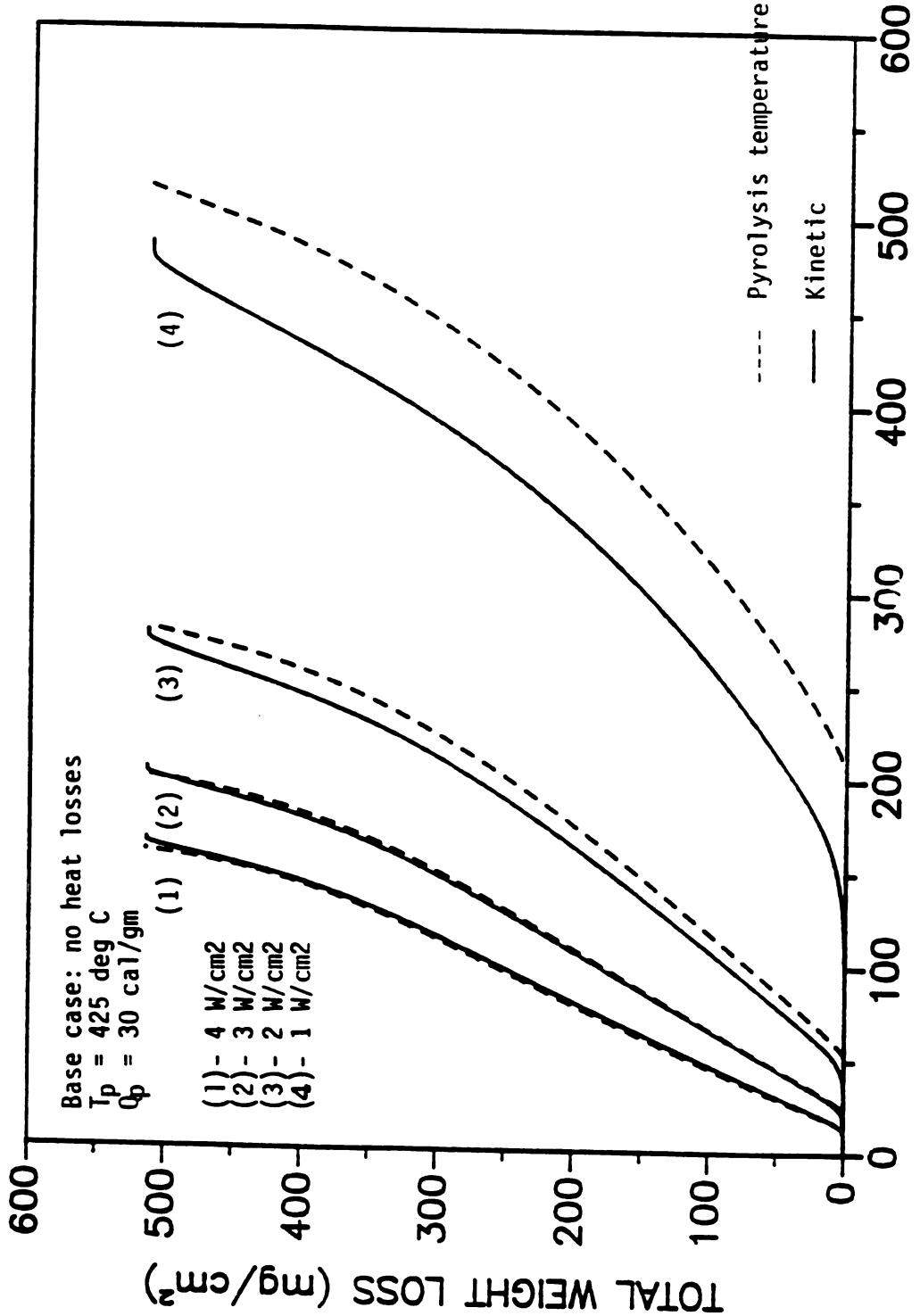

Figure 4.2c Total weight loss, with no heat losses at the front and back surfaces.

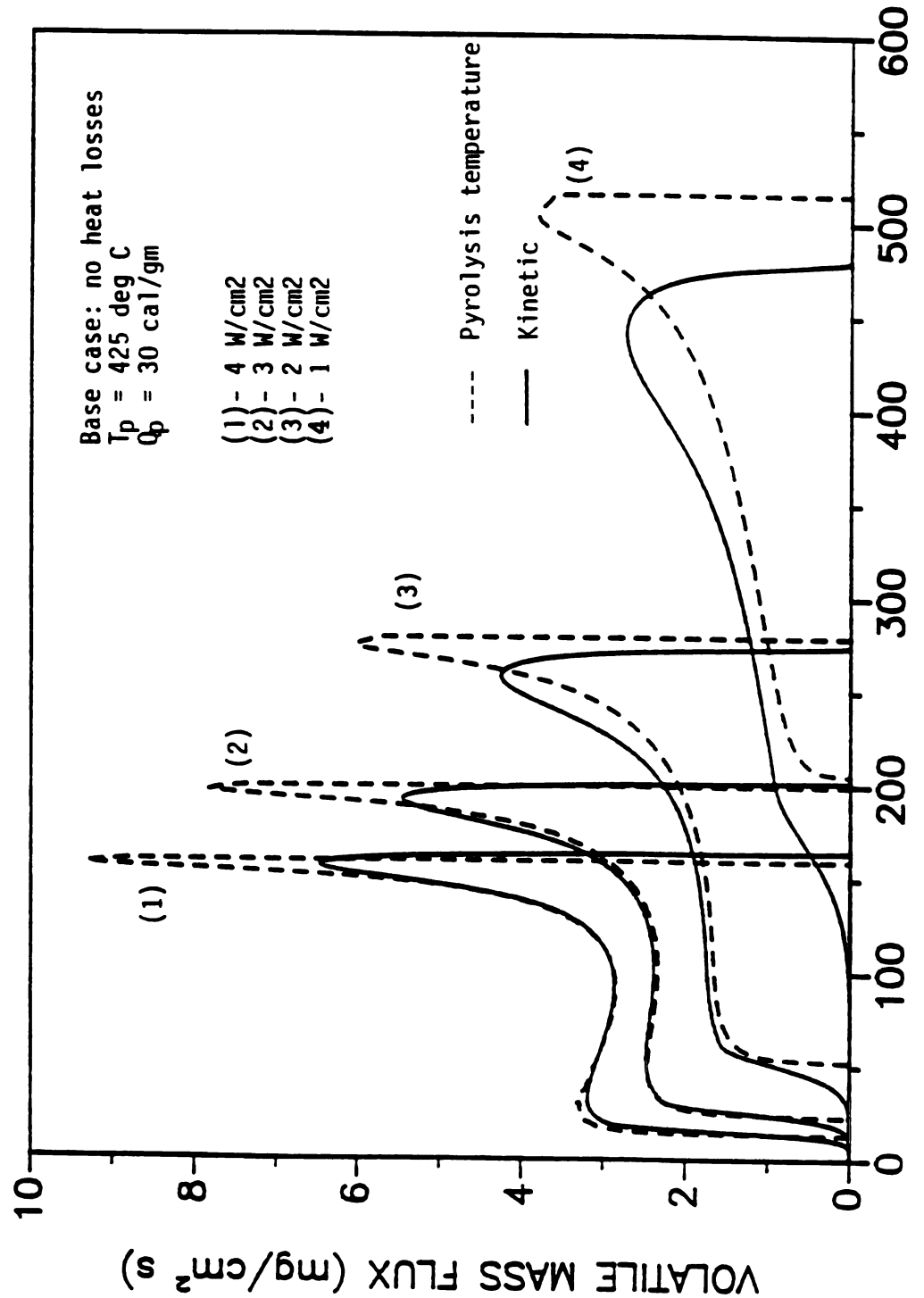

Figure 4.2d Weight loss rate, with no heat losses at the front and back surfaces.

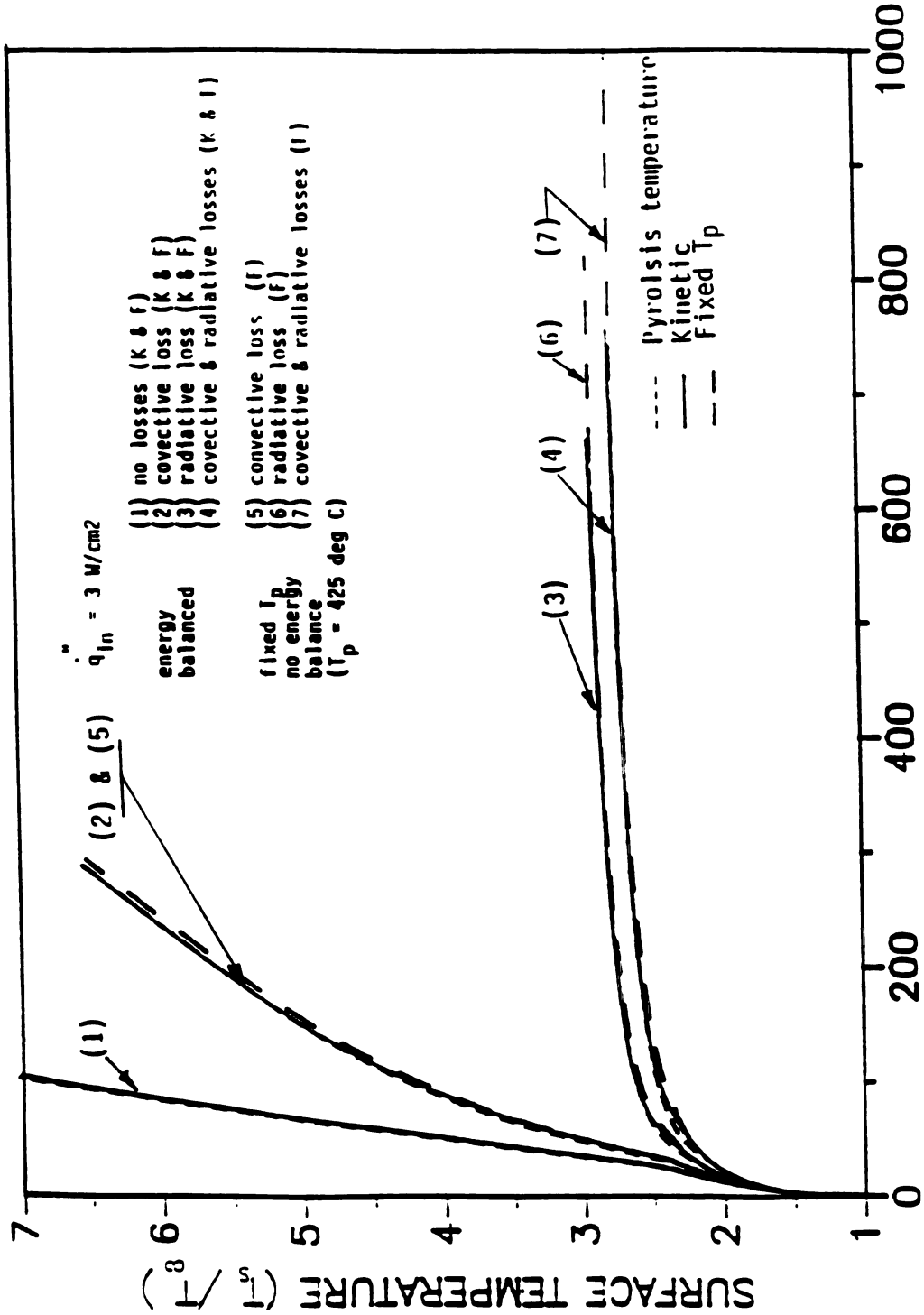

Figure 4.3a Surface temperature, with different front surface heat losses and back surface insulated.

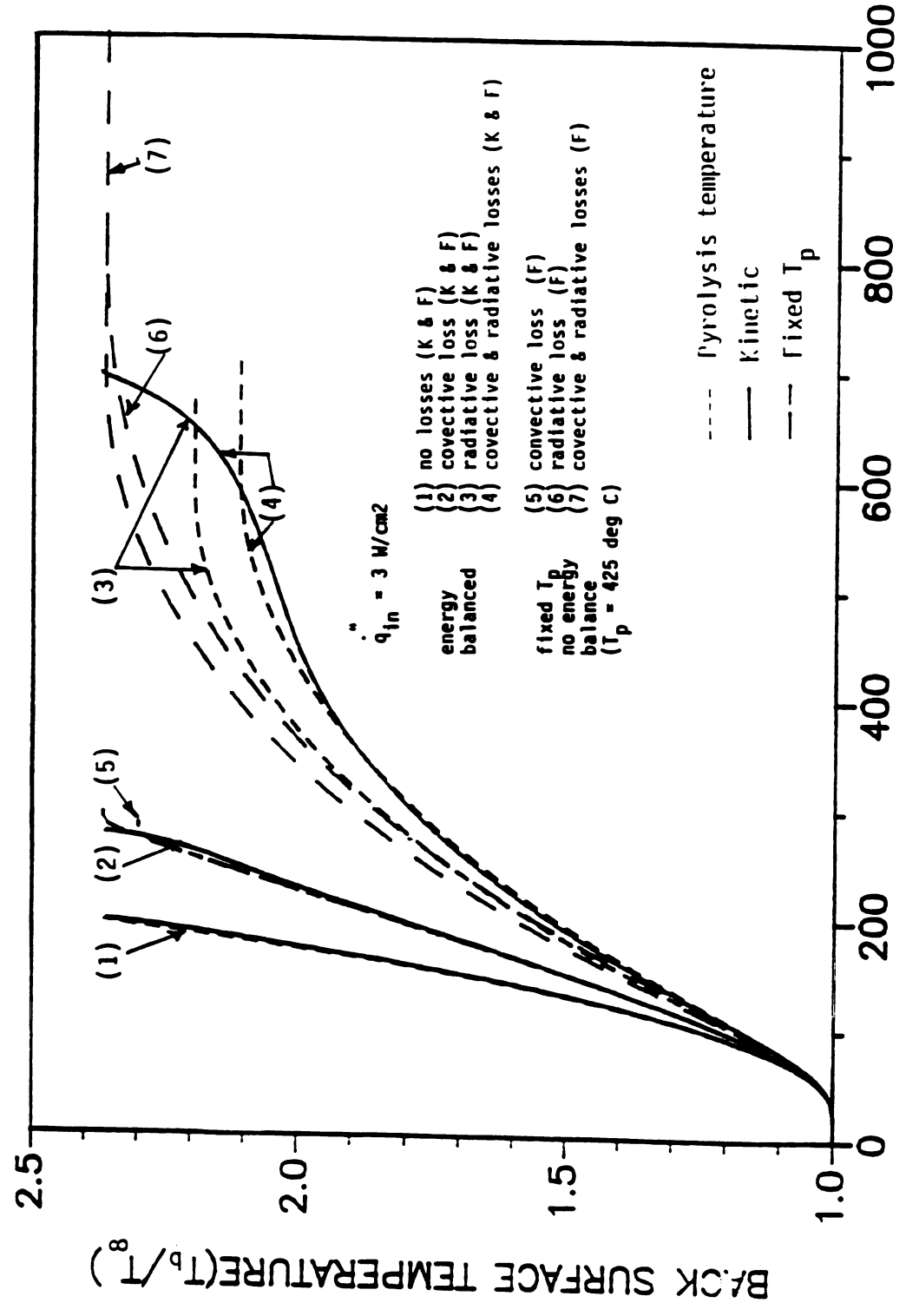

Figure 4.3b Back surface temperature, with different front surface heat losses and back surface insulated.

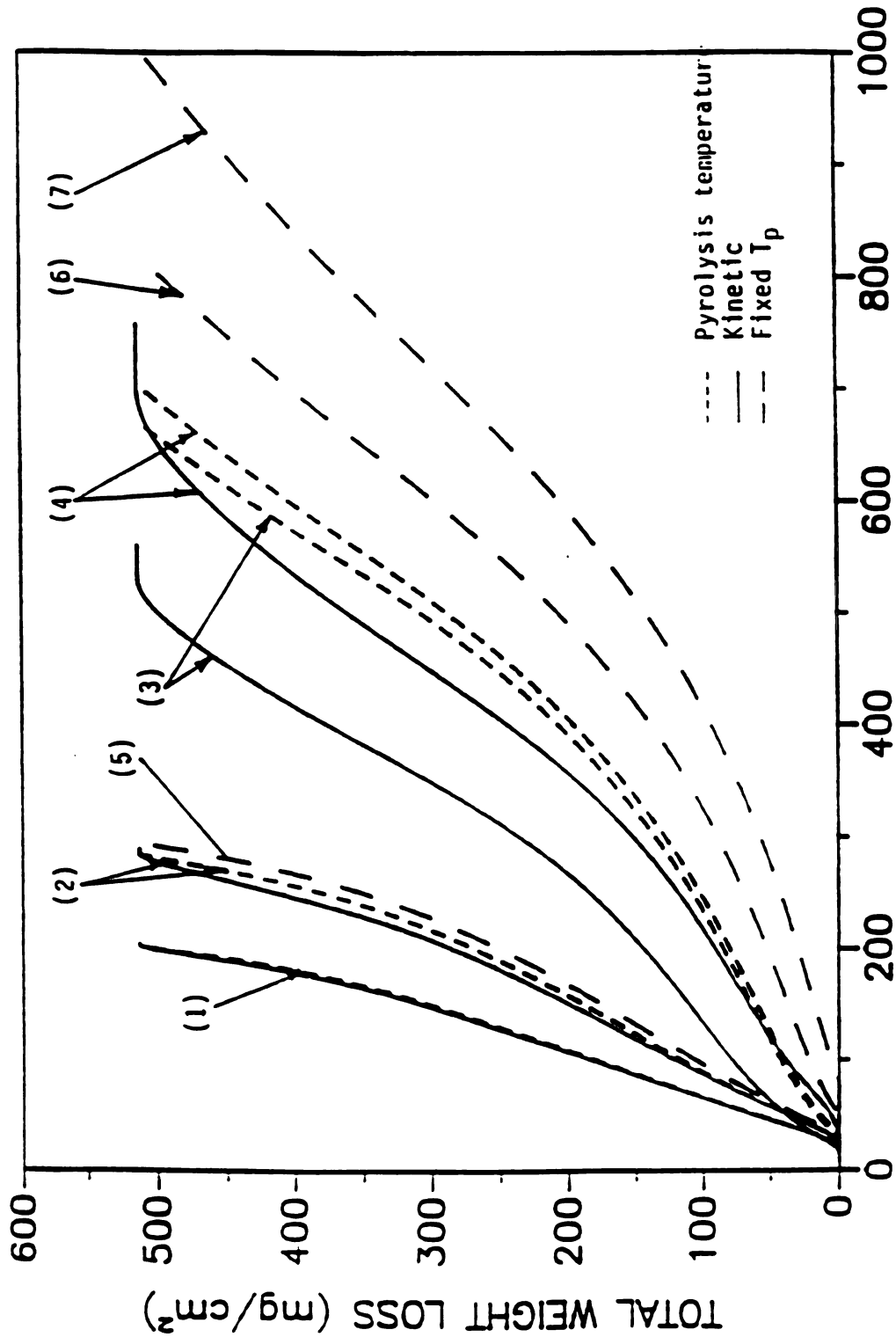

Figure 4.3c Total weight loss, with different front surface heat losses and back surface insulated.

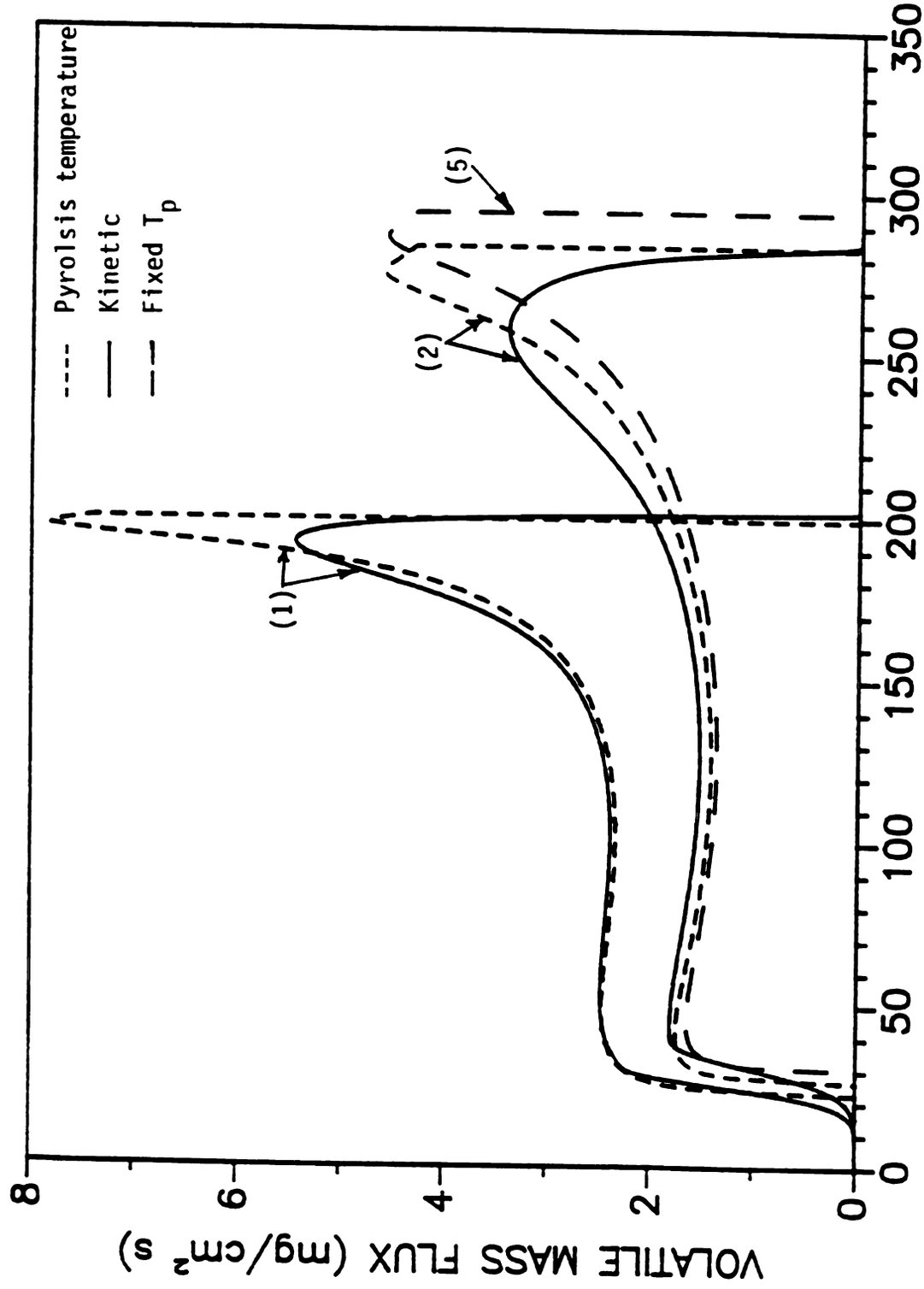

Figure 4.3d Weight loss rate, with different front surface leat losses and back surface insulated.

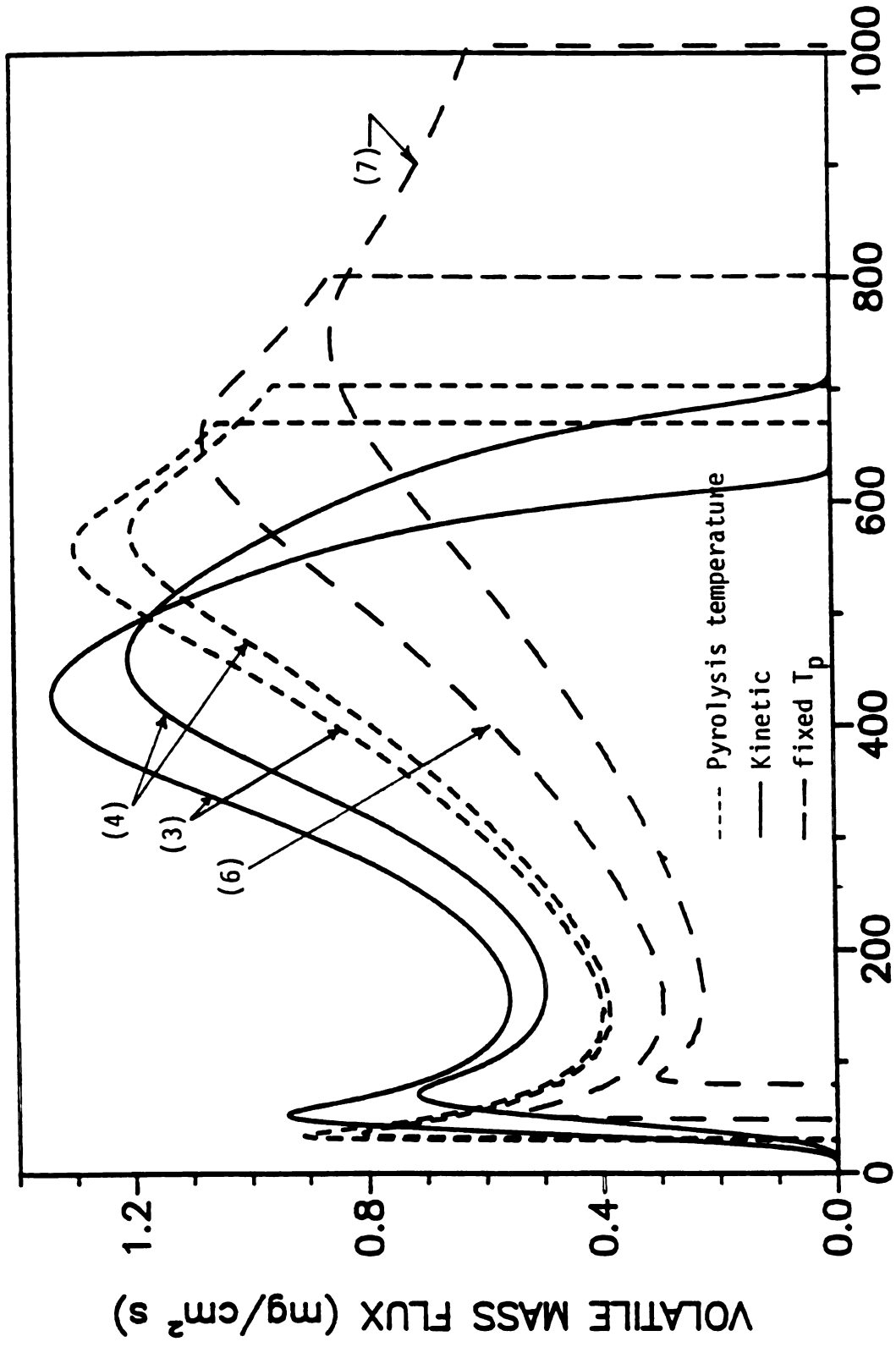

Figure 4.3e Weight loss rate, with different front surface heat losses and back surface insulated.

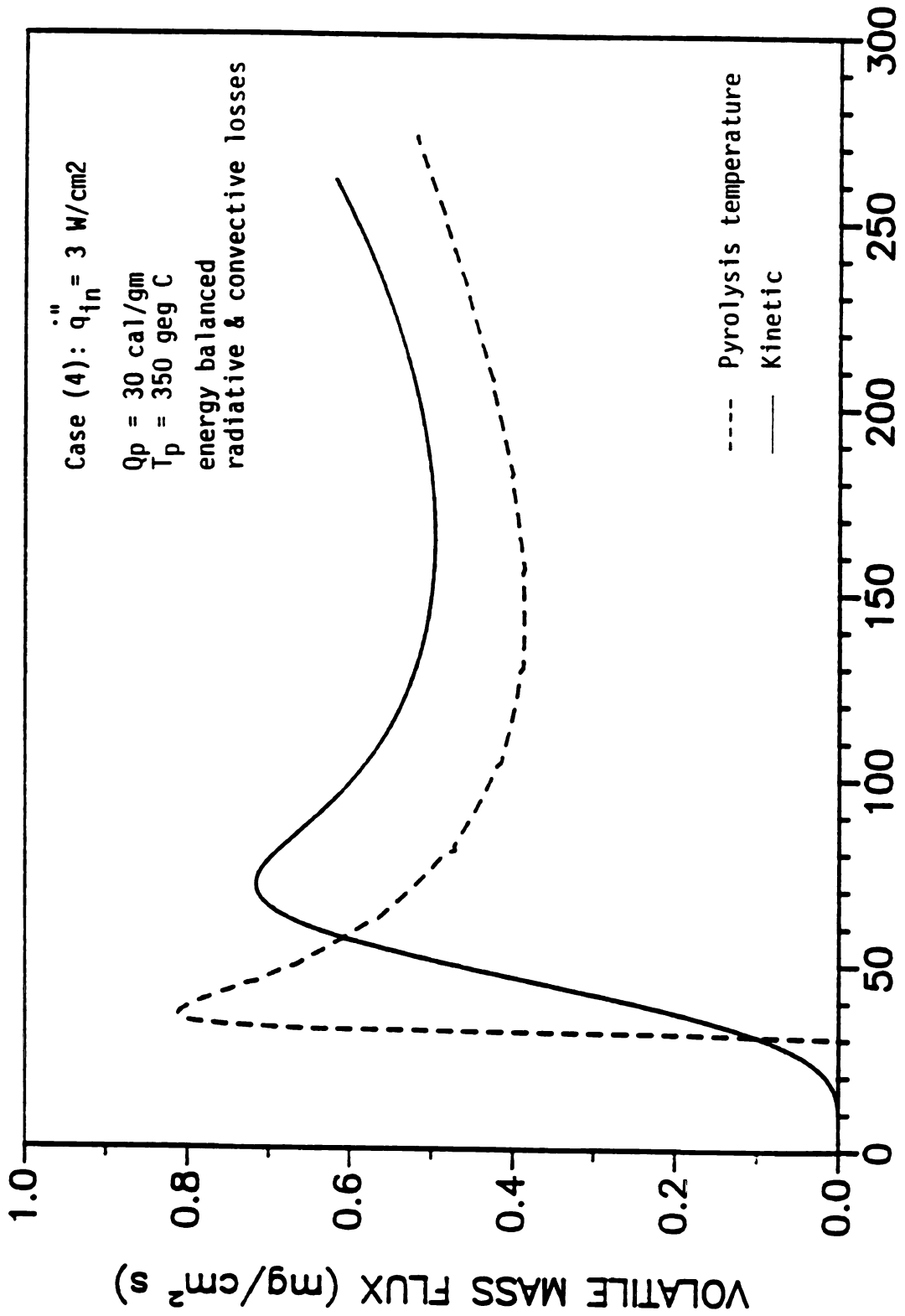

Figure 4.3f Weight loss rate at early times of pyrolysis.

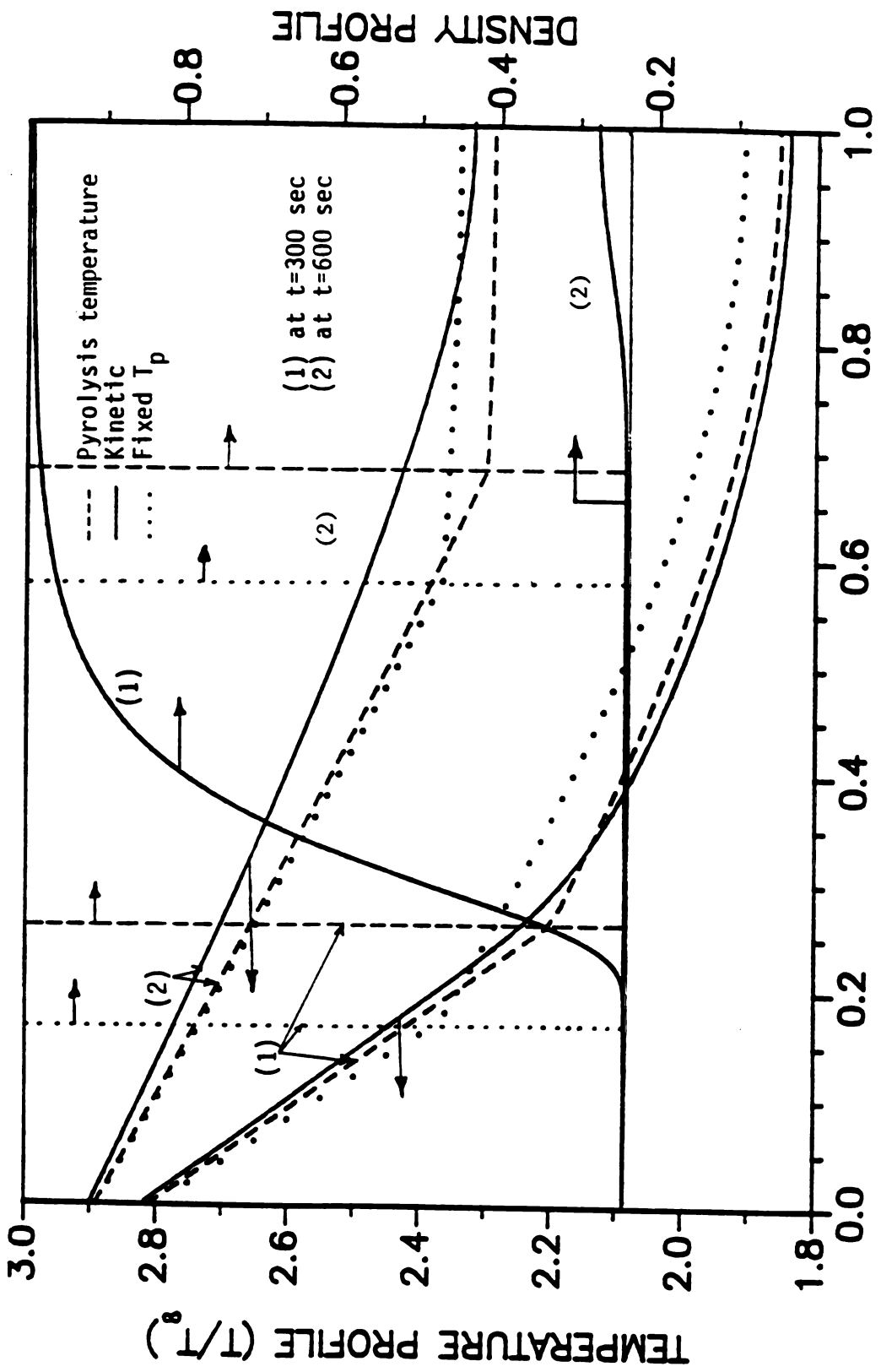

Figure 4.3g Indepth temperature and density profiles in the wood slab with the radiative heat loss at the front surface and the back surface insulated.

Effect of heat of pyrolysis (

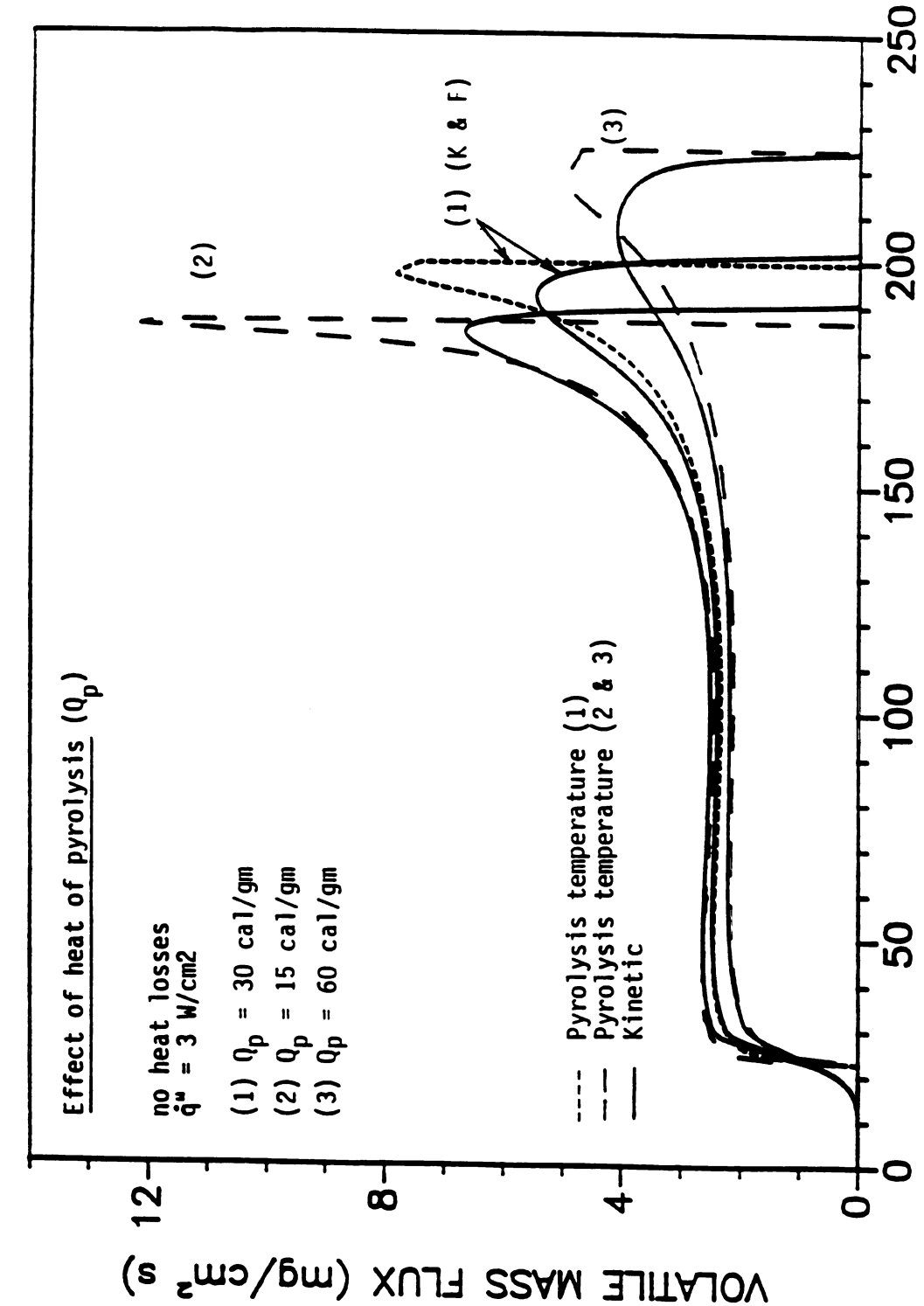

Figure 4.4 Weight loss rates.

Chapter Five

Conclusions and Recommendations

In this work, pyrolysis of thick samples of wood was experimentally investigated. Pyrolysis experiments under different levels of external heat flux and moisture content of wood were conducted in air and in nitrogen atmospheres. A unique small scale combustion-wind tunnel was constructed for these experiments which is useful for obtaining simultaneous transient measurements of several physical and chemical variables. Transient quantitative data on mass flux and pyrolysis products were obtained. In addition, a new approach in the chemical measurements was adopted. For this purpose a simple, but very efficient, catalytic combustor was constructed. A sample of pyrolysis products was burned in this tube. From the products of combustion after the tube, char yield, empirical chemical composition of pyrolysis volatiles, and their heat of combustion were determined. These are new

findings that provide understanding about changes in the chemical and physical parameters during pyrolysis. In the theoretical part, the concept of 'pyrolysis temperature' was investigated.

5.1 Experimental Work

The physical and chemical data obtained during pyrolysis experiments indicate that:

1. External heat flux has the strongest influence on the rate of gasification and temperature distribution. Rate of production of fuel volatiles increases and the char yield decreases as heat flux is increased.

2. Ambient oxygen significantly increases the pyrolysis rate and char oxidation provides additional energy which supplements the external heat flux. Surface and in-depth temperatures, char depth and pyrolysis products show increase in oxygen containing atmosphere.

3. The pyrolysis mass flux does not show a negative one-half power dependency on time. This is conclusive for experiments conducted in air. In the experiments conducted in nitrogen atmosphere in this work the surface temperature (and visual observation) do not show any evidence of char oxidation due to leakage of small amount of air (less than 5%) into the tunnel. However, the comparison of the results with the results of similar experiments in the literature indicates that presence of even small amount of O_2 in the atmosphere may affect the gasification rate.

4. Flow geometery, i.e., position of the sample in the boundary layer flow, can have significant effect on the gasification rate and time of occurrence of its maxima. When the boundary layer starts from the sample edge, it is not convectively well defined and heat and mass transfer are not uniform along the sample.

5. It was found that at lower temperatures in air, chemisorption of oxygen into the surface of freshly produced hot char may occur which reduces the pyrolysis mass flux. This is followed by smoldering and glowing combustion as temperature rises and char oxidation initiates. Therefore, extreme care is needed to provide well defined conditions for experimental study of wood pyrolysis.

6. Moisture content of wood primarily effects the physics of pyrolysis and ignition and its effect on the chemistry of pyrolysis is not significant. It cools the solid as it desorbs and reduces the tar evolution rate and delays ignition time in air. At lower heat fluxes for moist wood, mainly water is desorbed.

7. Char yield in pyrolysis of wood is not constant. It changes during pyrolysis as well as with changes in the external heat flux and moisture content of wood. Lower heat flux and higher moisture contents result in higher char yield.

8. Chemical composition of the pyrolysis products changes during the course of heating as well as with changes in the heating rate and moisture content. Most of the heavy hydrocarbons (tar) evolve at the early times of pyrolysis and more 'carbon' stays inside the solid as char thickens.

5.2 Theoretical work

1. The gasification rate of thermally thick charring materials was investigated. Two models were developed for this purpose; one with infinitely fast decomposition kinetics (pyrolysis temperature model) and the other with finite rate decomposition chemistry (kinetic model).

2. The pyrolysis temperature, which is often treated as a known constant is neither known nor is it a constant. It depends on the net heat flux entering the solid, which in turn depends upon the boundary conditions and the thermal properties of the solid. Each new problem requires a new value of the pyrolysis temperature. An improper choice of this temperature will produce serious errors in the predicted fuel

mass evolution rate.

3. For a given problem, a proper pyrolysis temperature may be chosen by enforcing the overall energy and mass balance between the two models.

4. Despite large differences in the fuel mass evolution rate, the front and back surface temperatures calculated by the two models are in reasonable agreement. This is because the same boundary conditions and heat of pyrolysis are used for both the models. However, significant differences exist in the in-depth temperature and density profiles.

5. The effect of the heat of pyrolysis on both models was similar and no significant differences in the predicted fuel mass flux was observed.

6. Although the pyrolysis temperature assumption considerably simplifies the solution of the governing equations, the results are incomplete because the pyrolysis temperature is unknown.

5.3 Recommendations

There are several topics that can be recommended to extend the present study in the future.

1. Experiments may be conducted in nitrogen atmosphere with only weight loss and surface temperature measurements. The pressure inside the tunnel should be allowed to be slightly above atmosphere in order to prevent any leakages of air into the tunnel and to eliminate any possibility of char oxidation. The results can be compared with the literature to accurately confirm the trend of fall-off of mass loss rate.

2. Similar experiments may be performed in air and in nitrogen with gas phase thermocouple installed very close to the surface of the solid without concerning about weight measurement. This data will show the exothermic gas phase reactions at the

present of O_2 and will help to clerify the question of exothermicity in wood pyrolysis.

3. From the temperature measurements obtained in this study, changes in the thermal properties of the solid can be obtained using an appropriate model.

4. To interpret the experimental results, and for prediction purposes, a detailed numerical model for wood pyrolysis should be developed. Such a model must include moisture desorption and cracking of char. Experimentally obtainad char yield and thermal properties of active material can be incorporated in this model. This model can be extended to include char oxidation as well.

5. It would be interesting to extend the "pyrolysis temperature" model to contain desorption of moisture as a second front traveling inside the solid. Such a model can be compared with a decomposition kinetic model which contains a finite rate kinetics term for moisture desorption.

Appendix A

Appendix A

Data Processing Procedure

As mentioned in section (2.9), the data acquisition system in the fast mode was able to collect data for more than 20 channels in every second. In a typical experiment period of 20 to 30 minutes between 1200 to 1800 data points were collected for more than 20 channels. In many cases 23 channels (12 thermocouples and 11 instruments) were used. During the same period the number of data points for weight loss was 5 to 6 times as much. These data were processed separately for each channel. The data processing procedure consisted of two major steps, namely, smoothing (curve fitting) and lag and response time correction. The FORTRAN code was the one developed by Atreya et. al. (1983). This code was used with minor modifications.

A.1 Smoothing

The raw experimental data curve showed different degrees of fluctuations primarily caused by the electrical disturbances of the equipments. In the case of weight loss measurement in addition to the electronic noise, small fluctuations were caused by the flow within the tunnel and motion of the air within the room. The experimental data had to be smoothed in such a way that while the main characteristics of data were preserved the unwanted disturbances were damped out. For weight loss data this task

was much more critical because the rate of weight loss, which is equal to the pyrolysis mass flux, had to be numerically calculated. Any small discontinuities in the weight loss data are highly magnified in the weight loss rate curves. The curve fitting scheme must ensure continuity of value and continuity of slope as much as possible. The data fitting program fits piece-wise polynomials to a given data set. A small segment* of data points was read into the computer and fitted with an orthogonal polynomial using the least square criterion. For each segment the highest polynomial fit (between 10th degree and a cubic) with no more than one inflection point in the fitted range was chosen. This was done because not more than one inflection point was expected to occur in the physical phenomena.

In order to preserve the continuity in value and slope, a segment was divided into 7 sub-segments and $\frac{6}{7}$ of the neighboring splines were made to overlap. The curve fitted data points were then extracted only from the central $\frac{1}{7}$ portion of the splines. Since the recorded number of data points were too large, the smoothed data were stored every 5 seconds. The results show that this scheme was quite satisfactory and no significant discontinuity was observed in the smoothed data. Only if there was a very sudden change (almost step-wise) in the data, small discontinuities were observed because continuity was not enforced mathematically. Figure A.1 shows a weight loss curve, smoothed data curve, and its derivative which is equivalent to the pyrolysis mass flux (weight loss rate of wood samples). Figure A.2 shows the original (raw) and curve fitted data points for a typical CO_2 measurement. The smoothed data was then corrected for lag and response time.

* The number of data points in a segment (LPOINT) could be varried to obtain the desired degree of smoothness. Typically 35 to 70 number of data points were taken for all signals. For weight about 280 data points were used. Special attention was paid to the selection of LPOINT in order to preserve sharp real which were usually experienced in weight loss rates and chemical species concentrations measurements.

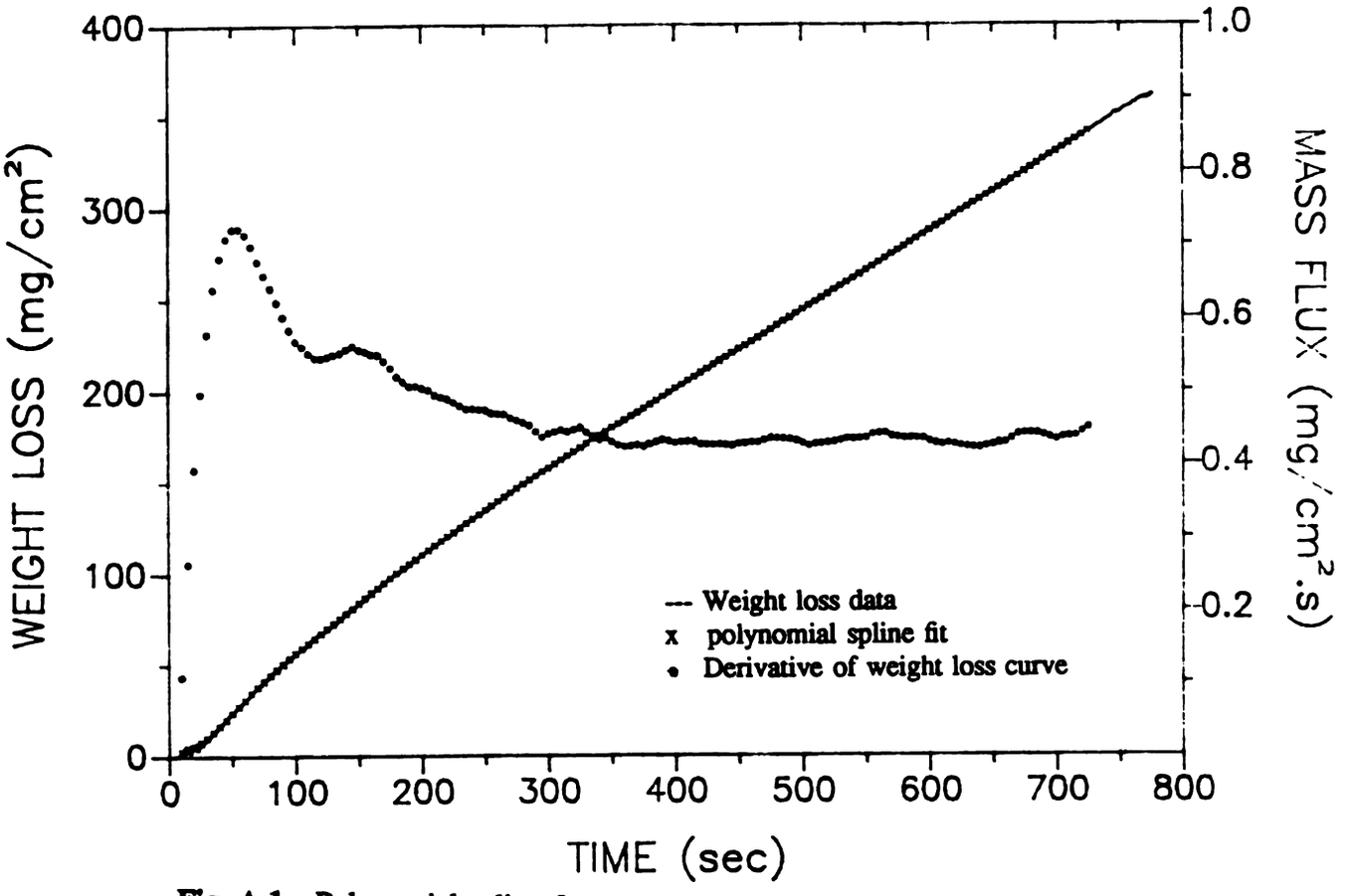

Fig. A.1 Polynomial spline fit and rate calculation of weightloss data.

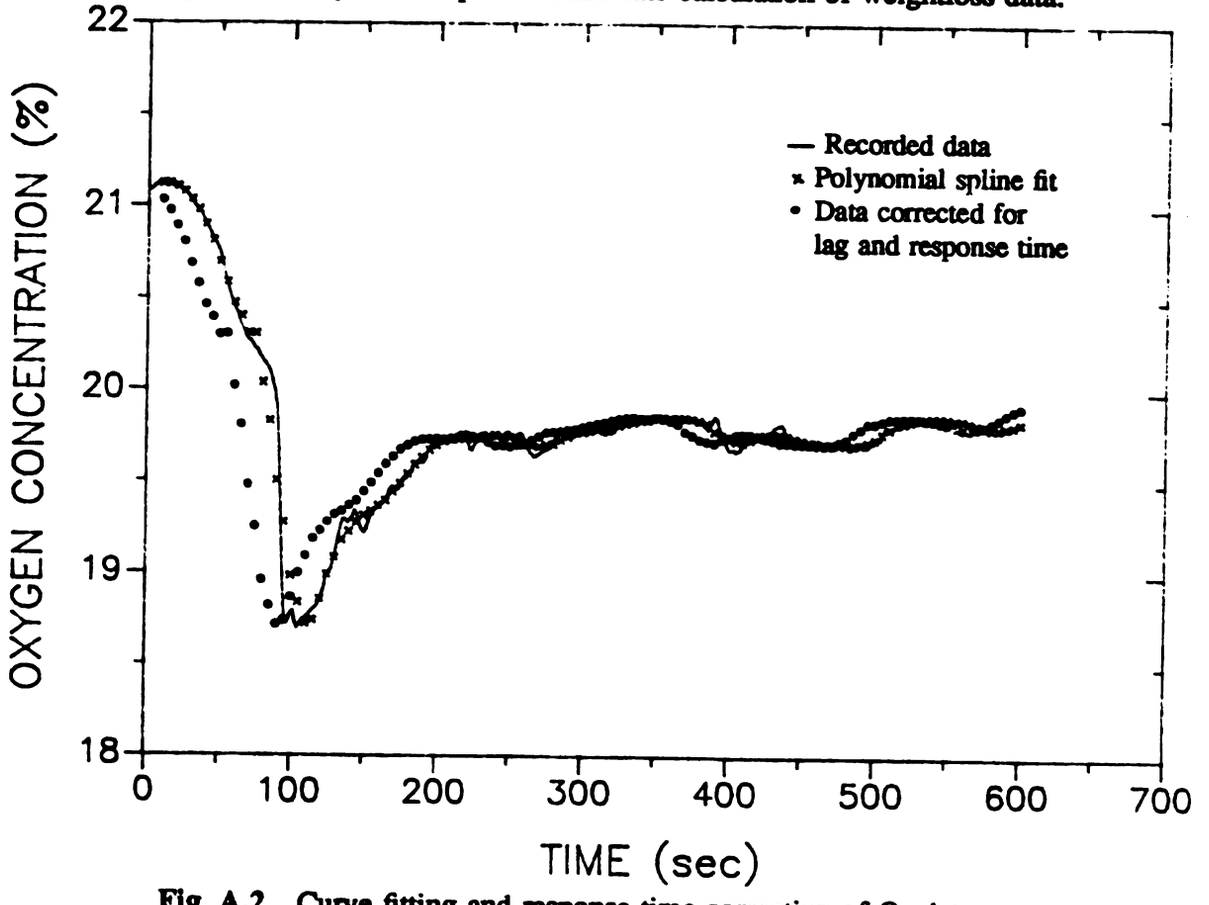

Fig. A.2 Curve fitting and response time correction of O_2 data.

A.2 Lag Time and Response Time Corrections

During the experiment some measurements such as weight loss, temperature, heat flux and pressure are fast enough to be considered instantaneous.For others, such as gas analysis equipment it takes some time for the information to reach the instrument. This time lag can be measured and simply subtracted from the recorded time. Further, the instrument has a response time which it takes before it can react to the information. The recorded data, therefore, has to be corrected for this response time. The response time of each instrument has to be determined experimentally.

The correction method described below and the computer program was adapted from Atreya (1983).It utilizes the response of the measuring system to a unit step. A typical recorded output of an instrument to a unit step input is typically shown in Figure A.4. The instrument response is the same as the recorded output corrected for the lag time. This is modeled as a transient process within the instrument.

Consider a gas analyzer where the gases are completely mixed while passing through the it. The outlet concentration, therefore, will be the same as concentration of the gases within the instrument at any instant. This is similar to a lumped heat capacitance system in which it is assumed that the instantanuous temperature T of every point within the body is the same at any time. Figure A.3 schematically represents such a well stirred system.

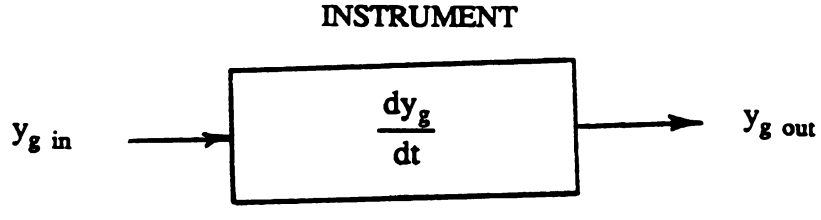

Figure A.3 A well stirred system.

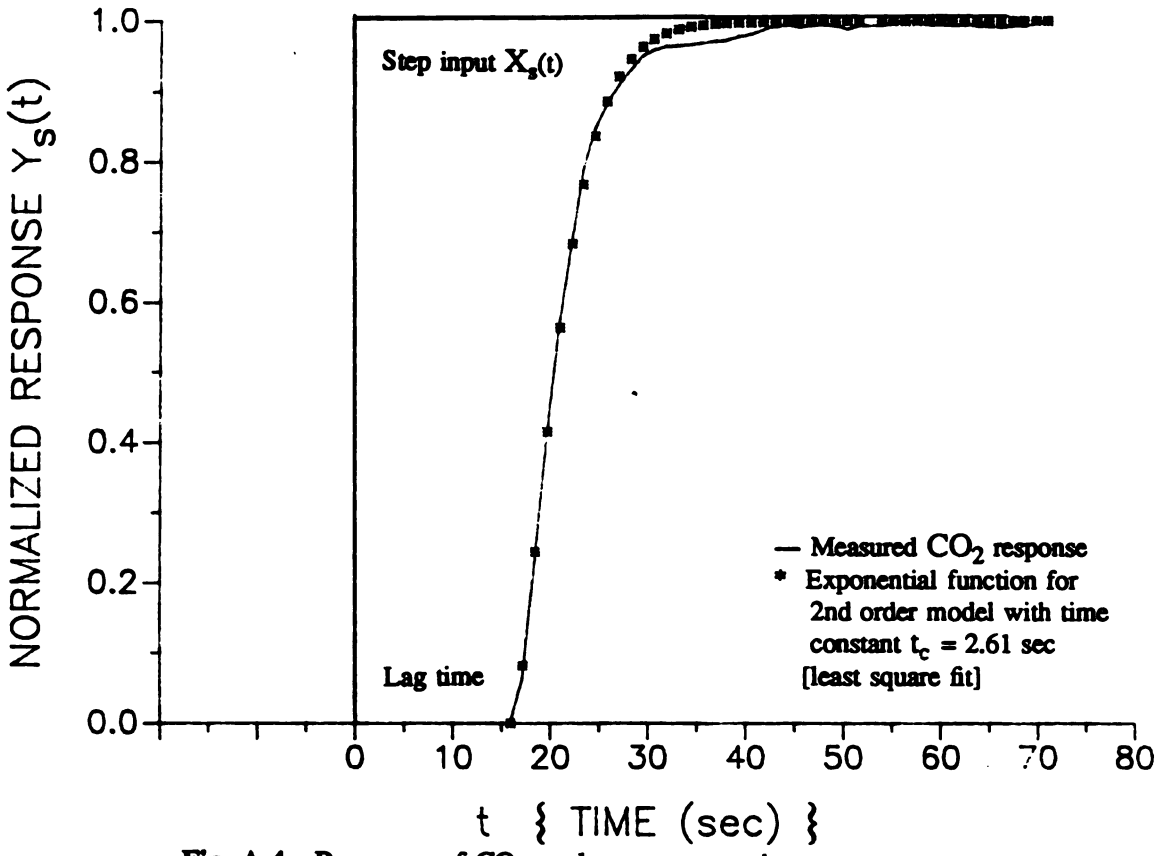

Fig. A.4 Response of CO_2 analyzer to a step input.

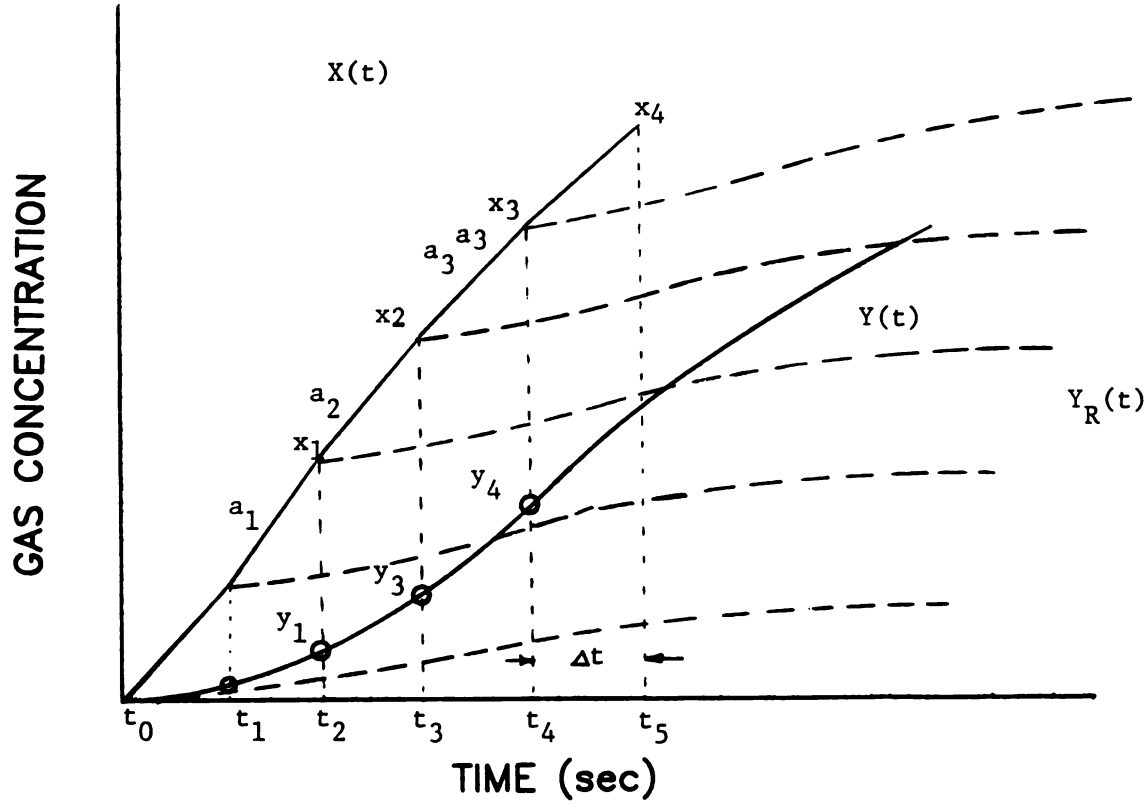

Fig. A.5 Recorded response to a peice-wise linear input.

Species mass balance for the stirred reactor of volume V is given by

$$\frac{\rho V}{\dot{m}}\left(\frac{dY_g}{dt}\right) = Y_{g,in} - Y_{g,out} . \qquad \text{(A-1)}$$

in which ρ is the density of the gas, $\dot{m}$ is the mass flux and Y_g is the mole fraction of the specie in the mixture..ps 12 Using $Y_{g,out} = Y_g$ and letting $\frac{\rho V}{\dot{m}} = t_c$ we will get:

$$\left[1 + t_c \frac{d}{dt}\right] Y_g = Y_{g,in} . \qquad \text{(A-2)}$$

This equation represents the instrument response Y_g to the input signal $Y_{g,in}$.

Some instruments are better modeled as containing two well stirred reactors in series. The governing equation for such systems is:

$$\left[t_c^2 \frac{d^2}{dt^2} + 2t_c \frac{d}{dt} + 1\right] Y_g = Y_{g,in} \qquad \text{(A-3)}$$

The response of the first order system modeled by equation (A-1) to a unit step input is

$$Y_s(t) = 1 - e^{-\frac{t}{t_c}} , \qquad \text{(A-4)}$$

and the response of the second order system modeled by equation (A-2) is given by

$$Y_s(t) = 1 - \left(1 + \frac{t}{t_c}\right) \exp\left(1 - \frac{t}{t_c}\right) . \qquad \text{(A-5)}$$

The only unknown in these equations is the time constant, t_c which is experimentally determined. For a more complicated time dependent input data X(t), the instrument response (for a sufficiently linear instrument) can be found by adding up the responses of the instrument to step inputs according to the Duhamel's superposition integral

$$Y(t) = \int_0^t Y_s(t-\tau)\,\frac{dx}{dt}\,d\tau \qquad \text{(A-6)}$$

Here, Y(t) is the measured output and $Y_s(t)$ is given by equation (A-4) or (A-5) for first or second order systems. Y(t) consists of a set of measured values $Y_i\,(t_i)$ at fixed time intervals $\Delta t\ (= t_{i+1} - t_i)$, and we want to find out a corresponding set of input values $X_i\,(t_i)$.

Assuming that the input X(t) to be piece-wise linear [Figure A.5], then the corresponding recorded output, Y(t), can be reconstructed by superposition of the ramp inputs. Each linear input ramp will be $X_j = a\,\tau_j + b$. The response of the analyzer to a ramp input is obtained from integrating equation (A-6) with Y_s from (A-5):

$$Y_{R_j}(t) = a_j \int_{t_{j-1}}^{t_j} \left(1 - e^{-\frac{t-\tau}{t_c}} - \frac{t-\tau}{t_c} e^{-\frac{t-\tau}{t_c}}\right) d\tau$$

$$= a_j \left(\Delta t + (t_j - t - 2t_c)\, e^{-\frac{t-t_j}{t_c}} - (t_{j+1} - t - 2t - 2t_c)\, e^{-\frac{t-t_{j-1}}{t_c}}\right) \qquad \text{(A-7)}$$

and for j=i and $t = t_i$

$$Y_{Ri}(t) = a_i \left[\Delta t - 2t_c - (-\Delta t - 2t_c)\, e^{-\frac{\Delta t}{t_c}}\right] \qquad \text{(A-8)}$$

The recorded output $Y_i(t_i)$ at any instant t_i, [Figure A.5], is the sum of responses of ramp inputs at previous times (t_{j-1}, with j=0 to i) plus response of ramp input at time i [Eq. (A-4)]. Therefore,

$$Y_i(t_i) = \sum_{j=0}^{i-1} Y_{R_j}(t_i) + Y_{R_i}(t_i)$$

$$= \sum_{j=0}^{i-1} Y_{R_j}(t_i) + a_i \left[\Delta t - 2t_c + (\Delta t + 2t_c)\, e^{-\frac{\Delta t}{t_c}}\right] \qquad \text{(A-9)}$$

In this equation the only unknown is a_i. Once a_i is known the input (piece-wise linear) will be $X_i(t_i) = X_{i-1} + a_i \Delta t$. The time constant of each instrument was found by introducing a known step input and using a least square method to match approximately with a first or second order system.

A calculation scheme where a_i (i=1,2,...,n) and hence X_i (i=1,2,...,n) were successfully determined from the knowledge of t_c, t_i, and Y_i (i=0,1,...,n) was used for the response time corrections of CO, CO_2, O_2, H_2O, and [THC] analyzers. The response of the dew point hygrometer was better modeled by a first order system and, except for the change in equation (A-1), an identical procedure was used.

The error due to the response time of instruments is basically due to the uncertainty of predicting the slope of the piece-wise linear input from the recorded output (Appendix A). Atreya (1983) discussed the error in the prediction of these values. He showed that for stability of the numerical criterion with a given measurement error, it may be necessary to use a fixed constant time correction factor t_{cb}, and in each time t_i shoot for the current time ($t_i - t_{cb}$) instead of the time step Δt. The values of t_{cb} were determined such that the prediction of the input signals be stable. Values of t_{cb} were typically between 10 to 40 percent of the instruments time

constants. Since both the instruments and the data reduction procedure were mainly the same as used by Atreya (1983), the discussion will not be repeated here.

Appendix B

Appendix B

Finite Difference Equations and Methods of Solution

In this appendix the numerical methods for solving the "pyrolysis temperature" and the "decomposition kinetics" models which were formulated in chapter 4 are described and the finite-difference equations are presented.

B.1 Pyrolysis Temperature Model

The numerical method for solving this problem is similar to that of Ehrlich (1954) with several modifications to improve the accuracy of the results and the stability of the numerical scheme. There exist several different methods in the literature for solving this Stefan-type problem. Most of these methods, however, primarily address the prediction of temperature profiles and the time dependent location of the phase change interface, corresponding to a "charring front" in this problem. These methods fail to correctly predict the rate of the propagation of the interface at the early times of phase-change process. Physically, the phase change rate

may not start at a finite value, but it has to begin from zero and increase subsequently. The method adopted in this work successfully predicts the charring rate of wood (as a phase-change problem) at the starting times as well as the large times.

B.2 Nondimensioalization

The governing equations and boundary conditions are normalized by defining:

$$\theta = \frac{T}{T_\infty},\ \eta = \frac{x}{L},\ \tau = \frac{k_w t}{\rho_w C_{p_w} L^2},\ \beta = \frac{\alpha_w}{\alpha_c},$$

$$\gamma = \frac{k_c}{k_w},\ r = \frac{\Delta\tau}{\Delta\eta^2} = \frac{k}{h^2} \qquad \text{(B-1)}$$

Phase I. Inert heating of wood slab

Before onset of pyrolysis; for t > 0 and $T_s < T_p$

$$G.E. \qquad \frac{\partial\theta_w}{\partial\tau} = \frac{\partial^2\theta_w}{\partial\eta^2} \qquad \text{(B-2)}$$

Boundary conditions:

$$1)\quad -\frac{\partial\theta_w}{\partial\eta}(0,\tau) = (b_1 + b_2 + b_3) - \theta_1(b_2\theta_1^3 + b_3) \qquad \text{(B-3)}$$

$$2)\quad -\frac{\partial\theta_w}{\partial\eta}(1,\tau) = 0 \qquad \text{(B-4)}$$

where

$$b_1 = \frac{L}{k_w T_\infty}\dot{q}''_{in}$$

$$b_2 = \frac{\sigma\,\varepsilon\,L\,T_\infty^3}{k_w}$$

$$b_3 = \frac{h\,L}{k_w}$$

Initial condition:

$$\theta\,(\eta,0) = 1 \qquad \text{(B-5)}$$

Phase II. Charring of Wood

Governing Equations:

I) On the wood side:

$$\frac{\partial\theta_w}{\partial\tau} = \frac{\partial^2\theta_w}{\partial\eta^2} \qquad \text{(B-6)}$$

II) On the char side:

$$\frac{\partial\theta_c}{\partial\tau} = \frac{1}{\beta}\,\frac{\partial^2\theta_c}{\partial\eta^2} \qquad \text{(B-7)}$$

Boundary conditions:

$$1)\quad -\frac{\partial\theta_c}{\partial\eta}(0,\tau) = \frac{1}{\gamma}\,(\,b_1 + b_2 + b_3\,) - \theta_1(\,b_2\theta_1^{\,3} + b_3) \qquad \text{(B-8)}$$

$$2)\quad -\frac{\partial\theta_c}{\partial\eta}(1,\tau) = 0 \qquad \text{(B-9)}$$

At the interface of char and wood, i.e., at $x=x_p$

$$\eta_p(\tau) = (w-1)\,\Delta\eta + s\,(\tau)\,\Delta\eta = [(w-1) + s\,(\tau)\,h] \qquad \text{(B-10)}$$

and

$$\gamma\,\frac{\partial\theta_c}{\partial\eta} - \frac{\partial\theta_w}{\partial\eta} = b_4\,h\,\frac{ds}{d\tau} \qquad \text{(B-11)}$$

where $b_4 = \dfrac{Q_p}{C_{p_w} T_\infty}$

B.3 The Finite Difference Equations

The basic method is Crank-Nicolson with a linear temperature profile within a nodal control volume. fully implicit scheme is used for some "special" cases to improve the stability of the numerical scheme. The set of finite difference equations for the phase I are as follows:

Node 1 : (implicit)

$$\left[3+4rh\left(\frac{1}{h}+b_2X_1+b_3\right)\right]\theta_1^{j+1} + (1+4r)\,\theta_2^{j+1}$$

$$= \left[3-4rh\left(\frac{1}{h}+b_2X_1+b_3\right)\right]\theta_1^{j} + (1+4r)\theta_2^{j} + 8rh(b_1+b_2+b_3) \qquad \text{(B-12)}$$

in which

$$X_1 \equiv (\theta_1^{j+1})^3 = \left[\frac{\theta_1^{j+1}+\theta_1^{j}}{2}\right]^3$$

Interior Nodes:

$$\left[\frac{1-4r}{6+8r}\right]\theta_{i-1}^{j+1} + \theta_i^{j+1} + \left[\frac{1-4r}{6+8r}\right]\theta_{i+1}^{j+1}$$

$$= \left[\frac{1+4r}{6+8r}\right]\left(\theta_{i-1}^{j} + \theta_{i+1}^{j}\right) + \left[\frac{6-8r}{6+8r}\right]\theta_i^{j} \qquad \text{(B-13)}$$

Last node (insulated); (implicit)

$$\left(\frac{1}{4}-r\right)\theta_N^{j+1} + \left(\frac{3}{4}+r\right)\theta_{N+1}^{j+1} = \left(\frac{3}{4}-r\right)\theta_{N+1}^{j} + \left(\frac{1}{4}+r\right)\theta_N^{j} \qquad \text{(B-14)}$$

B.4 Phase II: Charring of Wood

1. Node 1 at the start of charring (implicit):

$$\left[\frac{\beta}{2r}s^2_{j+1} + (\frac{b_2 h}{\gamma} + \frac{b_3 h}{\gamma})s_{j+1} + 1\right] =$$

$$\frac{\beta}{2r}s^2_{j+1}\,\theta_1^{\,j} + \theta_p + \frac{hs_{j+1}}{\gamma}(b_1+b_2+b_3) \qquad \text{(B-15)}$$

2. First node when the first slice is all charred; (implicit):

$$\left[3\beta\gamma+4rh(\frac{\gamma}{h}+b_2X_1+b_3)\right]\theta_1^{\,j+1} + (\beta\gamma-4rh)\theta_2^{\,j+1}$$

$$= \left[3\beta\gamma-4rh(\frac{\gamma}{h}+b_2X_2+b_3)\right]\theta_1^{\,j} + (\beta\gamma+4rh)\theta_2^{\,j} + 8rh\,(b_1+b_2+b_3) \qquad \text{(B-16)}$$

3. "Regular" nodes on the char side:

$$\left[\frac{\beta-4r}{6\beta+8r}\right]\theta_{i-1}^{\,j+1} + \theta_i^{j+1} + \left[\frac{\beta-4r}{6\beta+8r}\right]\theta_{i+1}^{\,j+1}$$

$$= \left[\frac{\beta+4r}{6\beta+8r}\right](\theta_{i-1}^{\,j}+\theta_{i+1}^{\,j}) + \left[\frac{6\beta-8r}{6\beta+8r}\right]\theta_i^{\,j} \qquad \text{(B-17)}$$

4. Node w adjacent to the interface on the char side; (implicit):

$$-\left[\frac{2rs_{j+1}}{1+s_{j+1}}\right]\theta_{w-1}^{\,j+1} + (2r+\beta s_{j+1})\theta_w^{\,j+1} = s_{j+1}\beta\theta_w^{\,j} + \frac{2r}{1+s_{j+1}}\theta_p \qquad \text{(B-18)}$$

5. Node w+1 adjacent to the interface on the wood side; (implicit):

$$(2-s_{j+1})(1+2r-s_{j+1})\theta_{w+1}{}^{j+1} - 2r(1-s_{j+1})\theta_{w+2}{}^{j+1} =$$

$$(2-sj+1)(1-s_{j+1})\theta_{w+1}{}^{j} + 2r\theta_p \qquad \text{(B-19)}$$

6. "Regular" nodes on the wood side; (Crank-Nicolson):

$$\left[\frac{1-4r}{6+8r}\right]\theta_{i-1}{}^{j+1} + \theta_i{}^{j+1} + \left[\frac{1-4r}{6+8r}\right]\theta_{i+1}{}^{j+1} =$$

$$\left[\frac{1+4r}{6+8r}\right](\theta_{i-1}{}^{j}+\theta_{i+1}{}^{j}) + \left[\frac{6-8r}{6+8r}\right] \qquad \text{(B-20)}$$

7. Last node when charring: (implicit)

$$\left[(1-s_{j+1})^2+2r\right]\theta_{N+1}{}^{j+1} = 2r\theta_{N+1}{}^{j} + (1-s_{j+1})^2\theta_{N+1}{}^{j} \qquad \text{(B-21)}$$

Finite difference equations for char-wood interface:

a. At the start of charring: at $\eta = 0$,

$$\frac{\partial\theta_c}{\partial\eta} = -\frac{b_1}{\gamma} \qquad \text{(B-22)}$$

expanding $\frac{\partial\theta_c}{\partial\eta}$ about $(0, \tau)$ and using

$$\frac{\partial\theta_c}{\partial\tau} = \frac{1}{\beta}\frac{\partial^2\theta_c}{\partial\eta^2}$$

we get

$$\frac{\partial\theta_c}{\partial\eta} = \frac{1}{\gamma}\Delta_2 \qquad \text{(B-23)}$$

where

$$\Delta_2 = -\frac{b_1 h}{\gamma} + \beta\, s_{j+1}\frac{\theta_1^{(j+1)} - \theta_1^{j}}{r} \tag{B-24}$$

This equation will be used until there are at least two nodes on the char side.

b.1 As the charring continues

$$\frac{\partial \theta_c}{\partial \tau} = \frac{1}{h}\Delta_2 \tag{B-25}$$

where

$$\Delta_2 = \left[\frac{s_{j+1}}{1+s_{j+1}}\theta_{w-1}^{\,j+1} - \frac{1+s_{j+1}}{s_{j+1}}\theta_w^{\,j+1} + \frac{1-2s_{j+1}}{s_{j+1}(1+s_{j+1}}\theta_p\right] \tag{B-26}$$

and

$$\frac{\partial \theta_w}{\partial \tau} = \frac{1}{h}\Delta_1 \tag{B-27}$$

where

$$\Delta_1 = \left[\frac{2-s_{j+1}}{1-s_{j+1}}\,\theta_{w+1}^{\,j+1} - \frac{1-s_{j+1}}{2-s_{j+1}}\,\theta_{w+2}^{\,j+1} - \frac{1-2(1-s_{j+1})}{(1-s_{j+1})(2-s_{j+1})}\theta_p\right] \tag{B-28}$$

c. when $s_{j+1} \to 0$ or $s_{j+1} \to 1$, we will have

$$\frac{\partial \theta_c}{\partial \tau} = \frac{1}{2h}\Delta_2 \tag{B-29}$$

where

$$\Delta_2' = \left[(1-2s_{j+1})\theta_{w-2}^{\,j+1} - 4(1-2s_{j+1})\theta_{w-1}^{\,j+1} + (3-2s_{j+1})\theta_w^{\,j+1}\right] \tag{B-30}$$

and

$$\frac{\partial \theta_w}{\partial \tau} = \frac{1}{2h}\Delta_1 \tag{B-31}$$

where

$$\Delta_1' = \left[-(5-2s_{j+1})\,\theta_{w+1}^{j+1} + 4(2-s_{j+1})\theta_{w+2}^{j+1} - (3-2s_{j+1})\,\theta_{w+3}^{j+1} \right] \tag{B-32}$$

B.5 The Method of Solution

The above equations when, considered for the related cases, provide a system of N+1 equations that have to be solved simultaneously. The N+1 unknown temperatures and the location of char-wood interface or alternatively s_{j+1} being the other unknown for which the interface equation provides the extra equation needed. For the approximation of the new location of the interface we will use:

$$s_{j+1} = \frac{r}{a_4}(\gamma\,\Delta_2 - \Delta_1) + s_j \tag{B-33}$$

such that

If $\eta_{j+1} < 1.25$ use Δ_2' in (B-33)

If $0.75 < s_{j+1} < 0.25$ use Δ_1' in (B-33)

If $0 < s_{j+1} < 0.25$ use w_{j+1} in Δ

otherwise use () as is.

For the initial approximation of s_{j+1} value at the onset of charring, the exact solution to the melting of a metal slab with ablation [Landau (1949)] is used to determine $\frac{ds}{dt}$ as follows:

$$\frac{ds}{dt} = \frac{2}{\pi}\frac{\dot{q}_{in}C_{pw}L}{k_w Q_{p0}}\,arctan\left[\frac{\tau}{\tau_p}-1\right]^{\frac{1}{2}} \tag{B-34}$$

in which τ_p is the time when pyrolysis begins. The initial approximation for s_{j+1} will be $s_{j+1} = \frac{ds}{dt}\Delta\tau$. For every new approximation of s_{j+1} the tridiagonal system of N+1

equations are solved iteratively for temperatures using the recursion solution given by Carnahan et. al. (1969). Once the solution converges for temperatures a new value for s_{j+1} is approximated and the procedure continues until s_{j+1} is also converged. To accelerate the convergence of the iteration process every new guess for s_{j+1} is found by using an underrelaxation or an interpolation between the old value of s_{j+1} and its new value. The underrelaxation factor ω was determined by trial and error such that the best convergence was achieved.

The process continues until the char interface comes very close to the next node at the boundary of two adjacent slices. when $| s_{j+1}-1 |$ is less than a pre-specified error criterion, charring of that slice is completed. Here, to avoid passage of the interface from across a nodal boundary before convergence, the time step is cut shorter successively until it converges. The validity of the results was examined by comparing the numerical solution for phase change problems at constant surface temperature with the exact solution [Carslaw and Jaeger (1959)] for freezing of water and the results were in very close agreement.

B.6 The Decomposition Kinetics Model

Using the Crank-Nicolson scheme, the finite-difference form of the governing equations will be:

$$\left[\rho_a C_{p_a}+\rho_c C_{p_c}\right]\left[\frac{T_i^{j+1}-T_i^j}{\Delta t}\right]\Delta x = k_s\left[\frac{T_{i+1}^{j+\frac{1}{2}}-2T_i^{j+\frac{1}{2}}+T_{i-1}^{j+\frac{1}{2}}}{\Delta x}\right] - \Delta x\left[\frac{\partial \rho_s}{\partial t}\right]_i^{j+\frac{1}{2}}\left[Q_p+h_s\right]_i^{j+\frac{1}{2}} \tag{B-35}$$

in which

$$\left[\frac{\partial \rho_s}{\partial t}\right]_i^{j+\frac{1}{2}} = -A\,\frac{\rho_{s,i}^{j+\frac{1}{2}}-\rho_f}{1-\frac{\rho_f}{\rho_i}}\exp\left[\frac{E}{RT_i^{j+\frac{1}{2}}}\right] \tag{B-36}$$

For the interface nodes $1<i<N+1$ we'll get

$$m_i\,T_{i-1}^{j+1} + u_i\,T_i^{j+1} + f_i\,T_{i+1}^{j+1} = b_i \tag{B-37}$$

where

$$m_i = -\frac{k_s}{2\Delta x} \tag{B-38}$$

$$u_i = \left[(\rho_a C_{p_a}+\rho_c C_{p_c})\frac{\Delta x}{\Delta t} + \frac{k_s}{\Delta x}\right] \tag{B-39}$$

$$f_i = -\frac{k_s}{2\Delta x} \tag{B-40}$$

$$b_i = \left(\frac{k_s}{2\Delta x}\right) T_{i-1}^{j} + \left[(\rho_c C_{p_c}) - \frac{k_s}{\Delta x}\right]T_i^j + \frac{k_s}{2\Delta x} + D_i \tag{B-41}$$

and

$$D_i = -\Delta x\left[\frac{\partial \rho_s}{\partial t}\right]_i^{j+\frac{1}{2}}\left[Q_p + (h_a-h_c)\,\frac{\frac{\rho_f}{\rho_w}}{1-\frac{\rho_f}{\rho_w}}\right]_i^{j+\frac{1}{2}} \tag{B-42}$$

$$h_a^{j+\frac{1}{2}} = C_{P_a}(\overline{T}_i - T_\infty) \tag{B-43}$$

$$h_{c,i}^{j+\frac{1}{2}} = C_{P_c}(\overline{T}_i - T_\infty) \tag{B-44}$$

$$\overline{T}_i = \frac{\overline{T}_i^{j+1} + \overline{T}_i^{j}}{2} \tag{B-45}$$

For the surface Node i=1

$$u_1 T_1^{j+1} + f_1 T_2^{j+1} = b_1 + c_1 \tag{B-46}$$

where

$$u_1 = \frac{1}{2}(\rho_a C_{p_a} + \rho_c C_{p_c})\frac{\Delta x}{\Delta t} + \frac{k_s}{2\Delta x} + \frac{h}{2} + \frac{1}{2}\varepsilon\sigma\left[T_1^{j+\frac{1}{2}}\right]^3 \tag{B-47}$$

$$f_1 = -\frac{k_s}{2\Delta x} \tag{B-48}$$

$$b_1 = \left[\frac{1}{2}(\rho_a C_{p_a} + \rho_c C_{p_c})\frac{\Delta x}{\Delta t} - \frac{k_s}{2\Delta x} - \frac{h}{2} - \frac{1}{2}\varepsilon\sigma(T_1^{j+\frac{1}{2}})^3\right]T_1^j + \frac{k_s}{2\Delta x}T_2^j + D_1 \tag{B-49}$$

and

$$D_1 = -\frac{1}{2}\Delta x\left[\frac{\partial \rho_s}{\partial t}\right]_1^{j+\frac{1}{2}}\left[Q_p + h_s\right]_1^{j+\frac{1}{2}} \tag{B-50}$$

$$c_1 = \dot{q}_{in} + h\,T_\infty + \varepsilon\sigma\,T_\infty^4 \tag{B-51}$$

For i = N+1 (insulated)

$$\frac{1}{2}(\rho_a C_{p_a})(\rho_c C_{p_c})\left[\frac{T_{n+1}^{j+1} - T_{n+1}^{j}}{\Delta t}\right]\Delta x$$

$$= k_s \frac{T_n^{j+\frac{1}{2}} - T_{n+1}^{j+\frac{1}{2}}}{\Delta x} - \frac{\Delta x}{2}\left[\frac{\partial \rho_s}{\partial t}\right]_{N+1}^{j+\frac{1}{2}} (Q + h_s)_{N+1}^{j+\frac{1}{2}} \qquad \text{(B-52)}$$

B.7 Method of Solution

The method of solution of the decomposition kinetic model is described in detail by Atreya (1983). The system of (N+1) linear equations are solved to determine the (N+1) unknown temperatures ($T_i^{j+\frac{1}{2}}$). In this case, the density of the solid is continuously changing as the wood is heated. Changes in 'ρ_s' are calculated from equation (B-36) and the mean density during a time step ($\rho_{s,i}^{j+\frac{1}{2}}$) is obtained. Then the system of N+1 linear equations is solved to determine new values of $T_i^{j+\frac{1}{2}}$, i=1,...., N+1. The convergence is checked based on the difference between the new predicted value and the previous one. The iteration continues until it is converged. The next time step is evaluated and the procedure is repeated for the new time step.

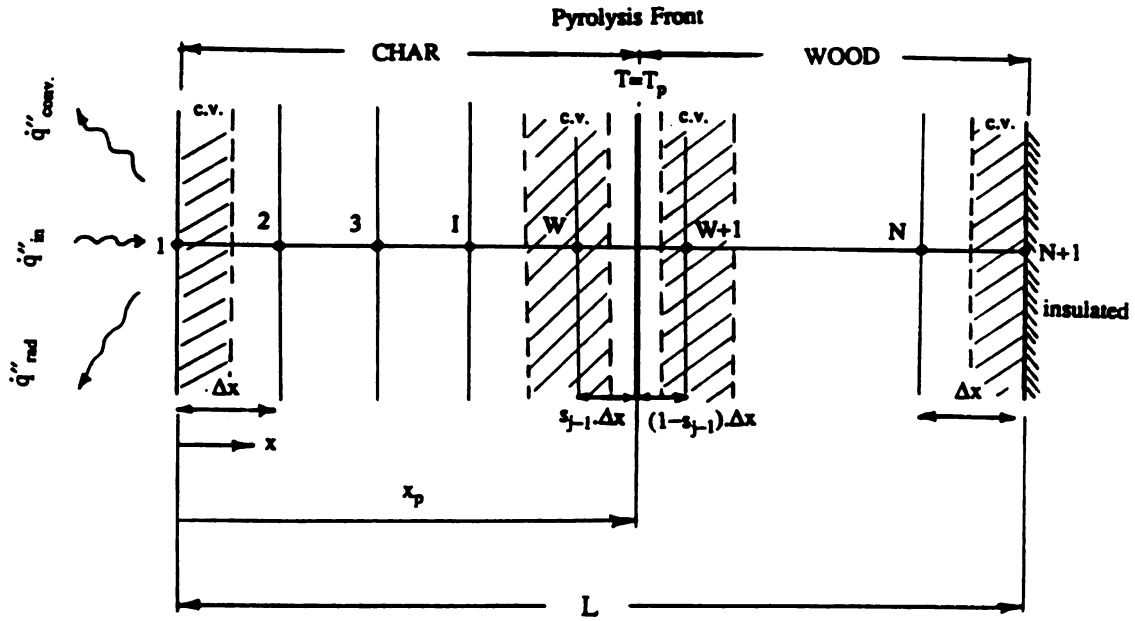

Figure B.1 Schematic of finite-difference numerical method for pyrolysis temperature model.

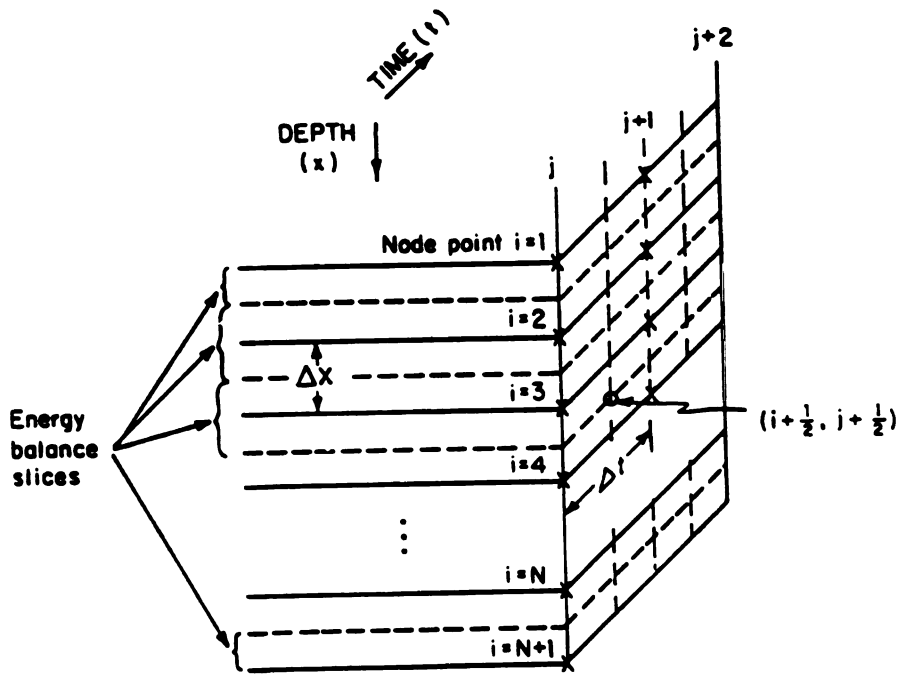

Figure B.2 Schematic of finite-difference method for decomposition model.

Appendix C

Appendix C

Data From Pyrolysis Experiments

In this appendix data obtained from the pyrolysis experiments are presented in the following order:

I. Experiments conducted in nitrogen atmosphere:

I.1 Exeriments conducted on dry wood.

I.2 Experiments conducted on 8-9% moist wood.

I.3 Experiments conducted on 17% moist wood.

II. Experiments conducted in air:

II.1 Experiments conducted on dry wood.

II.2 Experiments conducted on 8-9% moist wood.

II.3 Experiments conducted on 17% moist wood.

In each set of experiments the results are presented for 4, 3, 2, and 1 W/cm^2 external heat fluxes respectively. For each experiment in nitrogen atmosphere the measured and derived chemical quantities are given in the following order:

Fig. S1xxx Pyrolysis products (direct measurement).

Fig. S2xxx Pyrolysis products after burning in the catalytic combustor.

Fig. PSxxx Products of pyrolysis as percent of total mass flux.

Fig. CHxxx Number of C and H atoms in C_xH_yO.

Fig. YCxxx Char yield (gram char/gram wood).

Fig. GGxxx Gram[ ]/gram of C_xH_yO.

Fig. TMxxx Total mass balance for pyrolysis products.

Fig. ERxxx Error in total mass balance for pyrolysis products.

Fig. HVxxx Heat of combustion of pyrolysis products.

For experiments in air only the first six sets of data are presented. This order for every two consecutive experiments may have been altered to save space. Some of the low heat flux data curves are not presented due to high order of scateredness. Selected data on temperature measurements are given following the above data in the same order. In these notations xxx stands for every experiment and are consistent with notations summarized in table 3.1

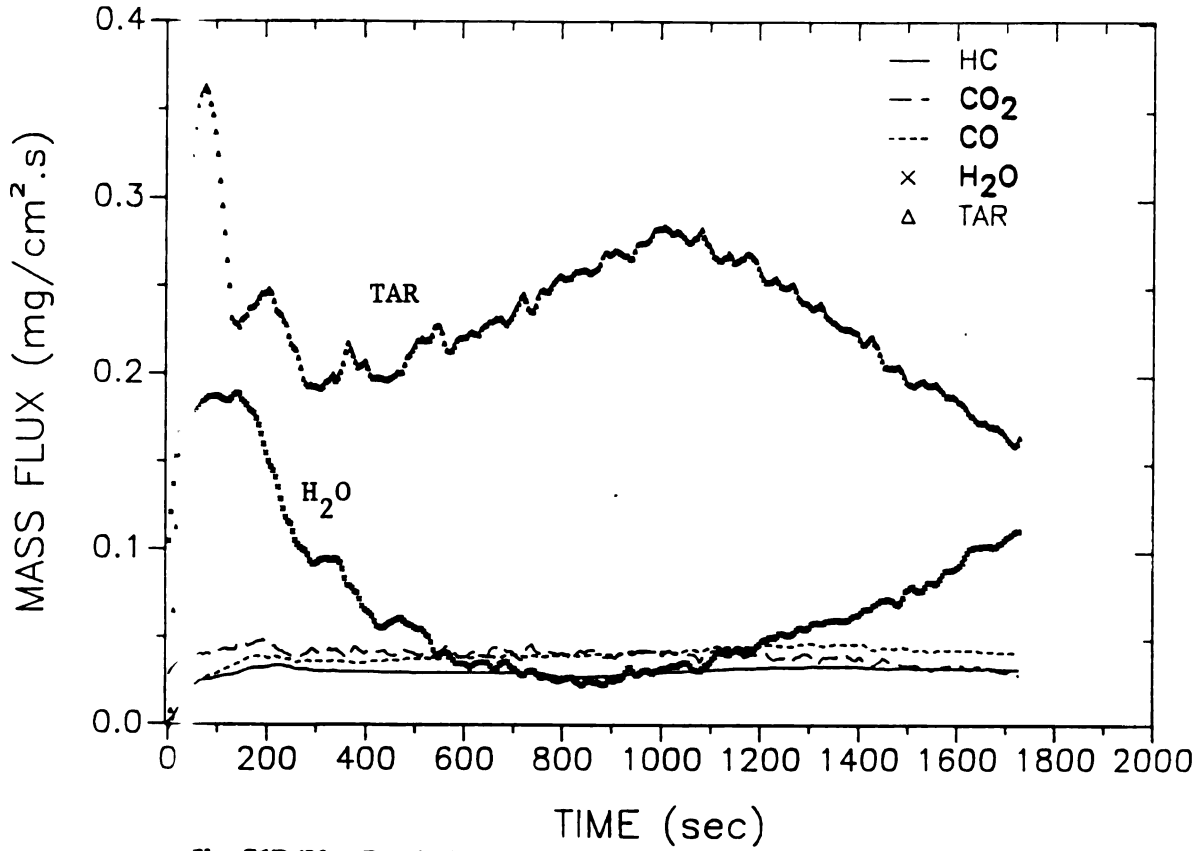

Fig. S1D4N Pyrolysis products (direct measurement); EXP. D4N

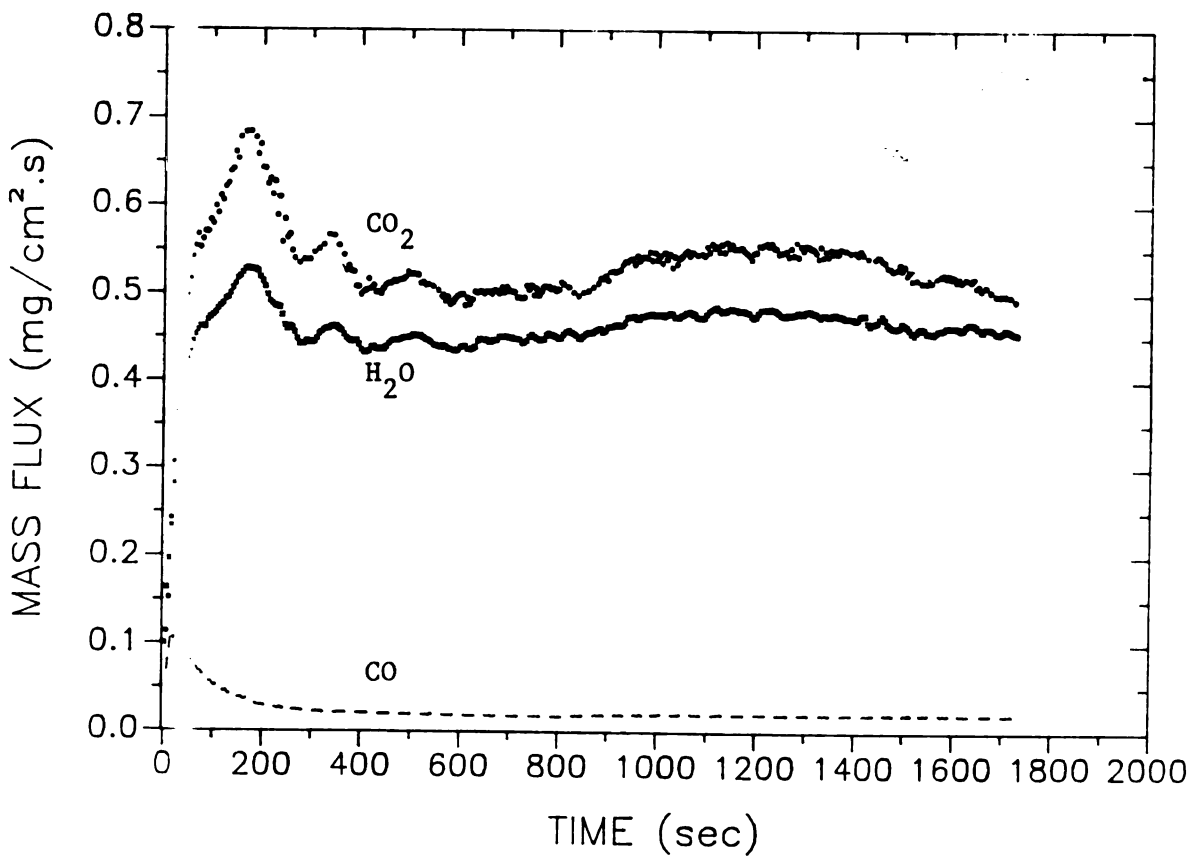

Fig. S2D4N Pyrolysis products (after catalytic combustor); EXP. D4N

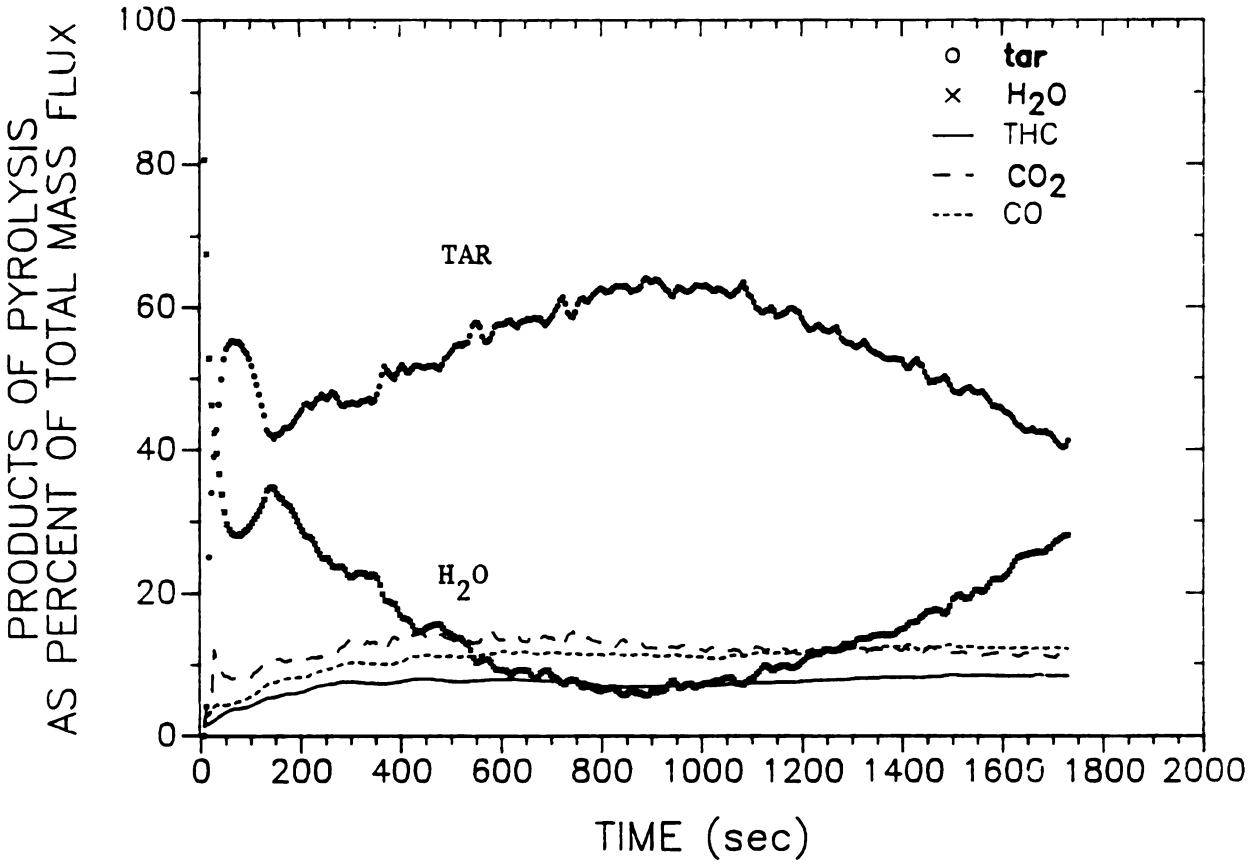

Fig. PSD4N Products of pyrolysis as percent of total mass flux; EXP. D4N

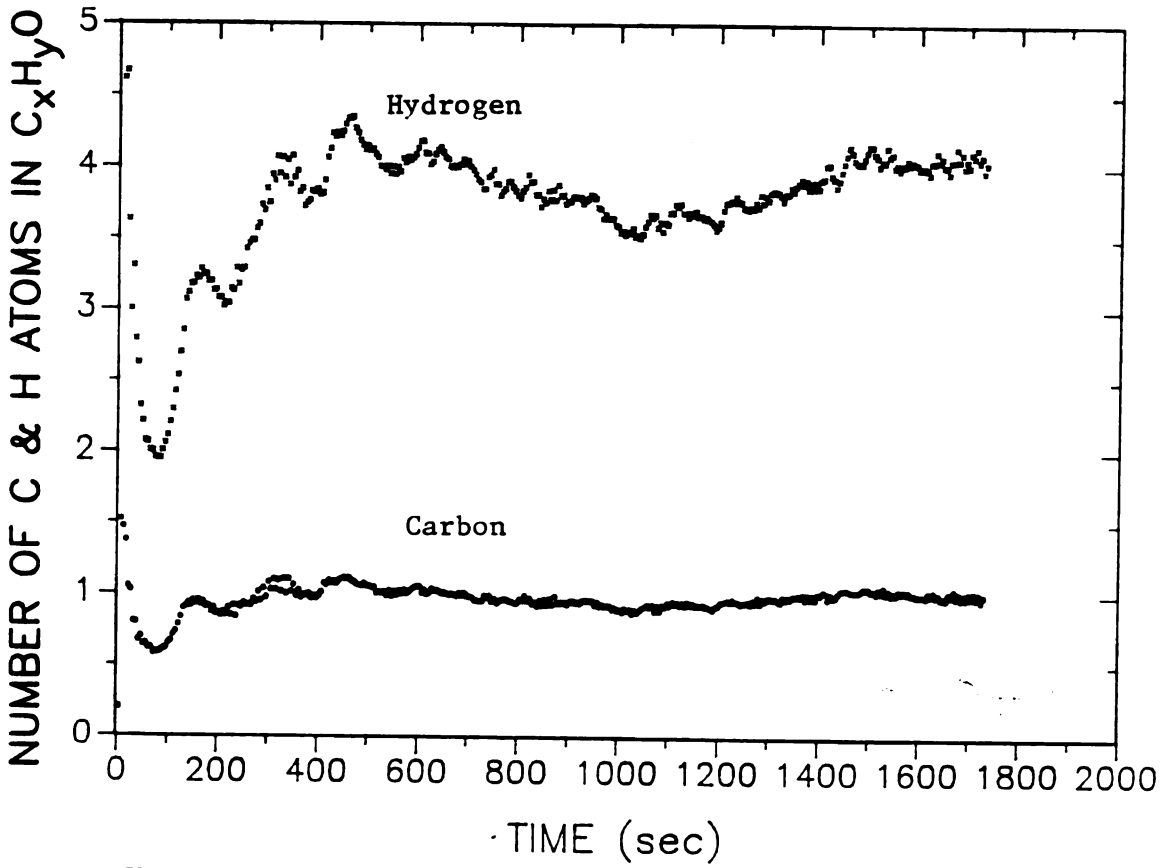

Fig. CHD4N Number of C and H atoms in the products of pyrolysis; EXP. D4N

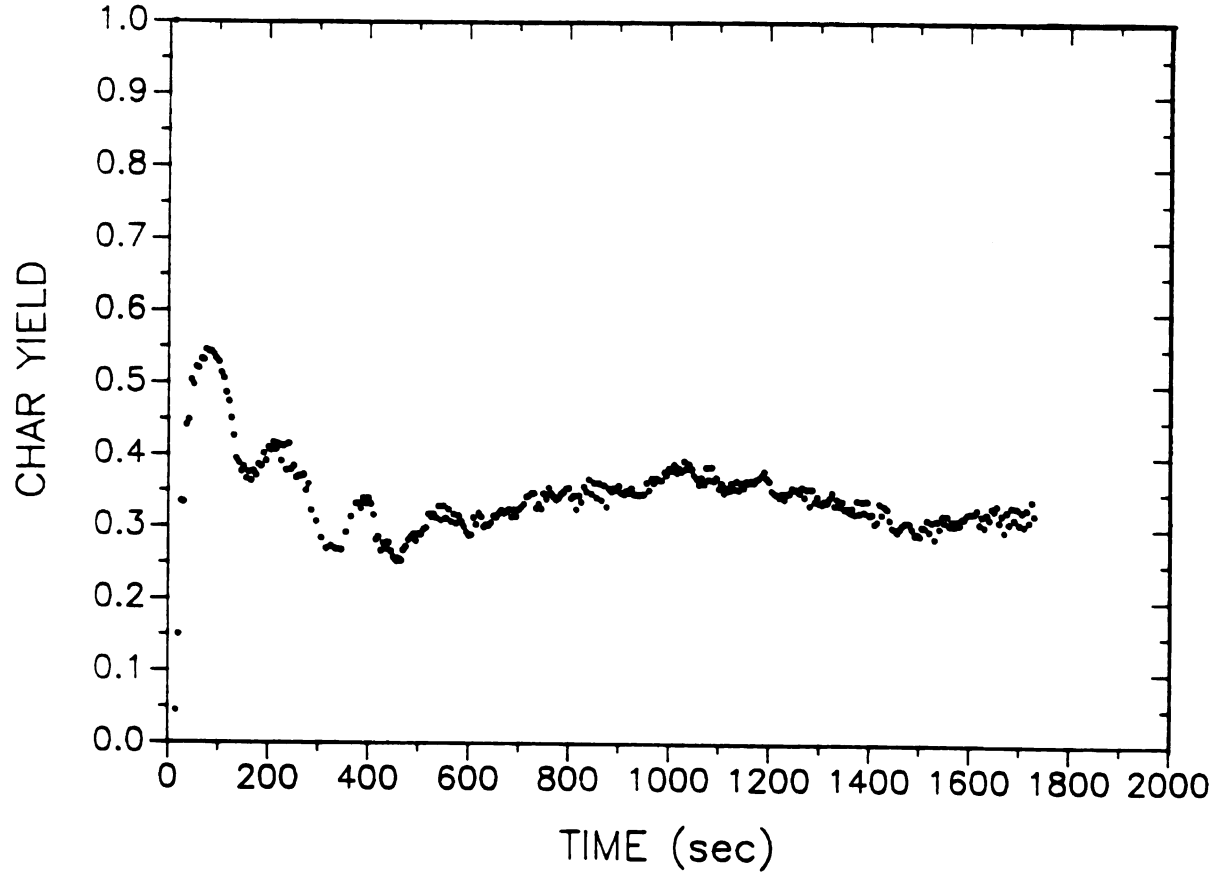

Fig. YCD4N Char yield (gram char/gram wood); EXP. D4N

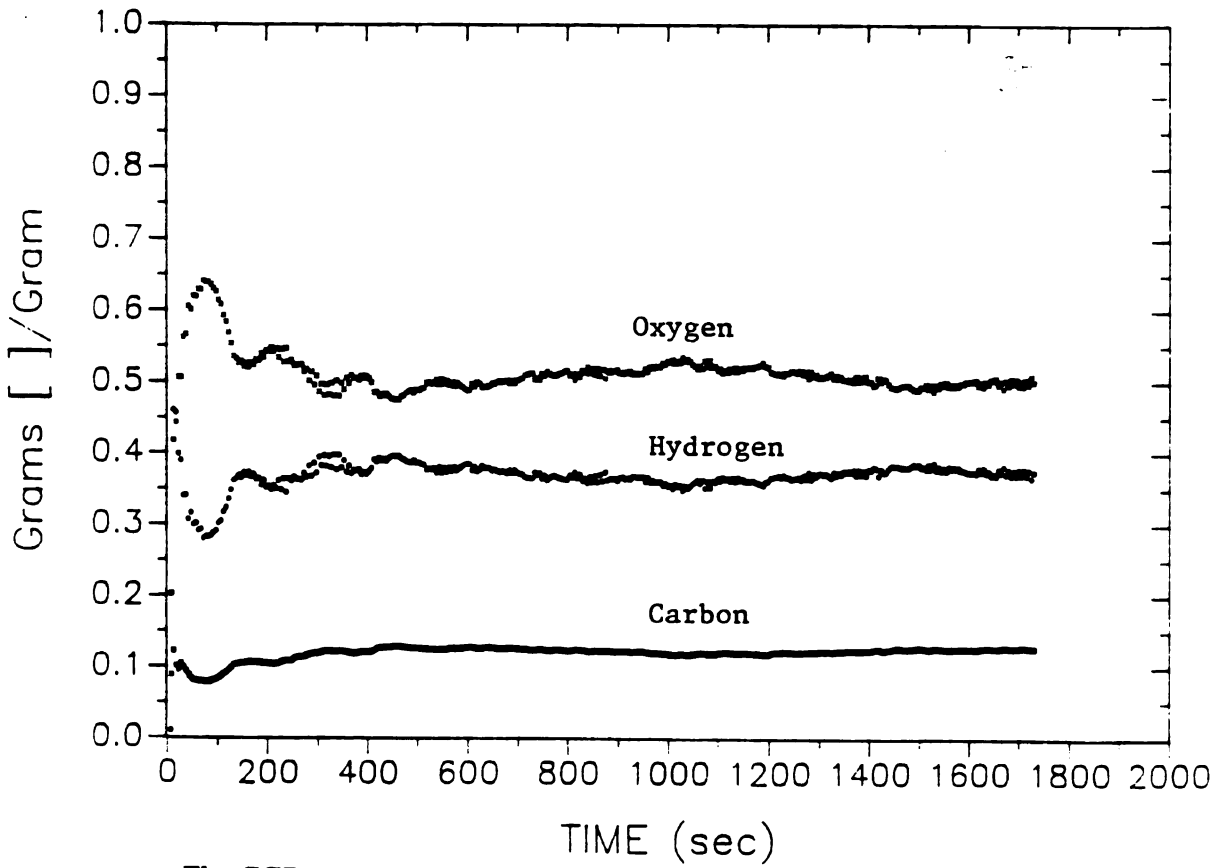

Fig. GGD4N Gram [ ]/gram of C_xH_yO; EXP. D4N

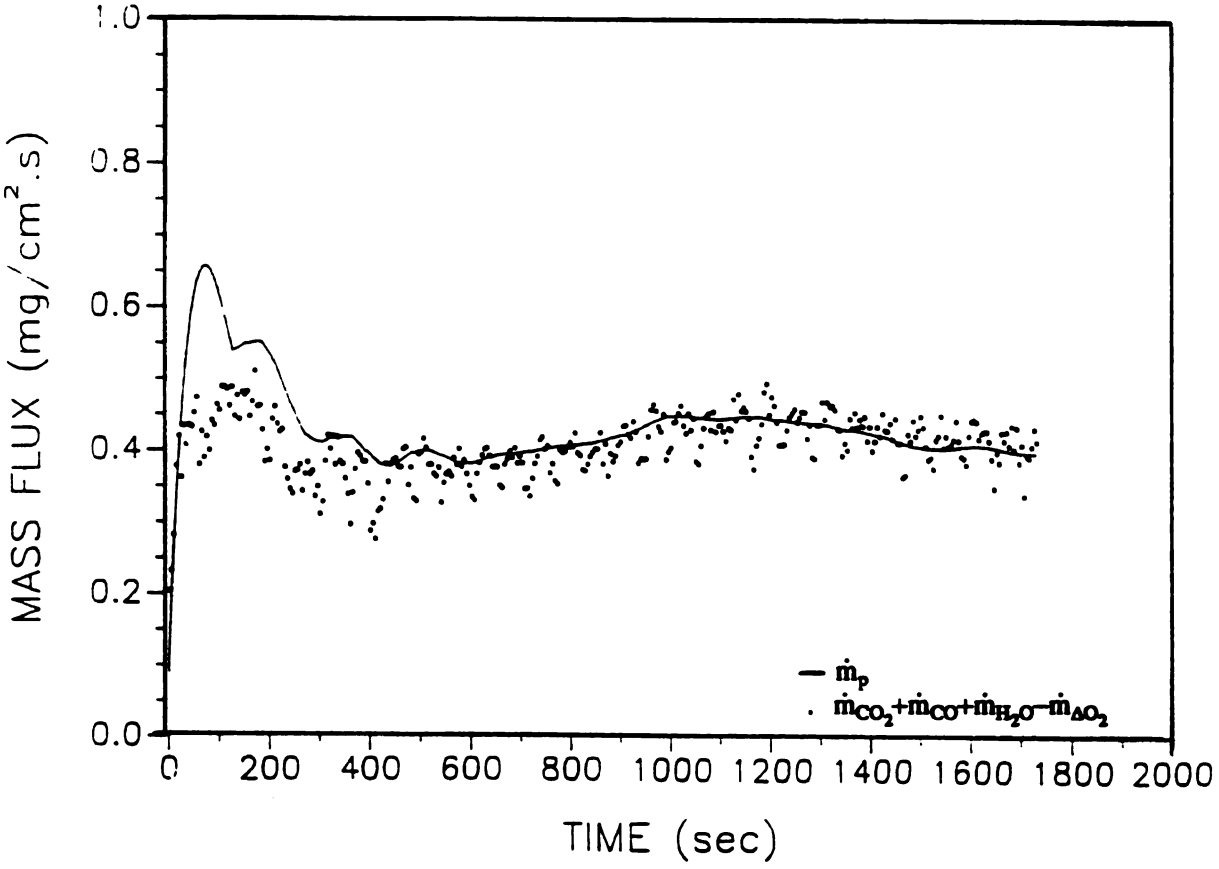

Fig. TMD4N Total mass balance for pyrolysis products; EXP. D4N

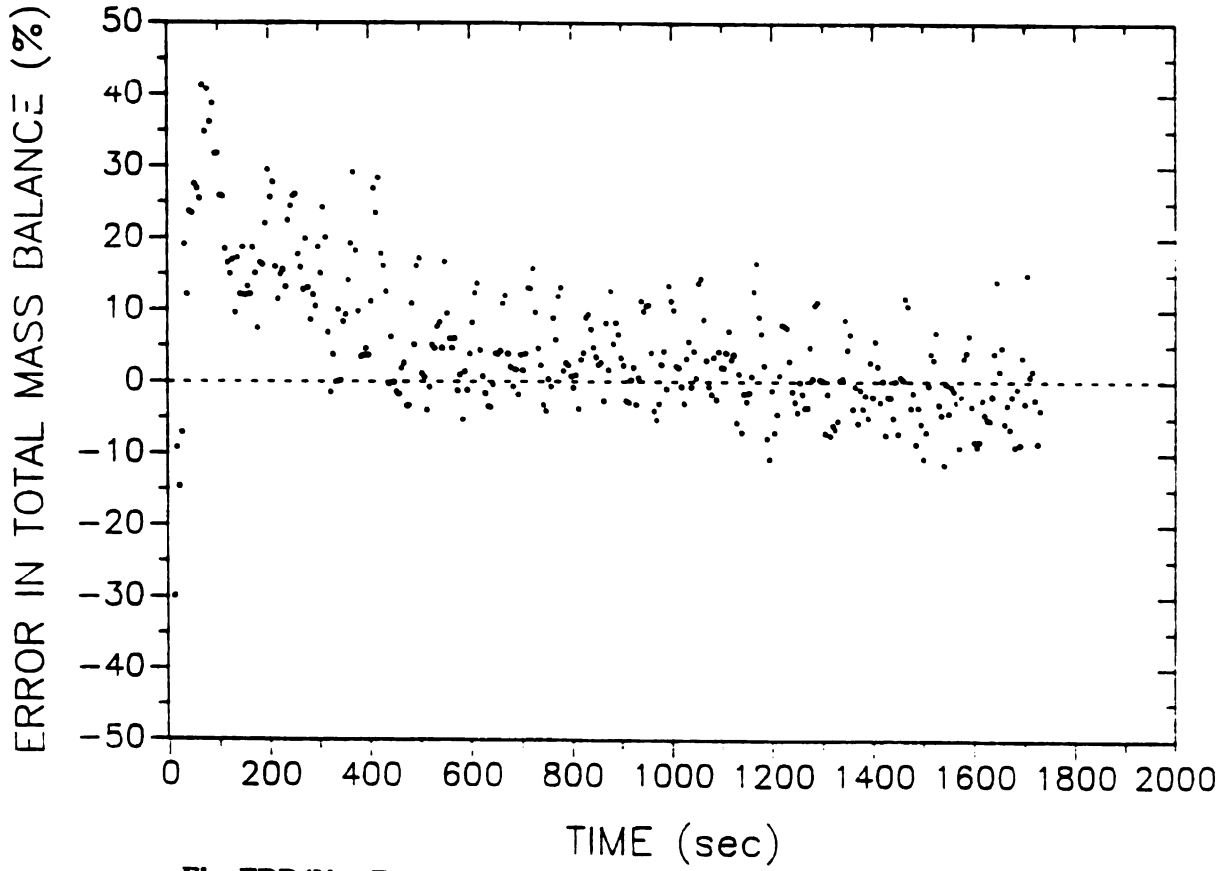

Fig. ERD4N Error in total mass balance for pyrolysis products; EXP. D4N

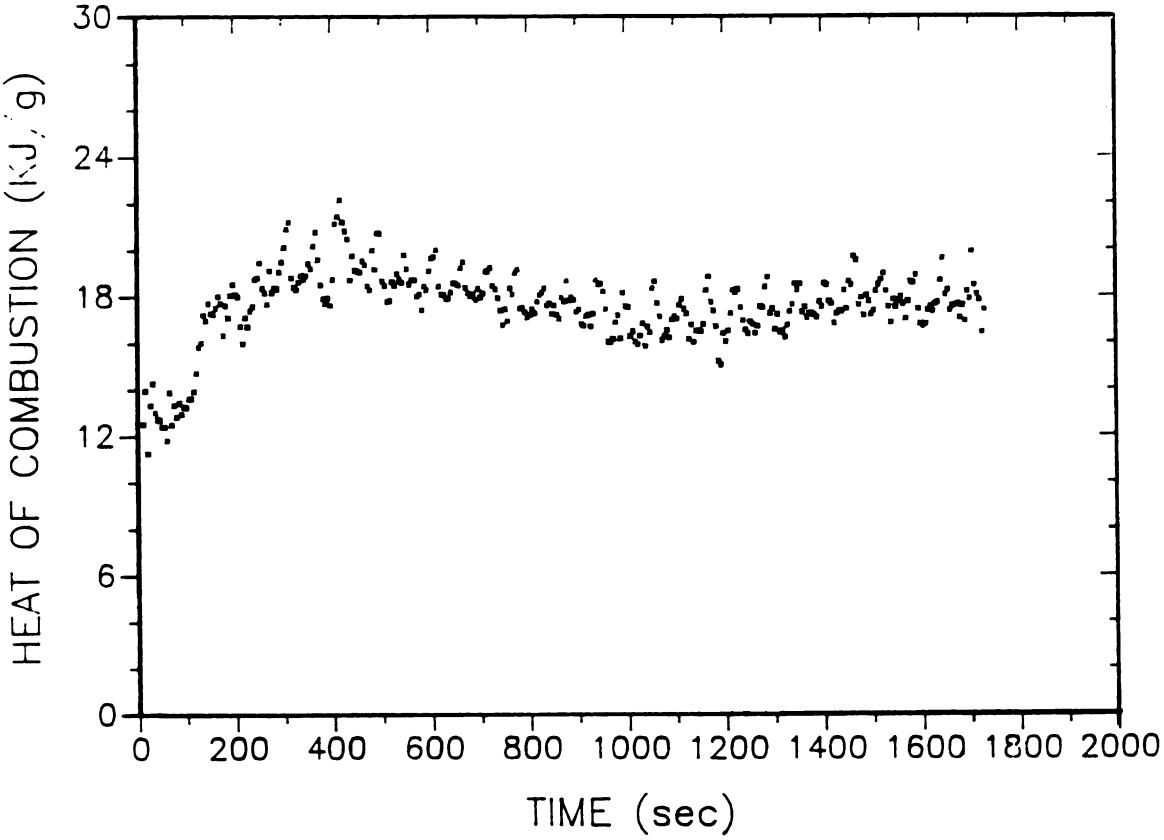

Fig. HVD4N Heat of combustion of pyrolysis products; EXP. D4N

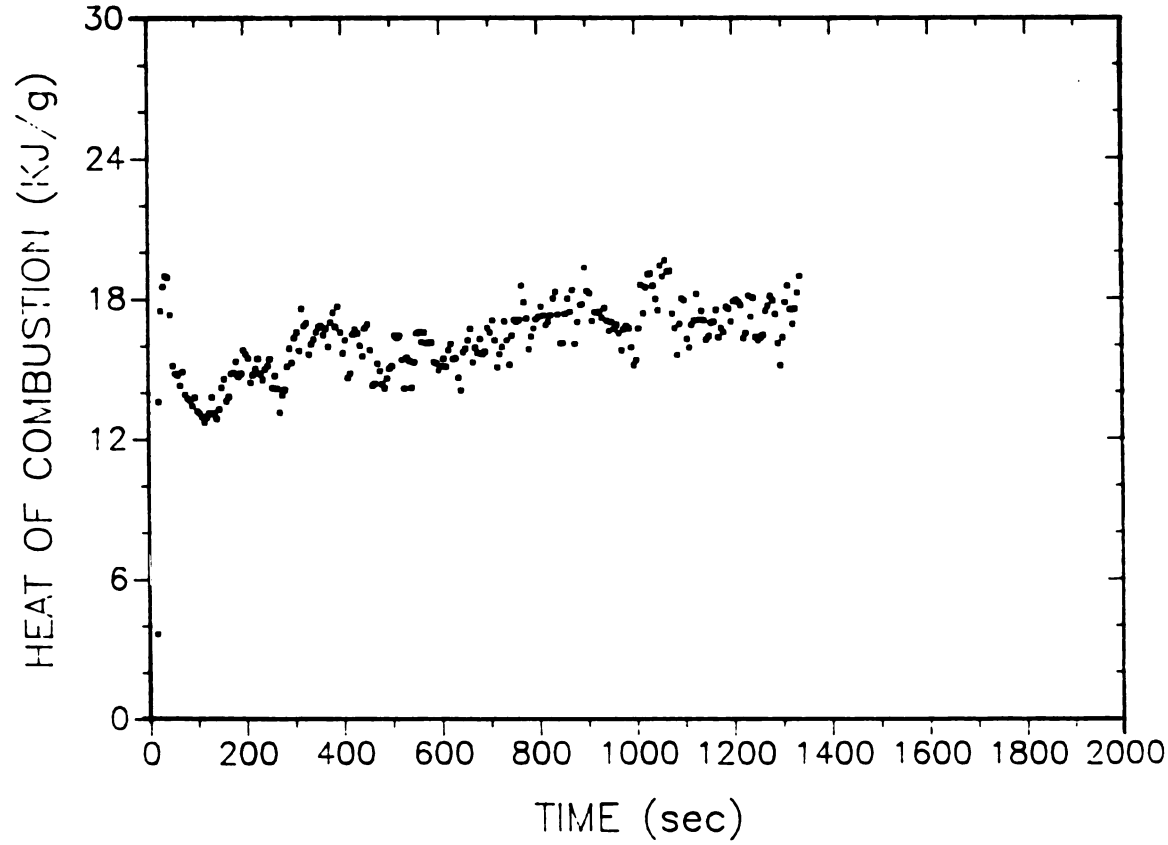

Fig. HVD3N Heat of combustion of pyrolysis products; EXP. D3N

MASS FLUX (mg/cm².s)

MASS FLUX (mg/cm².s)

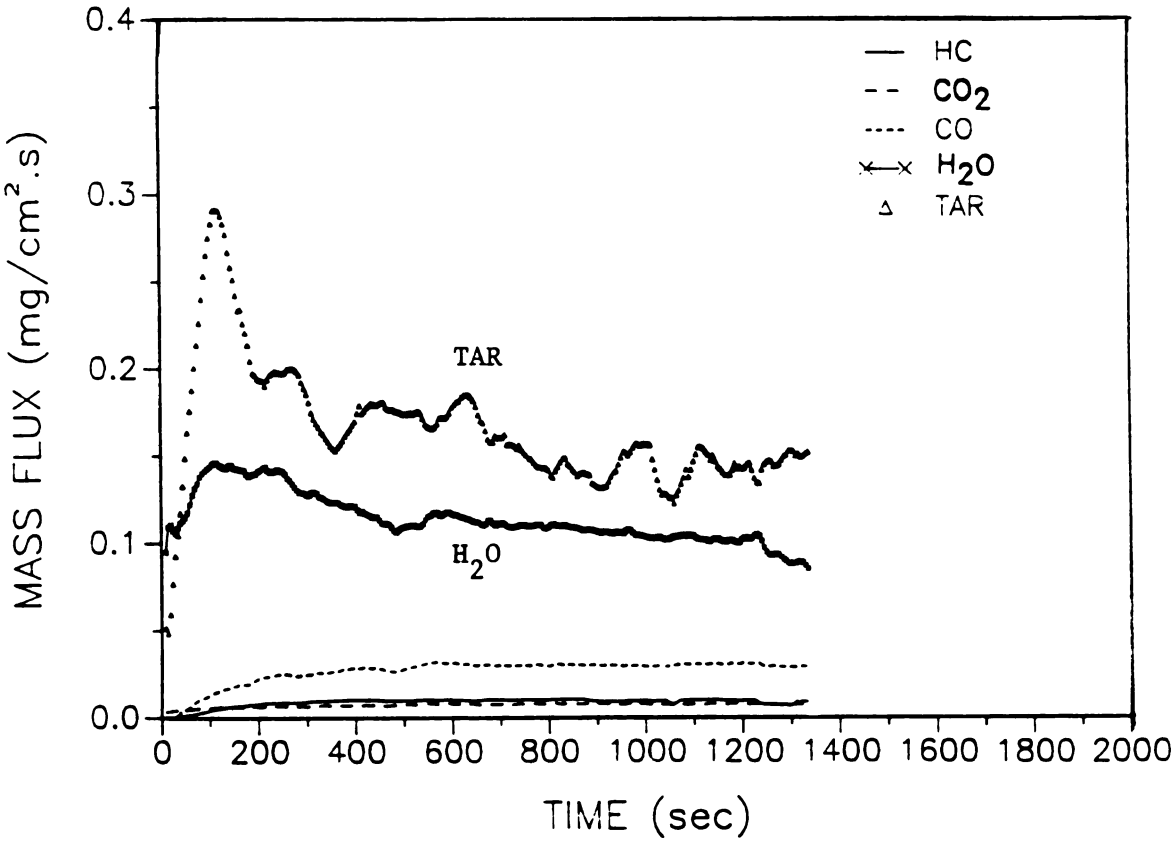

Fig. S1D3N Pyrolysis products (direct measurment); EXP. D3N

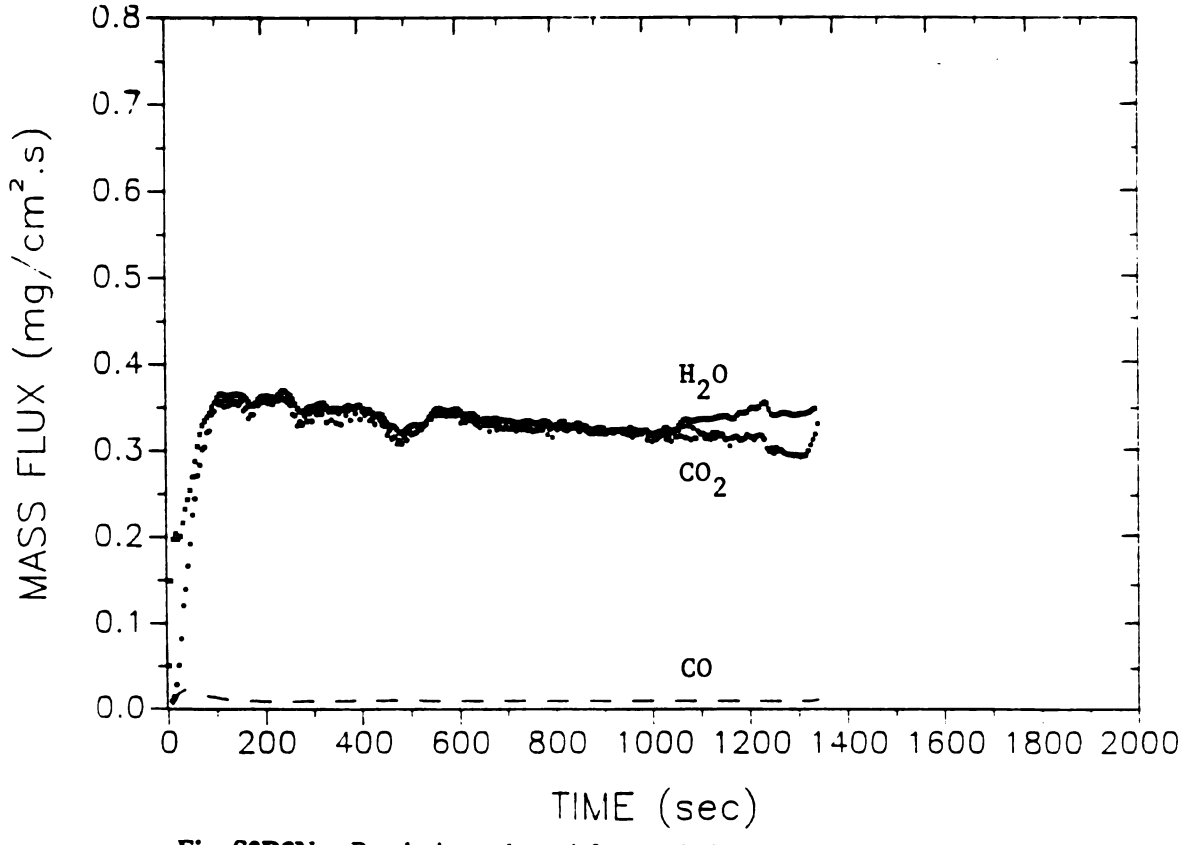

Fig. S2D3N Pyrolysis products (after catalytic combustor); EXP. D3N

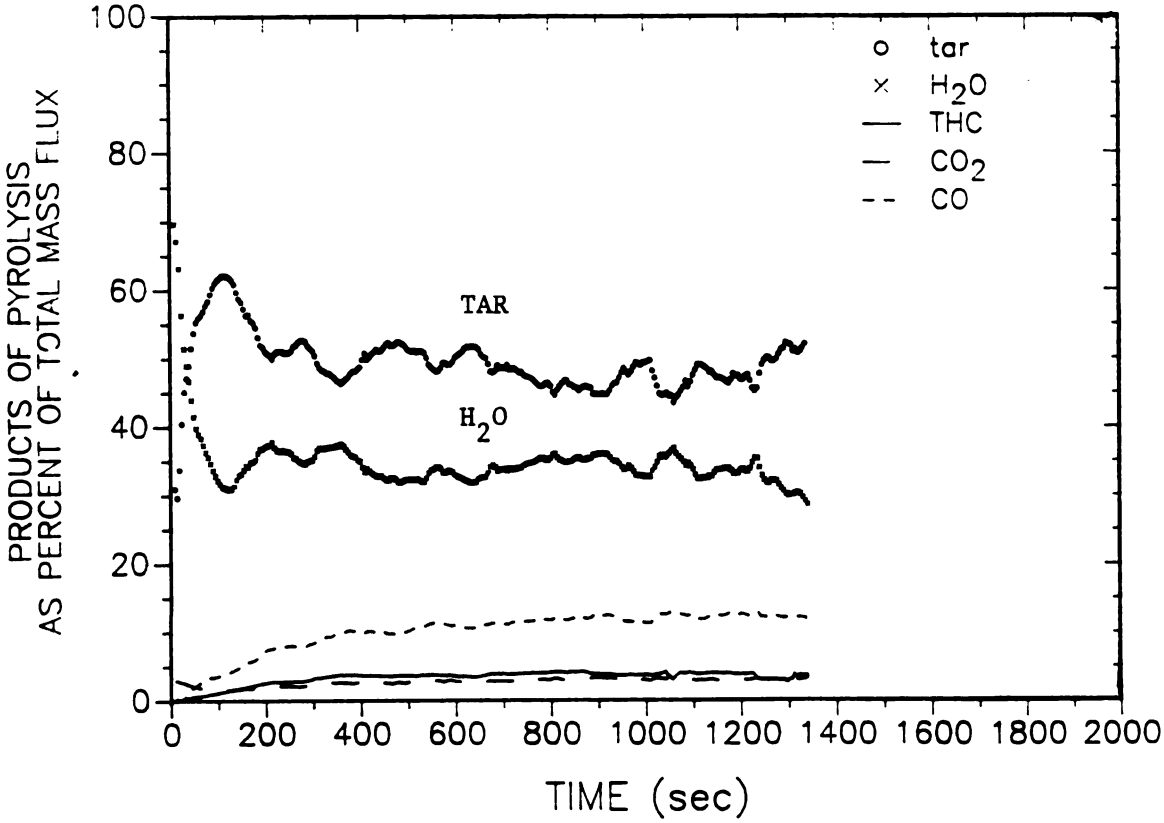

Fig. PSD3N Products of pyrolysis as percent of total mass flux; EXP. D3N

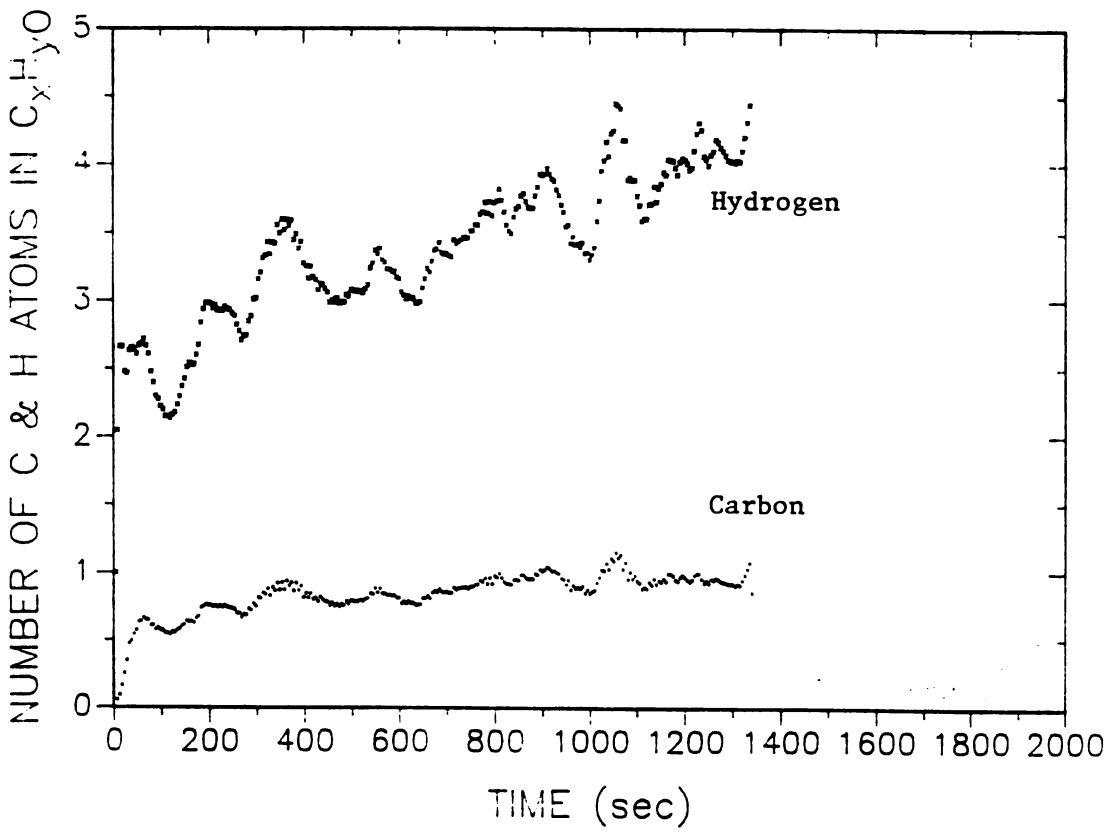

Fig. CHD3N Number of C and H atoms in the products of pyrolysis; EXP. D3N

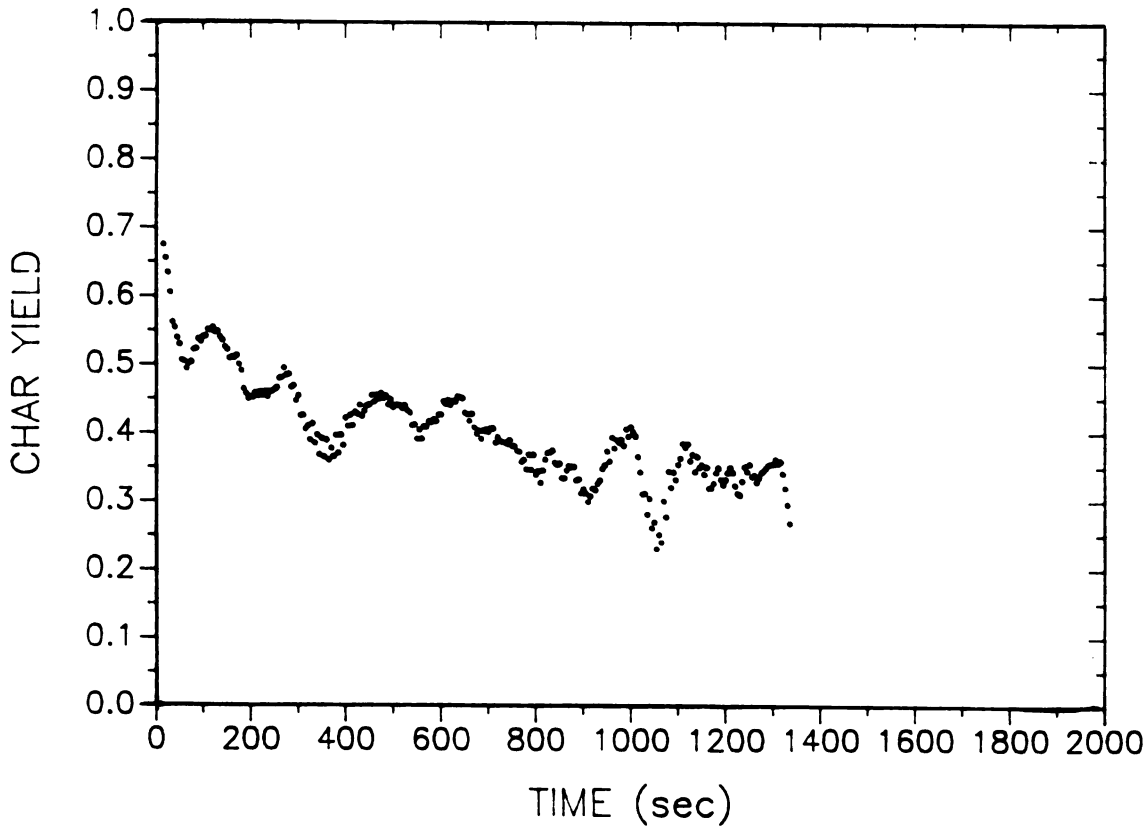

Fig. YCD3N Char yield (gram char/gram wood); EXP. D3N

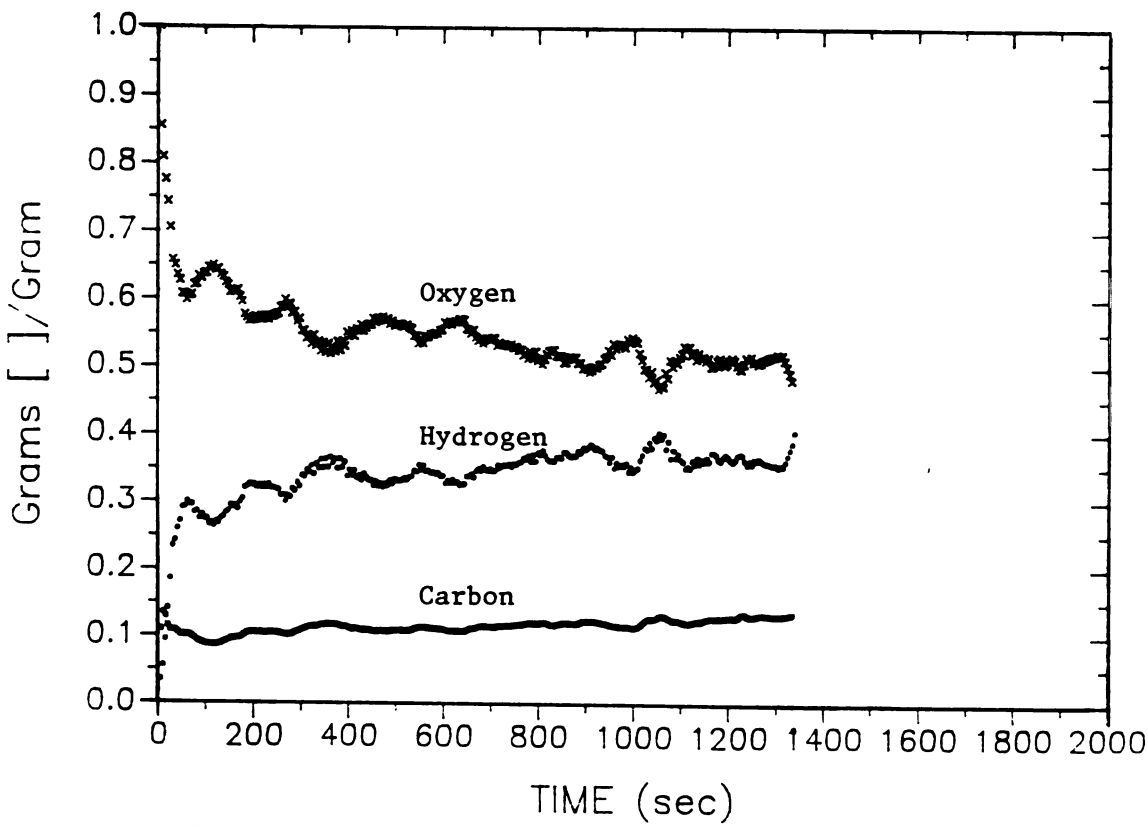

Fig. GGD3N Gram [ ]/gram of C_xH_yO; EXP. D3N

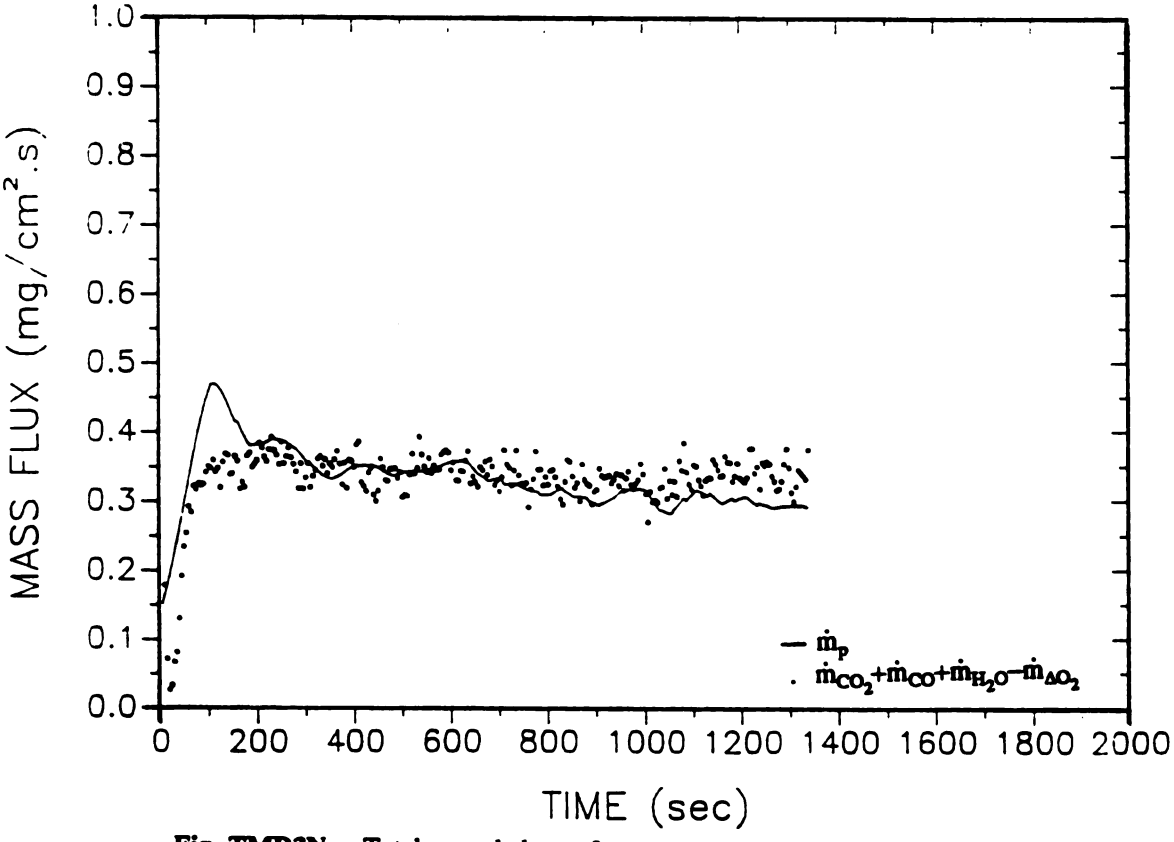

Fig. TMD3N Total mass balance for pyrolysis products; EXP. D3N

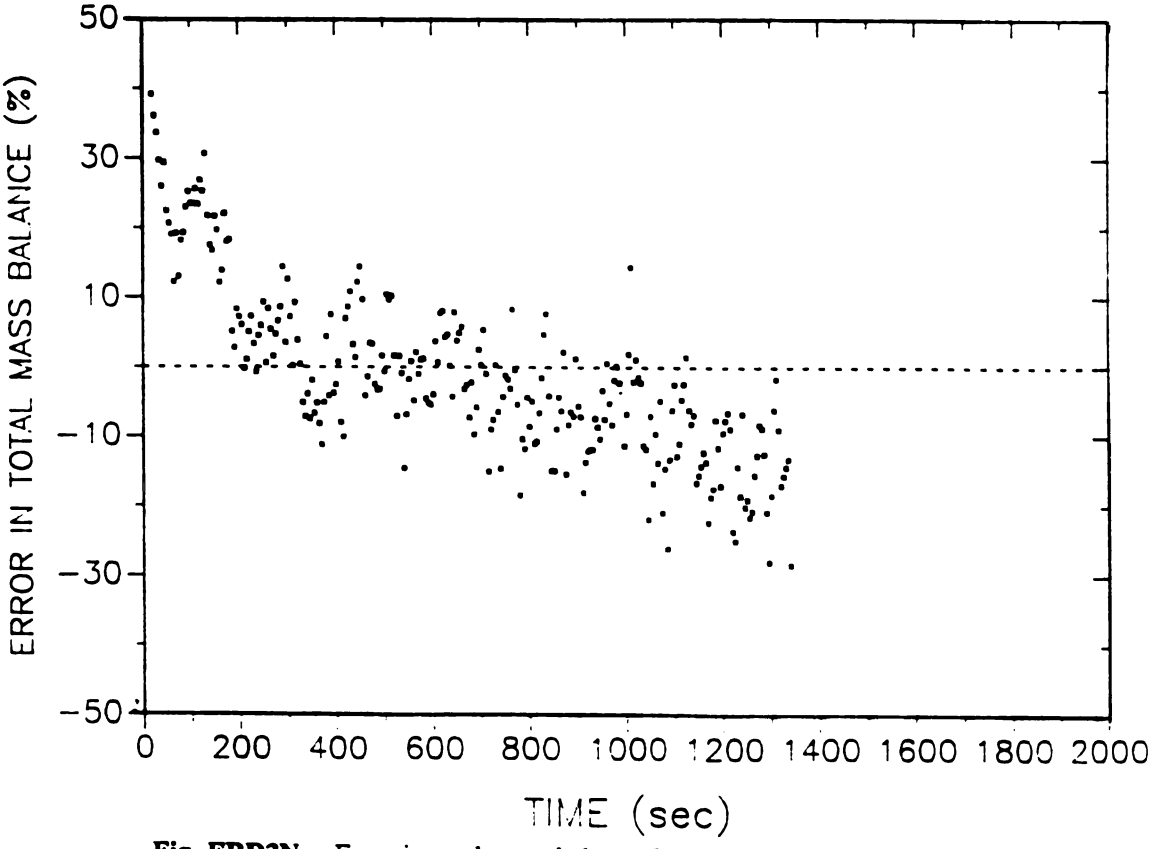

Fig. ERD3N Error in total mass balance for pyrolysis products; EXP. D3N

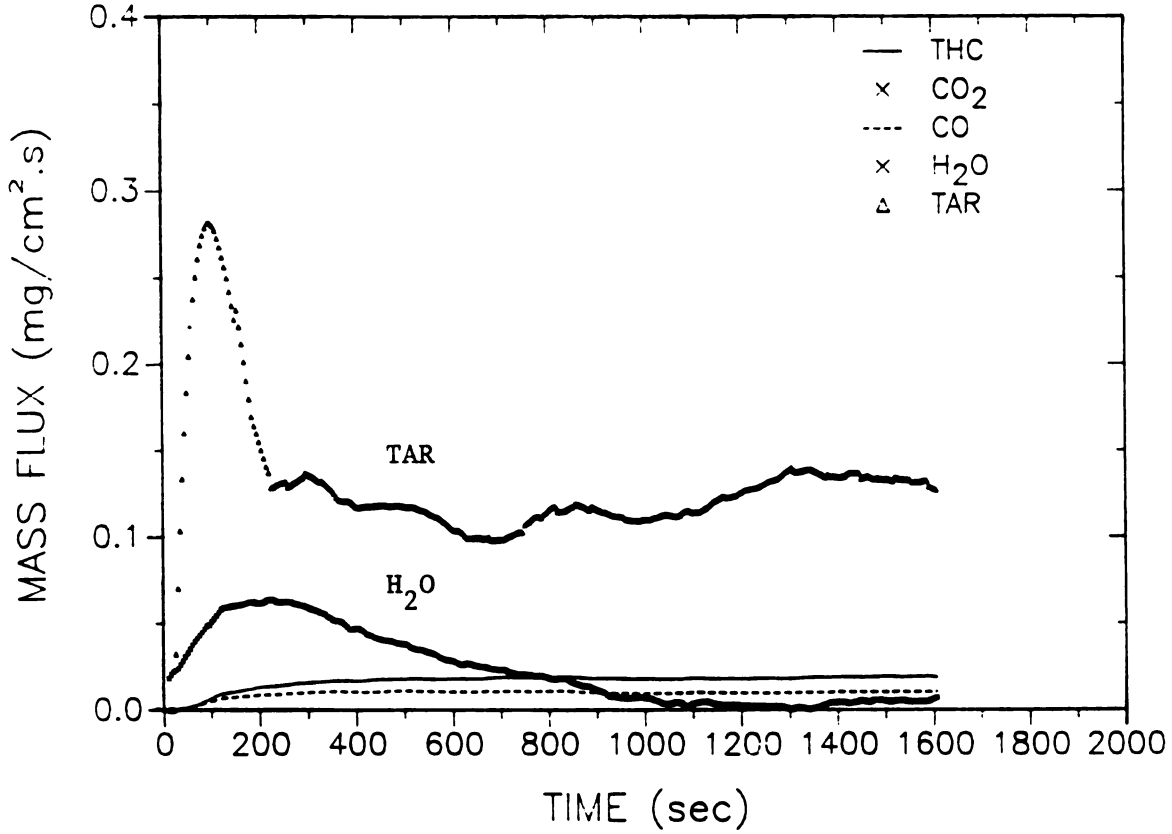

Fig. S1D2N Pyrolysis products (direct measurment); EXP. D2N

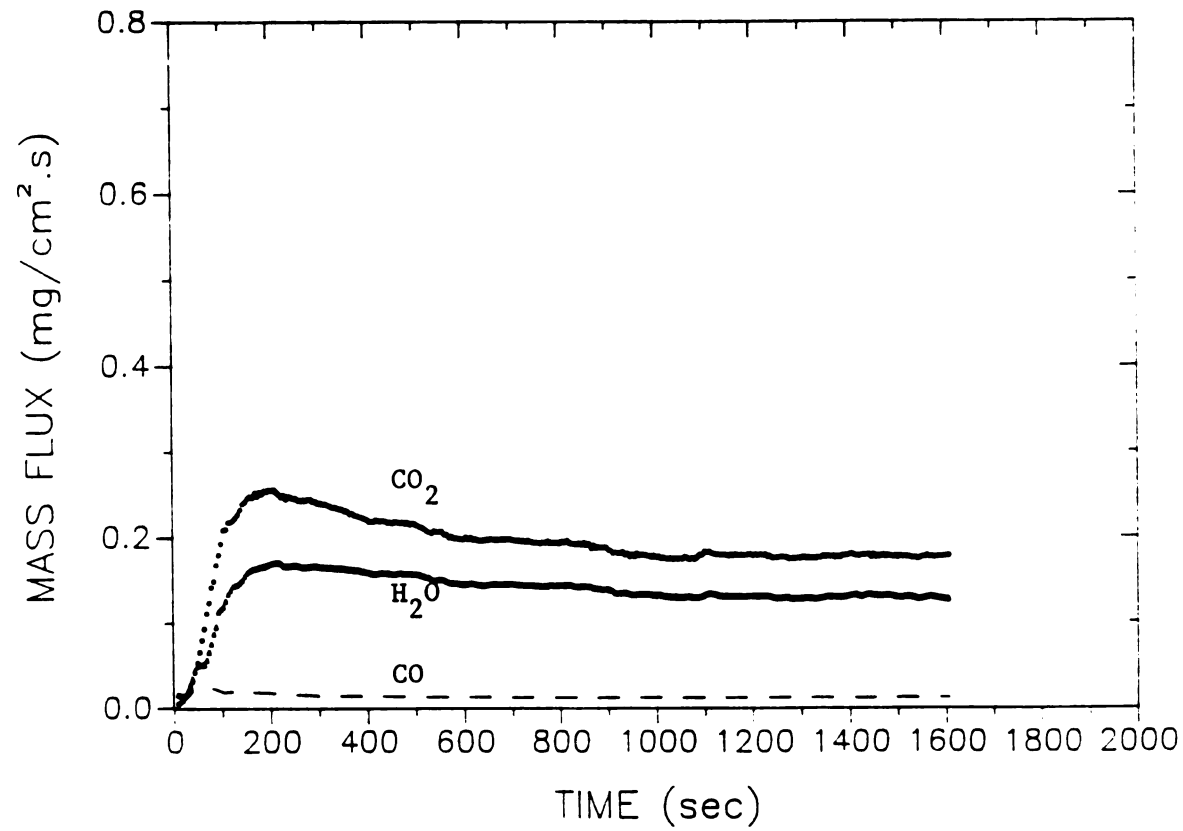

Fig. S2D2N Pyrolysis products (after catalytic combustor);EXP. D2N

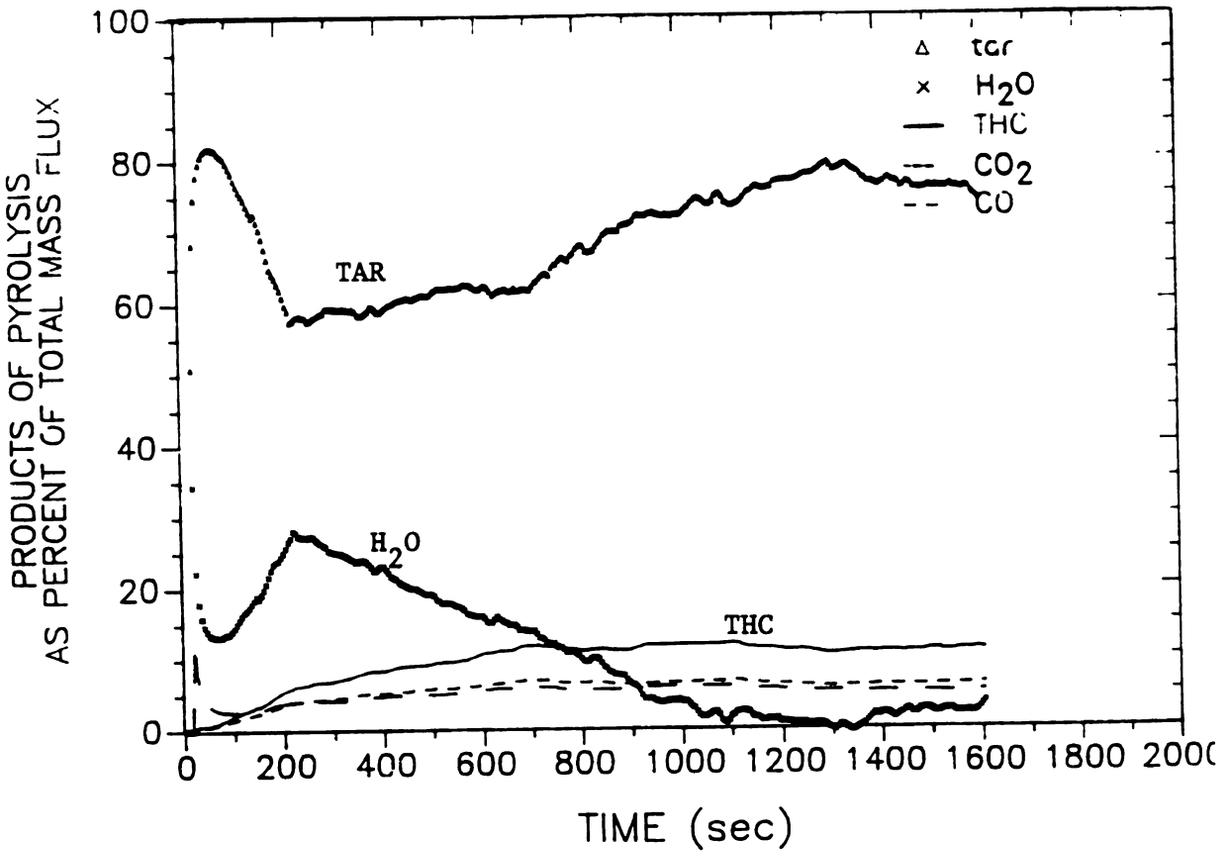

Fig. PSD2N Products of pyrolysis as percent of total mass flux; EXP. D2N

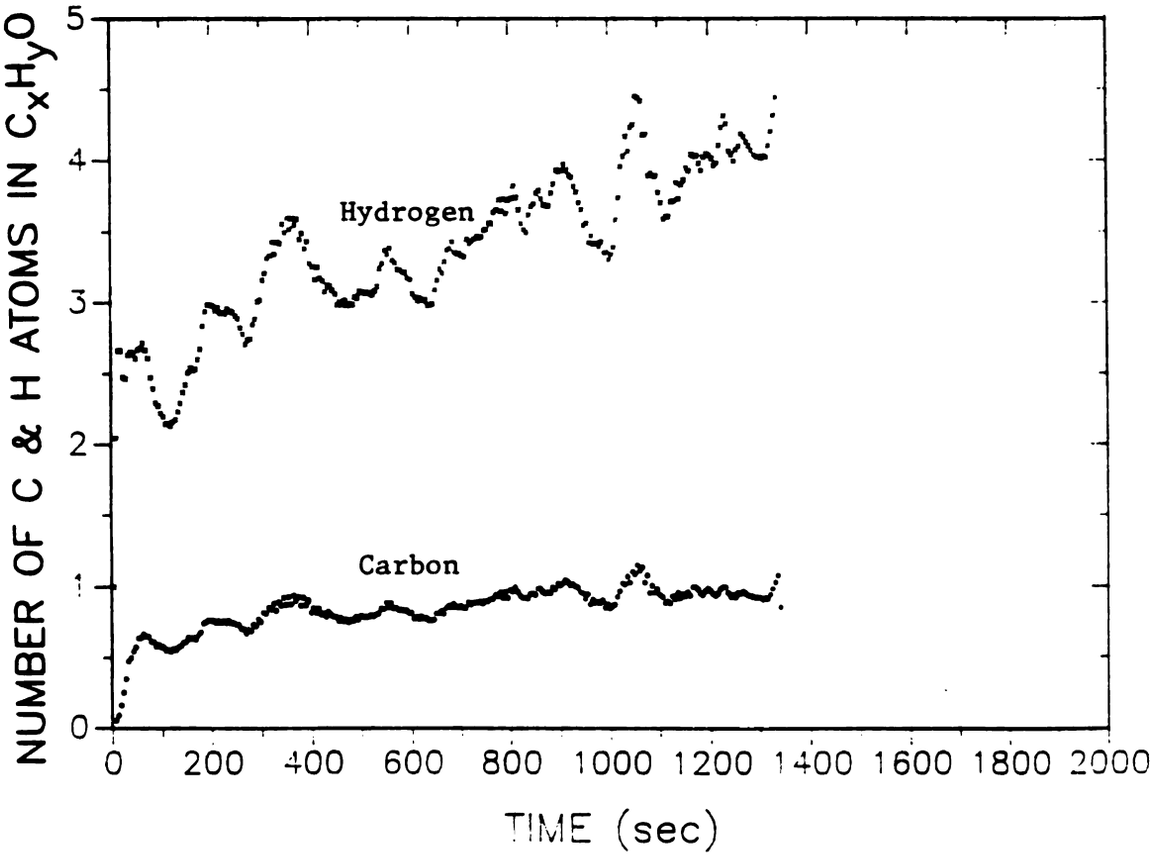

Fig. CHD2N Number of C and H atoms in the products of pyrolysis; EXP.

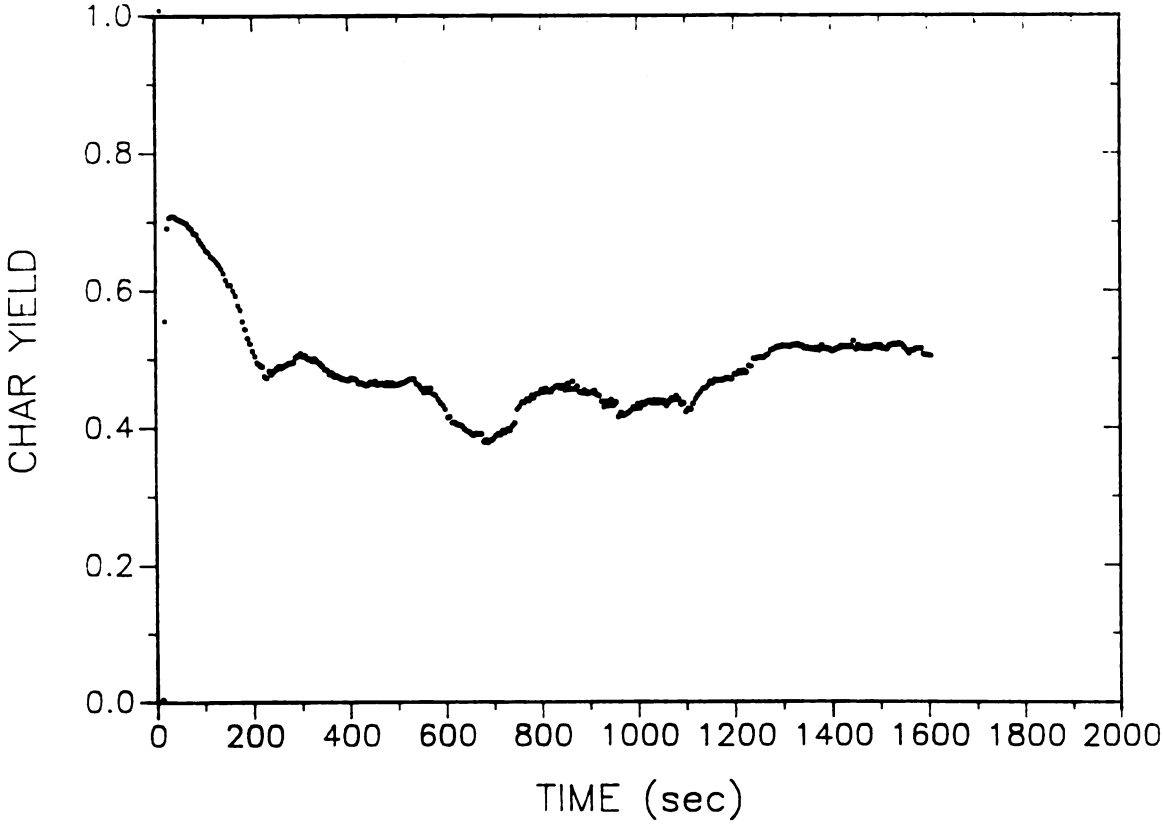

Fig. YCD2N Char yield (gram char/gram wood); EXP. D2N

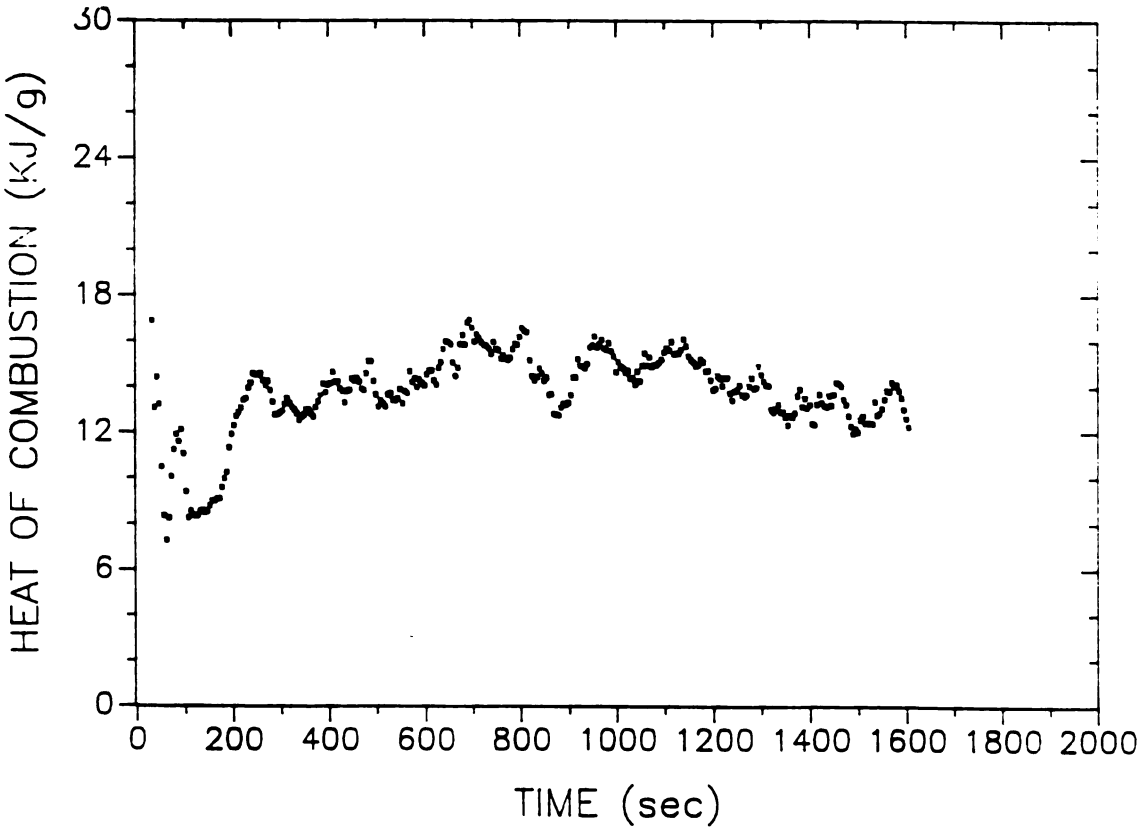

Fig. HVD2N Heat of combustion of pyrolysis products; EXP. D2N

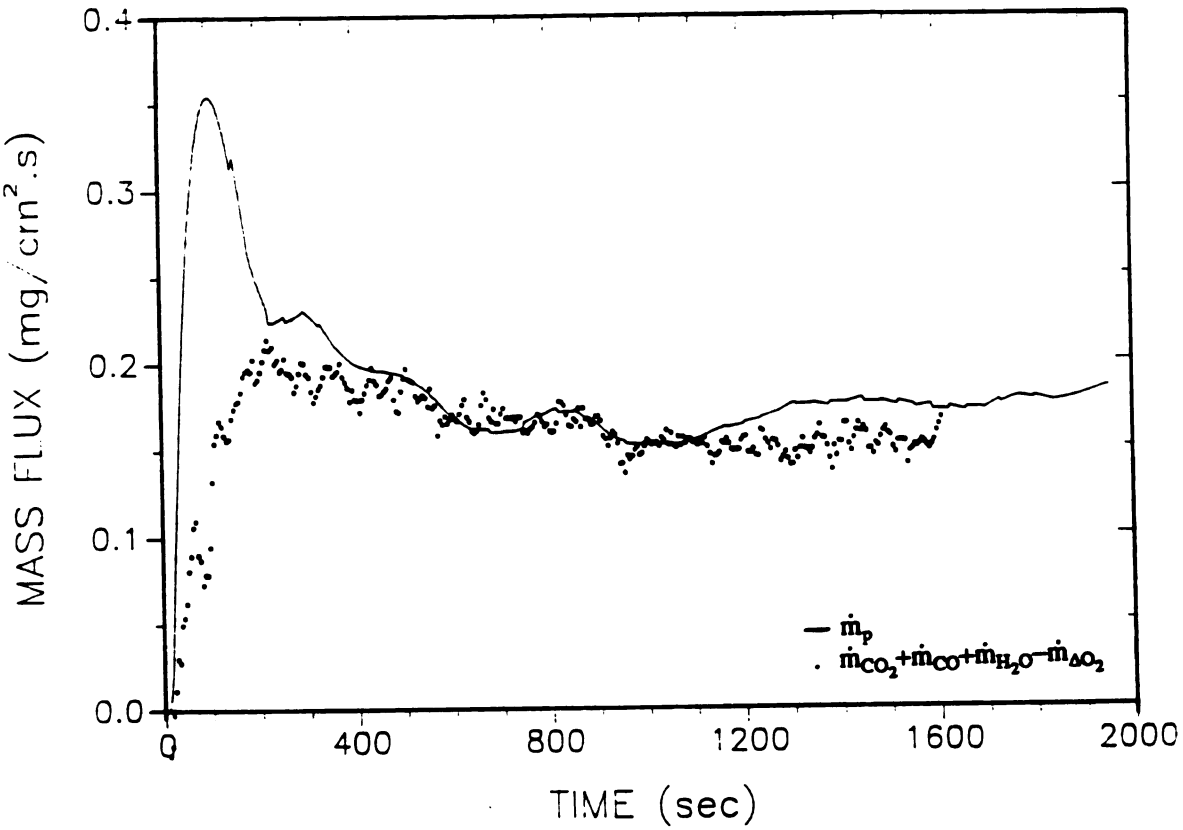

Fig. TMD2N Total mass balance for pyrolysis products; EXP. D2N

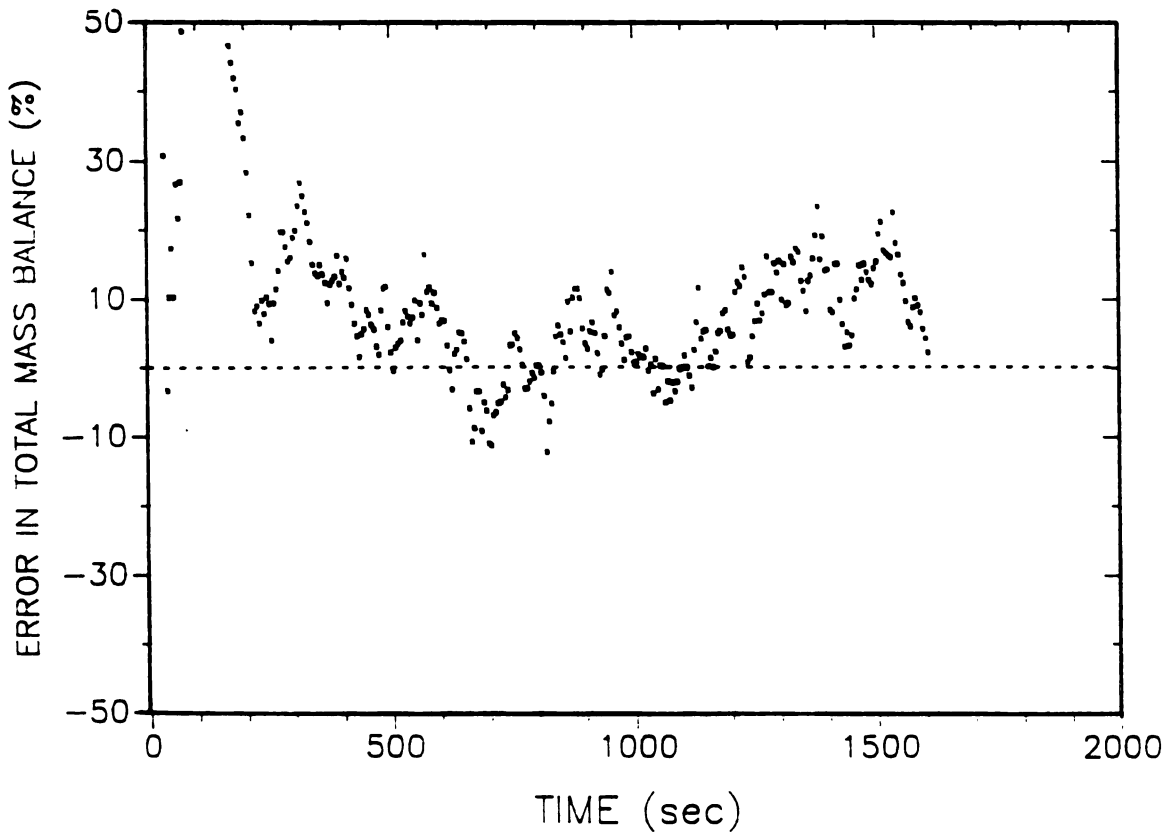

Fig. ERD2N Error in total mass balance for pyrolysis products; EXP. D2N

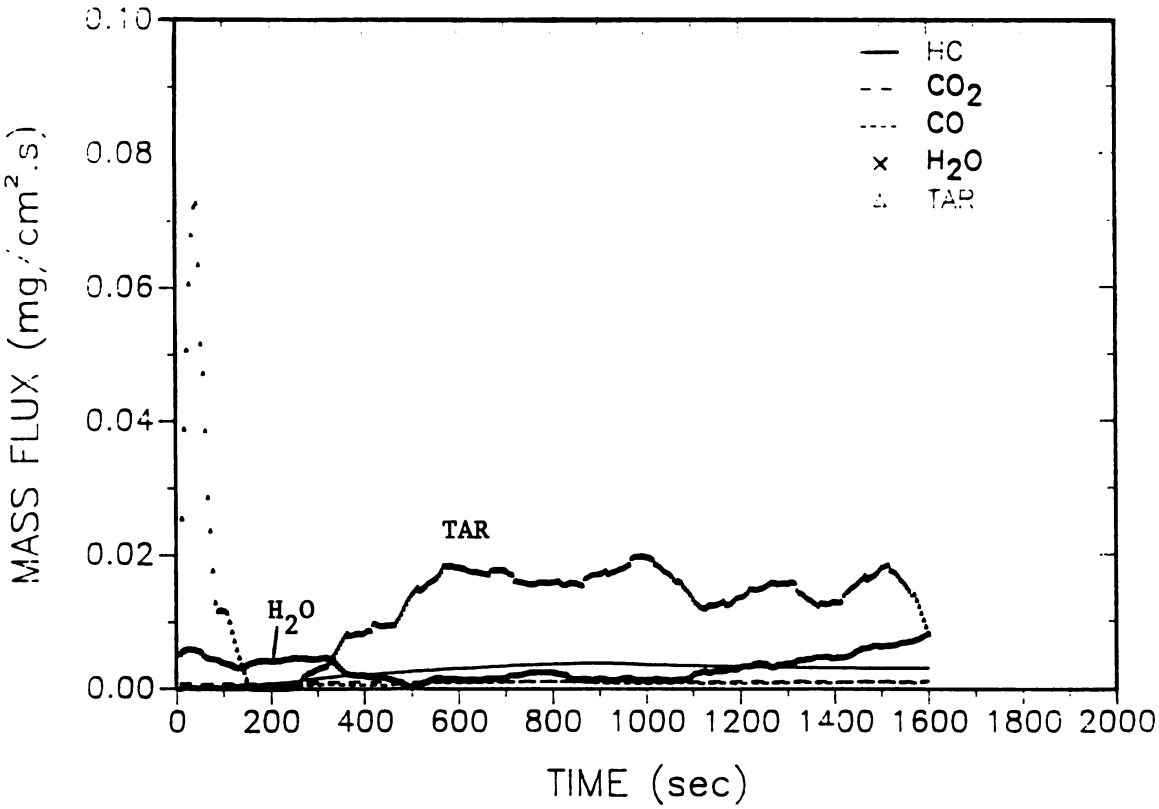

Fig. S1D1N Pyrolysis products (direct measurment); EXP. D1N

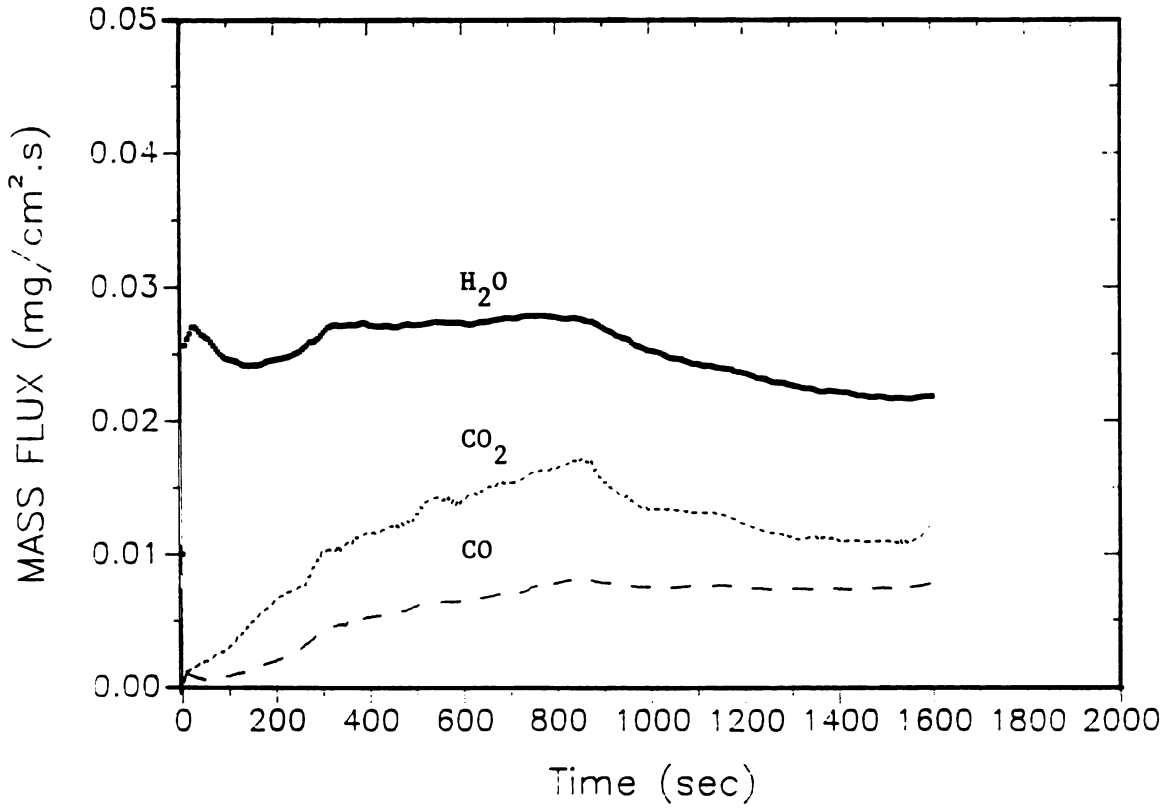

Fig. S2D1N Pyrolysis products (after catalytic combustor); EXP. D1N

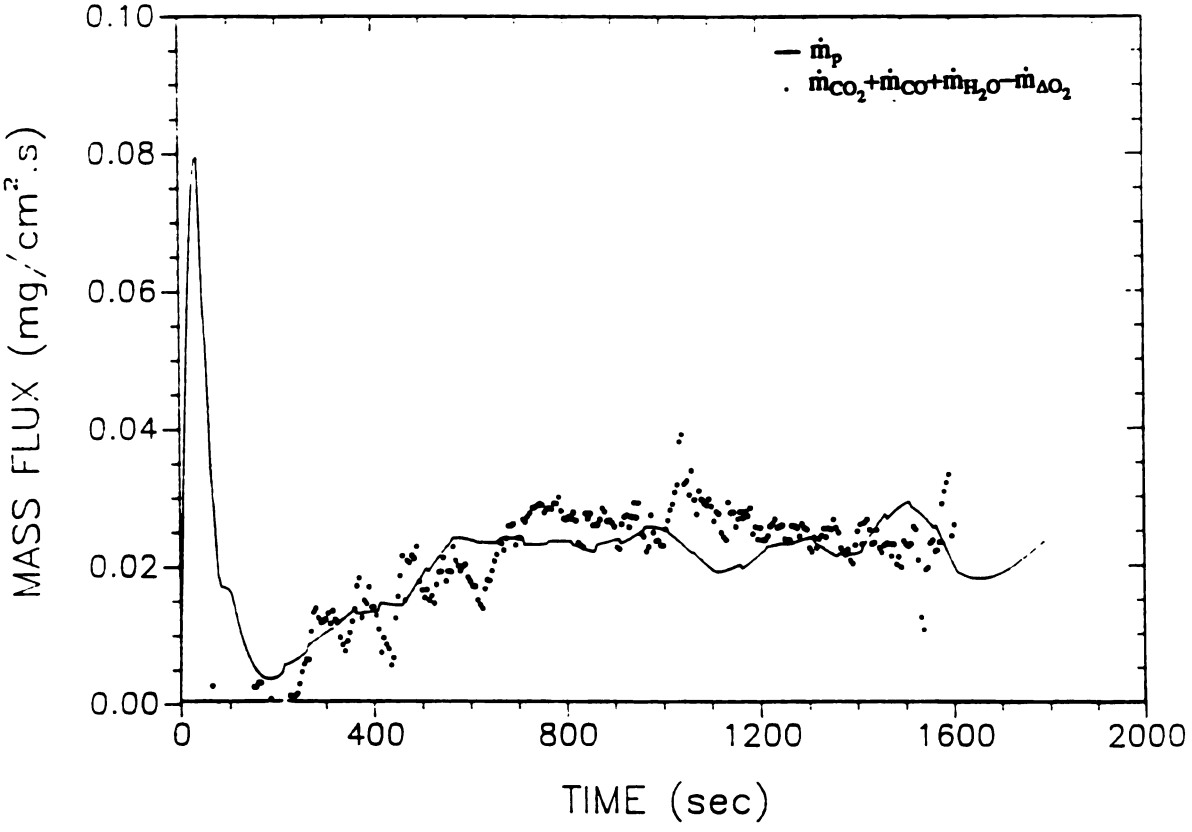

Fig. TMD1N Total mass balance for pyrolysis products; EXP. D1N

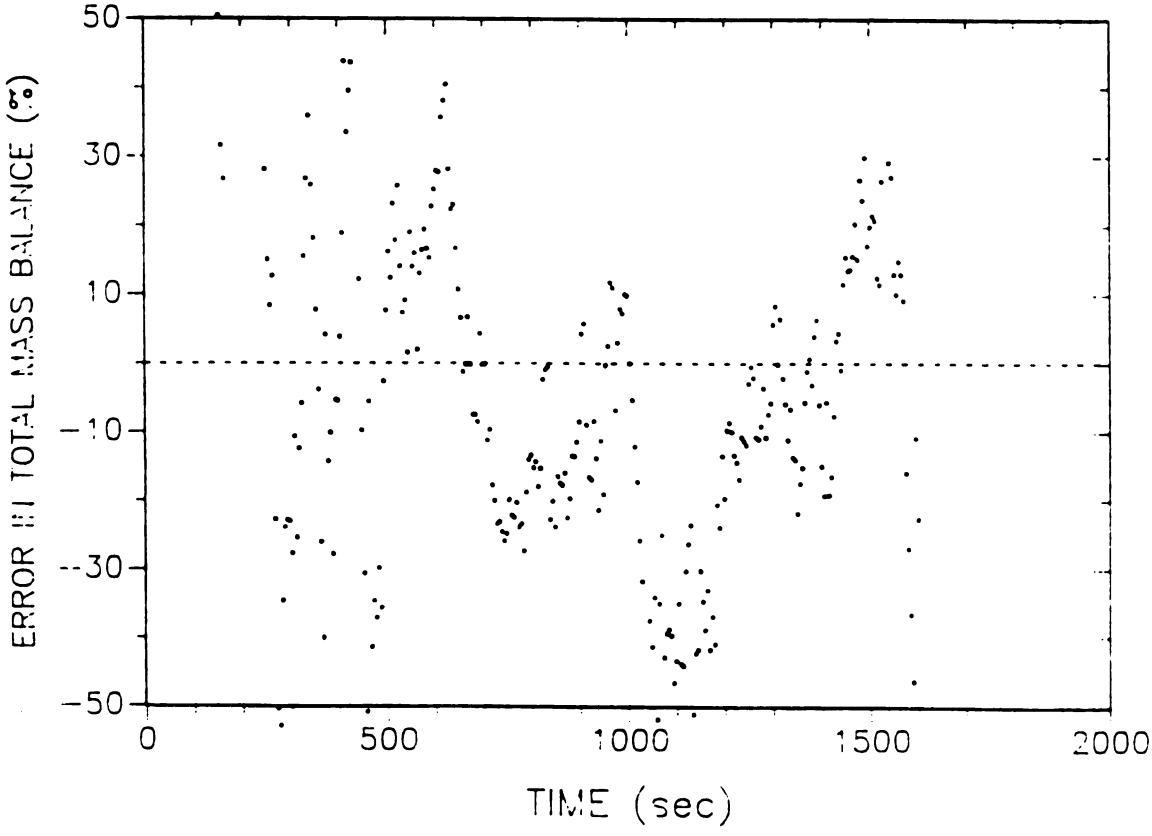

Fig. ERD1N Error in total mass balance for pyrolysis products; EXP. D1N

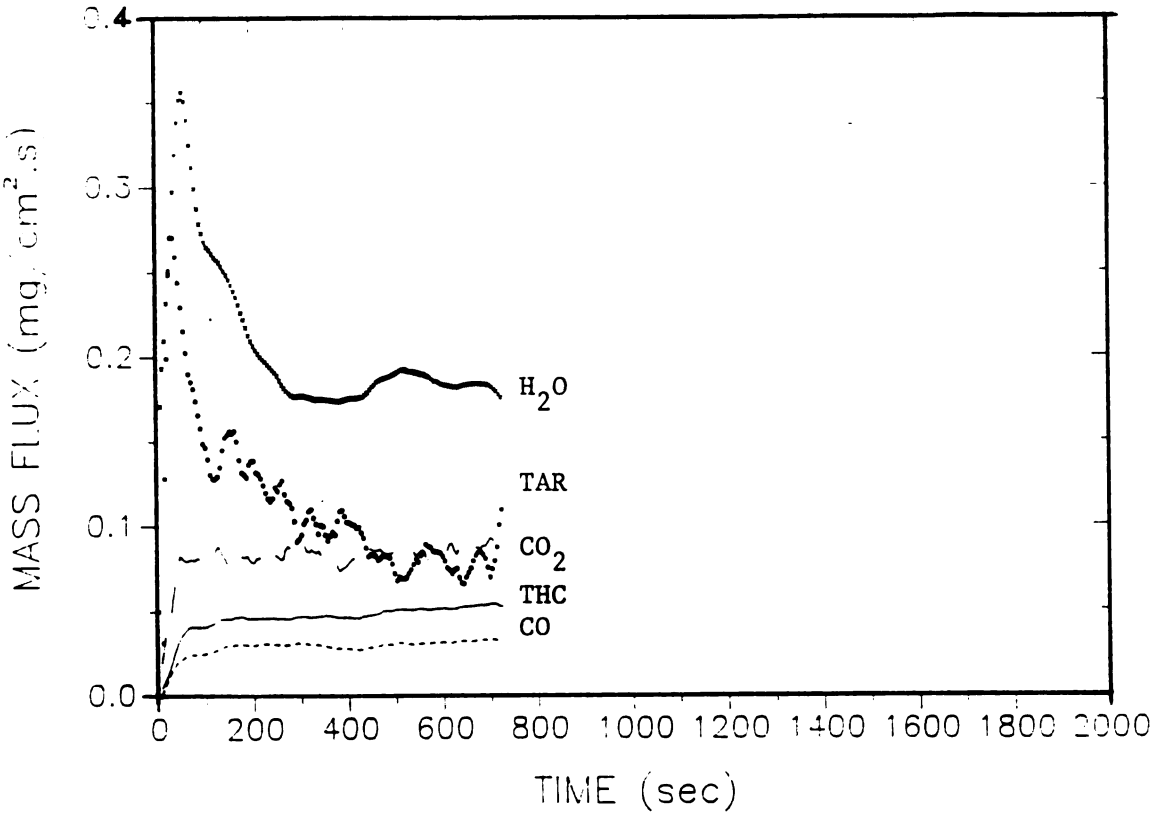

Fig. S1R4N Pyrolysis products (direct measurement); EXP. R4N

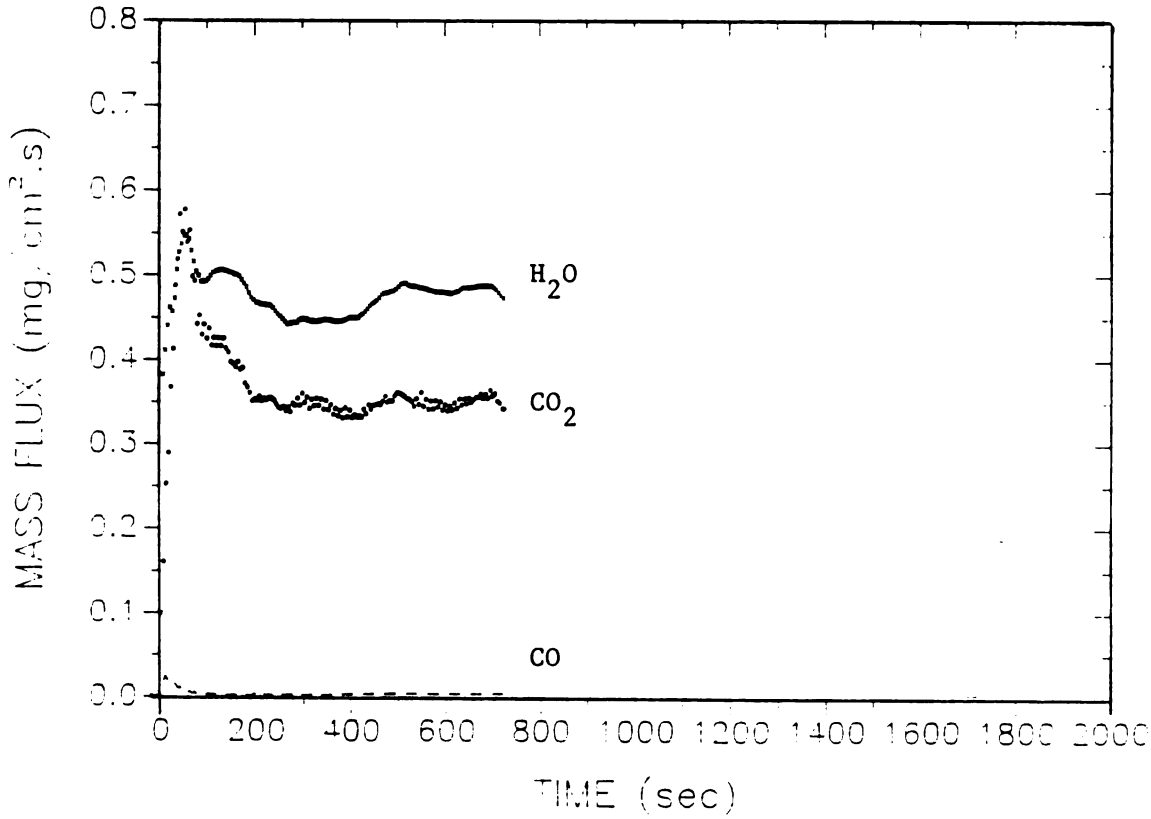

Fig. S2R4N Pyrolysis products (after catalytic combustor); EXP. R4N

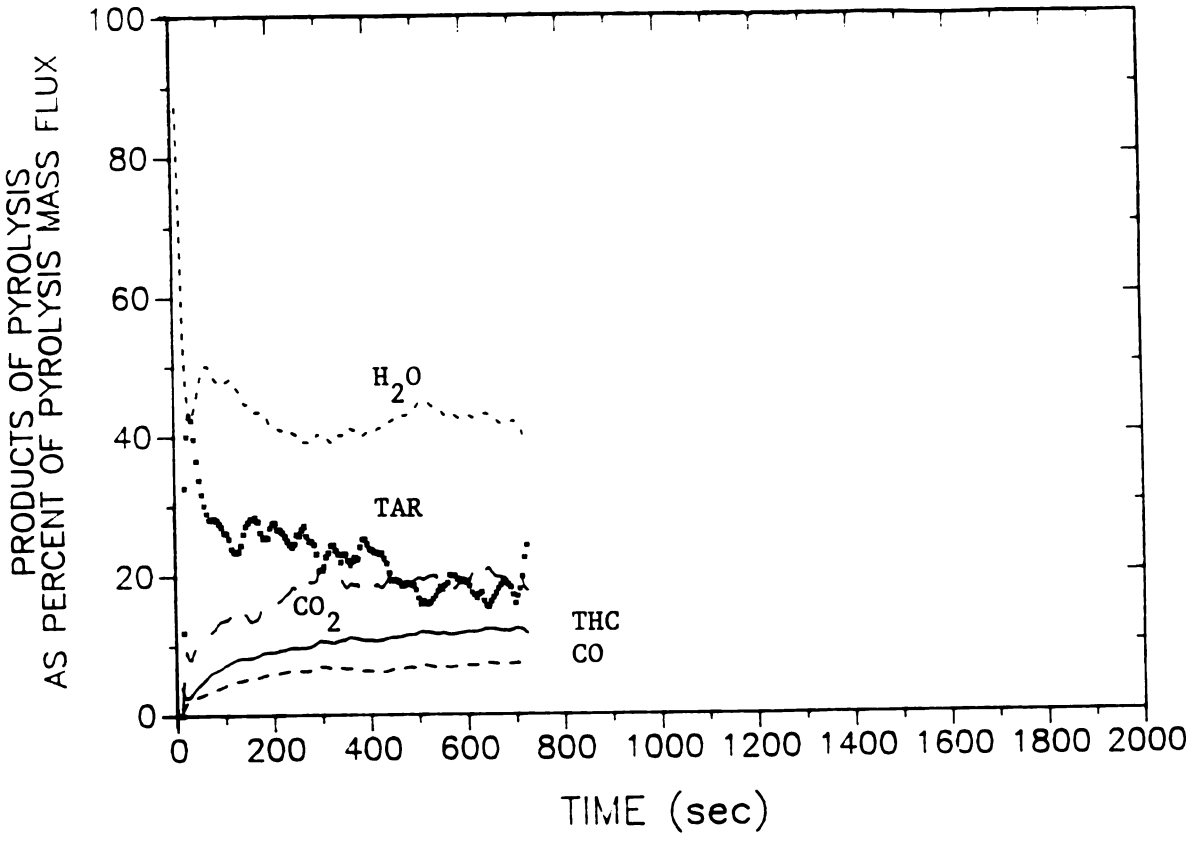

Fig. PSR4N Products of pyrolysis as percent of total mass flux; EXP. R4N

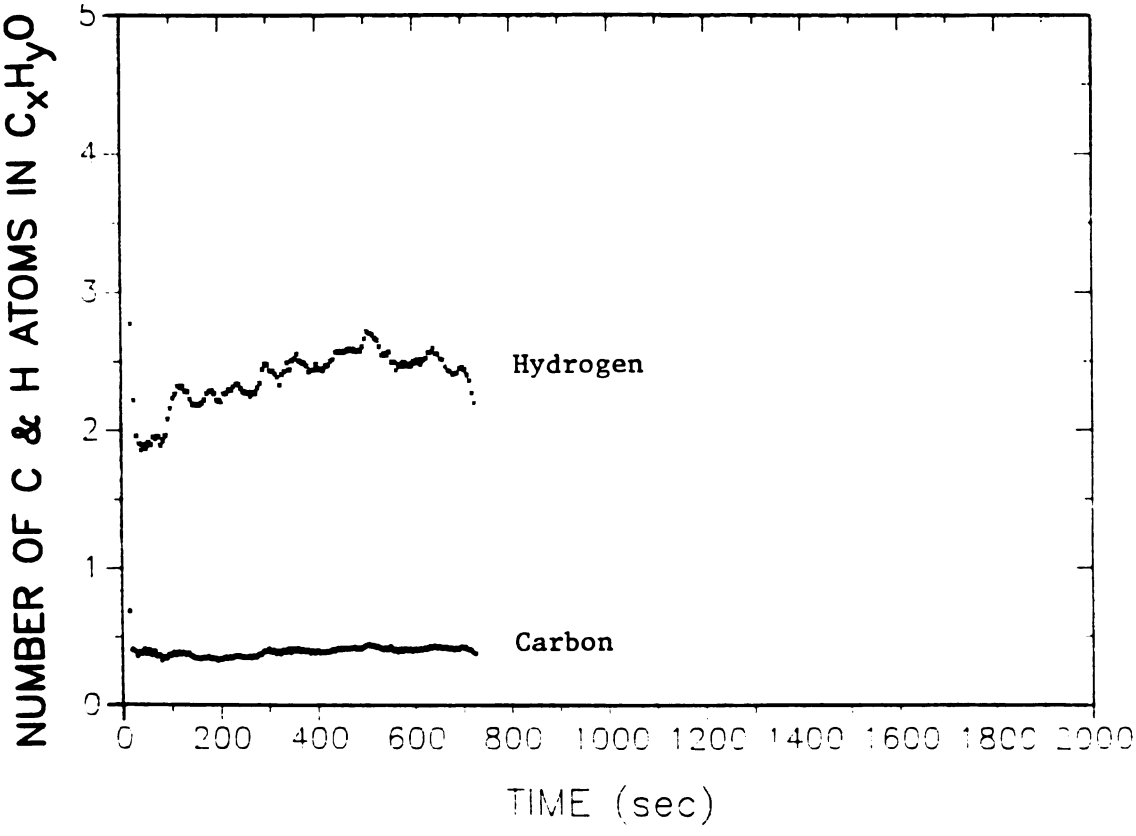

Fig. CHR4N Number of C and H atoms in the products of pyrolysis; EXP.

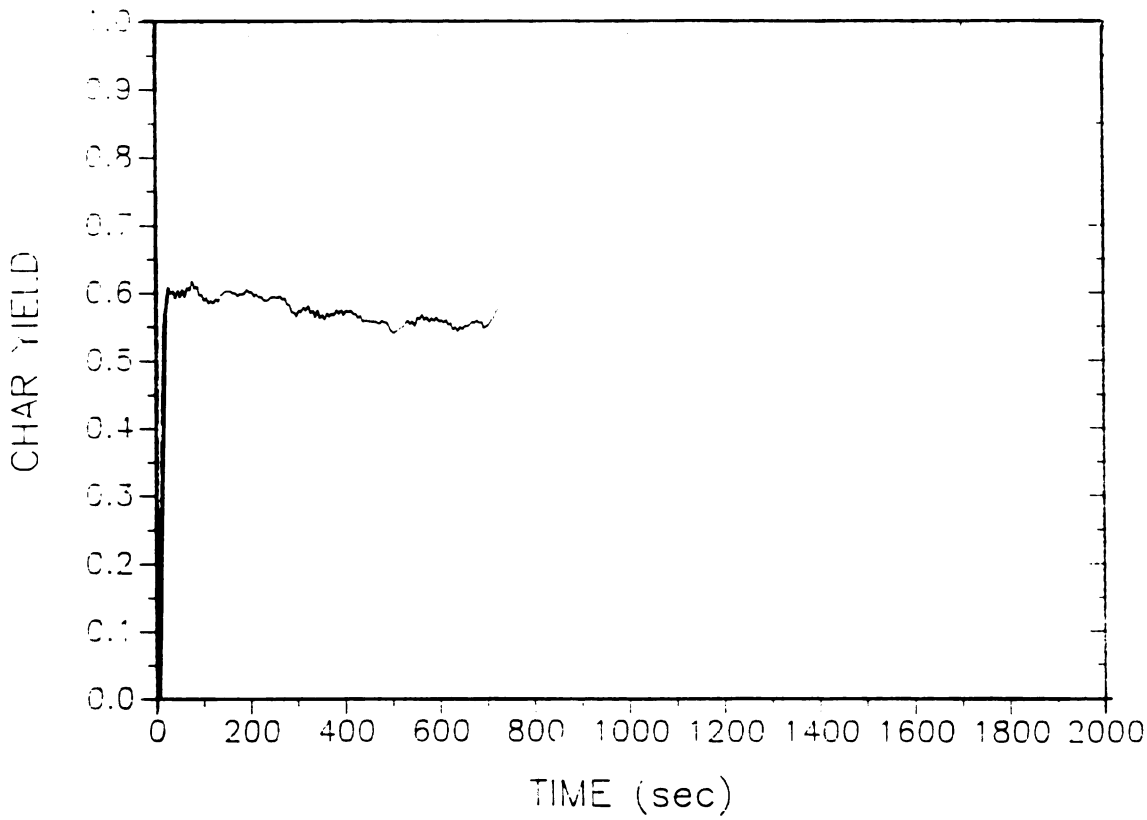

Fig. YCR4N Char yield (gram char/gram wood); EXP. R4N

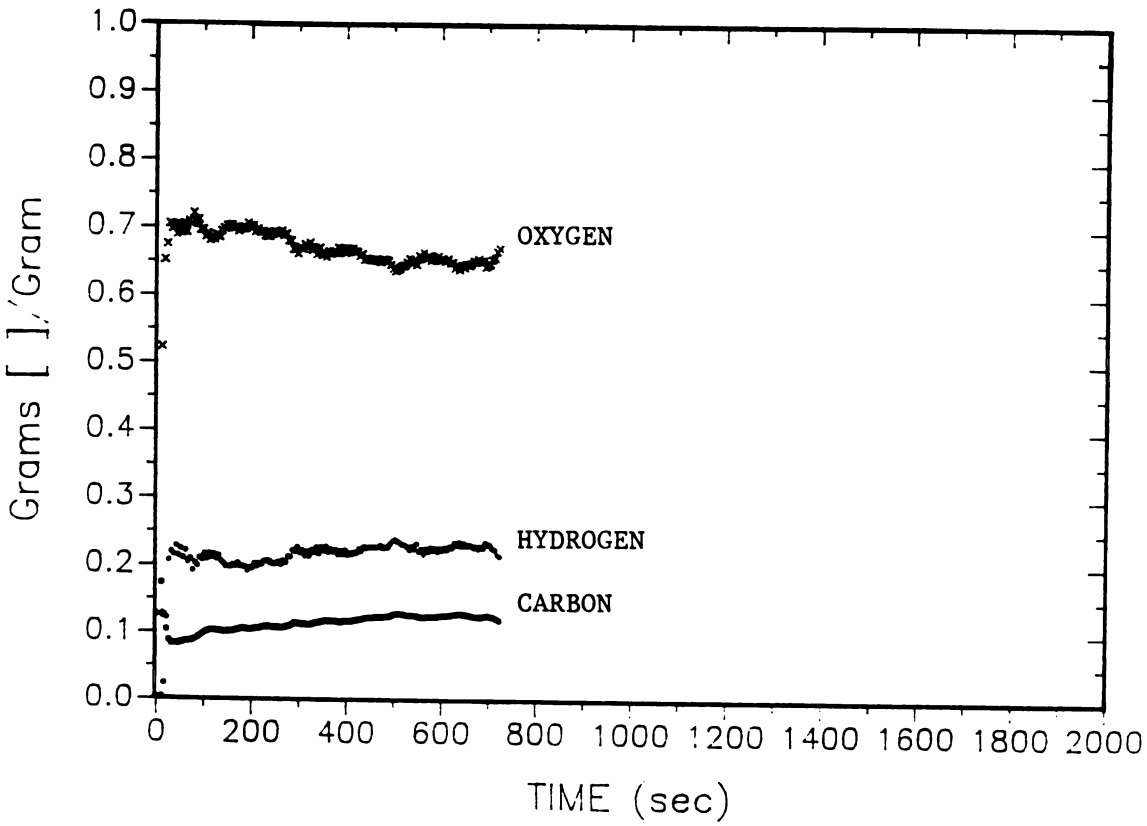

Fig. GGR4N Gram [ ]/gram of C_xH_yO; EXP. R4N

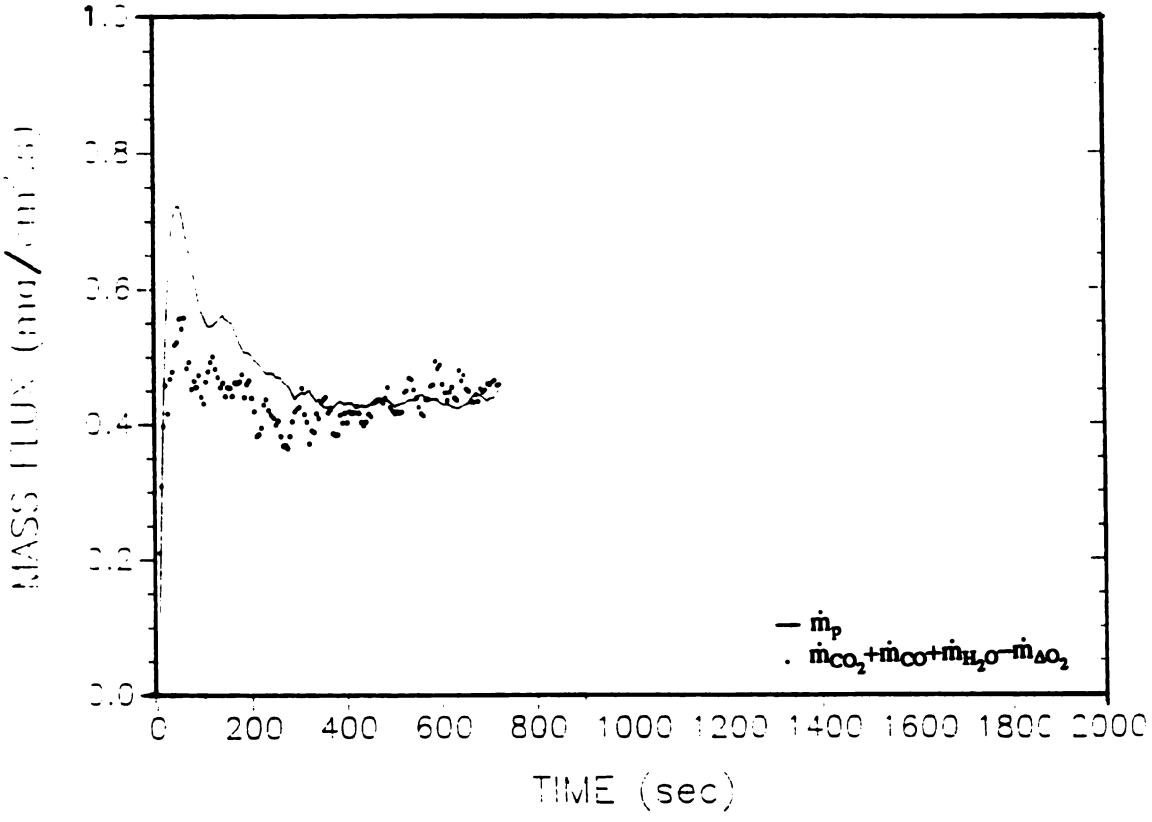

Fig. TMR4N Total mass balance for pyrolysis products; EXP. R4N

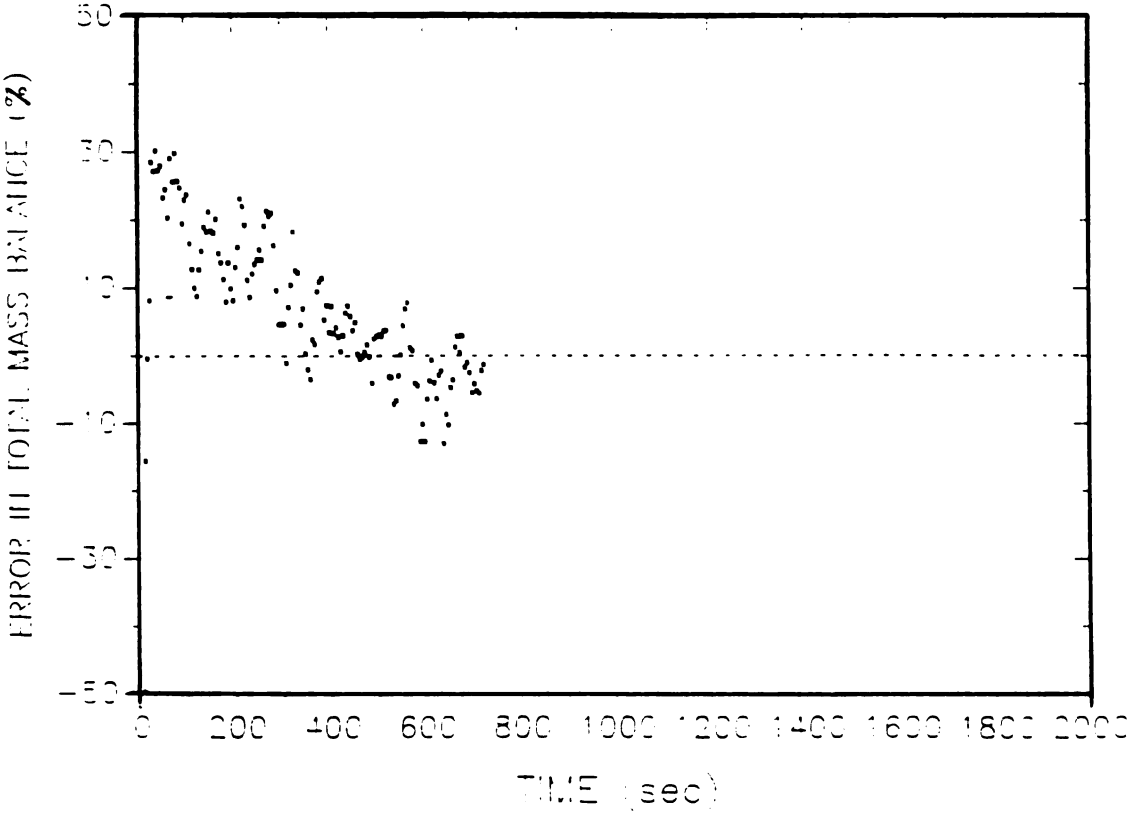

Fig. ERR4N Error in total mass balance for pyrolysis products; EXP. R4N

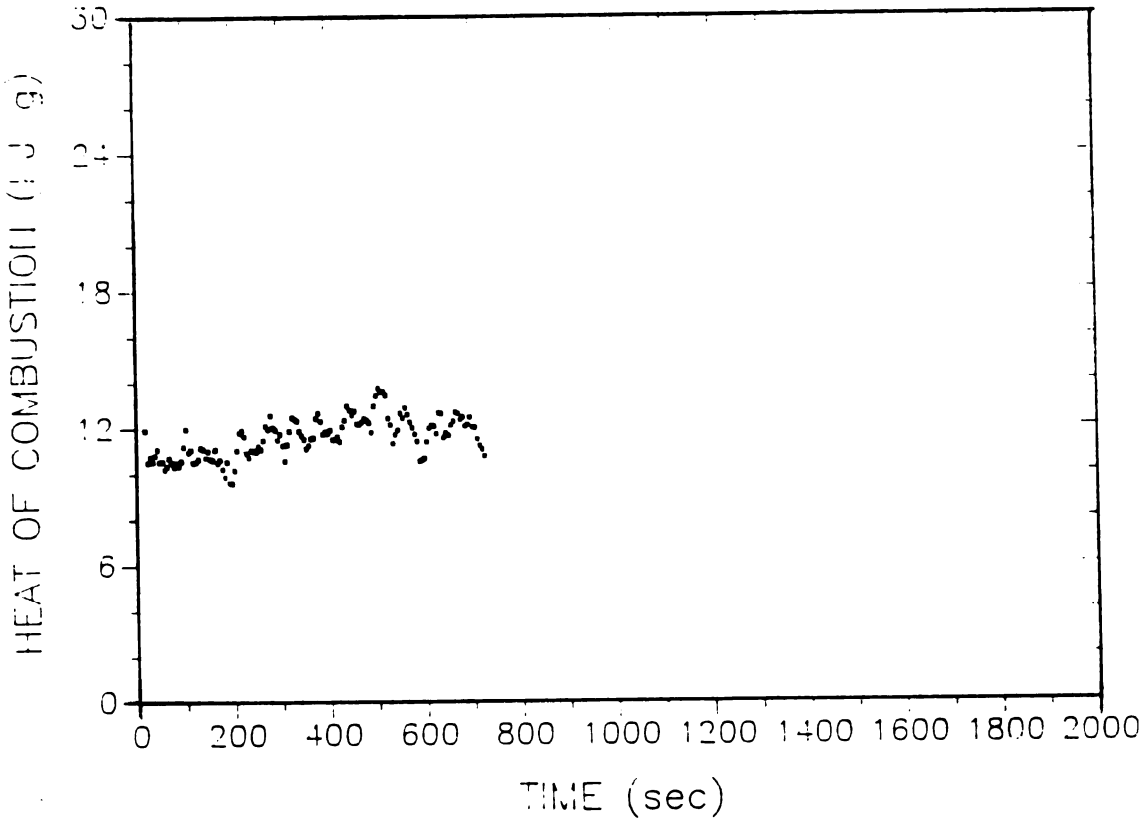

Fig. HVR4N Heat of combustion of pyrolysis products; EXP. R4N

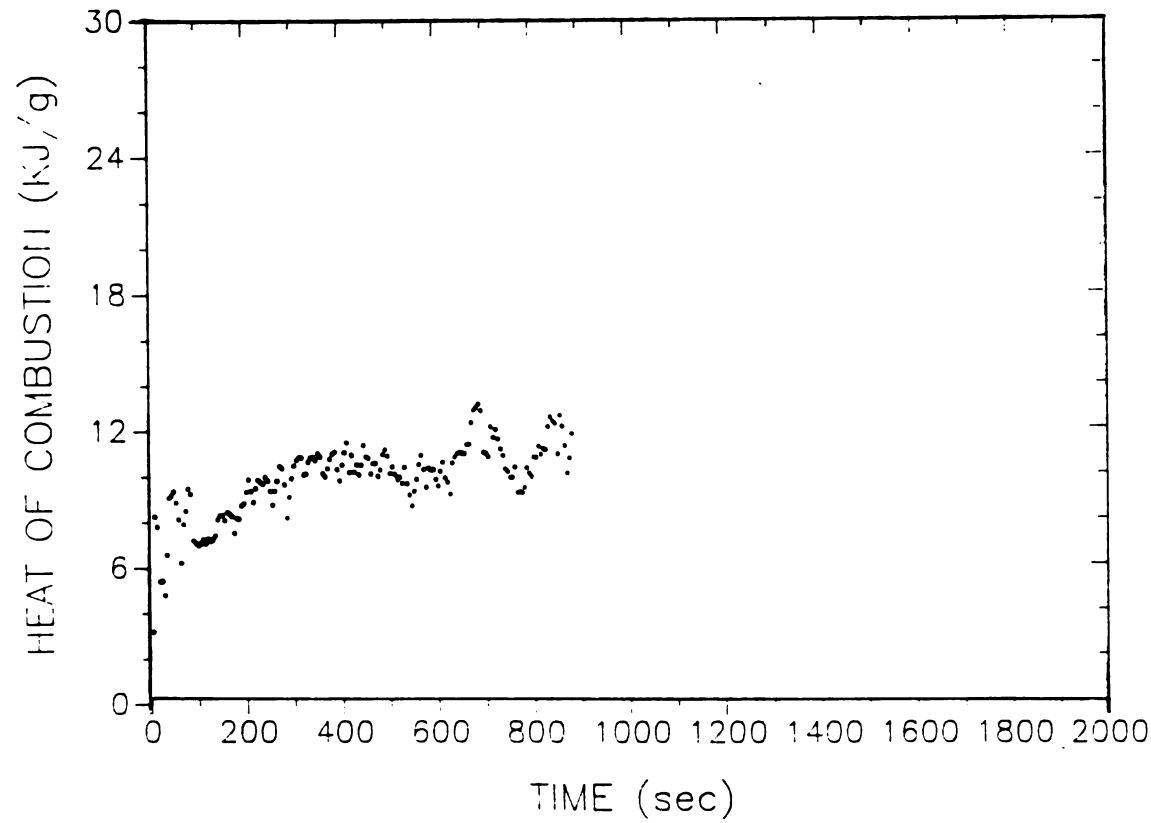

Fig. HVR3N Heat of combustion of pyrolysis products; EXP. R3N

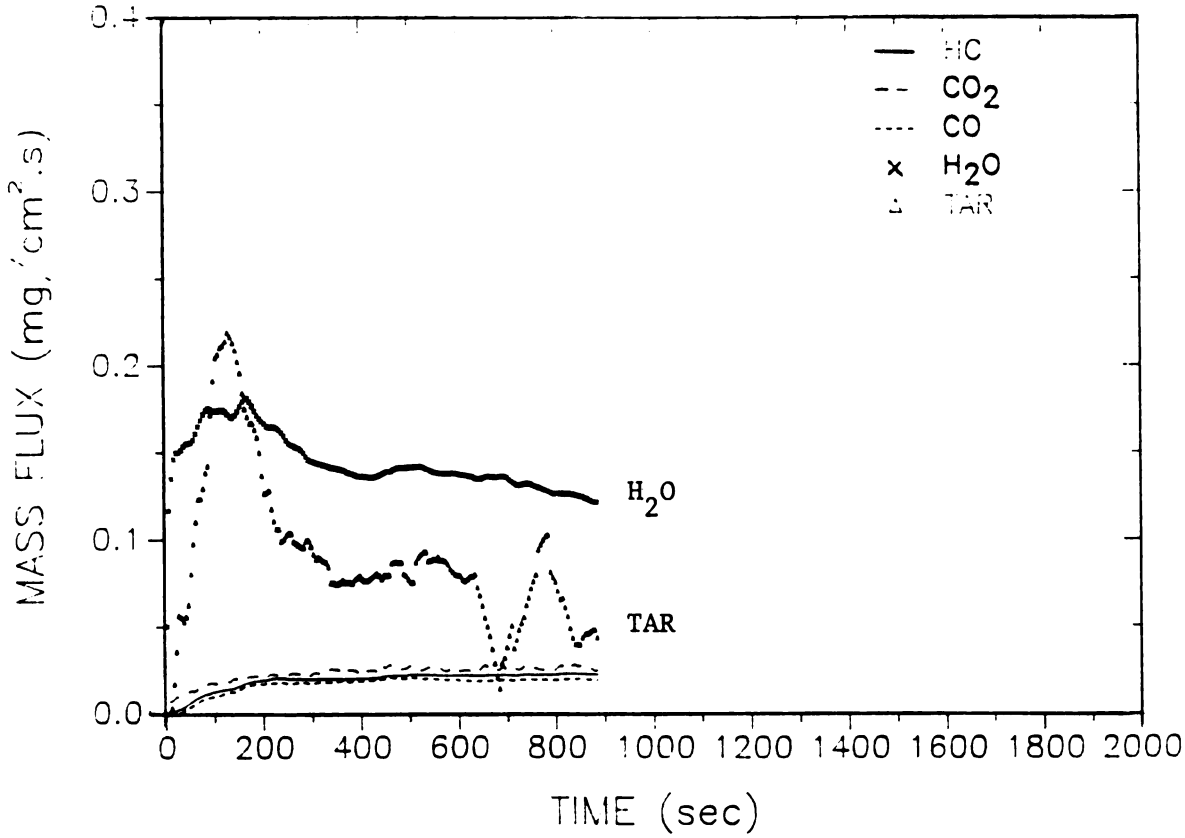

Fig. S1R3N Pyrolysis products (direct measurement); EXP. R3N

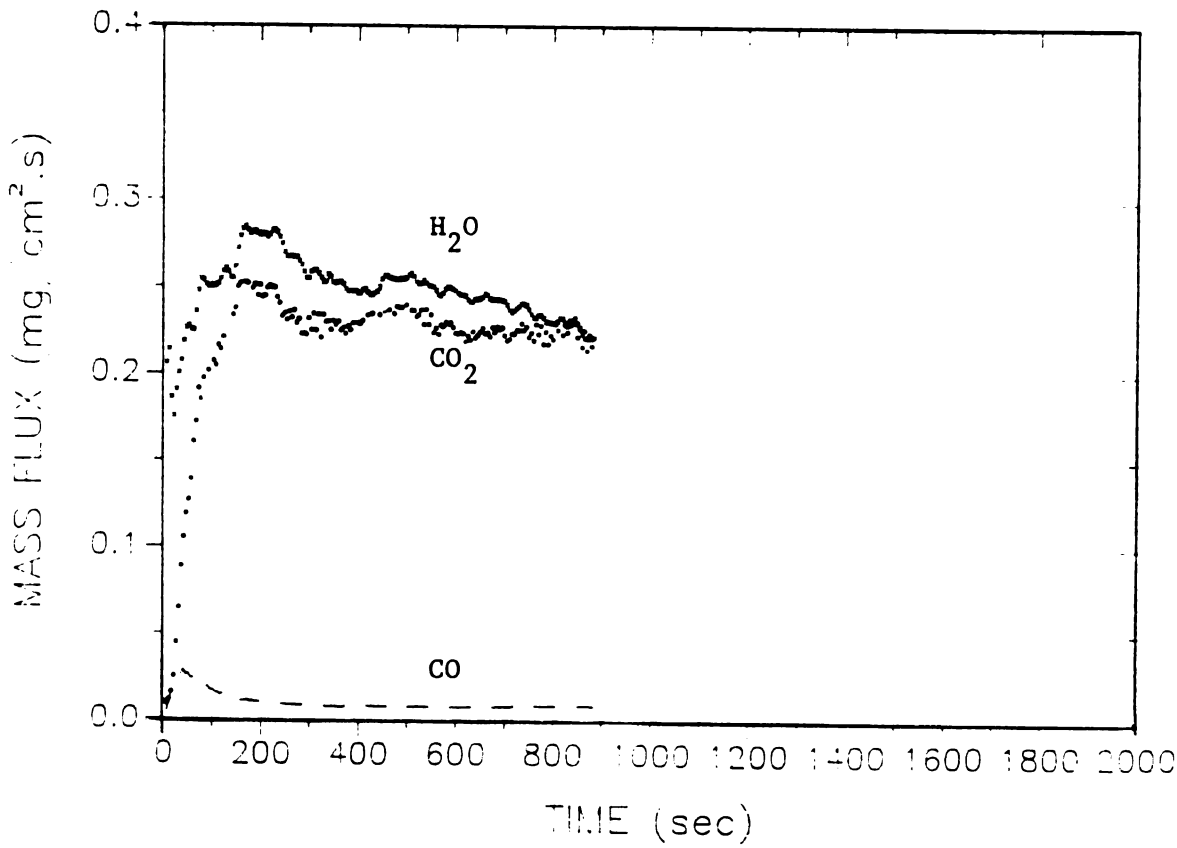

Fig. S2R3N Pyrolysis products (after catalytic combustor); EXP. R3N

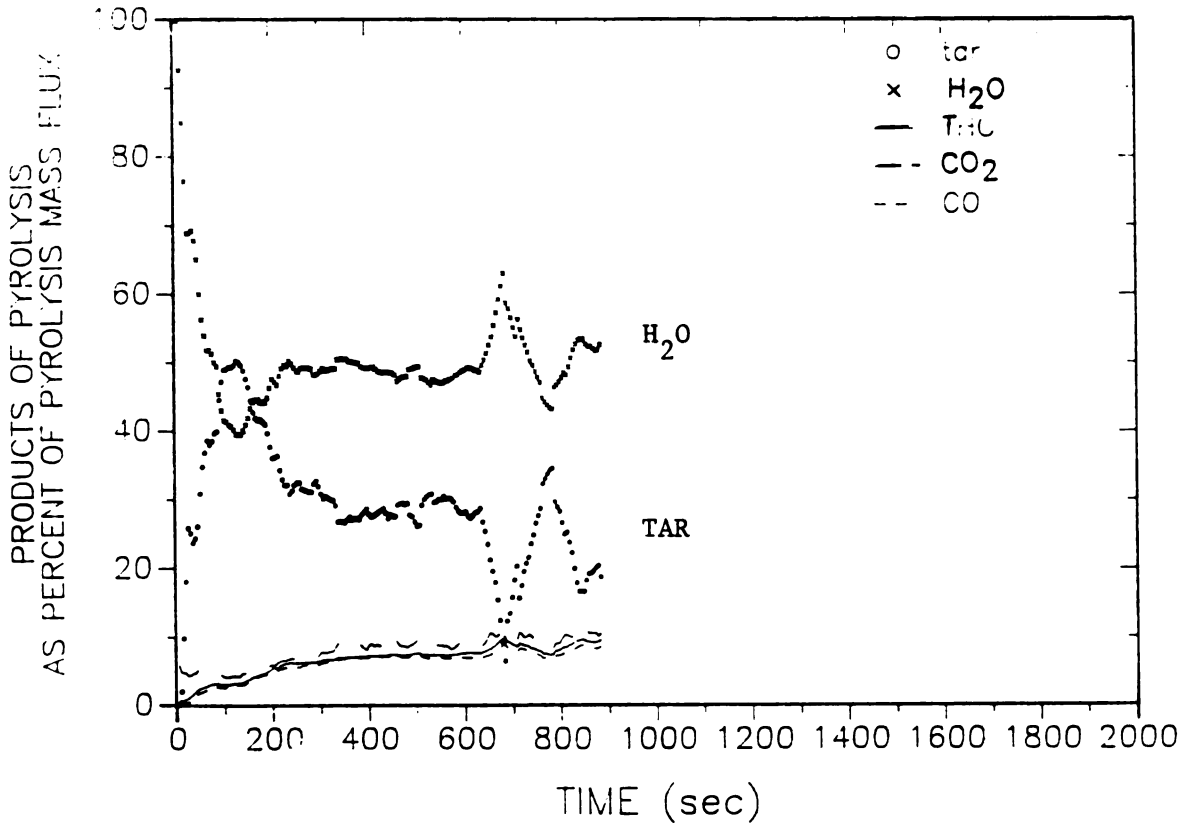

Fig. PSR3N Products of pyrolysis as percent of total mass flux; EXP. R3N

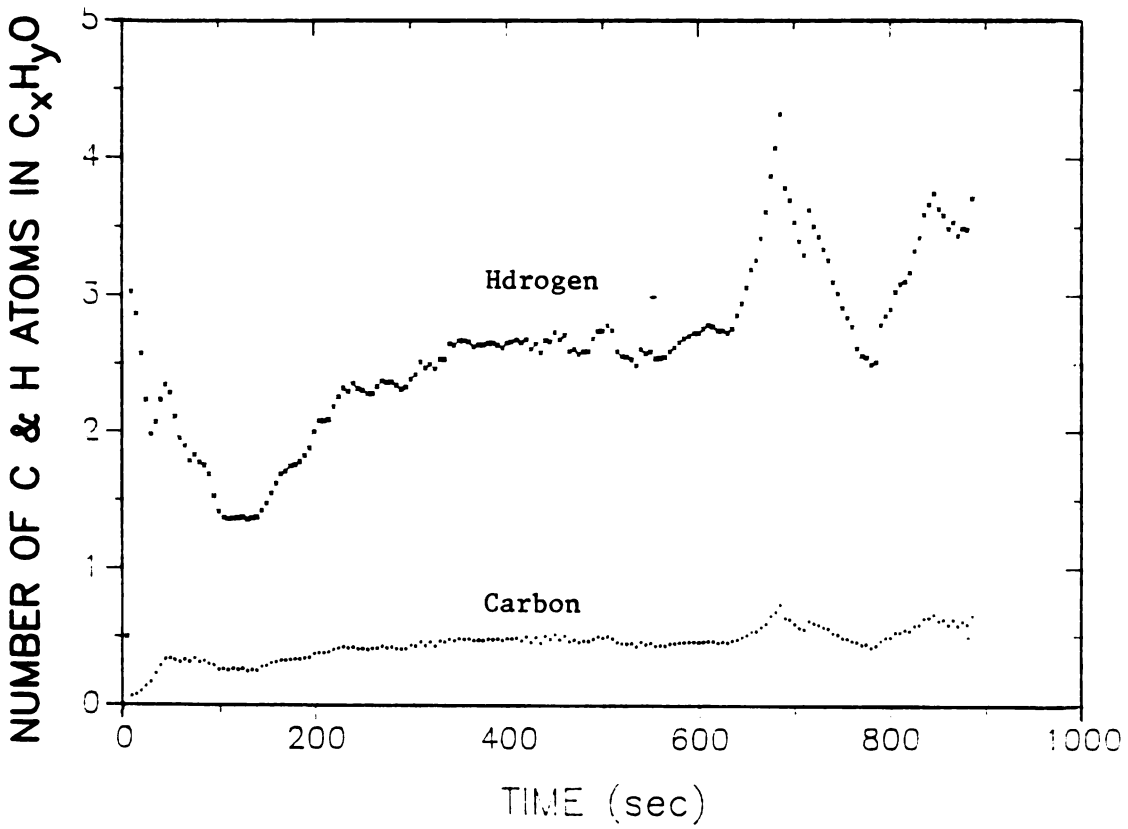

Fig. CHR3N Number of C and H atoms in the products of pyrolysis; EXP. R3N

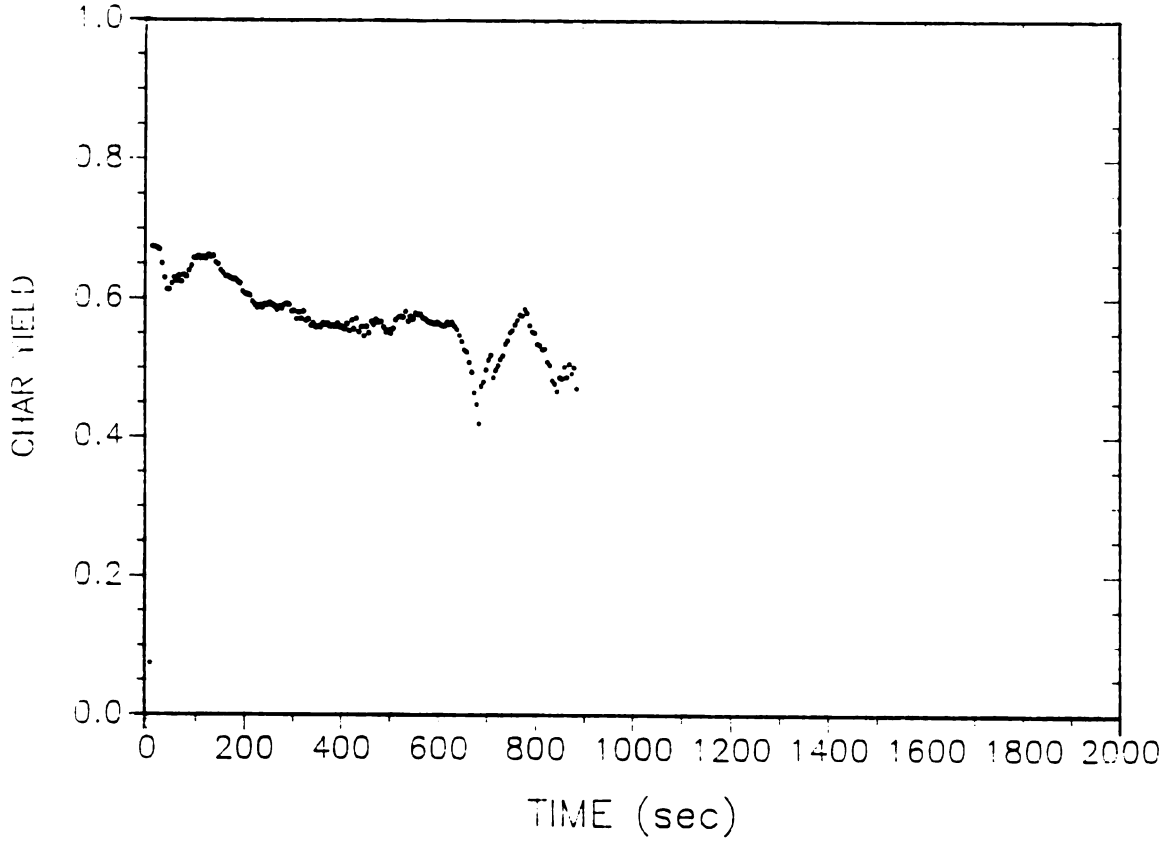

Fig. YCR3N Char yield (gram char/gram wood); EXP. R3N

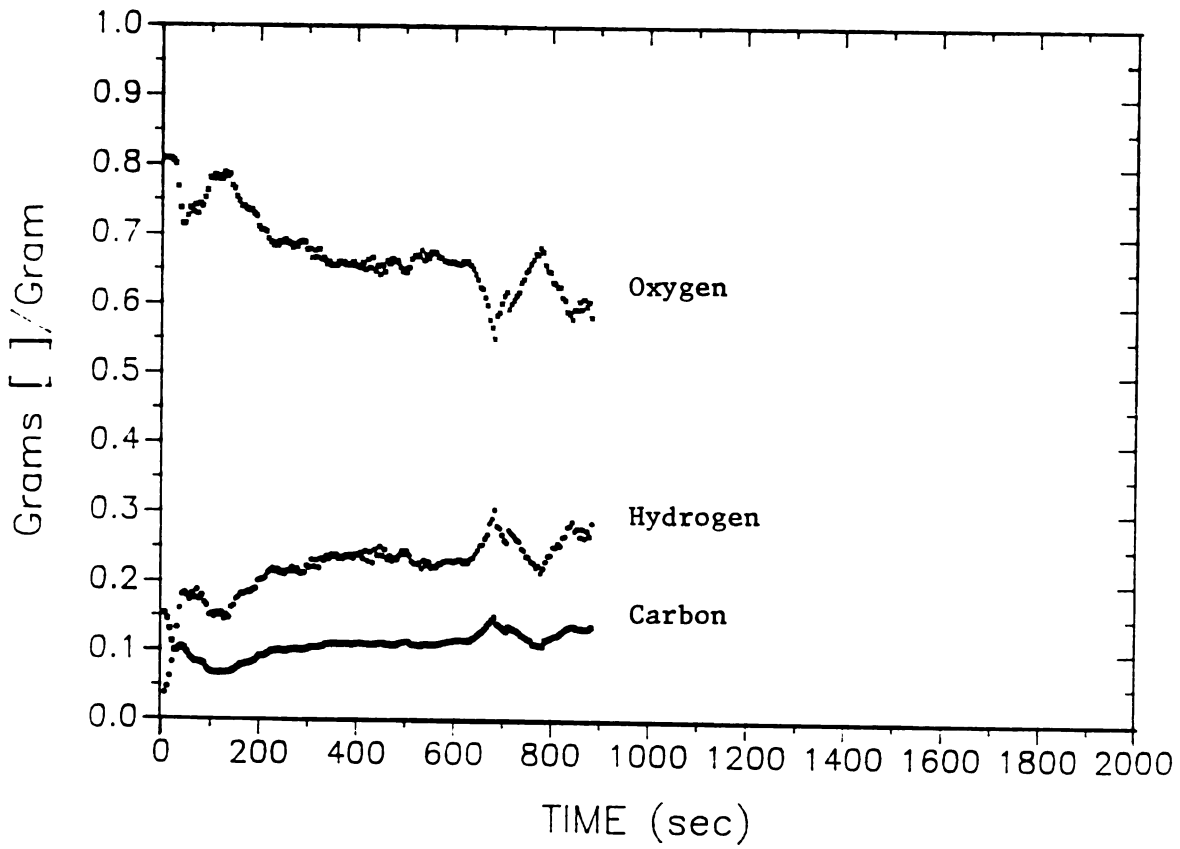

Fig. GGR3N Gram [ ]/gram of C_xH_yO; EXP. R3N

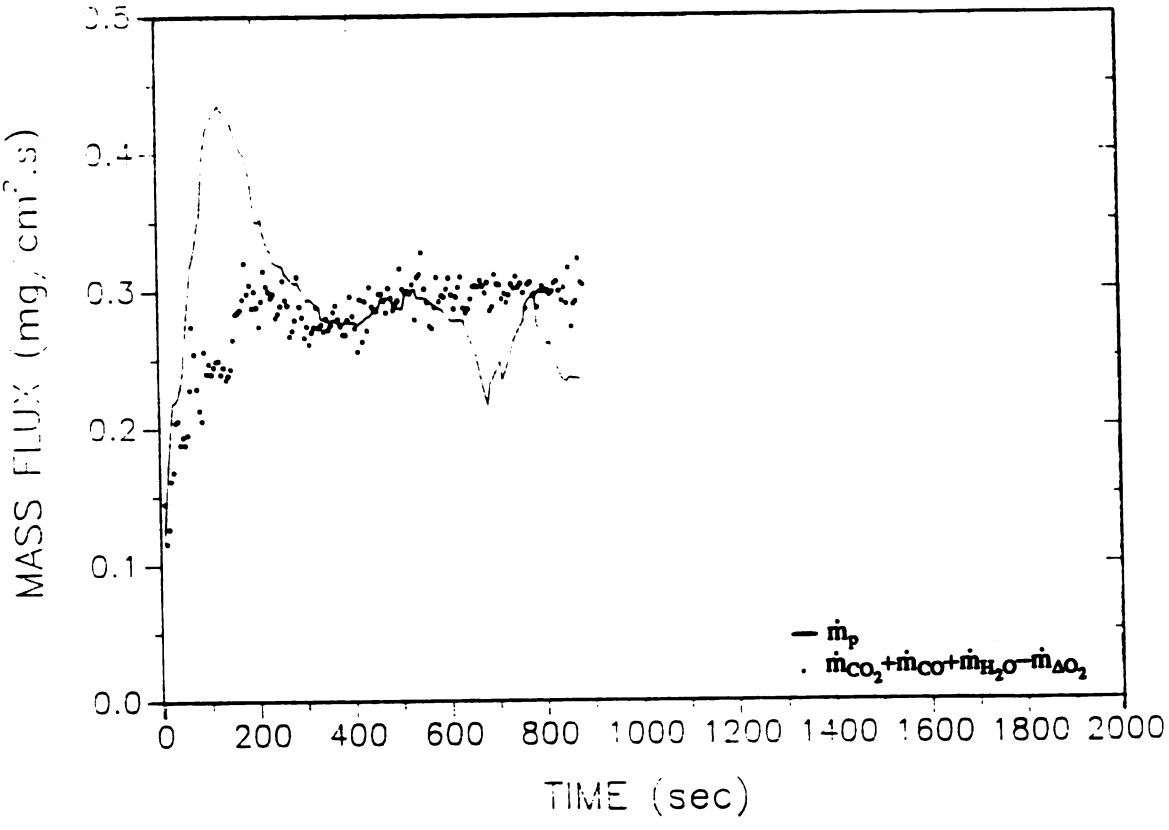

Fig. TMR3N Total mass balance for pyrolysis products; EXP. R3N

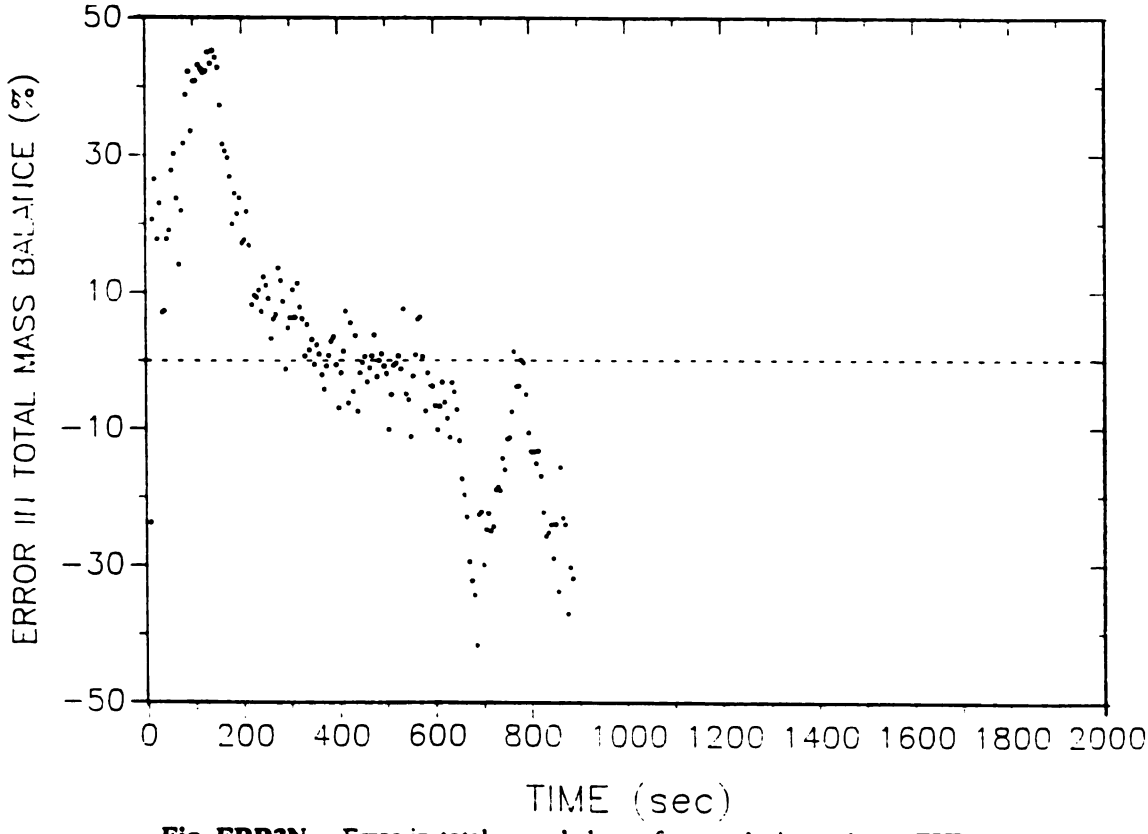

Fig. ERR3N Error in total mass balance for pyrolysis products; EXP. R3N

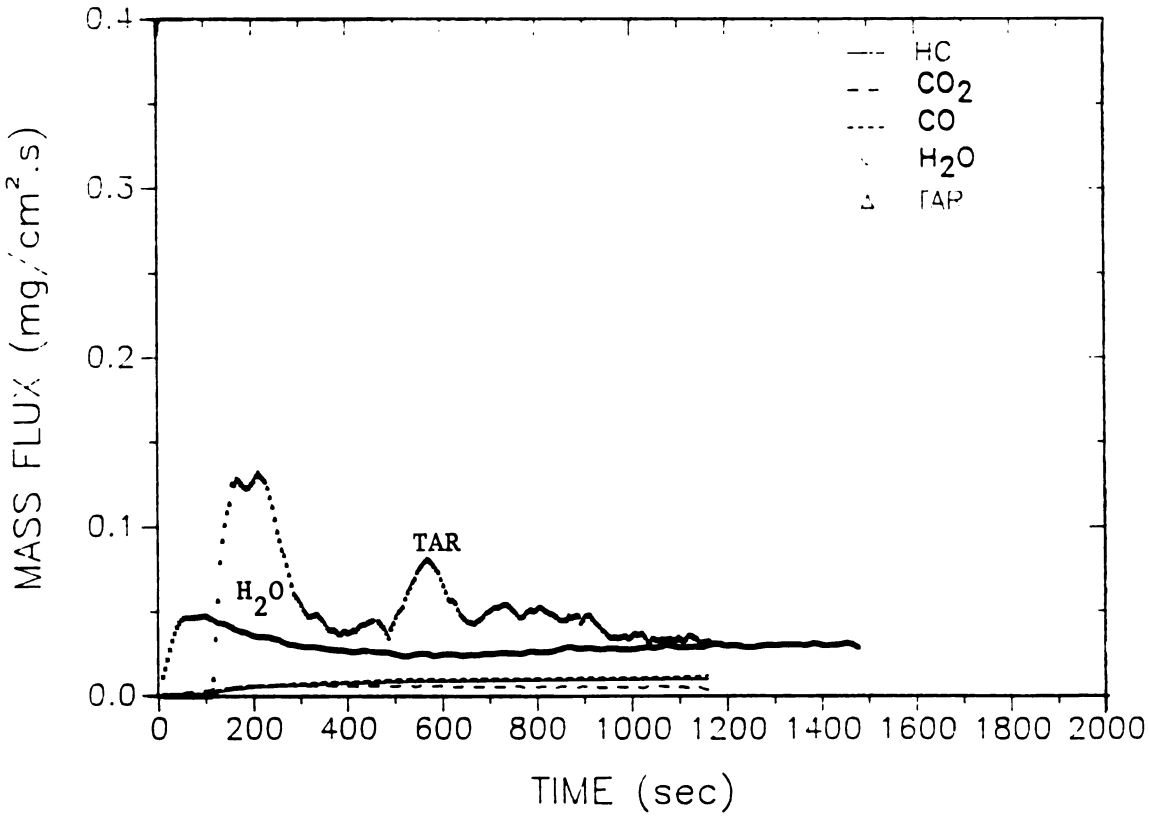

Fig. S1R2N Pyrolysis products (direct measurement); EXP. R2N

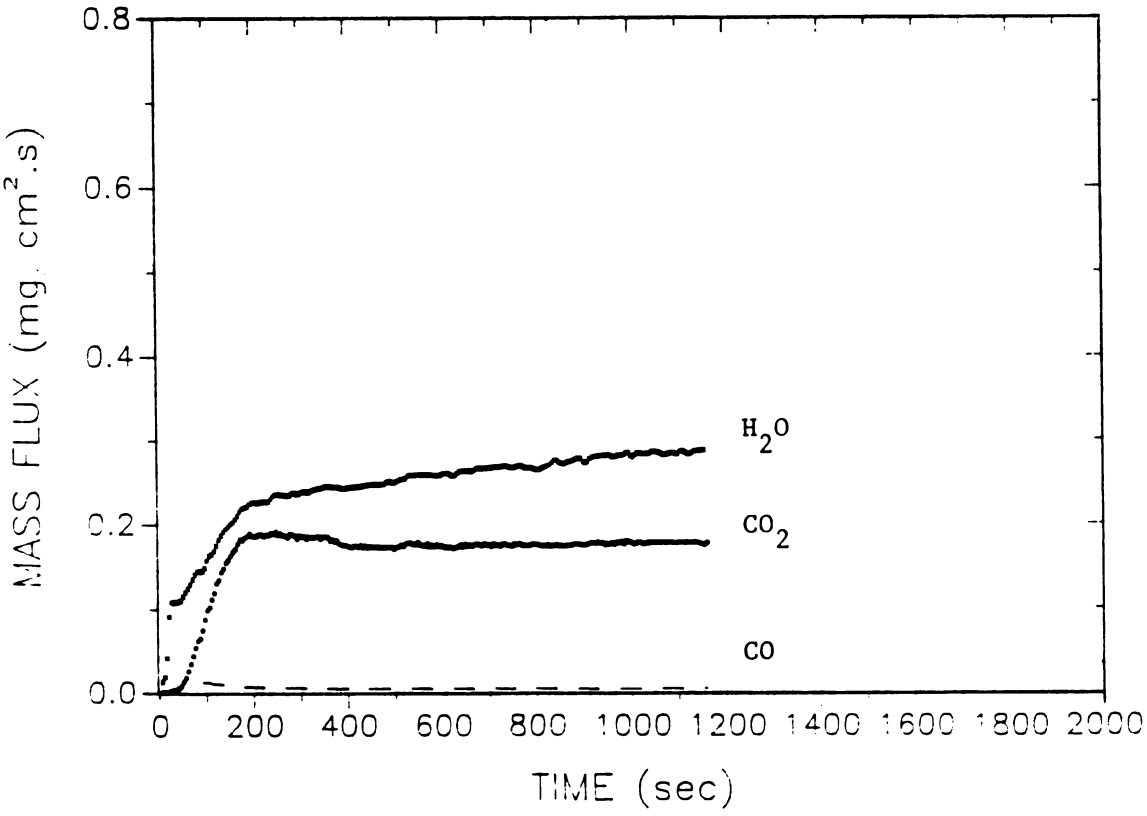

Fig. S2R2N Pyrolysis products (after catalytic combustor); EXP. R2N

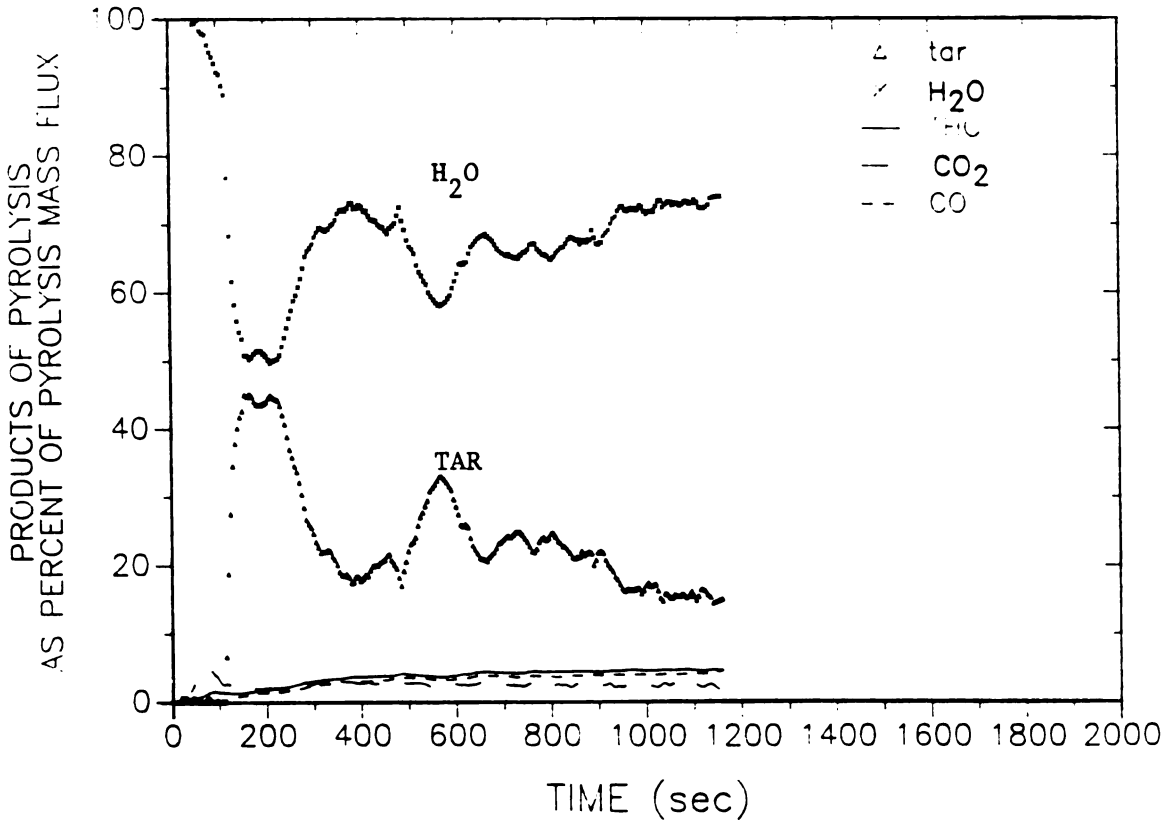

Fig. PSR2N Products of pyrolysis as percent of total mass flux; EXP. R2N

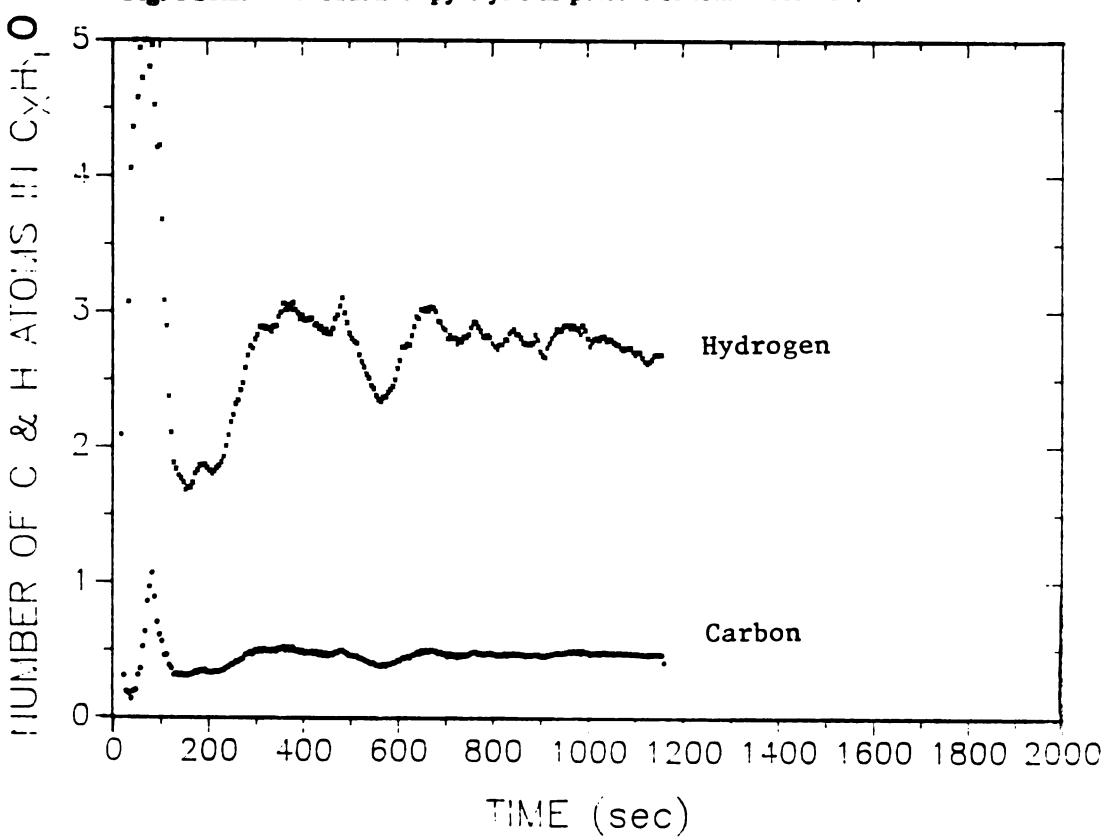

Fig. CHR2N Number of C and H atoms in the products of pyrolysis; EXP.

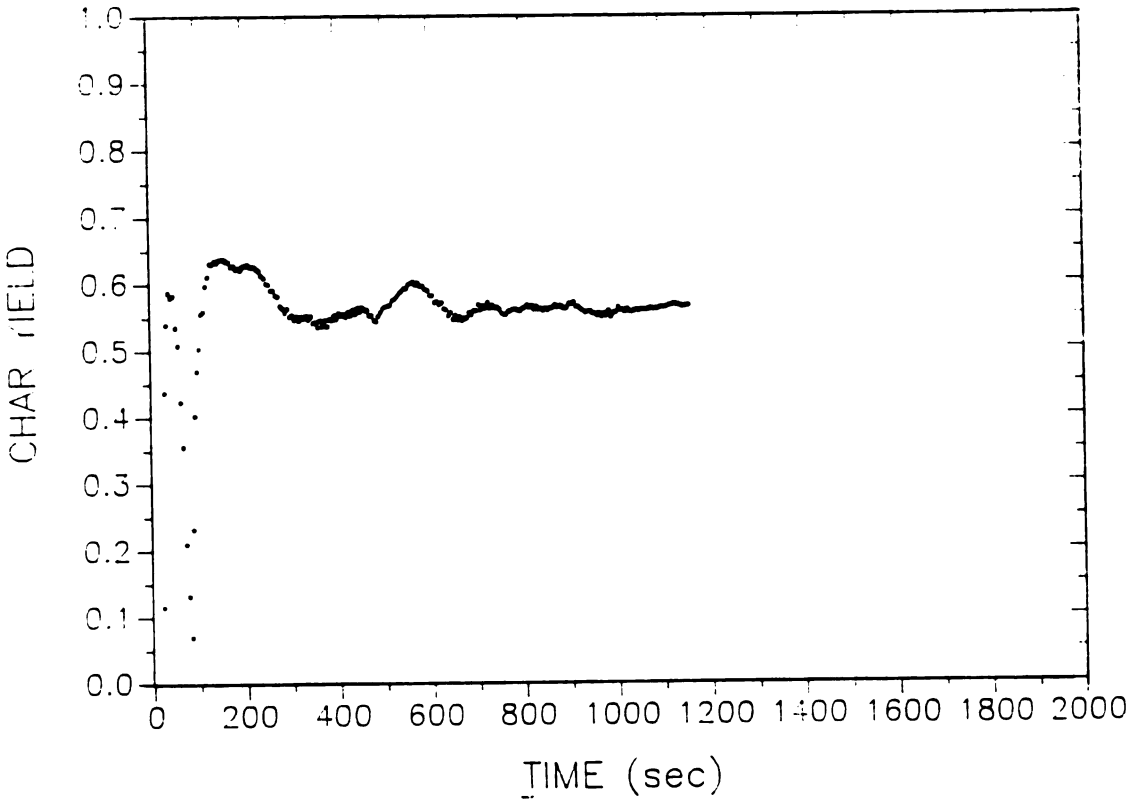

Fig. YCR2N Char yield (gram char/gram wood); EXP. R2N

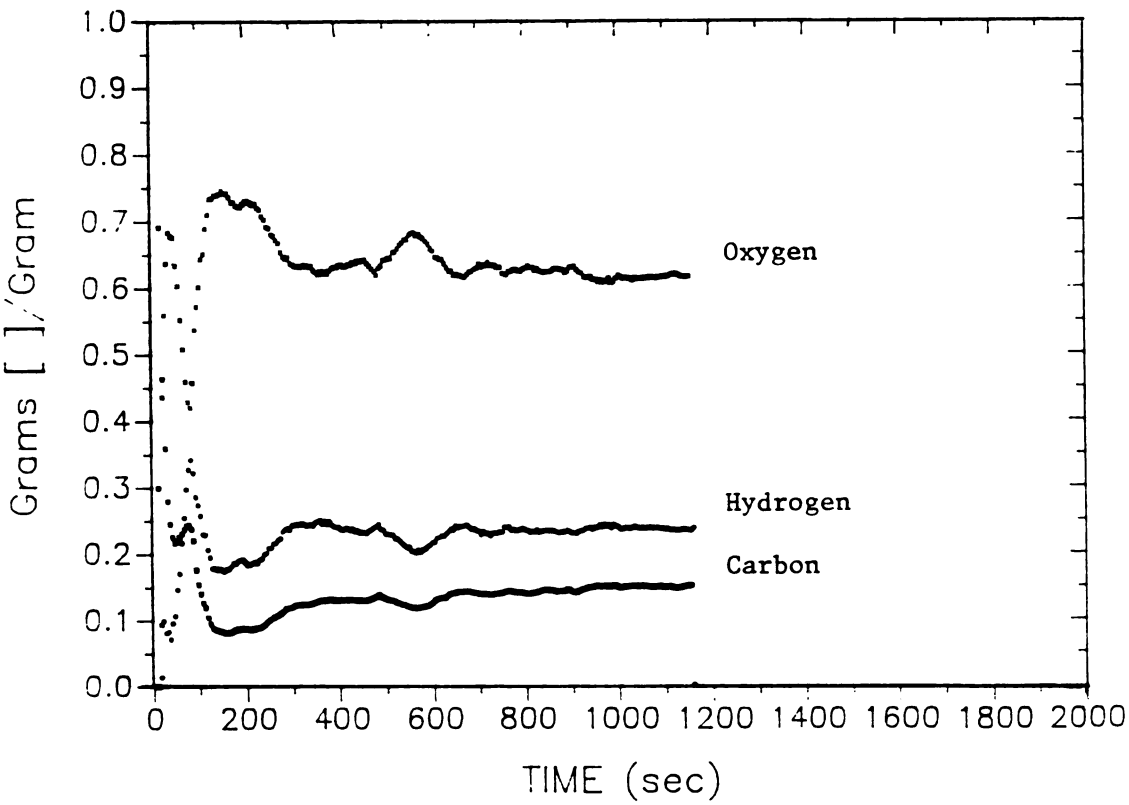

Fig. GGR2N Gram [ ]/gram of C_xH_yO; EXP. R2N

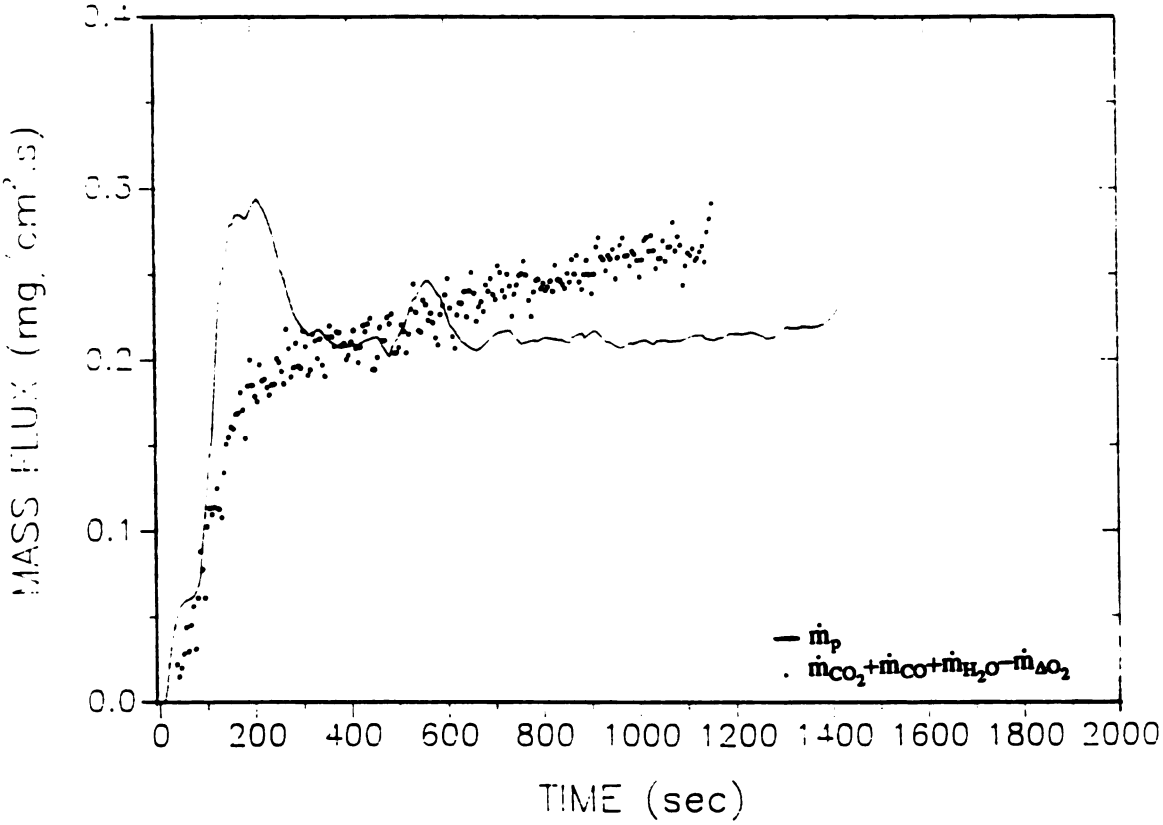

Fig. TMR2N Total mass balance for pyrolysis products; EXP. R2N

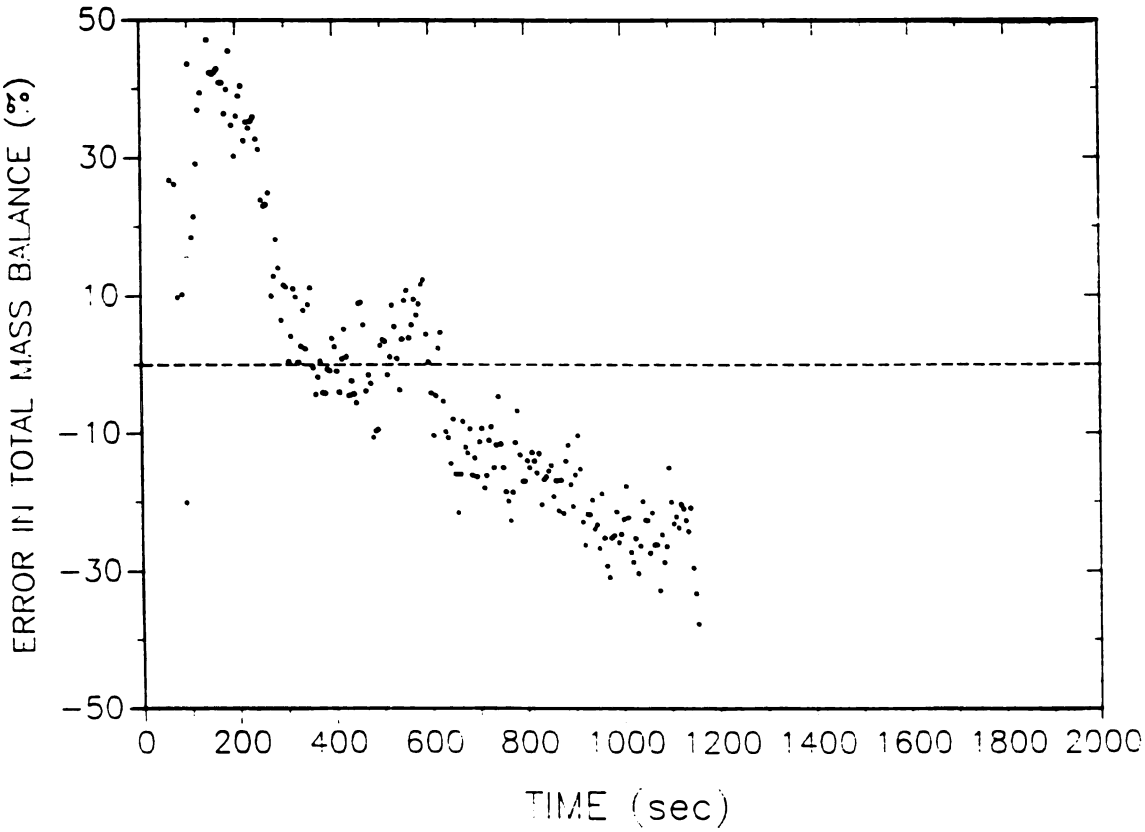

Fig. ERR2N Error in total mass balance for pyrolysis products; EXP. R2N

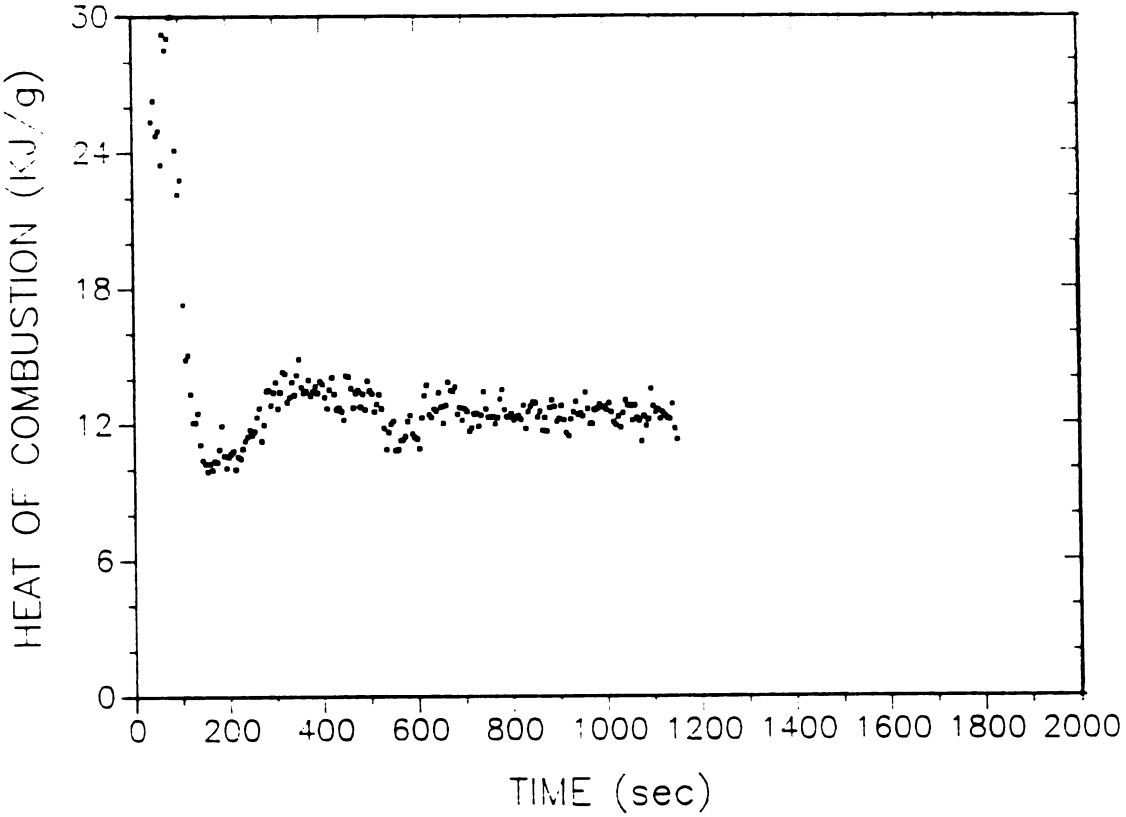

Fig. HVR2N Heat of combustion of pyrolysis products; EXP. R2N

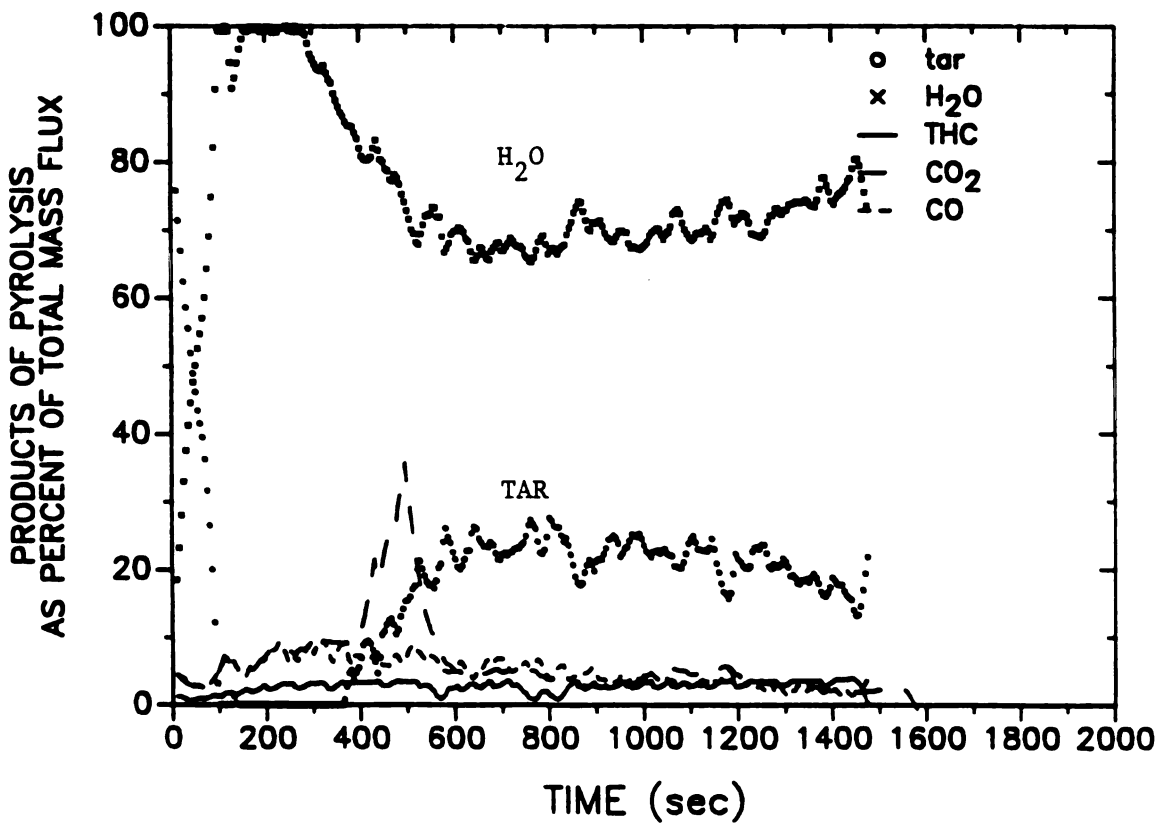

Fig. PSR1N Products of pyrolysis as percent of total mass flux; EXP. R1N

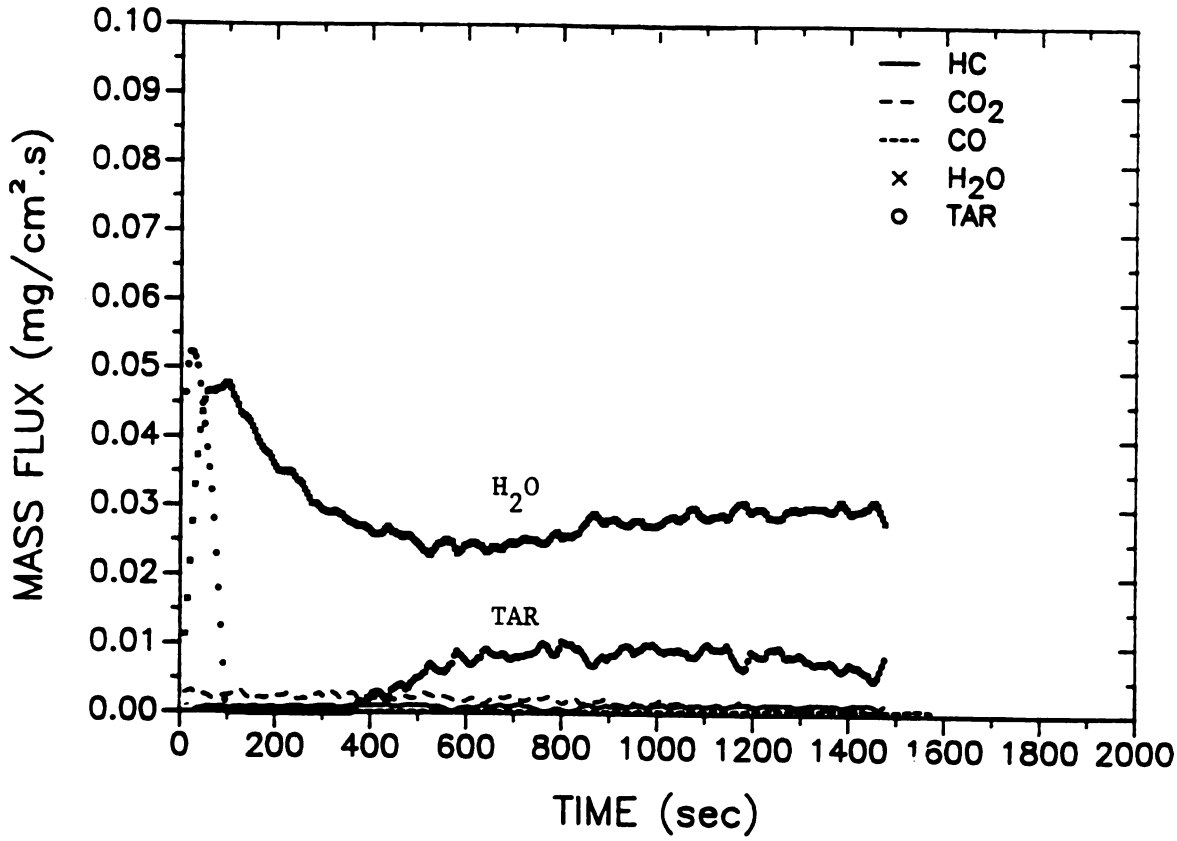

Fig. S1R1N Pyrolysis products (direct measurement); EXP. R1N

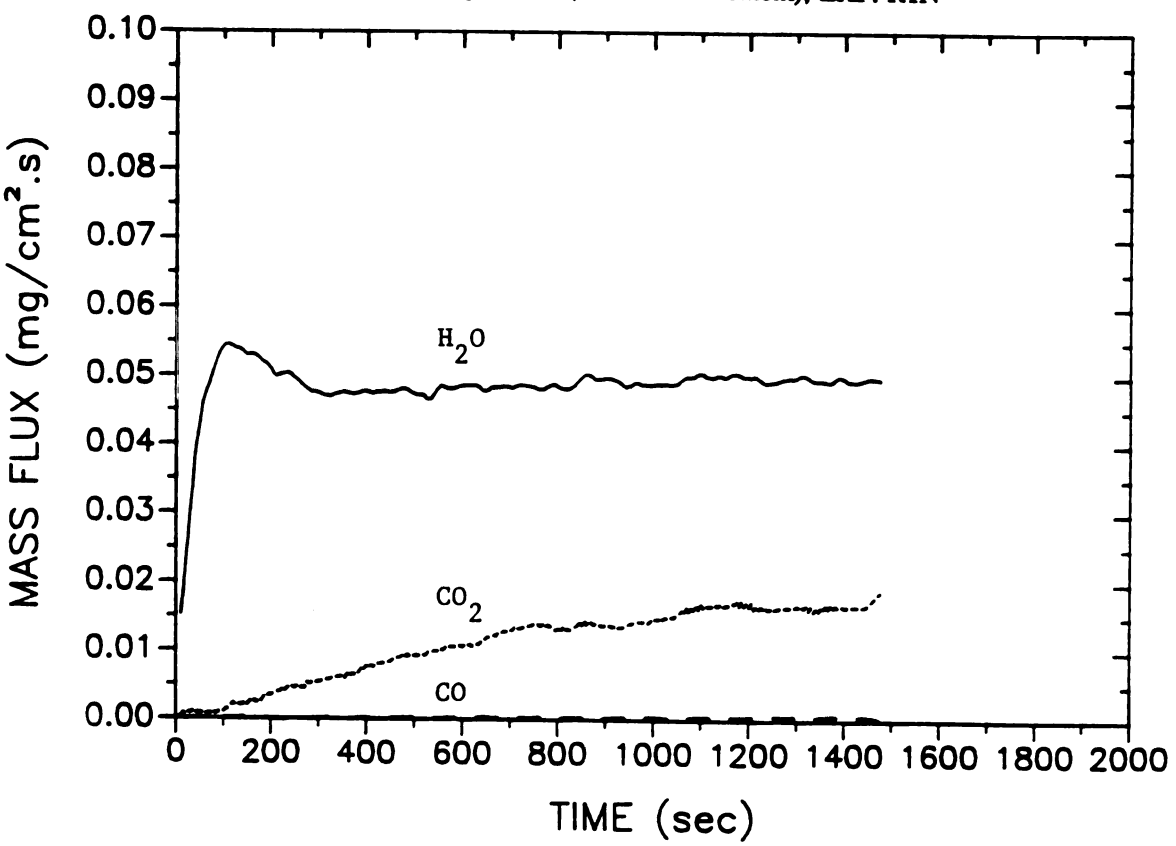

Fig. S2R1N Pyrolysis products (after catalytic combustor); EXP. R1N

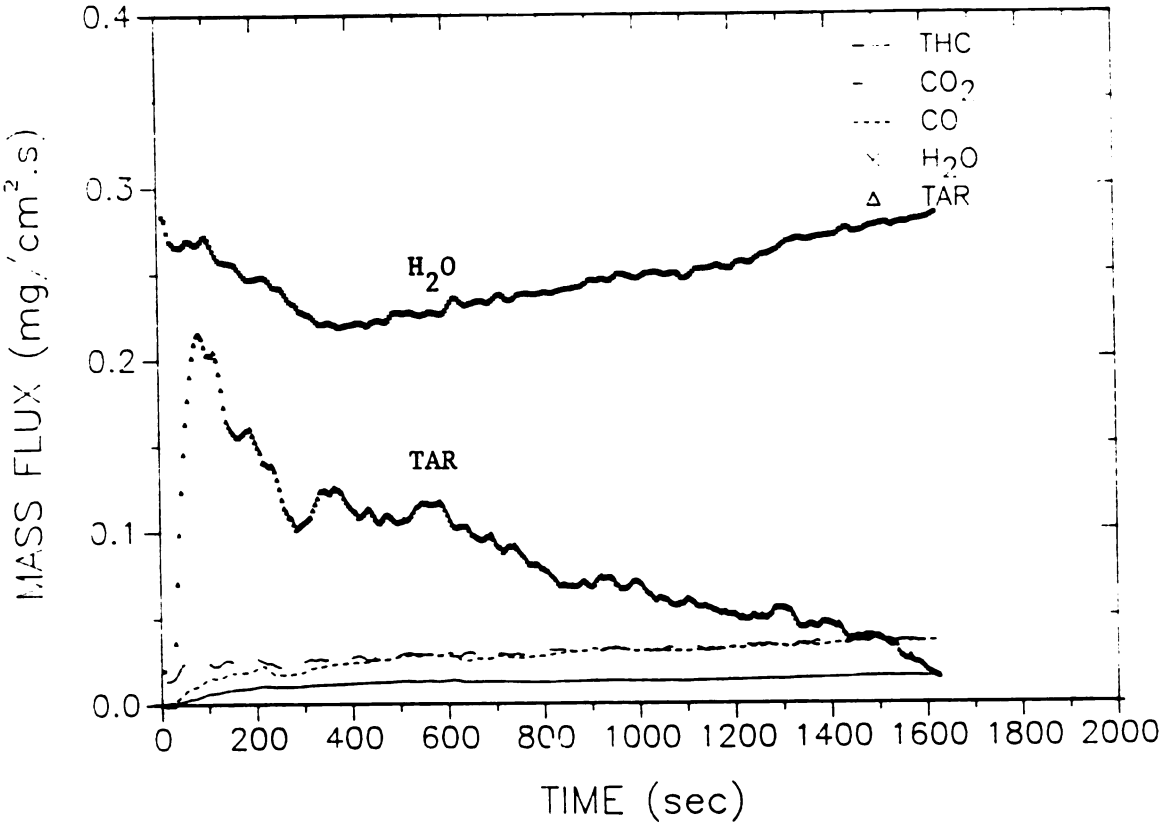

Fig. S1M4N Pyrolysis products (direct measurement); EXP. M4N

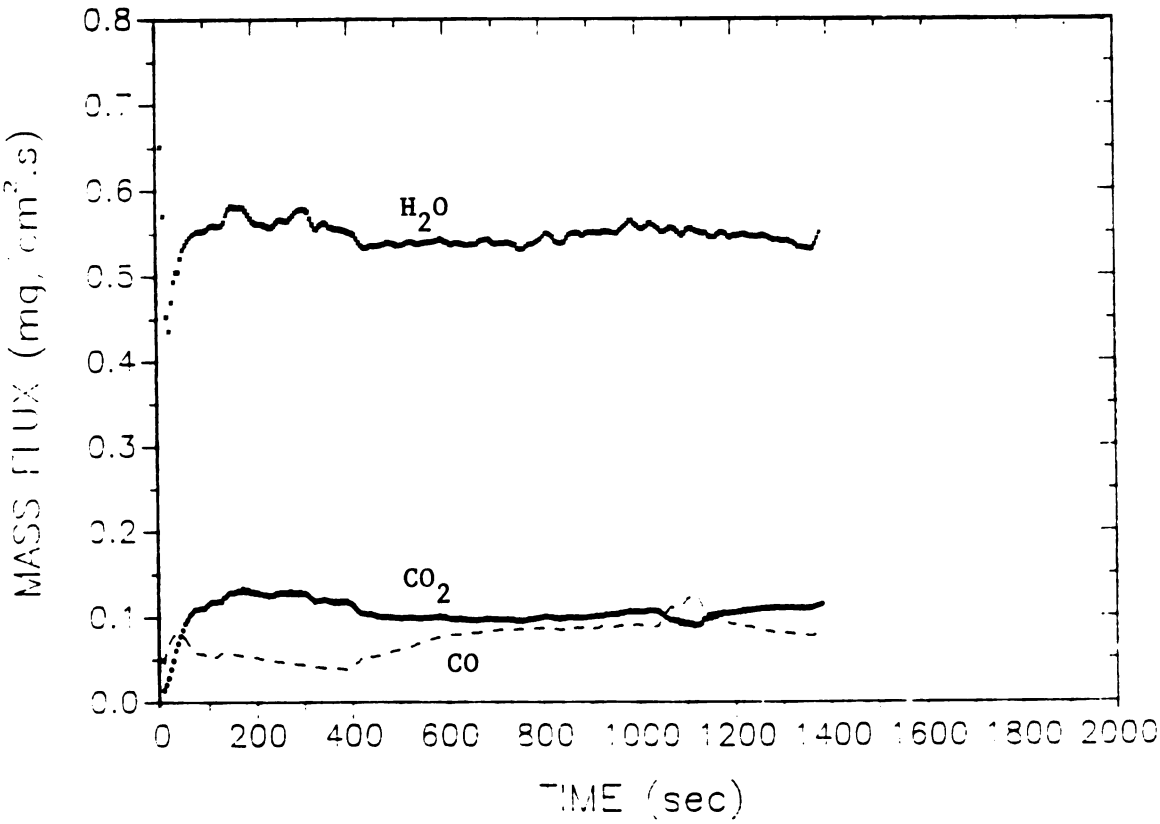

Fig. S2M4N Pyrolysis products (after catalytic combustor); EXP. M4N

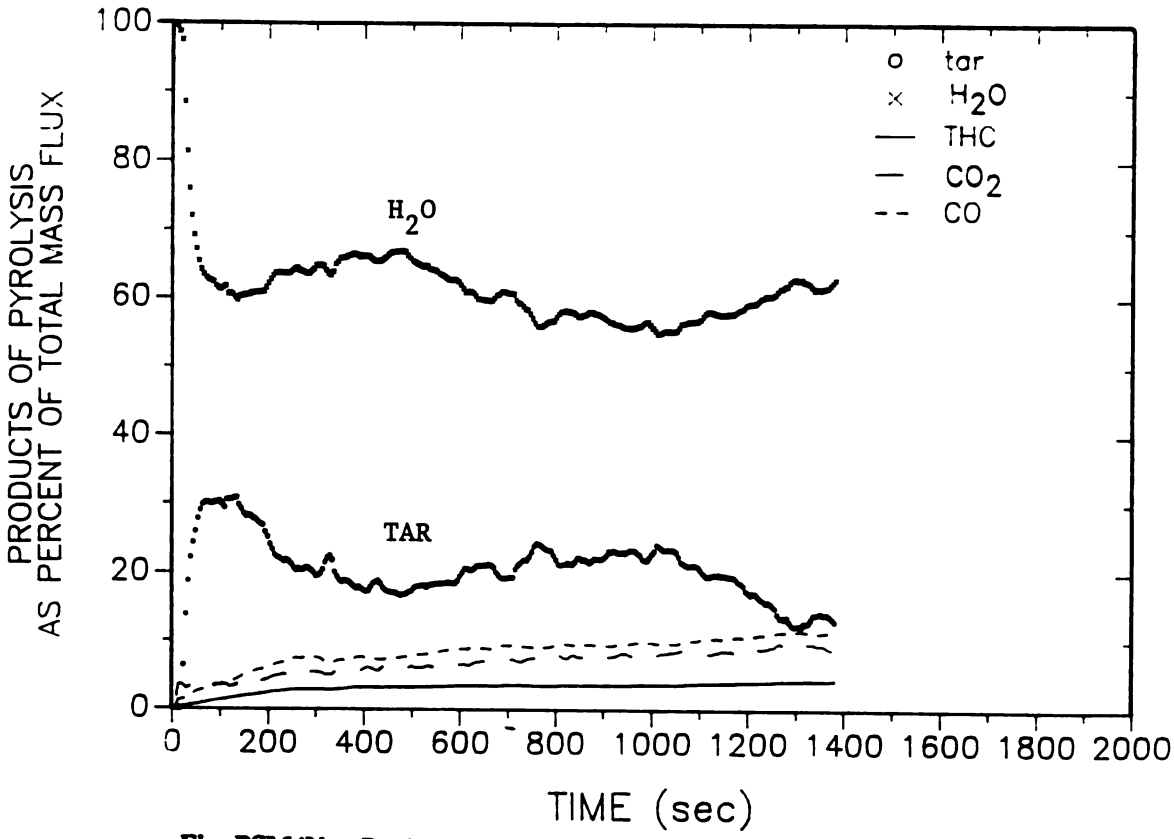

Fig. PSM4N Products of pyrolysis as percent of total mass flux; EXP. M4N

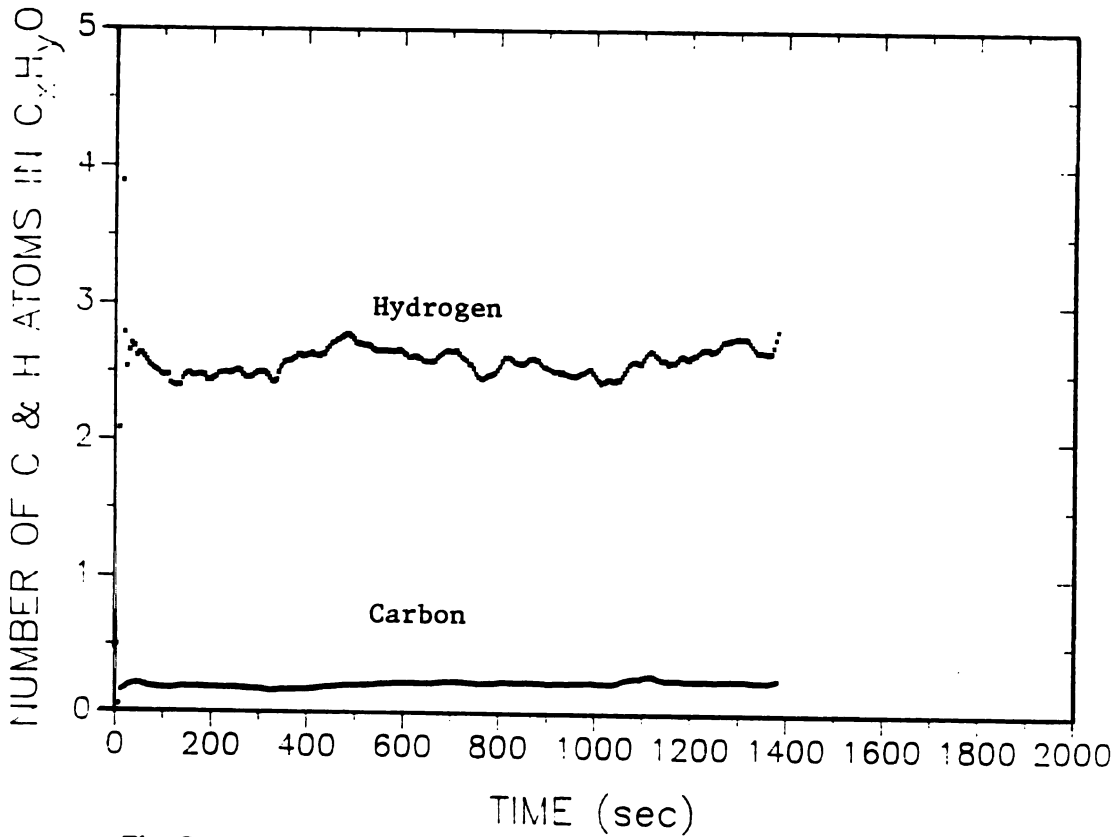

Fig. CHM4N Number of C and H atoms in the products of pyrolysis; EXP. M4N

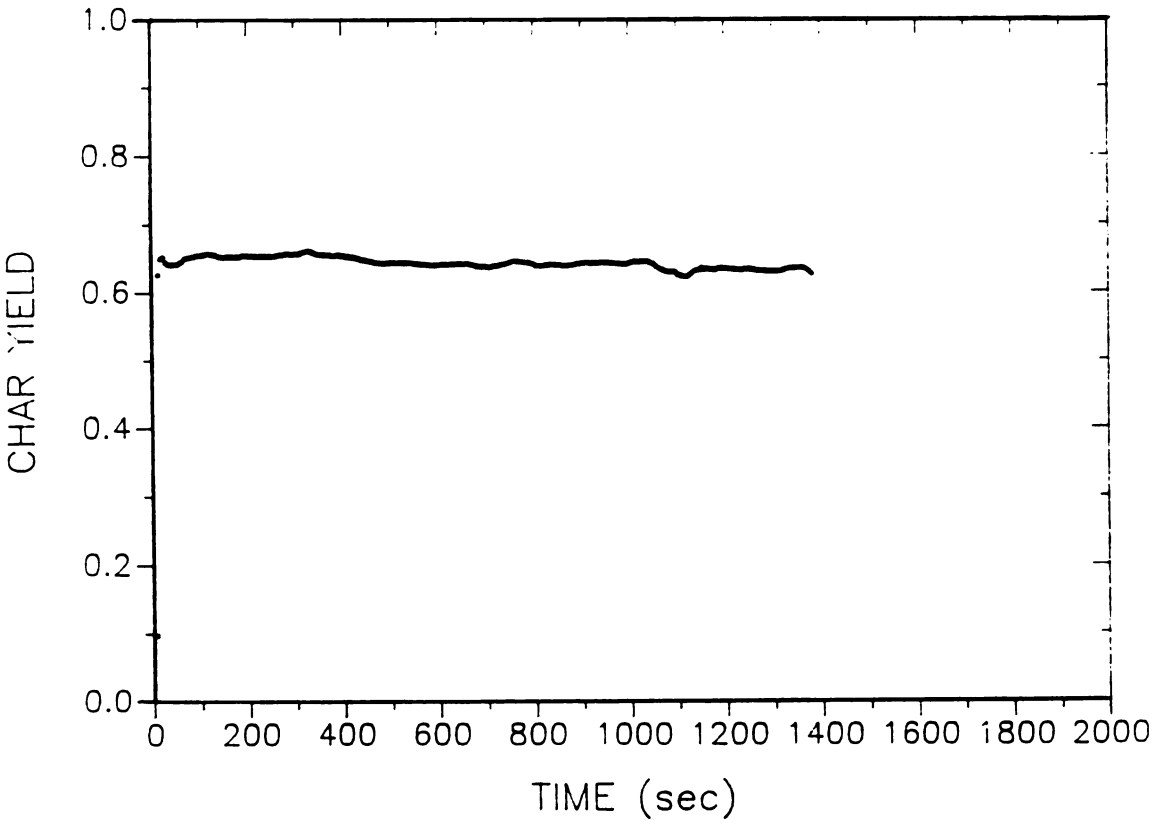

Fig. YCM4N Char yield (gram char/gram wood); EXP. M4N

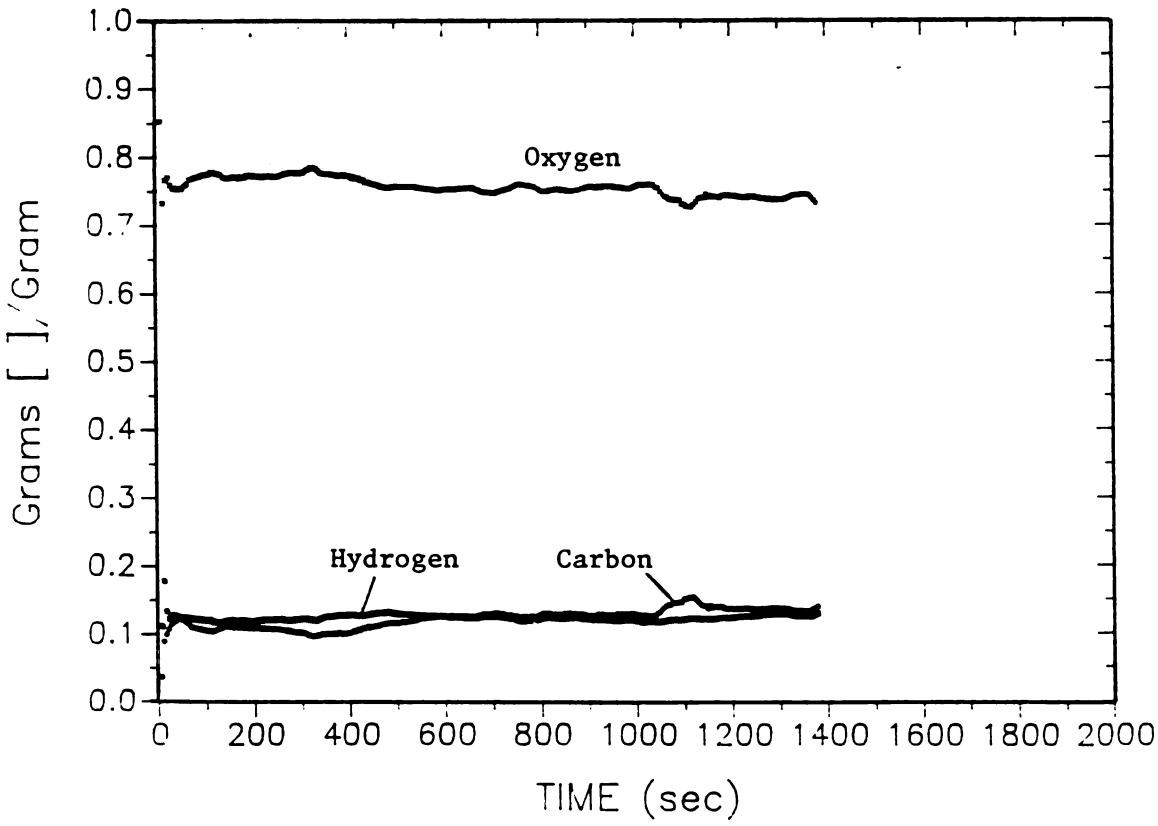

Fig. GGM4N Gram [ ]/gram of C_xH_yO; EXP. M4N

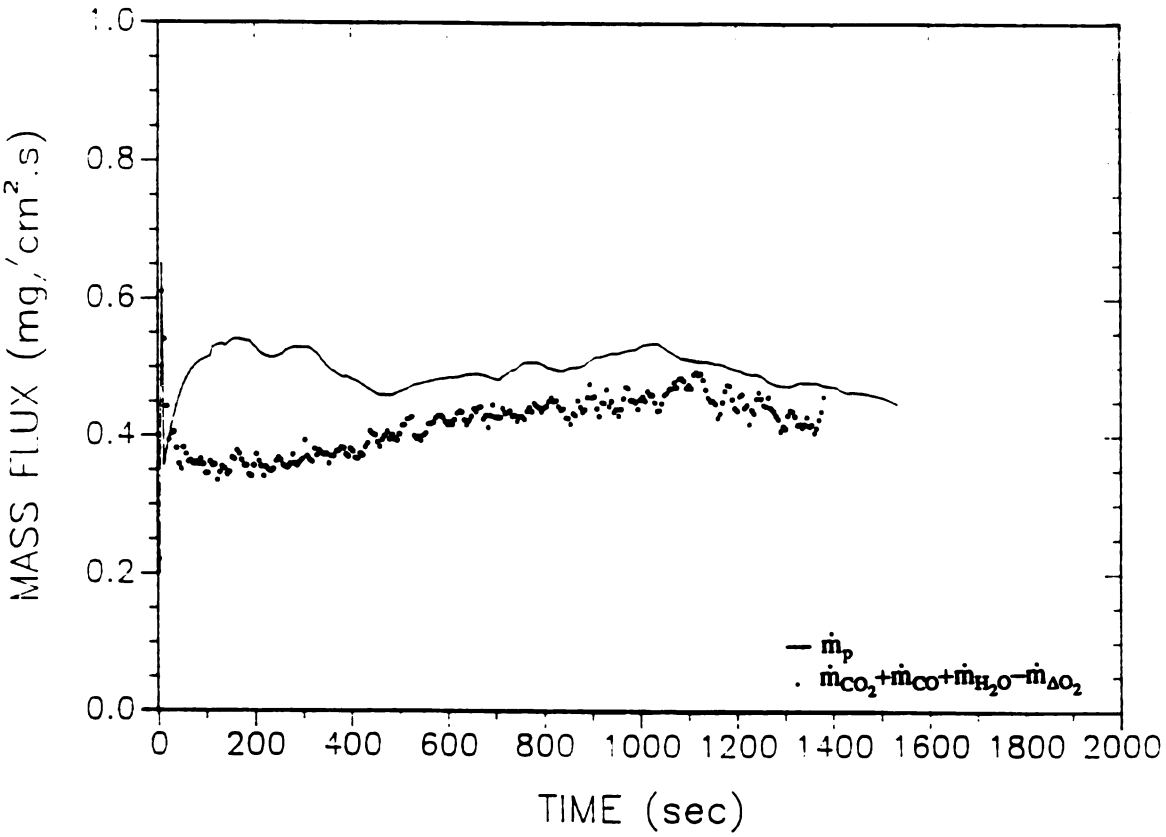

Fig. TMM4N Total mass balance for pyrolysis products; EXP. M4N

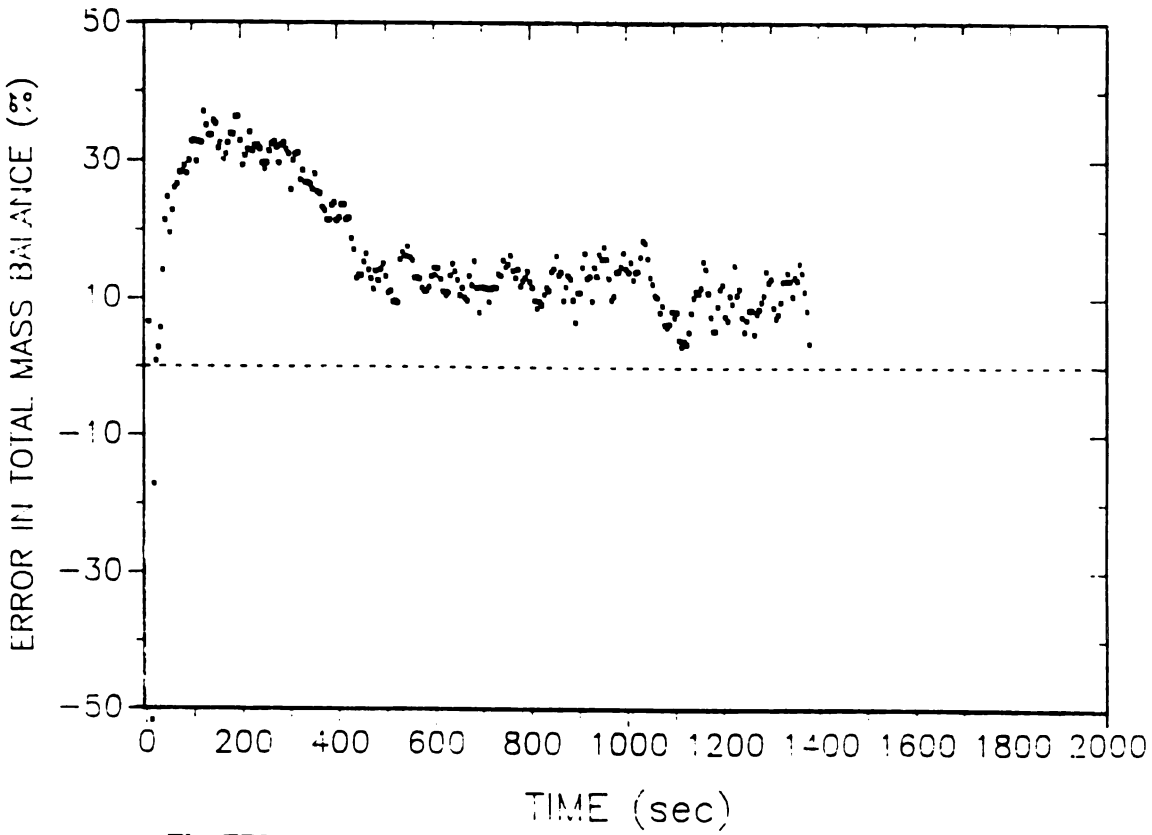

Fig. ERM4N Error in total mass balance for pyrolysis products; EXP. M4N

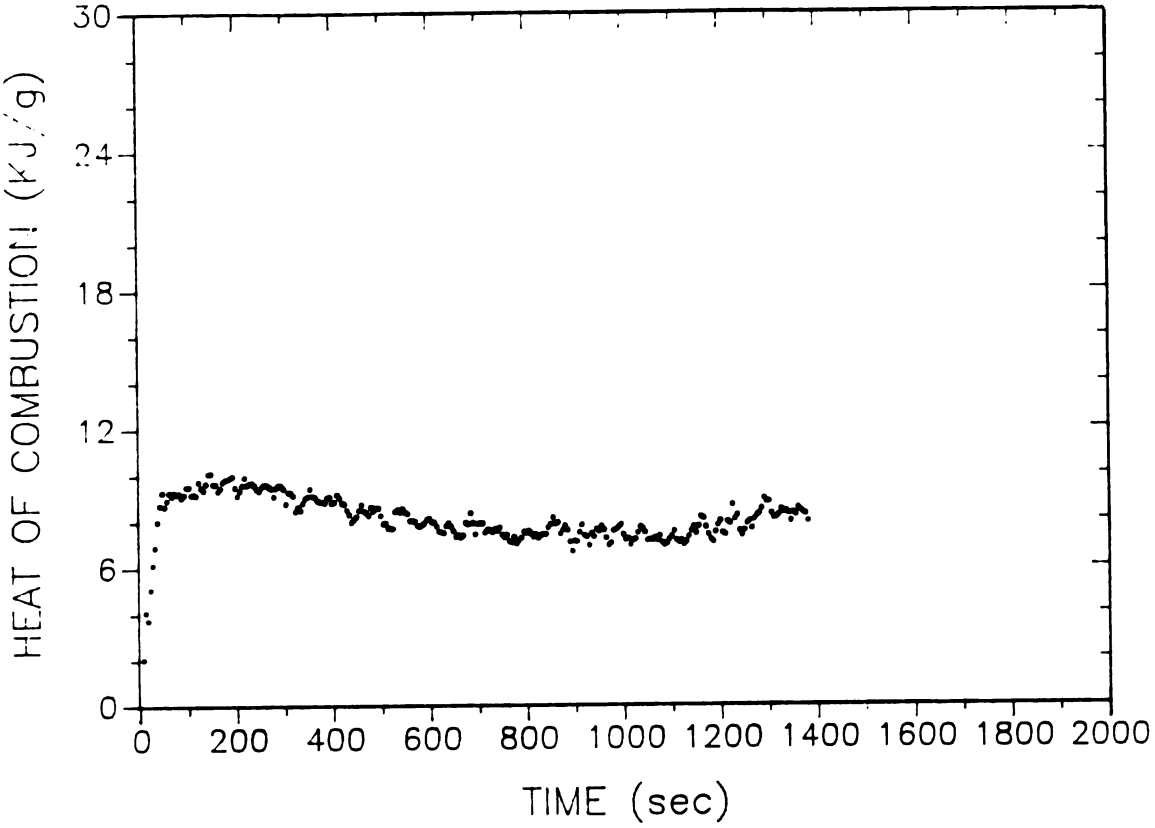

Fig. HVM4N Heat of combustion of pyrolysis products; EXP. M4N

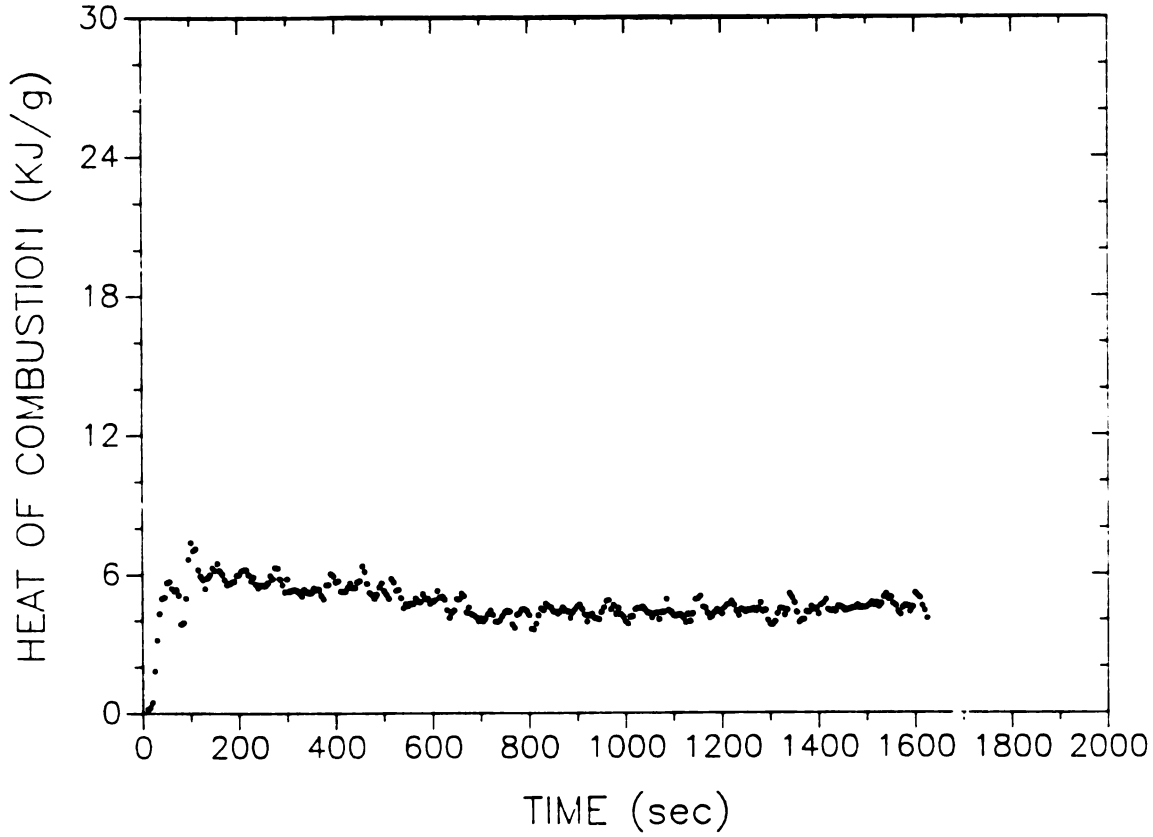

Fig. HVM3N Heat of combustion of pyrolysis products; EXP. M3N

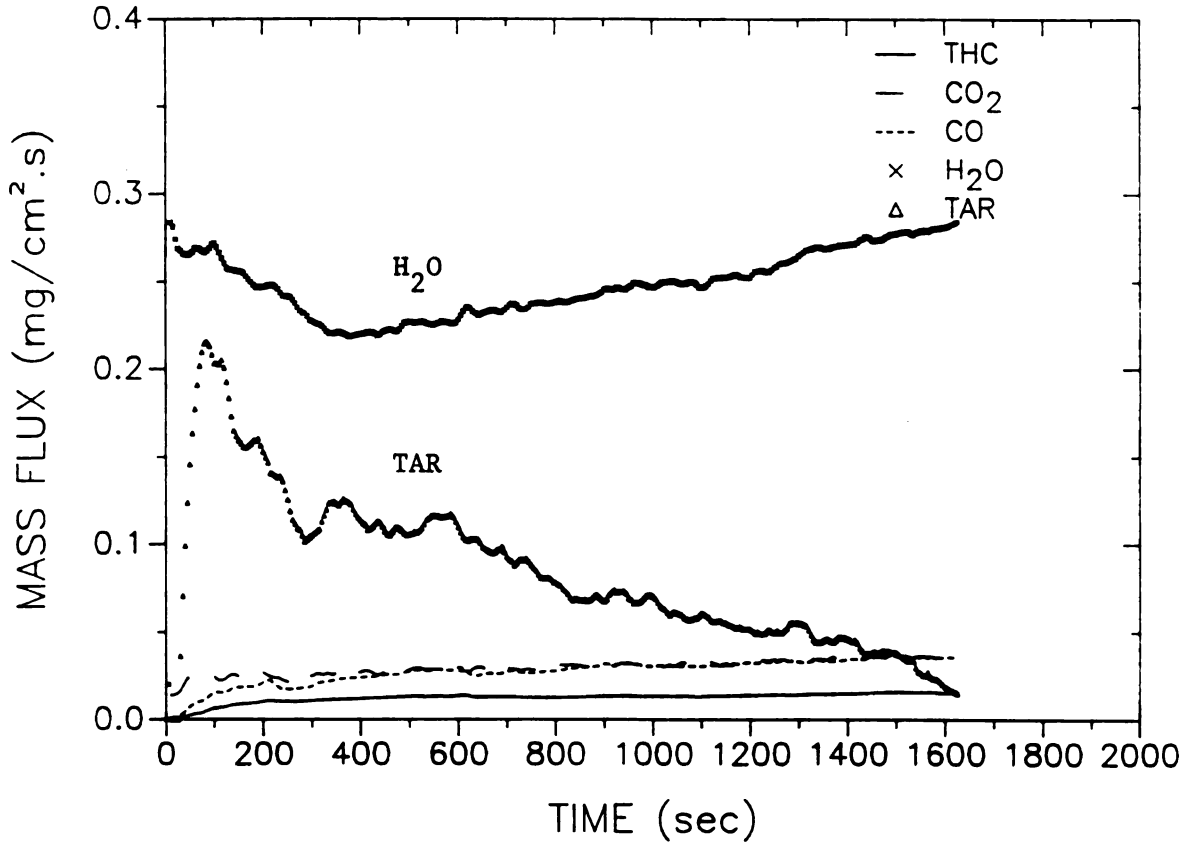

Fig. S1M3N Pyrolysis products (direct measurement); EXP. M3N

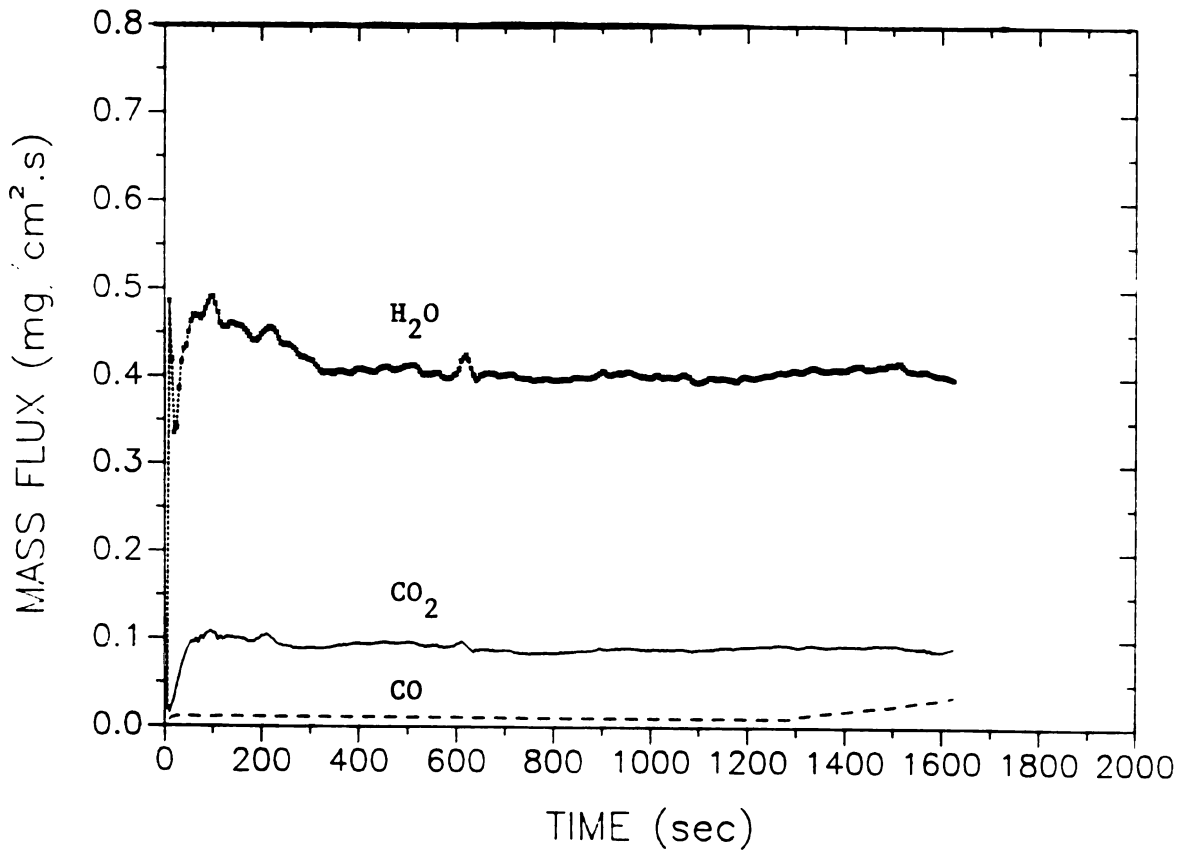

Fig. S2M3N Pyrolysis products (after catalytic combustor); EXP. M3N

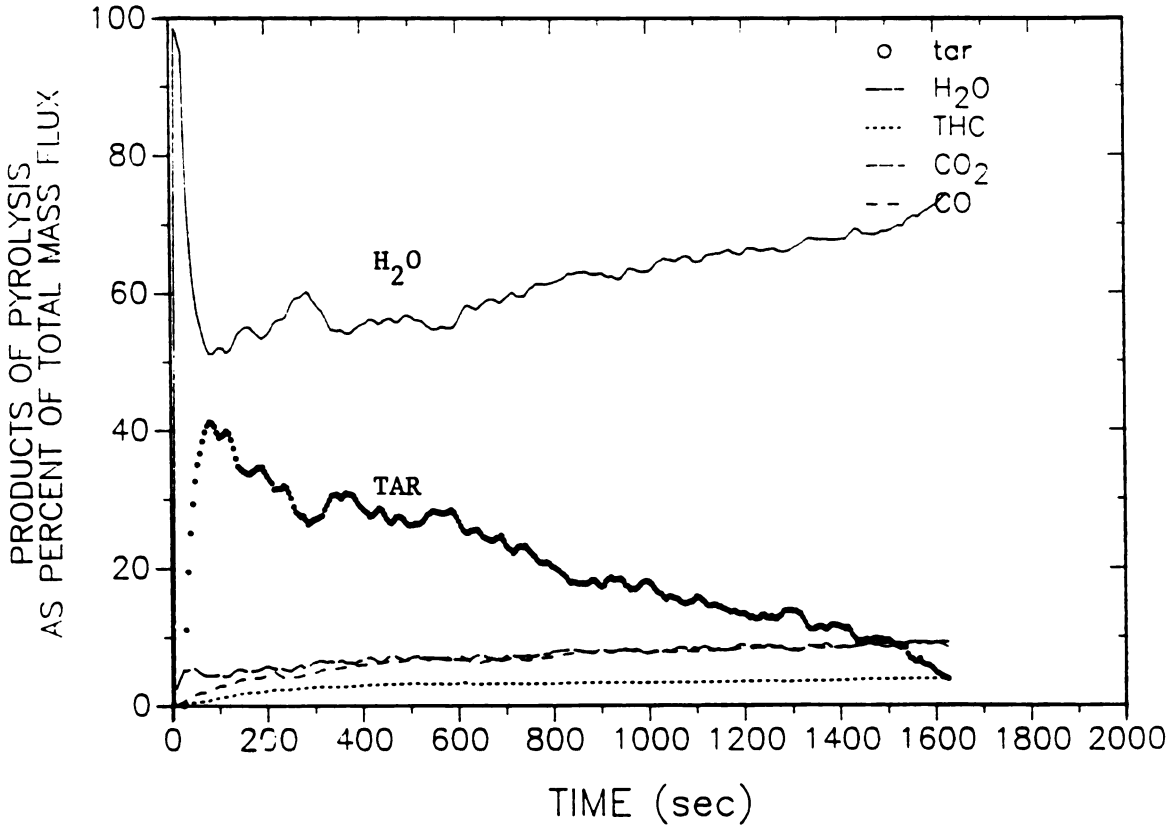

Fig. PSM3N Products of pyrolysis as percent of total mass flux; EXP. M3N

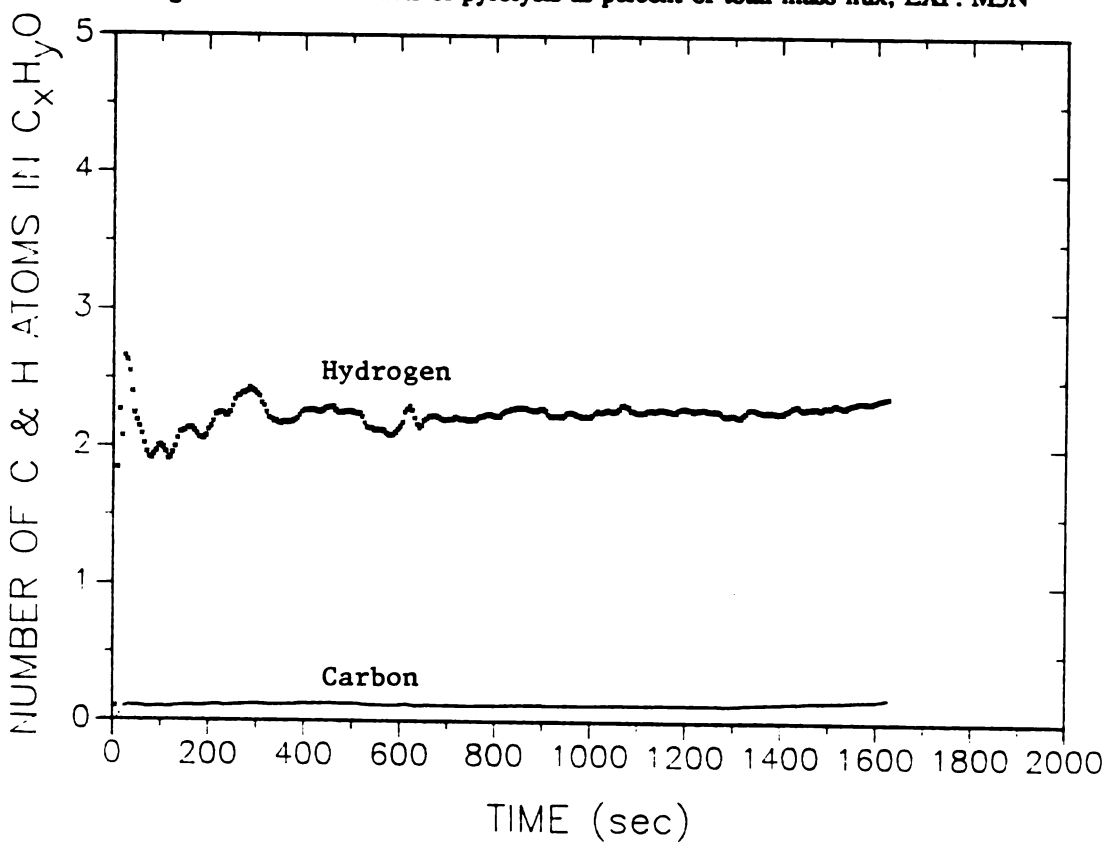

Fig. CHM3N Number of C and H atoms in the products of pyrolysis; EXP. M3N

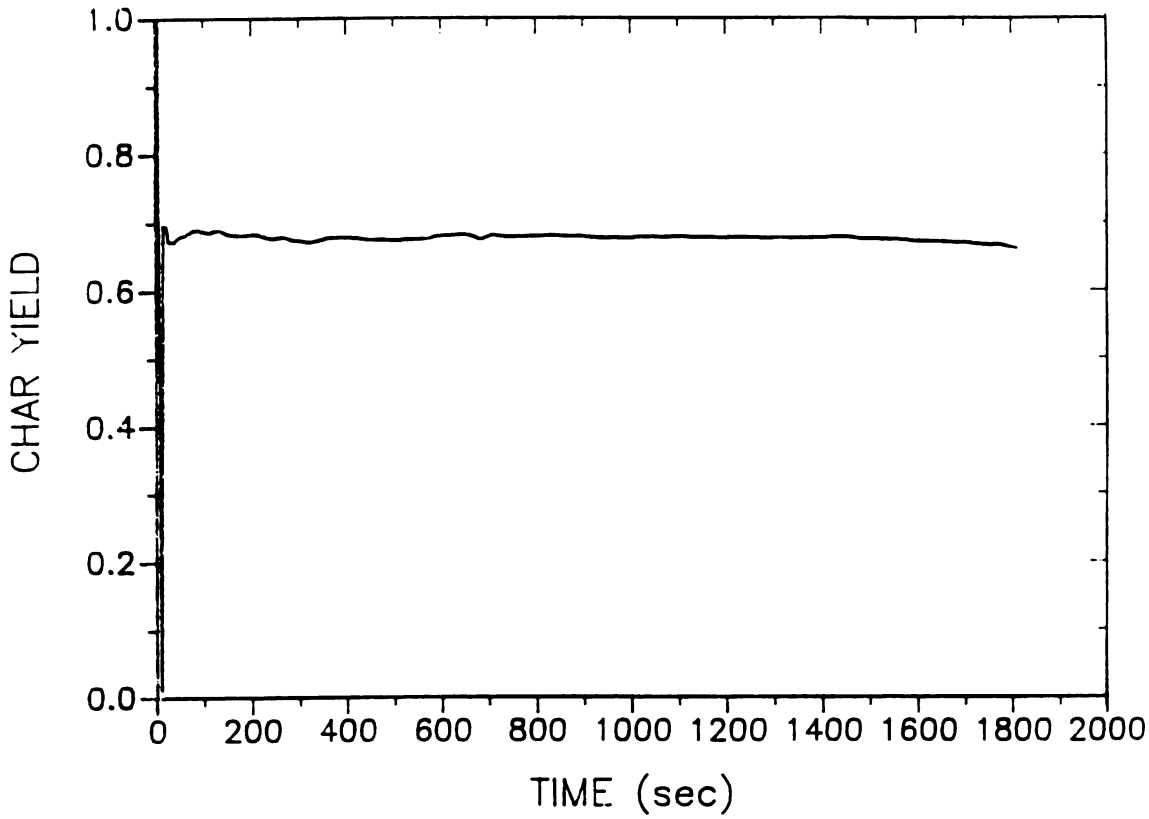

Fig. YCM3N Char yield (gram char/gram wood); EXP. M3N

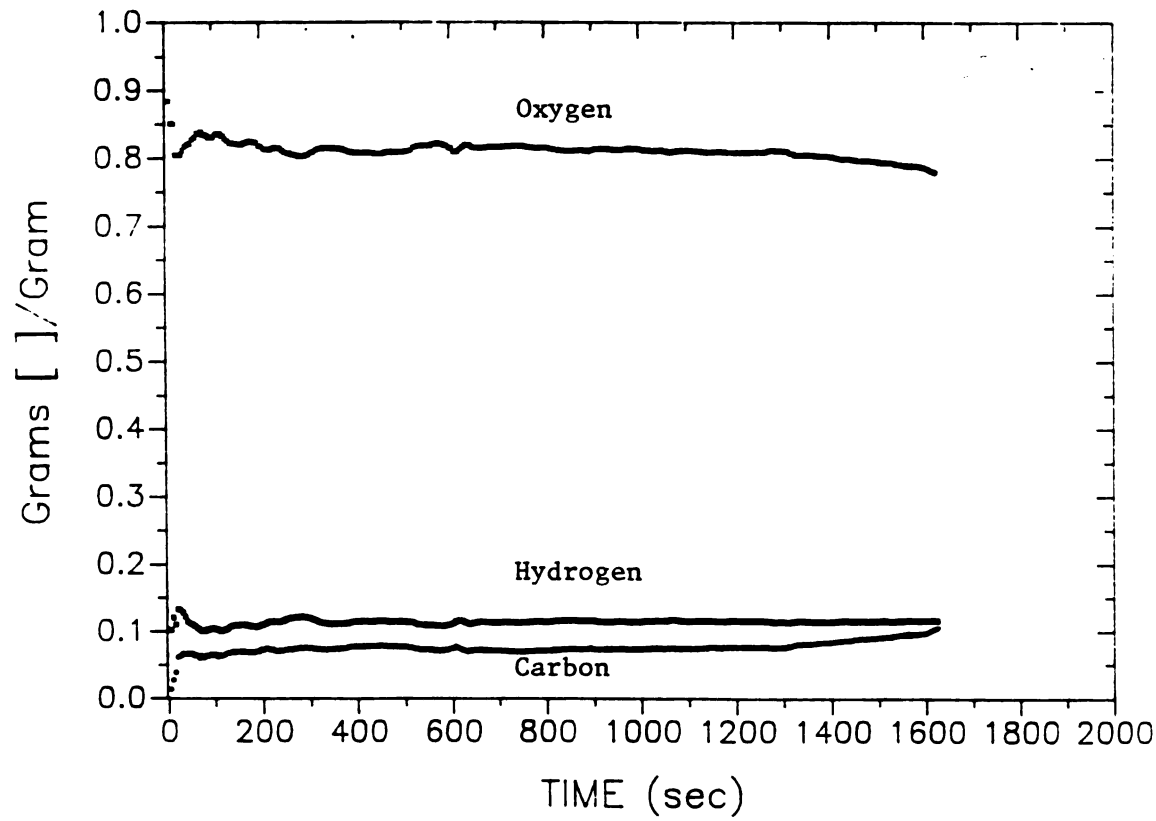

Fig. GGM3N Gram [ ]/gram of C_xH_yO; EXP. M3N

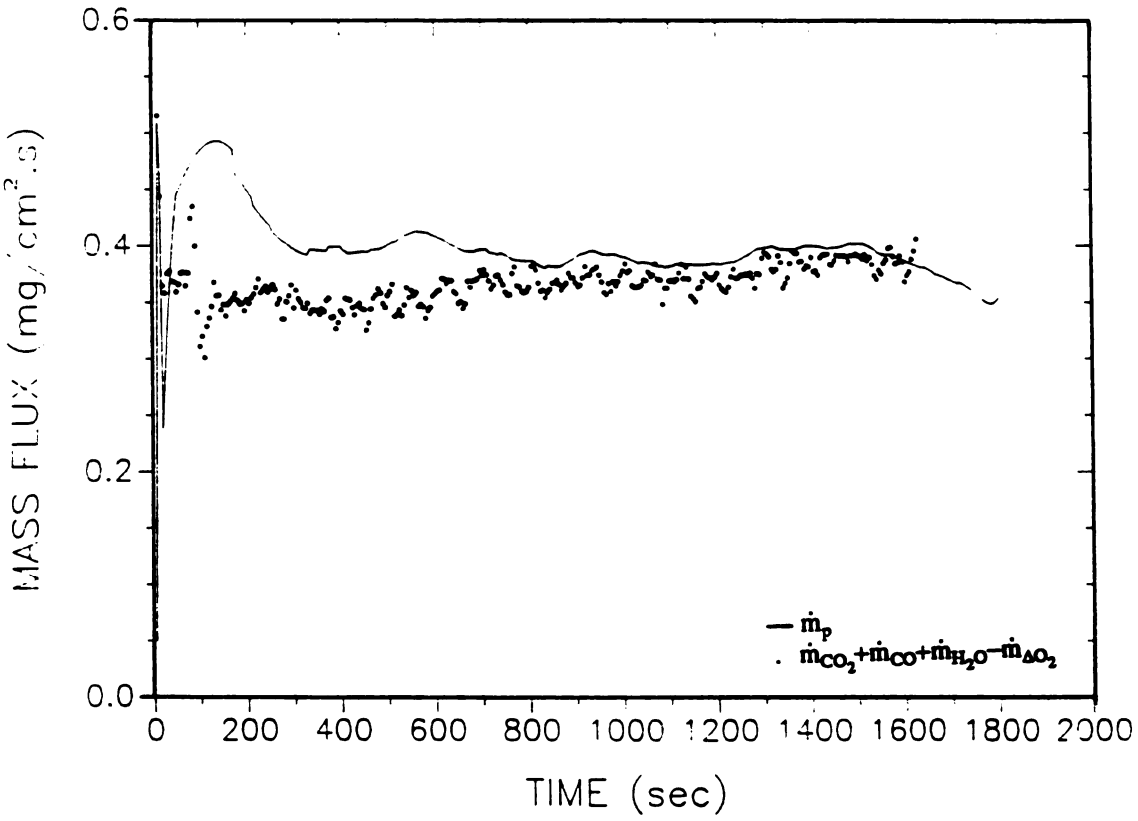

Fig. TMM3N Total mass balance for pyrolysis products; EXP. M3N

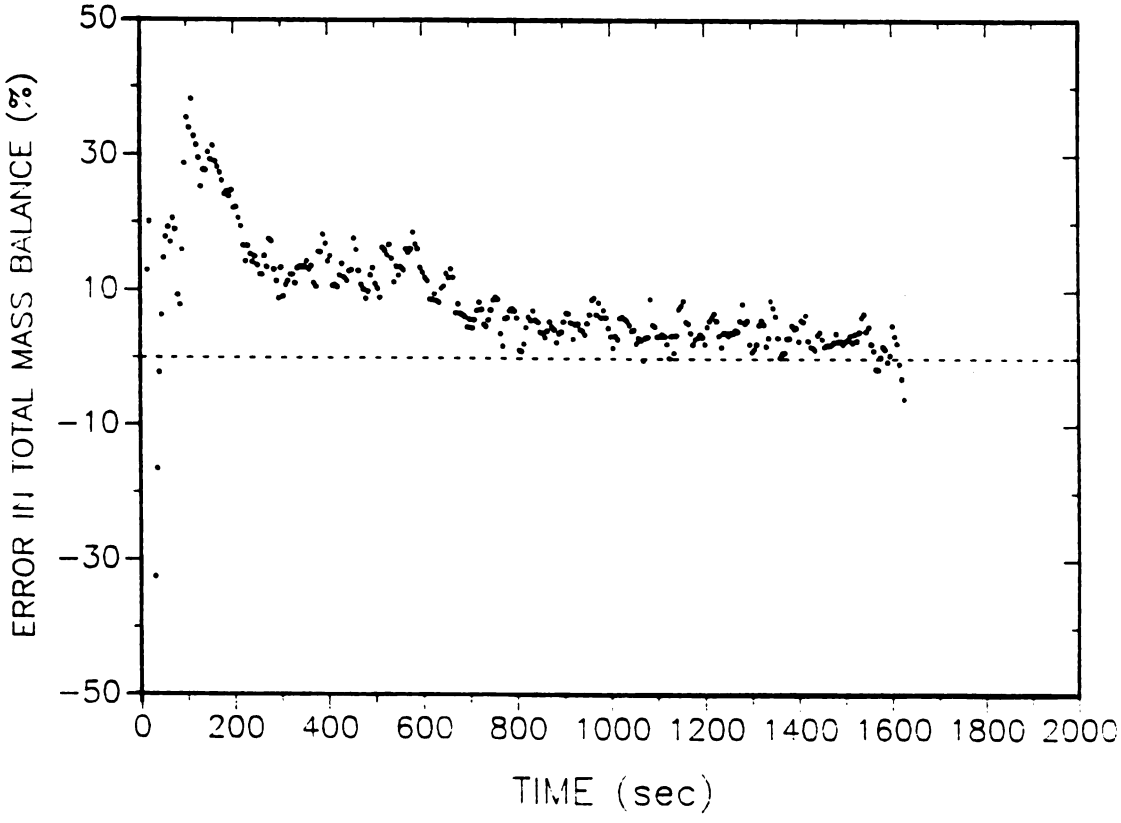

Fig. ERM3N Error in total mass balance for pyrolysis products; EXP. M3N

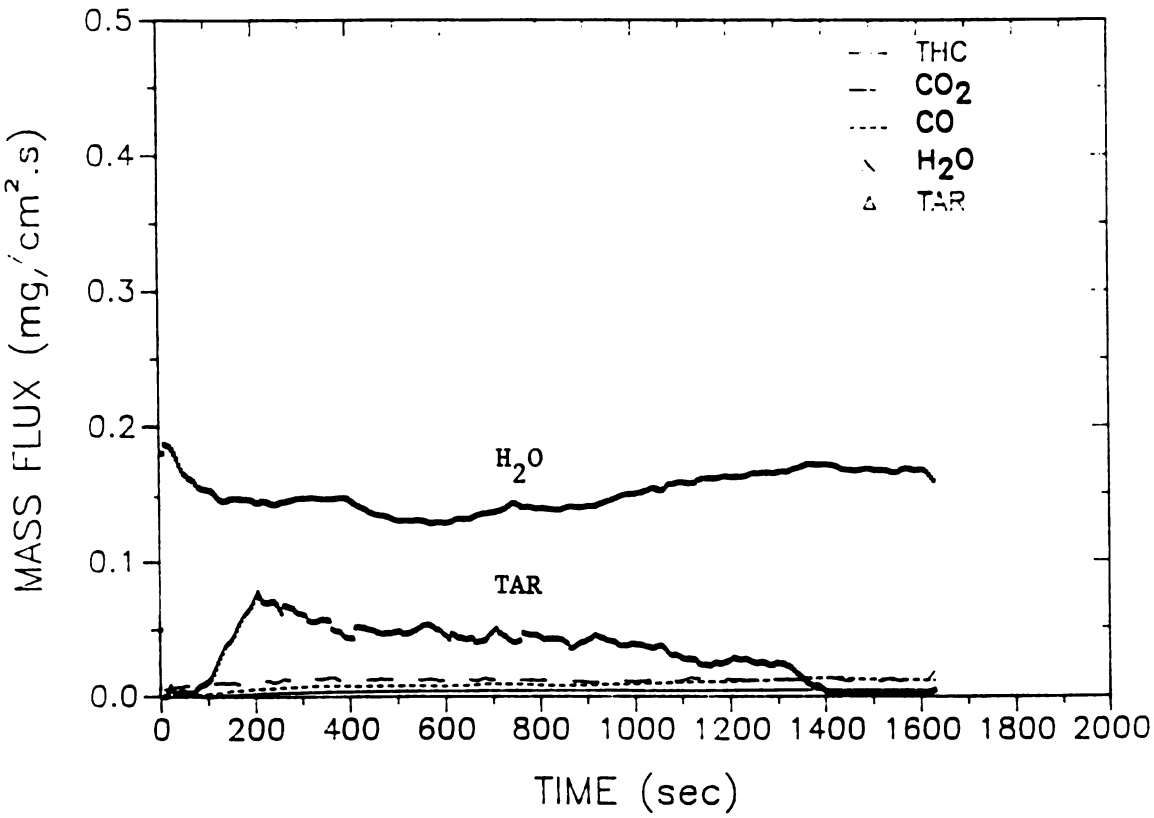

Fig. S1M2N Pyrolysis products (direct measurement); EXP. M2N

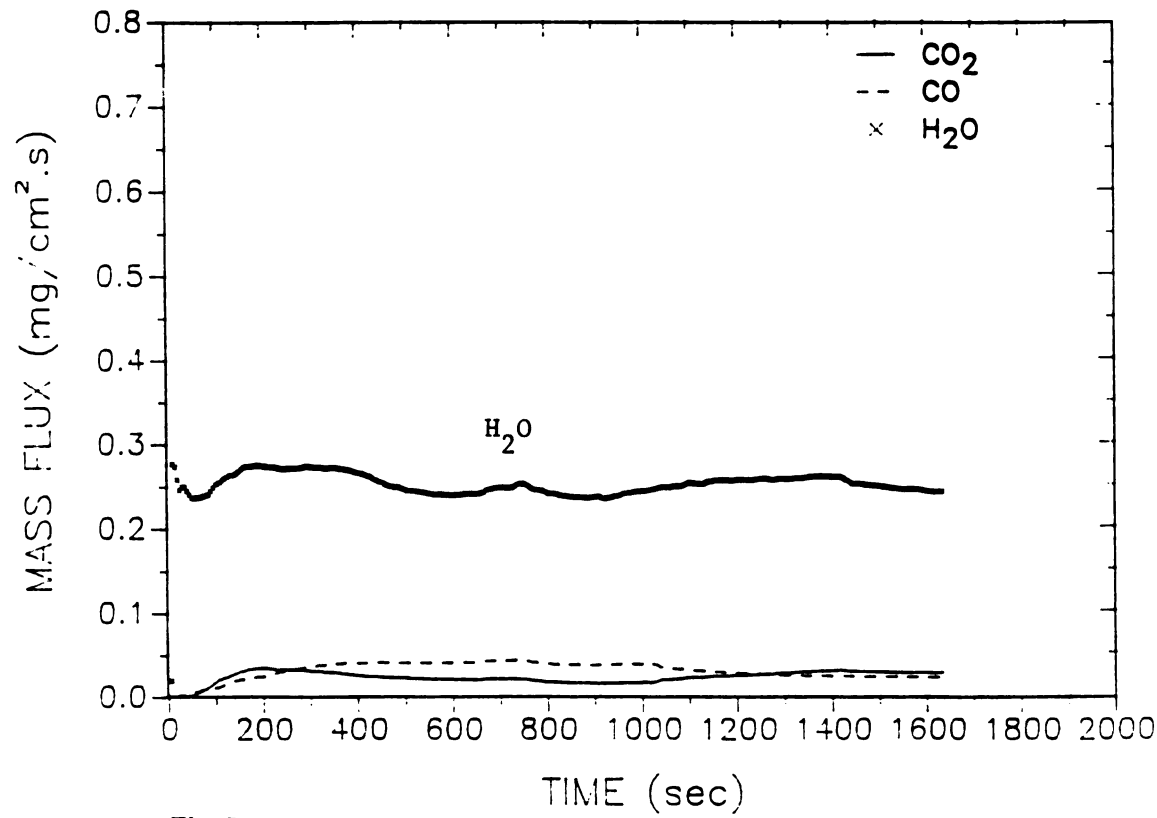

Fig. S2M2N Pyrolysis products (after catalytic combustor); EXP. M2N

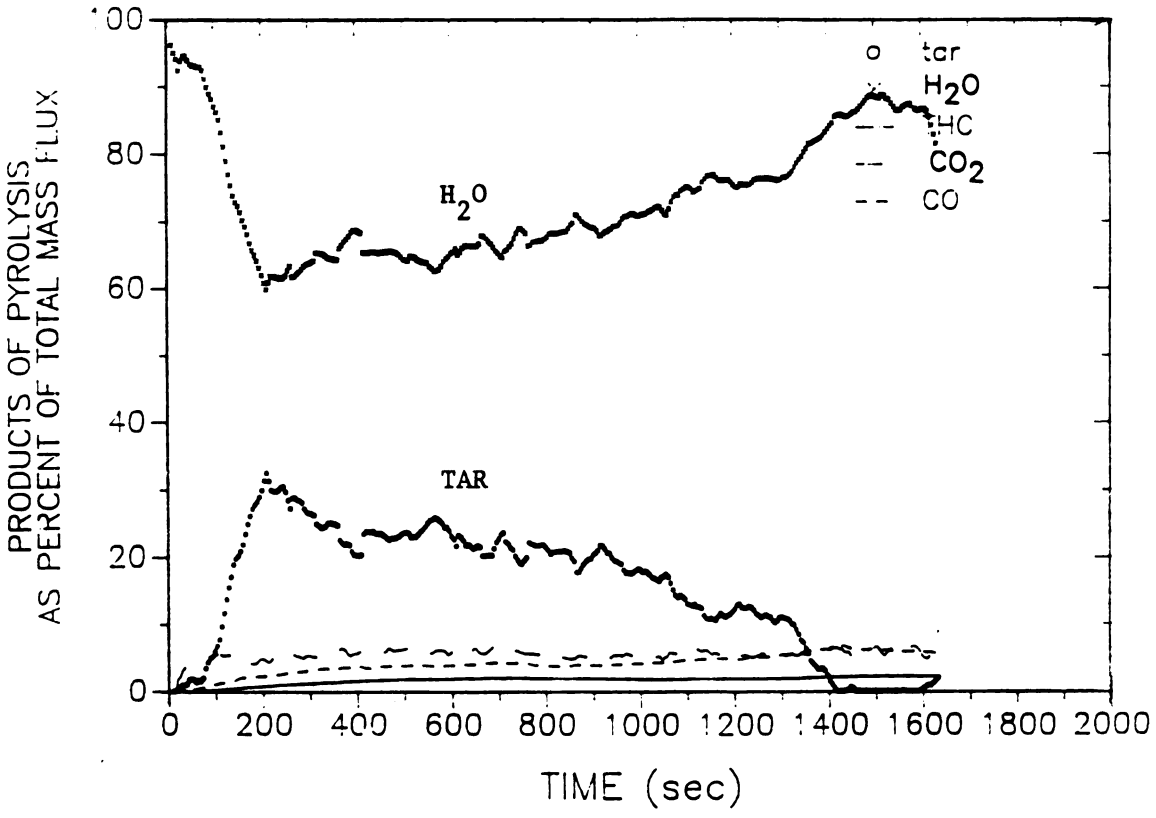

Fig. PSM2N Products of pyrolysis as percent of total mass flux; EXP. M2N

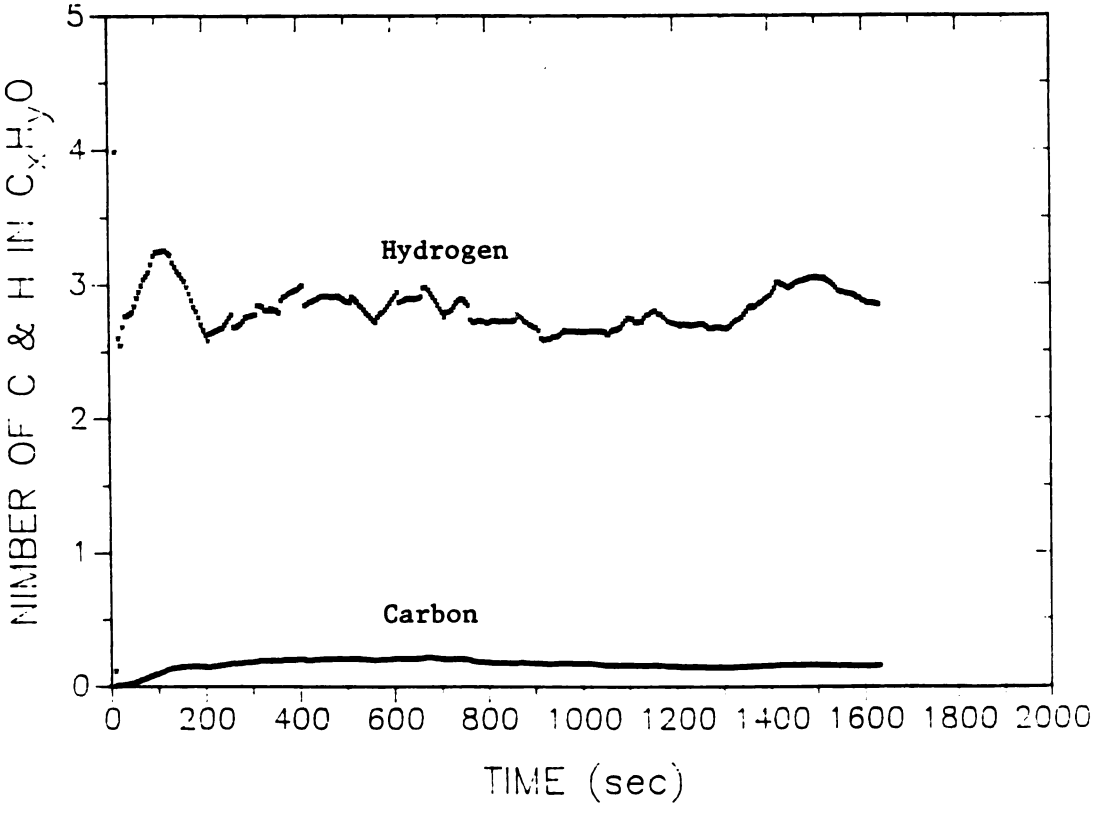

Fig. CHM2N Number of C and H atoms in the products of pyrolysis; EXP. M2N

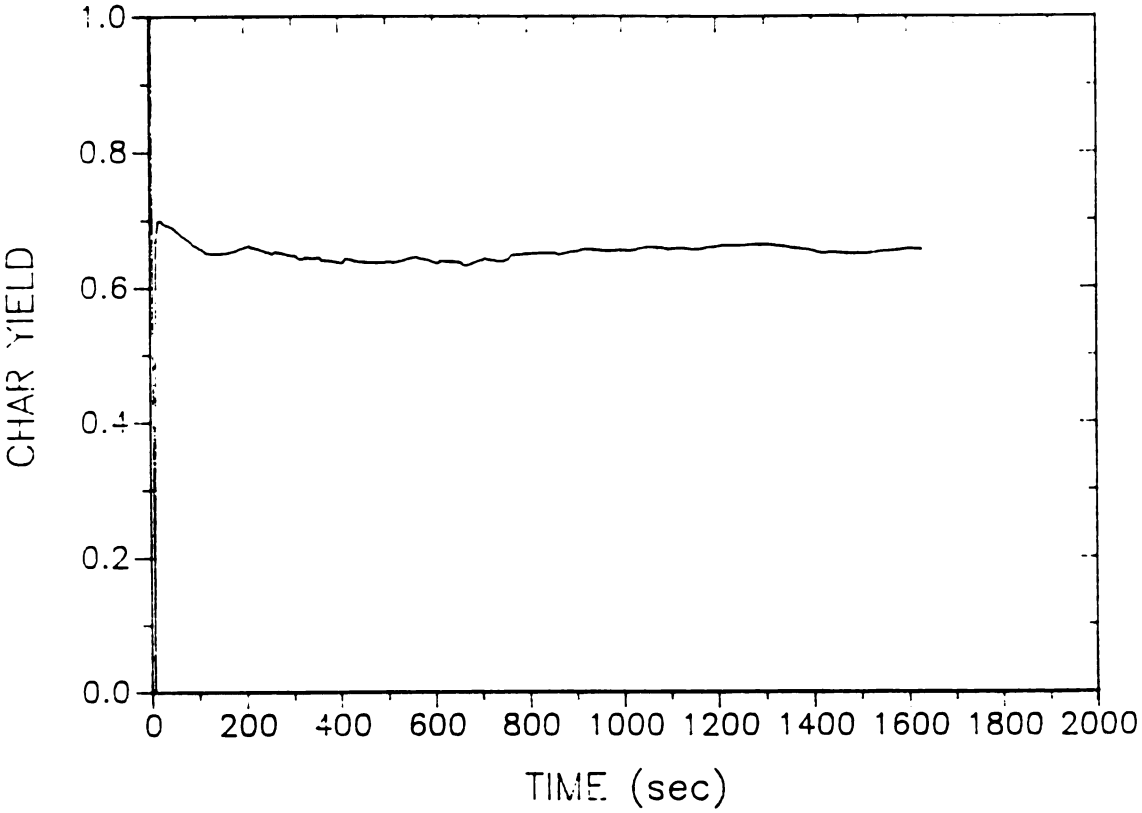

Fig. YCM2N Char yield (gram char/gram wood); EXP. M2N

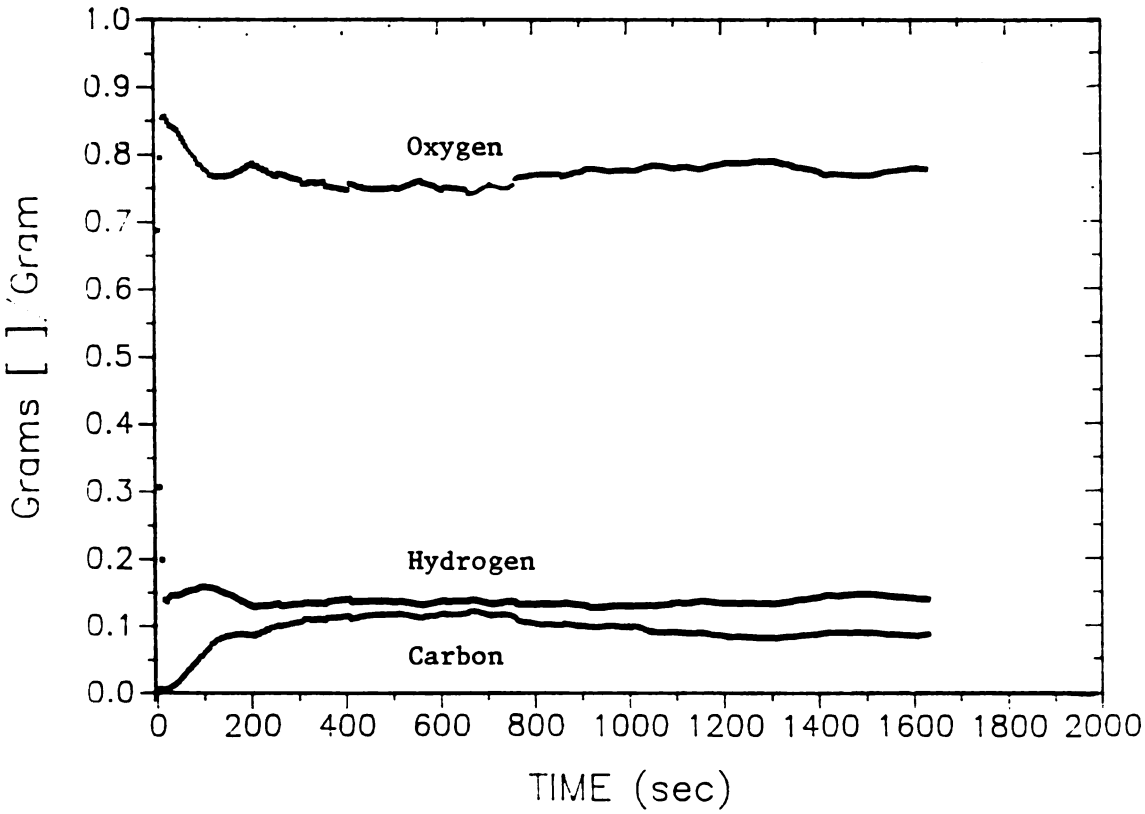

Fig. GGM2N Gram [ ]/gram of C_xH_yO; EXP. M2N

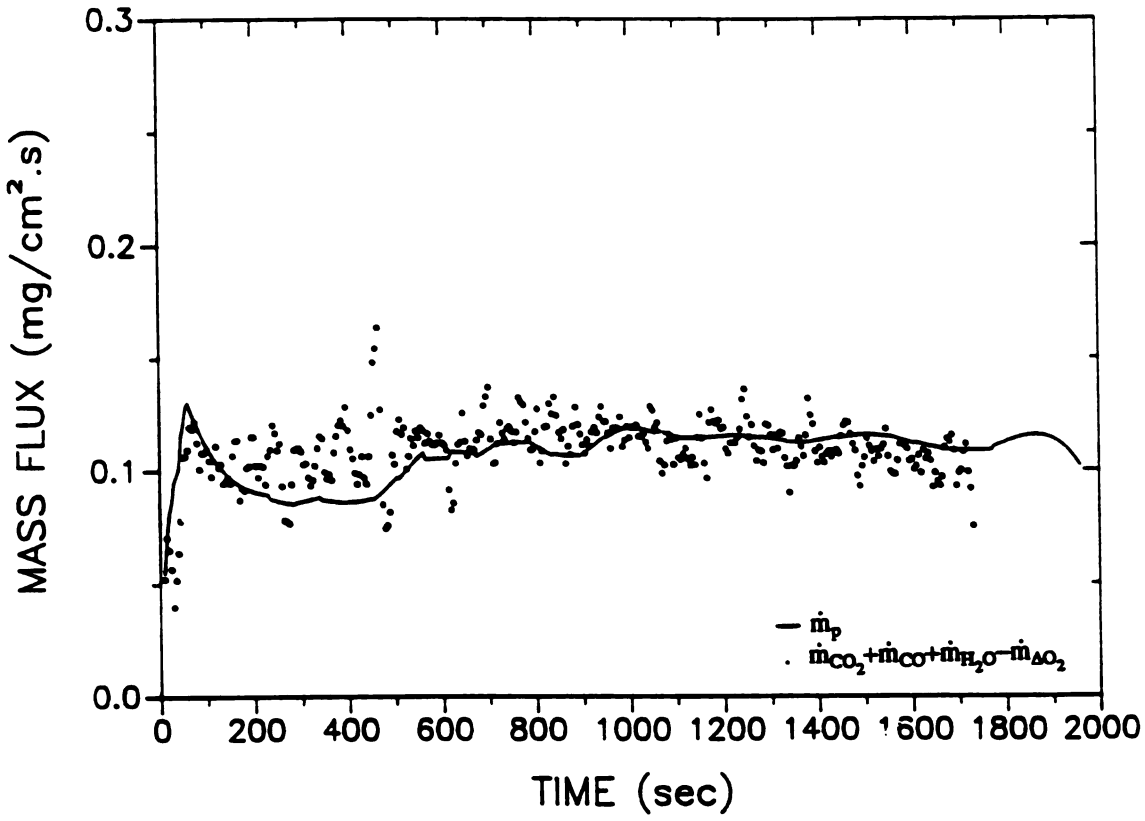

Fig. TMM1N Total mass balance for pyrolysis products; EXP. M1N

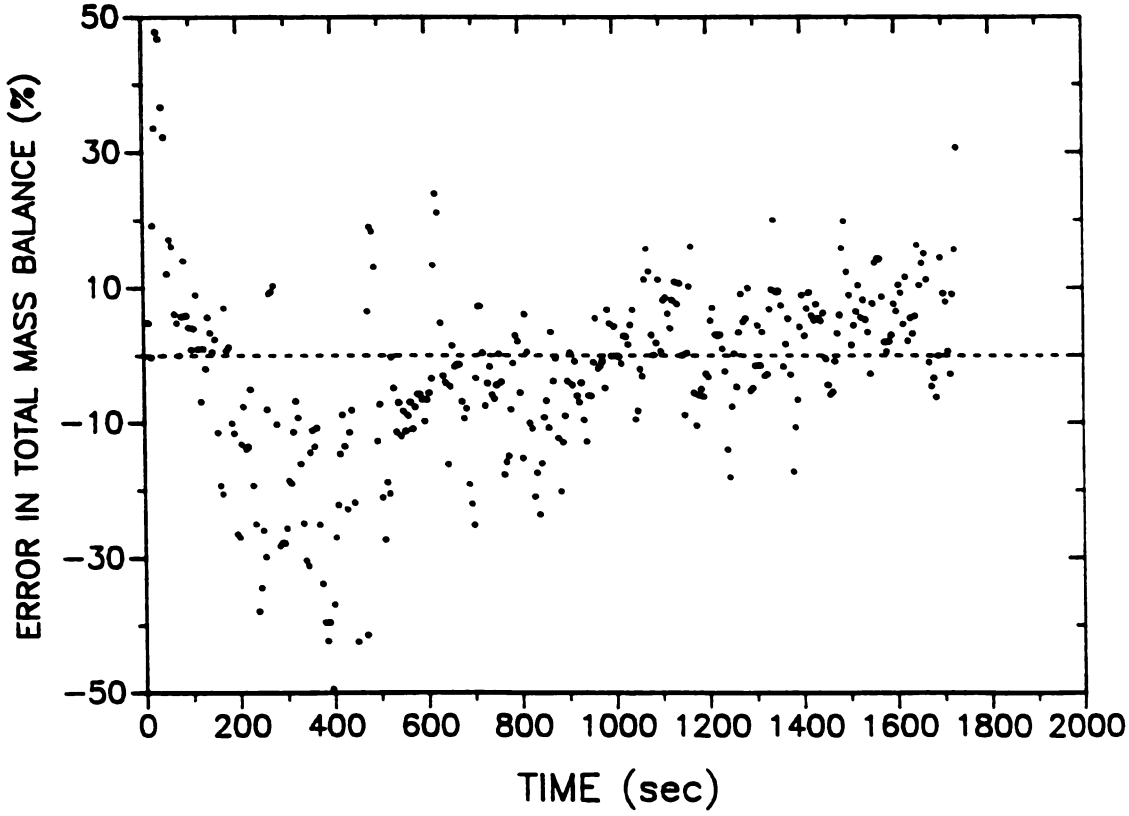

Fig. ERM1N Error in total mass balance for pyrolysis products; EXP. R1N

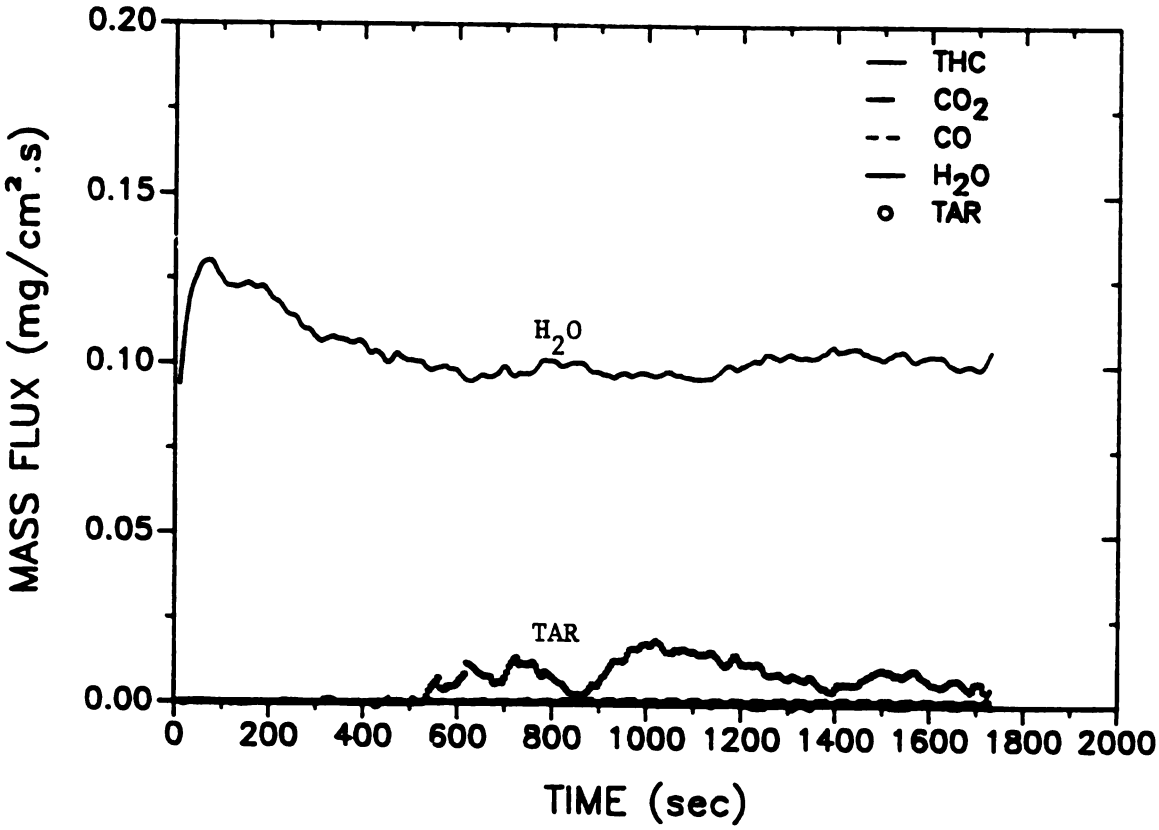

Fig. S1M1N Pyrolysis products (direct measurement); EXP. M1N

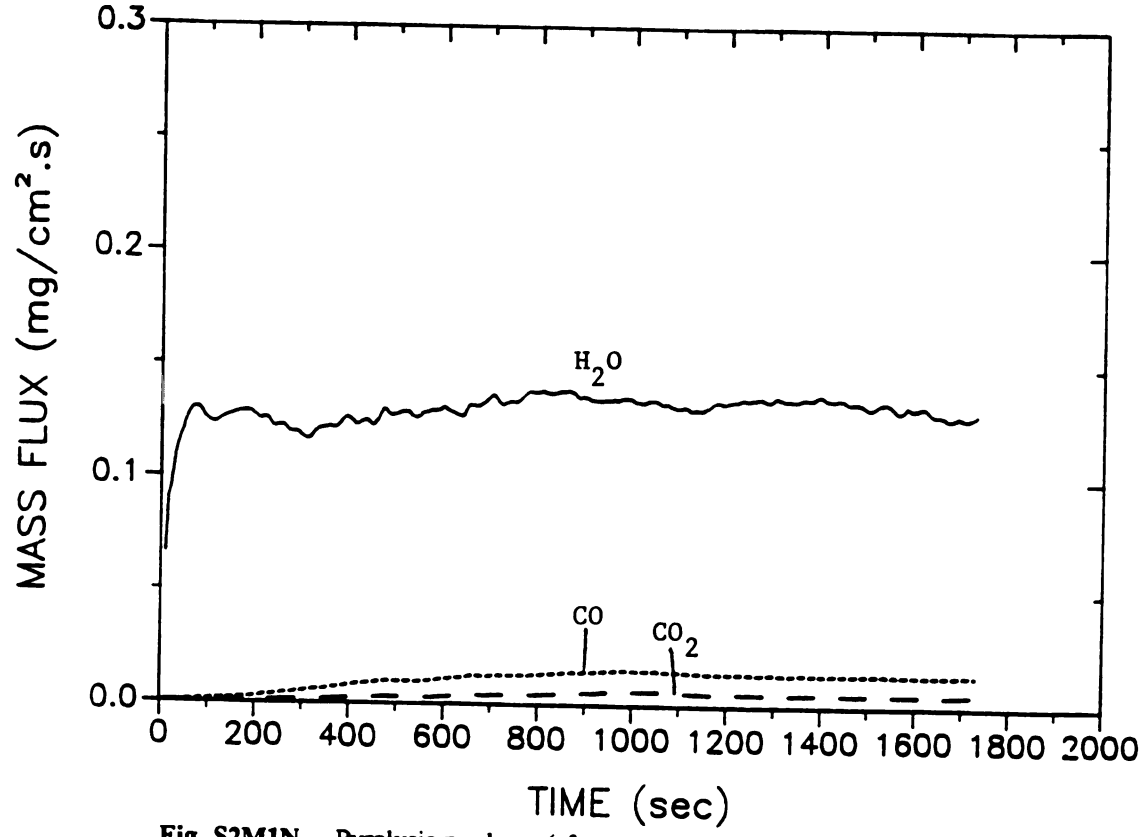

Fig. S2M1N Pyrolysis products (after catalytic combustor); EXP. M1N

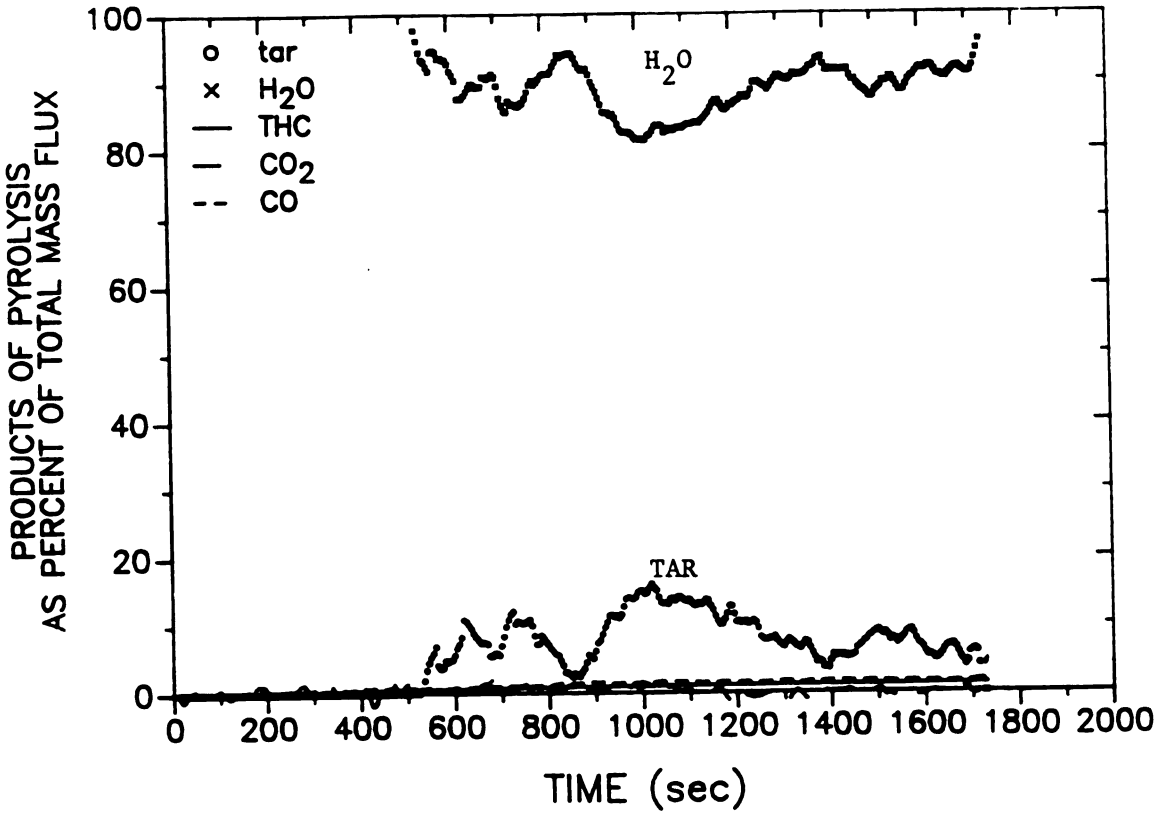

Fig. PSM1N Products of pyrolysis as percent of total mass flux; EXP. M1N

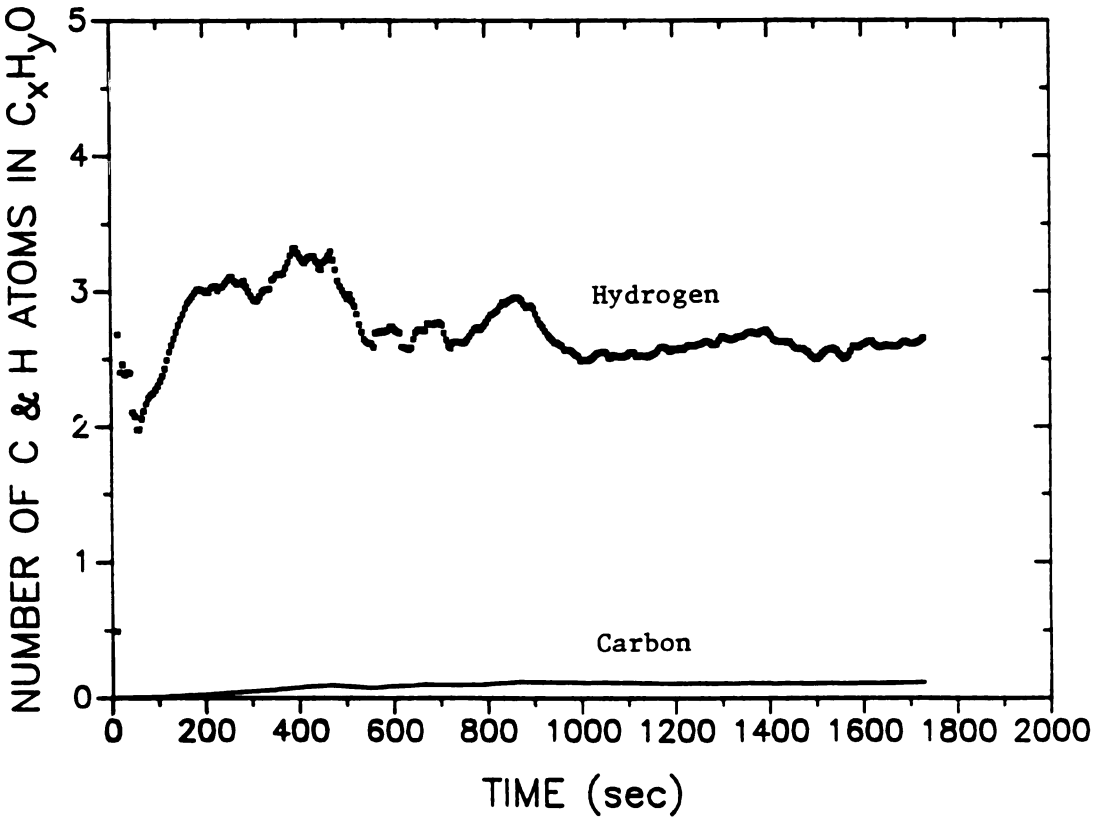

Fig. CHM1N Number of C and H atoms in the products of pyrolysis; EXP. M1N

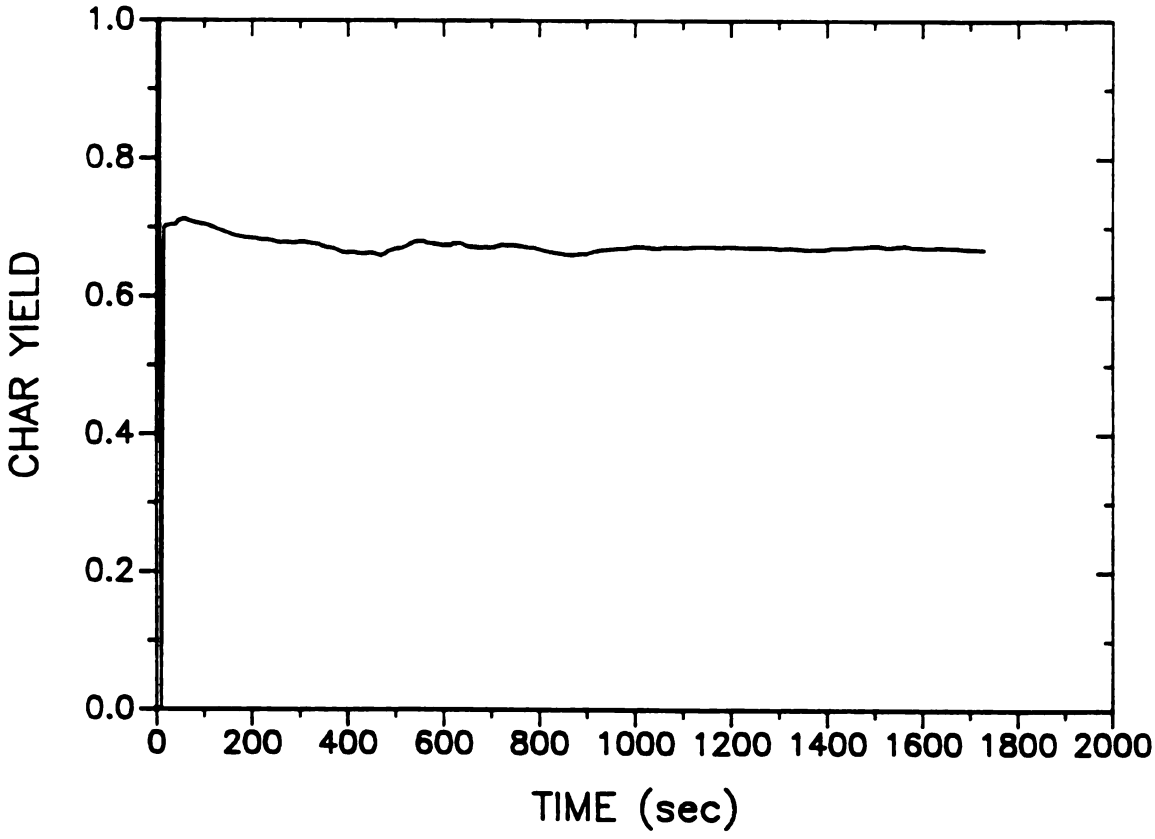

Fig. YCM1N Char yield (gram char/gram wood); EXP. M1N

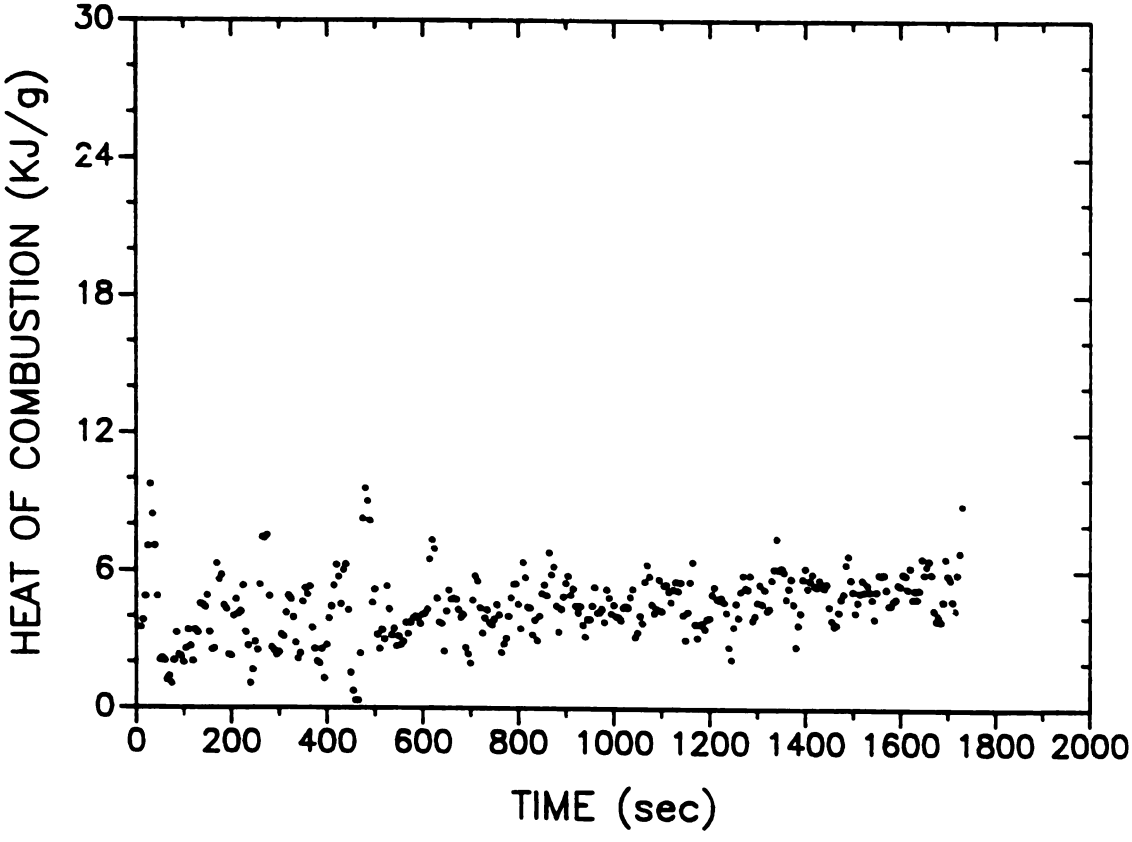

Fig. HM1N Heat of combustion of pyrolysis products; wood; EXP. M1N

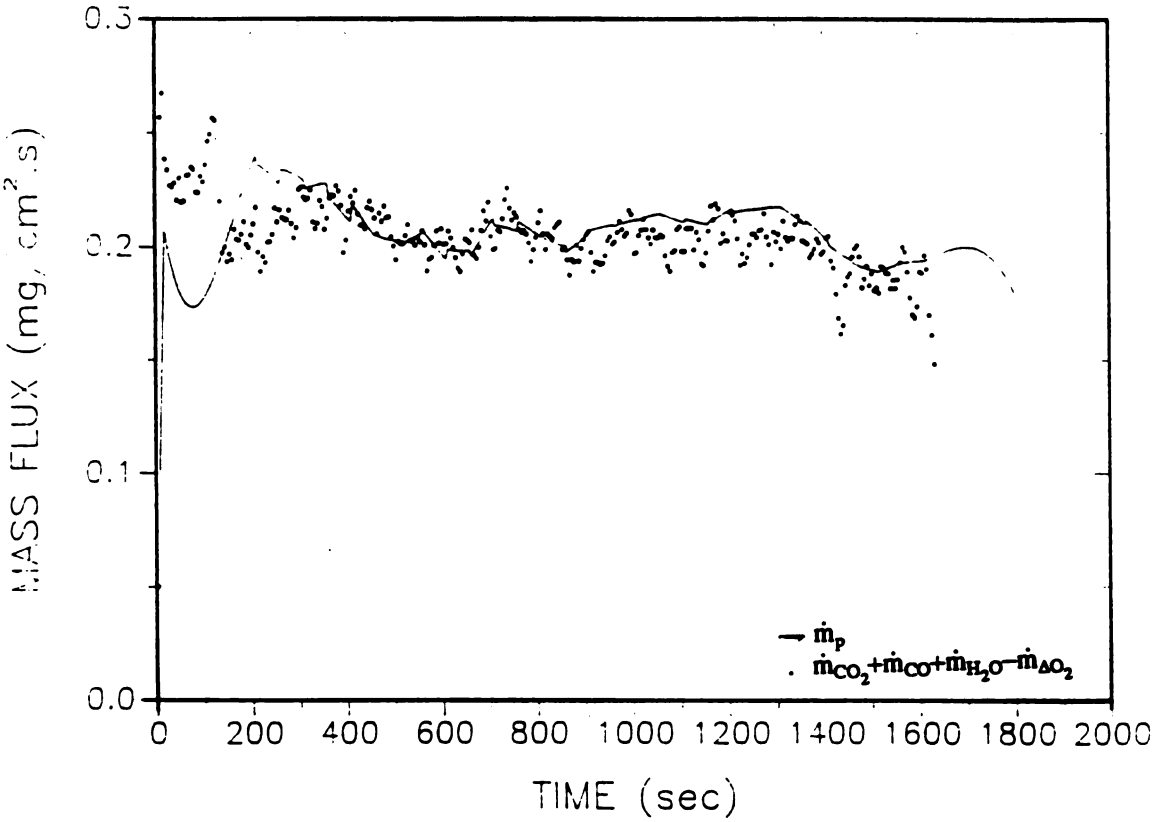

Fig. TMM2N Total mass balance for pyrolysis products; EXP. M2N

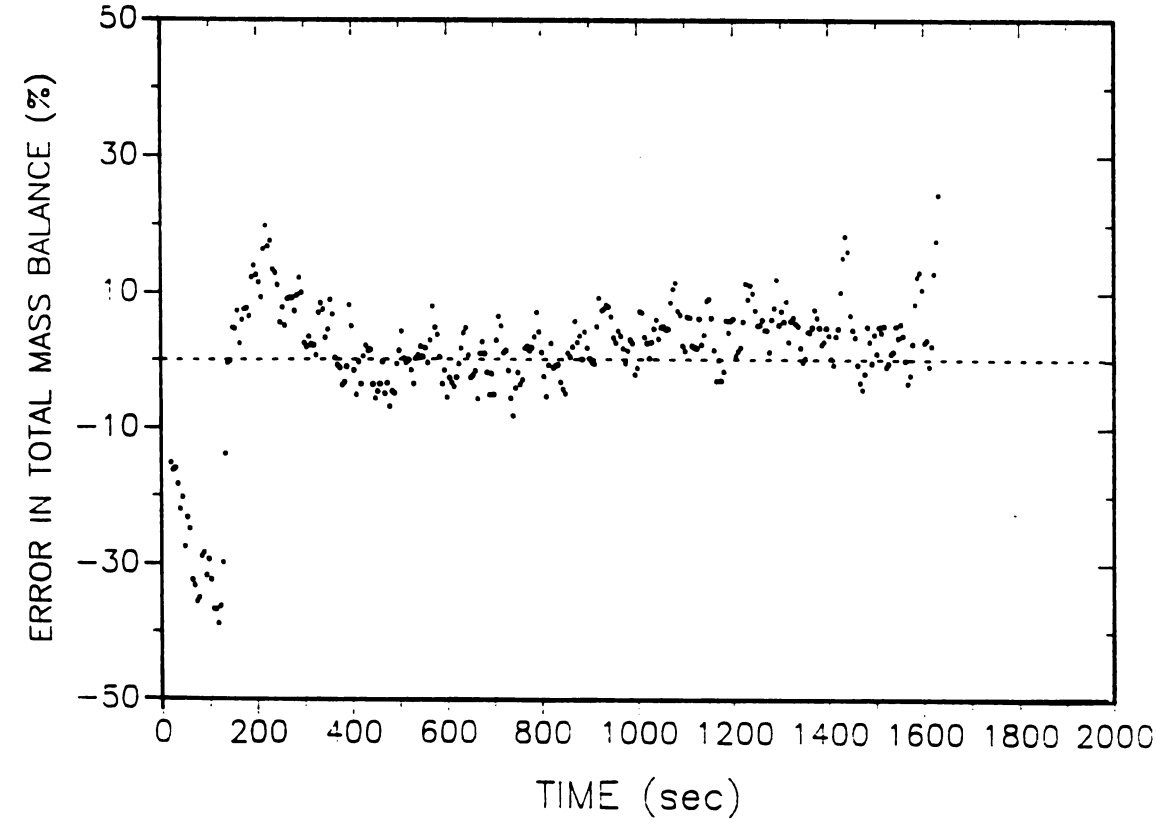

Fig. ERM2N Error in total mass balance for pyrolysis products; EXP. R2N

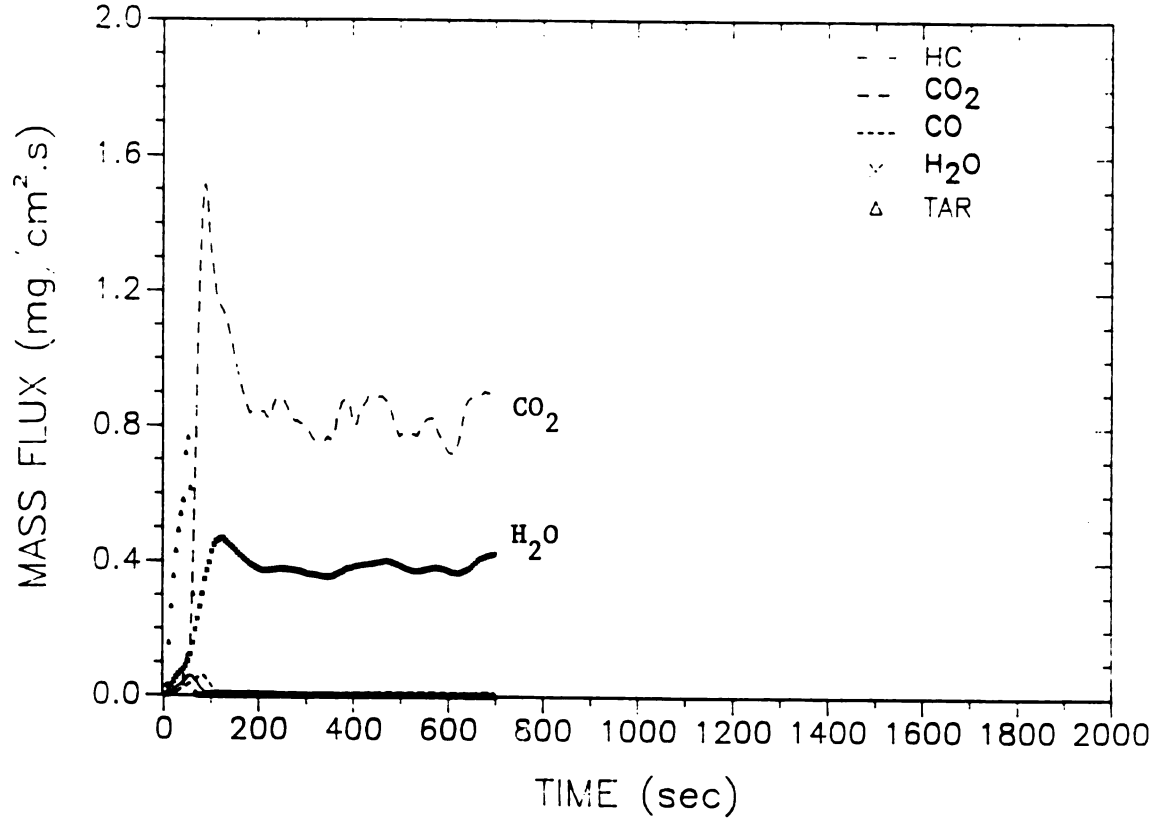

Fig. S1D4A Pyrolysis products (direct measurement); EXP. D4A

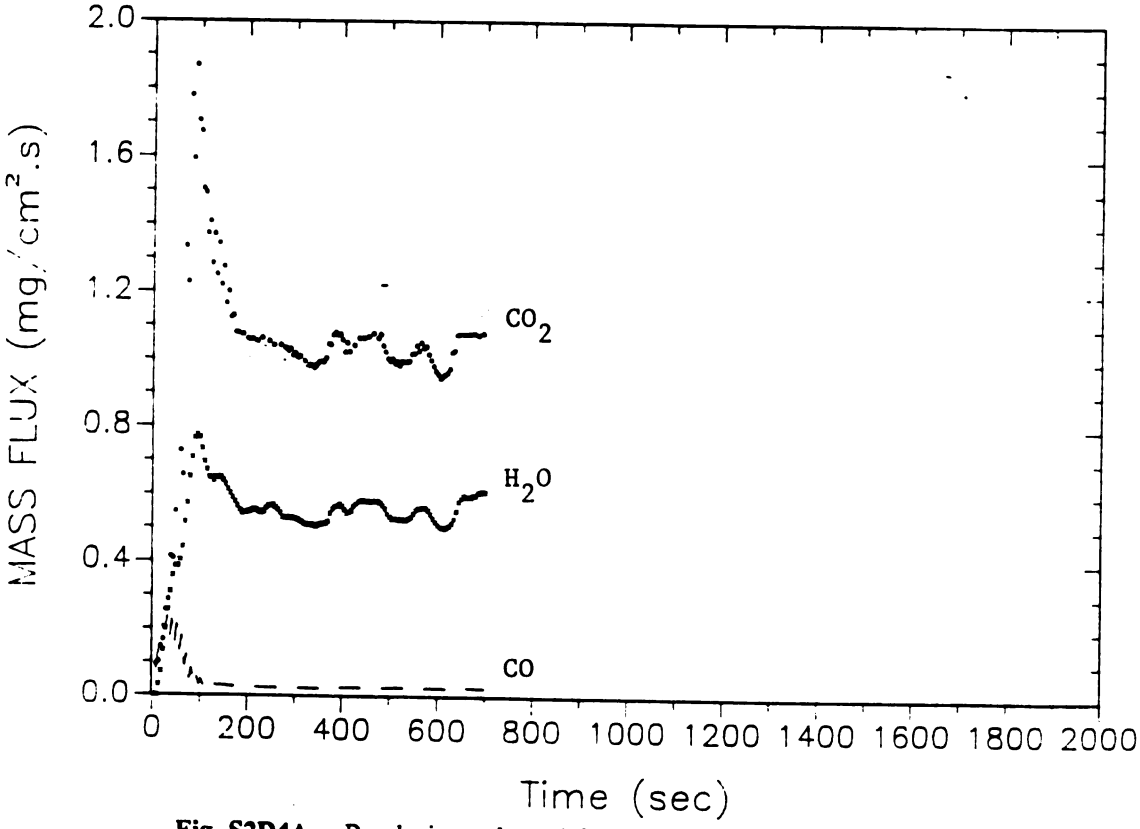

Fig. S2D4A Pyrolysis products (after catalytic combustor); EXP. D4A

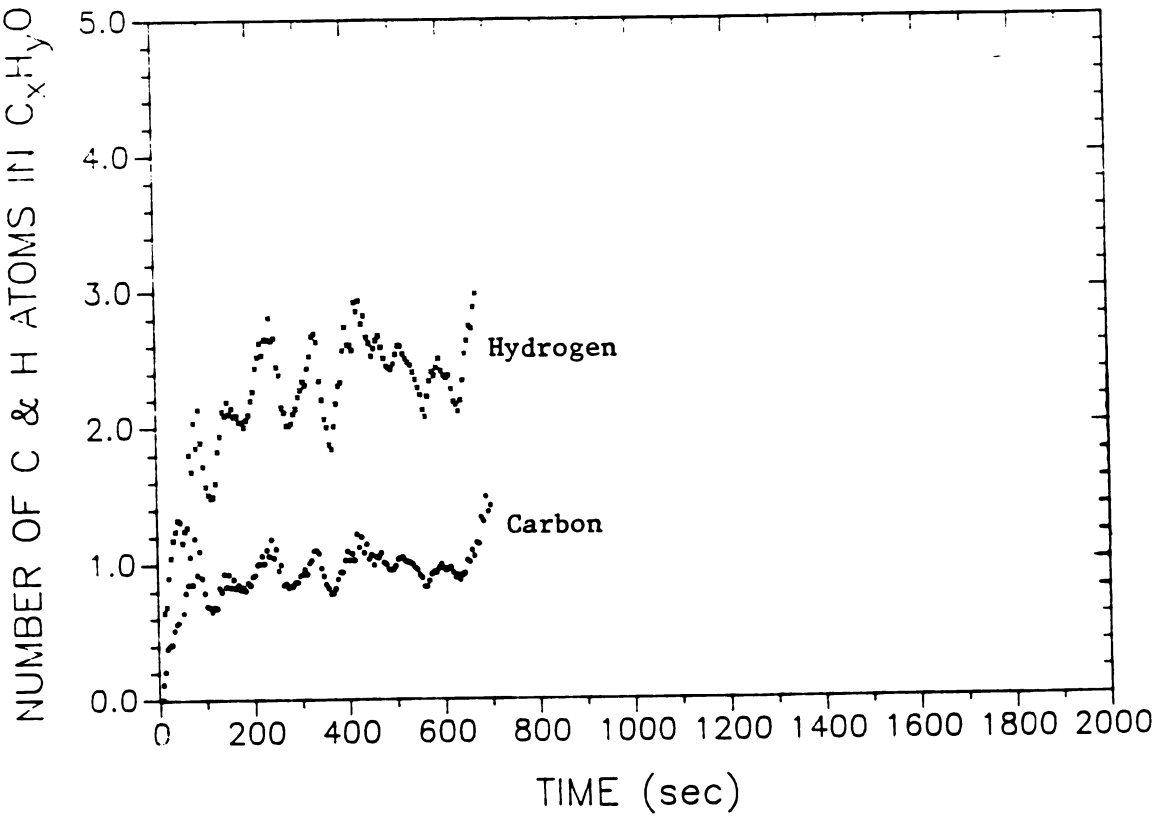

Fig. CHD4A Number of C and H atoms in the products of pyrolysis; EXP. D4A

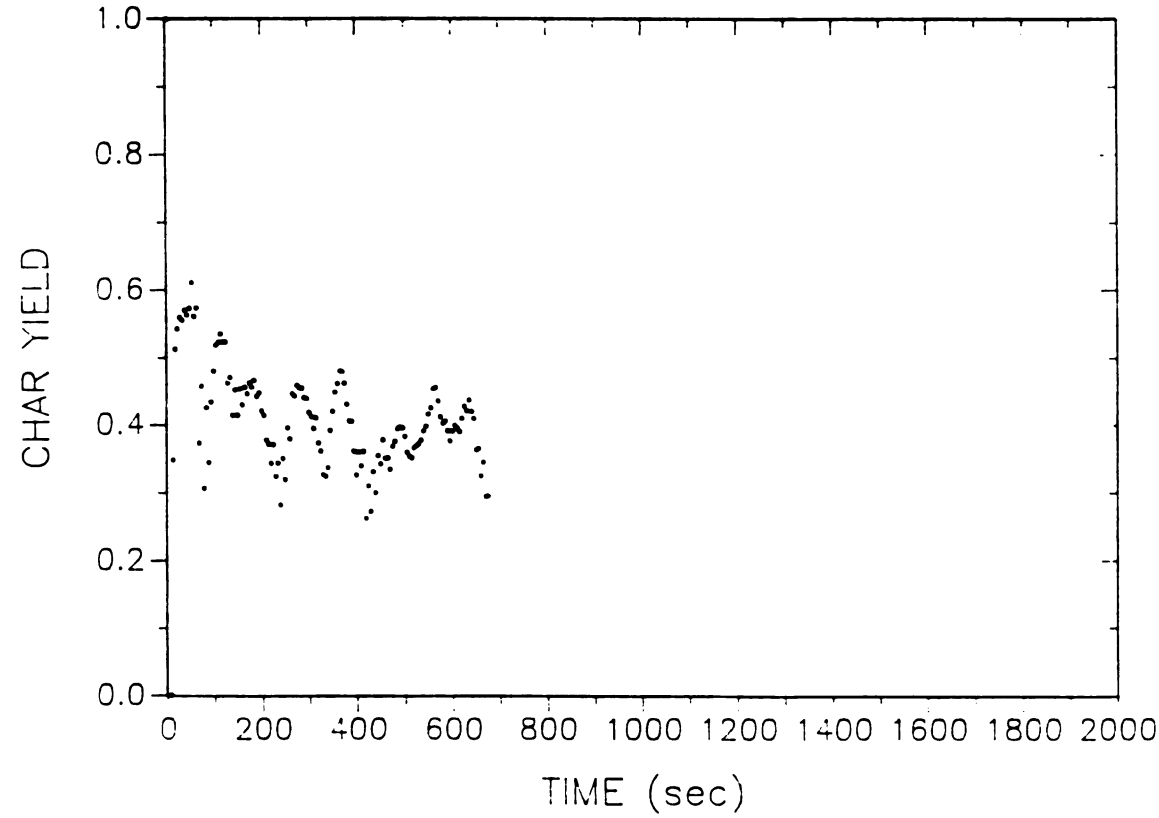

Fig. YCD4A Char yield (gram char/gram wood); EXP. D4A

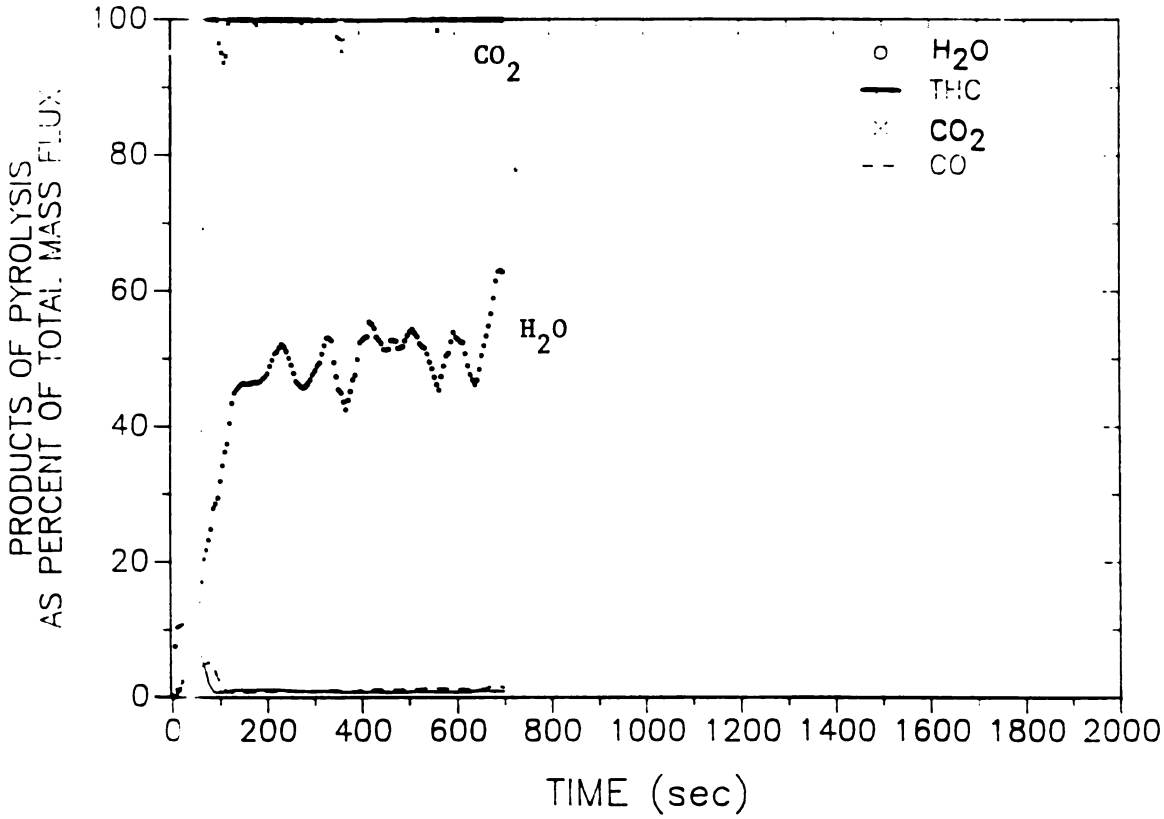

ig. PSD4A Products of pyrolysis as percent of total mass flux; EXP. D4A

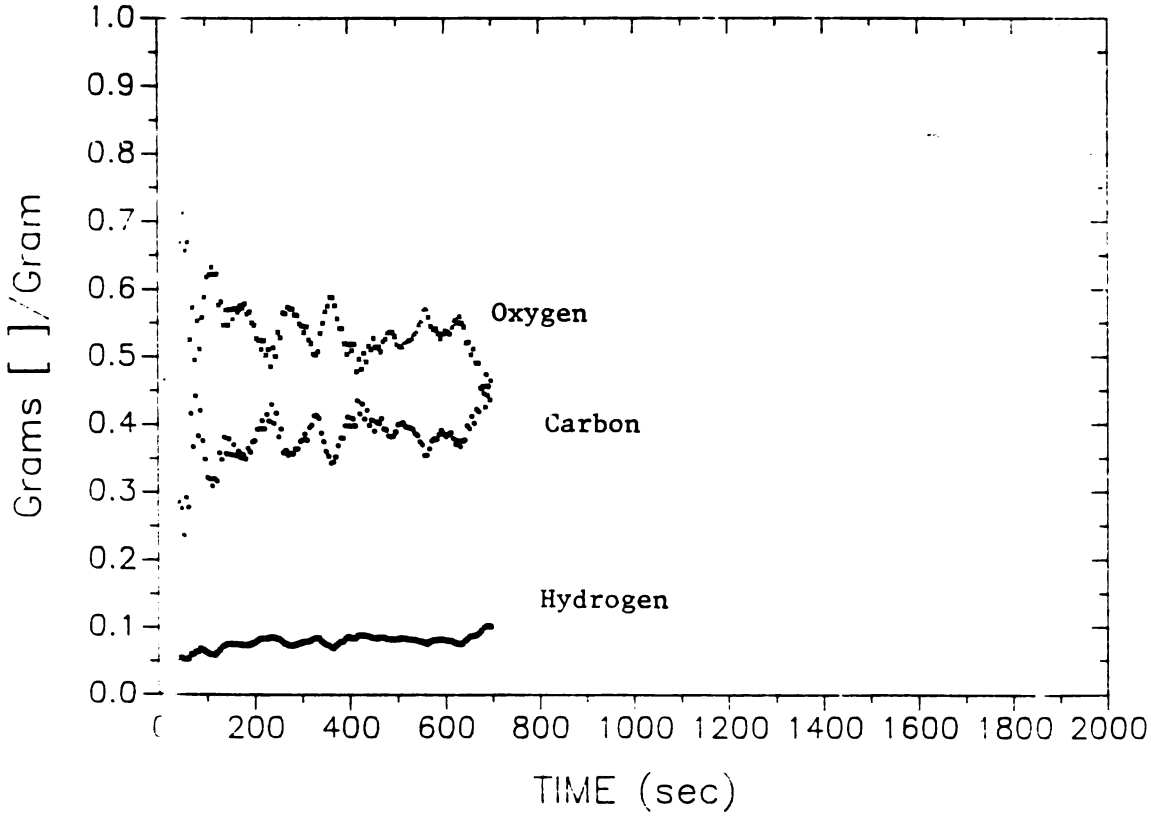

ig. GGD4A Gram [ ]/gram of C_xH_yO; EXP. D4A

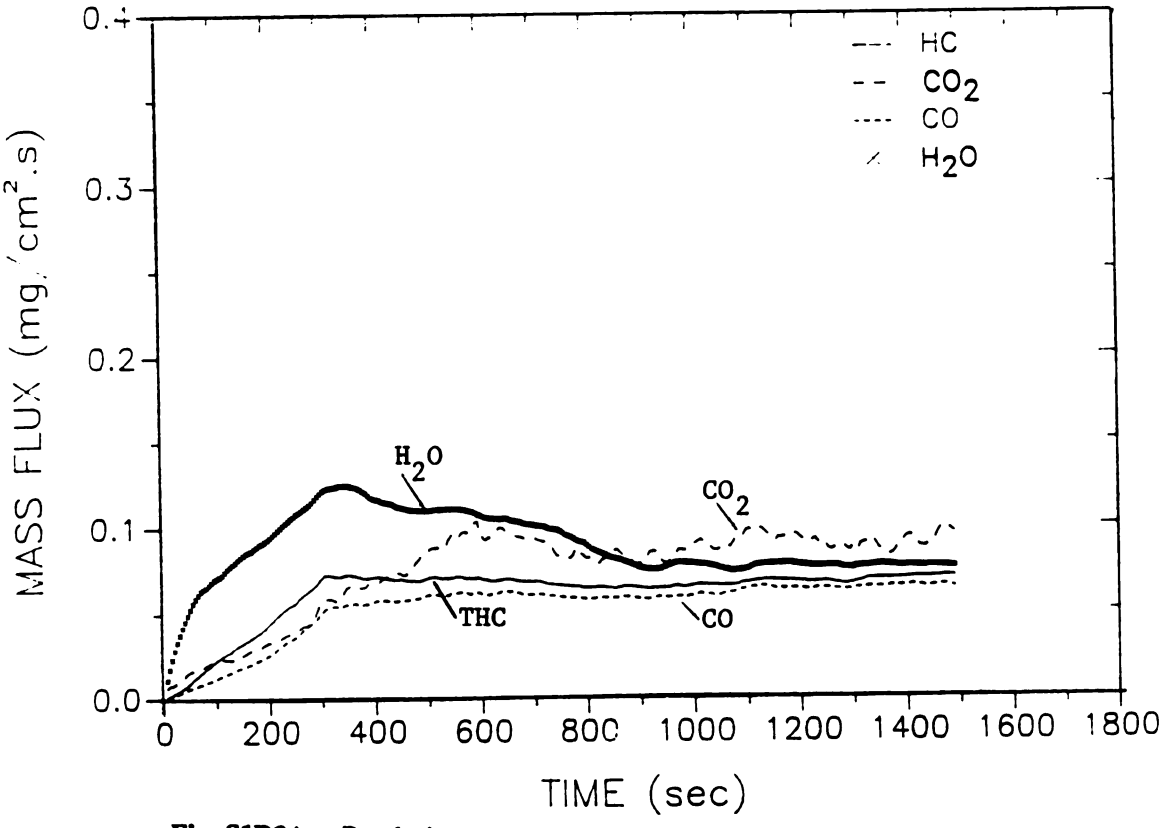

Fig. S1D3A Pyrolysis products (direct measurement); EXP. D3A

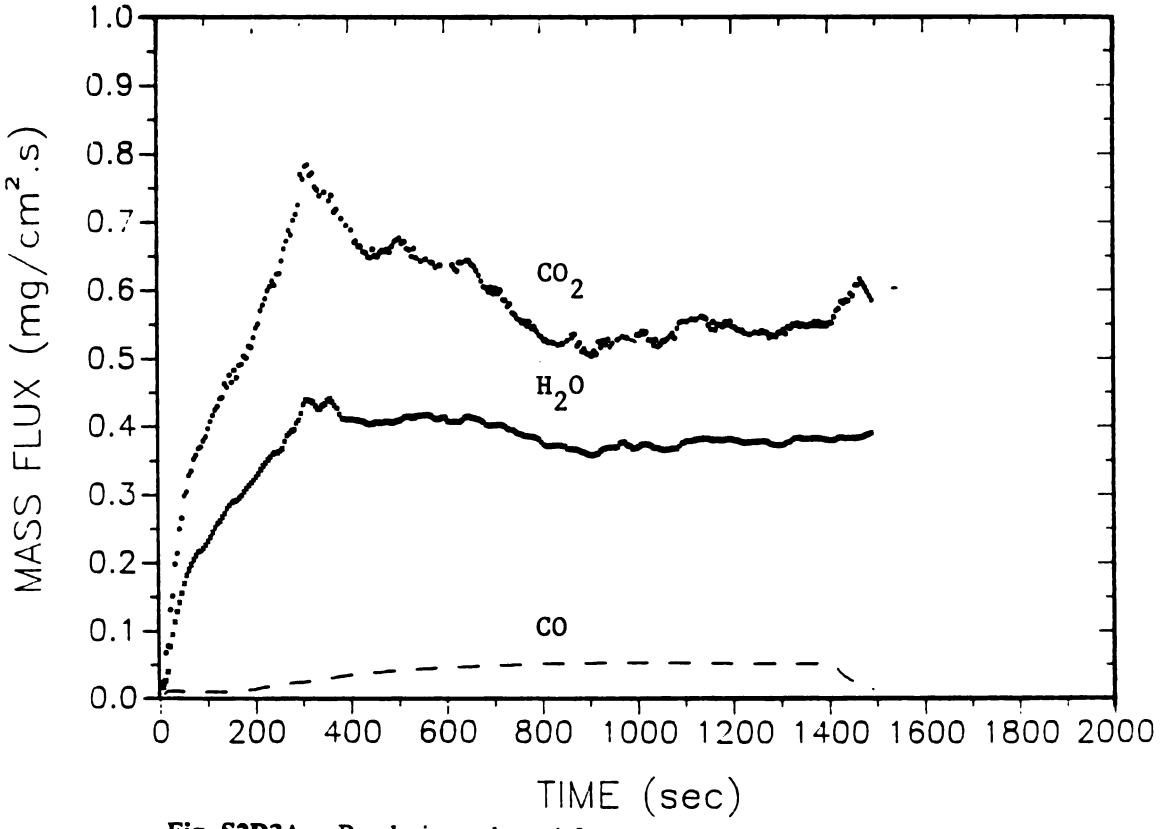

Fig. S2D3A Pyrolysis products (after catalytic combustor); EXP. D3A

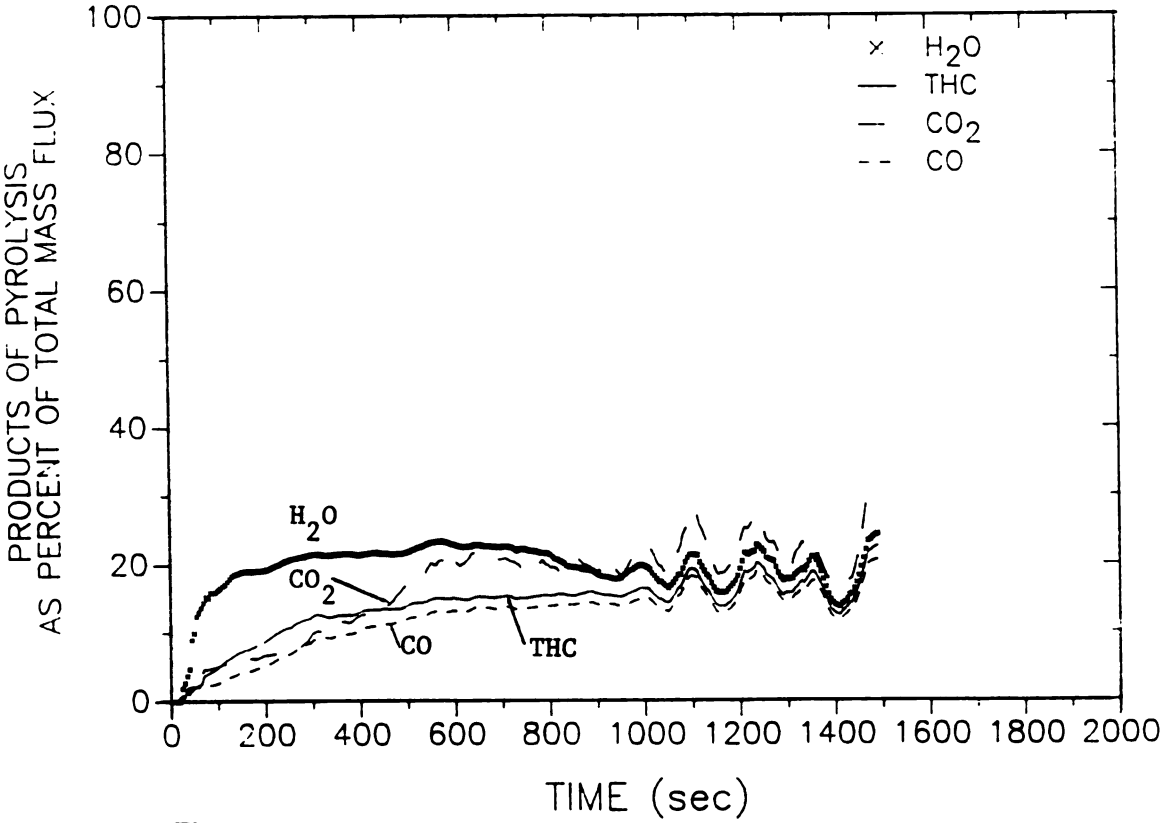

Fig. PSD3A Products of pyrolysis as percent of total mass flux; EXP. D3A

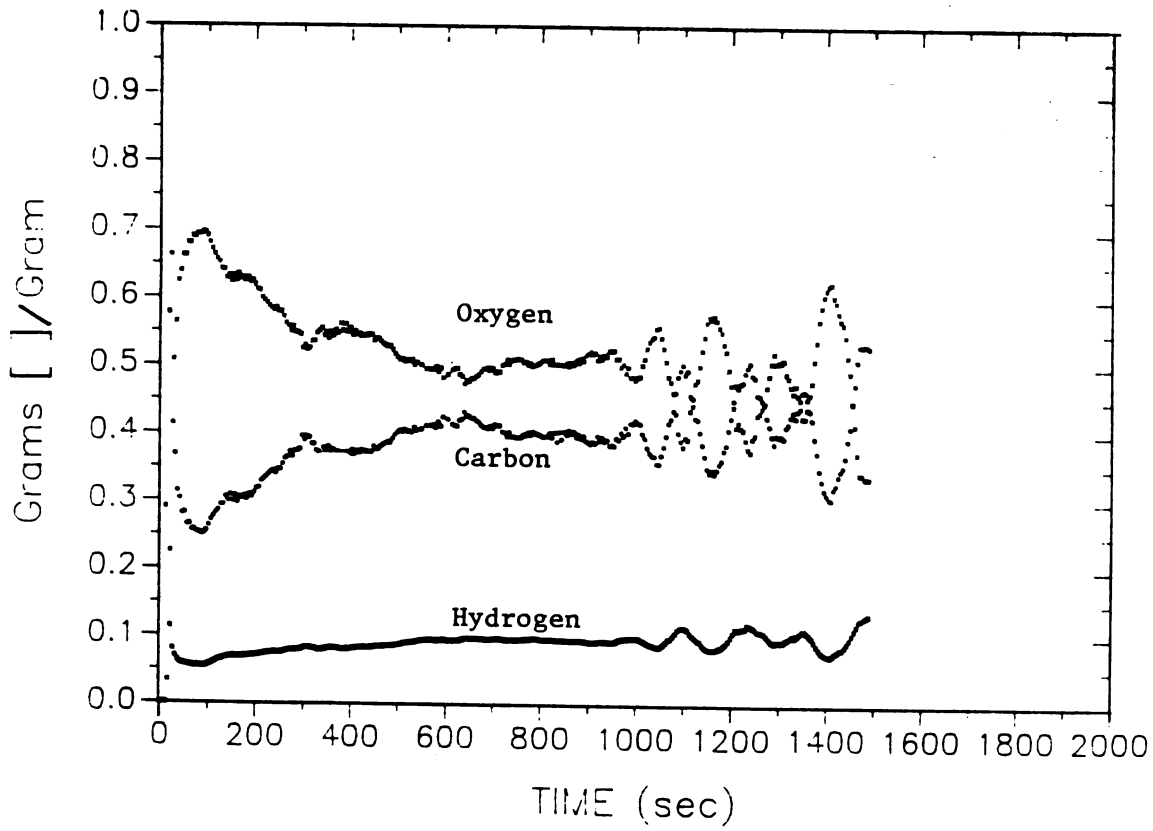

Fig. GGD3A Gram [ ]/gram of C_xH_yO; EXP. D3A

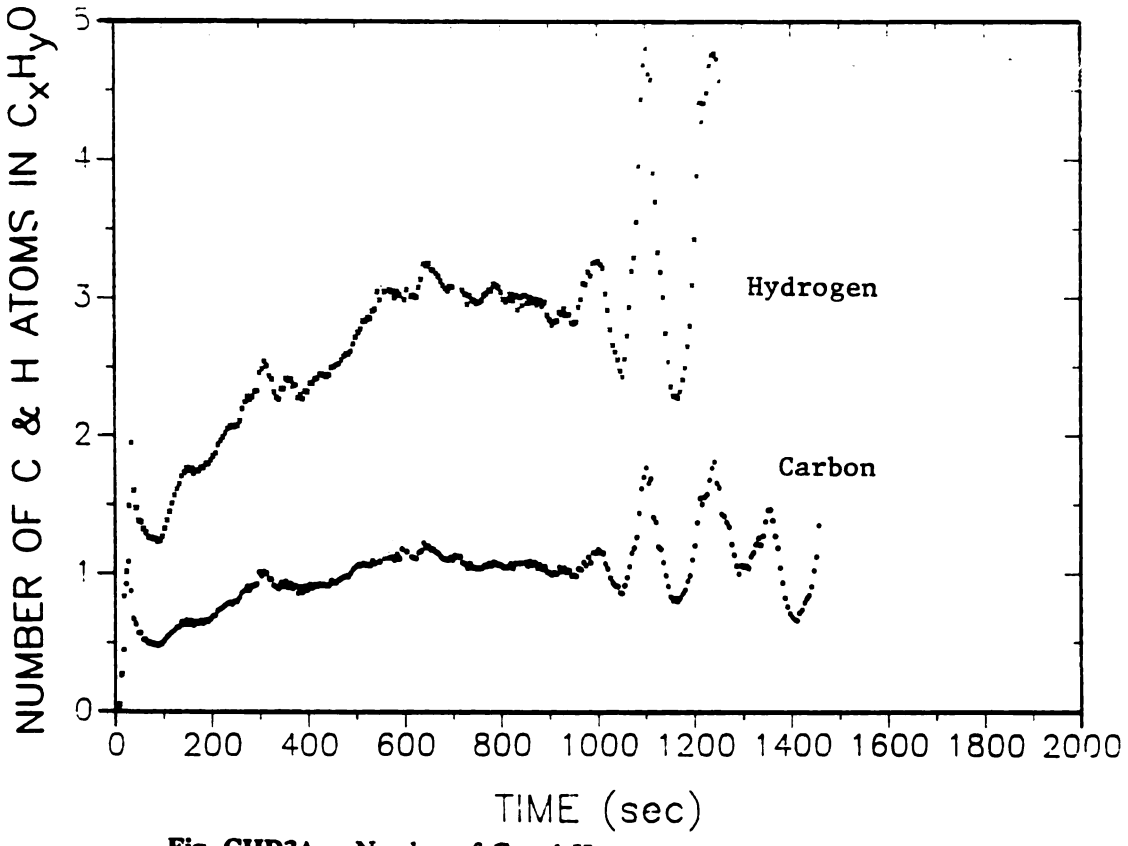

Fig. CHD3A Number of C and H atoms in the products of pyrolysis; EXP. D3A

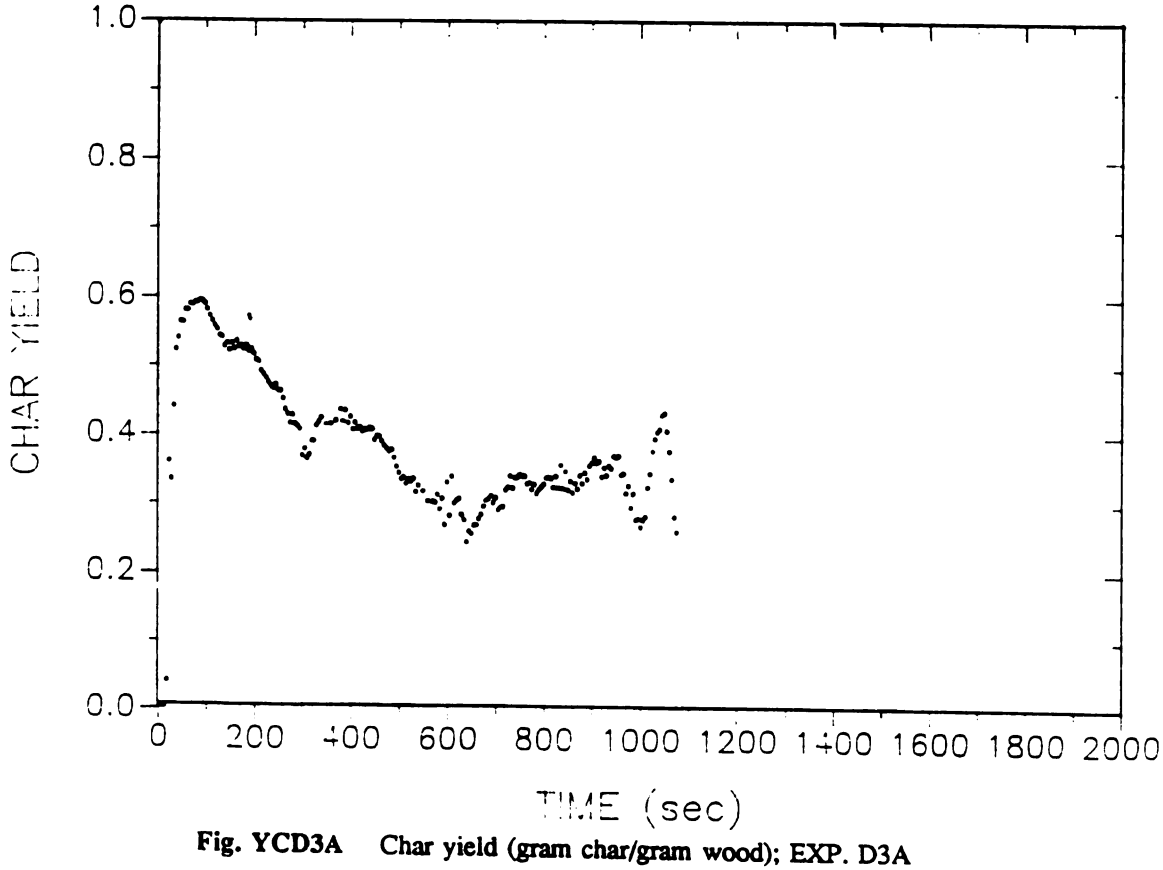

Fig. YCD3A Char yield (gram char/gram wood); EXP. D3A

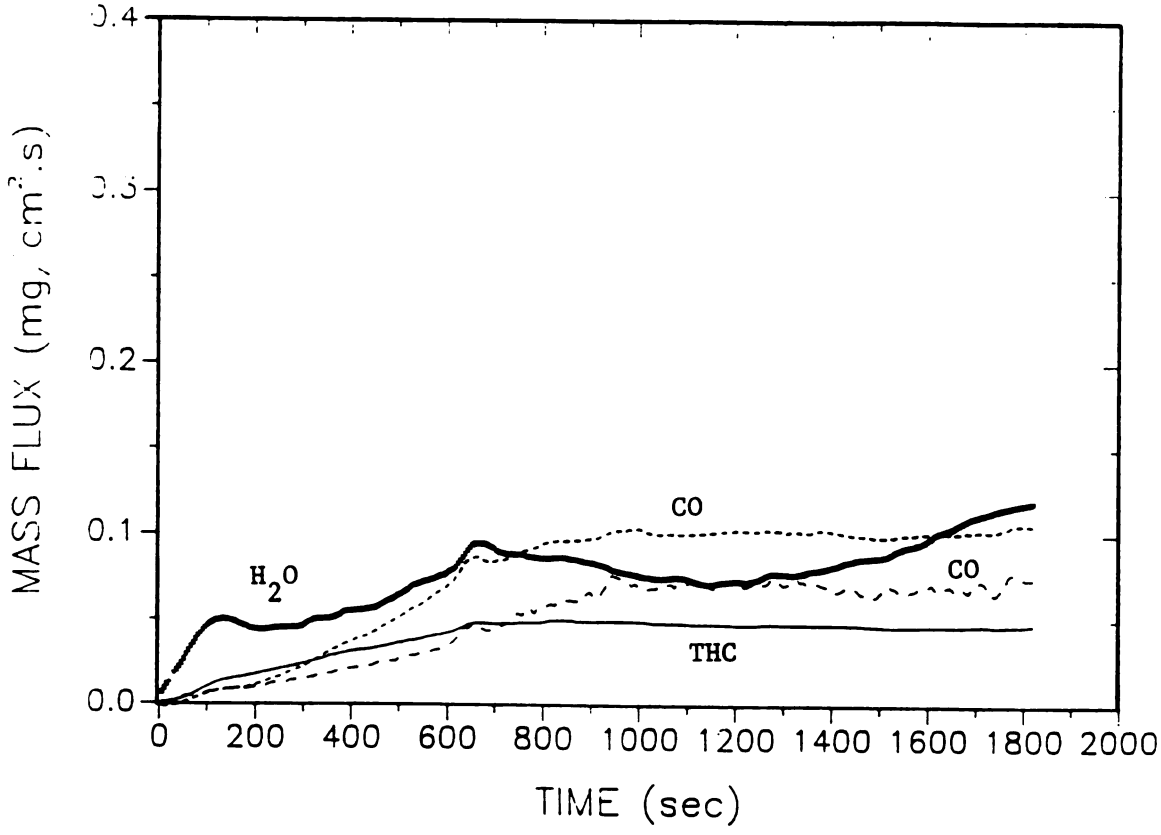

Fig. S1D2A Pyrolysis products (direct measurement); EXP. D2A

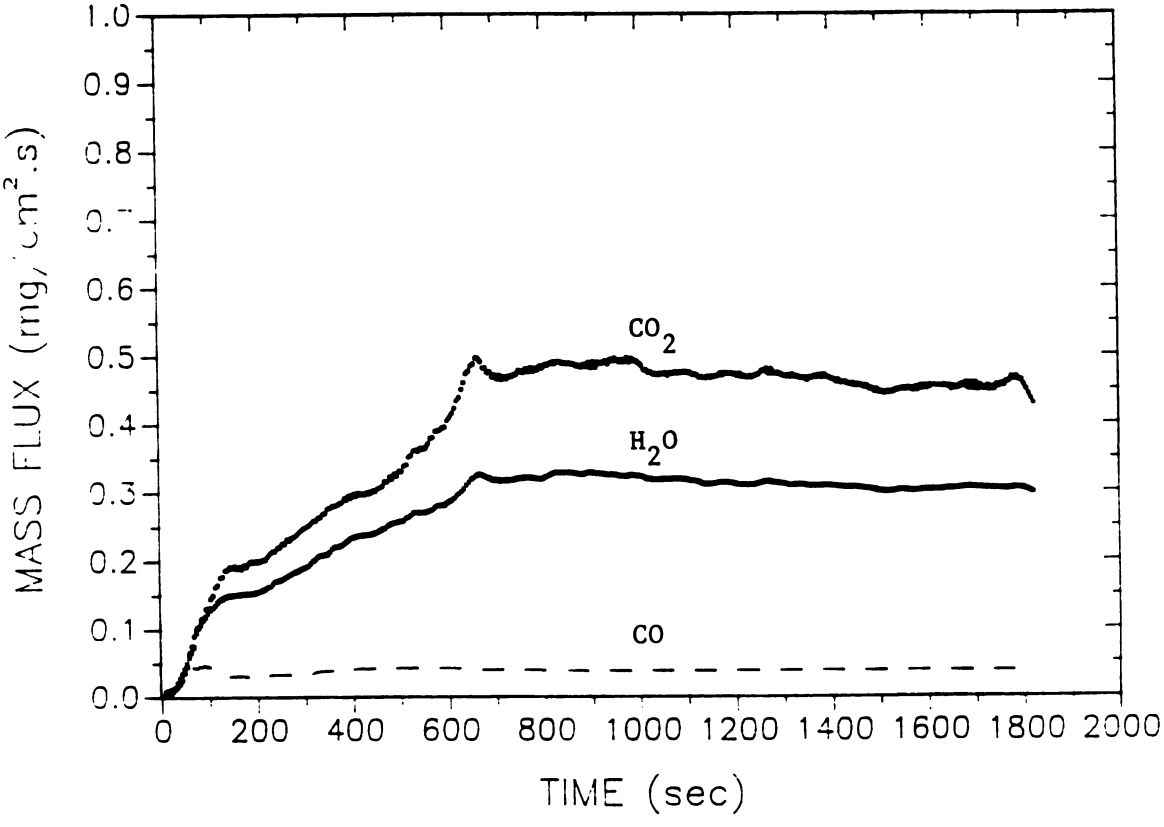

Fig. S2D2A Pyrolysis products (after catalytic combustor);EXP. D2A

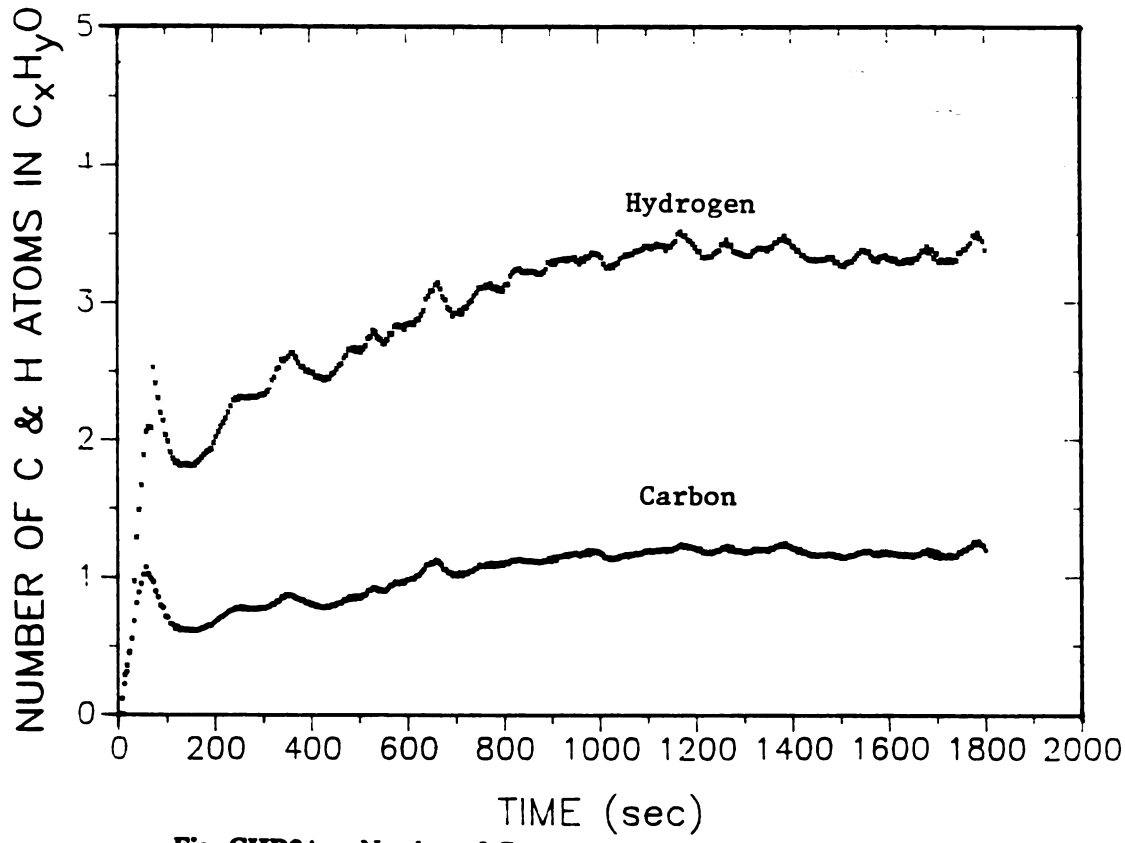

Fig. CHD2A Number of C and H atoms in the products of pyrolysis; EXP. D2A

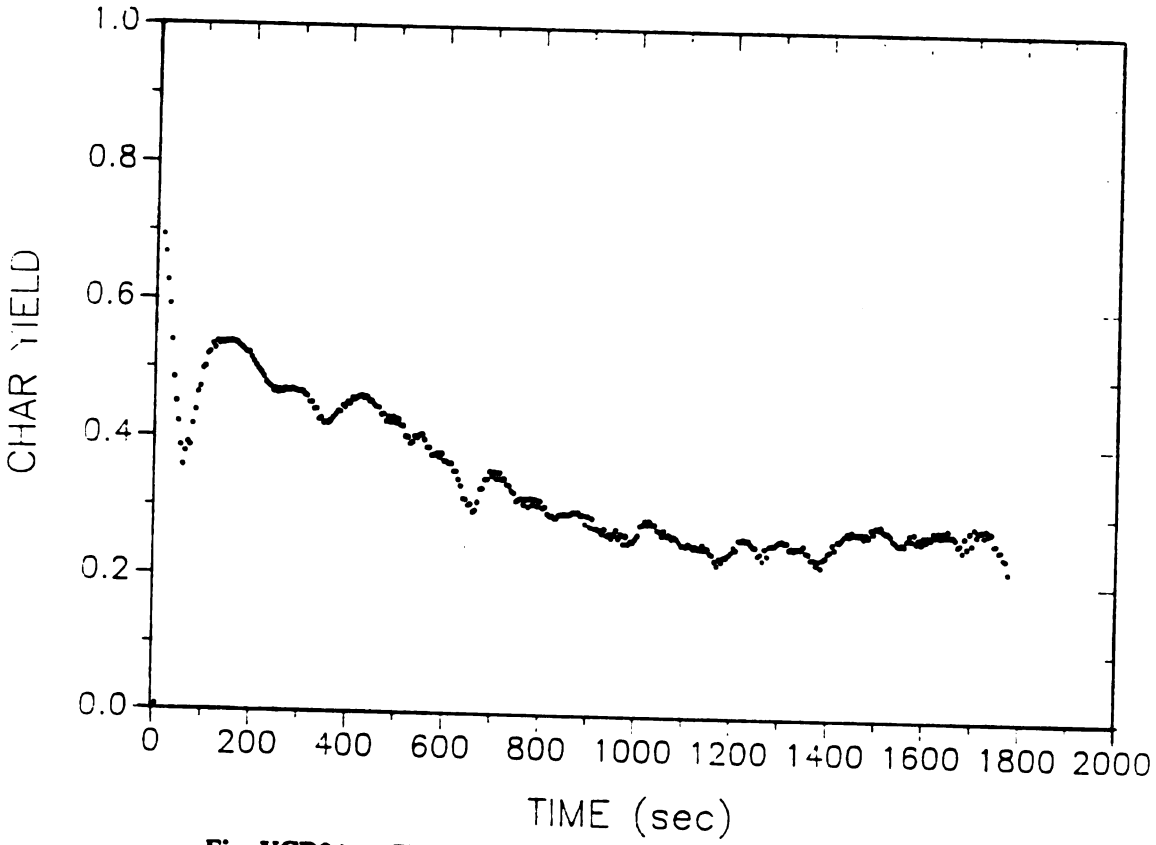

Fig. YCD2A Char yield (gram char/gram wood); EXP. D2A

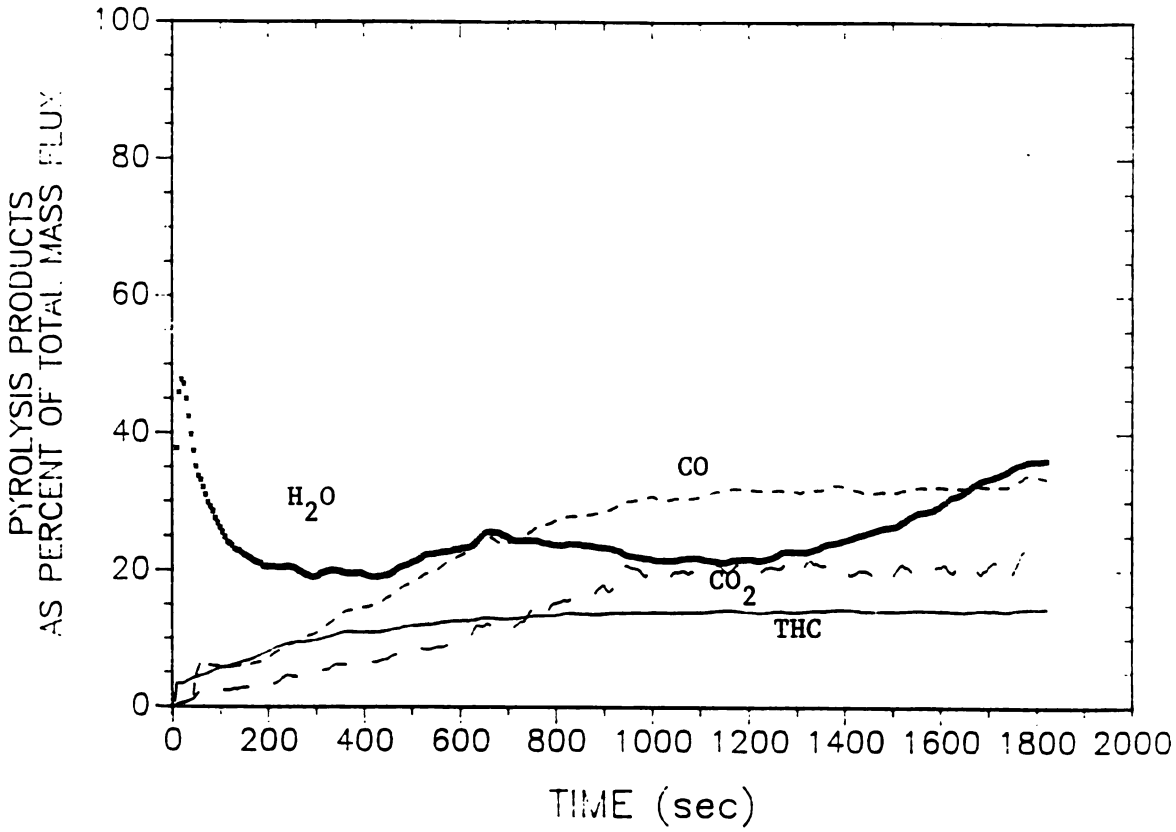

Fig. PSD2A Products of pyrolysis as percent of total mass flux; EXP. D2A

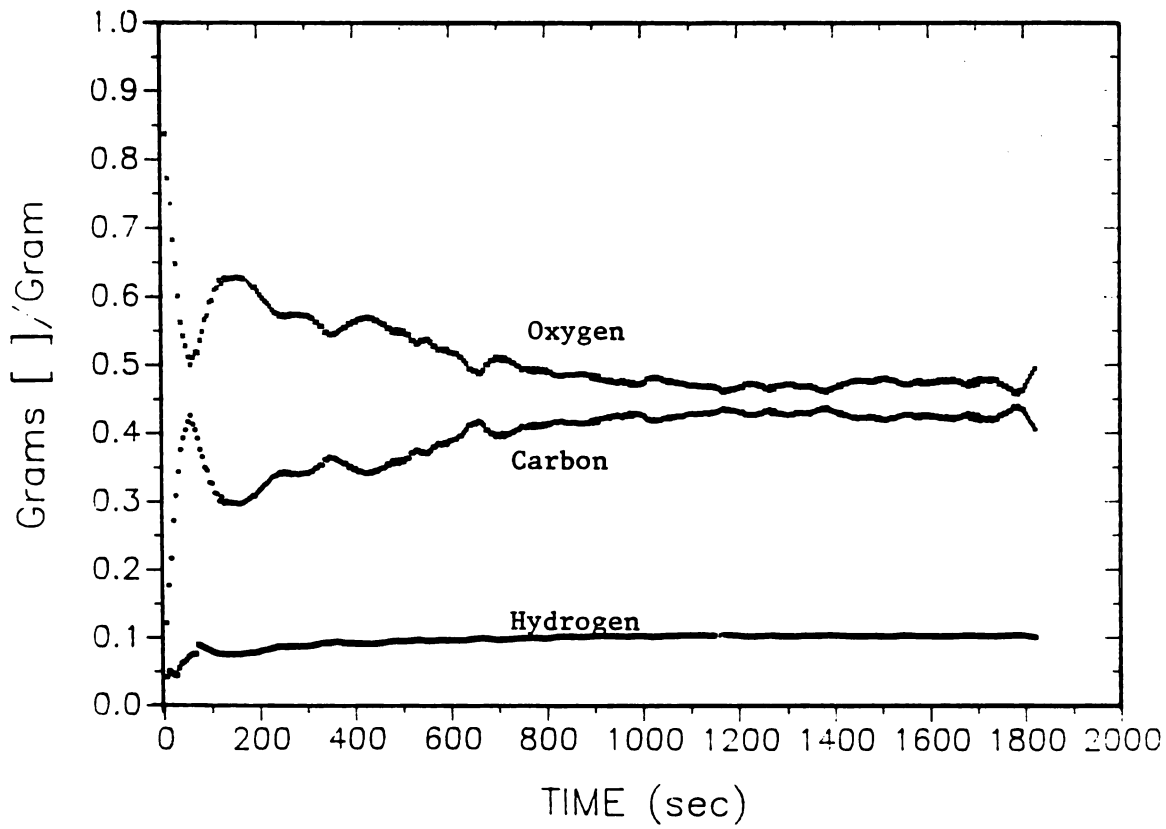

Fig. GGD2A Gram [ ]/gram of C_xH_yO; EXP. D2A

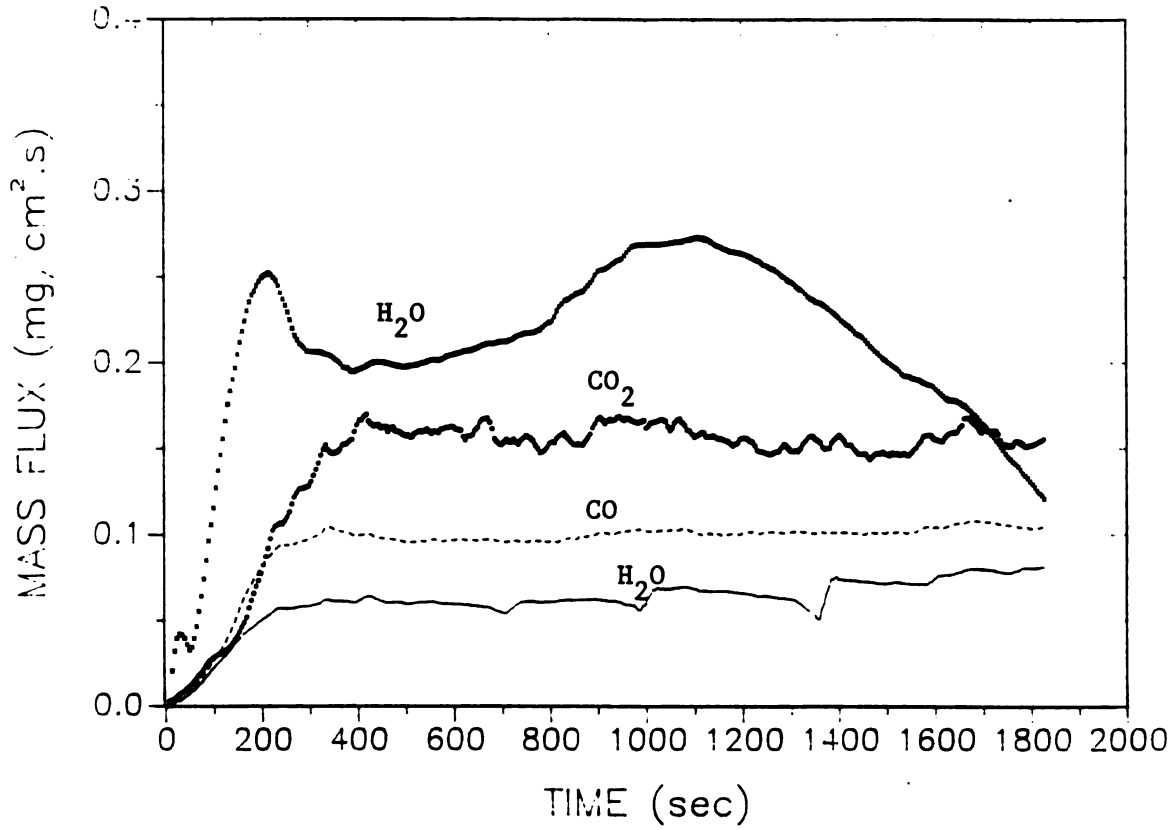

Fig. S1R3A Pyrolysis products (direct measurement); EXP. R3A

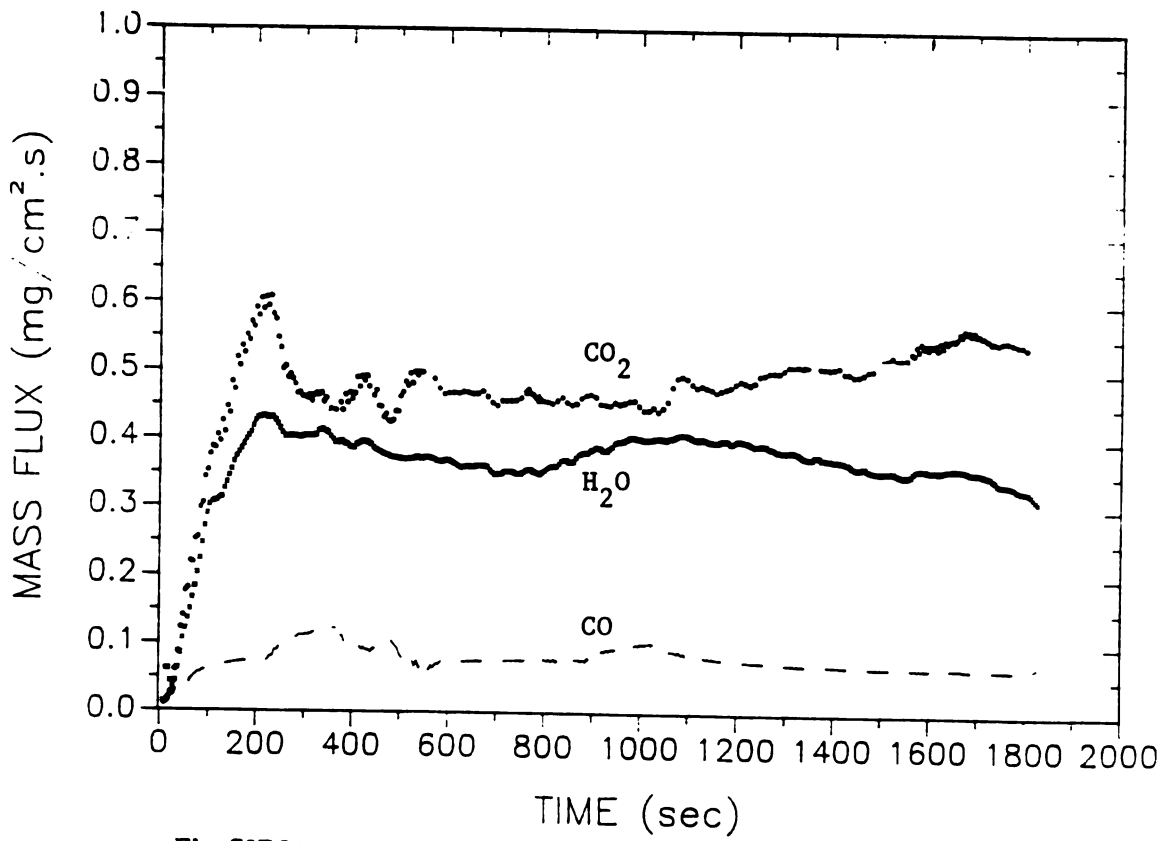

Fig. S2R3A Pyrolysis products (after catalytic combustor); EXP. R3A

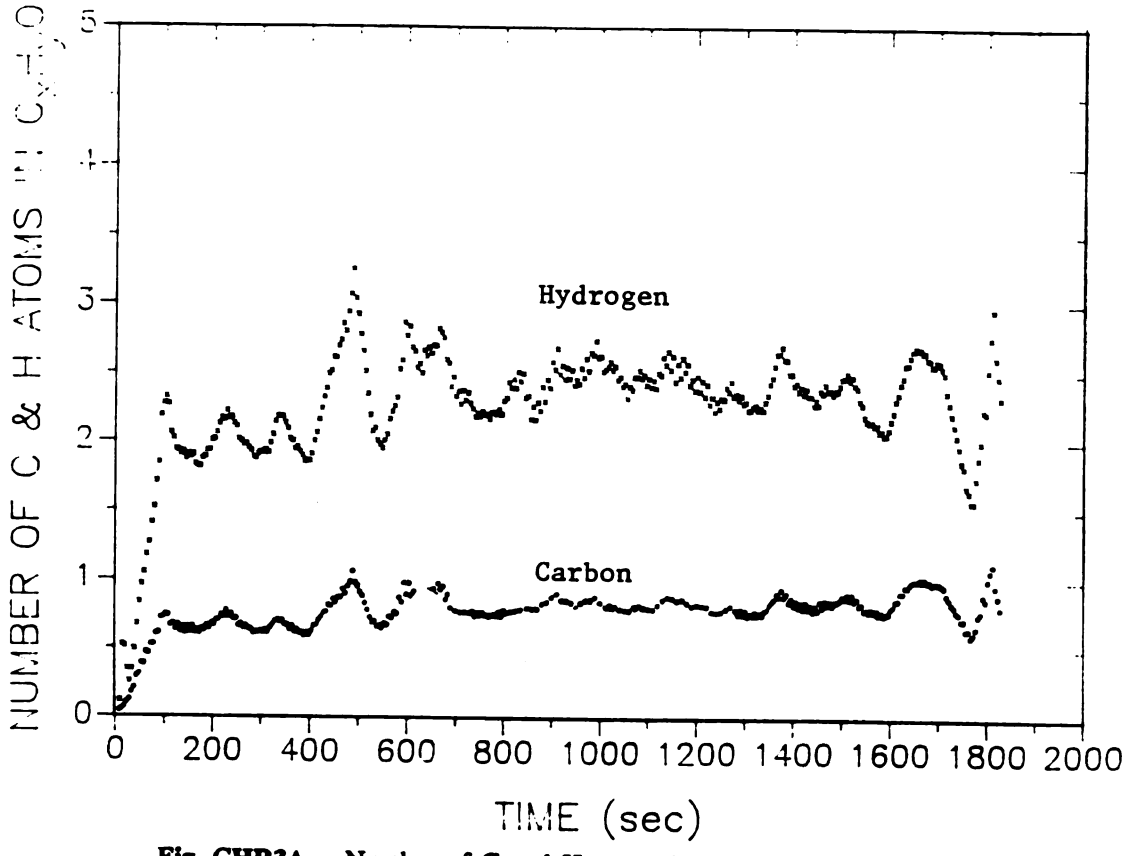

Fig. CHR3A Number of C and H atoms in the products of pyrolysis; EXP. R3A

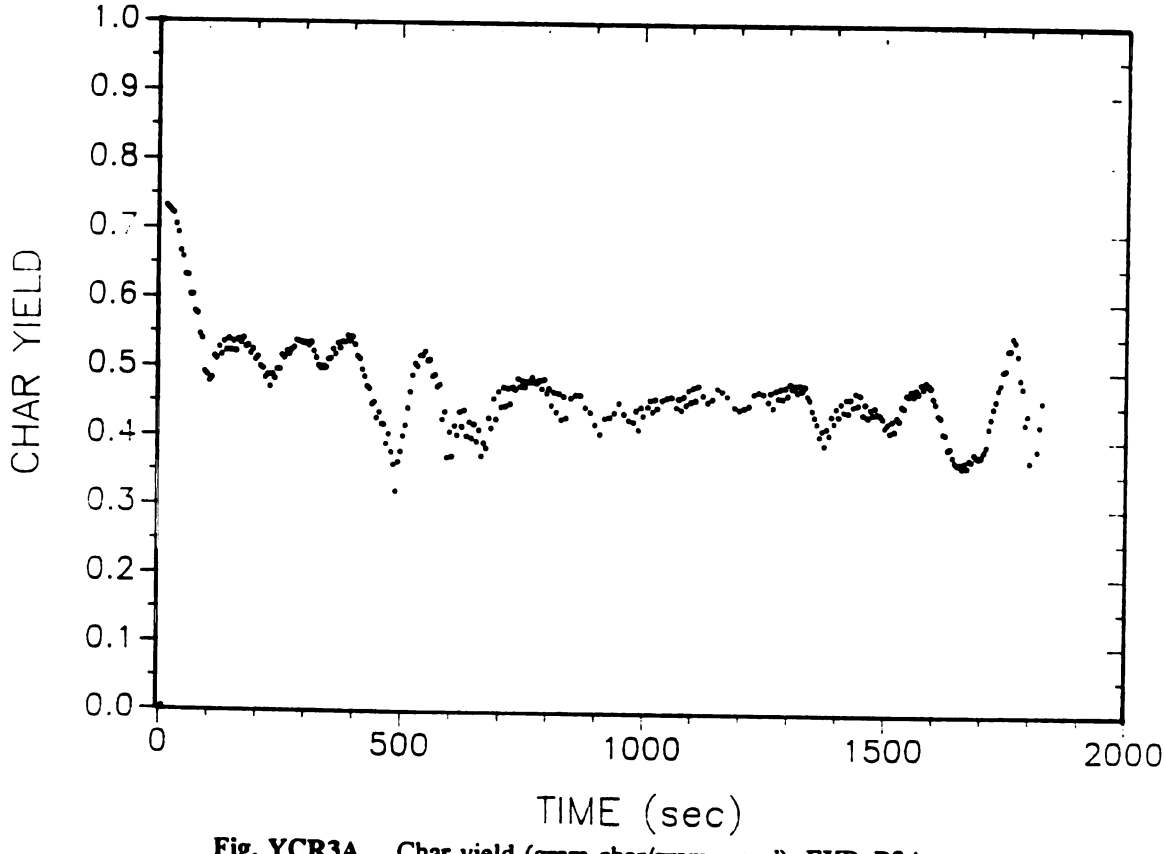

Fig. YCR3A Char yield (gram char/gram wood); EXP. R3A

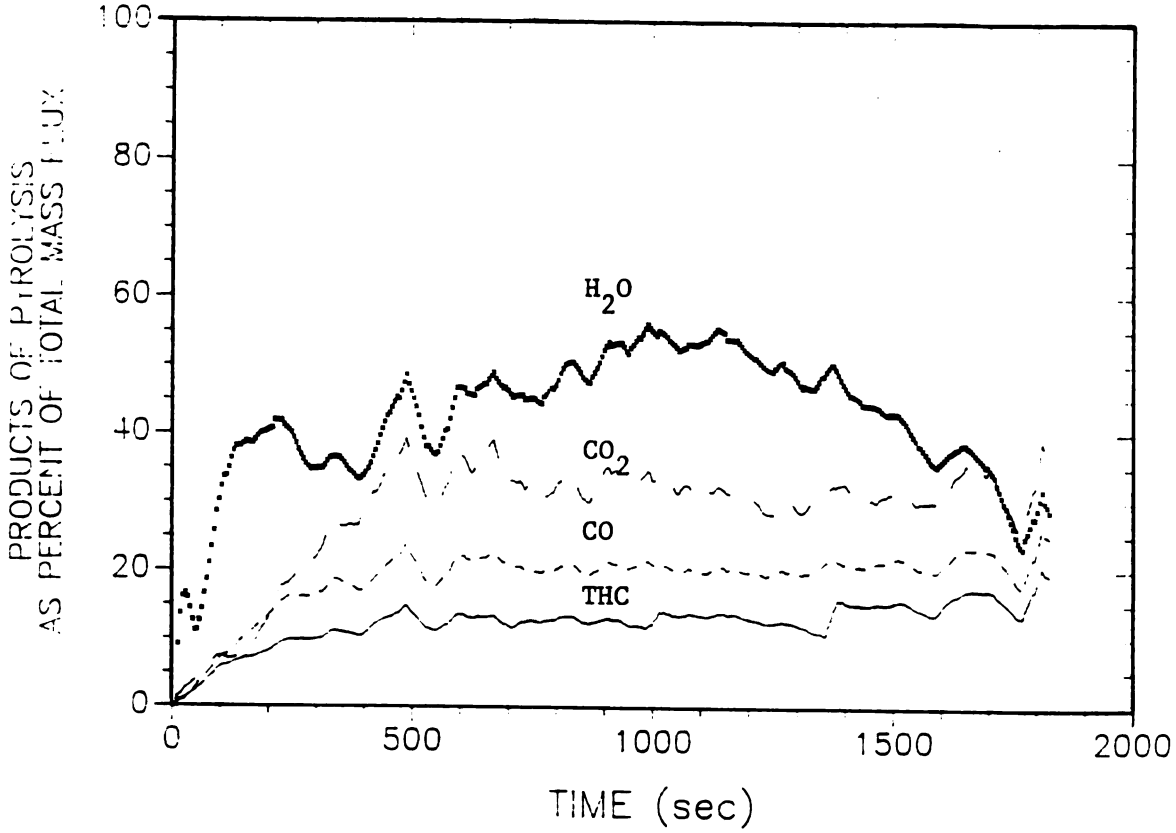

Fig. PSR3A Products of pyrolysis as percent of total mass flux; EXP. R3A

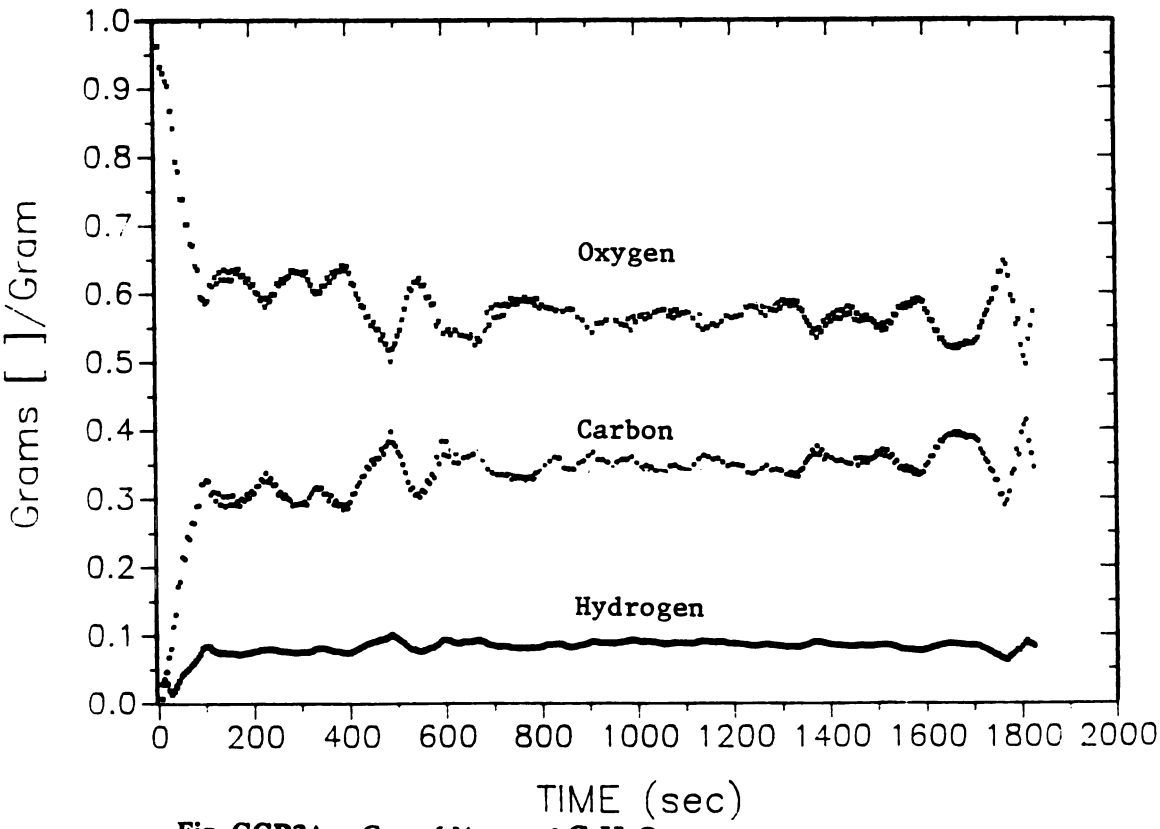

Fig. GGR3A Gram [ ]/gram of C_xH_yO; EXP. R3A

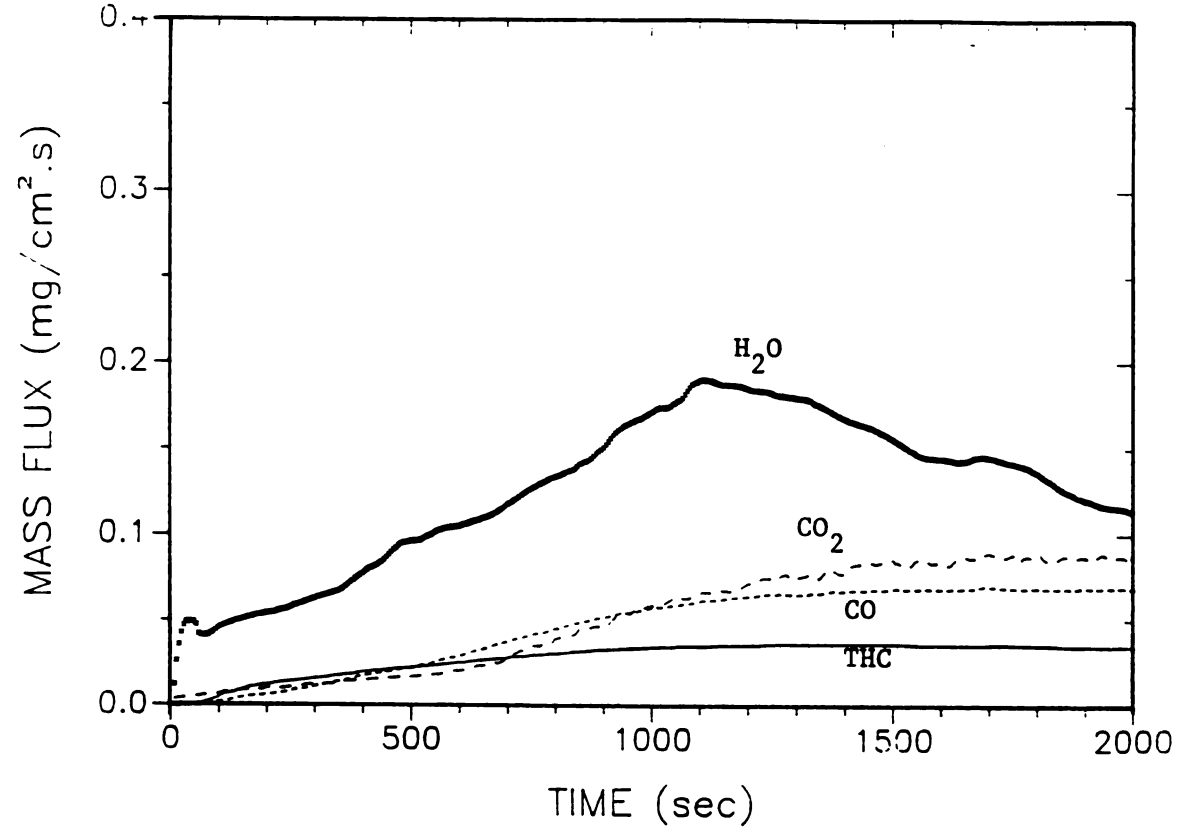

Fig. S1R2A Pyrolysis products (direct measurement); EXP. R2A

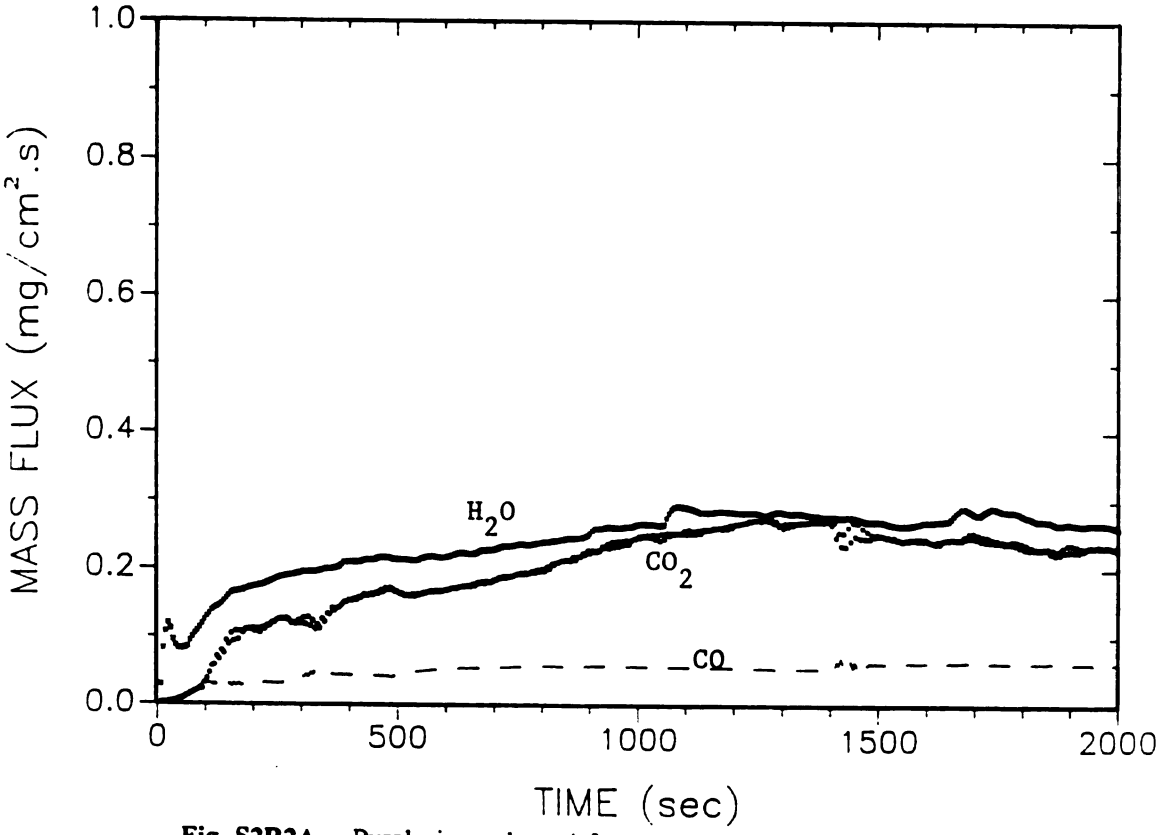

Fig. S2R2A Pyrolysis products (after catalytic combustor); EXP. R2A

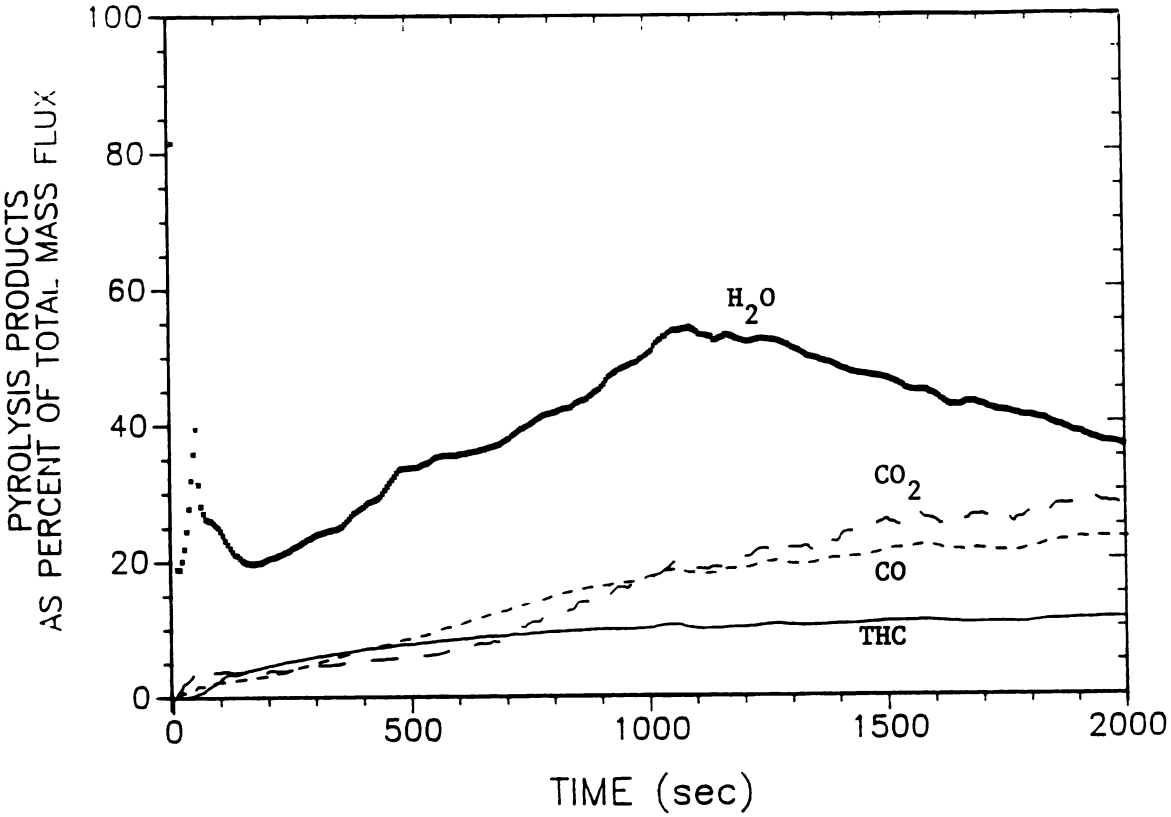

Fig. PSR2A Products of pyrolysis as percent of total mass flux; EXP. R2A

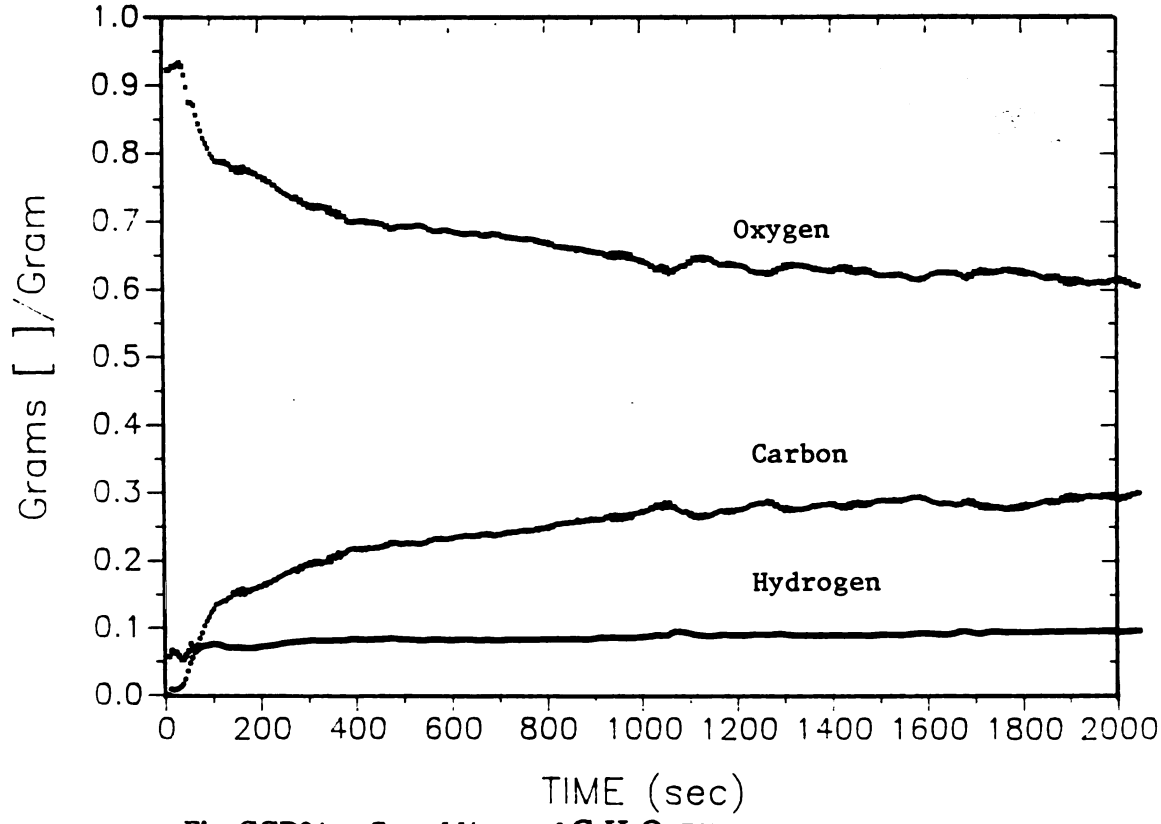

Fig. GGR2A Gram [ ]/gram of C_xH_yO; EXP. R2A

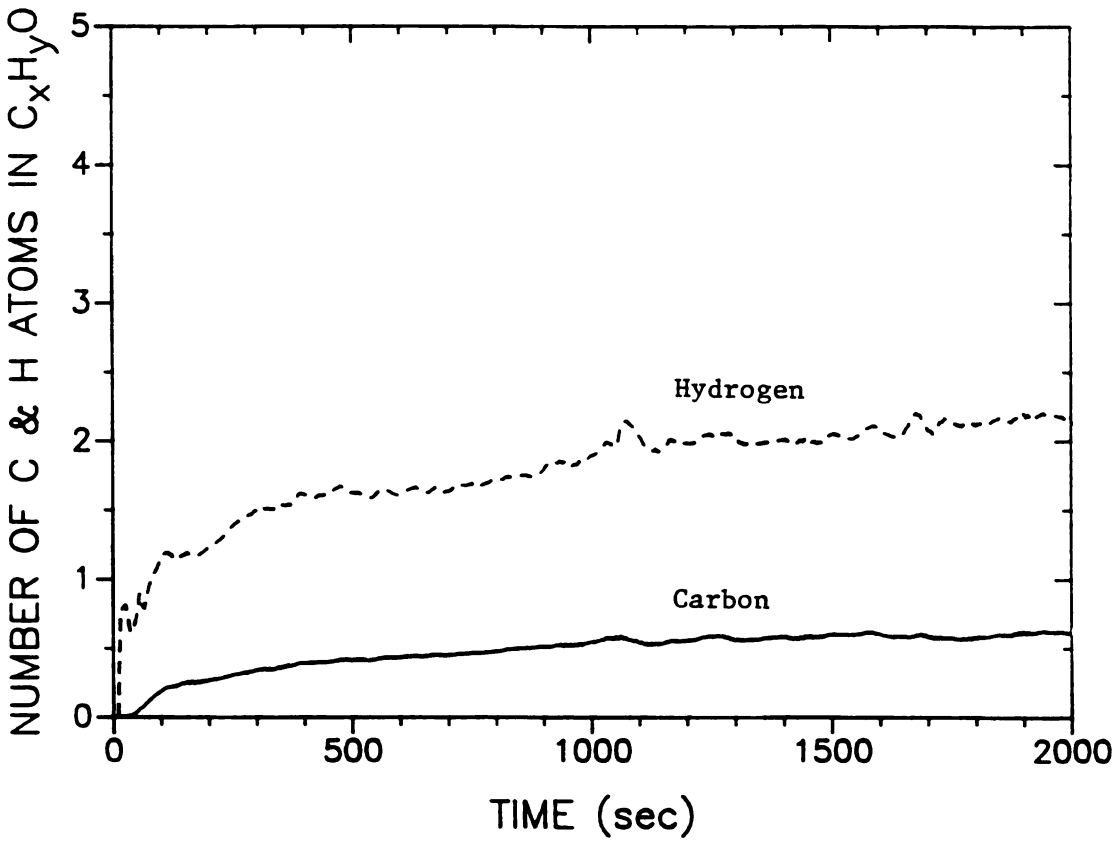

Fig. CHR2A Number of C and H atoms in the products of pyrolysis; EXP. R2A

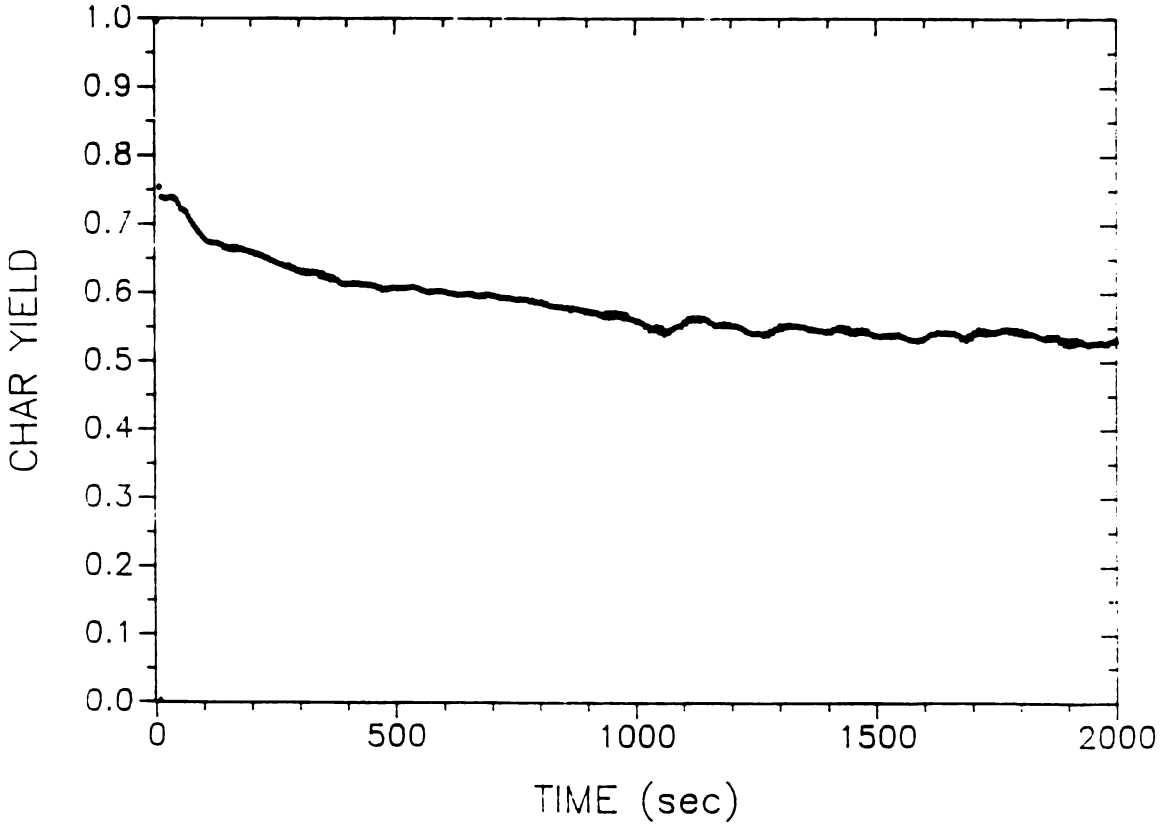

Fig. YCR2A Char yield (gram char/gram wood); EXP. R2A

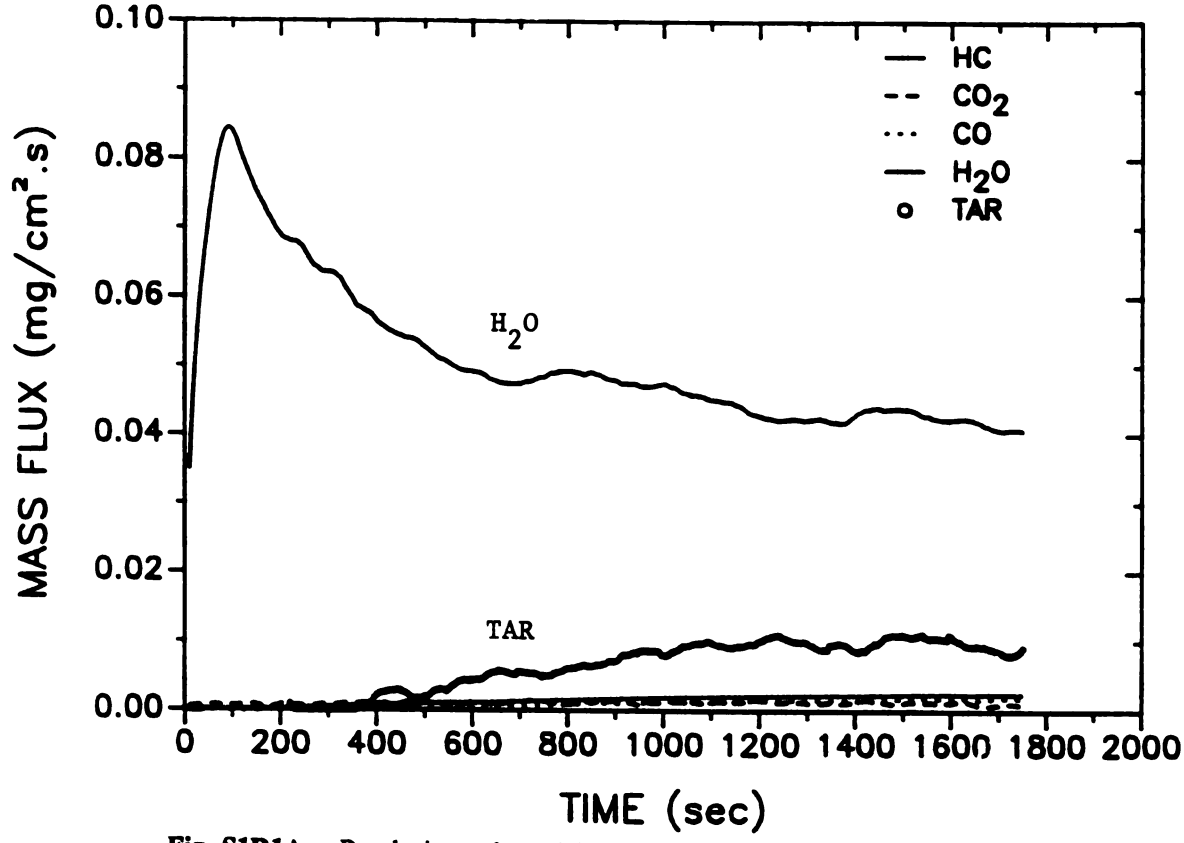

Fig. S1R1A Pyrolysis products (direct measurement); EXP. R1A

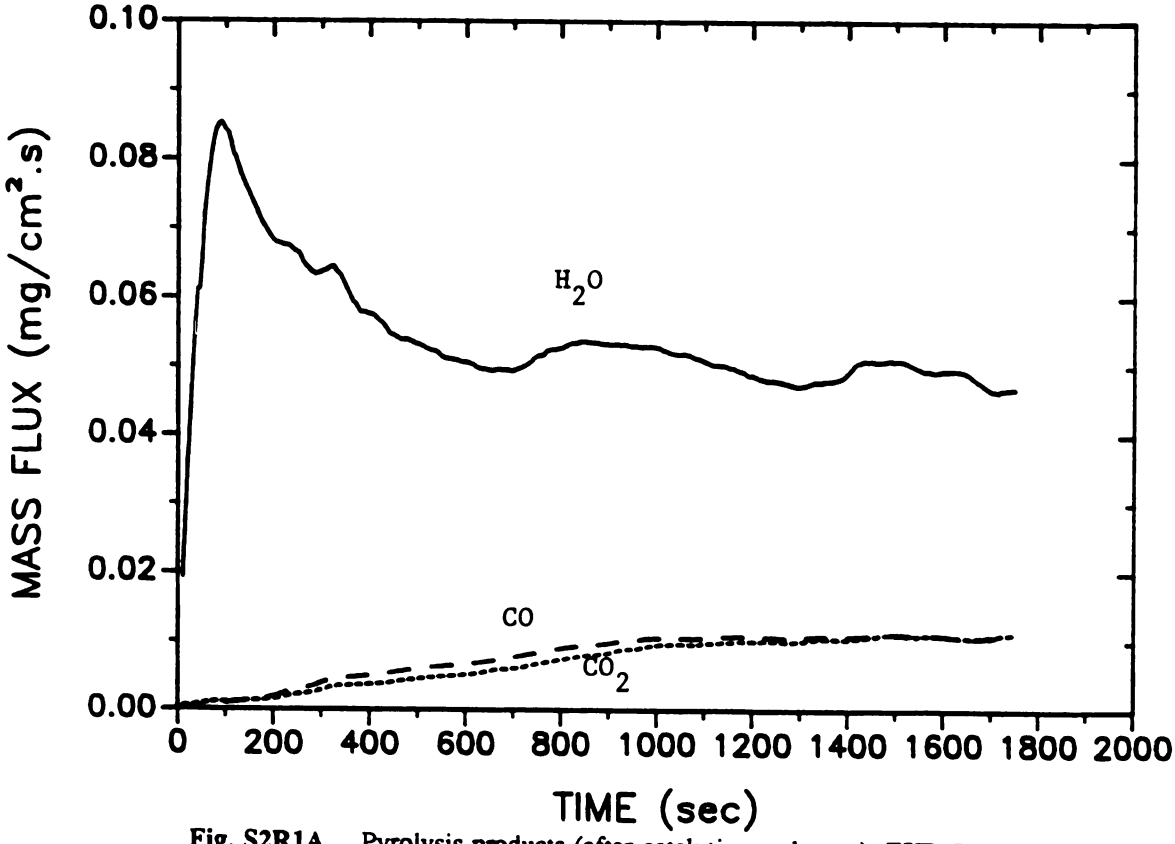

Fig. S2R1A Pyrolysis products (after catalytic combustor); EXP. R1A

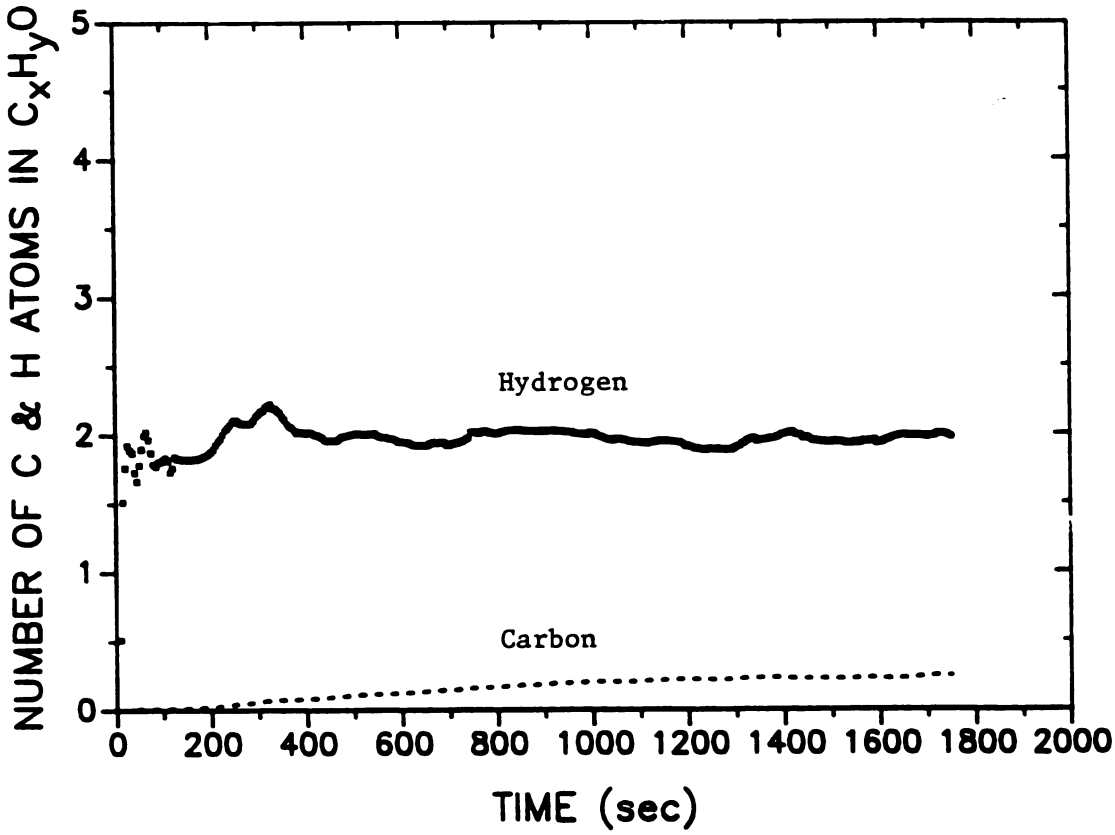

Fig. CHR1A Number of C and H atoms in the products of pyrolysis; EXP. R1A

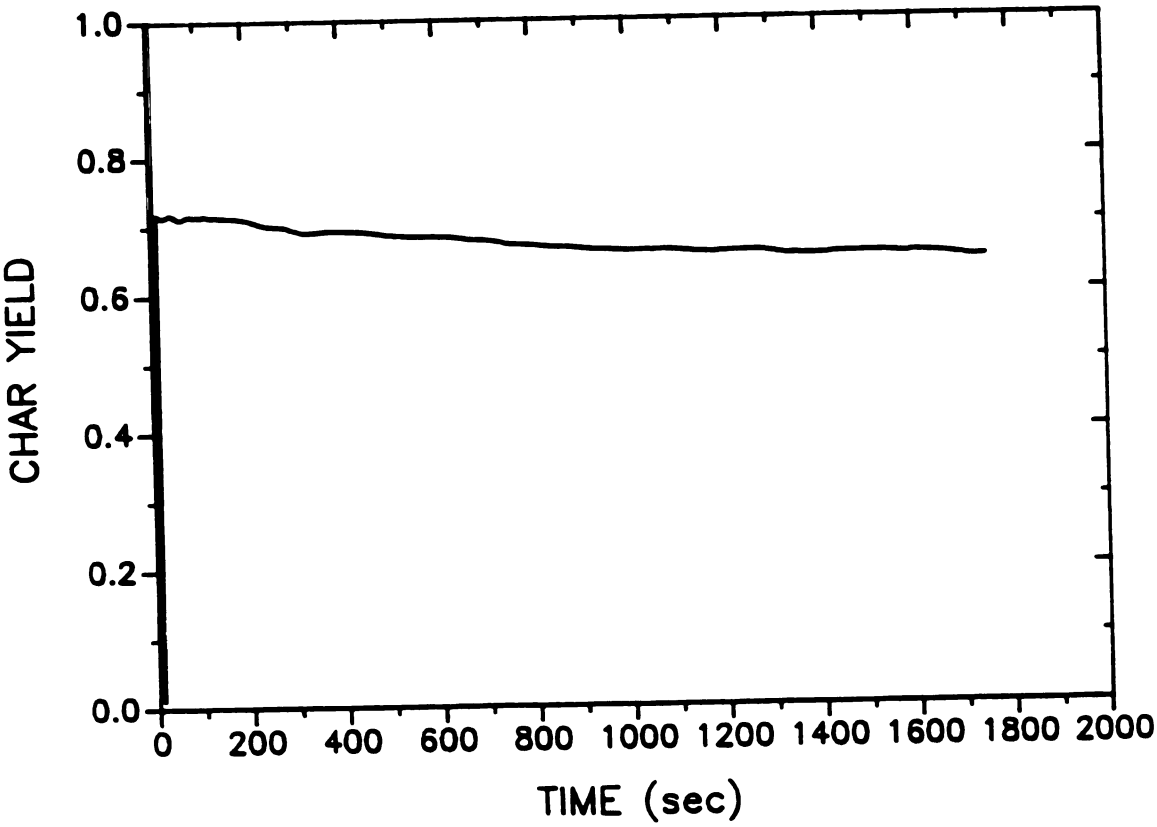

Fig. YCR1A Char yield (gram char/gram wood); EXP. R1A

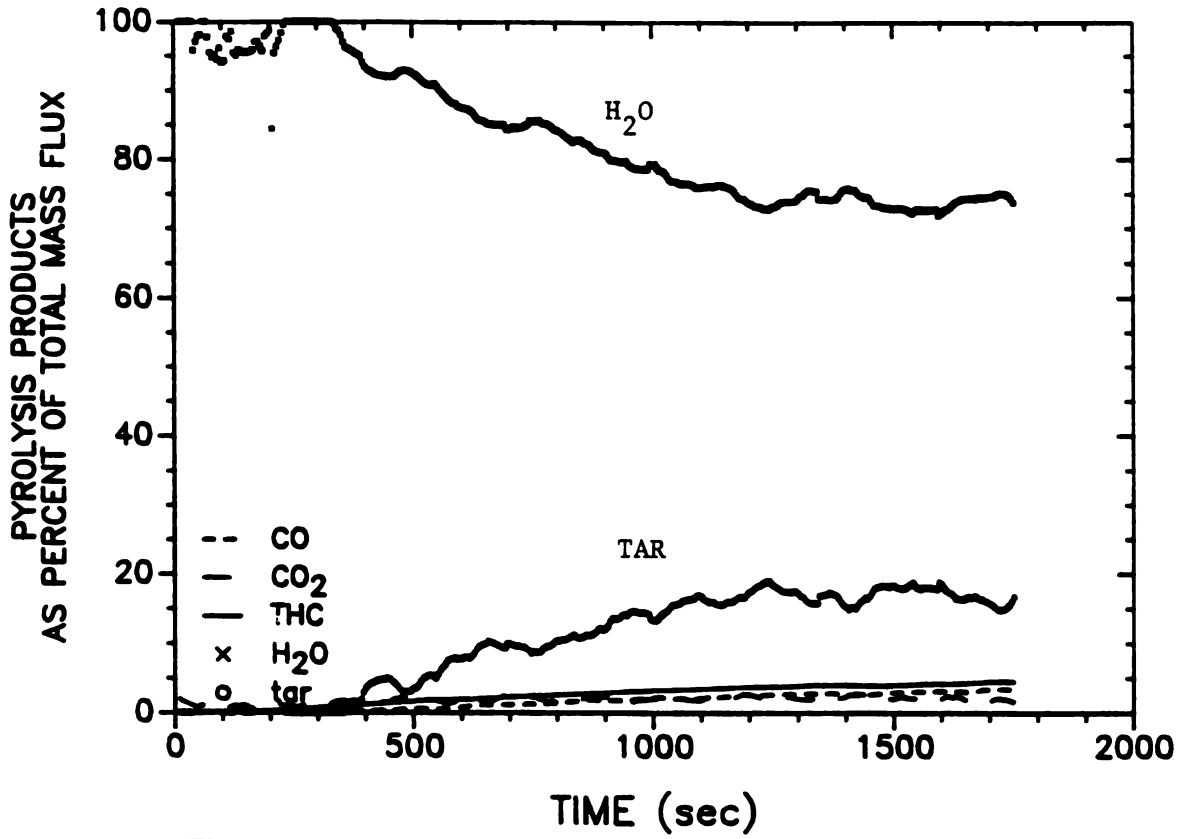

Fig. PSR1A Products of pyrolysis as percent of total mass flux; EXP. R1A

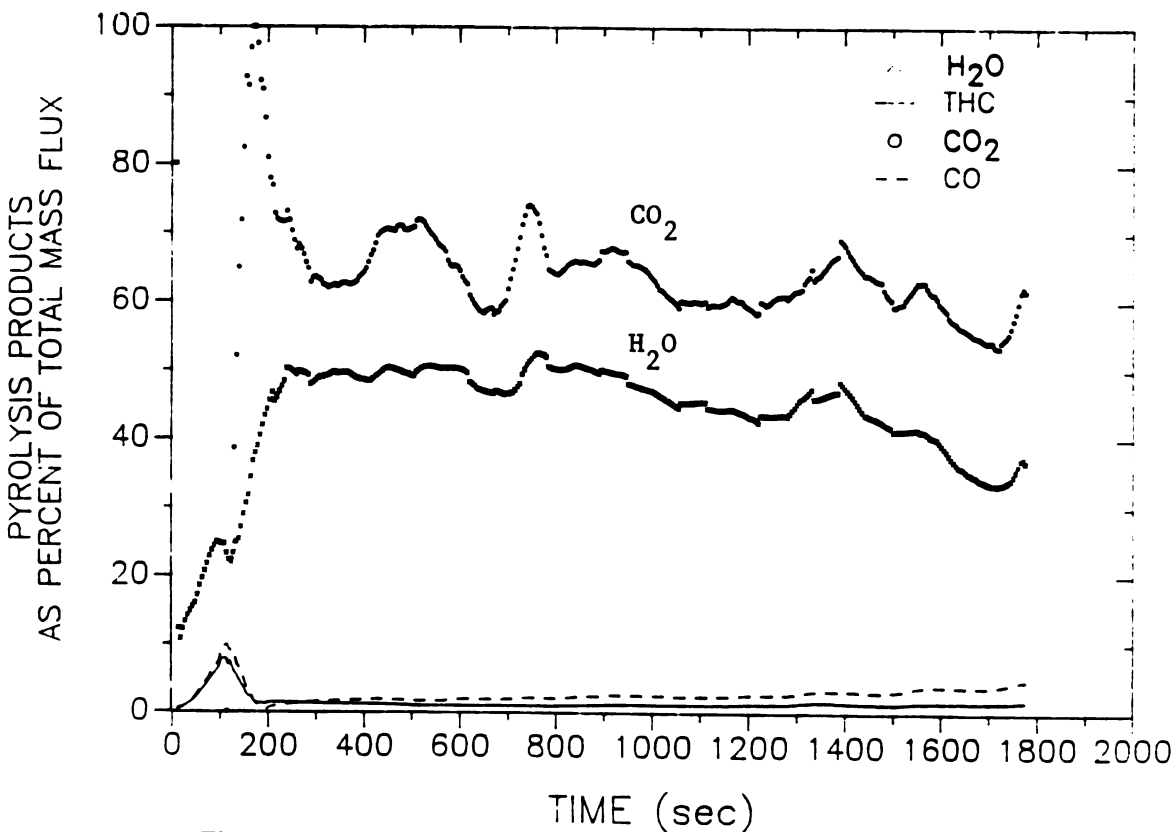

Fig. PSM4A Products of pyrolysis as percent of total mass flux; EXP. M4A

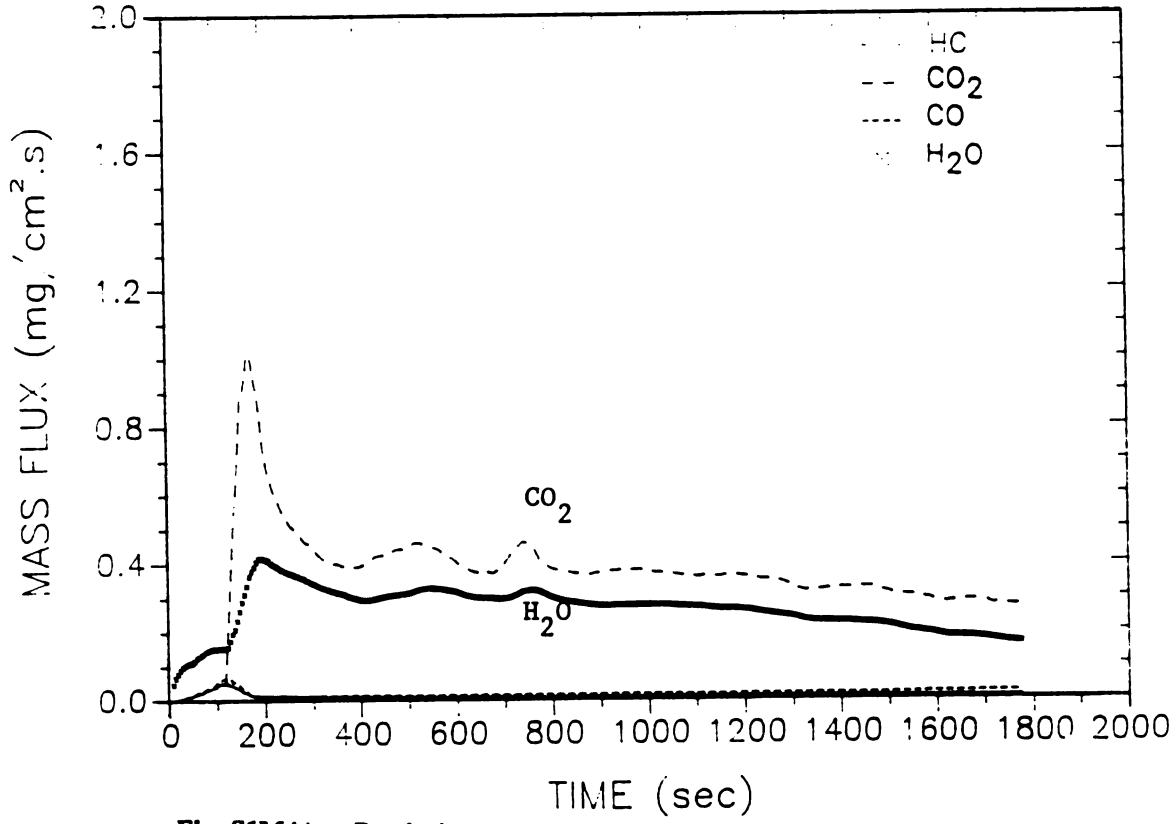

Fig. S1M4A Pyrolysis products (direct measurement); EXP. M4A

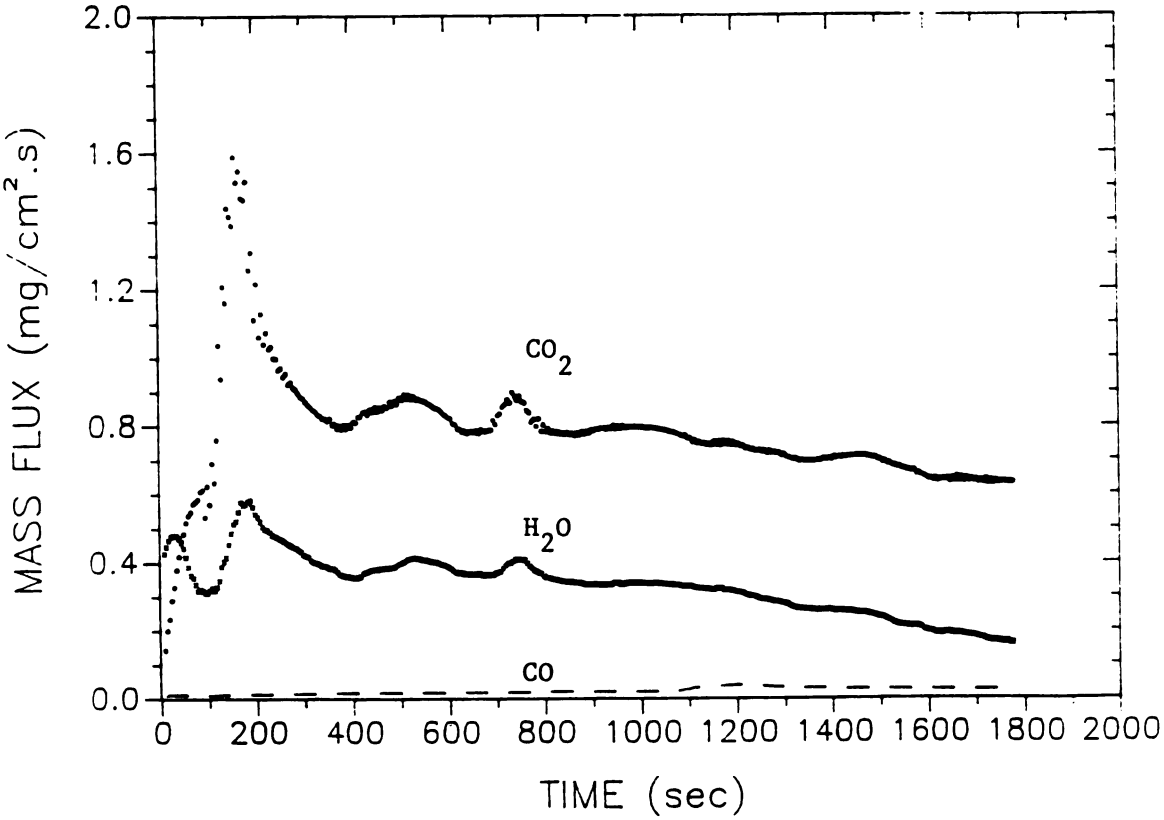

Fig. S2M4A Pyrolysis products (after catalytic combustor); EXP. M4A

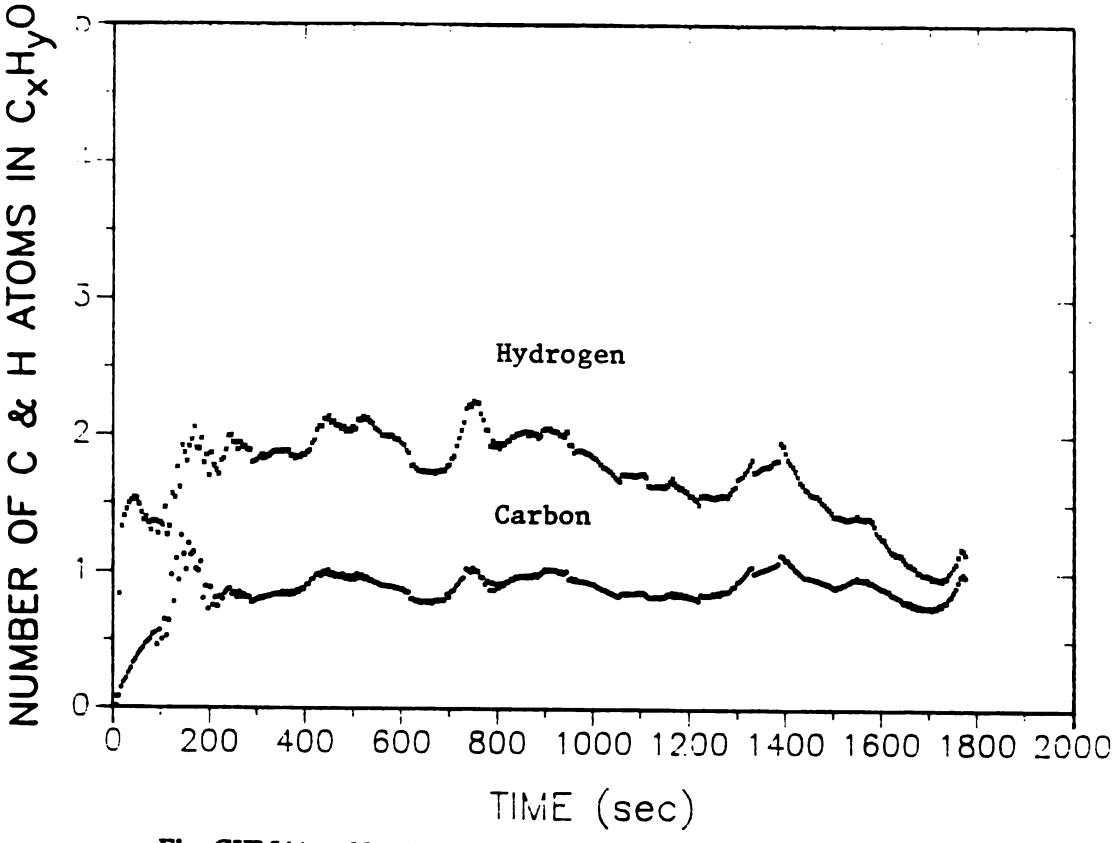

Fig. CHM4A Number of C and H atoms in the products of pyrolysis; EXP. M4A

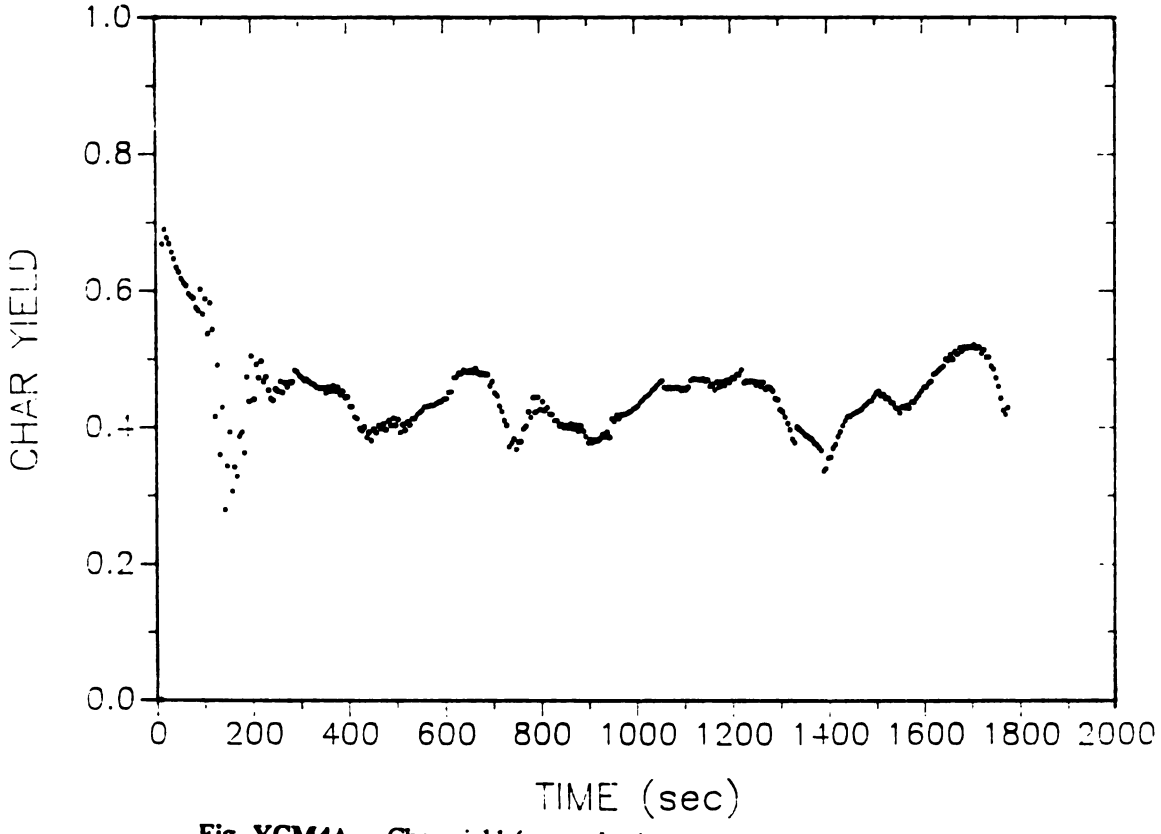

Fig. YCM4A Char yield (gram char/gram wood); EXP. M4A

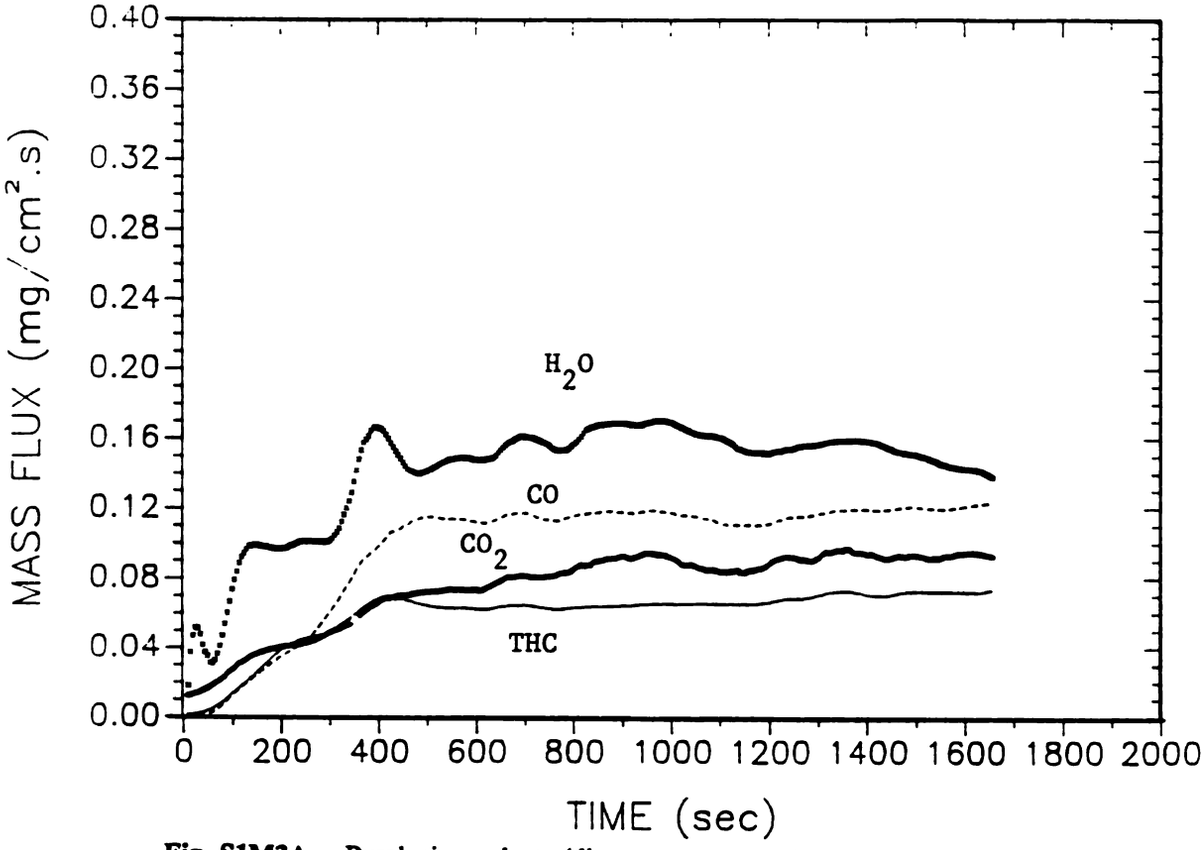

Fig. S1M3A Pyrolysis products (direct measurement); EXP. M3A

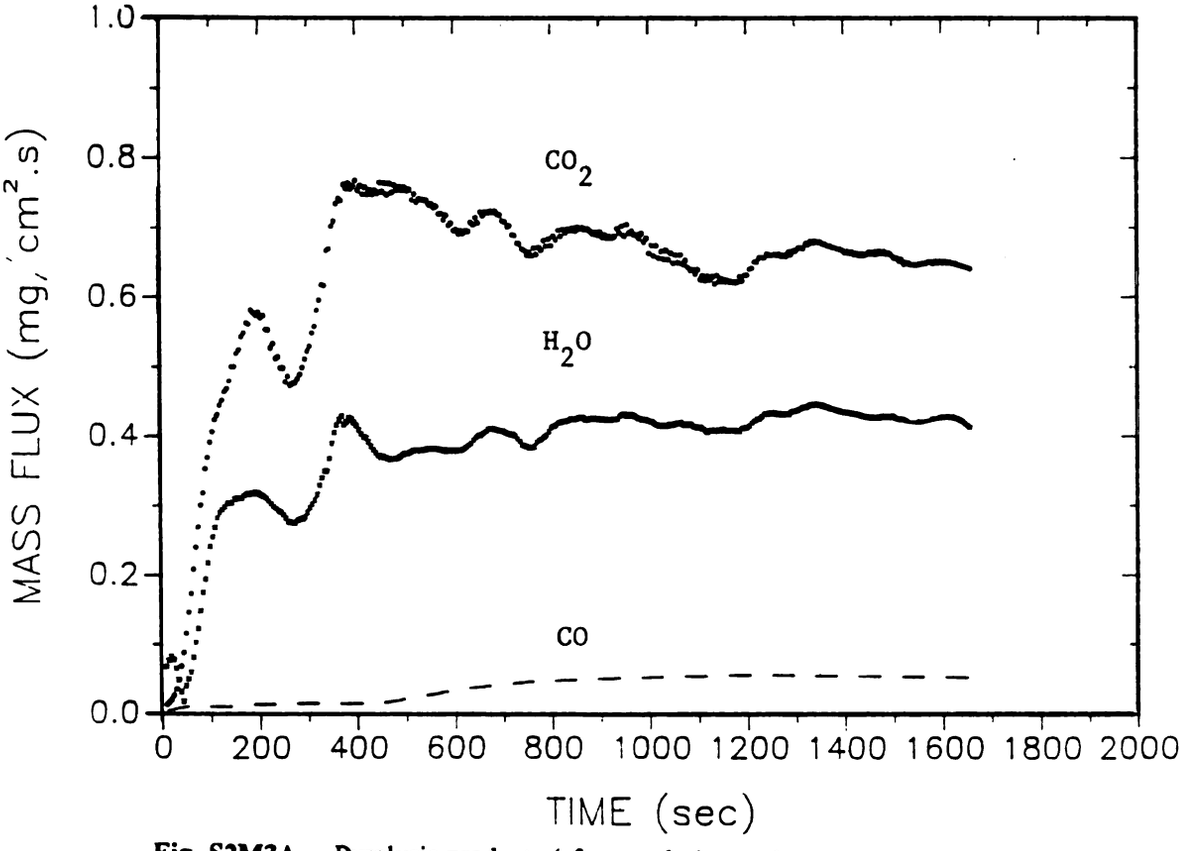

Fig. S2M3A Pyrolysis products (after catalytic combustor); EXP. M3A

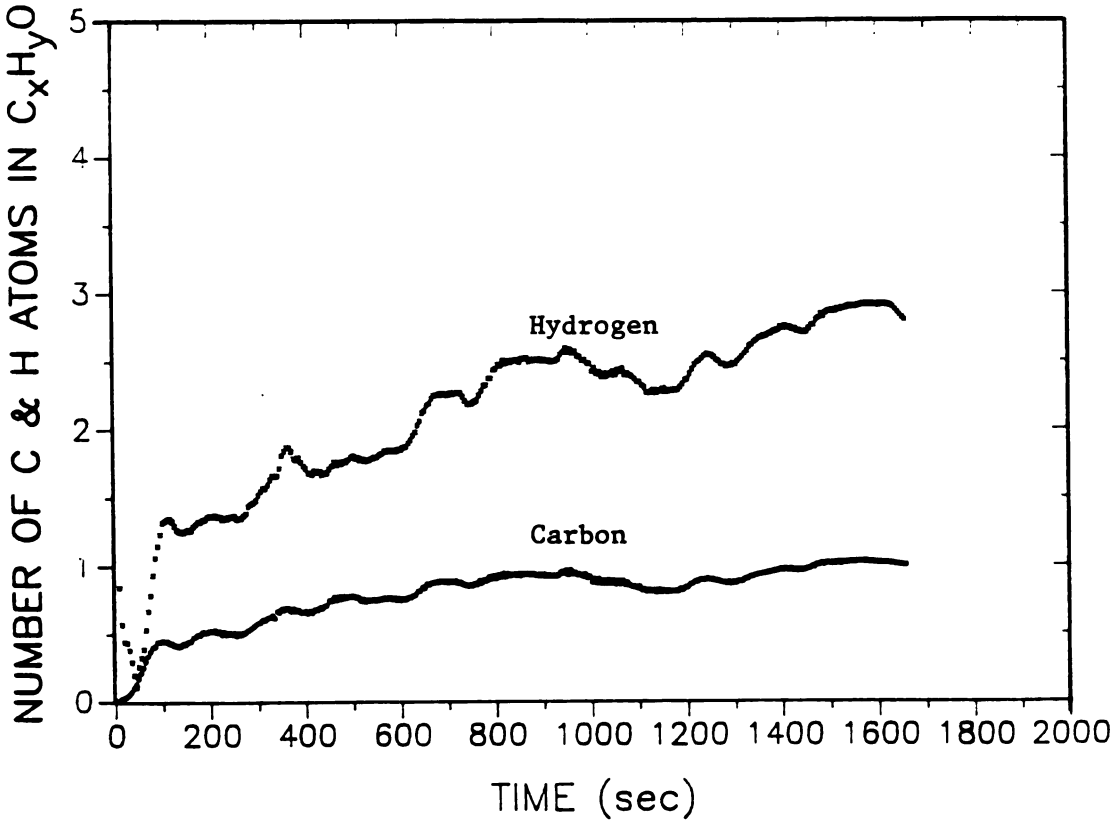

Fig. CHM3A Number of C and H atoms in the products of pyrolysis; EXP. M3A

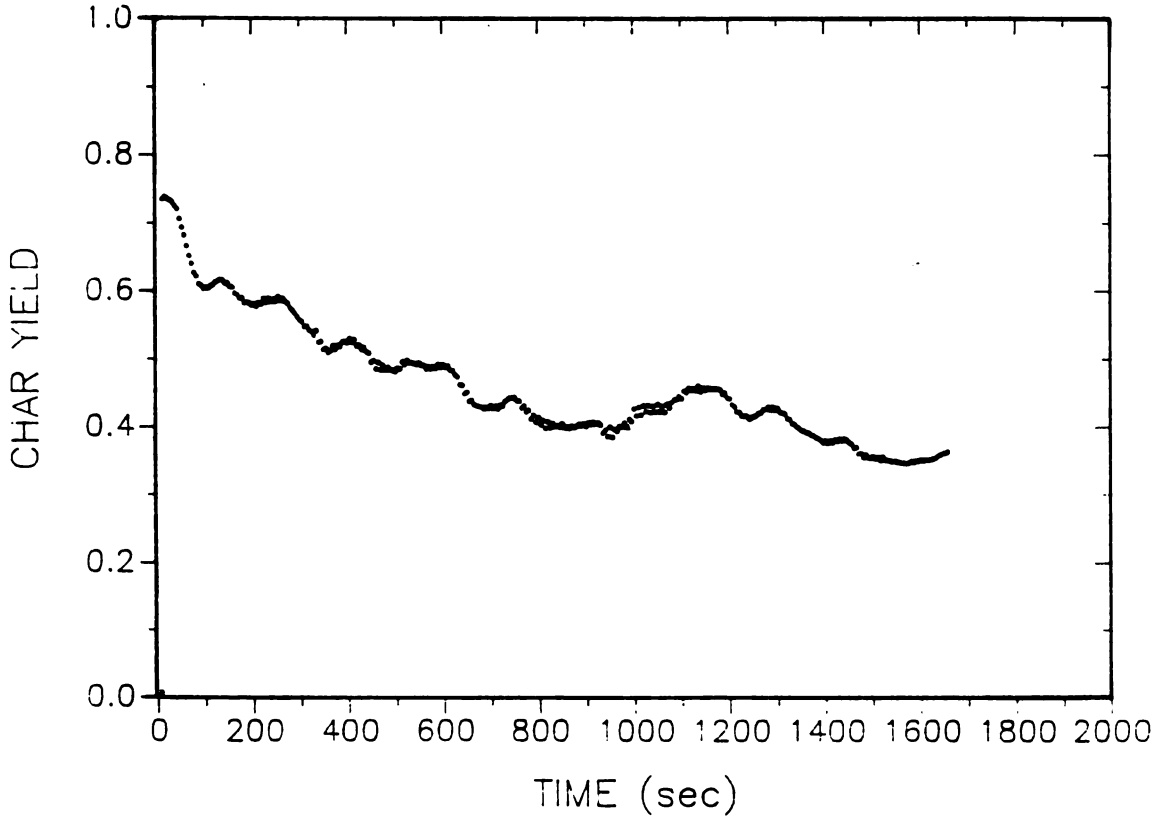

Fig. YCM3A Char yield (gram char/gram wood); EXP. M3A

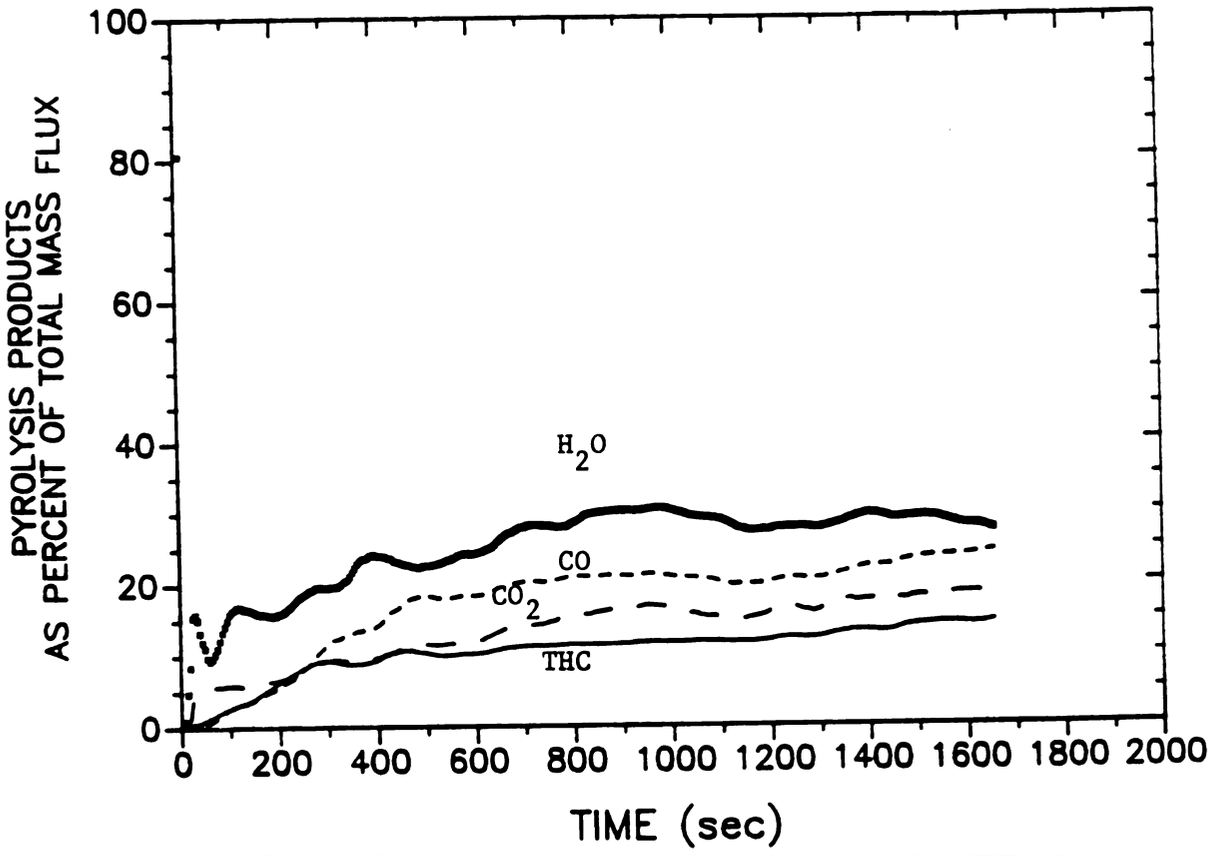

Fig. PSM3A Products of pyrolysis as percent of total mass flux; EXP. M3A

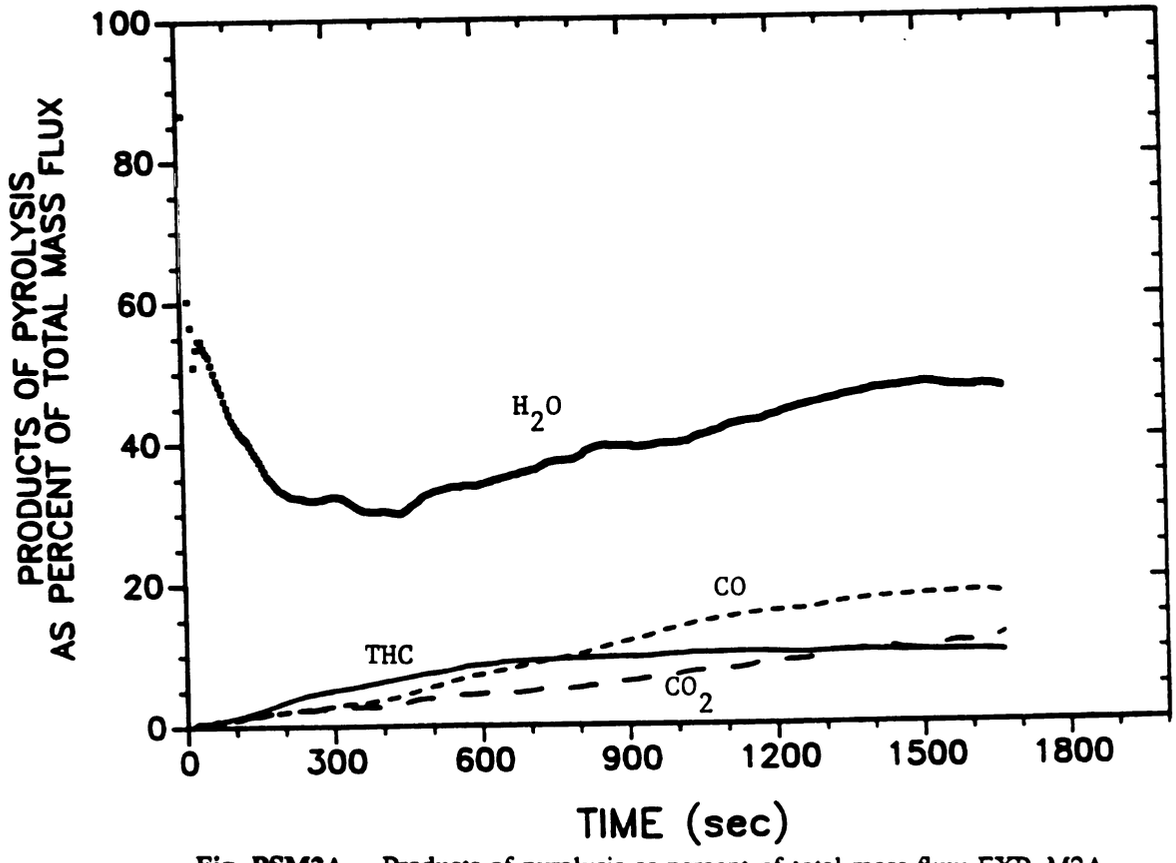

Fig. PSM2A Products of pyrolysis as percent of total mass flux; EXP. M2A

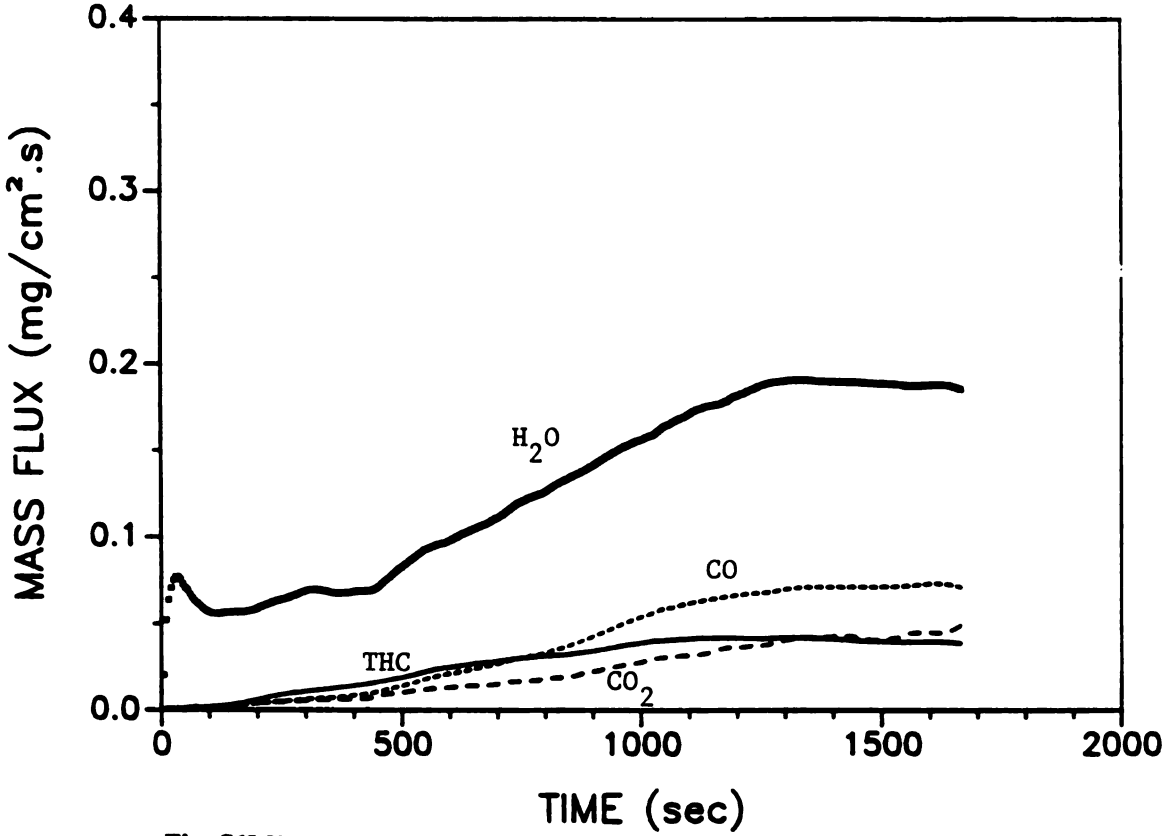

Fig. S1M2A Pyrolysis products (direct measurement); EXP. M2A

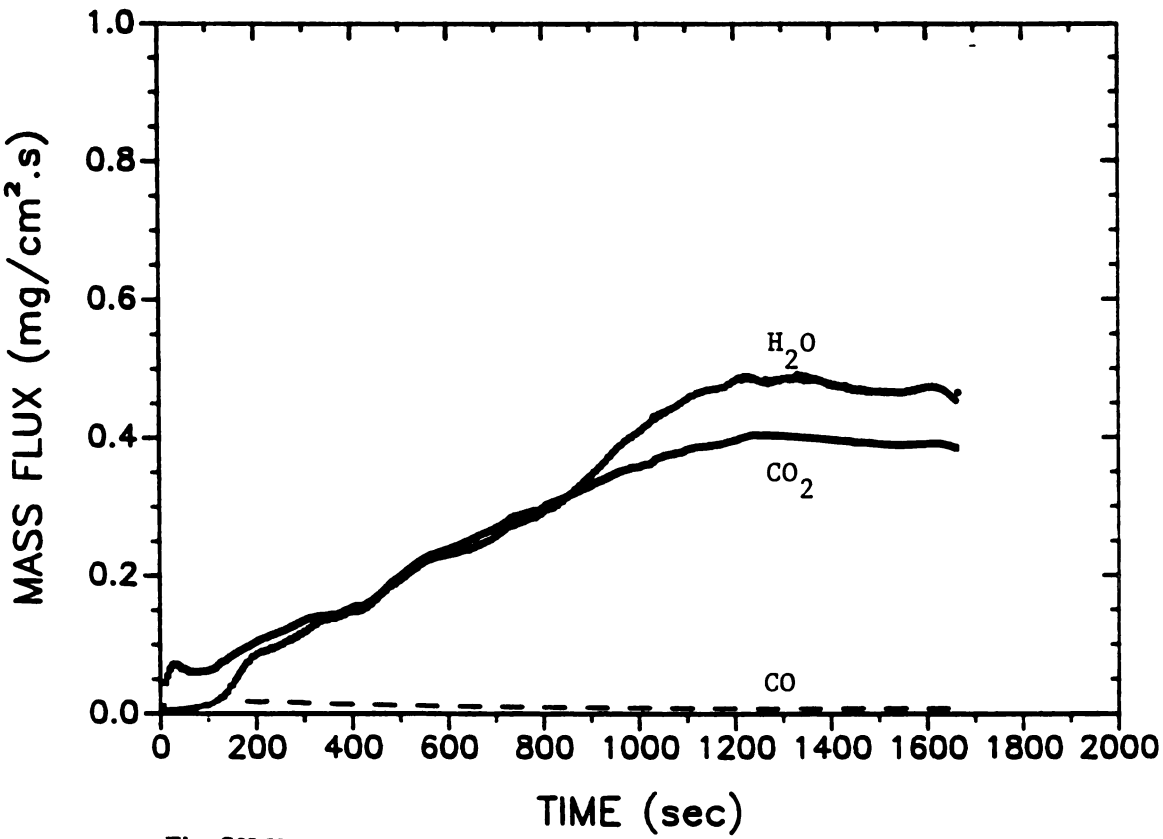

Fig. S2M2A Pyrolysis products (after catalytic combustor); EXP. M2A

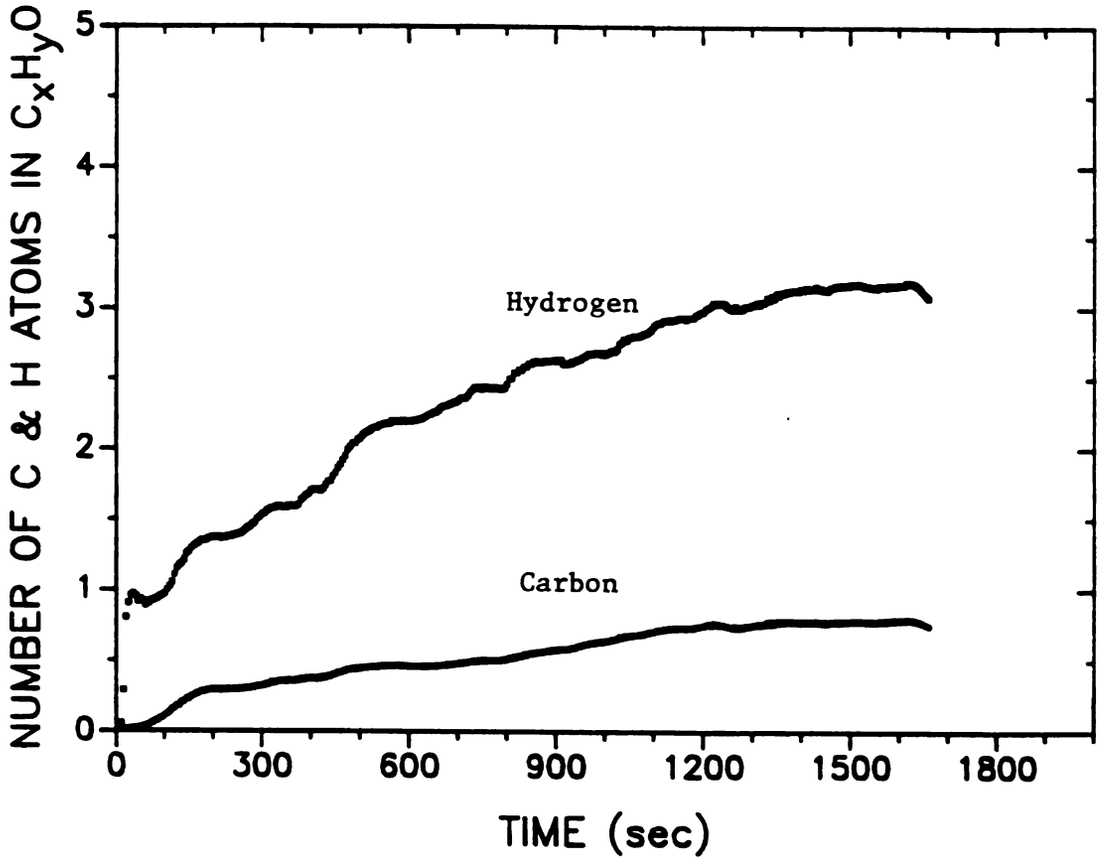

Fig. CHM2A Number of C and H atoms in the products of pyrolysis; EXP. M2A

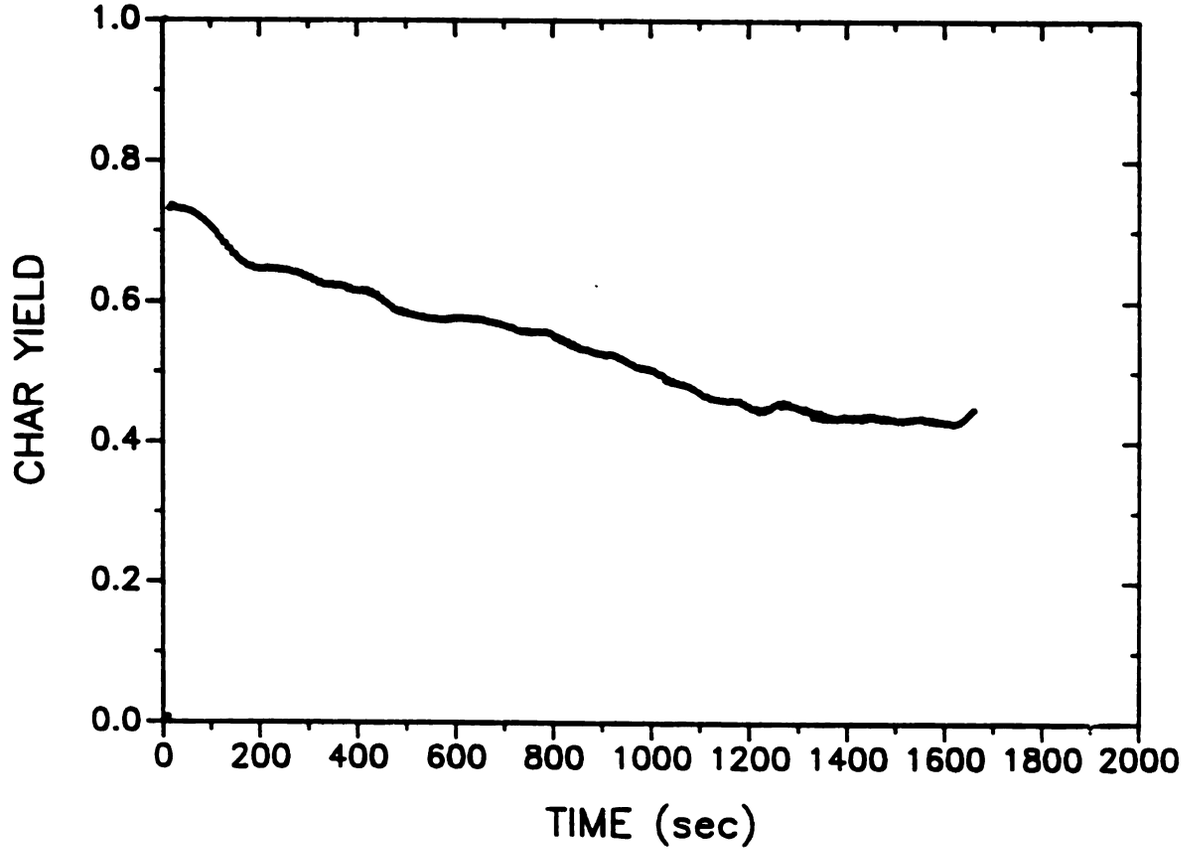

Fig. YCM2A Char yield (gram char/gram wood); EXP. M2A

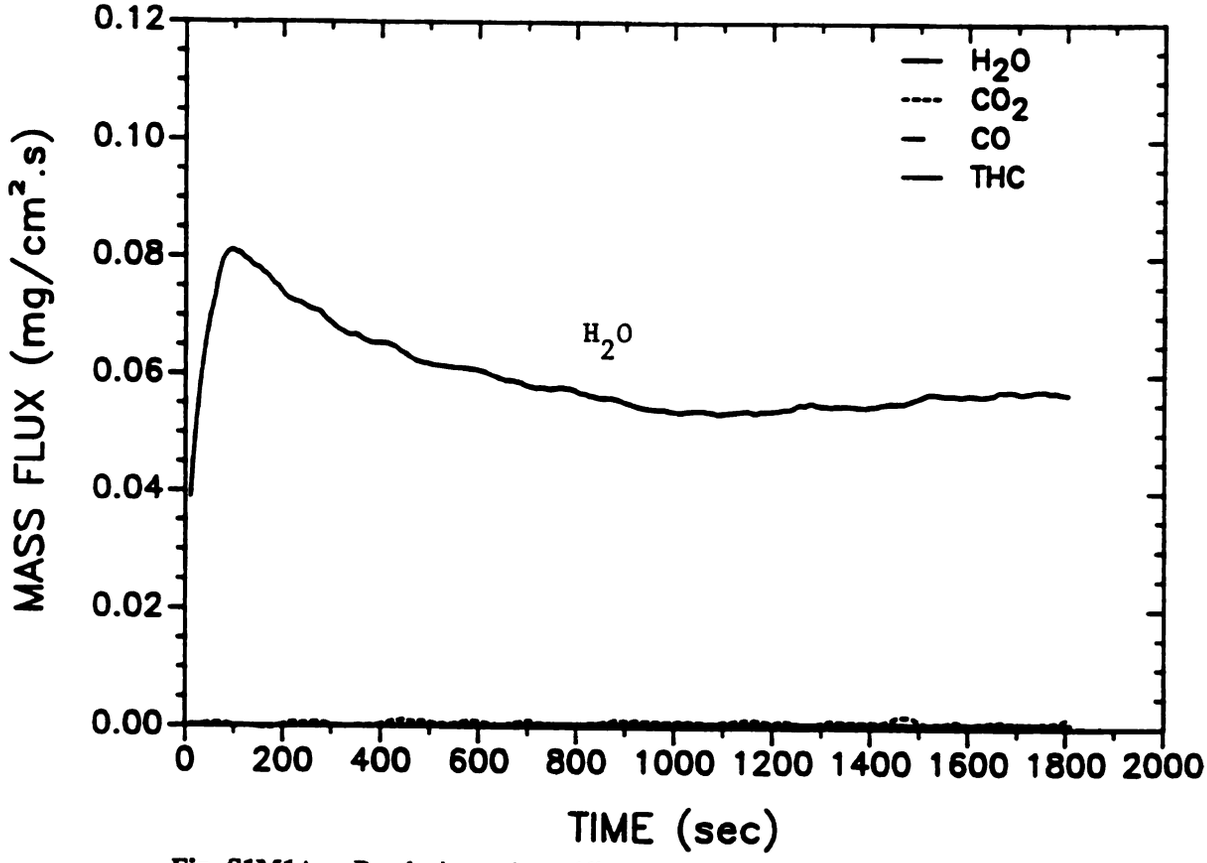

Fig. S1M1A Pyrolysis products (direct measurement); EXP. M1A

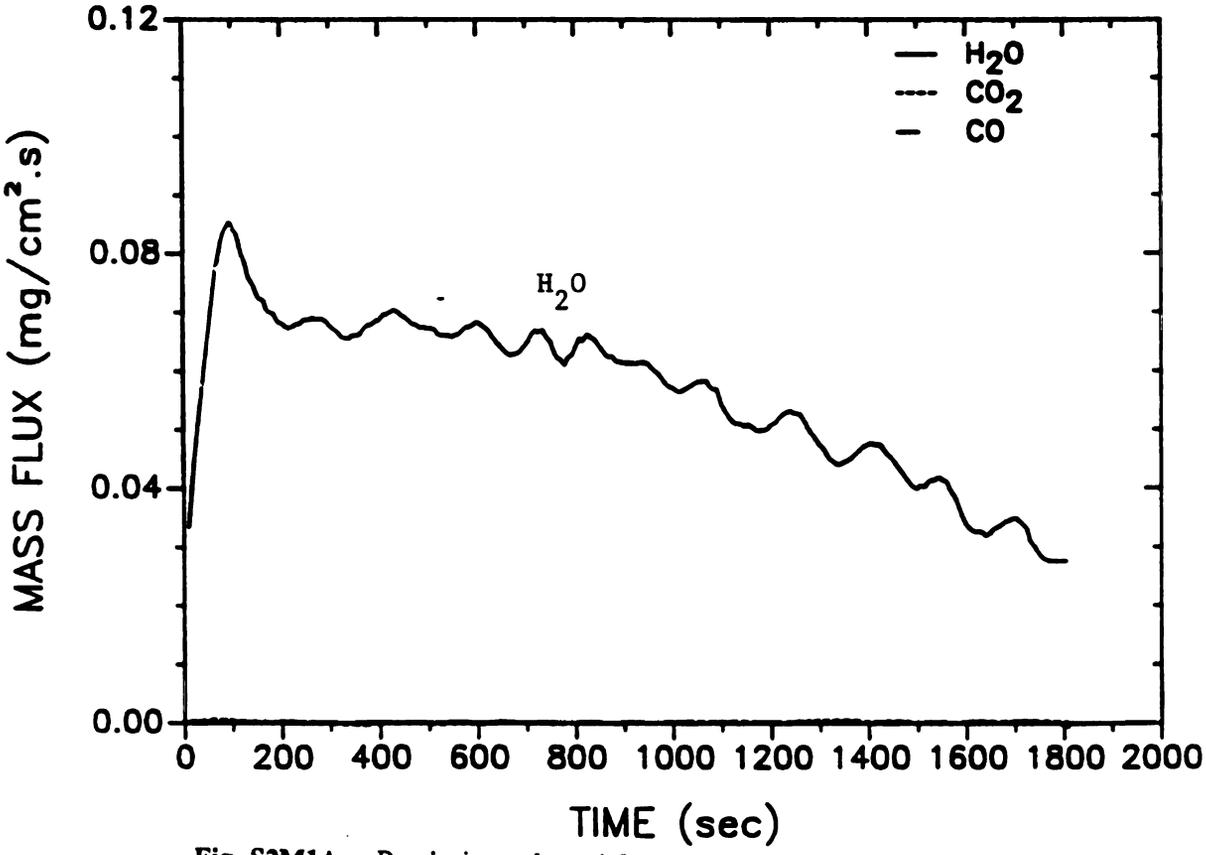

Fig. S2M1A Pyrolysis products (after catalytic combustor); EXP. M1A

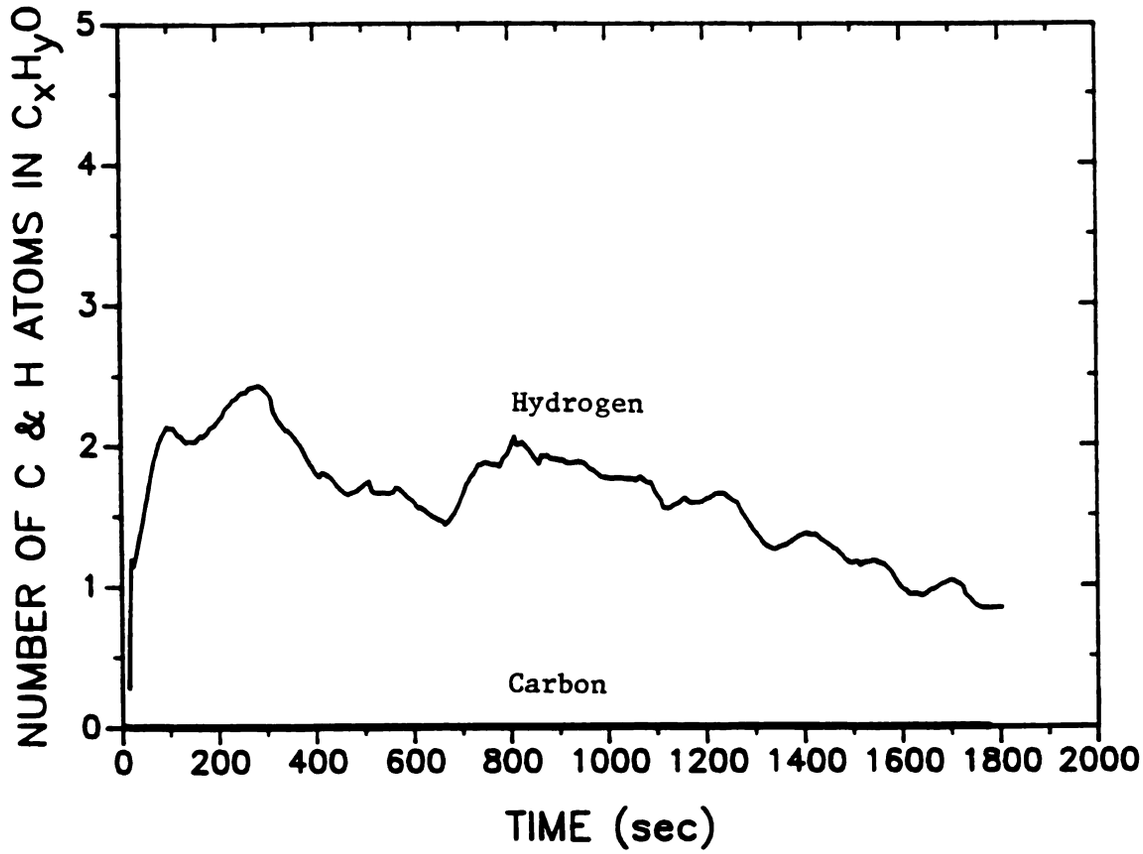

Fig. CHM1A Number of C and H atoms in the products of pyrolysis; EXP. M1A

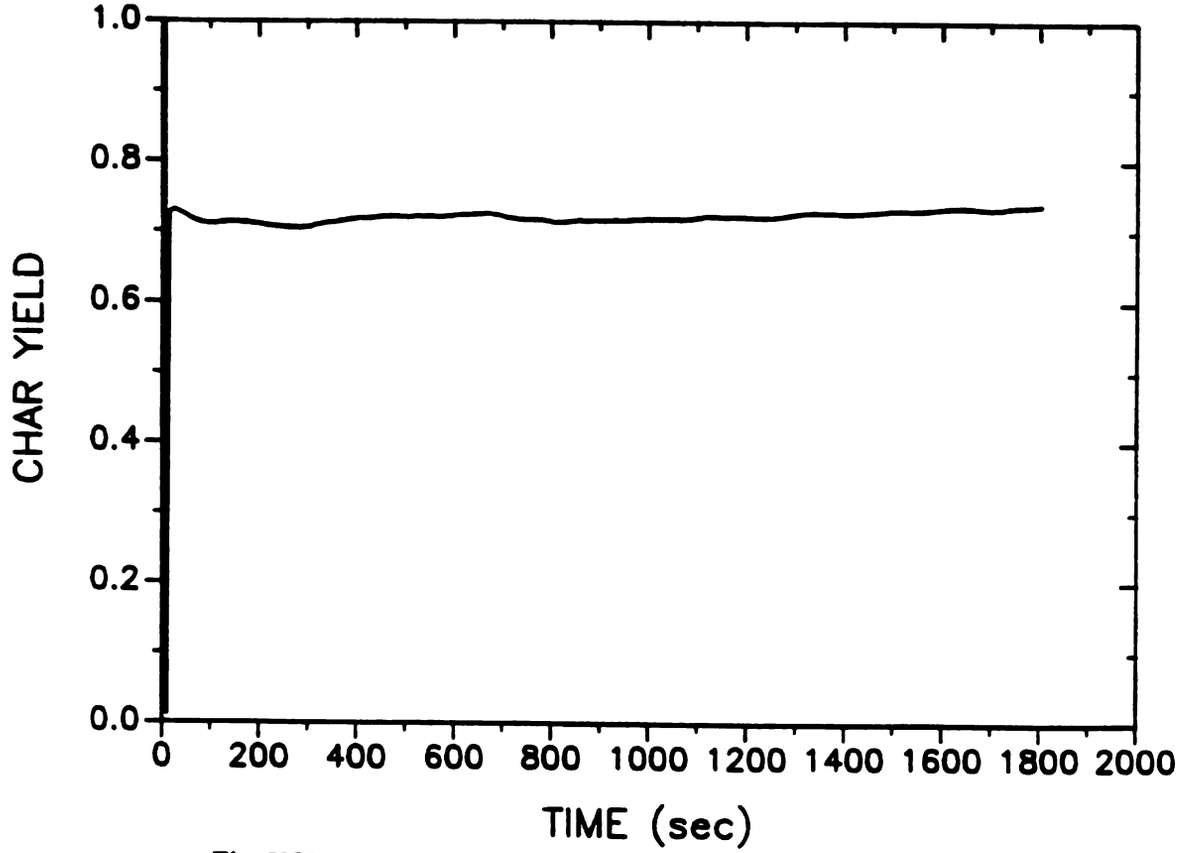

Fig. YCM1A Char yield (gram char/gram wood); EXP. M1A

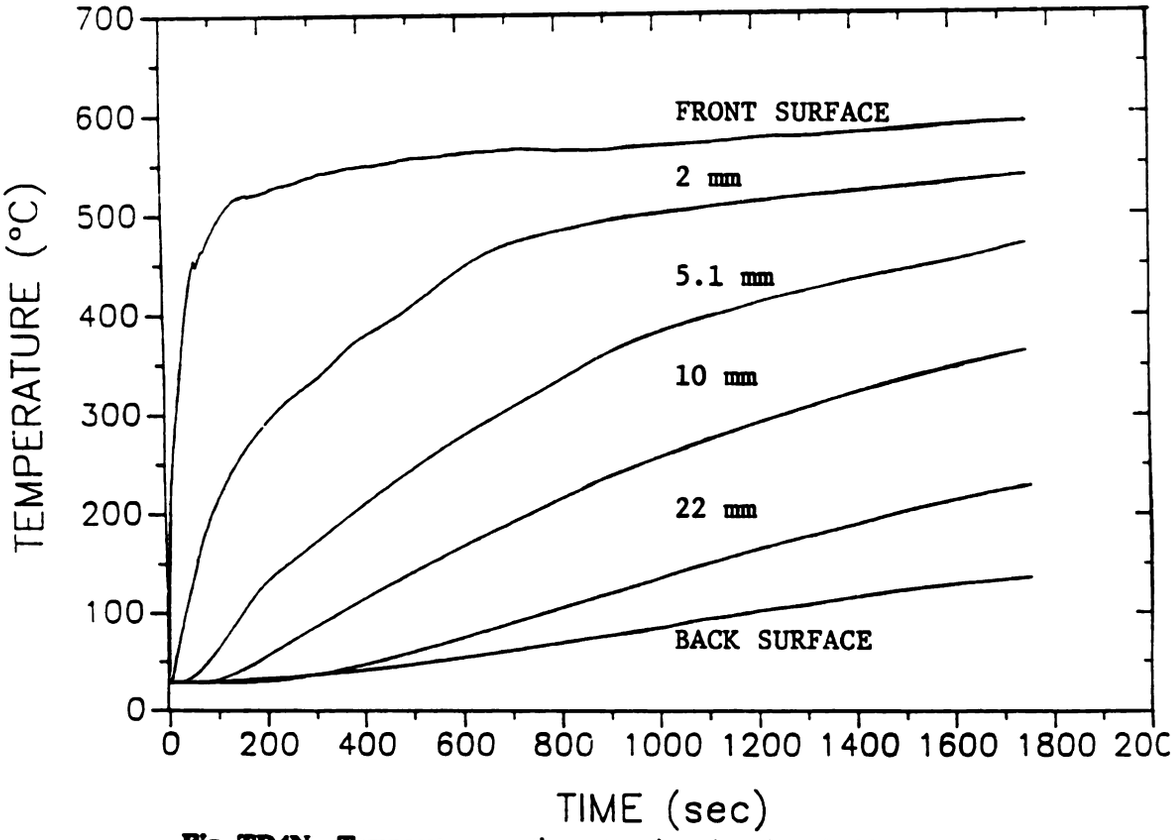

Fig. TD4N Temperature vs. time at various locations inside the wood; EXP. D4N

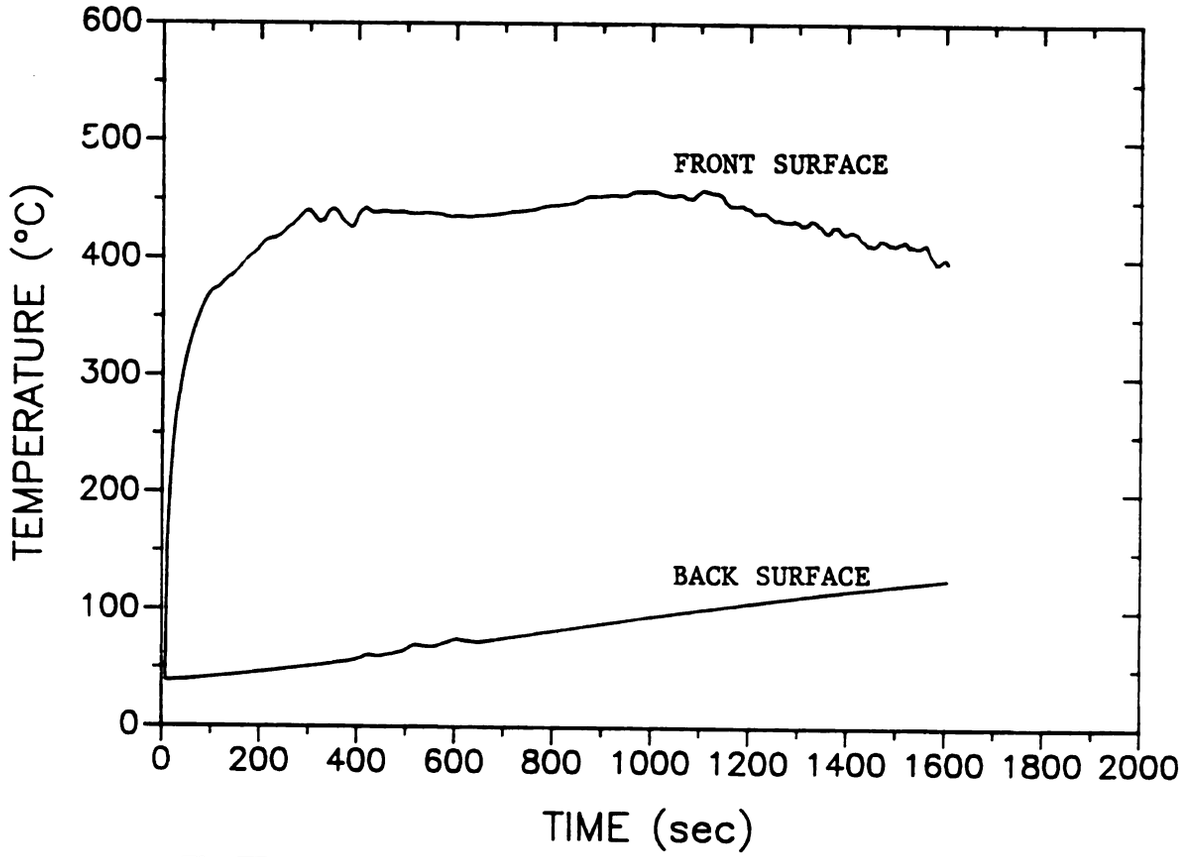

Fig. TD2N Temperature vs. time at various locations inside the the wood; EXP. D2N

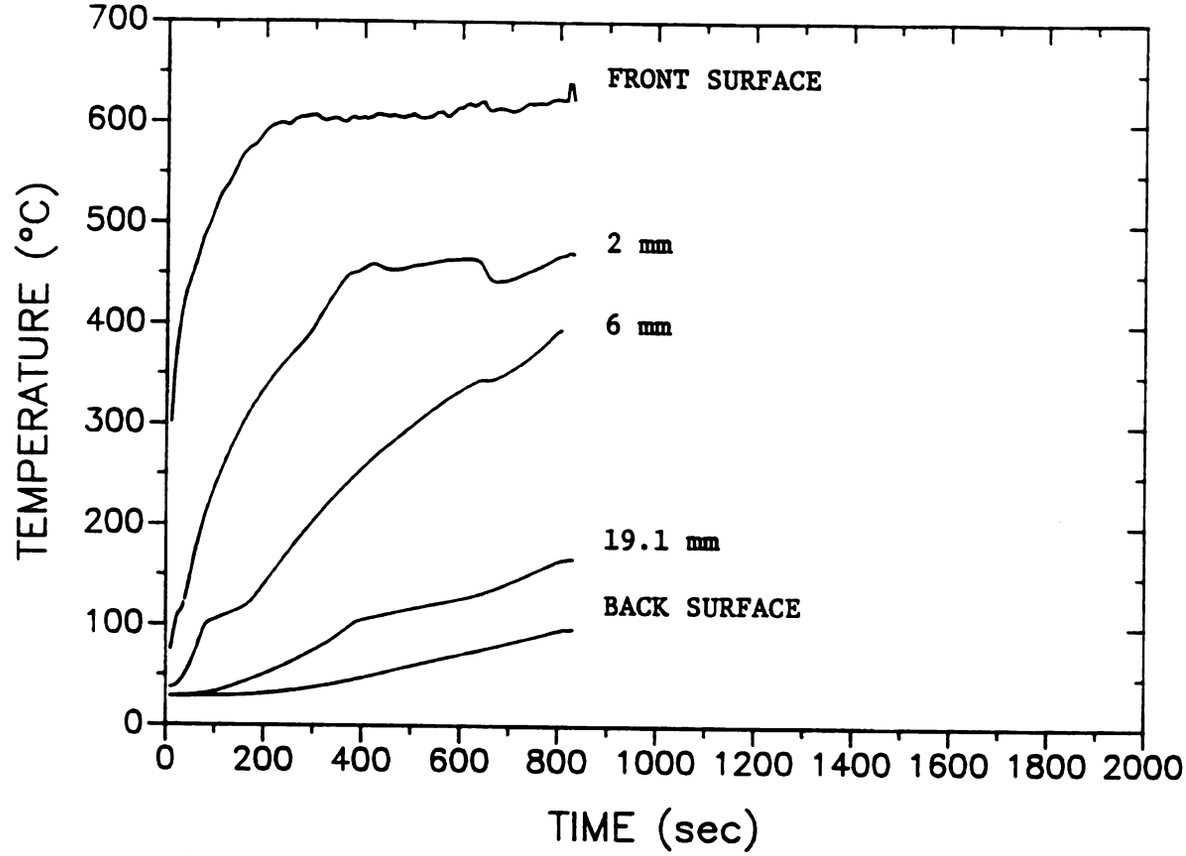

Fig. TR4N Temperature vs. time at various locations inside the wood; **EXP. R4N**

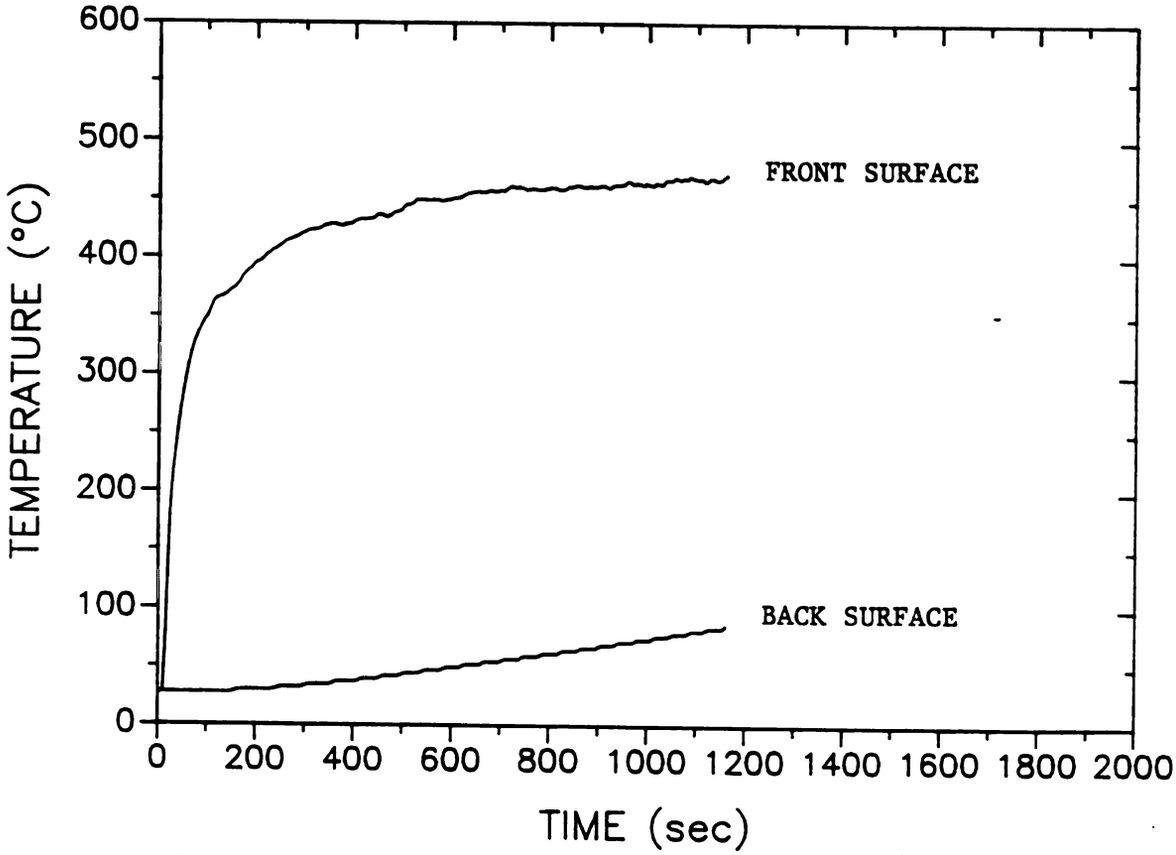

Fig. TR2N Temperature vs. time at various locations inside the wood; **EXP. R2N**

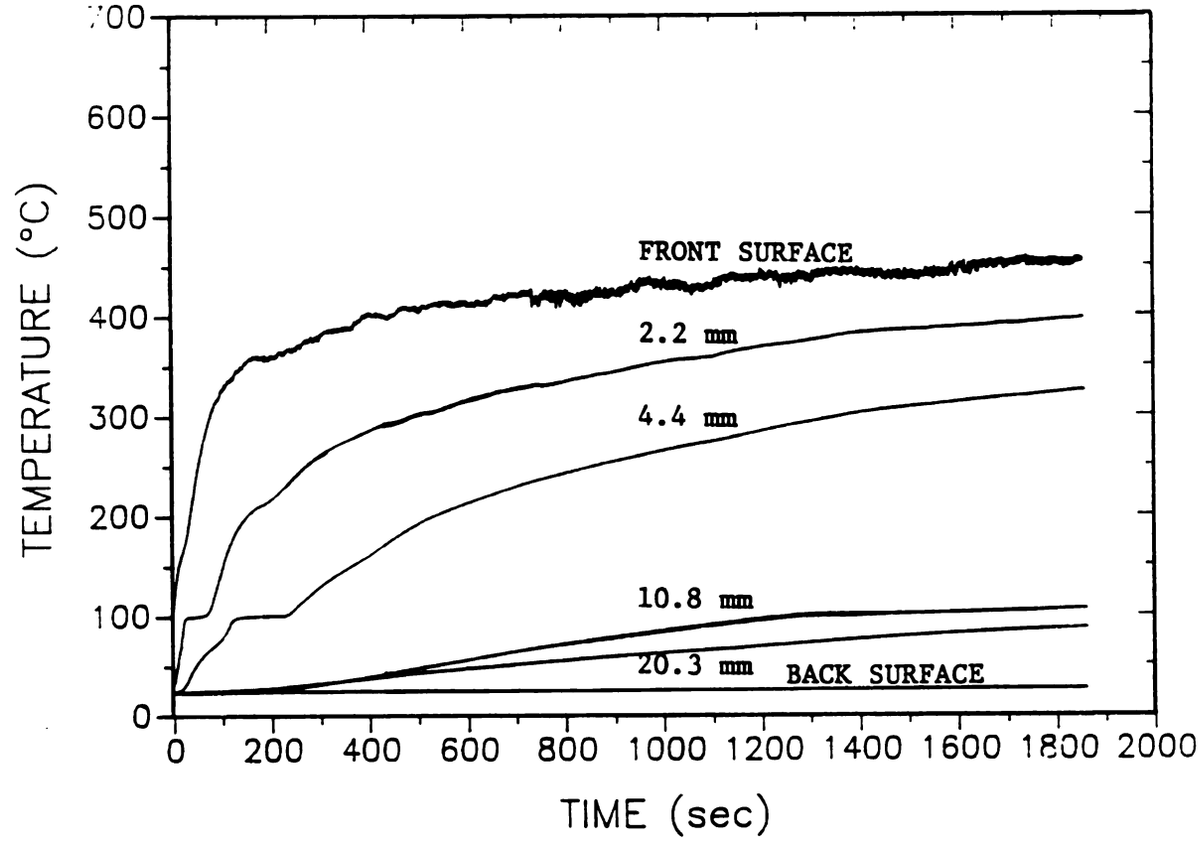

Fig. TM2N Temperature vs. time at various locations inside the wood; **EXP. M2N**

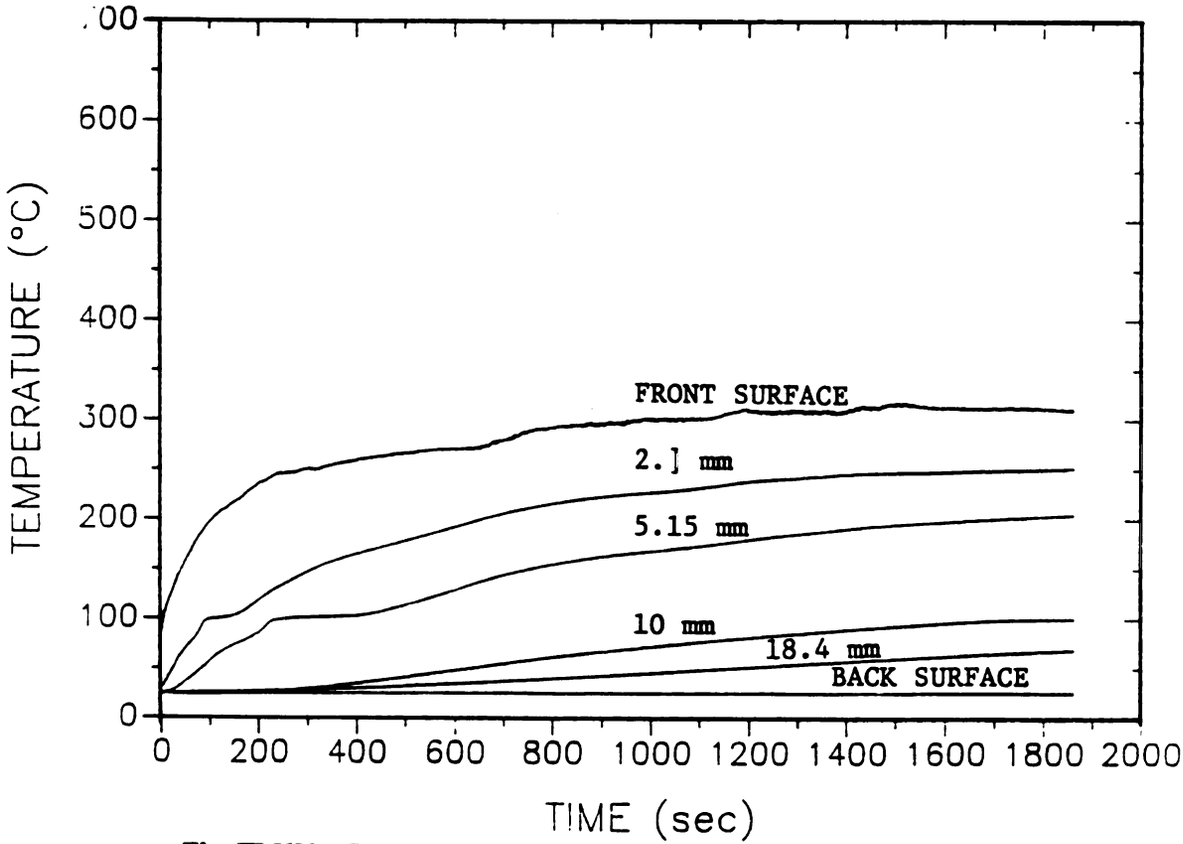

Fig. TM1N Temperature vs. time at various locations inside the wood; **EXP. M1N**

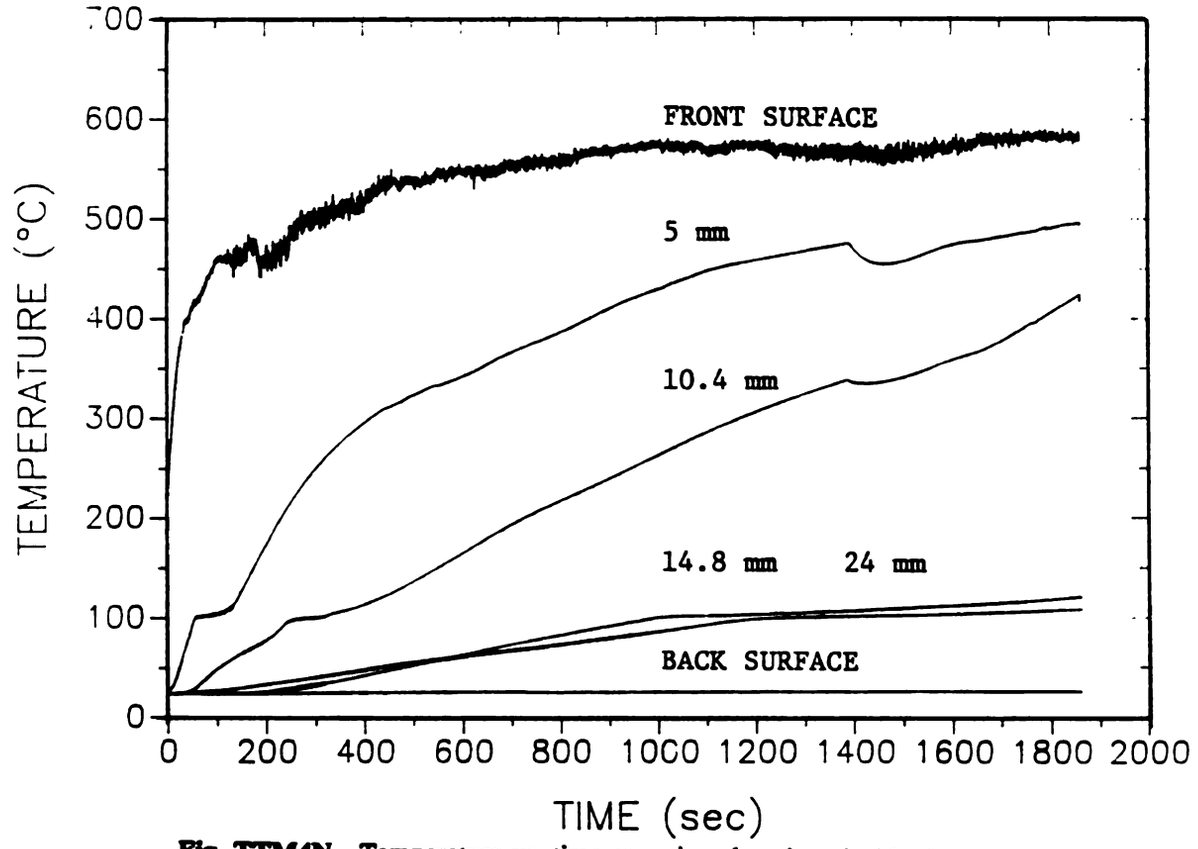

Fig. TTM4N Temperature vs. time at various locations inside the wood; EXP. T M4N

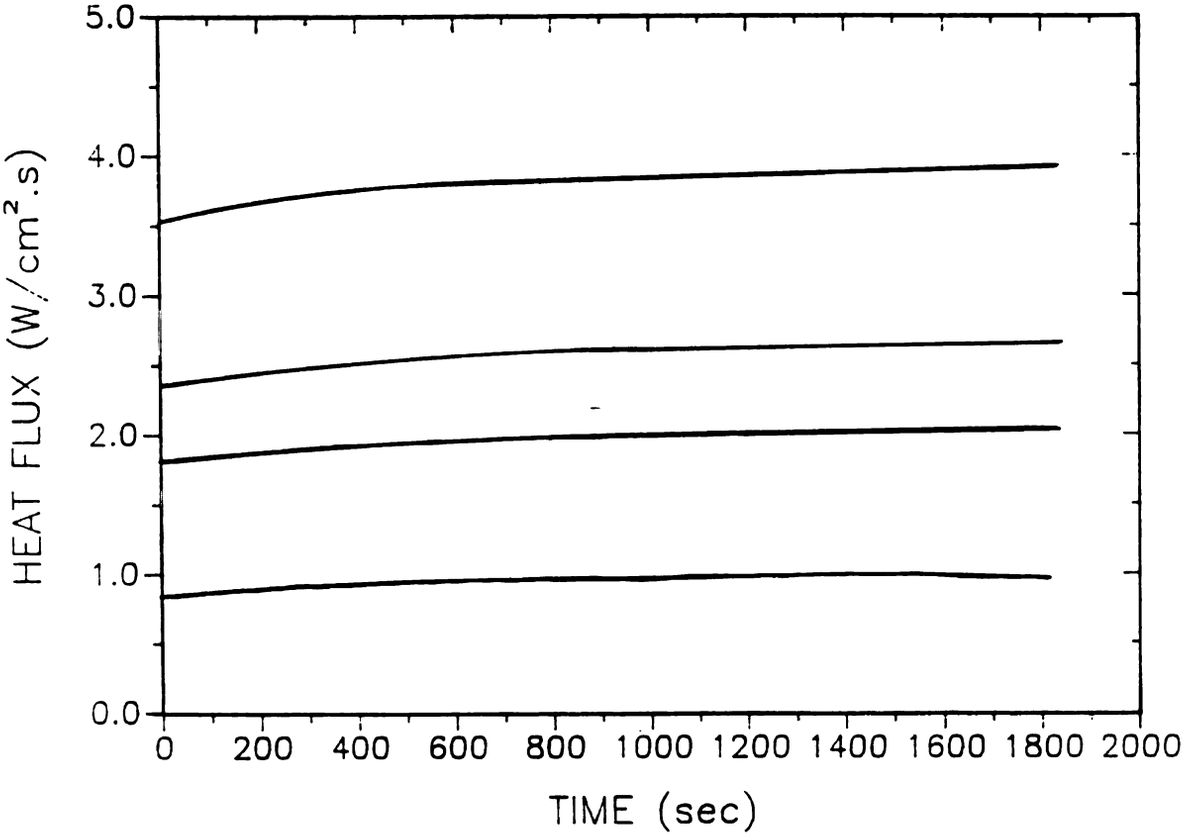

Fig. THFMN External heat fluxes for experiments on 17% moist wood.

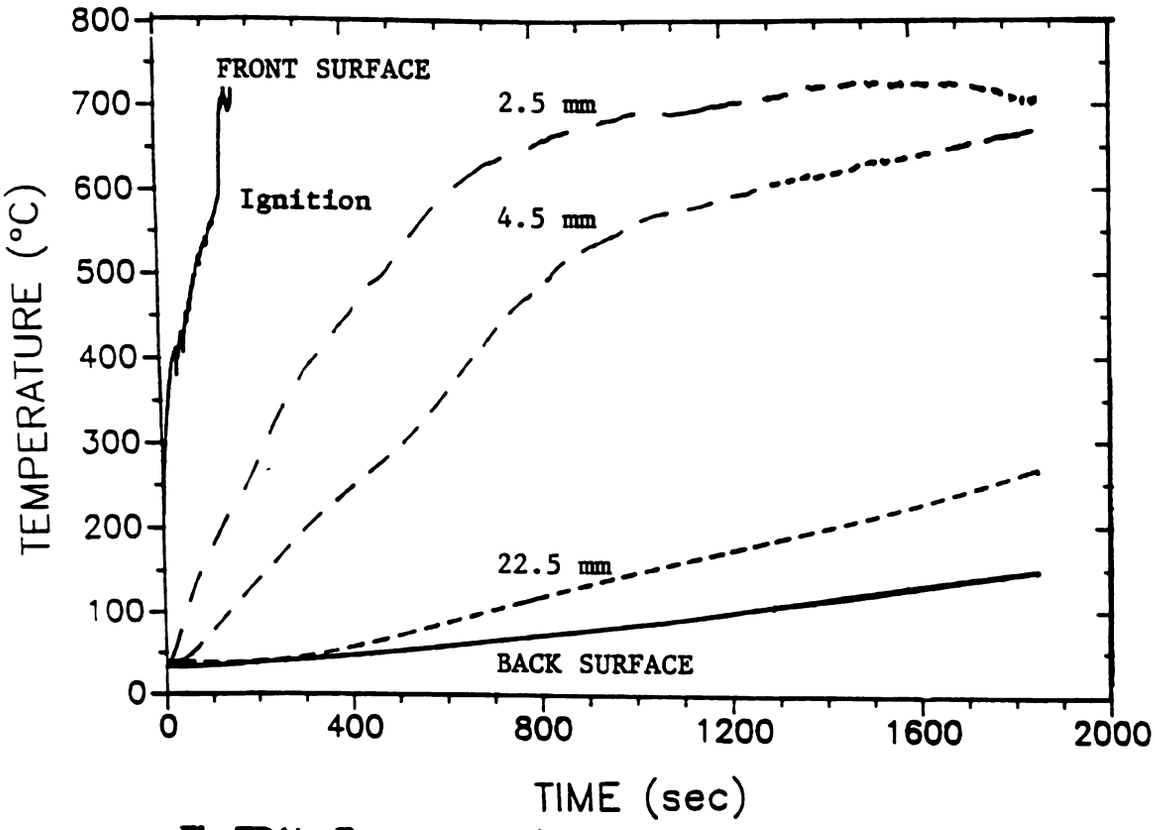

Fig. TD4A Temperature vs. time at various locations inside the wood; **EXP. D4A**

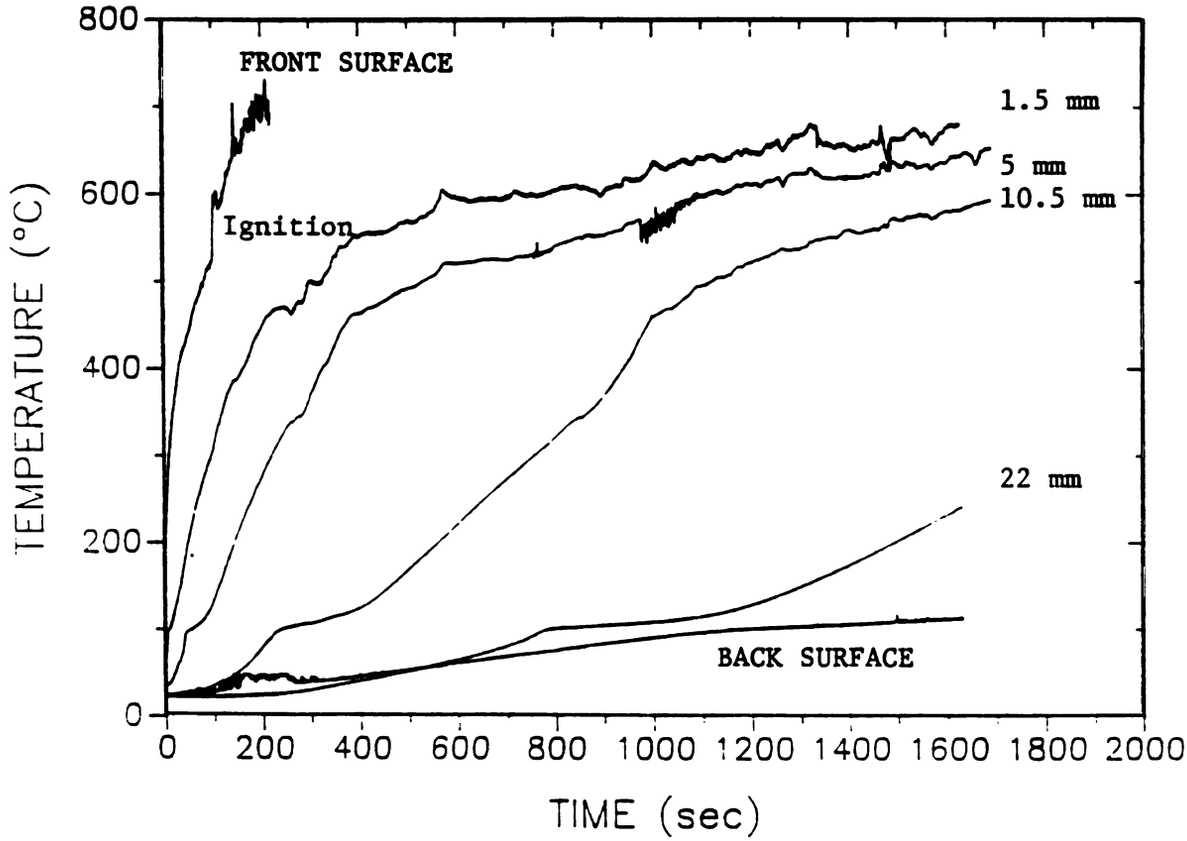

Fig. TR4A Temperature vs. time at various locations inside the wood; **EXP. R4A**

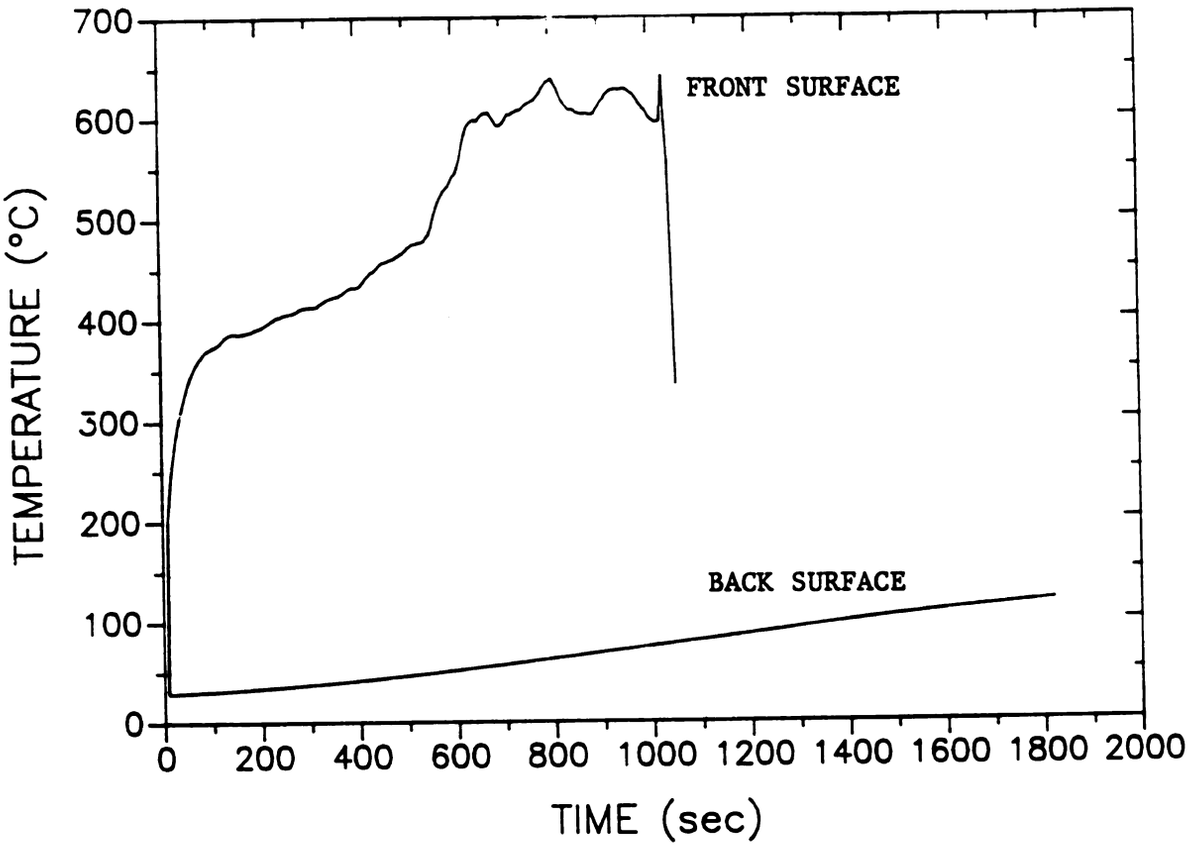

Fig. TD2A Temperature vs. time at various locations inside the wood; EXP. D2A

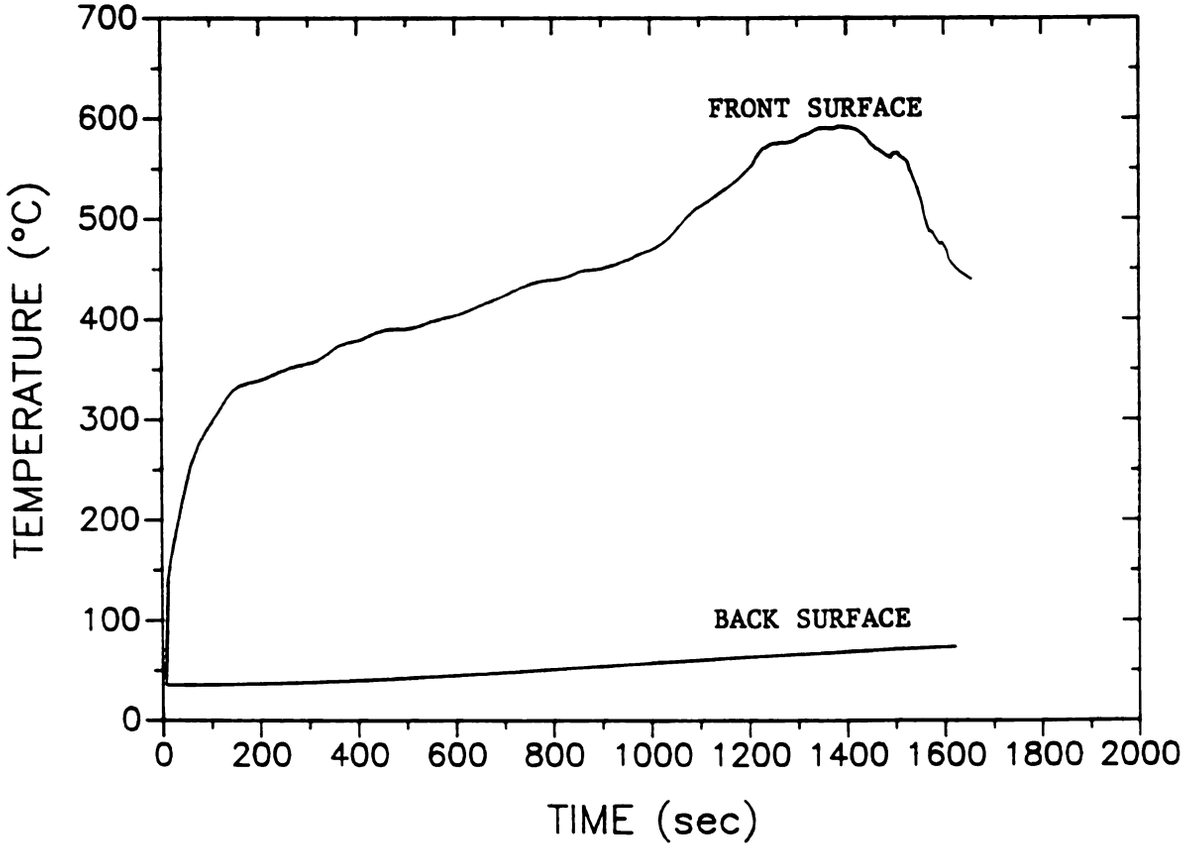

Fig. TM2A Temperature vs. time at various locations inside the wood; EXP. M2A

LIST OF REFERENCES

LIST OF REFERENCES

Atreya. A., "Pyrolysis, Ignition and Fire Spread on Horizontal Surface of Wood," *Ph.D. Thesis*, Harvard University, Cambridge, MA. (1983). Also published as a National Bureau of Standards report, NBS-GCR-83-449, March 1984.

Bamford, C.H. Crank, J., and Malans D.H., "The Combustion of Wood Part I," *Proc. Cambridge Phil. Soci.*, **42**, pp. 166-182 (1945).

Bradbury, A.G.W., and Shafizadeh, F., "Role of Oxygen Chemisorption in Low-Temperature Ignition of Cellulose," FI Combustion and Flame, **37**, pp. 85-89, (1980).

Broido, A., and Nelson, M.A., "Char Yield on Pyrolysis of Cellulose," *Combustion and Flame*, **24**, pp.263-268, (1975).

Carnahan, B., Luther, H.A., Wilkes, J.O., "Applied Numerical Methods," Wiley Publishing Co. (1969).

Carslaw, H.S., and Jaeger, J.C., "Conduction of Heat in Solids," 2nd edition, Oxford University Press, 1959.

Chan, W.C.R., "Analysis of Chemical and Physical Processes During The Pyrolysis of Large Biomass Pellets," *Ph.D. Thesis*, U of Washington, (1983).

Chan, W.C.R., Kelbon, M., and Krieger, B.B., "Products Formation in the Pyrolysis of Lrage Wood Particles," Preprint. To be published in *Fundamentals of Thermochemical Biomass Conversion*, (1984).

Chan, W.C.R., and Kreiger, B.B., "Modeling of Physical Processes of a Large Biomass Pellets with Experimental Verification, *ASC Fuel Div.*, Preprint, (1984).

Croce, P.A., *Combustion Science and Technology*, **14**, pp 221-228, (1975).

Cullis, C.F., Hirsciller, R.P., Townsend, R.P., and Visanuvimol, v., "The Pyrolysis of Cellulose under Conditions of Rapid Heating," *Combustion and Flame*, **49**, pp. 235-248, (1983).

Delichatsios, M.A., and de Ris, J. (1983), "An Analytical Model for the Pyrolysis of Charring Materials," Fall Technical Meeting, Eastern Section, *The Combustion Institute*, p.68, (1983).

Ehrlich, L.W., "A numerical Method of Solving a Heat Flow Problem With Moving Boundries," *JACM*, **5(2)**, pp. 161-176, (1958).

Eckert, E.R.G., and Drake, R.M. "Analysis of Heat and Mass Transfer," McGraw-Hill Publishers, New-York, (1972).

Goos, A.W., "The Thermal Decomposition of Wood," *Wood Chemistry*, **11**, ACS Nomograph Series, No. 97, 2nd Ed., Reinhold Pub. Co., New York (1952).

Havens, JA., Welker, J.R., and Sliepcevich, C.M., "Pyrolysis of Wood - A Thermoanalysis," *J. of Fire and Flammability*, **2**, p 32. (1971)

Havens, J.A., Hashemi, H.T., Brown, L.E., and Welker, J.R., "A Mathematical Model of the Thermal Decomposition of Wood," *Combustion Science and Technology*, **5**, pp. 91-98 (1972).

Hileman, F.D., Wojcik, L.H., Futrel, J.M., and Einhorn, I.N., "Thermal Uses and Properties of Carbohydrates and Lignin," Academic Press, New York, p. 49 (1976).

Kansa, E.J., Perlee, H.E., and Chaiken, R.F., "Mathematical Model of Wood Pyrolysis Including Internal Forced Convection," *Combustion and Flame*, **29**, pp. 311-324 (1977).

Kanury, M.A., "Burning of Wood. A Pure Transient Conduction Model," *J. of Fire and Flammability*, **2**, p. 191 (1971).

Kanury, M.A., "Rate of Burning of Wood. (A Simple Thermal Model)," *Combustion Science and Technology*, **5**, pp. 135-146, (1972).

Kanury, M.A., "Rate of Charring Combustion in a Fire," *14th Symposium (Int'l) on Combustion*, The Combustion Institute, Pittsburgh, PA, p. 1131 (1973).

Kanury, A.M., and Blackshear, P.L., "On the Combustion of Wood. II: The Influence of Internal Convection on Transient Pyrolysis of Cellulose," *Combustion Science and Technology*, **2**, pp. 5-9 (1970).

Kanury, A.M., and Blackshear, P.L., "Pyrolysis Effect in the Transfer of Heat and Mass in Thermally Decomposing Organic Solids," *Eleventh Symposium (Int'l) on Combustion*, p 517 (1967).

Kanury, A.M., and Backshear, P.L., "Some Considerations Pertaining to the Problem of Wood-Burning," *Combustion Sciences and Technology*, **1**, pp. 339-355 (1970).

Kanury, M.A., and Holve, D.J., "Transient Conduction With Pyrolysis (Approximate Solutions For Charring of Wood Slabs," *J. of Heat Transfer*, Transactions of ASME, 104, p.338, (1982).

Kashiwagi, T., "Radiative Ignition Mechanism of Solid Fuels," *Fire Safety Journal*, **3**, 185-200, (1981).

Kashiwagi, T., Ohlemiller, T.J., Werner, K., "Effects of External Radiant Flux and Ambient Oxygen Concentration on Nonflaming Gasification Rates and Evolved Products of White Pine," *Combustion and Flame* **69**, pp. 331-345, (1987).

Kashiwagi, T., T.J. Ohlemiller, K. Werner, "Wood Gasification at Fire Level Heat Fluxes," *Combustion and Flame*, **69**, pp. 155-170, (1987).

Kilzer, F.J., and Broido, A., *Pyrodynamics*, **2**, pp. 151-163 (1965).

Krause. Jr., R.F., and Gann, R.G., "Rate of Heat Release Measurments Using Oxygen Consumption," *J. of Fire and Flammability*, **12** pp. 117 (1980).

Kung, H.C., "A Mathematical Model of Wood Pyrolysis," *Combustion and Flame*, **20**, pp. 185-195, (1972).

Kung, H.C., "The Burning of Vertical Wooden Slabs," *15th Symposium (Int'l) on Combustion*, The Combustion Institute, Pittsburgh, PA, p. 243, (1975).

Kung, H.C., and Kalelkar, A.S., "On the Heat of Reaction in Wood Pyrolysis," *Combustion and Flame*, **20**, pp. 91-103, (1973).

Landau, H.G., "Heat Conduction in a Melting Solid," *Quarterly of Appl. Math.* FBVIII, No. 1, (1949).

Lee, C., and R.F. Chaiken, and J.M. Singer, "Charring Pyrolysis of Wood in Fires by Laser Simulation," *16th Symposium (Int'l) on Combustion*, (1976).

Lee, C.K., and J.R. Diehl, "Combustion of Irradiated Dry and Wet Oak," *Combustion and Flame*, **42**, pp. 123-138, (1981).

Lewellen, P.C., W.A. Peters, and J.B. Howard, "Cellulose Pyrolysis Kinetics and Char Formation Mechanism," *16th Symposium (Int'l) on Combustion*, p. 1471, (1976).

Loehrke, R.I., and Nagib, H.M., "Control of Free-Stream Turbulence by Means of Honeycombs: A Balance Between Suppression and Generation," *Journal of Fluids Engineering*, (September 1976).

Madorsky, S.L., "Thermal Degradation of Organic Polymers," R.E. Kreiger Publishers, New York, (1975).

Madorsky, S.L., V.E. Hart, and S.J. Staus, Res. Nat'l Bur. Stad., **56** (6), pp. 343-354 (1956).

Martin, S., *Tenth Symposium (Int'l) on Combustion*, pp. 877-896 (1965).

Matsumoto, T., T. Fujiwaru, and J. Kondo "Nonsteady Thermal Decomposition of Plastics," *12th Symposium (int'l) on Combustion*, p. 515 (1969).

Min, K., and H.W. Emmons "Drying of Porous Media," *Heat Transfer Fluid Mechanics Institute*, pp. 1-18 (1972).

Mitchel, U., and Frobel, E. "Lower Limit for the Velocity Fluctuation Level in Wind Tunnels," *Experiments in Fluids*, **6**, pp. 49-54, (1988).

Myers, G.E., "Analytical Methods in Conduction Heat Transfer," McGraw-Hill Publishers, New York, (1971).

Panton, R.L., and Rittmann, J.G., *13th Symposium (Int'l) on Combustion*, The Combustion Institute, Pittsburgh, PA, p. 881, (1971).

Parker, W.J., "Determination of the Kinetic Parameters and the Heat of Combustion of the Volatiles for Wood," Preprint. Center for Fire Research, NBS, (1985).

Quintiere, J., *Fire and Materials*," **5**, p. 51 (1981).

Roberts, A.F., and Clough, G., "Thermal Decomposition of Wood in an Inert Atmosphere," *9th Symposium (Int'l) on Combustion*, the Combustion Institute, Pittsburgh, PA, p. 158, (1963).

Roberts, A.F., "A Review of Kinetics for the Pyrolysis of Wood and Related Substances," *Combustion and Flame*, **14**, pp. 261-272 (1970).

Roberts, A.F. "Problems Associated with the Theoretical Analysis of Burning of Wood," *13th Symposium (Int'l) on Combustion*, p. 893, (1971).

Roberts, A.f. "Heat of Reaction During Pyrolysis of Wood," Combustion and Flame, **17**, p.79 (1971).

Rogers, F.E., and Ohlemiller, T.J., "Cellulosic Insulation Materials, I. Overal Degradation Kinetics and Reaction Heats," *Combustion Sciences and Technology*, **24**, 129, (1980).

Rohsenow, W.M. and Hartnett, J.P., "Handbook of Heat Transfer," McGraw-Hill Book Co. (1973).

Shafizadeh, F., Sarkanen, K.V., and Tillman, D.A., "Thermal Uses and Properties of Carbohydrates and Lignins," Academic Press, New York, (1976).

Shafizadeh, F., "Chemistry of Pyrolysis and Combustion of Wood," *Int'l Conference on Residential Solid Fuels*, Oregan Graduate Center, Portland, Oregan (1981).

Shivadev, U.K., and Emmons, H.W., "Thermal degradation and Spontaneous Ignition of paper Sheets in Air by Irradiation," *Combustion and Flame*, **22**, p. 223 (1974).

Siau, F.J., "Flow in Wood," Syracuse University Press, Syracuse, New York (1971).

Simms, D.L., and Law, M., "The Ignition of Wet and Dry Wood by Radiation," *Combustion and Flame*, **11**, p. 377 (1967).

Susott, R.A., "Characterization of the Thermal Properties of Forest Fuels by Combustible Gas Analysis," *Forest Science*, **28**, 2, pp. 404-420 (1982).

Tang, W.K., "Effects of Inorganic Salts on Pyrolysis of Wood, Alpha-Cellulose, and Lignin Determined by Dynamic Thermogravimetry," *U.S. Forest Services Research Paper*, FPL71, Forest Products Laboratory, Madison, Wisconsin (1967).

Tinney, E.R., "The Combustion of Wooden Dowels in Heated Air," *10th Symposium (Int'l) on Combustion*, pp. 925-930 (1965).

Volvlle, C., Delfau, "Mass Loss Rate Measurment on Solid Materials Under Radiative

Heating," *Combustion Science and Technology*, **36**, pp. 1-18, (1984).

Volvelle, C., Akrich, R. and Delfau,J.L., "Thermal Degradation of Solid Materials Under A Variable Radiant Heat flux," *20th Symposium (Int'l) on Combustion*, The Combustion Institute, Pittsburgh, PA, p. 1674, (1984).

Volvelle, C., Delfau, J.L., Reuillon, M., Bransier, J., Laraqui, N., "Experimental and Numerical Study of the Thermal Degradation of PMMA," *Combustion Science and Technology*, **53**, pp.187-201, (1987).

Welker, J.R., "The Pyrolysis and Ignition of Cellulosic Materials: A Literature Review," *J. of Fire and Fammability*, **1**, p.12 (1970).

Wesson, H.R., Welker, J.R., and Sliepcevich, C.M., "The Piloted Ignition of Wood by Thermal Radiation," *Combustion and Flame*, **16** p.303 (1970.

Wichman, W.S., and Atreya, A., "A Simplified Model for the Pyrolysis of Charring Materials," *Combustion and Flame*, **68**, pp.231-247, (1987).

Wilson, D.G., Solomon, A.D. and Boggs, P.T., "Moving Boundry Problems," Academic Press, New York, (1978).

Zardy, C.A., and Pyle, D.L. Proceedings of the Indians Academy of Sciences, *J. of Engineering Sciences*, **5**, part 4, p. 264 (1982).